frontiers | Research Topics

Acetic acid bacteria

Edited by
Isidoro García-García, Maria Gullo, Fusheng Chen and Teresa Garcia-Martinez

Published in
Frontiers in Microbiology

ISSN 1664-8714
ISBN 978-2-83251-665-2
DOI 10.3389/978-2-83251-665-2

About Frontiers

Frontiers is more than just an open access publisher of scholarly articles: it is a pioneering approach to the world of academia, radically improving the way scholarly research is managed. The grand vision of Frontiers is a world where all people have an equal opportunity to seek, share and generate knowledge. Frontiers provides immediate and permanent online open access to all its publications, but this alone is not enough to realize our grand goals.

Frontiers journal series

The Frontiers journal series is a multi-tier and interdisciplinary set of open-access, online journals, promising a paradigm shift from the current review, selection and dissemination processes in academic publishing. All Frontiers journals are driven by researchers for researchers; therefore, they constitute a service to the scholarly community. At the same time, the *Frontiers journal series* operates on a revolutionary invention, the tiered publishing system, initially addressing specific communities of scholars, and gradually climbing up to broader public understanding, thus serving the interests of the lay society, too.

Dedication to quality

Each Frontiers article is a landmark of the highest quality, thanks to genuinely collaborative interactions between authors and review editors, who include some of the world's best academicians. Research must be certified by peers before entering a stream of knowledge that may eventually reach the public - and shape society; therefore, Frontiers only applies the most rigorous and unbiased reviews. Frontiers revolutionizes research publishing by freely delivering the most outstanding research, evaluated with no bias from both the academic and social point of view. By applying the most advanced information technologies, Frontiers is catapulting scholarly publishing into a new generation.

What are Frontiers Research Topics?

Frontiers Research Topics are very popular trademarks of the *Frontiers journals series*: they are collections of at least ten articles, all centered on a particular subject. With their unique mix of varied contributions from Original Research to Review Articles, Frontiers Research Topics unify the most influential researchers, the latest key findings and historical advances in a hot research area.

Find out more on how to host your own Frontiers Research Topic or contribute to one as an author by contacting the Frontiers editorial office: frontiersin.org/about/contact

Acetic acid bacteria

Topic editors

Isidoro García-García — University of Cordoba, Spain
Maria Gullo — University of Modena and Reggio Emilia, Italy
Fusheng Chen — Huazhong Agricultural University, China
Teresa Garcia-Martinez — University of Cordoba, Spain

Citation

García-García, I., Gullo, M., Chen, F., Garcia-Martinez, T., eds. (2023). *Acetic acid bacteria*. Lausanne: Frontiers Media SA. doi: 10.3389/978-2-83251-665-2

Table of contents

frontiers | Frontiers in Microbiology

TYPE Editorial
PUBLISHED 31 January 2023
DOI 10.3389/fmicb.2023.1142659

OPEN ACCESS

EDITED AND REVIEWED BY
Aldo Corsetti,
University of Teramo, Italy

*CORRESPONDENCE
Isidoro Garcia-Garcia
✉ isidoro.garcia@uco.es

SPECIALTY SECTION
This article was submitted to Food Microbiology, a section of the journal Frontiers in Microbiology

RECEIVED 11 January 2023
ACCEPTED 13 January 2023
PUBLISHED 31 January 2023

CITATION
Garcia-Garcia I, Gullo M, Chen F and Garcia-Martinez T (2023) Editorial: Acetic acid bacteria. *Front. Microbiol.* 14:1142659. doi: 10.3389/fmicb.2023.1142659

Editorial: Acetic acid bacteria

Isidoro Garcia-Garcia[1]*, Maria Gullo[2], Fusheng Chen[3] and Teresa Garcia-Martinez[4]

[1]Department of Inorganic Chemistry and Chemical Engineering, Agrifood Campus of International Excellence ceiA3, Chemical Institute for Energy and Environment (iQUEMA), University of Córdoba, Córdoba, Spain, [2]Department of Life Sciences, University of Modena and Reggio Emilia, Reggio Emilia, Italy, [3]Food Biotechnology and Food Safety Laboratory, College of Food Science and Technology, Huazhong Agriculture University, Wuhan, China, [4]Department of Agricultural Chemistry, Edaphology and Microbiology, Agrifood Campus of International Excellence ceiA3, University of Córdoba, Córdoba, Spain

KEYWORDS

acetic acid bacteria, oxidative fermentation, vinegar, omics, exopolysaccharides, taxonomy, acid resistance, genetic improvement

Editorial on the Research Topic
Acetic acid bacteria

Acetic acid bacteria (ABB) are strictly aerobic organisms that can be found in a wide variety of natural and industrial environments. Their versatility and metabolic adaptability make them microorganisms of high interest to study the optimization of obtaining their multiple products and the essential mechanisms that allow them to grow under extreme conditions. Their metabolism, particularly the role of membrane-bound and soluble dehydrogenases, may offer new opportunities in the development of innovative processes based on their capability for carrying out the incomplete oxidation of several substrates. On the other hand, the resistance of AAB to some extreme conditions, i.e., low pH values, and adaptability to many different habitats make them highly competitive bacteria; so, their interaction with other organisms and plants is a very important topic to be studied. The ability of AAB in producing exopolysaccharides is also of great interest for both research and industrial purposes. They are considered as model organisms for understanding the mechanisms of cellulose synthesis and they are until now the most efficient organisms for producing it, under controlled conditions. Finally, the current state of omic technologies and efficient genetic modification methods can be applied for a greater understanding of the physiological behavior, the recovery of new strains and/or those occurring in complex environments as well as to exploit the full potential of AAB for oxidative bioconversions.

Taking all of the above into account, this Research Topic aims to address some of the most recent advances and challenges that arise around AAB, considering some of the main areas of study: taxonomy, physiology, products and processes, microbiota analysis, omic aspects, adaptation and genetic modification and others.

Considering the taxonomic revisions and the recent advances, which include a progressive increase of species as well as the description of new genera, especially within genera that are today recognized of great biotechnological relevance, a systematic of AAB is a hot topic. From the taxonomic point of view, until 2021, 19 genera of AAB have been reported (He et al.).

The high versatility of AAB in performing microbial bioconversion is industrially exploited mainly in foods and beverages, biomedical, pharmaceutical, cosmetics and agronomical fields. Some of the main products obtained by AAB, resulting from the activity of cytoplasmic membrane-bound dehydrogenases, are sorbose, dihydroxyacetone, miglitol and acetic, gluconic, gulonic and galactonic acids; up to now, at least 86 products of this type have been reported in the literature (see Figure 1, He et al.).

AAB, traditionally known for their ability to incompletely oxidize many sugars and alcohols, appear as the responsible organisms for vinegar production. Vinegar is, probably, one of the best known products of AAB and one of the most economically important. For this reason, and because many aspects remain still unknown, it is not surprising that there is an important field of work on it. Next references, published in this Research Topic, show some examples of topics under research on vinegar: Mizzi J et al.; Qian et al.; Román-Camacho, Mauricio et al.; Román-Camacho, García-García et al.; Xia et al.; Yang et al.

Mizzi et al. study the isolation, identification and fermentation performance of indigenous AAB from local raw materials.

On the other hand, Qian et al. are studying another of the problems that affect the behavior of the complex microbiota responsible for acetification in the production of vinegar; specifically, the interactions between prophages and the microbiota itself. The study evaluates the co-evolution of prophages and the genus *Acetobacter*; evidencing the important influence it has on the stability of the bacterial genome and thus affecting the industrial production of vinegar.

Using omic techniques, Román-Camacho, Mauricio et al.; Román-Camacho, García-García et al. approach the difficult problem of identifying and characterizing the complex microbial communities responsible for the production of vinegar, as well as the influence of the use of various culture media. Both through metaproteomics and metagenomics recognize that the microbial composition during industrial vinegar production include mainly *Komagataeibacter* members, especially *Komagataeibacter europaeus* strains. Likewise, the works show the ability of bacteria to adapt to different culture media through metabolic versatility.

Many of the products obtained by AAB are the result of complex microbial communities, either formed by AAB exclusively, or by AAB and other microorganisms. For example, the cereal vinegars produced in China are one more example of these complex ecosystems. The work of Xia et al. studies the interactions between AAB and lactic acid bacteria (LAB) during the solid-state fermentation of Shanxi aged vinegar. In this same context of complex microbial communities, Bouchez et al. carried out a review of the role of AAB in the production of sour beers. The identification, activities and, especially, the interactions at the molecular level between all microorganisms, is one of the problems in which these bacteria are almost always involved.

Another aspect that also receives a lot of attention is the one related to the study of how AAB resist the aggressive environments in which they are normally found, for example, the high acidity values during the industrial production of vinegar. Using RNA-Seq transcriptomic analysis, Yang et al. study gene regulation changes to find possible relationships with the acidity of the medium.

As previously mentioned, there are multiple products that can be obtained by AAB, for example, new sweeteners such

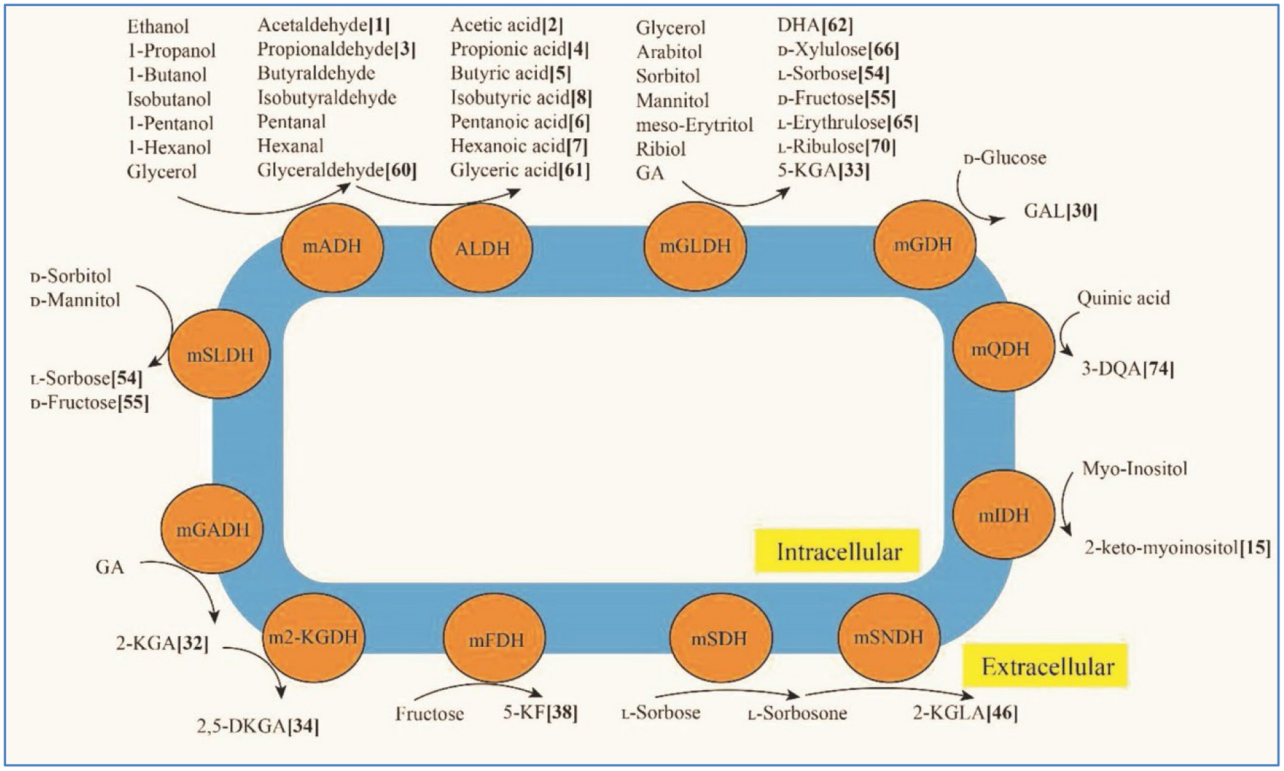

FIGURE 1
Figure 3 in He et al.. Typical membrane-binding dehydrogenases in acetic acid bacteria and their main oxidative fermentation products. mADH: membrane-binding alcohol dehydrogenase; mALDH: membrane-binding acetaldehyde dehydrogenase; mGADH: membrane-binding gluconate dehydrogenase; m2-KGDH: membrane-binding 2-keto-D-gluconate dehydrogenase; mFDH: membrane-binding D-fructose dehydrogenase; mSLDH: membrane-binding D-sorbitol dehydrogenase; mGDH: membrane-binding glucose dehydrogenase; mGLDH: membrane-binding glycerol dehydrogenase; mQDH: membrane-binding quinic acid dehydrogenasw; mIDH: membranebinding inositol dehydrogenase; mSDH: membrane-binding sorbose dehydrogenase; mSNDH: membrane-binding sorbone dehydrogenase; GA: gluconic acid; 2-KGA: 2-keto-Dgluconic acid; 2, 5-DKGA: 2, 5-diketo-D-gluconic acid; 5-KF: 5-keto-D-fructose; DHA: dihydroxyacetone; 3-QDA: 3-dehydroquinic acid; 2-KGLA: 2-keto-l-gulonic acid.

as 5-keto-D-fructose (5-KF) from the oxidation of fructose (see Figure 1). Although it is important to know all the aspects of its synthesis, it is also important to evaluate the properties of all these products from the point of view of the final use that is intended to be made of them. In this case, in the context of the search for new, healthier sweeteners, the work presented by Hövels et al. reveals the cytotoxic potential of 5-KF for both eukaryotic and prokaryotic cells. Therefore, its use in the food sector is not recommended.

Another of the products that can be obtained with AAB and with great potential for various applications is bacterial cellulose. Anguluri et al. carry out a study on *Komagataeibacter xylinus* K2G30 to evaluate its adaptation capacity on mannitol and even on D-fructose. The strain used shows a great adaptability for the production of cellulose. All this reveals the metabolic versatility of *K. xylinus* K2G30, which suggests the possibility of developing new strategies to produce bacterial cellulose without the need to use other approaches through genetic engineering.

As already mentioned, the most important product obtained by AAB is acetic acid in the context of vinegar production, and in this sense, other microorganisms cannot compete with them. However, if we consider the possibility of using AAB for the synthesis of acetic acid for producing it as a pure commodity they cannot compete with the chemical synthesis. For this reason, Krusong et al., selected a *Paenibacillus azoreducens* strain, which presents some metabolic advantages over *Acetobacter pasteurianus* (UMCC 2951) and which, in combination with AAB, might be used for the production of acetic acid as a non-food grade commodity.

New and highly efficient methods of genetic modification can further expand the potential of this group of bacteria. In this context, Fricke et al., study the use of the L-rhamnose regulator and its target promoters from *Escherichia coli* to act on the repression or activation of certain genes in *Gluconobacter oxydans*; all this is highly interesting to achieve the redirection of carbon flows in the context of metabolic engineering. On the other hand, another extremely interesting strategy to deduce the carbon flux is through a genomic analysis using an *in-silico* approach, which allows the simulation of reconstructing genome-scale metabolic models (GEMs). An example of this can be found in Pelicaen et al., in the context of the complex fermentation of cocoa where there are species, *Acetobacter ghanensis* and *Acetobacter senegalensis*, over which others clearly prevail, *Acetobacter pasteurianus*. In this way, it is possible to deepen the knowledge of bacterial metabolism and, thus, its adaptation to different substrates and conditions and some progress could be made in many aspects, for instance, in the preparation of optimal starter cultures for this fermentation.

Author contributions

All authors listed have made a substantial, direct, and intellectual contribution to the work and approved it for publication.

Acknowledgments

We would like to thank all the authors and peer reviewers for their valuable contributions to this special issue. This issue would not be possible without their valuable and professional work. In addition, we would also like to take the opportunity to show our gratitude to the Frontiers editorial team for their work.

Conflict of interest

The authors declare that the research was conducted in the absence of any commercial or financial relationships that could be construed as a potential conflict of interest.

Publisher's note

frontiers | Frontiers in Microbiology

ORIGINAL RESEARCH
published: 29 April 2022
doi: 10.3389/fmicb.2022.840119

Unraveling the Role of Acetic Acid Bacteria Comparing Two Acetification Profiles From Natural Raw Materials: A Quantitative Approach in *Komagataeibacter europaeus*

Juan J. Román-Camacho[1], Juan C. Mauricio[1], Inés M. Santos-Dueñas[2], Teresa García-Martínez[1] and Isidoro García-García[2]*

[1] Department of Agricultural Chemistry, Edaphology and Microbiology, University of Córdoba, Córdoba, Spain, [2] Department of Inorganic Chemistry and Chemical Engineering, Institute of Nanochemistry (IUNAN), University of Córdoba, Córdoba, Spain

OPEN ACCESS

Edited by:
Lisa Solieri,
University of Modena and Reggio Emilia, Italy

Reviewed by:
Isao Yumoto,
National Institute of Advanced Industrial Science and Technology (AIST), Japan
Zheng-Hong Xu,
Jiangnan University, China

***Correspondence:**
Juan C. Mauricio
mi1gamaj@uco.es

Specialty section:
This article was submitted to Food Microbiology, a section of the journal Frontiers in Microbiology

Received: 20 December 2021
Accepted: 25 February 2022
Published: 29 April 2022

Citation:
Román-Camacho JJ, Mauricio JC, Santos-Dueñas IM, García-Martínez T and García-García I (2022) Unraveling the Role of Acetic Acid Bacteria Comparing Two Acetification Profiles From Natural Raw Materials: A Quantitative Approach in Komagataeibacter europaeus. Front. Microbiol. 13:840119. doi: 10.3389/fmicb.2022.840119

The industrial production of vinegar is carried out by the activity of a complex microbiota of acetic acid bacteria (AAB) working, mainly, within bioreactors providing a quite specific and hard environment. The "omics" sciences can facilitate the identification and characterization analyses of these microbial communities, most of which are difficult to cultivate by traditional methods, outside their natural medium. In this work, two acetification profiles coming from the same AAB starter culture but using two natural raw materials of different alcoholic origins (fine wine and craft beer), were characterized and compared and the emphasis of this study is the effect of these raw materials. For this purpose, the composition and natural behavior of the microbiota present throughout these profiles were analyzed by metaproteomics focusing, mainly, on the quantitative protein profile of *Komagataeibacter europaeus*. This species provided a protein fraction significantly higher (73.5%) than the others. A submerged culture system and semi-continuous operating mode were employed for the acetification profiles and liquid chromatography with tandem mass spectrometry (LC-MS/MS) for the protein analyses. The results showed that neither of two raw materials barely modified the microbiota composition of the profiles, however, they had an effect on the protein expression changes in different biological process. A molecular strategy in which *K. europaeus* would prevail over other species by taking advantage of the different features offered by each raw material has been suggested. First, by assimilating the excess of inner acetic acid through the TCA cycle and supplying biosynthetic precursors to replenish the cellular material losses; second, by a previous assimilation of the excess of available glucose, mainly in the beer medium, through the glycolysis and the pentose

phosphate pathway (PPP); and third, by triggering membrane mechanisms dependent on proton motive force to detoxify the cell at the final moments of acetification. This study could complement the current knowledge of these bacteria as well as to expand the use of diverse raw materials and optimize operating conditions to obtain quality vinegars.

Clinical Trial Registration: [www.ClinicalTrials.gov], identifier [PXD031147].

Keywords: ***Komagataeibacter europaeus*, vinegar, fine wine, craft beer, proteomics, submerged culture**

INTRODUCTION

The industrial elaboration of vinegar is carried out through an acetification process from an alcoholic raw material obtaining a final product with high acetic acid content. The incomplete oxidation of the ethanol into acetic acid is performed by acetic acid bacteria (AAB), strictly aerobic microorganisms that, among their several biotechnological applications, are primarily responsible for this process of biotransformation that occurs within industrial reactors (García-García et al., 2007; Mamlouk and Gullo, 2013).

The quality of the vinegar depends on many factors including the microbial composition, the raw material, and operating conditions (Mas et al., 2014; Li et al., 2015). Regarding microbial composition, several studies have demonstrated that vinegar is a product resulting from the metabolism of a complex AAB microbiota, not by pure species (Trček et al., 2016; Román-Camacho et al., 2020). This microbiota is mostly composed of species from the genera *Acetobacter* and *Komagataeibacter* (many of them relocated from *Gluconacetobacter*) which are imposed because of their high capabilities for vinegar production, although species from other genera might coexist with the best-adapted ones (Gullo et al., 2014; Wang et al., 2015). The raw material employed as acetification substrate plays an essential role in the quality of the final product. High-quality wines allow to elaborate some of the most appreciated vinegars in the world, however, other alcoholic substrates including cereals (rice, malt, wheat, corn, and among others), fruits, and apple cider are also well-known (Hidalgo et al., 2013; Trček et al., 2016; Zhang et al., 2019; Kandylis et al., 2021; Peng et al., 2021). Conversely, vinegar is mainly produced at the industrial scale by submerged cultures in reactors that continuously supply very fine air bubbles into the medium as an aeration mechanism. The submerged system has several advantages over other techniques, such as solid-state fermentation or surface fermentation including high yield and process speed (Gullo et al., 2014). Through a semi-continuous operating mode, in which each cycle starts by loading the tank with fresh medium to a preset volume and finishes when a part of the volume is unloaded after depleting ethanol to an also preset concentration, high productivity and stability are ensured (Jiménez-Hornero et al., 2020). This working mode allows part of the biomass produced in each cycle to rapidly start the next one. Also, the operational variables can be used to maintain the average substrate and product concentrations within appropriate ranges for AAB to operate, which in turn, facilitates self-selection and adjustment to the specific medium (García-García et al., 2019).

The particular growing conditions and metabolic characteristics of AAB hinder their isolation outside the environments in which they carry out their activity fully (Fernández-Pérez et al., 2010; Mamlouk and Gullo, 2013). This fact limits the study of the richness and biodiversity of these microbiota that inhabit aggressive media as is the case of vinegar. The "omics" sciences can facilitate the analysis of the identification and function of complex microbiomes and resolve the hurdles of traditional methods for the characterization of either non-cultivable or hard to cultivate microorganisms (Andrés-Barrao et al., 2016; Xia et al., 2016; Zhu et al., 2018; Jiang et al., 2019; Verce et al., 2019). Recently, the microbiota of an acetification process using an alcohol medium as a reference has been characterized at a metaproteomic level (Román-Camacho et al., 2020, 2021). The *Komagataeibacter* species were predominant throughout the process and *K. europaeus* provided the major fraction of proteins, far above the others. This species has been described as one of the most suitable AAB for the industrial production of vinegar because of its growing conditions that include high ethanol-oxidizing ability, acetic acid requirement, and tolerance to both low [7–9% (w/v)] and high acidity levels [10–20% (w/v)] (Trček et al., 2007; Yamada et al., 2012; Gullo et al., 2014; Peng et al., 2021).

The present work aims to characterize and compare two acetification profiles using the same starter culture, coming from an acetification of previous works (Román-Camacho et al., 2020, 2021) making alcohol vinegar, but using different raw materials. For this purpose, the composition and natural behavior of the microbiota present throughout both processes were compared employing a metaproteomic analysis and especially, focusing on the protein profile of *K. europaeus* from an exhaustive quantitative approach. This species has been selected, as in our previous studies, because it provides a considerable amount (73.5%) of the metaproteome and plays an essential role in the microbial community function. A comparison of vinegar profiles using two natural raw materials (fine wine and craft beer), with a higher nutritional richness than the reference synthetic alcohol medium (Román-Camacho et al., 2020, 2021), under a strategy that employs a submerged culture and a semi-continuous operating mode, could elucidate the effect of the raw materials

on the organoleptic properties and quality of industrially elaborated vinegars.

MATERIALS AND METHODS

Raw Material

Two different alcoholic substrates were used as fermentation media: a dry fine wine from the Montilla-Moriles region (Bodegas Alvear S.A., Montilla, Córdoba, Spain) and a craft beer (Mahou-San Miguel, Córdoba, Spain). The dry fine wine contained an initial ethanol concentration of 15% (v/v) and an amino acids content of 0.72 ± 0.20 mM for L-proline, 0.24 ± 0.03 mM for L-aspartic acid, 0.23 ± 0.21 mM for ammonium ion, 0.21 ± 0.00 mM for L-γ-aminobutyric acid, 0.19 ± 0.02 mM for L-glutamic acid, 0.16 ± 0.01 mM for L-lysine, 0.15 ± 0.01 mM for L-arginine, 0.11 ± 0.01 mM for L-tyrosine, 0.06 ± 0.01 mM for L-leucine, 0.05 ± 0.01 mM for L-valine, 0.04 ± 0.01 mM for L-histamine, 0.03 ± 0.01 mM for L-glycine, 0.02 ± 0.01 mM for L-threonine, and 0.01 ± 0.01 mM for L-tryptophan. Conversely, the craft beer was obtained from a medium containing 35% of total sugars, remaining without fermenting 7% and composed, roughly, half, and half between maple syrup and muscovado sugar. The ethanol content was 17% (v/v) and the amino acids content of 3.66 ± 0.05 mM for L-γ-aminobutyric acid, 1.44 ± 0.03 mM for L-aspartic acid, 1.21 ± 0.02 mM for L-glutamic acid, 1.05 ± 0.02 mM for L-arginine, 0.92 ± 0.02 mM for ammonium ion, 0.90 ± 0.13 mM for L-proline, 0.55 ± 0.01 mM for L-glutamine, 0.47 ± 0.01 mM for L-glycine, 0.39 ± 0.01 mM for L-phenylalanine, 0.30 ± 0.01 mM for L-tryptophan, 0.18 ± 0.01 mM for L-leucine, 0.17 ± 0.01 mM for L-tyrosine, 0.13 ± 0.01 mM for L-histidine, 0.11 ± 0.03 mM for L-threonine, 0.04 ± 0.01 mM for L-histamine, and 0.02 ± 0.01 mM for L-lysine. Both raw materials were diluted with distilled water to adjust the ethanol concentration to the working conditions [≈ 10% (v/v)] reaching 9.8 ± 0.3 and 9.5 ± 0.3% (v/v) for fine wine and beer, respectively; the initial acetic acid concentration was of 0.2 ± 0.1% (w/v).

Microorganism

The starter culture consisted of a mixed broth coming from a fully active acetification process making alcohol vinegar, concretely harvested from the end of the ethanol exhausting phase, see microbial composition in **Supplementary File 1** (Román-Camacho et al., 2020). This original alcohol medium was composed of 10% ethanol, glucose (1 g/L), calcium pantothenate (13 mg/L), calcium citrate (0.1 g/L), potassium citrate (0.1 g/L), diammonium phosphate (0.5 g/L), magnesium sulfate (0.1 g/L), manganese sulfate (5 mg/L), and iron chloride (1 mg/L) following the method of Llaguno (1991) with yeast extract (0.25 g/L) and peptone (0.5 g/L) additionally supplied. A previous stage using each specific raw material, including several cycles of acetification, is necessary to adapt the inoculum and achieve a repetitive system behavior.

Operating Mode

Acetification cycles were carried out in a fully automated 8 L Frings bioreactor (Heinrich Frings GmbH & Co., KG, Bonn, Germany) working in a semi-continuous operating mode. Each cycle is started by a loading phase that replenishes the reactor with a fresh medium to the working volume (8 L) without exceeding a preset ethanol concentration of 5% (v/v). Then, an exhausting stage occurs depleting ethanol in the culture broth to a preset concentration of 1.0–1.5% (v/v). Finally, 50% of the volume is fast unloaded and the remaining content is used as inoculum of the next cycle. A constant temperature of 31°C, a fast-loading rate of 1.3 L/h, and an air-flow rate of 7.5 L/(h L medium) were employed. Sigmaplot 12.0 (Systat Software Inc., CA, United States) was used for graphical representation of the acetification profiles after monitoring the system data by LabView application (National Instruments, TX, United States). **Figure 1** shows the profiles of the main variables.

Sampling

Sampling was performed at two relevant times of the acetification cycle: at the end of the loading phase (EL), when final working volume or preset ethanol concentration of 5% (v/v) is reached, whichever occurs first; and just before the unloading phase, at the end of the ethanol exhaustion (UL). A total of 15 acetification cycles for each vinegar profile were performed including some previous cycles (7–10) necessary to achieve a semi-continuous repetitive state of the system. Six samples were harvested from fine wine vinegar: three at EL (cycles 12, 14, and 15) and three at UL (cycles 11, 13, and 14); and seven samples from beer vinegar: four at EL (cycles 11, 12, 13, and 14) and three at UL (cycles 12, 13, and 14).

Analytical Methods

System variables including the volume of the medium (L), ethanol concentration % (v/v), and temperature (°C) were constantly measured using an EJA 110 differential pressure probe (Yokogawa Electric Corporation, Tokyo, Japan), an Alkosens® probe (Heinrich Frings GmbH & Co., KG, Bonn, Germany), and a temperature probe, respectively. The automatization of the system allows the continuous recording of data as well as testing the high reproducibility of the method. Acetic acid concentration %, (w/v) was determined by acid-base titration with 0.5 N NaOH. Viable cells concentration, the difference between total and no viable cells, were directly counted using a light microscope (Olympus BX51), a Neubauer chamber (Blaubrand™, 7178-10) with 0.02 mm depth and rhodium-coated bottom, and propidium iodide (VWR, Inc., PA, United States). Though the chamber was subdivided into 25 square groups, composed of 16 squares each, 5 square groups (0.04 mm^2 each) on the diagonal were used for cell counting following the method of Baena-Ruano et al. (2006); samples were quantified by triplicate and standard error was calculated. These variables were exclusively measured at sampling times. The efficiency of the process was evaluated by mean acetification rate (r_A) and

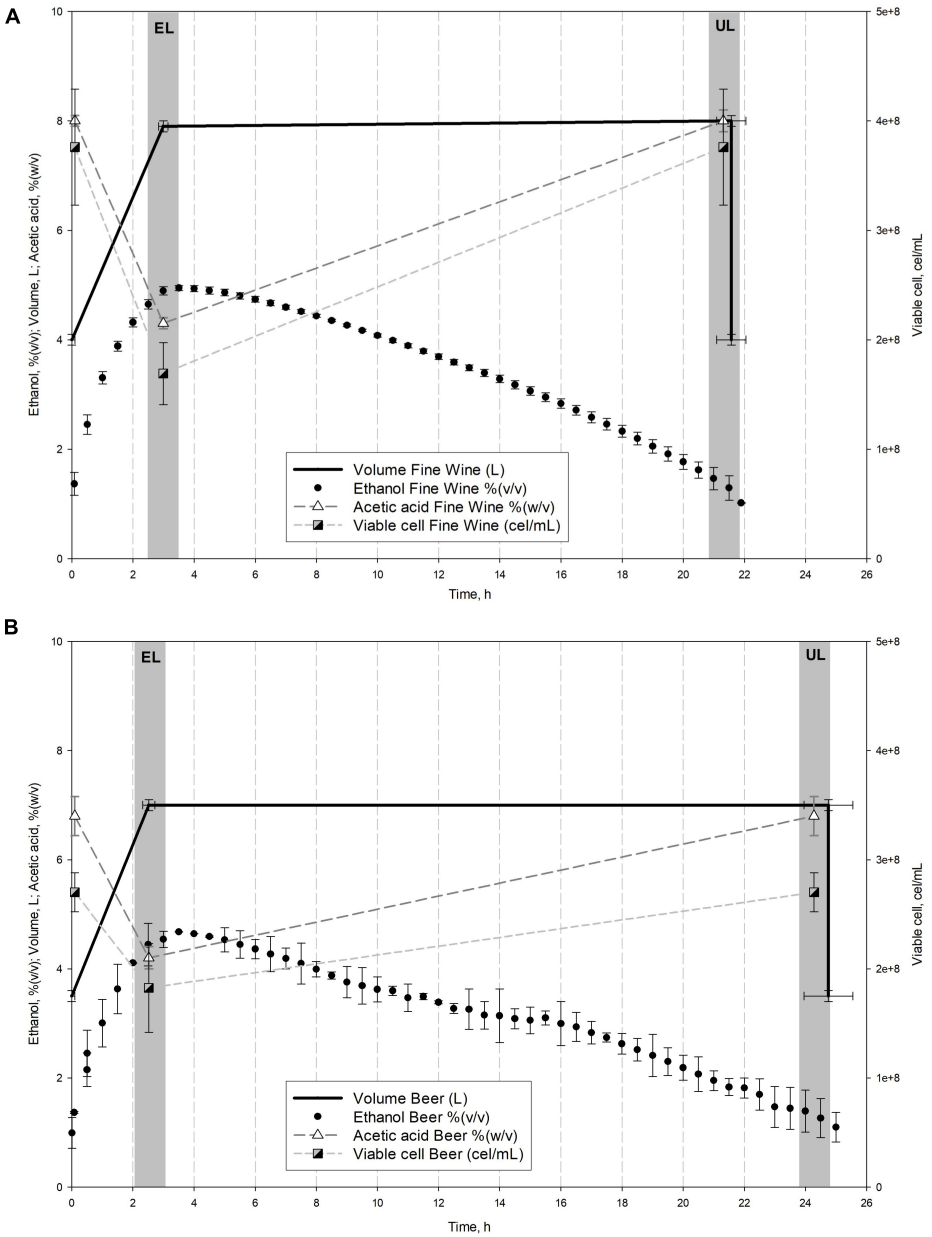

FIGURE 1 | Comparison of the main system variables throughout fine wine **(A)** and beer **(B)** vinegar profiles. Mean values and standard deviation (*SD*) of the variables of stable cycles performed are represented. Sampling times (EL, end of loading; UL, just before unloading) are also shown.

global production of acetic acid (p_A) which were calculated as follows:

$$r_A = \frac{\begin{array}{c}Final\ acetic\ acid\ concentration\ (\%,\ w/v)\\ \times Unloaded\ volume\ (L)\end{array}}{Total\ cycle\ time\ (h)\ \times\ Mean\ cycle\ volume\ (L)}$$

$$p_A = \frac{\begin{array}{c}Final\ acetic\ acid\ concentration\ (\%,\ w/v)\\ \times\ Unloaded\ volume\ (L)\end{array}}{Total\ cycle\ time\ (h)}$$

Proteomics

Sample Processing

Vinegar samples were harvested by directly unloading a volume of 300 mL from the pilot acetator, dividing it into six fractions of 50 mL each, and putting them in centrifuge tubes on ice. Cells were separated by centrifugation and then, twice cleaned using cold sterile distilled water; the resulting pellets were stored at −80°C. Then, cell extracts were broken by several cycles using glass beads and sonication after adding extraction buffer (100 mM Tris-HCl buffer pH 8.0, 2 mM dithiothreitol (DTT), 1 mM ethylenediaminetetraacetic acid (EDTA), and

1 mM phenylmethylsulphonyl fluoride (PMSF) supplemented with Protease Inhibitor Cocktail tablets). The protein fraction was precipitated, vacuum dried, solubilized, and its concentration was quantified by Bradford (1976) assays. A volume of each protein sample containing 50 μg was injected into LC-MS/MS analysis at Research Support Central Service (SCAI), University of Córdoba, Spain. All proteomic procedures were performed following the methodology previously developed by our group (Román-Camacho et al., 2020).

Protein Identification by Database Searching

Mass spectrometry raw data were processed using Proteome Discoverer (version 2.1.0.81, Thermo Fisher Scientific, MA, United States). MS/MS spectra were searched with SEQUEST engine against Uniprot.[1] Peptides obtained from tryptic digestion were searched setting the following parameters: up to one missed cleavage, cysteine carbamidomethylation as a fixed modification, and methionine oxidation as a variable one. Precursor mass tolerance was 10 ppm while ion products were searched at 0.1 Da tolerances. Peptide spectral matches (PSM) validation was performed at a 1% FDR using a percolator based on *q*-values. Peptide quantification was carried out by calculating precursor ion areas by Precursor Ion Area Detector and normalizing by Total Peptide Amount mode of Proteome Discoverer. The parsimony law was applied to obtain protein groups and filtered to 1% FDR.

The mass spectrometry proteomics data have been deposited to the ProteomeXchange Consortium via the PRIDE [1] partner repository with the dataset identifier PXD031147.

Raw Data Analysis

Proteins identified in the metaproteome were first screened removing those with score < 2 and number of peptides ≤ 2. Then, proteins in at least 50% out of total samples (three or four) in at least one sampling time were maintained. Exclusive proteins were obtained by the difference between those aforementioned and those identified in at least 50% out of total samples in each sampling time. From those, a GO Term analysis using Uniprot and Gene Ontology (GO) annotation tool[2] was performed to detail the metaproteome function. Subsequently, an enrichment analysis LC-MS[2] of the proteome of *K. europaeus* was performed and quantitative changes throughout each acetification profile were compared. Protein values were normalized by dividing each one by the sample global intensity and then multiplied by the mean value of global intensity from all samples. First, those proteins obtained in at least 50% of samples in one sampling time were retained and plotted in an intersection diagram ("UpSetR" R library). For the hierarchical clustering and heat map analysis, proteins identified in at least 50% of samples in each sampling time were used. Mean quantification values were previously scaled, centered by z-score transformation, and then, Pearson correlation was applied with method "complete" ("hclust" function in stats package from R). One-Way ANOVA followed by HSD Tukey's test was calculated by R functions "lm" and "anova" and *q*-value was used to calculate *p*-value multiple testing correction. Proteins identified only in one biological replicate were eliminated from the overall count.

Furthermore, the biological function of the protein clusters was studied by building protein-protein interaction network maps (INM) by using STRING database v11.[3] High confidence interaction (score = 0.70–0.90) and protein annotations based on the databases Uniprot (see text footnote 1) and KEGG[4] were used (see **Supplementary File 2**). Because *K. europaeus* is not available in the database, as in previous works (Román-Camacho et al., 2021), *K. xylinus* E25, a closely related species (MUM index of 0.21, according to Ryngajłło et al., 2018), was used as a model organism due to the high genome homology.

RESULTS

Description of Fine Wine and Beer Acetification Profiles: A Comparison

Figure 1 shows a comparison of the mean cycle of main system variables throughout fine wine (**Figure 1A**) and beer (**Figure 1B**) profiles, while **Table 1** lists the mean values of the aforementioned variables. The fine wine profile showed a fast-loading phase up to reach the working volume (8.0 ± 0.1 L) and an ethanol concentration of 4.9 ± 0.0% (v/v) at the end of the stage, at 3.0 ± 0.0 h. An exhausting phase started with the depletion of ethanol content up to 1.3 ± 0.3% (v/v) and just then, 50% of the reactor volume was unloaded (4.0 ± 0.1 L), at 21.4 ± 0.1 h. During this period, both acetic acid concentration [from 4.3 ± 0.0 to 7.9 ± 0.2% (w/v)] and cell viable concentration (from 1.43 ± 0.33 to 1.47 ± 0.28 × 10^8 cel/mL) were increased. The beer profile was operated with a final working volume of 7.0 ± 0.2 L because of the excessive foaming. First, a continuous

[1]http://www.uniprot.org

[2]http://geneontology.org/

[3]https://string-db.org/

[4]https://www.genome.jp/kegg/

TABLE 1 | Main variables of the acetification profile including both the system variables constantly monitored and those exclusively measured at sampling times.

	Variable	FW_EL	FW_UL	B_EL	B_UL
Mean ± *SD*	Cycle time (h)	3.0 ± 0.0	21.4 ± 0.1	2.8 ± 0.4	24.3 ± 1.1
	Volume (L)	8.0 ± 0.1	8.0 ± 0.1	7.0 ± 0.2	7.0 ± 0.2
	Ethanol (% v/v)	4.9 ± 0.0	1.3 ± 0.3	4.7 ± 0.2	1.2 ± 0.1
	Acetic acid (% w/v)	4.3 ± 0.0	7.9 ± 0.2	4.2 ± 0.4	6.8 ± 0.7
	Viable cell (10^8 cel/mL)	1.43 ± 0.33	1.47 ± 0.28	0.84 ± 0.70	1.05 ± 0.70
		FW		B	
	Mean acetification rate (r_A) [g acetic acid/(L h)]	0.19 ± 0.01		0.16 ± 0.01	
	Global acetic acid production (p_A) (g acetic acid/h)	15.2 ± 0.5		11.3 ± 0.5	

Data show mean values of all variables at the sampling times (FW_EL, FW_UL, B_EL, B_UL) and their standard deviation (SD). Variables used to obtain the acetification efficiency of each profile are included.

fast loading was performed to the aforementioned volume and an ethanol concentration of 4.7 ± 0.2% (v/v), both achieved at 2.8 ± 0.4 h. The second phase (24.3 ± 1.1 h) concluded when ethanol concentration was depleted to 1.2 ± 0.1% (v/v) and 50% of the volume of the medium was unloaded (3.5 ± 0.1 L). At the same time, the acetic acid concentration [from 4.2 ± 0.4 to 6.8 ± 0.7% (w/v)] and cell viability (from 0.84 ± 0.70 to 1.05 ± 0.70 × 10^8 cel/mL) were increased throughout this exhausting period. The efficiency of each acetification profile was evaluated by the mean acetification rate (r_A) and global production of acetic acid (p_A), both calculated as described in section "Analytical Methods" (see **Table 1**).

It is interesting to note that the two raw materials used show some significant differences to evaluate the behavior of the microbiota as a function of the available nutrients. In particular, the significant presence of sugars in the craft beer medium could lead, as it will be discussed later in this work, to the activation of several metabolic pathways aimed at taking advantage of this resource. Similarly, fine wine, a substrate whose suitability as an acetification medium is well known, not only allows higher acetification rates, but also higher final acidity values, which leads to harsher environmental conditions. This fact can trigger the activation of metabolic pathways other than those mentioned above in response to stress.

Comparison of the Metaproteome of Fine Wine and Beer Vinegar

Microbial Composition

A total of 1,069 (EL, 934; UL, 945) and 1,268 (EL, 1,226; UL, 1,110) proteins were identified in the LC/MS-MS analysis in fine wine and beer vinegar samples, respectively, after removing contaminants and those proteins not found in at least 50% of the samples in at least one sampling time (see **Supplementary File 1**). Although proteins belonging to 84 different species from the *Acetobacteraceae* family were identified, only 13 of them constituted around 90% of the metaproteome (see **Supplementary Table 1**): 11 species from the *Komagataeibacter* genus (*K. europaeus*, *K. xylinus*, *K. intermedius*, *K. rhaeticus*, *K. diospyri*, *K. swingsii*, *K. medellinensis*, *K. nataicola*, *K. oboediens*, *K.* sp., and *K. sucrofermentans*) as well as *Acetobacter* sp. and *Gluconacetobacter* sp.; *K. europaeus* was the most abundant species providing the largest amount of proteins (73.5%: FW_EL, 75.9%; FW_UL, 75.0%; B_EL, 70.6%; B_UL, 72.6%), far above the rest of species. No relevant differences regarding the composition of the microbiota were observed between sampling times and profiles. Since none of the remaining species exceeds a mean frequency of 0.5%, the functional metaproteome analysis is mainly focused on this major amount, which is considered sufficiently representative of the total (Román-Camacho et al., 2021).

Gene Ontology Term Functional Analysis

Because a high amount of the metaproteome (834 proteins) was common when different raw materials were used during the acetification, a GO Term analysis of exclusive proteins at each sampling time was performed to compare accurately the natural behavior of the microbiota. A total of 259 (FW_EL: 124; FW_UL: 135) and 200 (B_EL: 158; B_UL: 42) exclusive proteins were identified and detailed in **Supplementary File 3**. As previously mentioned, this analysis is mostly focused on the major amount of the metaproteome.

At the end of the loading phase for the fine wine profile (FW_EL), the metabolism of amino acids, mostly aminoacyl-tRNA ligases, cell division, and, briefly, stress-related response (metabolism of glutathione and chaperones) was highlighted between most abundant species. At the end of the exhausting phase (FW_UL), the formation of peptide release factors, ribosomal subunits, and stress-related response (chaperones, redox activity, and synthesis of lipopolysaccharides) were some of the most reported GO Terms. The end of the loading phase for the beer profile (B_EL) showed the metabolism of amino acids, energy metabolism pathways, and redox activity as main functions; exclusively identified in *K. europaeus*, outer membrane proteins as ABC transporters, and porins. At the end of the exhausting phase (B_UL), the predominant species were involved in ATP-binding, redox processes, and cellular homeostasis while the minor fractions were in stress-response (chaperones). *K. europaeus* (73.5%) not only shared the main GO terms with other related and minor species but was involved in other exclusive ones. A quantitative proteomic description of this species could provide an accurate approach to the microbiota function under the comparison of two acetification profiles.

Comparative of Two Quantitative Proteomic Profiles in *Komagataeibacter europaeus*

After subjecting all the samples to an LC/MS^2 enrichment analysis, a total of 1,533 valid proteins were identified in *K. europaeus*. From them, 1,420 (B_EL: 1,264; B_UL: 1,245; FW_EL: 1,121; FW_UL: 1,152) were found in at least 50% of samples in one cycle time. The distribution of these proteins throughout the phases of two acetification profiles was summarized in an intersection plot shown in **Figure 2A**. Of the 1,420 proteins, 950 (66.9%) were common throughout both profiles, with 174 (12.3%) exclusive of the beer profile, and 90 (6.3%) of the fine wine profile. The amount of exclusive proteins at each sampling time was considerably minor: 39 out of 1,420 (2.7%) exclusive proteins at FW_UL were highlighted against 21 (1.5%) at B_EL, 6 (0.4%) at FW_EL, and 5 (0.4%) at B_UL. Then, 9 out of 1,420 (0.6%) proteins were found exclusively at the end of the loading phase (EL) and 6 (0.4%) before unloading (UL). The results evidenced that an important amount of the *K. europaeus* proteome was stable not affected by the change of phase or raw material.

Protein Clustering Analysis: Quantification Patterns and Interaction Networks

The proteome of *K. europaeus* was grouped according to the quantification pattern of each protein throughout each acetification profile. First, each protein quantification value in at least 50% of samples in all sampling times was normalized by z-score transformation and then clustered according to its pattern. **Figure 2B** shows a heatmap that summarized the

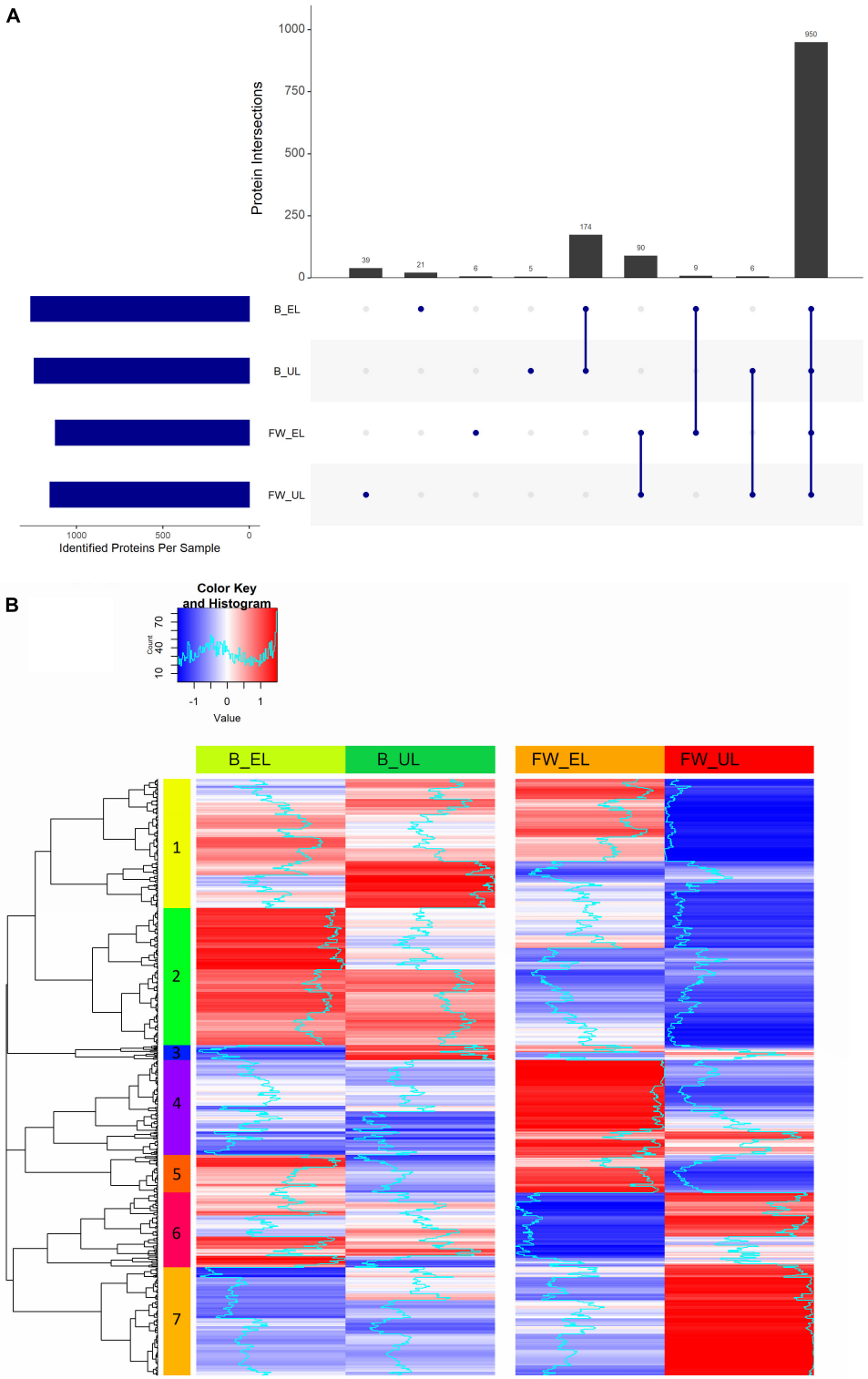

FIGURE 2 | (A) Intersection diagram of the proteins of *K. europaeus* identified in at least 50% of total samples in at least one phase. The number of proteins from each intersection group is represented on the bars. **(B)** Heat map showing the analysis of hierarchical clustering of the proteins identified in at least 50% of total samples in each phase. The number on each color represents each of the seven built clusters. Fine wine (FW), beer (B), end of loading (EL), just before unloading (UL).

hierarchical clustering carried out including a total of 832 proteins classified into seven clusters with different quantification patterns (more details can be found in **Supplementary Table 2**). Cluster 1 (n = 180) was characterized by a changing pattern throughout acetification of beer, but a marked decrease at the end of the exhausting phase in the fine wine vinegar (FW_UL). Cluster 2 (n = 191) was increased at the end of the loading phases, above all at B_EL, where quantification peaks were observed. Cluster 3 (n = 21), composed of a poor number of proteins, showed quantification peaks at B_UL. Clusters 4 (n = 132) and 5 (n = 53) were strongly upregulated at FW_EL, and also, Cluster 4 was decreased in the beer profile. Cluster 6 (n = 104) showed a changing pattern in the beer profile while in the fine wine profile, an increase just before unloading (FW_UL) was appreciated as in Cluster 7 (n = 151), where the quantification peaks were strongly observed (FW_UL).

Proteins from each cluster were then subjected to a protein-protein interaction analysis using the database STRING v11.0 to clarify the most relevant metabolic pathways related to each quantification pattern. **Figure 3** shows INM built from each cluster (six out of seven are represented), and those showed more interactions than expected (PPI enrichment p-value < 0.05):

- INM 1 (82 edges; PPI enrichment p-value, 1.71×10^{-13}) (**Figure 3A**) showed a high number of proteins related to the biosynthesis of amino acids (yellow nodes), mostly, L-glycine, L-serine, L-threonine, and L-lysine. A group of proteins at the top-left exhibited these proteins also involved in energy metabolism pathways [glycolysis (red nodes) and TCA cycle (purple nodes)]. Proteins related to the metabolism of purines (blue nodes) were found attached to it. Also, most of the alcohol dehydrogenase [ADH] subunits were classified in Cluster 1, even interaction groups that were not built (see **Supplementary Table 2**).
- INM 2 (123 edges; PPI enrichment p-value, 1.83×10^{-07}) (**Figure 3B**) exhibited a high number of proteins for the biosynthesis of aromatic amino acids (yellow nodes) (L-phenylalanine, L-tryptophane, and L-tyrosine), see middle-left group. Proteins related to the TCA cycle (red nodes) and the pyruvate metabolism (purple nodes) were also shown and connected to fatty acid biosynthesis proteins (light brown nodes), see middle and bottom-right groups. The metabolism of purines (blue nodes) and pyrimidines (light blue nodes) were observed evidencing a similarity to INM 1, although some particular groups were appreciated as biosynthesis of peptidoglycans (dark green nodes) and proteins (pink nodes), see bottom-left and top-right groups.
- INM 3 was not built because did not reach a PPI enrichment p-value < 0.05.
- INM 4 (86 edges; PPI enrichment p-value, 1.77×10^{-04}) (**Figure 3C**), similar to the previous INMs, showed groups relating processes like metabolism of amino acids (yellow nodes) to energy metabolism [TCA cycle (red nodes), pyruvate pathway (purple nodes)] and the purine (blue nodes) to pyrimidine metabolism (blue light nodes). Particularly, a group relating the biosynthesis of proteins (pink nodes) to aminoacyl-tRNA ligases (green nodes) was seen at the down-right.
- INM 5 (28 edges; PPI enrichment p-value, 2.95×10^{-4}) (**Figure 3D**) following the trend of previous INMs, predominated biosynthesis of amino acids (yellow nodes) (L-alanine, L-aspartate, and L-glutamate), proteins (pink nodes), metabolism of purines (blue nodes), and aminoacyl-tRNA ligases (green nodes).
- INM 6 (227 edges; PPI enrichment p-value, 1.00×10^{-16}) (**Figure 3E**) and INM 7 (353 edges; PPI enrichment p-value, 1.00×10^{-16}) (**Figure 3F**) presented both a highlighted central group composed mainly of ribosomal subunits, initiation, and elongation factors (pink nodes); ribosomal silencing and maturation factors were also found in INM 7. Around and/or attached to the central protein group, chaperones (dark green nodes), stress-response proteins (oxidoreductases, metabolism of glutathione, aldehyde dehydrogenase [ALDH] subunits, and outer membrane efflux pumps) (light brown nodes) were represented.

Differential Expression Analysis by Pairs: ANOVA and HSD Tukey's Test

A total of 141 proteins surpassed the statistical cut-off evidencing significant differences of quantification values in at least one pair comparison according to HSD Tukey's test corrected by multiple testing (q-value < 0.05) and $\log_2$ fold change in absolute value (FC) > 1: one protein for the pair B_UL/B_EL, 23 proteins for the pair FW_EL/B_EL, 76 for the pair FW_UL/B_UL, and 108 for FW_UL/FW_EL (see **Supplementary Table 3**). From these proteins, those that showed a strong significance (Tukey corrected by q-value < 0.01 and FC > 2) were represented in a radar chart and will be described below (see **Figure 4**). This Figure is an easy way to visualize the relationship between proteins and their abundance in each sample so that it can be quickly seen that the protein profile depends on both the sampling time (EL, UL) and the raw material (FW, B). Then, a detailed description of these protein groups can be carried out.

First, proteins that exhibited quantification peaks at B_EL (green) were mostly shown at the top-right of the radar chart. As observed in the corresponding clusters and INMs (1 and 2; see **Figures 2B**, **3A,B**) these proteins were involved in the metabolism of amino acids [glutathione reductase (gorAp), N-succinyl-transferase (dapDp)], of purines [adenine deaminase (adep)], aminoacyl-tRNA ligases [phenylalanine-tRNA ligase (pheSp)], and biosynthesis of proteins [riboflavin biosynthesis protein (ribFp), RNA polymerase sigma factor [RPOD] (rpoDp)]. Between them, rpoDp (cluster 1) was strongly down-regulated in the pairs FW_UL/B_UL and FW_UL/FW_EL (FC $\approx$ 3). One single protein presented the quantification peak at B_UL (yellow), DNA topoisomerase IV (parCp; cluster 1), essential in the segregation of chromosomes during DNA replication, especially down-regulated in the pair FW_UL/B_UL (FC $\approx$ 3).

Next, many proteins showed quantification peaks at FW_EL (blue), see clusters and INMs 4 and 5 (**Figures 2B**, **3C,D**): acetolactate synthase [large subunit] [ALS], involved in the

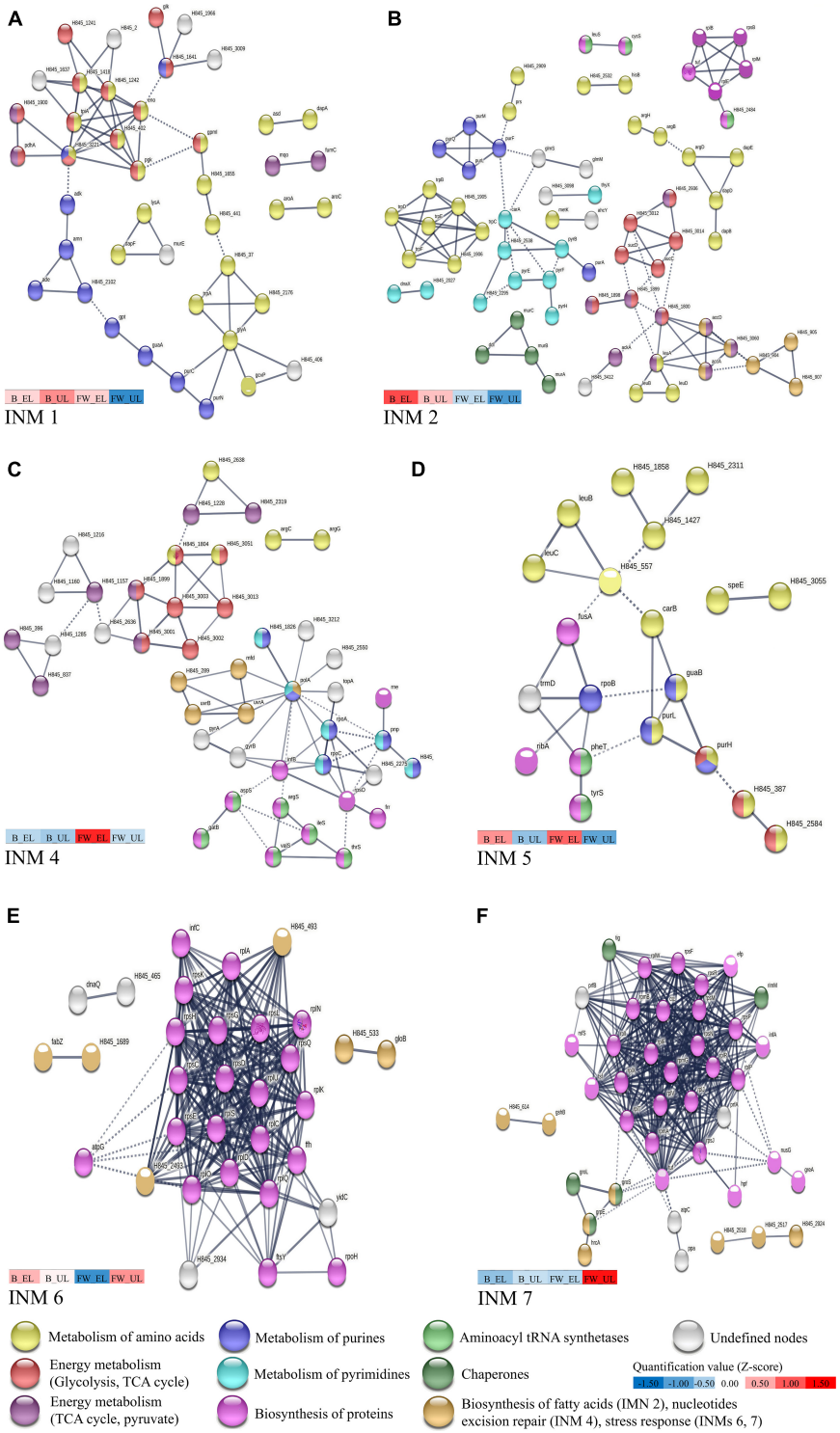

FIGURE 3 | High confidence protein-protein interaction network maps (INM) performed in *K. europaeus* of proteins from each cluster, shown in **Figure 2B**, with a PPI enrichment *p*-value < 0.05 using STRING v11.0. **(A)** INM 1 (Cluster 1), **(B)** INM 2 (Cluster 2), **(C)** INM 4 (Cluster 4), **(D)** INM 5 (Cluster 5), **(E)** INM 6 (Cluster 6), and **(F)** INM 7 (Cluster 7). Proteins are shown as nodes and interactions between them are represented by edges whose thickness indicates the strength of each interaction. Nodes with the same color represent a specific function based on protein annotations according to the databases Uniprot and KEGG. A color scale showing the mean quantification values (z-score) of clustered proteins (see **Figure 2B**) that compose each INM at each sampling time is represented. Undefined nodes (gray color) belong to proteins with a low prevalent or unknown function. *K. xylinus* E25 was used as a model organism due to the high homology (MUM index of 0.21 with the genome of *K. europaeus*; Ryngajłło et al., 2018). The list of total proteins subjected to STRING analysis and their respective annotations can be found in **Supplementary File 2**.

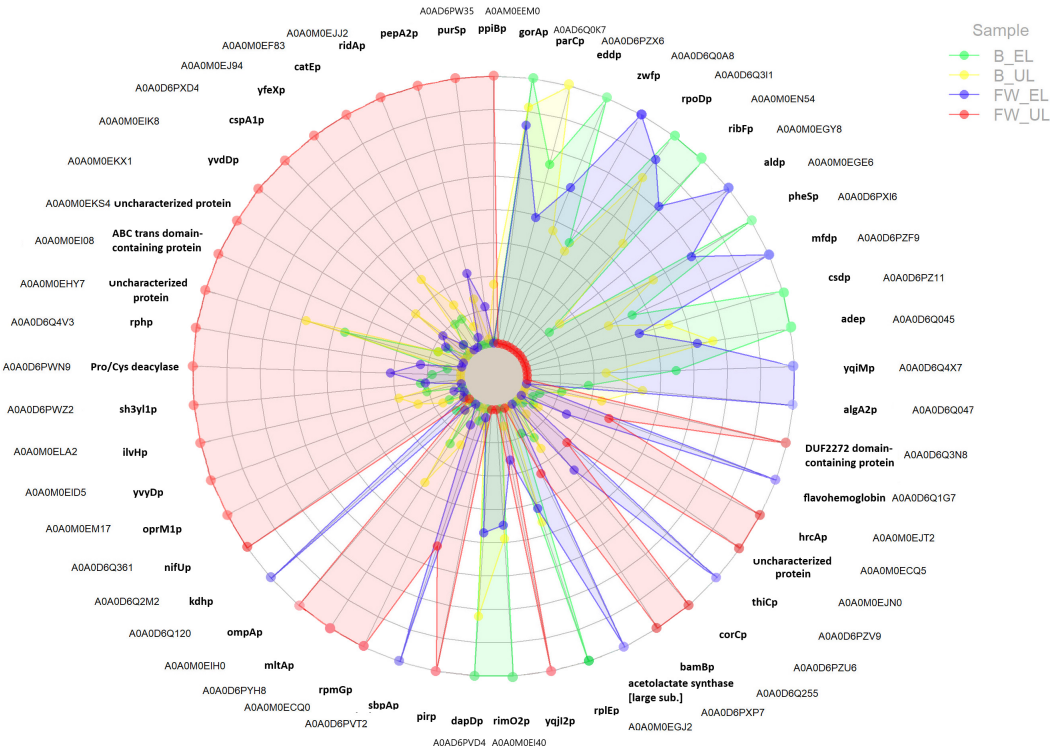

FIGURE 4 | Radar chart representing proteins showing the strongest significative differences according to HSD Tukey's test corrected by multiple testing (q-value < 0.01) and $\log_2$ fold change (in absolute value) > 2 (see **Supplementary Table 3**). The quantification area of each protein in each profile (FW, fine wine; B, beer) and sampling time (EL, end of loading; UL, just before unloading) is included.

biosynthesis of branched-chain amino acids (BCAA); other proteins related to energy metabolism activity like the pentose phosphate pathway (PPP) [glucose-6-phosphate dehydrogenase [GPDH] (zwfp)] and the TCA cycle [α-ketoglutarate dehydrogenase [αKDH] (kdhp), 3-succinoyl-semialdehyde dehydrogenase [SSADH] (aldp)]; flavohemoglobin and flavin oxidoreductase [NADH] (yqiMp), known to be involved in the biosynthesis of flavoproteins that catalyzes oxidoreduction processes while sulfate-binding protein (sbpAp) and phospho-methyl-pyrimidine synthase [THIC] (thiCp) may provide FeS clusters for the electron transport chain. Most of these proteins were upregulated in the pair FW_EL/B_EL and downregulated in FW_UL/FW_EL; for the first one, thiCp was remarked (FC = 4.68). Although the aforementioned proteins maintained acceptable levels of expression in the phases described (B_EL, B_UL, and FW_EL), all of them were characterized by a significant decrease at FW_UL (red).

A total of 28 proteins, mostly distributed at the half left of the radar chart (see **Figure 4**), were characterized by significant quantification peaks at FW_UL (red) against a marked decrease in the rest of the phases, see clusters and INMs 6 and 7 (**Figures 2B**, **3E,F**), and most of them were upregulated in FW_UL/B_UL and FW_UL/FW_EL pairs. Nitrogen-fixing thioredoxin (nifUp), iron-binding nuclear pirin (pirp), dehydrogenase PQQ (bamBp), and glyoxalase resistance protein (catEp) are related to oxidoreductase activity and maintain the redox balance. The outer membrane proteins ompAp and oprM1p, acting as porin of small solutes and efflux transport pump, respectively, and both playing a role in the outer membrane stability and resistance to environmental stress, were upregulated in the pair FW_UL/FW_EL (FC = 3.64 and 3.13 respectively). Other transmembrane proteins as ABC transporter (FC = 4.17) and murein hydrolase A [MLTA] (mltAp) (FC = 2.60) were then upregulated in the aforementioned pair while other proteins were related to the regulation of the translation: endoribonuclease [L-PSP] (ridAp), ribonuclease [RPH] (rphp), ribosome hibernation promoting factor [HPF] (yvyDp), and cold-shock protein [CSPA] (cspA1p). Acetolactate synthase [ILVH] (ilvHp) was shown, as occurred at FW_EL, while phospho-ribosylformylglycinamidine synthase [PURS] (purSp) catalyzed the first steps of the biosynthesis *de novo* of purines, and was one of the most upregulated proteins (FC = 5.58).

DISCUSSION

This study focused on the analysis of the acetification of two different substrates, aimed to delve into the behavior of the bacteria responsible for the process when the nutritional profile of the medium offers significant differences due to its

composition, especially, in regard to the availability of carbon sources additional to ethanol, namely carbohydrates. Indeed, if the microbiota responsible is able to adapt to the conditions of the environment by modifying its metabolism and taking advantage of the resources available in each case, it would be a proof of its great versatility and therefore, survive in different and particularly, aggressive environments. In previous studies by the authors, qualitative and quantitative proteomic analysis of one synthetic alcoholic medium acetification process were carried out. Now, a new study is being conducted for much more complex media (fine wine and a craft beer) from which the differences in proteomic profiles are being disclosed. Then, a novelty from this study is that even when using different raw materials, the microbiota composition is similar, but its metabolism, at a proteome level, is different. Next, a detailed discussion about these issues will be carried out while the main differences between both profiles and approached proposals about the metabolic differences are made.

As it is known in the vinegar industry, the total strength of the medium (ethanol plus acetic acid concentration), which remains constant throughout the cycle, can affect to the cell activity and concentration (García-García et al., 2007; Baena-Ruano et al., 2010). In the present study, a mild environment offering no special stressing conditions has been used to study some basic aspects of the complex microbiota of the process. Here, both media showed an initial ethanol concentration of around 10% (v/v), and the acetic acid level could be disregarded (see section "Raw Material"). The initial total strength [% (w/v) of acetic acid plus % (v/v) of ethanol] is 10 total degrees. Then, in each cycle, 3.5/4 L of medium containing 9.2 [7.9 ± 0.2% (w/v) plus 1.3 ± 0.3% (v/v)] and 8.0 [6.8 ± 0.7% (w/v) plus 1.2 ± 0.1% (v/v)] total degrees for fine wine and beer profiles, respectively, are unloaded. The differences between the initial total strength and unloaded product appear due to the volatile losses (around 8 and 20% in each medium, respectively). The foaming generated in the beer medium would favor the volatile losses (20%) and no special care was taken to avoid these losses since it would not affect the aim of the work. Regardless, 92 and 80% of the disappeared ethanol was used for acetic acid formation and the rest was stripped by air or transformed by bacteria for other uses (Jiménez-Hornero et al., 2020).

Regarding the protein composition of the microbiota, no relevant differences were appreciated between the sampling times of each acetification profile. This composition showed a strong similarity to results obtained in our previous work that characterized an alcohol vinegar profile (Román-Camacho et al., 2021). These results may be explained by the operating mode followed in this work in which the same starter culture, consisting of a mixed broth coming from the aforementioned alcohol medium acetification, concretely, from the end of the ethanol exhausting phase, was used for both acetification profiles. Under these working conditions, in which the fine wine and then, beer acetification were consecutively performed, the raw material change might not modify excessively the starter microbial composition despite the additional nutritional richness that these natural substrates might provide. Subsequently, the main functions of the exclusive proteins in each phase were detailed to compare the microbiota activity in each acetification profile. The predominant species of the microbiota exhibited a natural behavior according to other authors that worked using submerged biotransformation (Fernández-Pérez et al., 2010; Qi et al., 2014; Trček et al., 2016) while the minor species showed a high-stress response, probably trying to coexist along with the better-adapted ones. Even if the protein amount that provides each species affects its role in the metaproteome, all of them might participate in the whole function of the microbial community (Peng et al., 2021). *K. europaeus*, supplying a mean frequency of 73.5%, far above the rest, not only shared the main GO Terms with other species but was involved in other exclusive ones. It is worth noting that this species was also the most representative in our previous studies (Román-Camacho et al., 2020, 2021). Therefore, a quantitative proteomic description of *K. europaeus*, comparing two acetification profiles, might provide a prediction of the microbiota role and characterize the natural raw materials used.

K. europaeus is well-known as one of the main microorganisms responsible for industrial vinegar production. High ethanol-oxidizing ability, acetic acid requirement, and tolerance to high acidity levels [10–20% (w/v)] determine its suitability for this biotransformation (Trček et al., 2007; Yamada et al., 2012; Gullo et al., 2014). These capabilities allow it to perform an efficient incomplete oxidation reaction of the ethanol into acetic acid. This particular metabolic process consists of a two-step reaction (see **Figure 5**). First, alcohol dehydrogenase (ADH) binds to pyrroloquinoline quinone (PQQ) to oxidize the ethanol into acetaldehyde. Next, acetaldehyde is oxidized to acetic acid by aldehyde dehydrogenase (ALDH); both enzymes are located on the periplasmic side of the inner cell membrane (Adachi et al., 1980; Ameyama and Adachi, 1982). Further, NAD^+ and $NADP^+$ may be used as coenzymes by ADH-NAD and ALDH-NADP, located in the cytoplasm (Qin et al., 2021; Sriherfyna et al., 2021). The acetic acid produced at the periplasm is released into the medium increasing its external concentration which, in turn, triggers its diffusion and accumulation in the cytoplasm (Gullo et al., 2014; Qiu et al., 2021). The TCA cycle may assimilate the inner acetic acid through the input of acetyl-CoA providing biosynthetic precursors of amino acids and nucleic acids thus replenishing cell material throughout the loading phase and early stages of the ethanol depletion phase. The use of raw material with sugar content, as is the case of our craft beer, can lead to assimilating firstly, the available glucose and draining biosynthetic precursors directly from energy metabolic pathways as the PPP and the glycolysis. At the final moments of acetification, cells would trigger different membrane mechanisms dependent on proton motive force for the acetic acid release and detoxification. This molecular strategy, proposed in the present work, would allow *K. europaeus* to prevail over other species during the acetification process. These findings will be exhaustively detailed in the rest of the discussion based on hierarchical clustering, protein-protein interactions, and statistical analysis. Furthermore, it has been sectioned to facilitate the understanding of these microbial behavioral aspects at a quantitative level. In short, the discussion has been organized by analyzing the results obtained for the

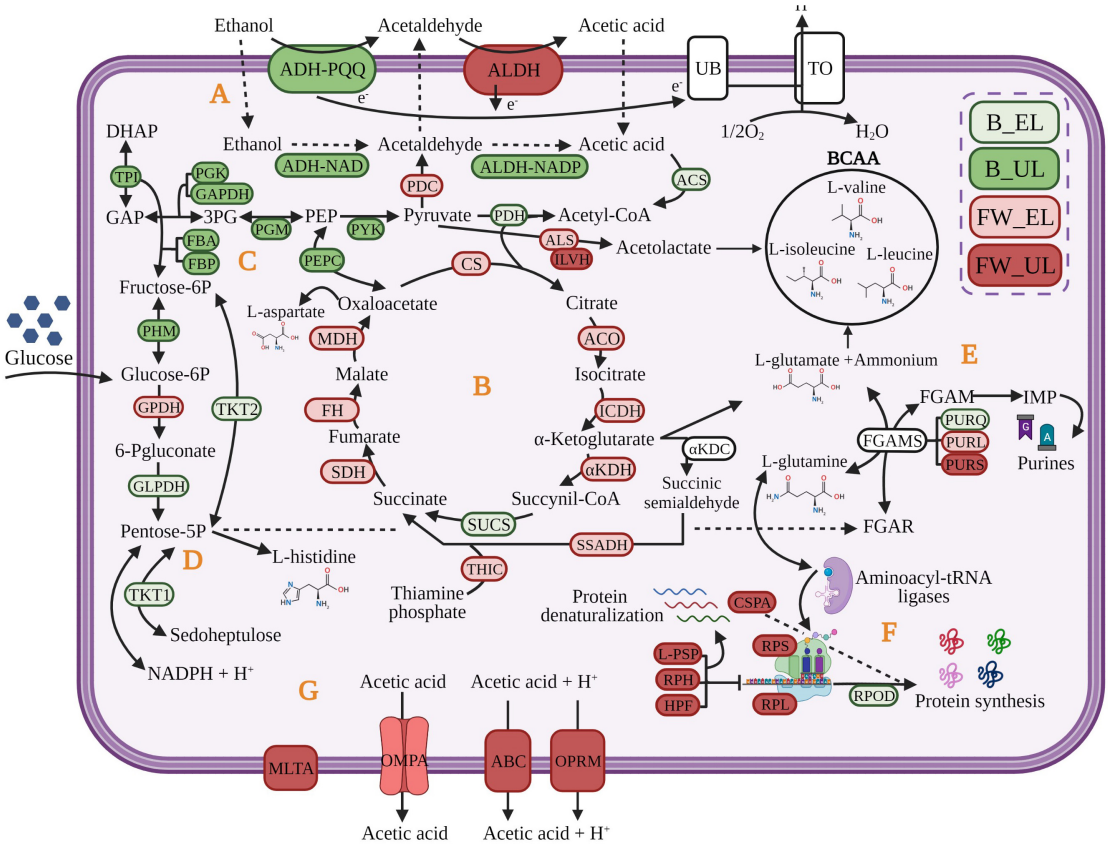

FIGURE 5 | Molecular strategy of *K. europaeus* proposed to prevail throughout acetification process. The colors of the proteins represent the phase in which the protein had the highest quantification value. Fine wine (FW), beer (B), end of loading (EL), just before unloading (UL). **(A)** oxidation of ethanol into acetic acid; **(B)** TCA cycle; **(C)** glycolysis; **(D)** pentose phosphate pathway; **(E)**, amino acids and purines formation from biosynthetic precursors; **(F)** regulation of protein synthesis; **(G)** membrane mechanisms for acetic acid release. GAP, glyceraldehyde 3-phosphate; DHAP, dihydroxyacetone phosphate; 3PG, 3-phosphoglycerate; PEP, phosphoenolpyruvate; FGAR, formylglycinamide ribonucleotide; FGAM, formylglycinamidine ribonucleotide; IMP, inosine monophosphate. The definitions of the protein abbreviations and their respective highest quantification values are given (see **Supplementary Table 4**). Created with BioRender.com (with publication license).

two raw materials as a whole according to the most relevant metabolic processes; and in this way, the differences existing in both acetification profiles can be better appreciated.

The Essential Role of the Biosynthesis of Amino Acids and Nucleic Acids From Metabolic Precursors Replenishing Cellular Material Losses

The metabolism of amino acids seems to be one of the most representative metabolic pathways of *K. europaeus*, as can be appreciated in most protein clusters, above all, in those showing quantification peaks at the end of the loading phase (Clusters 1, 2, 4, and 5). The amino acids are synthesized from intermediaries of the TCA cycle, the glycolysis, and the PPP through L-glutamate and L-glutamine, both acting as nitrogen sources that are self-regulated according to the cell requirements (Yin et al., 2017; Sankuan et al., 2020). These results suggest that AAB might use their high nitrogen recovery capability to convert continuously nitrogen sources like proteins, nucleic acids derived from raw materials, and apoptotic cells into amino acids and ammonium thus replacing their consumption and cell material losses during the loading phase (Álvarez-Cáliz et al., 2012; Kuypers et al., 2018). In this sense, ALS is related to the synthesis of BCAA and L-valine, L-leucine, and L-isoleucine, from pyruvate, are strongly upregulated at FW_EL. It is also interesting to note that ILVH was highly upregulated at FW_UL. BCAA may provide NH_3 and energy to neutralize the increase of acid final products during the exhausting phase and support intracellular pH balance through deamination, as proposed by other authors who reported different isoforms of acetolactate synthase in diverse acidophilic organisms (Santiago et al., 2012; Andrés-Barrao et al., 2016; Yin et al., 2017). Our findings supported the essential role of the metabolism of amino acids throughout acetification and especially, suggest the addition of BCAA to the fermentation culture as a possible system to protect the cellular integrity and increase productivity.

Conversely, the biosynthesis *de novo* of purines and pyrimidines requires the addition of amino acids to the pentose-5-phosphate, coming from the PPP, and metabolic

energy (ATP) as can be observed in INMs belonging to clusters showing quantification peaks at EL (1, 2, 4, and 5). To our knowledge, this pathway has been barely researched in AAB, but here, phosphoribosyl-formyl-glycinamidine synthase complex (FGAMS) has been found (see **Supplementary Table 2**). FGAMS, composed of three subunits (PURQ, PURL, and PURS), carries out the ATP-dependent formation of formyl-glycinamidine ribonucleotide [FGAM] converting L-glutamine to L-glutamate (Tanwar et al., 2012). In previous works characterizing an alcohol vinegar microbiota (Román-Camacho et al., 2020, 2021), some GO Terms related to the synthesis of organic heterocyclic aromatic compounds, concretely, nucleic acids were identified. In the present work, the main subunits showed quantification peaks at different phases (PURQ, B_EL; PURL, FW_EL; PURS, FW_UL) although along with others, most of them were highlighted at the end of the loading phase. This fact could indicate that the synthesis of nucleic acids is integrated with other metabolic pathways, being part of a biological system that aims to replenish cellular material losses caused after unloading, improving adaptability, and ensuring the survival of the microbiota, above all, *K. europaeus*.

The TCA Cycle as a Key Pathway in the Cytoplasmatic Acetic Acid Assimilation and Biosynthetic Precursors Source

The TCA cycle has been studied exhibiting an important function in the metabolism of AAB (Nakano and Fukaya, 2008; Kwong et al., 2017). The protein groups involved in this pathway were predominant in clusters whose quantification patterns were higher at EL phases (Clusters 1, 2, and 4). All the TCA cycle enzymes were found in the proteome of *K. europaeus* (see **Supplementary Table 2**) and all of them were downregulated, mainly in the fine wine profile (see **Figure 5**). In this work, αKDH, SSADH, and THIC were highlighted so they might play a critical role. Zhang and Bryant (2011) and Lei et al. (2018) investigated that αKDC and SSADH might form succinic acid via succinic semialdehyde by using cofactors of thiamine phosphate in *Synechococcus* sp. PCC7002. The TCA cycle can supply α-ketoglutarate to the synthesis of L-glutamate that provides amino groups in biosynthetic reactions, besides oxalacetate. For this purpose, the acetyl-CoA is provided to the TCA cycle by the conversion of pyruvate obtained in the glycolysis and of acetic acid derived from the ethanol oxidation (Mamlouk and Gullo, 2013; Qin et al., 2021). Because of the direct drain of intermediates from the TCA cycle to biomass, amino acids are partly derived from ethanol (Adler et al., 2014). In this sense, considering that AAB must cope with constant changes in ethanol, acetic acid, and cellular concentration because of the semi-continuous state of the cycles in our experiment, we suggest that the TCA cycle might be used for assimilating cytoplasmatic acetic acid, coming from ethanol, supplying energy, and biosynthetic precursors according to other authors (Ramírez-Bahena et al., 2013; Adler et al., 2014; Andrés-Barrao et al., 2016; Zheng et al., 2017).

The Pentose Phosphate Pathway and Glycolysis Are Used to Assimilate the Available Glucose Obtaining Rapidly Biomass and Energy for the Synthesis of Precursors

The pentose phosphate pathway (PPP) is the main metabolic route of AAB to incompletely oxidize the glucose of the medium providing several precursor metabolites, mainly pentose-5-phosphate, necessary for the biosynthesis of amino acids (L-histidine) and nucleic acids (Adler et al., 2014; García-García et al., 2017). Several authors have related the enhance of PPP to the generation of NADPH + H^+, also involved in biosynthetic processes even in reducing oxidative stress (Yin et al., 2017; Christodoulou et al., 2018; Sriherfyna et al., 2021). Although many of the species of *Acetobacter* and *Komagataeibacter* have demonstrated a higher preference for ethanol as a carbon source, in this analysis, most PPP enzymes were expressed when the ethanol concentration was higher (EL phases) (see **Supplementary Table 2**). Except for GPDH, which was strongly expressed in the fine wine profile (FW_EL), the rest of the PPP enzymes were higher quantified in the beer profile (B_EL) (see **Figure 5**). The remaining sugar content of the beer (7% before dilution) may provide glucose as a carbon source allowing AAB, mainly *K. europaeus*, to rapidly obtain biomass and energy for the synthesis of precursors (García-García et al., 2017; Qin et al., 2021). Indeed, the glycolysis enzymes were also higher expressed in the beer profile, in this case, and mostly upregulated (B_UL). Zheng et al. (2017) study showed that growing *A. pasteurianus* in a medium containing 1% initial acetic acid, PPP was decreased, and energy metabolism was enhanced by the production of pyruvate. Despite its ethanol preference, *K. europaeus* might assimilate, firstly, the glucose in the beer medium for rapid biosynthesis of precursors, which are not possible to obtain by other pathways, obtaining energy, and thus, prevail over other species that exhibit high glucose preference. This fact would explain the presence in our results of numerous protein groups involved in these pathways in clusters whose patterns showed quantification peaks during beer acetification (Clusters 1, 2, 4, and 5).

The Biosynthesis of Ribosomes and Proteins Is Regulated With the Increase of Acetic Acid Concentration

The biosynthesis of proteins has been reported by different authors as one of the most highlighted metabolic pathways in AAB throughout the acetification process (Andrés-Barrao et al., 2012; Xia et al., 2016; Román-Camacho et al., 2021). Here, the most of functional groups involved in this process, mainly composed of ribosomal subunits, showed quantification peaks at FW_UL (Clusters 6 and 7). However, few of them were significantly upregulated since proteins that surpassed the statistical cut-off were related to the regulation of the translation. Among them, L-PSP inhibits the synthesis of proteins by the degradation of mRNAs, HPF dimerizes the bacterial functional ribosomes into inactive 100S ribosomes (Matzov et al., 2019),

and RPH assists the maturation of tRNAs and the degradation of structured RNAs mainly in *E. coli* (Jain, 2012). Some authors have reported a decrease in the biosynthesis of proteins when the acidity levels increase in *A. pasteurianus* through functions as the recycling of ribosomes (Andrés-Barrao et al., 2012; Xia et al., 2016). Then, CSPA (see **Figure 5**), was strongly upregulated and its function has been discussed in *E. coli* as an RNA chaperone that prevents the protein refolding by ribonucleases (Rennella et al., 2017). When the acetic acid concentration is diluted during the loading phase the process of protein synthesis seems to occur efficiently through the presence of aminoacyl-tRNA ligases in Clusters 2, 4, and 5, binding tRNAs to specific amino acids and ensuring an accurate translation process (Román-Camacho et al., 2021). It is worth noting the drastic decrease of expression of initiation factors as RPOD with the increase of acetic acid level (FW_UL). In summary, these findings suggest that acetic acid accumulation generates a stress response thus regulating the formation of ribosomes and proteins.

Membrane Mechanisms of Response to Acetic Acid Stress Derived From the Incomplete Oxidation of Ethanol

The incomplete oxidation of the ethanol of the medium is carried out by membrane-bound systems directly coupled to respiratory chains and allowing that oxidation reaction to take place in the periplasm without a requirement of transport across the membrane (Qin et al., 2021; Qiu et al., 2021). In this work, numerous subunits of PQQ-ADH and ALDH were identified and mainly expressed at UL phases (see **Supplementary Table 2**), but in general, these enzymes were stable indicating that the oxidation of ethanol could be constantly active throughout acetification. The acetic acid produced in the periplasm is released into the medium, thus increasing its external concentration. However, when it occurs, this compound can diffuse and accumulate into the cytoplasm along with that generated inside by the activity of ADH-NAD and ALDH-NADP (Adler et al., 2014; Gullo et al., 2014). In this sense, some systems acting to detoxify the cell might be participating through the upregulated proteins at FW_UL. First, those related to redox homeostasis maintenance, particularly, implicated the maturation of iron-sulfur (FeS) clusters acting as cofactors in the electron transfer (nifUp), cell apoptosis (pirp), and detoxification (catEp) (Benoit et al., 2018). To our knowledge, this set of proteins had never been reported in AAB. Secondly, outer membrane proteins, as permeable porins of small solutes (OMPA) and efflux pumps (OPRM, putative ABC-transporter) (see **Figure 5**), might control the cellular output of acetic acid, whose concentration increases during the fermentation phase (Nakano and Fukaya, 2008; Confer and Ayalew, 2013). MLTA, participating in the maintenance of the peptidoglycan layer under these conditions, show even more evidence of the importance of the cell surface as an efficient mechanism against the acetic acid stress used by the species of *Komagataeibacter*, as other authors have well-studied (Wang et al., 2015; Andrés-Barrao et al., 2016).

CONCLUSION

A comparison of two acetification profiles using different raw materials was established to study the natural behavior of the involved microbiota through the metaproteome and, exhaustively, since it is the prevalent species, the quantitative proteomic profile of *K. europaeus*. Although the use of different raw materials seems not to affect the microbial composition, the microbiota behaved differently by significant changes in the expression of the proteome. In this work, it has been suggested that the inner acetic acid coming from the oxidation of ethanol might be assimilated in the TCA cycle providing biosynthetic precursors along with other metabolic pathways (PPP and glycolysis) if glucose is available, as is the case of one of the fermentation media studied (craft beer). These processes replenish the cell material losses (amino acids and nucleic acids) after unloading, throughout the loading phase. The excess of acetic acid in the cytoplasm would also be released to the medium by some cell membrane mechanisms proton motive-force dependent at the final stages of the acetification. This complete strategy has been reported in **Figure 5**, highlighting the phase at which each protein had a higher quantification value. The differences in the metabolic behavior throughout each acetification profile were more accentuated in the fine wine vinegar than in the craft beer vinegar. In this profile, FW_UL was a period significantly differentially based on statistical analysis. Metabolomic assays that would allow clarifying the differences between the associated metabolites to these raw materials, in more detail, are underway. These findings may lay the groundwork of a vinegar microbiota profile, at a protein level, under smooth operating conditions. Future studies might be undertaken to evaluate the effect on the microbiota of media with higher levels of ethanol and acetic acid and even comparatives studies to achieve a multi-omics integrative profile. This work might increase the knowledge of the use of diverse raw materials and optimize the operating conditions.

DATA AVAILABILITY STATEMENT

The datasets presented in this study can be found in online repositories. The names of the repository/repositories and accession number(s) can be found below: NCBI—PXD031147.

AUTHOR CONTRIBUTIONS

JR-C: methodology, validation, formal analysis, data curation, writing—original draft preparation, and visualization. JM and IG-G: conceptualization, investigation, resources, writing—review and editing, supervision, project administration, and funding acquisition. IS-D: methodology, validation, formal analysis, conceptualization, and visualization. TG-M: conceptualization, data curation, validation, and supervision. All authors contributed to the article and approved the submitted version.

FUNDING

This work has been co-funded by the "Programa Operativo FEDER de Andalucía 2014–2020" and "Plan Andaluz de Investigación, Desarrollo e Innovación (PAIDI 2020), Consejería de Economía, Conocimiento, Empresas y Universidad"; Ref. P20_00590.

ACKNOWLEDGMENTS

The kind help of the Proteomics and Bioinformatics staffs at the Central Research Support Service (SCAI) of the University of Córdoba with proteomic and bioinformatic analysis is, respectively, and gratefully acknowledged. Also, we would like to express our gratitude to Alvear Winery and Mahou San Miguel Group, production Center of Córdoba, for supplying us the craft beer. Special mention to Irene Sánchez-León for helping with the revision of tables and the manuscript.

SUPPLEMENTARY MATERIAL

The Supplementary Material for this article can be found online at: https://www.frontiersin.org/articles/10.3389/fmicb.2022.840119/full#supplementary-material

REFERENCES

Adachi, O., Tayama, K., Shinagawa, E., Matsushita, K., and Ameyama, M. (1980). Purification and characterization of membrane-bound aldehyde dehydrogenase from Gluconobacter suboxydans. *Agric. Biol. Chem.* 44, 503–515. doi: 10.1271/bbb1961.44.503

Adler, P., Frey, L. J., Berger, A., Bolten, C. J., Hansen, C. E., and Wittmann, C. (2014). The key to acetate: metabolic fluxes of *acetic acid bacteria* under cocoa pulp fermentation-simulating conditions. *Appl. Environ. Microbiol.* 80, 4702–4716. doi: 10.1128/AEM.01048-14

Álvarez-Cáliz, C., Santos-Dueñas, I. M., Cañete-Rodríguez, A. M., García-Martínez, T., Mauricio, J. C., and García-García, I. (2012). Free amino acids, urea and ammonium ion contents for submerged wine vinegar production: influence of loading rate and air-flow rate. *Acetic Acid Bact.* 1:e1. doi: 10.4081/aab.2012.e1

Ameyama, M., and Adachi, O. (1982). "Alcohol dehydrogenase from *acetic acid bacteria*, membrane bound," in *Methods in Enzymology*, ed. W. A. Wood (New York: Academic Press), 450–457. doi: 10.1016/S0076-6879(82)89078-2

Andrés-Barrao, C., Saad, M. M., Cabello-Ferrete, E., Bravo, D., Chappuis, M. L., Ortega-Pérez, R., et al. (2016). Metaproteomics and ultrastructure characterization of Komagataeibacter spp. involved in high-acid spirit vinegar production. *Food Microbiol.* 55, 112–122. doi: 10.1016/j.fm.2015.10.012

Andrés-Barrao, C., Saad, M. M., Chappuis, M. L., Boffa, M., Perret, X., Ortega-Pérez, R., et al. (2012). Proteome analysis of Acetobacter pasteurianus during acetic acid fermentation. *J. Proteome* 75, 1701–1717. doi: 10.1016/j.jprot.2011.11.027

Baena-Ruano, S., Jiménez-Ot, C., Santos-Dueñas, I. M., Cantero-Moreno, D., Barja, F., and García-García, I. (2006). Rapid method for total, viable and non-viable *acetic acid bacteria* determination during acetification process. *Process Biochem.* 41, 1160–1164. doi: 10.1016/j.procbio.2005.12.016

Baena-Ruano, S., Jiménez-Ot, C., Santos-Dueñas, I. M., Jiménez-Hornero, J. E., Bonilla-Venceslada, J. L., Álvarez-Cáliz, C., et al. (2010). Influence of the final ethanol concentration on the acetification and production rate in the wine vinegar process. *J. Chem. Technol. Biotechnol.* 85, 908–912. doi: 10.1002/jctb.2368

Benoit, S. L., Holland, A. A., Johnson, M. K., and Maier, R. J. (2018). Iron–sulfur protein maturation in *Helicobacter* pylori: identifying a Nfu-type cluster carrier protein and its iron–sulfur protein targets. *Mol. Microbiol.* 108, 379–396. doi: 10.1111/mmi.13942

Bradford, M. M. (1976). A rapid and sensitive method for the quantitation of microgram quantities of protein utilizing the principle of protein dye binding. *Anal. Biochem.* 72, 248–254. doi: 10.1016/0003-2697(76)90527-3

Christodoulou, D., Link, H., Fuhrer, T., Kochanowski, K., Gerosa, L., and Sauer, U. (2018). Reserve flux capacity in the pentose phosphate pathway enables *Escherichia coli*'s rapid response to oxidative stress. *Cell Syst.* 6, 569–578. doi: 10.1016/j.cels.2018.04.009

Confer, A. W., and Ayalew, S. (2013). The OmpA family of proteins: roles in bacterial pathogenesis and immunity. *Vet. Microbiol.* 163, 207–222. doi: 10.1016/j.vetmic.2012.08.019

Fernández-Pérez, R., Torres, C., Sanz, S., and Ruiz-Larrea, F. (2010). Strain typing of *acetic acid bacteria* responsible for vinegar production by the submerged elaboration method. *Food Microbiol.* 27, 973–978. doi: 10.1016/j.fm.2010.05.020

García-García, I., Cañete-Rodríguez, A. M., Santos-Dueñas, I. M., Jiménez-Hornero, J. E., Ehrenreich, A., Liebl, W., et al. (2017). Biotechnologically relevant features of gluconic acid production by *acetic acid bacteria*. *Acetic Acid Bact.* 6:6458. doi: 10.4081/aab.2017.6458

García-García, I., Cantero-Moreno, D., Jiménez-Ot, C., Baena-Ruano, S., Jiménez-Hornero, J., Santos-Dueñas, I., et al. (2007). Estimating the mean acetification rate via on-line monitored changes in ethanol during a semi-continuous vinegar production cycle. *J. Food Eng.* 80, 460–464. doi: 10.1016/j.jfoodeng.2006.05.028

García-García, I., Jiménez-Hornero, J. E., Santos-Dueñas, I. M., González-Granados, Z., and Cañete-Rodríguez, A. M. (2019). "Modeling and optimization of acetic acid fermentation," in *Advances in vinegar production*, ed. A. Bekatorou (Madrid, Spain: Taylor & Francis Group: CRC Press), doi: 10.1201/9781351208475

Gullo, M., Verzelloni, E., and Canonico, M. (2014). Aerobic submerged fermentation by *acetic acid bacteria* for vinegar production: process and biotechnological aspects. *Process Biochem.* 49, 1571–1579. doi: 10.1016/j.procbio.2014.07.003

Hidalgo, C., Torija, M. J., Mas, A., and Mateo, E. (2013). Effect of inoculation on strawberry fermentation and acetification processes using native strains of yeast and *acetic acid bacteria*. *Food Microbiol.* 34, 88–94. doi: 10.1016/j.fm.2012.11.019

Jain, C. (2012). Novel role for RNase PH in the degradation of structured RNA. *J. Bacteriol.* 194, 3883–3890. doi: 10.1128/JB.06554-11

Jiang, Y., Lv, X., Zhang, C., Zheng, Y., Zheng, B., Duan, X., et al. (2019). Microbial dynamics and flavor formation during the traditional brewing of Monascus vinegar. *Food Res. Int.* 125:108531. doi: 10.1016/j.foodres.2019.108531

Jiménez-Hornero, J. E., Santos-Dueñas, I. M., and García-García, I. (2020). Modelling acetification with Artificial Neural Networks and comparison with alternative procedures. *Processes* 8:749. doi: 10.3390/pr8070749

Kandylis, P., Bekatorou, A., Dimitrellou, D., Plioni, I., and Giannopoulou, K. (2021). Health Promoting Properties of Cereal Vinegars. *Foods* 10:344. doi: 10.3390/foods10020344

Kuypers, M., Marchant, H., and Kartal, B. (2018). The microbial nitrogen-cycling network. *Nat. Rev. Microbiol.* 16, 263–276. doi: 10.1038/nrmicro.2018.9

Kwong, W., Zheng, H., and Moran, N. (2017). Convergent evolution of a modified, acetate-driven TCA cycle in bacteria. *Nat. Microbiol.* 2:17067. doi: 10.1038/nmicrobiol.2017.67

Lei, G., Wang, X., Lai, C., Li, Z. M., Zhang, W., Xie, C., et al. (2018). Expression and biochemical characterization of α-ketoglutarate decarboxylase from cyanobacterium Synechococcus sp. PCC7002. *Int. J. Biol. Macromol.* 114, 188–193. doi: 10.1016/j.ijbiomac.2018.03.112

Li, S., Li, P., Feng, F., and Luo, L. X. (2015). Microbial diversity and their roles in the vinegar fermentation process. *Appl. Microbiol. Biotechnol.* 99, 4997–5024. doi: 10.1007/s00253-015-6659-1

Llaguno, C. (1991). "Definición y tipos de vinagre," in *El vinagre de vino*, eds C. Llaguno and M. C. Polo (Madrid, Spain: Consejo Superior de Investigaciones Científicas (CSIC)), 133–145.

Mamlouk, D., and Gullo, M. (2013). *Acetic acid bacteria*: physiology and carbon sources oxidation. *Indian J. Microbiol.* 53, 377–384. doi: 10.1007/s12088-013-0414-z

Mas, A., Torija, M. J., García-Parrilla, M. C., and Troncoso, A. M. (2014). *Acetic acid bacteria* and the production and quality of wine vinegar. *Sci. World J.* 2014:394671. doi: 10.1155/2014/394671

Matzov, D., Bashan, A., Yap, M. N. F., and Yonath, A. (2019). Stress response as implemented by hibernating ribosomes: a structural overview. *FEBS J.* 286, 3558–3565. doi: 10.1111/febs.14968

Nakano, S., and Fukaya, M. (2008). Analysis of proteins responsive to acetic acid in Acetobacter: molecular mechanisms conferring acetic acid resistance in *acetic acid bacteria*. *Int. J. Food Microbiol.* 125, 54–59. doi: 10.1016/j.ijfoodmicro.2007.05.015

Peng, M. Y., Zhang, X. J., Huang, T., Zhong, X. Z., Chai, L. J., Lu, Z. M., et al. (2021). Komagataeibacter europaeus improves community stability and function in solid-state cereal vinegar fermentation ecosystem: Non-abundant species plays an important role. *Food Res. Int.* 150:110815. doi: 10.1016/j.foodres.2021.110815

Qi, Z., Yang, H., Xia, X., Quan, W., Wang, W., and Yu, X. (2014). Achieving high strength vinegar fermentation via regulating cellular growth status and aeration strategy. *Process Biochem.* 49, 1063–1070. doi: 10.1016/j.procbio.2014.03.018

Qin, Z., Yu, S., Chen, J., and Zhou, J. (2021). Dehydrogenases of *acetic acid bacteria*. *Biotechnol. Adv.* 54:107863. doi: 10.1016/j.biotechadv.2021.107863

Qiu, X., Zhang, Y., and Hong, H. (2021). Classification of *acetic acid bacteria* and their acid resistant mechanism. *AMB Expr.* 11:29. doi: 10.1186/s13568-021-01189-6

Ramírez-Bahena, M. H., Tejedor, C., Martín, I., Velázquez, E., and Peix, A. (2013). Endobacter medicaginis gen. nov., sp. nov., isolated from alfalfa nodules in an acidic soil. *Int. J. Syst. Evol. Microbiol.* 63, 1760–1765. doi: 10.1099/ijs.0.041368-0

Rennella, E., Sára, T., Juen, M., Wunderlich, C., Imbert, L., Solyom, Z., et al. (2017). RNA binding and chaperone activity of the E. coli cold-shock protein CspA. *Nucleic Acids Res.* 45, 4255–4268. doi: 10.1093/nar/gkx044

Román-Camacho, J. J., Mauricio, J. C., Santos-Dueñas, I. M., García-Martínez, T., and García-García, I. (2021). Functional metaproteomic analysis of alcohol vinegar microbiota during an acetification process: a quantitative proteomic approach. *Food Microbiol.* 98:103799. doi: 10.1016/j.fm.2021.103799

Román-Camacho, J. J., Santos-Dueñas, I. M., García-García, I., Moreno-García, J., García-Martínez, T., and Mauricio, J. C. (2020). Metaproteomics of microbiota involved in submerged culture production of alcohol wine vinegar: a first approach. *Int. J. Food Microbiol.* 333:108797. doi: 10.1016/j.ijfoodmicro.2020.108797

Ryngajłło, M., Kubiak, K., Jędrzejczak-Krzepkowska, M., Jacek, P., and Bielecki, S. (2018). Comparative genomics of the Komagataeibacter strains–Efficient bionanocellulose producers. *Microbiologyopen* 8:e00731. doi: 10.1002/mbo3.731

Sankuan, X., Cuimei, Z., Bingqian, F., Yu, Z., Menglei, X., Linna, T., et al. (2020). Metabolic network of ammonium in cereal vinegar solid-state fermentation and its response to acid stress. *Food Microbiol.* 95:103684. doi: 10.1016/j.fm.2020.103684

Santiago, B., MacGilvray, M., Faustoferri, R. C., and Quivey, R. G. Jr. (2012). The branched-chain amino acid aminotransferase encoded by ilvE is involved in acid tolerance in Streptococcus mutans. *J. Bacteriol.* 194, 2010–2019. doi: 10.1128/JB.06737-11

Sriherfyna, F. H., Matsutani, M., Hirano, K., Koike, H., Kataoka, N., Yamashita, T., et al. (2021). The auxiliary NADH dehydrogenase plays a crucial role in redox homeostasis of nicotinamide cofactors in the absence of the periplasmic oxidation system in Gluconobacter oxydans NBRC3293. *Appl. Environ. Microbiol.* 87, e02155–20. doi: 10.1128/AEM.02155-20

Tanwar, A. S., Morar, M., Panjikar, S., and Anand, R. (2012). Formylglycinamide ribonucleotide amidotransferase from *Salmonella* typhimurium: role of ATP complexation and the glutaminase domain in catalytic coupling. *Acta Crystallogr. D* 68, 627–636. doi: 10.1107/S0907444912006543

Trček, J., Jernejc, K., and Matsushita, K. (2007). The highly tolerant acetic acid bacterium Gluconacetobacter europaeus adapts to the presence of acetic acid by changes in lipid composition, morphological properties and PQQ-dependent ADH expression. *Extremophiles* 11, 627–635. doi: 10.1007/s00792-007-0077-y

Trček, J., Mahnič, A., and Rupnik, M. (2016). Diversity of the microbiota involved in wine and organic apple cider submerged vinegar production as revealed by DHPLC analysis and next-generation sequencing. *Int. J. Food Microbiol.* 223, 57–62. doi: 10.1016/j.ijfoodmicro.2016.02.007

Verce, M., De Vuyst, L., and Weckx, S. (2019). Shotgun Metagenomics of a Water Kefir Fermentation Ecosystem Reveals a Novel Oenococcus Species. *Front. Microbiol.* 10:479. doi: 10.3389/fmicb.2019.00479

Wang, B., Shao, Y., and Chen, F. (2015). Overview on mechanisms of acetic acid resistance in *acetic acid bacteria*. *World J. Microbiol. Biotechnol.* 31, 255–263. doi: 10.1007/s11274-015-1799-0

Xia, K., Zang, N., Zhang, J., Zhang, H., Li, Y., Liu, Y., et al. (2016). New insights into the mechanisms of acetic acid resistance in Acetobacter pasteurianus using iTRAQ-dependent quantitative proteomic analysis. *Int. J. Food Microbiol.* 238, 241–251. doi: 10.1016/j.ijfoodmicro.2016.09.016

Yamada, Y., Yukphan, P., Lan-Vu, H. T., Muramatsu, Y., Ochaikul, D., Tanasupawat, S., et al. (2012). Description of Komagataeibacter gen. nov., with proposals of new combinations (*Acetobacteraceae*). *J. Gen. Appl. Microbiol.* 58, 397–404. doi: 10.2323/jgam.58.397

Yin, H., Zhang, R., Xia, M., Bai, X., Mou, J., Zheng, Y., et al. (2017). Effect of aspartic acid and glutamate on metabolism and acid stress resistance of Acetobacter pasteurianus. *Microb. Cell Factories* 16:109. doi: 10.1186/s12934-017-0717-6

Zhang, S., and Bryant, D. A. (2011). The Tricarboxylic Acid Cycle in Cyanobacteria. *Science* 334, 1551–1553. doi: 10.1126/science.1210858

Zhang, X., Wang, P., Dandan, X., Wang, W., and Zhao, Y. (2019). Aroma patterns of Beijing rice vinegar and their potential biomarker for traditional Chinese cereal vinegars. *Food Res. Int.* 119, 398–410. doi: 10.1016/j.foodres.2019.02.008

Zheng, Y., Zhang, R., Yin, H., Bai, X., Chang, Y., Xia, M., et al. (2017). Acetobacter pasteurianus metabolic change induced by initial acetic acid to adapt to acetic acid fermentation conditions. *Appl. Microbiol. Biotechnol.* 101, 7007–7016. doi: 10.1007/s00253-017-8453-8

Zhu, Y., Zhang, F., Zhang, C., Yang, L., Fan, G., Xu, Y., et al. (2018). Dynamic microbial succession of Shanxi aged vinegar and its correlation with flavor metabolites during different stages of acetic acid fermentation. *Sci. Rep.* 8:8612. doi: 10.1038/s41598-018-26787-6

Conflict of Interest: The authors declare that the research was conducted in the absence of any commercial or financial relationships that could be construed as a potential conflict of interest.

Publisher's Note: All claims expressed in this article are solely those of the authors and do not necessarily represent those of their affiliated organizations, or those of the publisher, the editors and the reviewers. Any product that may be evaluated in this article, or claim that may be made by its manufacturer, is not guaranteed or endorsed by the publisher.

frontiers | Frontiers in Microbiology

REVIEW
published: 24 May 2022
doi: 10.3389/fmicb.2022.879246

Oxidative Fermentation of Acetic Acid Bacteria and Its Products

Yating He[1,2], *Zhenzhen Xie*[1,2], *Huan Zhang*[1,2], *Wolfgang Liebl*[3], *Hirohide Toyama*[4] *and Fusheng Chen*[1,2]*

[1] Hubei International Scientific and Technological Cooperation Base of Traditional Fermented Foods, Huazhong Agricultural University, Wuhan, China, [2] College of Food Science and Technology, Huazhong Agricultural University, Wuhan, China, [3] Department of Microbiology, Technical University of Munich, Freising, Germany, [4] Department of Bioscience and Biotechnology, Faculty of Agriculture, University of the Ryukyus, Okinawa, Japan

Acetic acid bacteria (AAB) are a group of Gram-negative, strictly aerobic bacteria, including 19 reported genera until 2021, which are widely found on the surface of flowers and fruits, or in traditionally fermented products. Many AAB strains have the great abilities to incompletely oxidize a large variety of carbohydrates, alcohols and related compounds to the corresponding products mainly including acetic acid, gluconic acid, gulonic acid, galactonic acid, sorbose, dihydroxyacetone and miglitol *via* the membrane-binding dehydrogenases, which is termed as AAB oxidative fermentation (AOF). Up to now, at least 86 AOF products have been reported in the literatures, but no any monograph or review of them has been published. In this review, at first, we briefly introduce the classification progress of AAB due to the rapid changes of AAB classification in recent years, then systematically describe the enzymes involved in AOF and classify the AOF products. Finally, we summarize the application of molecular biology technologies in AOF researches.

Keywords: acetic acid bacteria, classification, membrane-bound dehydrogenase, oxidative fermentation, molecular biology

OPEN ACCESS

Edited by:
Albert Bordons,
University of Rovira i Virgili, Spain

Reviewed by:
Maria J. Valera,
Universidad de la República, Uruguay
Carla Jara,
University of Chile, Chile
Montserrat Poblet,
Rovira i Virgili University, Spain
Eveline Bartowsky,
Lallemand, Canada

***Correspondence:**
Fusheng Chen
chenfs@mail.hzau.edu.cn

Specialty section:
This article was submitted to Food Microbiology, a section of the journal Frontiers in Microbiology

Received: *19 February 2022*
Accepted: *25 April 2022*
Published: *24 May 2022*

Citation:
He Y, Xie Z, Zhang H, Liebl W, Toyama H and Chen F (2022) Oxidative Fermentation of Acetic Acid Bacteria and Its Products. Front. Microbiol. 13:879246. doi: 10.3389/fmicb.2022.879246

INTRODUCTION

Acetic acid bacteria (AAB) are a group of Gram-negative, strictly aerobic bacteria within the family Acetobacteraceae (Saichana et al., 2015), which habitat in a large variety of different sources, such as flowers or fruits (Trček and Barja, 2015), guts of some insects (Crotti et al., 2016), and various traditionally fermented foods including vinegar, lambic beer, kefir, kombucha and so on (De Roos and De Vuyst, 2018). AAB may be named after their abilities to produce acetic acid *via* ethanol oxidation (Nanda et al., 2001), but actually some AAB strains are unable to produce acetic acid from ethanol, such as some strains within AAB genera of *Asaia* (*As.*) and *Saccharibacter* (*Sa.*; Moore et al., 2002; Jojima et al., 2004). Meanwhile, some AAB strains can fix nitrogen (Fuentes-Ramírez et al., 2001), produce pigment (Malimas et al., 2009), or exopolysaccharide (EPS; Gullo et al., 2017; La China et al., 2018). Very importantly, many AAB strains can incompletely oxidize various carbohydrates, alcohols and related compounds to yield the corresponding industrial products such as acetic acid, gluconic acid (GA), galactonic acid, 2-keto-L-gulonic acid (2-KGA), dihydroxyacetone (DHA), miglitol and so on (Mamlouk and Gullo, 2013), which have been successfully used in foods, cosmetics, medicines and other fields (Gullo et al., 2014; Saichana et al., 2015). These partial oxidation processes of AAB are named as AAB oxidative fermentation (AOF).

In AOF, the membrane-binding dehydrogenases (mDH) localized on the periplasmic side of the cytoplasmic membrane of AAB can deprive electrons from the substrates, followed by transferring them to ubiquinone (UQ, also called as coenzyme Q), which is then reduced to ubiquinol (UQH_2), and eventually, the terminal oxidases (TO) transfer the electrons from UQH_2 to oxygen to produce UQ, H_2O, and the energy (ATP; Adachi et al., 2003; Matsushita et al., 2016; Zhang and Chen, 2022). Therefore, besides the common electronic respiratory chain which is located in the bacterial cell membrane, another special respiratory chain (hereinafter referred to as AOF respiratory chain) also co-exist in AAB cells, and make them rapidly get the energy released from AOF (Matsushita et al., 1994, 2004; Yakushi and Matsushita, 2010). The AAB strains with oxidative fermentation capacity are called as oxidative bacteria. It is worth mentioning that the oxidative fermentation and its corresponding respiratory chain not only exist in AAB cells, but also in other aerobic bacteria such as *Pseudomonas* spp. and *Enterobacter* spp. (Matsushita et al., 2016). In **Figure 1** the two respiratory chains of alcohol (ethanol) in AAB are showed.

Since AOF takes place on the periplasmic side of the cytoplasmic membrane of AAB, its products are directly released extracellular, and avoid the transport limitation from intracellular to extracellular, resulting that AAB cells are considered as very ideal biocatalysts to produce corresponding products (Matsushita et al., 2016; Sengun, 2017). In this review, we have collected 86 AOF products which have been published, and introduced the relative enzymes with AOF. In addition, we have summarized the advance of the AAB classification and molecular biotechnology.

AAB CLASSIFICATION ADVANCE

The first AAB genus, *Acetobacter* (*A.*) was proposed by Beijerinck in 1898 (Wang and Chen, 2014). It was not until 37 years later (1935) that the second AAB genus, *Gluconobacter* (*G.*) was described by Asai (1968) and Yamada and Yukphan (2008). By the year of 1989, only 3 genera and 10 species of AAB were generally recognized (Wang and Chen, 2014). Since then the discovery and identification of AAB genera and species have been achieving rapid progress thanks to the development of molecular biology techniques (Wang and Chen, 2014). At the end of 2021, 19 genera and 110 species of AAB have been reported (https://lpsn.dsmz.de/; **Supplementary Table 1**).

The early classification and identification of AAB were mainly based on the phenotypic traits such as colony and microscopic morphologies, catalase test, Gram staining, chemotaxonomical characteristics mainly including UQ types (UQ9 or UQ10) and the profile of fatty methyl esters in AAB cells. For example, in Yamada and Kondo (1984) divided the genus of *Acetobacter*

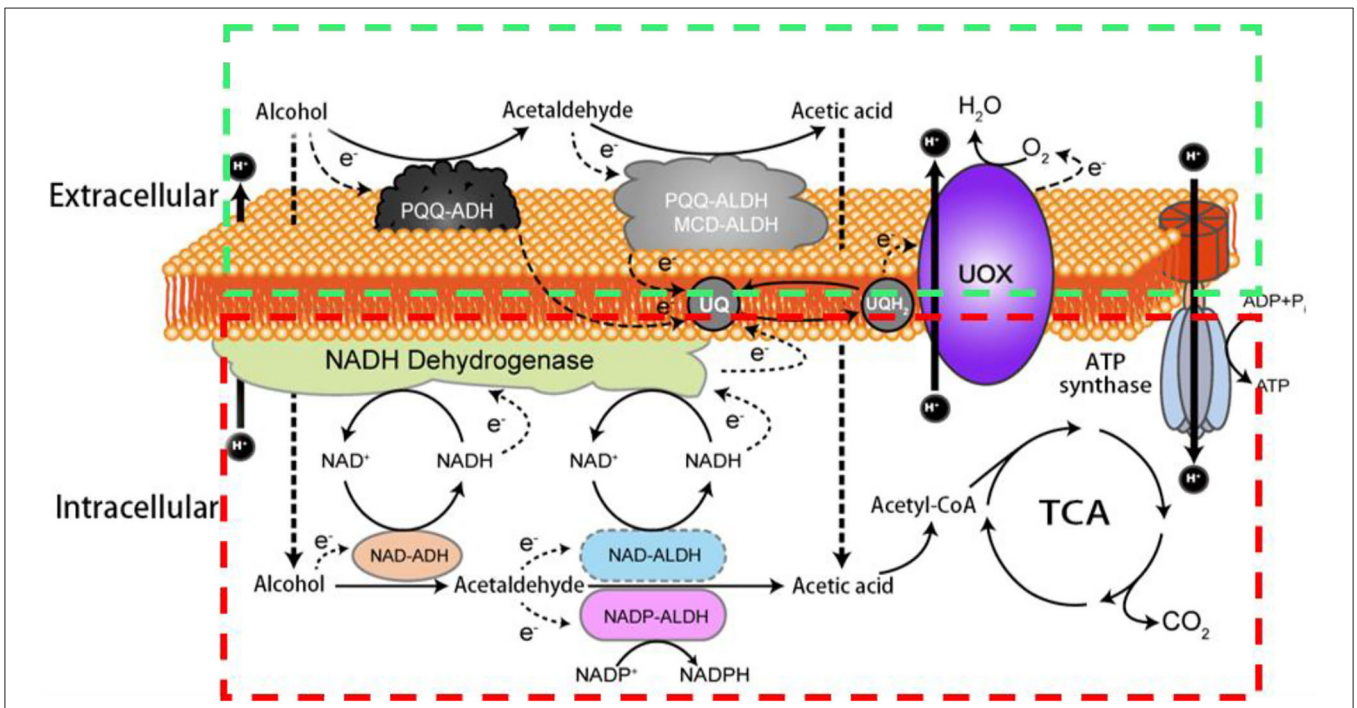

FIGURE 1 | Schematic diagram of two respiratory chains of alcohol in acetic acid bacteria. PQQ-ADH: pyrroloquinoline quinone dependent alcohol dehydrogenase; PQQ-ALDH: pyrroloquinoline quinone dependent acetaldehyde dehydrogenase; MCD-ALDH: molybdenum-molybdopterin cytosine dinucleotide dependent acetaldehyde dehydrogenase; NAD-ADH: nicotinamide adenine dinucleotide dependent alcohol dehydrogenase; NAD- ALDH: nicotinamide adenine dinucleotide dependent acetaldehyde dehydrogenase; NADP-ALDH: nicotinamide adenine dinucleotide phosphate dependent acetaldehyde dehydrogenase; UQ: ubiquinone; UQH2: ubiquinol; UOX: ubiquinol oxidase; ATP: the energy; TCA: tricarboxylic acid cycle; The green box shows the AOF respiratory chain including PQQ-ADH, PQQ-ALDH (MCD-ALDH), UQ, UQH2; UOX and ATP synthase; the red box indicates the common respiratory chain including NAD-ADH, NAD-ALDH (NADP-ALDH), UQ, UQH2; UOX and ATP synthase.

into two subgenera: *Acetobacter* subgenus with UQ9 and *Gluconoacetobacter* (*Ga.*) subgenus with UQ10, and Urakami et al. (1989) combined phenotypic characteristics, UQ types and the profile of fatty methyl esters to establish a new AAB genus—*Acidomonas* (*Ac.*), which was the third AAB genus recognized at that time.

In recent decades, with the development of molecular biology technologies, especially those related to rRNA, the AAB classification has developed very quickly, leading that some former AAB species or genera have excluded of the AAB group, meanwhile some new species and genera of AAB are proposed or independent from the former AAB (sub) species or (sub)genera. For instance, based on the phylogenic tree of 16S rRNA gene sequences, the genus *Gluconacetobacter*, which once belonged to the subgenus of *Acetobacter*, was elevated to the genus level (Yamada et al., 1997). Later, Yamada and his colleagues discovered that the 16S rRNA gene phylogenetic tree indicated two subclusters within the genus *Gluconacetobacter*, resulting that a new AAB genus *Komagataeibacter* (*K.*) was independent from the genus *Gluconacetobacter* (Yamada and Yukphan, 2008; Yamada et al., 2012a,b), and *Ga. kakiaceti*, *Ga. Medellinesis*, and *Ga. maltaceti* were re-classified into *K. kakiaceti*, *K. medellinesis*, and *K. maltaceti*, respectively (Yamada, 2014).

In **Table 1**, we have summarized the classification changes of AAB genera and species in recent decades.

However, only adopting the molecular biology methods related to rRNA may bring an error in AAB classification and identification. For example, according to the 16S rRNA phylogenic tree, the AAB genera of *Asaia* (*As.*), *Kozakia* (*Ka.*), *Swaminathania* (*Sa.*), and *Neoasaia* (*N.*) (**Supplementary Table 1**) could be categorized as one single genus, but their phenotypes warranted their distinction on the different genus level (Kersters et al., 2006). Therefore, internal transcribed spacer (ITS) of 16S-23S rRNA gene, restriction fragment length polymorphisms of genomic DNA and DNA-DNA hybridization (Janda and Abbott, 2007; Trček and Barja, 2015; Yamada, 2016) were also applied in AAB taxonomic studies. Moreover, the sequences of some genes were applied to identify AAB. For example, Trcek et al. (2006) used the nucleotide sequence of gene *adhA* for AAB identification, while genes of *nifD* and *nifH* were applied to identify nitrogen-fixing AAB species (Loganathan and Nair, 2004; Dutta and Gachhui, 2006). And multilocus sequence analysis of the three genes (*dnaK*, *groEL*, and *rpoB*) was performed to differentiate AAB species (Cleenwerck et al., 2010).

In the future, in order to obtain more objective, precise and reliable AAB classification, there is no doubt that a multidimensional method of the morphological classification combined with multiple molecular biological methods such as different genes or/ and the complete genome comparison, should be utilized for the classification and identification of AAB strains (Wang and Chen, 2014; Yamada, 2016).

TABLE 1 | The changes of classification status of AAB genera and species in recent decades.

Current species names	Once used species names	References
Acidomonas (*Ac.*) *methanolica*	*A. methanolicus*	Urakami et al., 1989
Frateuria aurantia (not AAB)	*A. aurantius*	Swings et al., 1980
Ga. diazotrophicus	*diazotrophicus, G. diazotrophicus*	Gillis et al., 1989; Yamada et al., 1997
Ga. liquefaciens	*A. liquefaciens, G.liquefaciens*	Yamada et al., 1997
G. japonicas	*G. industrius, G. nephelii*	Malimas et al., 2008
G. oxydans	*G. suboxydans, G. uchimurae, G. melanogenus*	Gosselé et al., 1983; Li et al., 2017
G. sphaericus	*G. oxydans* subsp. *sphaericus*	Malimas et al., 2008
G. thailandicus	*G. suboxydans, G. oxydans*	Tanasupawat et al., 2004
Ketogulonicigenium vulgare (not AAB)	*G. oxydans*	Urbance et al., 2001
K. europaeus	*A. europaeus*, *Ga. europaeus*	Yamada et al., 2012a
K. hansenii	*A. hansenii*, *Ga. hansenii*	Yamada et al., 2012a
K. intermedius	*A.intermedius, Ga. Intermedius*	Yamada et al., 2012b
K. kakiaceti	*Ga. kakiaceti*	Yamada, 2014
K. kombuchae	*Ga. kombuchae*, *Ga. hansenii*	Yamada et al., 2012a
K. maltaceti	*Ga. Maltaceti*	Yamada, 2014
K. medellinensis	*Ga. xylinus*, *Ga. medellinensis*	Marič et al., 2020
K. nataicola	*Ga. nataicola*	Yamada et al., 2012a
K. oboediens	*A. oboediens, Ga. oboediens*	Yamada, 2000; Yamada et al., 2012b
K. rhaeticus	*Ga. Rhaeticus*	Yamada et al., 2012b
K. saccharivorans	*Ga. saccharivorans*	Yamada et al., 2012b
K. sucrofermentans	*A. xylinum* subsp. *sucrofermentans, Ga. sucrofermentans*	Yamada et al., 2012a
K. swingsii	*A. xylinum* subsp. *nonacetooxidans, Ga. Swingsii*	Yamada et al., 2012b
K. xylinus	*A. xylinus, A. aceti* subsp. *xylinum, Ga. xylinus*	Yamada et al., 1997, 2012a,b

A., Acetobacter; Ac., Acidomonas; G., Gluconobacter; Ga., Gluconoacetobacter; K., Komagataeibacter.

AAB OXIDATIVE FERMENTATION

Due to their long existence in sugar-rich environments such as fruits and flowers, some AAB strains are adaptively evolved their abilities to rapidly incompletely oxidize sugars, sugar alcohols, or/and alcohols by mDH to produce corresponding products like aldehydes, ketones, acids, and other products, and yield ATP *via* the AOF respiratory chain (**Figure 1**; Matsushita et al., 1994, 2002; Saichana et al., 2015).

In addition to AOF, AAB can also completely oxidize sugars, sugar alcohols, alcohols, organic acids, and other substances to CO_2 and H_2O through the Embden–Meyerhof–Parnas pathway, the tricarboxylic acid cycle, the pentose phosphate pathway, the Entner–Doudoroff pathway, and/or the glyoxylate pathway, and produce intermediates for cell growth and ATP through the common respiratory chain (**Figure 1**). Although both complete and incomplete oxidation systems simultaneously exist in AAB cells, usually two systems rarely show similar activities in the same growth period of AAB strains. In an environment of a high concentration of sugars, alcohols, and/or acids, AAB cells mainly carry out AOF in the early growth period and complete oxidation in the late growth period. Aldehydes, ketones, or/and acids accumulated *via* AOF can inhibit the growth of other microorganisms, subsequently, when substrates are almost consumed by AOF, AAB can utilize these AOF products to continue to grow through the complete oxidation, resulting in AAB cells possessing the good growth and survival competitiveness. From the view of ecological evolution, AOF should be considered as a unique characteristic for AAB to adapt to the growth and survival environments, so it leading the carbon sources used by AAB is very complex, especially when multiple carbon sources such as sugars and alcohols are simultaneously present in the media (Gupta et al., 2001; Deppenmeier et al., 2002; Adachi et al., 2003; Raspor and Goranovič, 2008; Mamlouk and Gullo, 2013; Nishikura-Imamura et al., 2014; Saichana et al., 2015). The strategies of AAB to cope with changes in their growth and survival environments (culture conditions) by adjusting AOF were summarized in the reference (Qin et al., 2022).

Since the dehydrogenases (DHs) involved in AOF are located in the cell membrane, they are called as mDHs, while DHs in the cytoplasm is called as cytoplasmic DHs (cDHs). When AAB are exposed to a high concentration of substrate such as sugars and/or alcohols, the DH activity in AAB cells is mainly reflected by mDH, whereas cDH is almost inactive, but with the decrease of concentration of substrates, the cDH activity gradually increases, while the mDH activity decreases or hardly functions (Baldrian, 2006; Hölscher and Görisch, 2006). There are great differences in the coenzymes between mDHs and cDHs, mDHs ones are quite diverse, mainly including pyrroloquinoline quinone (PQQ), molybdenum-molybdopterin cytosine dinucleotide (MCD), flavin adenine dinucleotide (FAD), nicotinamide adenine dinucleotide (NAD), or/and nicotinamide adenine dinucleotide phosphate (NADP; **Table 2**), while cDHs ones mainly include NAD or/and NADP (**Figure 1**; Matsushita et al., 1994). The electrons and protons (H^+) from the substrate are deprived by both mDHs and cDHs, and transferred to UQ to produce UQH_2, which is then oxidized to produce a proton potential between intracellular and extracellular by terminal oxidase (TO), thereby driving ATP synthase to yield ATP (**Figure 1**).

Based on the coenzyme difference, the AAB mDH can be divided into five categories: quinoprotein-cytochrome complex, molybdoprotein-cytochrome complex, flavoprotein–cytochrome complex, quinoprotein, and others (**Table 2**). The mDH's types and characteristics vary in different genera, species, or strains of AAB. For example, membrane-binding alcohol dehydrogenase (mADH) from the genus *Gluconobacter* can oxidize ethanol into acetic acid, and can also oxidize D-glucose, GA, D-sorbitol, and glycerol into the corresponding products. In contrast, mADH from the genus *Acetobacter* or *Komagataeibacter* can only oxidize ethanol, almost impossible to oxidize other substrates (Matsushita et al., 2016).

TO is another key enzyme in the AOF respiratory chain, which can transfer electrons and protons from UQH_2 to O_2 to generate H_2O_2 or H_2O. The TOs from AAB and other aerobic bacteria can be divided into heme-copper oxidase (HCO) and heme *bd* type oxidase (HBD-O). Among them, HCO includes cytochrome *c* oxidase (COX) which can accept electrons from cytochrome *c*, and ubiquinol oxidase (UOX) which can accept electrons from UQH_2, and have binuclear O_2-reducing sites consisting of heme *a*, *o* or/and *b* and one copper atom (Matsutani et al., 2014). Bacteria with COX are called "oxidase-positive" bacteria, such as strains from the genera of *Paracoccus* and *Pseudomonas*, while bacteria with UOX are called "oxidase-negative" bacteria, such as *Escherichia coli* and AAB strains. In addition, HBD-O of AAB is also one kind of UOX that can accept electrons from UQH_2, but its oxygen reduction site contains heme *b* and *d*, which has a strong affinity for oxygen and can perform aerobic respiration under low oxygen conditions. Moreover, HBD-O has no proton pump function but has a certain proton release capacity that can produce part of the proton potential. In a word, the TOs of AAB mainly include UOX and HBD-O (Qin et al., 2022).

Membrane-Binding Dehydrogenase (mDH) in AOF

mDHs involved in the AOF drive functions are usually present in the form of heterotrimer or heterodimer. The structures and functions for some mDHs from AAB cells that have been clearly studied at present are shown in **Figure 2**.

Quinoprotein–Cytochrome Complex

The mDH of quinone protein-cytochrome complex clearly studied at present is mADH [EC.1.1.1.1], which is a constitutive ethanol ubiquinone oxidoreductase, and can catalyze the oxidation of ethanol to aldehyde and the reduction of UQ to UQH_2 (**Table 2**). The mADH isolated from the cell membrane of *Gluconobacter* spp. consists of three subunits: the large subunit (I) containing one PQQ and a heme *c* binding-sites, respectively, can oxidize ethanol to acetaldehyde; the cytochrome *c* subunit (II) including three heme *c* binding sites, can reduce UQ to UQH_2; and the small subunit (III) without any coenzyme binding site may be involved in cell membrane binding (Adachi et al., 2007; Masud et al., 2010). However, mADHs from *K. europaeus* and *A. peroxydans* (currently *A. pasteurianus*) contain only subunits I and II, no subunit III (Tayama et al., 1989; Trcek et al., 2006). When the dissociation of subunits I and II, the mADH enzyme activity of subunit I decrease significantly, but its enzyme activity is recovered after it re-combinates with subunit II, indicating that the complex of subunits I and II is necessary to maintain the mADH activity. The mADH contains a high-affinity UQ binding site and a catalytic site for the UQ oxidation-reduction enzyme activity, and UQ

TABLE 2 | The membrane-binding dehydrogenases in acetic acid bacteria based on their coenzyme differences.

Category	Enzyme and code number	Substrate	Product	Subunit[a]	Prosthetic group1[b]	Prosthetic group2[b]	Electron acceptor[c]
Quinoprotein-cytochrome complex	mADH (EC 1.1.1.1)	Ethanol	Acetaldehyde	I-II-III or I-II	PQQ	4 heme *c*	UQ
Molybdoprotein-cytochrome complex	mALDH (EC 1.2.1.10)	Acetaldehyde	Acetic acid	II-III or I-II	MCD or PQQ	[2Fe-2S] and 3 heme *c*; [2Fe-2S] and heme *b*; or heme *b* and *c*	UQ*
Flavoprotein-cytochrome complex	mGADH (EC 1.1.99.3)	D-Gluconic acid	2-KGA	I-II-III	FAD	3 heme *c*	UQ
	m2-KGDH (EC 1.1.99.4)	2-KGA	2, 5-DKGA	I-II-III	FAD	3 heme *c*	UQ*
	mFDH (EC 1.1.99.11)	D-Fructose	5-KF	I-II-III	FAD	3 heme *c*	UQ*
	mSLDH (EC 1.1.99.21)	D-Sorbitol	L-Sorbose	I-II-III	FAD	3 heme *c*	UQ*
Membrane-binding quinoprotein	mGDH (EC 1.1.99.17)	D-Glucose	GAL	I-II	PQQ	—[d]	UQ
	mGLDH (EC 1.1.1.6)	Polyalcohol	Ketone	I-II	PQQ	—	UQ
	mQDH (EC 1.1.99.25)	Quinic acid	3-DQA	I-II	PQQ	—	UQ
	mIDH (EC 1.1.1.18)	Myo-inositol	2-Keto-myoinositol	I-II	PQQ	—	UQ*
Other	mSDH (EC 1.1.99.12)	L-Sorbose	L-Sorbone	—[4]	FAD	—	UQ
	mSNDH (EC 1.1.1.-)	L-Sorbosone	2-KGLA	—	NAD or NADP or PQQ	—	UQ*

[a] *I-II-III: three subunits (large, medium-sized and small) complex; I-II: two subunits (large and medium-sized) complex.*
[b] *Prosthetic groups 1 and 2 are involved in substrate oxidation and electron transfer.*
[c] *UQ is experimentally verified by the experiments, and UQ* means that it has not been experimentally verified.*
[d] *"—": indicates that no such prosthetic group or subunit complex exists.*
mADH, membrane-binding alcohol dehydrogenase; mALDH, membrane-binding acetaldehyde dehydrogenase; mGADH, membrane-binding gluconate dehydrogenase; m2-KGDH, membrane-binding 2-keto-D-gluconate dehydrogenase; mFDH, membrane-binding D-fructose dehydrogenase; mSLDH, membrane-bindingD-sorbitol dehydrogenase; mGDH, membrane-binding glucose dehydrogenase; mGLDH, membrane-binding glycerol dehydrogenase; mQDH, membrane-binding quinic acid dehydrogenase; mIDH, membrane-binding inositol dehydrogenase; [2Fe-2S], 2 iron-sulfur clusters; mSDH, membrane-binding sorbose dehydrogenase; mSNDH, membrane-binding sorbone dehydrogenase; 2-KGA, 2-keto-D-gluconic acid; 2, 5-DKGA, 2, 5-diketo-D-gluconic acid; 5-KF, 5-keto-D-fructose; GAL, gluconic acid-δ-lactone; 3-QDA, 3-dehydroquinic acid; 2-KGLA, 2-keto-L-gulonic acid; PQQ, pyrroloquinoline quinone; MCD, molybdenum-molybdopterin cytosine dinucleotide; FAD, flavin adenine dinucleotide; NAD, nicotinamide adenine dinucleotide; NADP, nicotinamide adenine dinucleotide phosphate; UQ, ubiquinone.

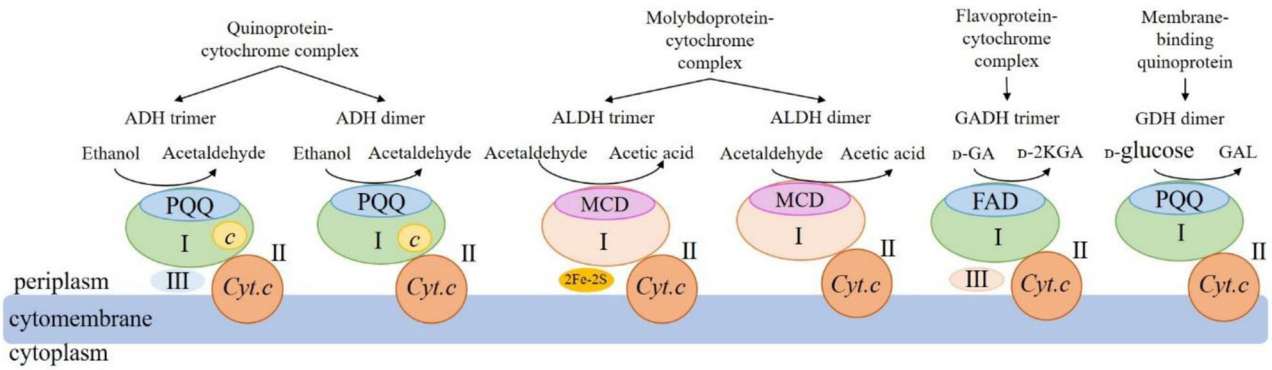

FIGURE 2 | Schematic of structures and functions of the four main membrane-binding dehydrogenases from acetic acid bacteria. ADH: membrane-binding alcohol dehydrogenase; ALDH: membrane-binding acetaldehyde dehydrogenase; GADH: membrane-binding gluconate dehydrogenase; GDH: membrane-binding glucose dehydrogenase; PQQ: pyrroloquinoline quinone; MCD: molybdenum-molybdopterin cytosine dinucleotide; FAD: flavin adenine dinucleotide; c: heme c; Cyt.c: cytochrome c; UQ: ubiquinone; UQH2: reduced ubiquinone; 2Fe-2S: 2 iron-sulfur clusters; I: large subunits; II: medium-size subunits; III: small subunits; GA: gluconic acid; 2-KGA: 2-keto-D-gluconic acid; GAL: gluconic acid-ă-lactone.

is involved in electron transfer among heme *c*, UQ, and UQH_2. In summary, based on the current research results, the AAB mADH is a heterotrimer (I-II-III) or a dimer (I-II) membrane-binding quinoprotein-cytochrome complex and includes prosthetic groups: PQQ and heme *c* (**Table 2** and **Figure 2**).

The substrate specificity of AAB mADH usually is very poor. Except for methanol, short-chain alcohols such as ethanol, 1-propanol, 1-butanol, 1-pentanol, and 1-hexanol can be utilized as its substrates (Shinagawa et al., 2006). In addition, mADH can also produce glyceraldehyde from glycerol, although it only has a low affinity for glycerol. Especially when the glycerol concentration is greater than 10% (W/V), its ability to oxidize glycerol is significantly improved (Habe et al., 2009). Moreover, aldehydes can be applied as substrates of mADH, too, and their oxidation rates by mADHs are almost same as those of the corresponding alcohols (Gómez-Manzo et al., 2008). Therefore, mADH alone can carry out the entire oxidation process from ethanol to acetaldehyde to acetic acid without the involvement of membrane-binding acetaldehyde dehydrogenase (mALDH) [EC 1.2.1.10] (Gómez-Manzo et al., 2015). In addition, although mADH cannot oxidize methanol, it can oxidize formaldehyde so that mADH can be developed as a formaldehyde scavenger (Shinagawa et al., 2006).

Molybdoprotein–Cytochrome Complex

The well-studied molybdoprotein-cytochrome complex mDH at present is mALDH, which is an acetaldehyde ubiquinone oxidoreductase. It is generally considered to be a heterotrimer (I-II-III) consisting of a large subunit (I) with MCD as one coenzyme, a medium-size subunit (II) with three heme *c* as prosthetic groups, and a small subunit (III) with two iron-sulfur clusters [2Fe-2S] as prosthetic groups (**Table 2** and **Figure 2**). However, mALDHs are very different in various AAB strains. For instance, in term of the subunit composition, mALDHs from both *A. aceti* and *K. europaeus* are heterotrimers (I-II-III), while the mALDH from *A. peroxydans* (currently *A.pasteurianus*) is a heterodimer (I-II; Gómez-Manzo et al., 2010). In term of the prosthetic groups, the mALDH ones from *K. europaeus* include heme *b*, [2Fe-2S] cluster and MCD, while the mALDH ones from *Ga. diazotrophicus* include PQQ, heme *b* and *c* (Thurner et al., 1997; Gómez-Manzo et al., 2010).

As with mADH, mALDH possesses a poor substrate specificity, which can oxidize acetaldehyde, 1-propionaldehyde, 1-butyraldehyde, isobutyraldehyde, glutaraldehyde, and other major short-chain aldehydes except for formaldehyde (Toyama et al., 2007).

Flavoprotein–Cytochrome Complex

The flavoprotein-cytochrome complex mDH of AAB mainly includes membrane-binding gluconate dehydrogenase (mGADH) [EC 1.1.99.3], 2-keto-D-gluconate dehydrogenase (m2-KGDH) [EC 1.1.99.4], D-fructose dehydrogenase (mFDH) [EC 1.1.99.11], and D-sorbitol dehydrogenase (mSLDH) [EC 1.1.99.21] (Toyama et al., 2005; Kawai et al., 2013; Kataoka et al., 2015). These mDHs generally consist of a large subunit (I) with FAD as a coenzyme, a medium-size subunit (II) containing three heme *c* prosthetic groups, and a small subunit (III) with unknown function (**Table 2** and **Figure 2**; Toyama et al., 2007).

mGADH, m2-KGDH, mFDH, and mSLDH are all UQ oxidoreductases with high substrate specificity. mGADH is also called GA 2-DH because it can oxidize the C-2 hydroxyl group of GA to produce 2-KGA. mGADH can only oxidize GA, and m2-KGDH can only oxidize 2-KGA to produce 2, 5-DKGA. mFDH can just oxidize fructose to produce 5-KF, which can be used as a biometric recognition molecule of the fructose biosensor. mSLDH can oxidize D-sorbitol to L-sorbose, and also weakly oxidize D-mannitol, whereas pentitol and erythritol are not oxidized by mSLDH (Shinagawa et al., 1982, 1984).

Membrane-Binding Quinoprotein

The membrane-binding quinoprotein AAB mDHs mainly include glucose dehydrogenase (mGDH) [EC 1.1.99.17], glycerol dehydrogenase (mGLDH) [EC 1.1.1.6], quinic acid dehydrogenase (mQDH) [EC 1.1.99.25], and inositol dehydrogenase (mIDH) [EC 1.1.1.18], which are composed of an N-terminal transmembrane domain and a C-terminal catalytic domain, including a large subunit (I) and a medium-size subunit (II). The coenzyme of the large subunit is PQQ, which plays a catalytic role, while the medium-size subunit does not contain any coenzyme and is only responsible for binding to the cell membrane (**Table 2** and **Figure 2**).

mGDH is a D-glucose ubiquinone oxidoreductase, which can oxidize the C-1 hydroxyl group of D-glucopyranose to gluconic acid-δ-lactone (GAL; Ameyama et al., 1981), and GAL can be transformed into GA spontaneously or by one of glucolactonases on the cell membrane. mGDH has been developed as a glucose sensor because of its high substrate specificity, which can oxidize only glucose but not hexose and pentose. mGLDH is a glycerol ubiquinone oxidoreductase with the poor substrate specificity, which can oxidize glycerol to dihydroxyacetone, arabitol, sorbitol, mannitol, erytritol, ribiol, and other polyols to the corresponding ketones (Sugisawa and Hoshino, 2002), and GA to 5-KGA (Matsushita et al., 2003). Industrially, mGLDH from *Glucobacter* spp. has been used to produce L-sorbate, DHA, erythrose, and 5-KGA (Shinjoh et al., 2002; Sugisawa and Hoshino, 2002; Hoshino et al., 2003). mQDH is a quinic acid ubiquinone oxidoreductase, which can oxidize the C3 hydroxyl group of quinic acid to 3-dehydroquinic acid (3-DQA), then 3-DQA is transformed to shikimic acid and protocatechuic acid successively by mQDH, of which activity is only one fourth of that of quinic acid (Vangnai et al., 2010). mIDH is an inositol ubiquinone oxidoreductase, which can oxidize the C2 hydroxyl group of inositol to 2-keto-inositol (Holscher et al., 2007).

Other Membrane-Binding Dehydrogenases (mDH)

Other types of AAB mDHs include membrane-binding sorbose dehydrogenase (mSDH) [EC 1.1.99.12] and sorbosone dehydrogenase (SNDH) [EC 1.1.1.-] (**Table 2**). mSDH is an L-sorbose ubiquinone oxidoreductase with FAD as a coenzyme, which can oxidize the C1 hydroxyl group of sorbose to L-sorbosone (Sugisawa et al., 1991). mSDH has a high substrate specificity, which can only oxidize L-sorbose, not other sugars and alcohols (Pappenberger and Hohmann, 2013). There are 2 classes of SNDH, the first class of SNDH is a L-sorbosone ubiquinone oxidoreductase with NAD or NADP as a coenzyme, and can oxidize the C1 hydroxyl group of L-sorbosone to produce 2-keto-L-gulonic acid (2-KGLA; Pappenberger and Hohmann, 2013), present in the cytosol (Sugisawa et al., 1991; Shinjoh and Hoshino, 1995); the other class exists on the

plasma membrane(mSNDH), are PQQ-dependent enzymes with L-sorbosone oxidation activity (Yakushi et al., 2020). Recently, it has been suggested that the substrate of mSNDH is the hemiacetal of L-sprbitol-1,5-pyranose (an isoform of L-sorbitol), that oxidized to 2-keto-L-gulone-1,5-pyranose(2-KGLL), and 2-KGLL will spontaneously be hydrolyzed into 2-KGLA under neutral pH conditions, but the substrate specificity, dynamics and structure of such mSNDH still need further investigation (Yakushi et al., 2020).

Terminal Oxidase (TO) in AOF

The TOs involved in the AOF respiratory chain mainly include UOX and HBD-O. Up to now, the TOs from *G. oxydans* and *A. aceti* have been intensively investigated.

Terminal Oxidases (TOs) in G. oxydans

The TOs in *G. oxydans* include cytochrome bo_3-UOX and HBD-O (Prust et al., 2005; Miura et al., 2013; Richhardt et al., 2013; Matsushita et al., 2016). When bo_3-UOX is absent, the early growth of *G. oxydans* is severely affected, whereas when HBD-O is absent, the early growth of cells is not affected (Matsushita et al., 1984). Further studies have indicated that at the early growth stage of *G. oxydans*, when the media pH is neutral, bo_3-UOX is the major TO, and with the accumulation of acid and other products, when the media pH decrease to acid, HBD-O can replace bo_3-UOX as the major TO, and act synergistically with cDH in the cytoplasm, leading that *G. oxydans* cells in acidic conditions continue to utilize organic acids and other products to grow (Miura et al., 2013; Richhardt et al., 2013).

Terminal Oxidases (TOs) in A. aceti

The TOs in *A. aceti* includes ba_3/bo_3-UOX, HBD-O, and two homologs of HBD-O, cyanide insensitive oxidase (CIO), CIO1, and CIO2, four TOs in total. Among them, ba_3/bo_3-UOX, CIO1 and CIO2 have a low affinity with oxygen, but a high turnover rate (efficiency), whereas HBD-O has a high affinity with oxygen, and can perform aerobic respiration under hypoxic conditions (Cunningham et al., 1997). Compared with HBD-O, CIO1 and CIO2, ba_3/bo_3-UOX have the stronger ability to form transmembrane proton potential and produce ATP, leading that ba_3/bo_3-UOX is the major TO in *A. aceti* (Matsutani et al., 2014).

NATURAL PRODUCTS YIELDED BY AOF

Through various mDHs in AOF, AAB can oxidize various alcohols, sugars, sugar alcohols, acids and so on to the corresponding products such as acetic acid, GA, galactonic acid, 2-KGA, DHA, miglitol and so on (Mamlouk and Gullo, 2013), which have been successfully used in foods, cosmetics, medicines and other fields (Gullo et al., 2014; Saichana et al., 2015). The schematic diagram of typical mDHs from AAB strains and their main AOF products is shown in **Figure 3**. Up to now, 86 AOF products have been reported, and each AOF product is given a bold Arabic numeral (**Supplementary Table 2**). Based on the numbers in square brackets after each AOF product, the molecular and structural formula of the corresponding AOF compound can be found in **Supplementary Table 2**.

AOF Products From Alcohols

AAB can partly oxidize a great number of primary, secondary and diol alcohols to yield the corresponding products, which have been utilized in foods, chemicals, and medicines.

Products From Primary Alcohols

The oxidation of ethanol to acetic acid may be the first-known AOF process from the AAB genus *Acetobacter* (Atkinson, 1956). The ethanol oxidation into acetic acid is a typical AOF process, which is divided into two steps (Matsushita et al., 1994). Ethanol is first oxidized to acetaldehyde [**1**] by PQQ-mADH, then converted to acetic acid [**2**] by PQQ-mALDH or MCD-mALDH. Besides the genus *Acetobacter*, the strains from *Komagataeibacter* spp. have very strong abilities to convert ethanol to acetic acid. Moreover, both of them have a high tolerance to ethanol and acetic acid, therefore they are the main species and strains in the vinegar production in the world (Adachi et al., 1978; Kanchanarach et al., 2010).

Except for methanol, mADH and mALDH can incompletely oxidize primary aliphatic normal alcohols with carbon chain length $\leq$6 to corresponding aldehydes and/or acids due to their poor substrate specificities (Adachi et al., 1978; Toyama et al., 2007), resulting in propionaldehyde [**3**] to propionic acid [**4**] from propanol, and butyric acid [**5**], pentanoic acid [**6**], hexanoic acid [**7**], isobutyric acid [**8**], and isovaleraldehyde [**9**] from butanol, pentanol, hexanol, isobutanol, and isoamyl alcohol, respectively (Švitel and Kutnik, 1995; Švitel and Šturdík, 1995; Molinari et al., 1996; Noyori, 2002).

Moreover, mADH and mALDH can also covert aromatic and other primary alcohols to the respective aldehydes and/or acids including phenylacetaldehyde [**10**], phenylacetic acid [**11**], 2-chloropropionic acid [**12**], (S)-2-phenyl-1-propionic acid [**13**], 2-methylbutanoic acid [**14**] and 2-keto-myoinositol [**15**] from 2-phenyl-ethanol, 2-chloropropanol, race-2-phenyl-1- propanol, 2-methylbutanol and myo-inositol, respectively (Molinari et al., 1996, 1999; Romano et al., 2002; Gandolfi et al., 2004; Hölscher and Görisch, 2006; Keliang and Dongzhi, 2006). Wei et al. (2016) found that racemic 1-(4-methoxyphenyl) ethanol (race-MOPE) could be oxidized to enantiopure (S)-MOPE [**16**] and 4-methoxyacetophenone [**17**] by mADH from *Acetobacter* sp. CCTCC M209061.

Products From Secondary Alcohols and Diols

Švitel and Kutnik (1995) found that *G. oxydans* CCM1783 could oxidize isopropanol and 2-butanol to acetone [**18**] and 2-buranone [**19**], respectively. Some AAB strains can also stereoselectively oxidize 2-methy-1,3-propanediol to (R)-β-hydroxyisobutyric acid [**20**] which is an important chiral building block in the synthesis of drugs (León et al., 2009).

The diols can be oxidized by some AAB strains, too. For example, 1,3-butandiol, 2,3- butandiol, (2R,3R)-2,3-butandiol, *N*-2-1,4-nonanodiol, 1,2-propanediol, ethanediol (ethylene glycol), racemical-1,2-butanediol, 1,3-propanediol and (R)-1-phenyl-1,2-ethanediol are oxidized to 3-hydroxybutyric acid [**21**] (Romano et al., 2002), (S)-acetoin [**22**] (Romano et al., 2002; Wang et al., 2013; Zhou et al., 2018), diacetyl [**23**], γ-nonanoic lactone [**24**] (Romano et al., 2002), (R)-2-hydroxy-propionic acid (D-(-)-lactic acid) [**25**] (Su et al., 2004), glycolic acid [**26**] (Wei

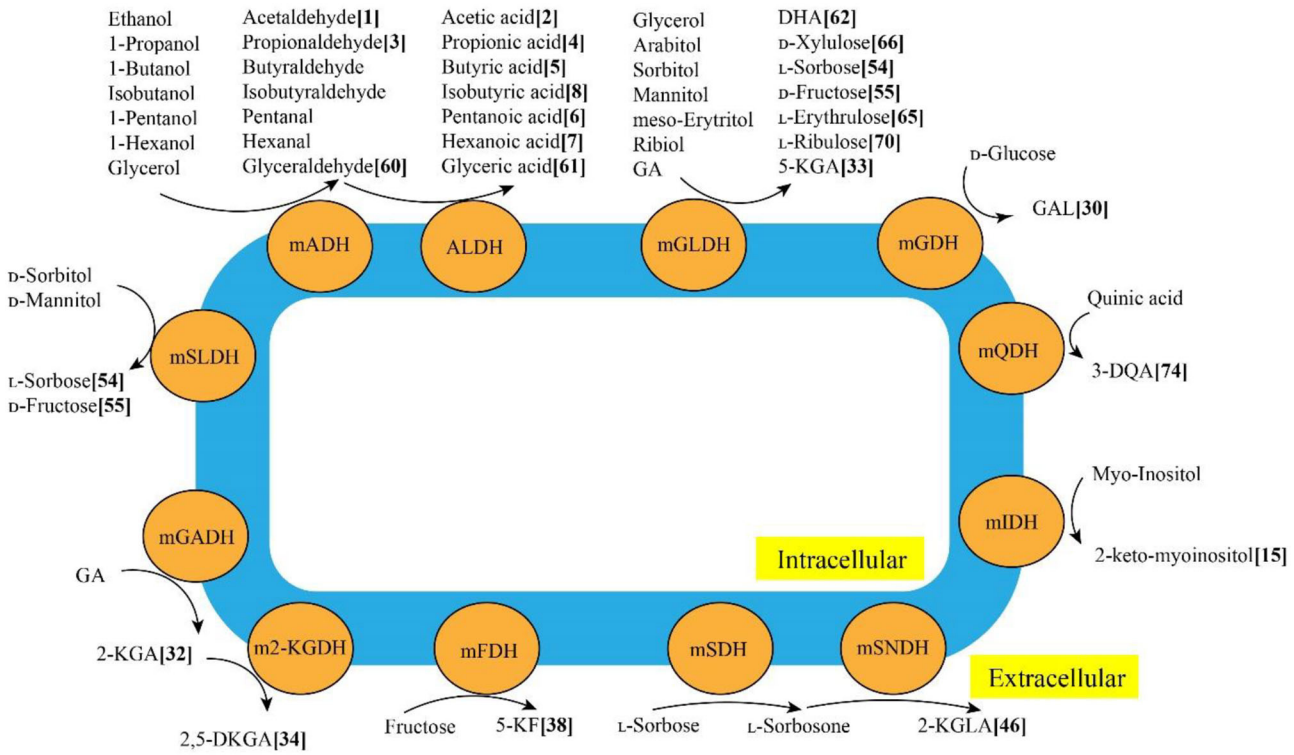

FIGURE 3 | Typical membrane-binding dehydrogenases in acetic acid bacteria and their main AOF products. mADH: membrane-binding alcohol dehydrogenase; mALDH: membrane-binding acetaldehyde dehydrogenase; mGADH: membrane-binding gluconate dehydrogenase; m2-KGDH: membrane-binding 2-keto-D-gluconate dehydrogenase; mFDH: membrane-binding D-fructose dehydrogenase; mSLDH: membrane-binding D-sorbitol dehydrogenase; mGDH: membrane-binding glucose dehydrogenase; mGLDH: membrane-binding glycerol dehydrogenase; mQDH: membrane-binding quinic acid dehydrogenasw; mIDH: membranebinding inositol dehydrogenase; mSDH: membrane-binding sorbose dehydrogenase; mSNDH: membrane-binding sorbone dehydrogenase; GA: gluconic acid; 2-KGA: 2-keto-Dgluconic acid; 2, 5-DKGA: 2, 5-diketo-D-gluconic acid; 5-KF: 5-keto-D-fructose; DHA: dihydroxyacetone; 3-QDA: 3-dehydroquinic acid; 2-KGLA: 2-keto-l-gulonic acid.

et al., 2009), (R)-2-hydroxybutyric acid [**27**] (Gao et al., 2012), 3-hydroxypropionic acid [**28**] (Dishisha et al., 2015; Zhu et al., 2018), and (R)-mandelic acid [**29**] (Li et al., 2014), respectively.

Products From Sugars and Disaccharides *via* AOF

Through AOF, AAB can partially oxidize various sugars and disaccharides like glucose, fructose, arabinose, ribose, xylose, sorbose, lactose, isomaltose, gentiobiose, and melibiose to the corresponding products.

Products From Glucose

During AOF, glucose is first converted into gluconic acid-δ-lactone [**30**] (Shinagawa et al., 2009), then changed into GA [**31**] spontaneously or by membrane-binding gluconic acid-δ- lactonase (Shinagawa et al., 2009). GA can further be oxidized to 2-KGA [**32**] by GA dehydrogenase, or to 5-KGA [**33**] by PQQ dependent glycerol dehydrogenase (PQQ-GLDH); 2-KGA can be catalyzed to 2,5-DKGA [**34**] by FAD-dependent 2-keto-D-gluconic acid dehydrogenase (FAD-GADH; Matsushita et al., 2003; Shinagawa et al., 2009). 2,5-DKGA can be transferred to 4-keto-D-arabinose [**35**], which is further catalyzed to 4-keto-D-arabonate [**36**] by 4-keto-D-aldopentose-1-dehydrogenase (Adachi et al., 2011a). 2,5-DKGA can be decarboxylated to form D-lyxuronic acid [**37**], too (Kondô and Ameyama, 1958).

Glucose oxidative fermentation of AAB is not only closely related to glucose concentration and reaction pH (Qazi et al., 1991) but also to the sugars of the culture medium. When glucose in the medium is depleted, small amounts of 2-KGA and 5-KGA secreted in the medium can be transported to AAB cells by transporters and then reduced to GA by 2-KGA reductase (2-KGAR) or 5-KGA reductase (5-KGAR) in the cytoplasm, and utilized by AAB through the pentose phosphate pathway (PPP), allowing AAB to reproduce again and present a secondary growth curve (Saichana et al., 2015). The kinds of products obtained from glucose oxidation by AAB are also affected by pH, for example, when the pH of the culture medium is at 3.4-4.0, AAB oxidized glucose produces only 5-KGA. Therefore, when producing GA, 2-KGA, and 5-KGA using AAB species, to prevent them from being further consumed by AAB utilization, culture conditions with high glucose concentration, low pH and high O_2 must be applied and fermentation terminated before the appearance of the secondary growth curve (Mamlouk and Gullo, 2013).

Products From Fructose, Arabinose, Ribose, Xylose, Sorbose, and Galactose

D-fructose can be oxidized to 5-keto-D-fructose **[38]** *via* mFDH and D-pentonate-4- dehydrogenase (P-4-DH) from AAB cells (Adachi et al., 2011b; Ano et al., 2017). mFDH possesses a high substrate specificity, whereas P-4-DH does not, which can oxidize D-psicose to 5-keto-D-psicose **[39]** (Ano et al., 2017), and shows mGLDH activity, too. In addition, fructose turns to glucosone **[40]** *via* a series of oxidized directly by *G. roseus* (Takahashi and Asai, 1932; Ikeda, 1955).

AAB strains can also transform D-arabinose to 4-keto-D-arabinose **[35]** and 4-keto-D-arabonate **[36]** (Adachi et al., 2010); D-ribose to 4-keto-D-ribose **[41]** and 4-keto-D-ribonate **[42]** (Adachi et al., 2011a); xylose to xylonic acid **[43]** (Buchert et al., 1988; Hahn et al., 2020), D-xylulose to xylitol **[44]** (Qi et al., 2016), sorbose to sorbitol **[45]** and 2-keto-D-gulonic acid **[46]** (Sugisawa et al., 1991; Adachi et al., 1999a), and D-galactose to D-galactonic acid **[47]** (Švitel and Šturdik, 1994). Adachi et al. (2013) also found that AAB cells could use 2-deoxy-D-ribose as a substrate to produce 2-deoxy-4-keto-D-ribose **[48]** and 2-deoxy-4-keto-D-ribonate **[49]**, which are under the action of membrane-binding D-aldopentose 4-dehydrogenase and 4-keto-D-1-dehydrogenase, respectively (Adachi et al., 2013).

Products From Disaccharides

The strain *A. orientalis* KYG 22 can oxidize lactose to lactose acid **[50]** with the aid of D-glucose by mGDH (Kiryu et al., 2014). mGDH from some strains of *Gluconobacter*, *Ga. hansenii* NBRC 14816 and *K. medellinensis* NBRC 3288 can also oxidize isomaltose, gentiobiose and melibiose to isomaltobionic acid **[51]**, gentiobionic acid, **[52]**, and melibionic acid **[53]**, respectively (Kiryu et al., 2020).

Products From Sugar Alcohols Through AOF

The sugar alcohols such as D-sorbitol, glycerol, D-mannitol, D-arabinol, D-erythritol and D-ribitol are transferred by AOF into L-sorbose, DHA, L-erythrose, D-xylulose, D-fructose, and L-ribulose, respectively (Cummins et al., 1957; Sugisawa and Hoshino, 2002; Prust et al., 2005; Adachi et al., 2007; Mamlouk and Gullo, 2013).

Products From Sorbitol

Sorbitol may be sequentially oxidized by two mDHs, sorbitol dehydrogenase and sorbose dehydrogenase from AAB cells, to L-sorbose **[54]** and D-fructose **[55]** (Cummins et al., 1957; Sato et al., 1967). Then sorbose is changed to 5-keto-D-fructose **[56]**, which will be converted into three γ-pyrone compounds including kojic acid **[57]**, 3-oxykojic acid, **[58]**, and 5-oxymaltol **[59]** (Sato et al., 1967). In addition, L-sorbosone can enter AAB cells, then transformed to 2-keto-L-gulonic acid **[46]**, which is secreted extracellularly as an intermediate of vitamin C synthesis (Sugisawa and Hoshino, 2002; Matsushita et al., 2003; Adachi et al., 2007).

Products From Glycerol

The *G. frateurii* NBRC3262 strain can sequentially convert glycerol to glyceraldehyde **[60]** to D-glyceric acid **[61]** by mADH (Habe et al., 2009). Some *G. oxydans* strains can oxidize glycerol to DHA **[62]** *via* mGLDH (Habe et al., 2009; Hu et al., 2010). DHA is widely used in cosmetics as an active sunscreen ingredient, as well as utilized in weight loss, antioxidant, vitiligo treatment, and so on (Levy, 1992). Some *Acetobacter* strains can convert racemic glycidol to glycidic acid **[63]** (Geerlof et al., 1994; Švitel and Kutnik, 1995).

Products From Other Sugar Alcohols

A. suboxydans strains can make L-fucitol convert to L-duco-4-ketose **[64]** (Richtmyer et al., 1950). Meso-erythritol is changed to L-erythrulose **[65]** by AAB cells (Richtmyer et al., 1950). D-arabitol (the 2-epimer of eylitol) was firstly oxidized to D-xylulose **[66]** by D-arabitol dehydrogenase (AraDH), then reduced to xylitol **[67]** by NAD-dependent xylitol dehydrogenase (Suzuki et al., 2002; Liu et al., 2019). Xylitol, a natural pentahydroxy sugar alcohol, has a sweet compound similar to sucrose and serves as a substitute for natural sweeteners. It also plays a role in preventing tooth decay (Suzuki et al., 2002). *G. suboxydans* can produce D-fructose **[55]** from D-mannitol (Adachi et al., 1999b). *Ac. oxydans* and could oxidize allitol to L-allulose (L-ribo-hexulose or L-psicose) **[68]** (Carr et al., 1968; Takeshita et al., 1996), which is rare and not natural ketohexose. AAB cells can also oxidize ribitol to L-ribulose **[60]** by membrane-binding NAD(P) independent ribitol dehydrogenase (Adachi et al., 2001). Recently, Xu et al. (2021) reported that polyol galactitol can be oxidized to two rare sugars, D-tagatose **[70]** and L-xylo-3-hexulose **[71]** by PQQ-dependent L-arabinitol 4-dehydrogenase (PQQ-LAD) from *Acetobacter* sp. and *Gluconobacter* sp. strains.

Products Converted From Organic Acids

Products From Quinate

Whiting and Coggins (1967) firstly reported that quinate oxidase from *Ac. oxydans,* quinate-cytochrome 555 oxidoreductase, could oxidize D-dihydroshikimic acid into 3,4- dihydroxy-5-oxocyclohexane-1-carboxylic acid **[72]**. Quinate is oxidized to 3-dehydroquinate (DQA) **[73]** by NAD(P) independent quinate dehydrogenase (QDH, EC 1.1.99.25), then to 3-dehydroshikimate (DSA) **[74]** *via* DQA dehydratase (EC. 4.2.1.10), and DSA can be converted to protocatechuate **[75]** by DSA dehydratase (Adachi et al., 2006).

Products From Other Organic Acids

Benziman and Perez (1965) proved that malate was converted to oxaloacetate **[76]** by a FAD-protein from *A. xylinum* (currently *K. xylinus*). Dosoretz et al. (1992) reported that the pure cultures of *A. pasteurianus*, *G. cerinus* and *G. oxydans* could oxidize calcium magnesium (Ca-Mg) lactate to Ca-Mg acetate (CMA) **[77]**, which is considered to be a potentially noncorrosive and biodegradable deicing chemical. In 2015, Sato et al. discovered that some strains of *Acetobacter* spp. could partially oxidize L/D-lactate into pyruvate **[78]** by lactate dehydrogenase (Sato et al., 2015).

Products Converted From Other Substrates *via* AOF

Products From Hexosamine

In 1960, Takahashi and Kayamori discovered that *A. melanogenum* (currently *G. oxydans*) could transform glucosamine into glucosaminic acid **[79]**, which is used as a commercial chemical in daily life (Takahashi and Kayamori, 1960). In 2004, Moonmangmee et al. found that D-mannosamine and D-galactosamine were changed into D-mannosaminate **[80]** and D-galatosaminate **[81]** by *Gluconobacter* sp. IFO 3264, respectively (Moonmangmee et al., 2004).

Products From Furfural

Zhou et al. (2017) prove that *G. oxydans* ATCC 621H could change furfural or furfuryl alcohol into 2-furoic acid **[82]**, which is the raw material to produce many furoate esters and its derivatives widely used in the synthesis of pharmaceutical, agricultural and industrial chemicals (Zhou et al., 2017). Sayed et al. (2019) found that the resting cells of *G. oxydans* DSM 50049 were capable of highly selective production of 5-hydroxymethyl-2- furan-carboxylic acid **[83]**, which is used as a monomer of a variety of polymers with antibacterial and antitumor activities (Sayed et al., 2019).

Products From Others

Sugisawa et al. (2005) first found that *G. oxydans* DSM 4025 could produce L-ascorbic acid **[84]** from L-gulono-γ-lactone with L-gulonate-γ-lactone dehydrogenase. Landis et al. (2002) prove that the strains of *G. oxydans* could also selectively region oxidize the *N*- butylglucamine into 6-deoxy-6-butylaminosorbose **[85]** (Landis et al., 2002). Some AAB strains can yield 6-(2-hydroxy-ethyl) amino-6-deoxy-α-L-sorbofuranose **[86]** using *N*-2-hydroxyethyl glucamine as substrate, which is an important precursor of miglitol, a α-glucosidase inhibitor, which was approved by the Food and Drug Administration of United States for the treatment of type II diabetes in December 1996 (Keliang and Dongzhi, 2006).

MOLECULAR BIOLOGICAL METHODS FOR AOF

In recent decades, a lot of molecular biology techniques have been applied to investigate AOF, especially its mDHs. Hereinafter, we just make a brief introduction about the application of molecular biology technologies in AOF, especially the establishment of a marker-less gene deletion system, for more detailed information, please read our recent review article (Yang et al., 2022).

Establishment of Marker-Less Gene Deletion System and Its Application in AOF

To investigate the function of mDH's genes from AAB, gene deletion is doubtlessly a direct and powerful tool. In this context, using a marker-less strategy is preferable to other molecular biology methods due to the following reasons (Peters et al., 2013): (1) the number of available markers such as antibiotic-resistant gene markers is so limited that the construction of the multi-gene knockout strain is sometimes impossible with marker genes; (2) as about 50% of genes in prokaryotes are located in the operons, where genes are co-transcribed into a single polycistronic mRNA (Osbourn and Field, 2009), the insertion of marker genes into the operon may exert polar effects and suppress the expression of downstream genes in the same operon.

Marker-less gene deletion techniques are often carried out in a two-step procedure using a plasmid vector carrying an antibiotic resistance selection marker, a counter selection marker, as well as the fused flanking fragments of the target gene (Gao et al., 2006). In the first step, the non-replicating plasmid vector is introduced into the host cell. Subsequently, the clones with the vector integrated at either the upstream or downstream site of the target gene by the homologous recombination are screened by antibiotic resistance and will be used for the second homologous recombination, in which the clones without the vector will be obtained through the recombination of the other homologous flanking region and the counter selection marker. The second homologous recombination will yield either the wild type strain or the desired gene deletion mutant with the theoretical ratio of 1:1 (Yang et al., 2022).

Peters et al. (2013) reported such a gene deletion system for AAB. The system involves a kanamycin resistance gene to select for AAB cells harboring the vector after its integration at the target site of the genome, together with gene *upp*, encoding uracil phosphoribosyl- transferase for the subsequent counter-selection to lose the vector from the genome, which could result in the desired deletion mutant without any marker sequence. In this case, uracil phosphoribosyltransferase converts the counter selection agent 5-fluorouracil (FU) to toxic 5-fluorouridinemonophosphate (F-UMP) to kill the wild type. However, most AAB species, including *G. oxydans*, possess the *upp* gene in their genomes. Therefore, deletion of the *upp* gene is required prior to application of this deletion method.

In order to avoid the deletion of *upp* before knocking out other genes, an improved method was established by Kostner et al. (2013) using the *codA* gene from *Echerichia coli* as the counter selection marker. This gene codes for cytosine deaminase, converting the nontoxic counters election agent 5-fluorocytosine (FC) to FU, which is subsequently converted to toxic F-UMP by uracil phosphoribosyltransferase encoded by gene *upp*. In addition, they found that the co-expression of *codA* with *codB,* coding for cytosine permease that facilitate the uptake of FC, can significantly increase the efficiency of the deletion method. Thus, *codB* was introduced to the deletion vector and also became a part of counter selection marker together with *codA* in this newly developed system.

Using the *upp* marker-based counter selection approach, Peters et al. (2013) knocked out all mDH-coding genes in *G. oxydans* 621H in a sequential manner, creating a series of mutants lacking one or more mDH (s), including *G. oxydans* BP.9 without all mDH genes and *G. oxydans* BP.8 only with the gene of a polyol dehydrogenase. Subsequently, by adopting a whole-cell 2,6-dichlorophenolindophenol (DCPIP) activity assay, the substrate specificities of the mDHs were clarified. Mientus et al. (2017) analyzed the substrate spectra of the mDHs of *G. oxydans* by applying a shuttle vector to express each individual enzyme

in *G. oxydans* BP.9, and the substrate spectra of every one of the mDHs were defined by the whole-cell DCPIP assay. In addition, Peters et al. (2013) used *G. oxydans* BP.9 to express genes encoding mDHs from the metagenome of a mother of vinegar sample including many non-culturable AAB and other microorganisms. In 2019, Burger et al. applied *G. oxydans* BP.8 to investigate and optimize the production of L-erythrulose (Burger et al., 2019).

Molecular Biology Studies Regarding AOF Other Than Marker-Less Deletion

Besides the gene marker-less deletion method, a number of other molecular biological technologies have also been applied for AOF research. For example, PQQ-GLDH was once conferred different names owning to the diversity of its substrates, including D-gluconate, D-arabitol, and D-sorbitol (Shinagawa et al., 1999; Adachi et al., 2001; Sugisawa and Hoshino, 2002). It was not until the gene disruption experiments that people finally realized that these enzymes are actually the same (Miyazaki et al., 2002; Shinjoh et al., 2002). Later, the name PQQ-GLDH was confirmed by Matsushita et al. (2003).

The molecular techniques are also exploited with the aim of promoting AOF production. A typical example is the oxidation of D-glucose, which is the most common substrate for *G. oxydans* and can be transferred into a variety of different products, such as GA, 5-KGA, 2-KGA, and 2, 5-DKGA (Saichana et al., 2015). Therefore, in terms of GA production, further oxidation of GA to ketogluconate is unexpected, suggesting that promotion of GA could be achieved by suppressing the mDHs which can further oxidize GA (La China et al., 2018). On the other hand, an increase in the production of GA, 2-KGA, and 5-KGA could be achieved by over-expression of genes encoding FAD-dependent D-gluconate dehydrogenase (Shi et al., 2014), PQQ-GDH and PQQ-GLDH (Merfort et al., 2006), respectively. In addition, either enhancing the abundance of mRNA transcribed from PQQ-GLDH-coding genes through adding an A/T tail (Xu et al., 2014) or over-expression of genes responsible for PQQ biosynthesis (Wang et al., 2016) can lead to the improved production of L-sorbose, which could be used as the substrate for producing 2-keto-L-gulonic acid, a direct precursor of vitamin C (La China et al., 2018). Furthermore, Gao et al. (2014) heterologously expressed a different combination of genes encoding five L-sorbose mDHs and two L-sorbosone mDHs from *Ketogulonicigenium vulgare* in *G. oxydans* WSH-003, and screened the best recombinant strain *G. oxydans*/pGUC-*k*0203-GS-*k*0095 with the highest yield, achieving one-step production of 2-keto-L-gulonic acid from D-sorbitol, which was produced *via* a two-step process in the past.

CONCLUSION AND DISCUSSION

AAB is a large group of Gram-negative, strictly aerobic bacteria, some of which have the great ability to yield a number of products with commercial or potential commercial values by their unique oxidative fermentation (AOF). In this review, we first summarize the AAB classification progress, then systematically describe and classify AOF products and the relative enzymes. The application of molecular biology technologies in AOF research is also briefly introduced.

Although many research works have been carried out and remarkable progress has been made on AOF, some AOF products such as acetic acid (vinegar), bacterial cellulose, DHA and so on (La China et al., 2018), have been industrialized, there are still a lot of issues about AOF which need to be further investigated. For example, although we are pleased to witness the promising progress achieved in the research on the functions of AAB mDHs, as well as in the AOF application, 21 'orphan' mDHs with unknown substrate spectra in *G. oxydans* are still unexplored (Adachi and Yakushi, 2016), and few crystal structures of AAB mDHs have been published (Qin et al., 2022), which greatly hinders the understanding of substrate space- and enantio- specificities of AAB mDHs. Moreover, the relevant modern technologies, especially modern molecular biotechnology including omics, systems biology, combinatorial biology, synthetic biology, and metabolic engineering, should be utilized for constructing relevant engineering strains for efficient production of the target AOF products.

AUTHOR CONTRIBUTIONS

YH contribute to the data collection, collation, and writing of the first draft. ZX and HZ responsible for the data collection and collation. WL and HT provide brief article ideas and language modifications. FC propose the overall idea for this article, reviewed and revised the first draft, and provided the corresponding financial support. All authors contributed to the article and approved the submitted version.

FUNDING

This work was supported by the Fundamental Research Funds for the Central Universities (No. 2662019PY015), the Major Special Projects of Technological Innovation of Hubei Province, China (No. 2018ABA075), the Major Science and Technology Project in Zhenjiang City, Jiangsu Province, China (No. ZD2019001), Programs of the International S&T Cooperation, Ministry of Science and Technology, China (No. 2014DFG32380), and China Scholarship Council (202006760070).

SUPPLEMENTARY MATERIAL

The Supplementary Material for this article can be found online at: https://www.frontiersin.org/articles/10.3389/fmicb.2022.879246/full#supplementary-material

REFERENCES

Adachi, O., Ano, Y., Moonmangmee, D., Shinagawa, E., Toyama, H., Theeragool, G., et al. (1999a). Crystallization and properties of NADPH-dependent L-sorbose reductase from *Gluconobacter melanogenus* IFO 3294. *Biosci. Biotechnol. Biochem.* 63, 2137–2143. doi: 10.1271/bbb.63.2137

Adachi, O., Ano, Y., Toyama, H., and Matsushita, K. (2006). High shikimate production from quinate with two enzymatic systems of acetic acid bacteria. *Biosci. Biotechnol. Biochem.* 70, 2579–2582. doi: 10.1271/bbb.60259

Adachi, O., Ano, Y., Toyama, H., Matsushita, K., and KGaA, C. (2007). *Biooxidation With PQQ-and FAD- Dependent Dehydrogenases. Modern Biooxidation: Enzymes, Reactions Applications*. Weinheim: Wiley-VCH Verlag GmbH.

Adachi, O., Fujii, Y., Ano, Y., Moonmangmee, D., Toyama, H., Shinagawa, E., et al. (2001). Membrane-bound sugar alcohol dehydrogenase in acetic acid bacteria catalyzes L-ribulose formation and NAD-dependent ribitol dehydrogenase is independent of the oxidative fermentation. *Biosci. Biotechnol. Biochem.* 65, 115–125. doi: 10.1271/bbb.65.115

Adachi, O., Hours, R. A., Akakabe, Y., Shinagawa, E., Ano, Y., Yakushi, T., et al. (2013). Pentose oxidation by acetic acid bacteria led to a finding of membrane-bound purine nucleosidase. *Biosci. Biotechnol. Biochem.* 77, 1131–1133. doi: 10.1271/bbb.130066

Adachi, O., Hours, R. A., Akakabe, Y., Tanasupawat, S., Yukphan, P., Shinagawa, E., et al. (2010). Production of 4-keto-D-arabonate by oxidative fermentation with newly isolated *Gluconacetobacter liquefaciens*. *Biosci. Biotechnol. Biochem.* 74, 2555–2558. doi: 10.1271/bbb.100698

Adachi, O., Hours, R. A., Shinagawa, E., Akakabe, Y., Yakushi, T., and Matsushita, K. (2011a). Enzymatic synthesis of 4-pentulosonate (4-keto-D-pentonate) from D-aldopentose and D-pentonate by two different pathways using membrane enzymes of acetic acid bacteria. *Biosci. Biotechnol. Biochem.* 75, 2418–2420. doi: 10.1271/bbb.110575

Adachi, O., Hours, R. A., Shinagawa, E., Akakabe, Y., Yakushi, T., and Matsushita, K. (2011b). Formation of 4-keto-D-aldopentoses and 4-pentulosonates (4-keto-D-pentonates) with unidentified membrane-bound enzymes from acetic acid bacteria. *Biosci. Biotechnol. Biochem.* 75, 1801–1806. doi: 10.1271/bbb.110339

Adachi, O., Moonmangmee, D., Toyama, H., Yamada, M., Shinagawa, E., and Matsushita, K. (2003). New developments in oxidative fermentation. *Appl. Microbiol. Biotechnol.* 60, 643–653. doi: 10.1007/s00253-002-1155-9

Adachi, O., Tayama, K., Shinagawa, E., Matsushita, K., and Ameyama, M. (1978). Purification and characterization of particulate alcohol dehydrogenase from *Gluconobacter suboxydans*. *Agri. Biol. Chem.* 42, 2045–2056. doi: 10.1271/bbb1961.42.2045

Adachi, O., Toyama, H., and Matsushita, K. (1999b). Crystalline NADP-dependent D-mannitol dehydrogenase from *Gluconobacter suboxydans*. *Biosci. Biotechnol. Biochem.* 63, 402–407. doi: 10.1271/bbb.63.402

Adachi, O., and Yakushi, T. (2016). "Membrane-bound dehydrogenases of acetic acid bacteria," in *Acetic Acid bacteria: Ecology and Physiology*, eds K. Matsushita, H., Toyama, N., Tonouchi, A., Okamoto-Kainuma (Tokyo: Springer Japan), 273–297. doi: 10.1007/978-4-431-55933-7_13

Ameyama, M., Shinagawa, E., Matsushita, K., and Adachi, O. (1981). D-Glucose dehydrogenase of *Gluconobacter suboxydans*: solubilization, purification and characterization. *Agri. Biol. Chem.* 45, 851–861. doi: 10.1271/bbb1961.45.851

Ano, Y., Hours, R. A., Akakabe, Y., Kataoka, N., Yakushi, T., Matsushita, K., et al. (2017). Membrane- bound glycerol dehydrogenase catalyzes oxidation of D-pentonates to 4-keto-D-pentonates, D-fructose to 5-keto-D-fructose, and D-psicose to 5-keto-D-psicose. *Biosci. Biotechnol. Biochem.* 81, 411–418. doi: 10.1080/09168451.2016.1254535

Asai, T. (1968). *Acetic Acid Bacteria; Classification and Biochemical Activities*. Tokyo: University of Tokyo Press.

Atkinson, D. E. (1956). The oxidation of ethanol and tricarboxylic acid cycle intermediates by *Acetobacter peroxydans*. *J. Bacteriol.* 72, 195–198. doi: 10.1128/jb.72.2.195-198.1956

Baldrian, P. (2006). Fungal laccases–occurrence and properties. *FEMS Microbiol. Rev.* 30, 215–242. doi: 10.1111/j.1574-4976.2005.00010.x

Benziman, M., and Perez, L. (1965).The participation of vitamin K in malate oxidation by *Acetobacter xylinum*. *Biochem. Biophys. Res. Commun.* 19, 127–132. doi: 10.1016/0006-291X(65)90130-0

Buchert, J., Puls, J., and Poutanen, K. (1988). Comparison of *Pseudomonas fragi* and *Gluconobacter oxydans* for production of xylonic acid from hemicellulose hydrolyzates. *Appl. Microbiol. Biotechnol.* 28, 367–372. doi: 10.1007/BF00268197

Burger, C., Kessler, C., Gruber, S., Ehrenreich, A., Liebl, W., and Weuster-Botz, D. (2019). L-Erythrulose production with a multideletion strain of *Gluconobacter oxydans*. *Appl. Microbiol. Biotechnol.* 103, 4393-4404. doi: 10.1007/s00253-019-09824-w

Carr, J., Coggins, R., Hough, L., Stacey, B., and Whiting, G. (1968). Microbiological oxidation of allitol to l-ribo-hexulose by *Acetomonas oxydans*. *Phytochemistry*. 7, 1–4. doi: 10.1016/S0031-9422(00)88197-2

Cleenwerck, I., De Vos, P., and De Vuyst, L. (2010). Phylogeny and differentiation of species of the genus *Gluconacetobacter* and related taxa based on multilocus sequence analyses of housekeeping genes and reclassification of *Acetobacter xylinus* subsp. sucrofermentans as *Gluconacetobacter sucrofermentans* (Toyosaki et al. 1996) sp. nov., comb. nov. *Int. J. Systemat. Evol. Microbiol.* 60, 2277–2283. doi: 10.1099/ijs.0.018465-0

Crotti, E., Chouaia, B., Alma, A., Favia, G., Bandi, C., Bourtzis, K., et al. (2016). "Acetic acid bacteria as symbionts of insects," in *Acetic Acid Bacteria: Ecology and Physiology*, eds K. Matsushita, H. Toyama, N. Tonouchi and A. Okamoto-Kainuma. (Tokyo: Springer Japan), 121–142. doi: 10.1007/978-4-431-55933-7_5

Cummins, J. T., King, T. E., and Cheldelin, V. H. (1957). The biological oxidation of sorbitol. *J. Biol. Chem.* 224, 323–329. doi: 10.1016/S0021-9258(18)65031-8

Cunningham, L., Pitt, M., and Williams, H. D. (1997).The *cioAB* genes from *Pseudomonas aeruginosa* code for a novel cyanide-insensitive terminal oxidase related to the cytochrome bd quinol oxidases. *Mol. Microbiol.* 24, 579–591. doi: 10.1046/j.1365-2958.1997.3561728.x

De Roos, J., and De Vuyst, L. (2018). Acetic acid bacteria in fermented foods and beverages. *Curr. Opin. Biotechnol.* 49, 115–119. doi: 10.1016/j.copbio.2017.08.007

Deppenmeier, U., Hoffmeister, M., and Prust, C. (2002). Biochemistry and biotechnological applications of *Gluconobacte*r strains. *Appl. Microbiol. Biotechnol. Adv.* 60, 233–242. doi: 10.1007/s00253-002-1114-5

Dishisha, T., Pyo, S. H., and Hatti-Kaul, R. (2015). Bio-based 3-hydroxypropionic- and acrylic acid production from biodiesel glycerol *via* integrated microbial and chemical catalysis. *Microb Cell Fact.* 14:200. doi: 10.1186/s12934-015-0388-0

Dosoretz, C. G., Jain, M. K., and Grethlein, H. E. (1992). Oxidative fermentation of calcium-magnesium lactate to calcium-magnesium acetate deicing salt. *Biotechnol. Lett.* 14, 613–618. doi: 10.1007/BF01023951

Dutta, D., and Gachhui, R. (2006). Novel nitrogen-fixing *Acetobacter nitrogenifigens* sp. nov., isolated from Kombucha tea. *Int. J. Systemat. Evol. Microbiol.* 56, 1899–1903. doi: 10.1099/ijs.0.64101-0

Fuentes-Ramírez, L. E., Bustillos-Cristales, R., Tapia-Hernández, A., Jiménez-Salgado, T., Wang, E. T., Martínez-Romero, E., et al. (2001). Novel nitrogen-fixing acetic acid bacteria, *Gluconacetobacter johannae* sp. nov. and *Gluconacetobacter azotocaptans* sp. nov., associated with coffee plants. *Int. J. Systemat. Evol. Microbiol.* 51, 1305–1314. doi: 10.1099/00207713-51-4-1305

Gandolfi, R., Cavenago, K., Gualandris, R., Sinisterra Gago, J. V., and Molinari, F. (2004). Production of 2-phenylacetic acid and phenylacetaldehyde by oxidation of 2-phenylethanol with free immobilized cells of *Acetobacter aceti*. *Process Biochem.* 39, 749–753. doi: 10.1016/S0032-9592(03)00185-7

Gao, C., Zhang, W., Huang, Y., Ma, C., and Xu, P. (2012). Efficient conversion of 1,2-butanediol to (R)-2-hydroxybutyric acid using whole cells of *Gluconobacter oxydans*. *Bioresour. Technol.* 115, 75–78. doi: 10.1016/j.biortech.2011.11.009

Gao, L., Hu, Y., Liu, J., Du, G., Zhou, J., and Chen, J. (2014). Stepwise metabolic engineering of *Gluconobacter oxydans* WSH-003 for the direct production of 2-keto-L-gulonic acid from D-sorbitol. *Metabol. Eng.* 24, 30–37. doi: 10.1016/j.ymben.2014.04.003

Gao, W., Liu, Y., Giometti, C. S., Tollaksen, S. L., Khare, T., Wu, L., et al. (2006). Knock-out of SO1377 gene, which encodes the member of a conserved hypothetical bacterial protein family COG2268, results in alteration of iron metabolism, increased spontaneous mutation and hydrogen peroxide sensitivity in *Shewanella oneidensis* MR-1. *BMC Genom.* 7, 1–13. doi: 10.1186/1471-2164-7-76

Geerlof, A., Jongejan, J. A., van Dooren, T. J., Raemakers-Franken, P. C., van den Tweel, W. J., and Duine, J.A. (1994). Factors relevant to the production of (R)-(+)-glycidol (2, 3-epoxy-1-propanol) from racemic glycidol

by enantioselective oxidation with *Acetobacter pasteurianus* ATCC 12874. *Enzyme Microbial. Technol.* 16, 1059–1063. doi: 10.1016/0141-0229(94)90143-0

Gillis, M., Kersters, K., Hoste, B., Janssens, D., Kroppenstedt, R., Stephan, M., et al. (1989). *Acetobacter diazotrophicus* sp. nov., a nitrogen-fixing acetic acid bacterium associated with sugarcane. *Int. J. Systemat. Evol. Microbiol.* 39, 361–364. doi: 10.1099/00207713-39-3-361

Gómez-Manzo, S., Chavez-Pacheco, J., Contreras-Zentella, M., Sosa-Torres, M., Arreguín-Espinosa, R., Perez De La Mora, M., et al. (2010). Molecular and catalytic properties of the aldehyde dehydrogenase of *Gluconacetobacter diazotrophicus*, a quinoheme protein containing pyrroloquinoline quinone, cytochrome b, and cytochrome c. *J. Bacteriol.* 192, 5718–5724. doi: 10.1128/JB.00589-10

Gómez-Manzo, S., Contreras-Zentella, M., González-Valdez, A., Sosa-Torres, M., Arreguín-Espinoza, R., and Escamilla-Marván, E. (2008). The PQQ-alcohol dehydrogenase of *Gluconacetobacter diazotrophicus*. *Int. J. Food Microbiol.* 125, 71–78. doi: 10.1016/j.ijfoodmicro.2007.10.015

Gómez-Manzo, S., Escamilla, J. E., González-Valdez, A., López-Velázquez, G., Vanoye-Carlo, A., Marcial-Quino, J., et al. (2015).The oxidative fermentation of ethanol in *Gluconacetobacter diazotrophicus* is a two-step pathway catalyzed by a single enzyme: alcohol-aldehyde dehydrogenase (ADHa). *Int. J. Mol. Sci.* 16, 1293–1311. doi: 10.3390/ijms16011293

Gosselé, F., Swings, J., Kersters, K., and De Ley, J. (1983). Numerical analysis of phenotypic features and protein gel electropherograms of *Gluconobacter Asai* 1935 emend. mut. char. Asai, Iizuka, and Komagata 1964. *Int. J. Systemat. Evol. Microbiol.* 33, 65-81. doi: 10.1099/00207713-33-1-65

Gullo, M., Sola, A., Zanichelli, G., Montorsi, M., Messori, M., and Giudici, P. (2017). Increased production of bacterial cellulose as starting point for scaled-up applications. *Appl. Microbiol. Biotechnol.* 101, 8115–8127. doi: 10.1007/s00253-017-8539-3

Gullo, M., Verzelloni, E., and Canonico, M. (2014). Aerobic submerged fermentation by acetic acid bacteria for vinegar production: process and biotechnological aspects. *Process Biochem.* 49, 1571–1579. doi: 10.1016/j.procbio.2014.07.003

Gupta, A., Singh, V. K., Qazi, G., and Kumar, A. (2001).*Gluconobacter oxydans*: its biotechnological applications. *J. Mol. Microbiol. Biotechnol. Adv.* 3, 445–456.

Habe, H., Shimada, Y., Yakushi, T., Hattori, H., Ano, Y., Fukuoka, T., et al. (2009). Microbial production of glyceric acid, an organic acid that can be mass produced from glycerol. *Appl. Environ. Microbiol.* 75, 7760–7766. doi: 10.1128/AEM.01535-09

Hahn, T., Torkler, S., van Der Bolt, R., Gammel, N., Hesse, M., Möller, A., et al. (2020). Determining different impact factors on the xylonic acid production using *Gluconobacter oxydans* DSM 2343. *Process Biochem.* 94, 172–179. doi: 10.1016/j.procbio.2020.04.011

Hölscher, T., and Görisch, H. (2006). Knockout and overexpression of pyrroloquinoline quinone biosynthetic genes in *Gluconobacter oxydans* 621H. *J. Bacteriol.* 188, 7668–7676. doi: 10.1128/JB.01009-06

Holscher, T., Weinert-Sepalage, D., and Gorisch, H. (2007). Identification of membrane-bound quinoprotein inositol dehydrogenase in *Gluconobacter oxydans* ATCC 621H. *Microbiology*153, 499–506. doi: 10.1099/mic.0.2006/002196-0

Hoshino, T., Sugisawa, T., Shinjoh, M., Tomiyama, N., and Miyazaki, T. (2003). Membrane-bound D-sorbitol dehydrogenase of *Gluconobacter suboxydans* IFO 3255—enzymatic and genetic characterization. *Biochim. Biophys. Acta* 1647, 278–288. doi: 10.1016/S1570-9639(03)00071-2

Hu, Z. C., Liu, Z. Q., Zheng, Y. G., and Shen, Y. C. (2010). Production of 1, 3-dihydroxyacetone from glycerol by *Gluconobacter oxydans* ZJB09112. *J. Microbiol. Biotechnol. Lett.* 20, 340–345. doi: 10.4014/jmb.0907.07011

Ikeda, Y. (1955). A presumable pathway of kojic acid formation formation from fructose by *Gluconoeacter*. *J. General Appl. Microbiol. Biotechnol.* 1, 152–163. doi: 10.2323/jgam.1.152

Janda, J. M., and Abbott, S. L. (2007). 16S rRNA gene sequencing for bacterial identification in the diagnostic laboratory: pluses, perils, and pitfalls. *J. Clin. Microbiol.* 45, 2761–2764. doi: 10.1128/JCM.01228-07

Jojima, Y., Mihara, Y., Suzuki, S., Yokozeki, K., Yamanaka, S., and Fudou, R. (2004). *Saccharibacter floricola* gen. nov., sp. nov., a novel osmophilic acetic acid bacterium isolated from pollen. *Int. J. Systemat. Evol. Microbiol.* 54, 2263–2267. doi: 10.1099/ijs.0.02911-0

Kanchanarach, W., Theeragool, G., Inoue, T., Yakushi, T., Adachi, O., and Matsushita, K. (2010). Acetic acid fermentation of *Acetobacter pasteurianus*: relationship between acetic acid resistance and pellicle polysaccharide formation. *Biosci. Biotechnol. Biochem.* 2010:1007022033. doi: 10.1271/bbb.100183

Kataoka, N., Matsutani, M., Yakushi, T., and Matsushita, K. (2015). Efficient production of 2, 5-diketo-D-gluconate *via* heterologous expression of 2-ketogluconate dehydrogenase in *Gluconobacter japonicus*. *Appl. Environ. Microbiol.* 81, 3552–3560. doi: 10.1128/AEM.04176-14

Kawai, S., Goda-Tsutsumi, M., Yakushi, T., Kano, K., and Matsushita, K. (2013). Heterologous overexpression and characterization of a flavoprotein-cytochrome c complex fructose dehydrogenase of *Gluconobacter japonicus* NBRC3260. *Appl. Environ. Microbiol.* 79, 1654–1660. doi: 10.1128/AEM.03152-12

Keliang, G., and Dongzhi, W. (2006). Asymmetric oxidation by *Gluconobacter oxydans*. *Appl. Microbiol Biotechnol.* 70: 135–139. doi: 10.1007/s00253-005-0307-0

Kersters, K., Lisdiyanti, P., Komagata, K., and Swings, J. (2006). The family A*cetobacteraceae*: the genera *Acetobacter*, *Acidomonas*, *Asaia*, *Gluconacetobacter*, *Gluconobacter*, and *Kozakia*. *Prokaryotes* 5, 163–200. doi: 10.1007/0-387-30745-1_9

Kiryu, T., Kiso, T., Sato, H., and Murakami, H. (2020). Oxidation of isomaltose, gentiobiose, and melibiose by membrane-bound quinoprotein glucose dehydrogenase from acetic acid bacteria. *Biosci. Biotechnol. Biochem.* 84, 507–517. doi: 10.1080/09168451.2019.1689095

Kiryu, T., Yamauchi, K., Masuyama, A., Ooe, K., Kimura, T., Kiso, T., et al. (2014). Optimization of lactobionic acid production by *Acetobacter orientalis* isolated from Caucasian Fermented Milk, "Caspian Sea Yogurt". *Biosci. Biotechnol. Biochem.* 76, 361–363. doi: 10.1271/bbb.110608

Kondô, K., and Ameyama, M. (1958). Carbohydrate metabolism by acetobacter species: part I. oxidative activity for various carbohydrates. Part II. Ketogenic metabolism of glucose. Part III. Isolation and identification of d-lyxuronic acid on glucose oxidation by *A. melanogenum*. *J. Agri. Chem. Soc. Jap*. 22, 369–386. doi: 10.1080/03758397.1958.10857508

Kostner, D., Peters, B., Mientus, M., Liebl, W., and Ehrenreich, A. (2013). Importance of *codB* for new *codA*- based markerless gene deletion in *Gluconobacter* strains. *Appl. Microbiol. Biotechnol.* 97, 8341-8349. doi: 10.1007/s00253-013-5164-7

La China, S., Zanichelli, G., De Vero, L., and Gullo, M. (2018). Oxidative fermentations and exopolysaccharides production by acetic acid bacteria: a mini review. *Biotechnol. Lett.* 40, 1289–1302. doi: 10.1007/s10529-018-2591-7

Landis, B. H., McLaughlin, J. K., Heeren, R., Grabner, R. W., and Wang, P. T. (2002). Bioconversion of N-Butylglucamine to 6-Deoxy-6-butylamino Sorbose by *Gluconobacter o xydans*. *Org. Process Res. Dev.* 6, 547–552. doi: 10.1021/op0255128

León, R., Prazeres, D. M. F., Molinari, F., and Cabral, J. M. S. (2009). Microbial stereoselective oxidation of 2-methyl-1,3-propanediol to (R)-β-hydroxyisobutyric acid in aqueous/organic biphasic systems. *Biocatal. Biotransform.* 20, 201–207. doi: 10.1080/10242420290020723

Levy, S. B. (1992). Dihydroxyacetone-containing sunless or self-tanning lotions. *J. Am. Acad. Dermatol.* 27, 989–993. doi: 10.1016/0190-9622(92)70300-5

Li, D. H., Lin, J. P., and Wei, D. Z. (2014).Improving *Gluconobacter oxydans* performance in the *in situ* removal of the inhibitor for asymmetric resolution of racemic 1-phenyl-1,2-ethanediol. *Bioresour. Technol.* 159, 327–333. doi: 10.1016/j.biortech.2014.02.104

Li, L., Cleenwerck, I., De Vuyst, L., and Vandamme, P. (2017). Identification of acetic acid bacteria through matrix-assisted laser desorption/ionization time-of-flight mass spectrometry and report of *Gluconobacter nephelii* Kommanee et al. 2011 and *Gluconobacter uchimurae* Tanasupawat et al. 2012 as later heterotypic synonyms of *Gluconobacter japonicus* Malimas et al. 2009 and *Gluconobacter oxydans* (Henneberg 1897) De Ley 1961 (Approved Lists 1980) emend. Gosselé et al. 1983, respectively. *Systemat. Appl. Microbiol.* 40, 123–134. doi: 10.1016/j.syapm.2017.01.003

Liu, L., Zeng, W., Du, G., Chen, J., and Zhou, J. (2019). Identification of NAD-dependent xylitol dehydrogenase from *Gluconobacter oxydans* WSH-003. *ACS Omega* 4, 15074–15080. doi: 10.1021/acsomega.9b01867

Loganathan, P., and Nair, S. (2004). *Swaminathania salitolerans* gen. nov., sp. nov., a salt-tolerant, nitrogen-fixing and phosphate-solubilizing bacterium from

wild rice (*Porteresia coarctata* Tateoka). *Int. J. Systemat. Evol. Microbiol*. 54, 1185–1190. doi: 10.1099/ijs.0.02817-0

Malimas, T., Yukphan, P., Takahashi, M., Muramatsu, Y., Kaneyasu, M., Potacharoen, W., et al. (2008). *Gluconobacter sphaericus* (Ameyama 1975) comb. nov., a brown pigment-producing acetic acid bacterium in the Alphaproteobacteria. *J. General Appl. Microbiol.* 54, 211–220. doi: 10.2323/jgam.54.211

Malimas, T., Yukphan, P., Takahashi, M., Muramatsu, Y., Kaneyasu, M., Potacharoen, W., et al. (2009). *Gluconobacter japonicus* sp. nov., an acetic acid bacterium in the Alphaproteobacteria. *Int. J. Systemat. Evol. Microbiol*. 59, 466–471. doi: 10.1099/ijs.0.65740-0

Mamlouk, D., and Gullo, M. (2013). Acetic acid bacteria: physiology and carbon sources oxidation. *Indian J. Microbiol.* 53, 377–384. doi: 10.1007/s12088-013-0414-z

Marič, L., Cleenwerck, I., Accetto, T., Vandamme, P., and Trček, J. (2020). Description of *Komagataeibacter melaceti* sp. nov. and *Komagataeibacter melomenusus* sp. nov. isolated from apple cider vinegar. *Microorganisms* 8:1178. doi: 10.3390/microorganisms8081178

Masud, U., Matsushita, K., and Theeragool, G. (2010). Cloning and functional analysis of *adhS* gene encoding quinoprotein alcohol dehydrogenase subunit III from *Acetobacter pasteurianus* SKU1108. *Int. J. Food Microbiol.* 138, 39–49. doi: 10.1016/j.ijfoodmicro.2009.12.027

Matsushita, K., Fujii, Y., Ano, Y., Toyama, H., Shinjoh, M., Tomiyama, N., et al. (2003). 5-keto-D-gluconate production is catalyzed by a quinoprotein glycerol dehydrogenase, major polyol dehydrogenase, in *Gluconobacter* species. *Appl. Environ. Microbiol.* 69, 1959–1966. doi: 10.1128/AEM.69.4.1959-1966.2003

Matsushita, K., Patel, L., and Kaback, H. R. (1984). Cytochrome o oxidase from *Escherichia coli*. Characterization of the enzyme and mechanism of electrochemical proton gradient generation. *Biochemistry* 23, 4703–4714. doi: 10.1021/bi00315a028

Matsushita, K., Toyam,a, H., and Adachi, O. (2004). *Respiratory Chains in Acetic Acid Bacteria: Membranebound Periplasmic Sugar and Alcohol Respirations. Respiration in Archaea and Bacteria*. Dordrecht: Springer, 81–99. doi: 10.1007/978-1-4020-3163-2_4

Matsushita, K., Toyama, H., and Adachi, O. (1994). Respiratory chains and bioenergetics of acetic acid bacteria. *Adv. Microbial. Physiol.* 36, 247–301. doi: 10.1016/S0065-2911(08)60181-2

Matsushita, K., Toyama, H., Tonouchi, N., and Okamoto-Kainuma, A. (2016). *Acetic Acid Bacteria—— Ecology and Physiology*. Tokyo: Springer, Japan. doi: 10.1007/978-4-431-55933-7

Matsushita, K., Toyama, H., Yamada, M., and Adachi, O. (2002). Biotechnology quinoproteins: structure, function, and biotechnological applications. *Appl. Microbiol. Biotechnol.* 58, 13–22. doi: 10.1007/s00253-001-0851-1

Matsutani, M., Fukushima, K., Kayama, C., Arimitsu, M., Hirakawa, H., Toyama, H., et al. (2014). Replacement of a terminal cytochrome c oxidase by ubiquinol oxidase during the evolution of acetic acid bacteria. *Biochim. Biophys. Acta* 1837, 1810–1820. doi: 10.1016/j.bbabio.2014.05.355

Merfort, M., Herrmann, U., Bringer-Meyer, S., and Sahm, H. (2006). High-yield 5-keto-D-gluconic acid formation is mediated by soluble and membrane-bound gluconate-5-dehydrogenases of *Gluconobacter oxydans*. *Appl. Microbiol. Biotechnol.* 73, 443–451. doi: 10.1007/s00253-006-0467-6

Mientus, M., Kostner, D., Peters, B., Liebl, W., and Ehrenreich, A. (2017). Characterization of membrane-bound dehydrogenases of *Gluconobacter oxydans* 621H using a new system for their functional expression. *Appl. Microbiol. Biotechnol.* 101, 3189–3200. doi: 10.1007/s00253-016-8069-4

Miura, H., Mogi, T., Ano, Y., Migita, C. T., Matsutani, M., Yakushi, T., et al. (2013).Cyanide-insensitive quinol oxidase (CIO) from *Gluconobacter oxydans* is a unique terminal oxidase subfamily of cytochrome bd. *J. Biochem.* 153, 535–545. doi: 10.1093/jb/mvt019

Miyazaki, T., Tomiyama, N., Shinjoh, M., and Hoshino, T. (2002). Molecular cloning and functional expression of d-sorbitol dehydrogenase from *Gluconobacter suboxydans* IFO3255, which requires pyrroloquinoline quinone and hydrophobic protein SldB for activity development in *E. coli*. *Biosci. Biotechnol. Biochem.* 66, 262–270. doi: 10.1271/bbb.66.262

Molinari, F., Aragozzini, F., Cabral, J., and Prazeres D. (1996). Continuous production and in situ extraction of isovaleraldehyde in a membrane bioreactor. *Enzyme Microb. Technol.* 20, 604–611. doi: 10.1016/S0921-0423(96)80074-8

Molinari, F., Gandolfi, R., Aragozzini, F., Leon, R., and Prazeres, D. M. (1999). Biotransformations in two-liquid-phase systems: production of phenylacetaldehyde by oxidation of 2-phenylethanol with acetic acid bacteria. *Enzyme Microb. Technol.* 25, 729–735. doi: 10.1016/S0141-0229(99)00107-6

Moonmangmee, D., Adachi, O., Toyama, H., and Matsushita, K. (2004). D-hexosaminate production by oxidative fermentation. *Appl. Microbiol Biotechnol*. 66, 253–258. doi: 10.1007/s00253-004-1707-2

Moore, J. E., McCalmont, M., Xu, J., Millar, B. C., and Heaney, N. (2002). *Asaia* sp., an unusual spoilage organism of fruit-flavored bottled water. *Appl. Environ. Microbiol.* 68, 4130–4131. doi: 10.1128/AEM.68.8.4130-4131.2002

Nanda, K., Taniguchi, M., Ujike, S., Ishihara, N., Mori, H., Ono, H., et al. (2001). Characterization of acetic acid bacteria in traditional acetic acid fermentation of rice vinegar (komesu) and unpolished rice vinegar (kurosu) produced in Japan. *Appl. Environ. Microbiol.* 67, 986–990. doi: 10.1128/AEM.67.2.986-990.2001

Nishikura-Imamura, S., Matsutani, M., Insomphun, C., Vangnai, A. S., Toyama, H., Yakushi, T., et al. (2014). Overexpression of a type II 3-dehydroquinate dehydratase enhances the biotransformation of quinate to 3-dehydroshikimate in *Gluconobacter oxydans*. *Appl. Microbiol. Biotechnol. Adv.* 98, 2955–2963. doi: 10.1007/s00253-013-5439-z

Noyori, R. (2002). Asymmetric catalysis: science and opportunities (Nobel lecture). *Angewandte Chemie Int. Ed.* 41, 2008-2022. doi: 10.1002/1521-3773(20020617)41:12<2008::AID-ANIE2008>3.0.CO;2-4

Osbourn, A. E., and Field, B. (2009). Operons. *Cell. Mol. Life Sci.* 66, 3755–3775. doi: 10.1007/s00018-009-0114-3

Pappenberger, G., and Hohmann, H. P. (2013). Industrial production of L-ascorbic acid (vitamin C) and D-isoascorbic acid. *Biotechnol. Food Feed Additiv*. 143–188. doi: 10.1007/10_2013_243

Peters, B., Junker, A., Brauer, K., Mühlthaler, B., Kostner, D., Mientus, M., et al. (2013). Deletion of pyruvate decarboxylase by a new method for efficient markerless gene deletions in *Gluconobacter oxydans*. *Appl. Microbiol. Biotechnol.* 97, 2521–2530. doi: 10.1007/s00253-012-4354-z

Prust, C., Hoffmeister, M., Liesegang, H., Wiezer, A., Fricke, W. F., Ehrenreich, A., et al. (2005). Complete genome sequence of the acetic acid bacterium *Gluconobacter oxydans*. *Nat. Biotechnol*. 23, 195–200. doi: 10.1038/nbt1062

Qazi, G., Parshad, R., Verma, V., Chopra, C., Buse, R., Träger, M., et al. (1991).Diketo-gluconate fermentation by *Gluconobacter oxydans*. *Enzyme Microb. Technol*. 13, 504–507. doi: 10.1016/0141-0229(91)90010-8

Qi, X. H., Zhu, J. F., Yun, J. H., Lin, J., Qi, Y. L., Guo, Q., et al. (2016). Enhanced xylitol production: expression of xylitol dehydrogenase from *Gluconobacter oxydans* and mixed culture of resting cell. *J. Biosci. Bioeng.* 122, 257–262. doi: 10.1016/j.jbiosc.2016.02.009

Qin, Z., Yu, S., Chen, J., and Zhou, J. (2022). Dehydrogenases of acetic acid bacteria. *Biotechnol. Adv.* 54:107863. doi: 10.1016/j.biotechadv.2021.107863

Raspor, P., and Goranovič, D. (2008). Biotechnological applications of acetic acid bacteria. *Crit. Rev. Biotechnol.* 28, 101–124. doi: 10.1080/07388550802046749

Richhardt, J., Luchterhand, B., Bringer, S., Büchs, J., and Bott, M. (2013). Evidence for a key role of cytochrome bo 3 oxidase in respiratory energy metabolism of *Gluconobacter oxydans*. *J. Bacteriol*. 195, 4210–4220. doi: 10.1128/JB.00470-13

Richtmyer, N. K., Stewart, L. C., and Hudson, C. (1950). L-fuco-4-ketose, a new sugar produced by the action of *Acetobacter suboxydans* on L-Fucitol1. *J. Am. Chem. Soc.* 72, 4934–4937. doi: 10.1021/ja01167a025

Romano, A., Gandolfi, R., Nitti, P., Rollini, M., and Molinari, F. (2002). Acetic acid bacteria as enantioselective biocatalysts. *J. Mol. Catalysis B* 17, 235–240. doi: 10.1016/S1381-1177(02)00013-9

Saichana, N., Matsushita, K., Adachi, O., Frébort, I., and Frebortova, J. (2015). Acetic acid bacteria: a group of bacteria with versatile biotechnological applications. *Biotechnol. Adv.* 33, 1260–1271. doi: 10.1016/j.biotechadv.2014.12.001

Sato, J., Wakayama, M., and Takagi, K. (2015). Lactate dehydrogenase involved in lactate metabolism of *Acetobacter Pasteurianus*. *Proc. Environ. Sci.* 28, 67–71. doi: 10.1016/j.proenv.2015.07.010

Sato, K., Yamada, Y., Aida, K., and Uemura, T. (1967). On the formation of 5-keto-d-fructose and three γ-pyrone compounds from d-sorbitol by *Acetobacter suboxydans*. *Agri. Biol. Chem*. 31, 877–879. doi: 10.1080/00021369.1967.10858894

Sayed, M., Pyo, S.-H., Rehnberg, N., and Hatti-Kaul, R. (2019). Selective oxidation of 5-hydroxymethylfurfural to 5-hydroxymethyl-2-furancarboxylic

acid using *Gluconobacter oxydans*. *ACS Sustain. Chem. Eng.* 7, 4406–4413. doi: 10.1021/acssuschemeng.8b06327

Sengun, I. Y. (2017). *Acetic Acid Bacteria: Fundamentals and Food Applications*. Oxfordshire: Taylor & Francis Group. doi: 10.1201/9781315153490

Shi, L., Li, K., Zhang, H., Liu, X., Lin, J., and Wei, D. (2014). Identification of a novel promoter gHp0169 for gene expression in *Gluconobacter oxydans*. *J. Biotechnol.* 175, 69–74. doi: 10.1016/j.jbiotec.2014.01.035

Shinagawa, E., Ano, Y., Yakushi, T., Adachi, O., and Matsushita, K. (2009). Solubilization, purification, and properties of membrane-bound D-gluconodelta-lactone hydrolase from *Gluconobacter oxydans*. *Biosci. Biotechnol. Biochem.* 73, 241–244. doi: 10.1271/bbb.80554

Shinagawa, E., Matsushita, K., Adachi, O., and Ameyama, M. (1982). Purification and characterization of D-sorbitol dehydrogenase from membrane of *Gluconobacter suboxydans* var. *Agri. Biol. Chem.* 46, 135–141. doi: 10.1271/bbb1961.46.135

Shinagawa, E., Matsushita, K., Adachi, O., and Ameyama, M. (1984). D-Gluconate dehydrogenase, 2-keto-D-gluconate yielding, from *Gluconobacter dioxyacetonicus*: purification and characterization. *Agri. Biol. Chem.* 48, 1517–1522. doi: 10.1271/bbb1961.48.1517

Shinagawa, E., Matsushita, K., Toyama, H., and Adachi, O. (1999). Production of 5-keto-D-gluconate by acetic acid bacteria is catalyzed by pyrroloquinoline quinone (PQQ)-dependent membrane-bound D-gluconate dehydrogenase. *J. Mol. Catal. B. Enzym.* 6, 341–350.

Shinagawa, E., Toyama, H., Matsushita, K., Tuitemwong, P., Theeragool, G., and Adachi, O. (2006). A novel type of formaldehyde-oxidizing enzyme from the membrane of *Acetobacter* sp. SKU 14. *Biosci. Biotechnol. Biochem.* 70, 850–857. doi: 10.1271/bbb.70.850

Shinjoh, M., and Hoshino, T. (1995). Development of a stable shuttle vector and a conjugative transfer system for *Gluconobacter oxydans*. *J. Ferment. Bioeng.* 79, 95–99. doi: 10.1016/0922-338X(95)94074-2

Shinjoh, M., Tomiyama, N., Miyazaki, T., and Hoshino, T. (2002). Main polyol dehydrogenase of *Gluconobacter suboxydans* IFO 3255, membrane-bound D-sorbitol dehydrogenase, that needs product of upstream gene, sldB, for activity. *Biosci., Biotechnol. Biochem.* 66, 2314–2322. doi: 10.1271/bbb.66.2314

Su, W., Chang, Z., Gao, K., and Wei, D. (2004). Enantioselective oxidation of racemic 1,2-propanediol to D-(−)-lactic acid by *Gluconobacter oxydans*. *Tetrahedron* 15, 1275–1277. doi: 10.1016/j.tetasy.2004.03.009

Sugisawa, T., and Hoshino, T. (2002). Purification and properties of membrane-bound D-sorbitol dehydrogenase from *Gluconobacter suboxydans* IFO 3255. *Biosci. Biotechnol. Biochem.* 66, 57–64. doi: 10.1271/bbb.66.57

Sugisawa, T., Hoshino, T., Nomura, S., and Fujiwara, A. (1991). Isolation and characterization of membrane-bound L-sorbose dehydrogenase from *Gluconobacter melanogenus* UV10. *Agri. Biol. Chem.* 55, 363–370. doi: 10.1271/bbb1961.55.363

Sugisawa, T., Miyazaki, T., and Hoshino, T. (2005). Microbial production of L-ascorbic acid from D-sorbitol, L-sorbose, L-gulose, and L-sorbosone by *Ketogulonicigenium vulgare* DSM 4025. *Biosci. Biotechnol. Biochem.* 69, 659–662. doi: 10.1271/bbb.69.659

Suzuki, S., Sugiyama, M., Mihara, Y., Hashiguchi, K., and Yokozeki, K. (2002). Novel enzymatic method for the production of xylitol from D-arabitol by *Gluconobacter oxydans*. *Biosci. Biotechnol. Biochem.* 66, 2614–2620. doi: 10.1271/bbb.66.2614

Švitel, J., and Kutnik, P. (1995). Potential of acetic acid bacteria for oxidation of low-molecular monoalcohols. *Lett. Appl. Microbiol.* 20, 365–368. doi: 10.1111/j.1472-765X.1995.tb01322.x

Švitel, J., and Šturdik, E. (1994). D-Galactose transformation to D-Galactonic acid by *Gluconobacter oxydans*. *J. Biotechnol.* 37, 85–88. doi: 10.1016/0168-1656(94)90206-2

Švitel, J., and Šturdík, E. (1995). n-Propanol conversion to propionic acid by *Gluconobacter oxydans*. *Enzyme Microb. Technol.* 17, 546–550. doi: 10.1016/0141-0229(94)00088-9

Swings, J., Gillis, M., Kersters, K., De Vos, P., Gosselé, F., and De Ley, J. (1980). *Frateuria*, a new genus for "*Acetobacter aurantius*". *Int. J. Systemat. Evol. Microbiol.* 30, 547–556. doi: 10.1099/00207713-30-3-547

Takahashi, T., and Asai, T. (1932). On the formation of fructose and kojic acid by acetic acid bacteria. *Proc. Imperial Acad.* 8, 364–366. doi: 10.2183/pjab1912.8.364

Takahashi, T., and Kayamori, H. (1960). Studies on the formation of glucosamine acid by *Acetobacter melanogenum* Beijerinck and *Pseudomonas fluorescens liquefaciens*. *J. Agri. Chem. Soc. Jap.* 24, 231–234. doi: 10.1080/03758397.1960.10857663

Takeshita, K., Shimonishi, T., and Izumori, K. (1996). Production of L-psicose from allitol by *Gluconobacter frateurii* IFO 3254. *J. Ferment. Bioeng.* 81, 212–215. doi: 10.1016/0922-338X(96)82210-0

Tanasupawat, S., Thawai, C., Yukphan, P., Moonmangmee, D., Itoh, T., Adachi, O., et al. (2004). *Gluconobacter thailandicus* sp. nov., an acetic acid bacterium in the α-Proteobacteria. *J. General Appl. Microbiol.* 50, 159–167. doi: 10.2323/jgam.50.159

Tayama, K., Fukaya, M., Okumura, H., Kawamura, Y., and Beppu, T. (1989). Purification and characterization of membrane-bound alcohol dehydrogenase from *Acetobacter polyoxogenes* sp. nov. *Appl. Microbiol. Biotechnol. Adv.* 32, 181–185. doi: 10.1007/BF00165885

Thurner, C., Vela, C., Thöny-Meyer, L., Meile, L., and Teuber, M. (1997). Biochemical and genetic characterization of the acetaldehyde dehydrogenase complex from *Acetobacter europaeus*. *Archiv. Microbiol.* 168, 81–91. doi: 10.1007/s002030050473

Toyama, H., Furuya, N., Saichana, I., Ano, Y., Adachi, O., and Matsushita, K. (2007). Membrane-bound, 2-Keto-D-Gluconate-yielding D-gluconate dehydrogenase from *Gluconobacter dioxyacetonicus* IFO 3271: molecular properties and gene disruption. *Appl. Environ. Microbiol.* 73, 6551–6556. doi: 10.1128/AEM.00493-07

Toyama, H., Soemphol, W., Moonmangmee, D., Adachi, O., and Matsushita, K. (2005). Molecular properties of membrane-bound FAD-containing D-sorbitol dehydrogenase from thermotolerant *Gluconobacter frateurii* isolated from Thailand. *Biosci. Biotechnol. Biochem.* 69, 1120–1129. doi: 10.1271/bbb.69.1120

Trček, J., and Barja, F. (2015). Updates on quick identification of acetic acid bacteria with a focus on the 16S−23S rRNA gene internal transcribed spacer and the analysis of cell proteins by MALDI-TOF mass spectrometry. *Int. J. Food Microbiol.* 196, 137–144. doi: 10.1016/j.ijfoodmicro.2014.12.003

Trcek, J., Toyama, H., Czuba, J., Misiewicz, A., and Matsushita, K. (2006). Correlation between acetic acid resistance and characteristics of PQQ-dependent ADH in acetic acid bacteria. *Appl. Microbiol. Biotechnol. Adv.* 70, 366–373. doi: 10.1007/s00253-005-0073-z

Urakami, T., Tamaoka, J., Suzuki, K. I., and Komagata, K. (1989). *Acidomonas* gen. nov., incorporating *Acetobacter methanolicus* as *Acidomonas methanolica* comb. nov. *Int. J. Systemat. Evol. Microbiol.* 39, 50–55. doi: 10.1099/00207713-39-1-50

Urbance, J., Bratina, B., Stoddard, S., and Schmidt, T. (2001). Taxonomic characterization of *Ketogulonigenium vulgare* gen. nov., sp. nov. and *Ketogulonigenium robustum* sp. nov., which oxidize L-sorbose to 2-keto-L-gulonic acid. *Int. J. Systemat. Evol. Microbiol.* 51, 1059–1070. doi: 10.1099/00207713-51-3-1059

Vangnai, A., Promden, W., De-Eknamkul, W., Matsushita, K., and Toyama, H. (2010). Molecular characterization and heterologous expression of quinate dehydrogenase gene from *Gluconobacter oxydans* IFO3244. *Biochemistry* 75, 452–459. doi: 10.1134/S0006297910040085

Wang, B., and Chen, F. (2014). Taxonomy progress of acetic acid bacteria. *China Brewing* 33, 1–10. doi: 10.11882/j.issn.0254-5071.2014.12.001

Wang, P., Xia, Y., Li, J., Kang, Z., Zhou, J., and Chen, J. (2016). Overexpression of pyrroloquinoline quinone biosynthetic genes affects L-sorbose production in *Gluconobacter oxydans* WSH-003. *Biochem. Eng. J.*112, 70–77. doi: 10.1016/j.bej.2016.04.011

Wang, X., Lv, M., Zhang, L., Li, K., Gao, C., Ma, C., et al. (2013). Efficient bioconversion of 2, 3-butanediol into acetoin using *Gluconobacter oxydans* DSM 2003. *Biotechnol. Biofuels* 6, 1–9. doi: 10.1186/1754-6834-6-155

Wei, G., Yang, X., Zhou, W., Lin, J., and Wei, D. (2009). Adsorptive bioconversion of ethylene glycol to glycolic acid by *Gluconobacter oxydans* DSM 2003. *Biochem. Eng. J.* 47, 127–131. doi: 10.1016/j.bej.2009.07.016

Wei, P., Liang, J., Cheng, J., Zong, M. H., and Lou, W. Y. (2016). Markedly improving asymmetric oxidation of 1-(4-methoxyphenyl) ethanol with *Acetobacter* sp. CCTCC M209061 cells by adding deep eutectic solvent in a two-phase system. *Microb. Cell Fact.* 15:5. doi: 10.1186/s12934-015-0407-1

Whiting, G., and Coggins, R. J. (1967). The oxidation of D-quinate and related acids by *Acetomonas oxydans*. *Biochem. J.* 102, 283–293. doi: 10.1042/bj1020283

Xu, S., Wang, X., Du, G., Zhou, J., and Chen, J. (2014). Enhanced production of L-sorbose from D-sorbitol by improving the mRNA abundance of sorbitol dehydrogenase in *Gluconobacter oxydans* WSH-003. *Microb. Cell Factor*. 13, 1–7. doi: 10.1186/s12934-014-0146-8

Xu, Y., Chi, P., Lv, J., Bilal, M., and Cheng, H. (2021). L-xylo-3-hexulose, a new rare sugar produced by the action of acetic acid bacteria on galactitol, an exception to Bertrand Hudson's rule. *Biochim. Biophys. Acta Gen Subj.* 1865:129740. doi: 10.1016/j.bbagen.2020.129740

Yakushi, T., and Matsushita, K. (2010). Alcohol dehydrogenase of acetic acid bacteria: structure, mode of action, and applications in biotechnology. *Appl. Microbiol. Biotechnol*. 86, 1257–1265. doi: 10.1007/s00253-010-2529-z

Yakushi, T., Takahashi, R., Matsutani, M., Kataoka, N., Hours, R. A., Ano, Y., et al. (2020). The membrane-bound sorbosone dehydrogenase of *Gluconacetobacter liquefaciens* is a pyrroloquinoline quinone-dependent enzyme. *Enzyme Microb. Technol.* 137:109511. doi: 10.1016/j.enzmictec.2020.109511

Yamada, Y. (2000). Transfer of *Acetobacter oboediens* Sokollek et al 1998 and *Acetobacter intermedius* Boesch et al. 1998 to the genus *Gluconacetobacter* as *Gluconacetobacter oboediens* comb. nov. and *Gluconacetobacter intermedius* comb. nov. *Int. J. Systemat. Evol. Microbiol.* 50, 2225–2227. doi: 10.1099/00207713-50-6-2225

Yamada, Y. (2014). Transfer of *Gluconacetobacter kakiaceti*, *Gluconacetobacter medellinensis* and *Gluconacetobacter maltaceti* to the genus Komagataeibacter as *Komagataeibacter kakiaceti* comb. nov., *Komagataeibacter medellinensis* comb. nov. and *Komagataeibacter maltaceti* comb. nov. *Int. J. Systemat. Evol. Microbiol.* 64, 1670–1672. doi: 10.1099/ijs.0.054494-0

Yamada, Y. (2016). "Systematics of acetic acid bacteria," in *Acetic Acid Bacteria: Ecology and Physiology*, eds. K. Matsushita, H. Toyama, N. Tonouchi and A. Okamoto-Kainuma (Tokyo: Springer Japan), 1–50. doi: 10.1007/978-4-431-55933-7_1

Yamada, Y., Hoshino, K. I., and Ishikawa, T. (1997). The phylogeny of acetic acid bacteria based on the partial sequences of 16S ribosomal RNA: the elevation of the subgenus *Gluconoacetobacter* to the generic level. *Biosci. Biotechnol. Biochem*. 61, 1244–1251. doi: 10.1271/bbb.61.1244

Yamada, Y., and Kondo, K. (1984). *Gluconoacetobacter*, a new subgenus comprising the acetate-oxidizing acetic acid bacteria with ubiquinone-10 in the genus *Acetobacter*. *J. General Appl. Microbiol*. 30, 297–303. doi: 10.2323/jgam.30.297

Yamada, Y., and Yukphan, P. (2008). Genera and species in acetic acid bacteria. *Int. J. Food Microbiol*. 125, 15–24. doi: 10.1016/j.ijfoodmicro.2007.11.077

Yamada, Y., Yukphan, P., Vu, H. T. L., Muramatsu, Y., Ochaikul, D., and Nakagawa, Y. (2012b). Subdivision of the genus Gluconacetobacter Yamada, Hoshino and Ishikawa 1998: the proposal of *Komagatabacter* gen. nov., for strains accommodated to the *Gluconacetobacter xylinus* group in the α-Proteobacteria. *Ann. Microbiol*. 62, 849–859. doi: 10.1007/s13213-011-0288-4

Yamada, Y., Yukphan, P., Vu, H. T. L., Muramatsu, Y., Ochaikul, D., Tanasupawat, S., et al. (2012a). Description of *Komagataeibacter* gen. *nov., with proposals of new combinations (Acetobacteraceae). The Journal of general and applied microbiology*. 58, 397–404. doi: 10.2323/jgam.58.397

Yang, H., Chen, T., Wang, M., Zhou, J., Liebl, W., Barja, F., et al. (2022). Molecular biology: fantastic toolkits to improve knowledge and application of acetic acid bacteria. *Biotechnol. Adv*. 2022:107911. doi: 10.1016/j.biotechadv.2022.107911

Zhang, X. Y., and Chen, F. S. (2022). *Acetic Acid Bacteria and Their Application*. Beijing: Chemical Industry Press.

Zhou, X., Zhou, X., Xu, Y., and Chen, R. R. (2017). *Gluconobacter oxydans* (ATCC 621H) catalyzed oxidation of furfural for detoxification of furfural and bioproduction of furoic acid. *J. Chem. Technol. Biotechnol*. 92, 1285–1289. doi: 10.1002/jctb.5122

Zhou, X., Zhou, X., Zhang, H., Cao, R., and Xu, Y. (2018). Improving the performance of cell biocatalysis and the productivity of acetoin from 2, 3-butanediol using a compressed oxygen supply. *Process Biochem*. 64, 46–50. doi: 10.1016/j.procbio.2017.09.027

Zhu, J., Xie, J., Wei, L., Lin, J., Zhao, L., and Wei, D. (2018). Identification of the enzymes responsible for 3-hydroxypropionic acid formation and their use in improving 3-hydroxypropionic acid production in *Gluconobacter oxydans* DSM. *Bioresour. Technol*. 265, 328–333. doi: 10.1016/j.biortech.2018.06.001

Conflict of Interest: The authors declare that the research was conducted in the absence of any commercial or financial relationships that could be construed as a potential conflict of interest.

Publisher's Note: All claims expressed in this article are solely those of the authors and do not necessarily represent those of their affiliated organizations, or those of the publisher, the editors and the reviewers. Any product that may be evaluated in this article, or claim that may be made by its manufacturer, is not guaranteed or endorsed by the publisher.

frontiers | Frontiers in Microbiology

ORIGINAL RESEARCH
published: 21 June 2022
doi: 10.3389/fmicb.2022.935062

5-Keto-D-Fructose, a Natural Diketone and Potential Sugar Substitute, Significantly Reduces the Viability of Prokaryotic and Eukaryotic Cells

*Marcel Hövels[1], Nicole Gallala[1], Samara Lisa Keriakes[1], Anna Paulina König[1], Jacqueline Schiessl[1], Tobias Laporte[1], Konrad Kosciow[2] and Uwe Deppenmeier[1]**

[1] Institute for Microbiology and Biotechnology, University of Bonn, Bonn, Germany, [2] German Aerospace Center (DLR), Institute for the Protection of Terrestrial Infrastructures, Sankt Augustin, Germany

OPEN ACCESS

Edited by:
Maria Gullo,
University of Modena and Reggio Emilia, Italy

Reviewed by:
Salvatore La China,
University of Modena and Reggio Emilia, Italy
Armin Ehrenreich,
Technical University of Munich, Germany

***Correspondence:**
Uwe Deppenmeier
udeppen@uni-bonn.de

Specialty section:
This article was submitted to Food Microbiology, a section of the journal Frontiers in Microbiology

Received: 03 May 2022
Accepted: 30 May 2022
Published: 21 June 2022

Citation:
Hövels M, Gallala N, Keriakes SL, König AP, Schiessl J, Laporte T, Kosciow K and Deppenmeier U (2022) 5-Keto-D-Fructose, a Natural Diketone and Potential Sugar Substitute, Significantly Reduces the Viability of Prokaryotic and Eukaryotic Cells. Front. Microbiol. 13:935062. doi: 10.3389/fmicb.2022.935062

5-Keto-D-fructose (5-KF) is a natural diketone occurring in micromolar concentrations in honey, white wine, and vinegar. The oxidation of D-fructose to 5-KF is catalyzed by the membrane-bound fructose dehydrogenase complex found in several acetic acid bacteria. Since 5-KF has a sweetening power comparable to fructose and is presumably calorie-free, there is great interest in making the diketone commercially available as a new sugar substitute. Based on a genetically modified variant of the acetic acid bacterium *Gluconobacter oxydans* 621H, an efficient process for the microbial production of 5-KF was recently developed. However, data on the toxicology of the compound are completely lacking to date. Therefore, this study aimed to investigate the effect of 5-KF on the viability of prokaryotic and eukaryotic cells. It was found that the compound significantly inhibited the growth of the gram-positive and gram-negative model organisms *Bacillus subtilis* and *Escherichia coli* in a concentration-dependent manner. Furthermore, cell viability assays confirmed severe cytotoxicity of 5-KF toward the colon cancer cell line HT-29. Since these effects already occurred at concentrations of 5 mM, the use of 5-KF in the food sector should be avoided. The studies performed revealed that in the presence of amines, 5-KF promoted a strong Maillard reaction. The inherent reactivity of 5-KF as well as the Maillard products formed could be the trigger for the observed inhibition of prokaryotic and eukaryotic cells.

Keywords: 5-keto-D-fructose, toxicology, Maillard reaction, sugar substitutes, HT-29 cell line

INTRODUCTION

A growing body of epidemiological evidence supports the claim that excessive sugar consumption elevates the abundance of first-world diseases, such as insulin resistance, type 2 diabetes mellitus, obesity, metabolic syndrome, hypertension, and cardiovascular diseases (Johnson et al., 2007; Dekker et al., 2010; Hu and Malik, 2010; Malik et al., 2010; Tappy and Lê, 2010; Aragno and Mastrocola, 2017). This causality and the growing awareness among consumers about the adverse effects of excessive sugar consumption are leading to an increasing demand for suitable

sugar substitutes. Over the past decades, numerous sugar alcohols and synthetic sweeteners have been approved as sugar substitutes. Due to their reduced or non-existent caloric value, these substances are counteracting the spread of sugar-associated first-world diseases (Kroger et al., 2006; Chattopadhyay et al., 2014). However, many of the available sugar substitutes are characterized by unpleasant off-tastes (Schiffman et al., 1995) and have been shown to induce laxative effects, flatulence (Grembecka, 2015), or undesirable modulation of the gut microbiota (Suez et al., 2014). Unpleasant off-tastes are more prevalent among synthetic sweeteners such as saccharin or cyclamate, which taste bitter or metallic, for example (Chattopadhyay et al., 2014). Laxative effects and flatulence, on the other hand, are more likely caused by sugar alcohols due to their higher intake rates and water-pulling properties (Mäkinen, 2016).

The search for substances that provide a pleasant and sufficient sweetening power without triggering the mentioned side effects led to the discovery of 5-keto-D-fructose (5-KF, 5-ketofructose, 5-oxofructose, 5-dehydro-D-fructose, threo-2,5-hexodiulose), a natural diketone found in honey, white wine, and vinegar in low concentrations (Burroughs and Sparks, 1973; Schiessl et al., 2021). This potential sugar substitute can be produced by enzymatic oxidation of D-fructose, a reaction catalyzed by the membrane-bound fructose dehydrogenase complex (FDH_{SCL}) found in a variety of acetic acid bacteria (Mowshowitz et al., 1974; Ameyama et al., 1981; Kawai et al., 2013). After Terada et al. (1960) already reported a sweet taste of 5-KF in the 1960s, the compound was recently evaluated in a dedicated sensory study (Herweg et al., 2018). A trained tasting panel could not distinguish between iso-sweet solutions of D-fructose (60 mM) and 5-KF (70 mM), indicating that 5-KF is almost as sweet as D-fructose. In addition, the sensory evaluation revealed overall high taste quality and total absence of off-tastes for 5-KF (Herweg et al., 2018). Due to these promising features, great efforts have been made to develop a biotechnological production process for 5-KF based on suitable acetic acid bacteria. In this context, heterologous production of the FDH_{SCL} encoded in the genome of the strictly aerobic alphaproteobacterium *Gluconobacter* (*G.*) *japonicus* NBRC3260 in the closely related strain *G. oxydans* 621H proved to be most efficient. Fed-batch fermentation of the FDH_{SCL} overproducing strain *G. oxydans fdh* resulted in a 5-KF concentration of 489 g L^{-1} at a conversion efficiency of 98% (Herweg et al., 2018; Siemen et al., 2018). These results could pave the way for large-scale production and commercial distribution of the 5-KF (Herweg et al., 2020). However, dedicated analyses of the compound's uptake, distribution, metabolism, excretion, and corresponding toxicological studies are required prior to the application of 5-KF as a novel food compound. Although data are relatively sparse in this regard, 5-KF has been shown to be a suitable substrate for both rat and bovine liver fructokinase, leading to the formation of 5-keto-D-fructose-1-phosphate (Englard et al., 1972). This monophosphate was found to be a potent competitive inhibitor of the D-fructose-1-phosphate cleavage catalyzed by liver aldolase (Englard et al., 1972). Concerning microbial degradation, it was demonstrated that 5-KF could not be degraded by 15 members of the most common and abundant intestinal microorganisms (Schiessl et al., 2021). Thus, the sugar derivative seems to be an unsuitable growth substrate for prokaryotes in the human intestine. Besides, environmental bacteria such as *Tatumella morbirosei*, *Clostridium pasteurianum,* and *Gluconobacter* sp. were identified as capable of 5-KF consumption. Environmental accumulation, a phenomenon that has been reported recently for multiple synthetic sweeteners (Sang et al., 2014), is therefore unlikely in the case of 5-KF.

To further elucidate the effect of 5-KF on prokaryotic and eukaryotic cells, the compound was produced in larger quantities in this work, purified, and used for growth experiments and toxicological studies. The obtained results indicate that diketone significantly reduces the viability of gram-negative and gram-positive bacteria as well as HT-29 cells at concentrations $\geq$ 5 mM. The use of 5-KF in the food sector should therefore be reconsidered.

MATERIALS AND METHODS

Chemicals

Chemicals and reagents were purchased from Sigma-Aldrich (St. Louis, US), Carl Roth GmbH & Co., KG (Karlsruhe, Germany), PAN-Biotech GmbH (Aidenbach, Germany), and Promega GmbH (Walldorf, Germany).

Cultivation of Prokaryotic and Eukaryotic Cells

Shake Flask Cultivation of Microbial Strains

G. oxydans strains (**Table 1**) were cultured aerobically in shake flasks at 30°C, and 180 rpm in YMF-medium (6 g L^{-1} yeast extract, 0.6 g L^{-1} D-mannitol, and 0.06 g L^{-1} D-fructose) supplemented with 50 μg mL^{-1} cefoxitin. Cultures of the plasmid-bearing strain *G. oxydans fdh* were additionally supplemented with 50 μg mL^{-1} kanamycin.

Precultures of *Escherichia* (*E.*) *coli* DSM 498 were cultivated aerobically in shake flasks at 37°C and 180 rpm in modified Wilms-MOPS-medium (Wilms et al., 2001). The mineral medium consisted of 6.98 g L^{-1} $(NH_4)_2SO_4$, 3 g L^{-1} K_2HPO_4, 2 g L^{-1} Na_2SO_4, 41.85 g L^{-1} 3-(*N*-Morpholino)-propane sulfonic acid (MOPS), 0.5 g L^{-1} $MgSO_4 \times 7\ H_2O$, 0.01 g L^{-1} thiamine hydrochloride, 1 mL L^{-1} trace element solution (0.54 g L^{-1} $ZnSO_4 \times 7\ H_2O$, 0.48 g L^{-1} $CuSO_4 \times 5\ H_2O$, 0.3 g L^{-1} $MnSO_4 \times H_2O$, 0.54 g L^{-1} $CoCl_2 \times 6\ H_2O$, 41.76 g L^{-1} $FeCl_3 \times 6\ H_2O$, 1.98 g L^{-1} $CaCl_2 \times 2\ H_2O$, 33.4 g L^{-1} $Na_2EDTA \times 2\ H_2O$). Glucose was added as the carbon source at a final concentration of 20 g L^{-1}. The pH was adjusted to 7.5 using 1 M NaOH.

Precultures of *Bacillus* (*B.*) *subtilis* DSM 10 were cultivated aerobically in shake flasks at 30°C and 180 rpm in Spore minimal medium (Demain, 1958). To prepare the medium, 100 mL of a salt solution consisting of 30 g L^{-1} K_2HPO_4, 10 g L^{-1} KH_2PO_4, 5 g L^{-1} NH_4Cl, 1 g L^{-1} NH_4NO_3, 1 g L^{-1} Na_2SO_4, 0.1 g L^{-1} $MgSO_4 \times 7\ H_2O$, 0.01 g L^{-1} $MnSO_4 \times 4\ H_2O$, 0.01 g L^{-1} $FeSO_4 \times 7\ H_2O$, and 0.005 g L^{-1} $CaCl_2$ were added to 900 mL of a

solution containing 11.1 g L^{-1} glucose, 1 g L^{-1} L-alanine, 1.63 g L^{-1} L-glutamic acid, and 1.47 g L^{-1} L-asparagine. The pH of both solutions was adjusted to 6.9 with 1 M NaOH and 1 M HCl before autoclaving separately.

Plate-Reader Cultivation of Microbial Strains

The effect of 5-KF on the growth behavior of *E. coli* DSM 498 and *B. subtilis* DSM 10 was investigated by plate-reader assisted microplate cultivation. Cultures were grown in covered 48-well plates (Greiner CELLSTAR® multi-well plates for suspension culture) using a Tecan Infinite M200 plate reader (Tecan Group AG, Männedorf, Switzerland). Strains were cultivated in a 700-μL scale using Wilms-MOPS-medium or Spore minimal medium supplemented with varying concentrations of 5-KF (1 mM, 10 mM, and 20 mM). A 5-KF solution was produced for this purpose using resting cells of *G. oxydans fdh* (section "Production and Purification of 5-Keto-D-Fructose"). The required volume of 5-KF stock solution (158.8 mM) was added to 542.5 μL of the corresponding medium and filled up to 700 μL with H_2O_{demin}.

Plate reader cultivation was performed at 30°C in the case of *B. subtilis* DSM 10 and 37°C in the case of *E. coli* DSM 498. In cycles of 20 min, the plates were shaken linearly for 5 min with a shaking amplitude of 3 mm before detecting the optical density at 600 nm. To compensate for the backscatter effect of the OD_{600} measurement in undiluted cultures during plate reader cultivation, OD calibrations were performed for both strains. For this purpose, the OD_{600} values of several culture dilutions were measured in the plate reader setup and at appropriate dilutions ($OD_{600} < 0.3$) in a benchtop photometer. The OD_{600} values of the photometer were then plotted against the values of the plate reader, and the calibration equations were determined *via* quadratic regression through the zero point.

Due to a strong Maillard reaction observed in the cultures of *E. coli* DSM 498, the plate reader setup could not assess OD_{600} values. To circumvent this problem, cultures were centrifuged (8,000 × *g*, 20°C, 1 min) at the end of the incubation and washed twice in buffer W (100 mM Tris-HCl, 150 mM NaCl, 1 mM EDTA, pH 8). Since the washing volume was equal to the culture volume, the optical density could subsequently be measured at 600 nm.

Production and Purification of 5-Keto-D-Fructose

To produce 5-KF from D-fructose, a cryopreserved stock of *G. oxydans fdh* was streaked on YMF-plates (section "Shake Flask Cultivation of Microbial Strains") containing 1.5% [w/v] Agar-Agar, Kobe I, and the antibiotics cefoxitin and kanamycin at final concentrations of 50 μg mL^{-1}. To evaluate the impact of potential cellular contamination during 5-KF production on subsequent toxicological studies, a reference fructose solution was prepared using *G. oxydans* 621H Δ*hsdR*, which cannot oxidize D-fructose in the form of dormant cells. Thus, apart from potential contaminations with cellular components, a D-fructose solution emerges unchanged from whole-cell catalysis with resting cells of *G. oxydans* 621H Δ*hsdR*. After 48 h of incubation at 30°C, single colonies of each strain were used to inoculate 50 mL of YMF-precultures supplemented with the required antibiotics (see section "Shake Flask Cultivation of Microbial Strains"). Precultures were maintained in shake flasks at 30°C and 200 rpm for 48 h for the subsequent inoculation of the main cultures. Therefore, 250 mL of YMF medium were inoculated with 12.5 mL of preculture and incubated for 24 h at 30°C and 200 rpm. The cultivation was carried out in 2-L shake flasks to ensure sufficient oxygen supply. After cultures were harvested by centrifugation (8,000 × *g*, 10°C, 15 min), cell pellets were resuspended in 10 mL of 50 mM D-fructose solution and again centrifuged, applying the same conditions. This washing procedure was repeated two more times before the cells were finally resuspended in 5 ml of 50 mM D-fructose solution. Bioconversion of D-fructose to 5-KF was carried out at a 250-mL scale in 2-L shake flasks, using a 200 mM D-fructose solution adjusted to pH 6 by adding 5 mM of MES-buffer (pH 6). The washed cells of *G. oxydans* 621H Δ*hsdR* and *G. oxydans fdh* were added to separate flasks and incubated for 18 h at 30°C and 200 rpm. After cell removal by centrifugation (10,000 × g, 20°C, 20 min), the supernatants were treated with activated charcoal (Cabot Norit GAC 1240 Plus; Cabot Corporation, US, Boston). Therefore, 26 mg of activated charcoal were added

TABLE 1 | Overview of utilized strains and cell lines.

Strain/cell line	Genotype/description	Origin
G. oxydans 621H Δ*hsdR*	Δ*hsdR* (Δ*gox2567*) derivative of *G. oxydans* 621H (DSM 2343); Cef^R	S. Bringer-Meyer, Forschungszentrum Jülich, Germany
G. oxydans 621H Δ*hsdR* pBBR1-p264-fdhSLC-ST[a] (referred to as *G. oxydans fdh*)	*G. oxydans* 621H Δ*hsdR* expressing the fdh_{SCL}-operon (GenBank accession: AB728565.1) from *G. japonicus* NBRC3260 under control of the constitutive p264 promotor; Cef^R, Kan^R	Siemen et al., 2018
E. coli DSM 498	Type strain	DSMZ, Braunschweig, Germany,
B. subtilis DSM 10	Type strain	DSMZ, Braunschweig, Germany,
HT-29 ATCC HTB-38	Colon cell line with epithelial morphology	ATCC, Manassas, US

[a]*Naming of this strain is inconsistent within the literature. The existing synonyms G. oxydans 621H ΔhsdR pBBR1-p264-fdhSLC-ST (Siemen et al., 2018), G. oxydans 621H ΔhsdR pBBR1p264-FDH-Strep (Herweg et al., 2018), G. oxydans fdh (Hoffmann et al., 2020), and G. oxydans 621H pBBR1p264-fdhSCL-ST (Battling et al., 2020) are all describing the same strain.*

per mL supernatant and incubated under stirring for 1 h at 22°C. Subsequently, the suspension was subjected to a final centrifugation step (10,000 × *g*, 20°C, 10 min). The generated supernatants were first filtered through CHROMAFIL® RC-45/25 syringe filters (0.45 μm pore size) and sterilized by subsequent filtration using sterile PVDF syringe filters (0.22 μm pore size). Filtrates were stored at 8°C in sterile falcon tubes.

Chromatographic Analysis of 5-Keto-D-Fructose and D-Fructose Solutions Produced by Resting Cells of *Gluconobacter oxydans* 621H Strains

For qualitative and quantitative analysis of the prepared 5-KF and D-fructose solution, a Knauer Smartline HPLC-system (Knauer GmbH, Berlin, Germany) was used. The system was composed of a degasser (Knauer Smartline manager 5000), a pump (Knauer Smartline pump 1000), an autosampler (Knauer Smartline autosampler 3800), a column oven (Knauer Column-Thermostat Jetstream 2 Plus), an RI detector (AZURA RID 2.1L), and an ultraviolet (UV) detector (Knauer Smartline UV detector 2600), which measured the absorbance at a wavelength of 210 nm. Sample separation was achieved using the Eurokat H column (300 × 8 mm; Knauer GmbH) and a precolumn (30 × 8 mm; Knauer GmbH) heated to 65°C. The mobile phase, 5 mM H_2SO_4, was applied at a flow rate of 0.6 mL min^{-1}. The injection volume was set to 20 μL. Data evaluation and control of the HPLC system were accomplished using ClarityChrom® 8.2.3 (Knauer GmbH). Peak assignment and quantification were performed by applying external standards of D-fructose and 5-KF in concentrations of 0.5, 1, and 2 mM.

Ultraviolet-Vis Spectroscopy of 5-Keto-D-Fructose and D-Fructose Solutions Produced by Resting Cells of *Gluconobacter oxydans* 621H Strains

The produced and purified 5-KF solution was analyzed by UV-Vis spectroscopy using a JASCO V-650 spectrophotometer (JASCO Deutschland GmbH, Pfungstadt, Germany). Therefore, 1 ml of a diluted 5-KF solution (final concentration: 15.8 mM) was measured using a bandwith of 1.0 nm between a wavelength of 200 and 700 nm. The measurement was performed in an Eppendorf Uvette® (Eppendorf, Hamburg, Germany), which served as a blank in the empty state.

Endotoxin Quantification

The endotoxin levels in the prepared 5-KF and D-fructose solutions were quantified using the ToxinSensor Chromogenic LAL Endotoxin Assay Kit (Genscript Biotech, New Jersey, United States). The quantification was performed according to the manufacturer's instructions.

Toxicological Studies

MTT-Assay

To assess the cell viability of HT-29 cells in the presence or absence of 5-KF, the MTT assay was performed. Therefore, HT-29 cells (10,000/well) were plated in a 96-well plate and supplemented with 200 μL DMEM high glucose medium containing 10% fetal bovine serum (FBS) and antibiotic–antimycotic. Using six biological replicates, cells were supplemented with H_2O_{pure} (negative control), different concentrations of bortezomib (BTZ; positive control), 5-KF, or D-fructose. The latter two compounds were custom-made by whole-cell catalysis using dormant cells of *G. oxydans* 621H Δ*hsdR* and *G. oxydans fdh*. Following incubation at 37°C for 18 h in a humidified CO_2 (5%)/air (95%) atmosphere (referred to as 5% CO_2 atmosphere), the medium was removed and HT-29 cells were washed with PBS. 3-(4,5-dimethylthiazol-2-yl)-2,5-Diphenyltetrazolium bromide (MTT) was solved in sterile DMEM high glucose medium and added to each well at a concentration of 0.5 mg mL^{-1}. After 1 h of incubation at 37°C in a humidified 5% CO_2 atmosphere, MTT was removed and formazan crystals were resolved. Therefore, 100 μL of solubilizing solution (99.5% isopropanol, 0.4% 1 M HCl, and 0.1% Triton X-100) were added and incubated at 37°C until formazan crystals disappeared. The absorbance was measured at 570 nm using a Tecan Infinite 200 M Plex plate reader (Tecan Group AG).

RealTime-Glo™ MT Cell Viability Assay

Prior to the RealTime-Glo™ MT cell viability assay (Promega Corporation, Madison, US), HT-29 cells (1,500/well) were plated in a 96-well plate supplemented with 200 μL DMEM high glucose medium containing 10% fetal bovine serum (FBS) and antibiotic–antimycotic. The plate was incubated for 12 h at 37°C in a humidified 5% CO_2 atmosphere to promote cell adherence. Test compounds (bortezomib, 5-KF, and D-fructose) were diluted in a medium at a concentration 2-fold higher than the target concentration desired in the subsequent assay. The RealTime-Glo reagent (Promega Corp.) was prepared as a 2x stock in the test compound diluent. Following incubation, the medium was removed and the cells were treated with 100 μL of medium containing the respective test compound and 100 μL test compound diluent containing the 2x RealTime-Glo™ reagent. Afterward, cells were incubated at 37°C in a humidified 5% CO_2 atmosphere. In a discontinuous mode, the luminescence of each well was measured at 37°C using a Tecan Infinite 200 M Plex plate reader (Tecan Group AG). Per test compound, six biological replicates were performed.

Photometric Determination of 5-Keto-D-Fructose Induced Maillard Reaction

During the growth studies performed, intensive brown coloring was observed in *E. coli* DSM 498 cultures supplemented with 5-KF, indicating the formation of Maillard products. To investigate the impact of specific media components on the formation of Maillard products, photometric assays were performed in 96-well microtiter plates. Per well, 150 μL H_2O_{demin} was mixed with 7.5 μL Tris-HCl (1 M, pH 7), 30 μL of different dilutions (undiluted, 1:2, 1:4, 1:8, 1:16, and 1:32) of 0.4 M potassium phosphate, 24 μL of different dilutions (undiluted, 1:2, 1:4, 1:8,

1:16, and 1:32) of 0.5 M ammonium chloride, and 15 μL of 99 mM 5-KF solution. The plate was then incubated at 37°C in a Tecan Infinite M200 plate reader (Tecan Group AG), which measured the absorbance at 360 nm every 15 min for 20 h. The same experiment was repeated to investigate the impact of L-lysine on the formation of Maillard products in the presence of 5-KF. For this purpose, the experiment was repeated; however, the ammonium chloride solution was substituted with a 0.5 M L-lysine monohydrate solution.

To investigate the formation of fluorescent Maillard products, assays containing 150 μL H_2O_{demin}, 7.5 μL Tris-HCl (1 M, pH 7), 30 μL 0.4 M potassium phosphate, 24 μL 0.5 M ammonium chloride, and 15 μL 99 mM 5-KF were transferred to a 96 well plate and subjected to fluorescence spectroscopy. In control assays, 5-KF was substituted with H_2O_{demin}. Fluorescence was detected using an excitation wavelength of 365 nm and an emission wavelength of 445 nm. Incubation at 37°C and simultaneous measurement of the relative fluorescence units (RLUs) was achieved by an Infinite M Plex plate reader (Tecan AG Group). The experiment was conducted using biological triplicates.

Data Evaluation, Visualization, and Statistical Analysis

HPLC chromatograms, UV-spectra, and bacterial growth curves were visualized using the scientific plotting package Veusz 3.3.1 (Max-Planck-Institut für extraterrestische Physik, Garching, Germany). Bar charts and *X–Y* plots generated to present results of toxicological assays and studies on Maillard reaction were prepared using GraphPad Prism 9.3.1 (GraphPad Software, San Diego, US). Statistical analyses were performed using GraphPad Prism 9.3.1 (GraphPad Software). Assuming equal standard deviations, data obtained during growth experiments with *B. subtilis* DSM 10 and *E. coli* DSM 498 were tested by ordinary one-way analysis of variance (ANOVA). Applying Dunnett's multiple comparisons test, the means of individual data sets were compared to the mean of the respective water controls. Assuming equal standard deviations, data obtained during toxicological studies on HT-29 cells were tested by ordinary one-way ANOVA. Applying Tukey's multiple comparisons test, the means of the individual conditions were compared with the means of every other condition.

RESULTS

Production of 5-Keto-D-Fructose and D-Fructose by Resting Cells of *Gluconobacter oxydans* 621H *fdh* and *Gluconobacter oxydans* 621H

To evaluate the impact of the potential sugar substitute 5-KF on the viability of prokaryotic and eukaryotic cells, the diketone was produced from D-fructose using resting cells of *G. oxydans fdh*. A reference solution of D-fructose, incubated with the wild type strain *G. oxydans* 621H, served as a control to assess the effect of potential microbial contaminations during the production process on toxicological assays. After completion of the bioconversion and subsequent downstream processing, both solutions were analyzed by HPLC, revealing that D-fructose was efficiently oxidized to 5-KF by resting the cells of *G. oxydans fdh* (**Figure 1A**). No residual substrate was detectable in the final 5-KF solution, confirming the functionality of the production process. However, a tiny preceding peak was detected with a retention time of 8.3 min, most likely caused by a dimerized spirane structure of two 5-KF monomers (β-pyranose and β-furanose). Nonetheless, based on the chromatographic analyses, the purity of the 5-KF solution was found to be > 98%. The use of activated charcoal as an adsorbent thus proved to be extremely effective in removing potential by-products of the bioconversion. During the bioconversion with the wild type strain *G. oxydans* 621H, D-fructose remained untouched and a clean D-fructose peak was observed in the corresponding HPLC chromatogram (**Figure 1A**).

During UV-Vis spectroscopy, two clear absorption maxima were detected at 286 and 215 nm for the 5-KF solution (**Figure 1B**). Above a wavelength of 345 nm, no absorption was detected.

Using the ToxinSensor™ Chromogenic LAL Endotoxin Assay Kit (Genscript Biotech), it was confirmed that no microbial endotoxins were present in the prepared 5-KF and D-fructose solutions (data not shown).

Effect of 5-Keto-D-Fructose on the Viability of Prokaryotic Microorganisms

Growth experiments using *B. subtilis* DSM 10 and *E. coli* DSM 498 were designed to elucidate the effect of 5-KF on the viability of prokaryotic cells. Plate-reader-assisted cultivation in microtiter plates enabled high-throughput assessment of the optical densities at an exceptionally high measurement frequency.

In Spore minimal medium (Demain, 1958), *B. subtilis* DSM 10 exhibited typical bacterial growth, characterized by an initial lag phase, an exponential growth phase, and a stationary growth plateau (**Figure 2**). During the initial growth phase (2–7 h), doubling times of all cultures were comparable and ranged from 175 ± 2 to 230 ± 14 min. Subsequently, only the negative control lacking 5-KF maintained its high growth rate, reaching a maximum OD_{600} of 1.31 ± 0.03 after 28.5 h of incubation (**Figure 2**). Following the initial growth phase, cultures containing 5-KF showed elevated doubling times of 368 ± 13 (1 mM 5-KF), 453 ± 26 (10 mM 5-KF), and 444 ± 7 min (20 mM 5-KF).

Accordingly, after 28.5 h of incubation, significantly ($p < 0.0001$) lower OD_{600}-values of 1.11 ± 0.03 (1 mM 5-KF), 0.88 ± 0.02 (10 mM 5-KF), and 0.89 ± 0.02 (20 mM 5-KF) were detected in wells supplemented with 5-KF (**Figure 3**). Although cultures supplemented with 5-KF exhibited a reduced growth rate during the exponential growth phase, they reached similar optical densities as the negative control over the course of the 45-h experiment (**Figure 2**).

During growth studies with *E. coli* DSM 498, a strong browning of cultures supplemented with 5-KF was observed

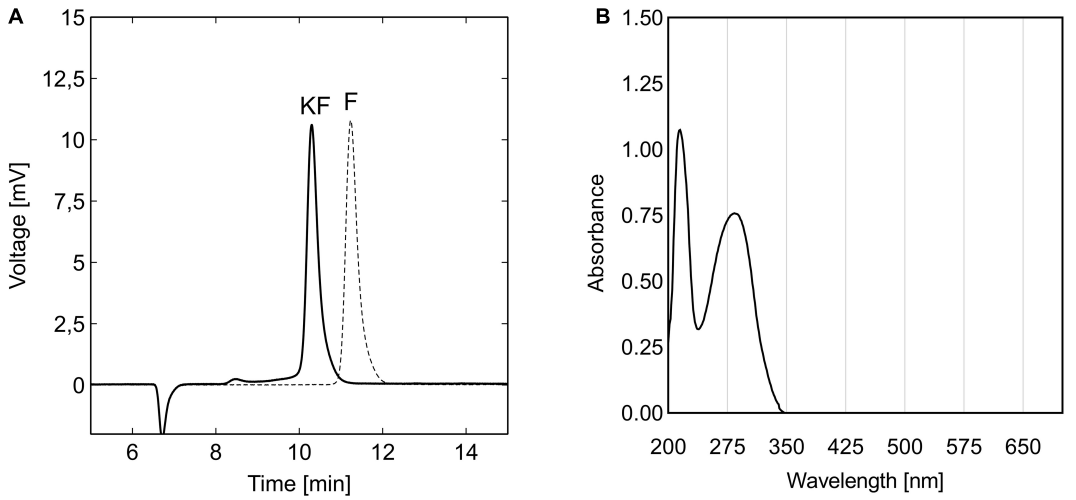

FIGURE 1 | HPLC chromatograms of 5-KF and D-fructose solutions **(A)** and UV-Vis spectrum of 5-KF **(B)** produced by resting cells of *G. Gluconobacter oxydans* 621H strains. After bioconversion of 200 mM D-fructose solution with *G. oxydans fdh* and *G. oxydans* 621H and subsequent downstream processing, final process solutions were analyzed by HPLC and UV-Vis spectroscopy. Chromatographic separation of 5-KF solution (solid line) and D-fructose solution (dotted line) was achieved using the Eurokat H column (300 × 8 mm; Knauer GmbH) heated to 65°C. The mobile phase, 5 mM H_2SO_4, was applied at a flow rate of 0.6 ml min^{-1}. Shown are the signals of the refractive index detector. UV-Vis spectroscopy was performed solely for 5-KF using a JASCO V-650 spectrophotometer (JASCO Deutschland GmbH).

(**Figure 3D**). This browning reaction was concentration-dependent and also occurred in a non-inoculated medium (**Supplementary Figure 1**), indicating reactivity between 5-KF and media components. This observation occurred exclusively with Wilms-MOPS-medium as non-inoculated Spore minimal medium displayed only a faint coloring, which did not affect the assessment of the bacterial biomass (**Supplementary Figure 1**). Due to the intense brown coloring in cultures of *E. coli* DSM 498, the optical density was not correctly detected by the plate reader platform used. To assess the viability and biomass yields of the cultures, cells were harvested by centrifugation after 45 h of incubation and washed twice in buffer W after discarding the browned supernatants. While the control culture reached an OD_{600} of 1.11 ± 0.06, cultures supplemented with 5-KF displayed decreased maximum optical densities (**Figure 3B**). This effect was concentration-dependent and significant ($p < 0.0001$) for cultures supplemented with 10 mM and 20 mM 5-KF.

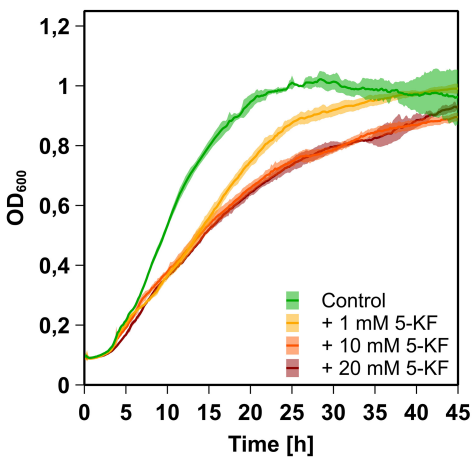

FIGURE 2 | Growth behavior of *B. subtilis* DSM 10 cultures supplemented with and without 5-KF. *B. subtilis* DSM 10 was grown in Spore minimal medium (Demain, 1958) at 30°C without 5-KF (green), or with 1 mM (yellow), 10 mM (orange), or 20 mM (red) 5-KF. OD_{600} was measured every 5 min by a Tecan Infinite M200 plate reader (Tecan Group AG). The dark, central line of the growth curves reflects the mean of each biological triplicate, while the lighter area above and below displays the standard deviation. After 28.5 h of incubation, when the control culture reached a maximum OD_{600}, all cultures treated with 5-KF displayed significantly lower optical densities ($p < 0.0001$). Dunnett's multiple comparisons test was performed using GraphPad 9.3.1 (GraphPad Software, San Diego, US) to determine statistical significance.

Unlike in the case of *B. subtilis* DSM 10, increasing the 5-KF concentration from 10 to 20 mM had a detrimental effect on the final optical density and thus on the viability of *E. coli* DSM 498. The lowest OD_{600} was observed in the presence of 20 mM 5-KF with 0.21 ± 0.01.

Effect of 5-Keto-D-Fructose on the Viability of Eukaryotic Cells

The effect of 5-KF on eukaryotic cell viability was investigated using the MTT assay and the RealTime-Glo™ MT Cell Viability assay. The first assay is based on the production of purple-colored formazan crystals from MTT by mitochondrial dehydrogenases of vital cells (Mosmann, 1983). In the second method, a membrane-permeable precursor substrate is reduced by vital cells. In reduced form, the said substrate can be converted by a NanoLuc® luciferase, generating a detectable luminescence signal (Riss et al., 2004). While the MTT assay only allows endpoint determination of cell viability, the RealTime-Glo MT

Cell Viability assay can be measured in real-time due to the biocompatibility of the assay components.

Assessment of HT-29 Cell Viability in the Presence of 5-Keto-D-Fructose Using the MTT Assay

The absorbance values detected following the MTT assay were used to determine the relative cell survival of the different approaches compared to control assays treated with H_2O_{pure} (**Figure 4**). Thereby, it was shown that the apoptosis inducer bortezomib led to a significant reduction ($p < 0.0001$) of cell viability at a concentration of 0.01 μM. The relative cell survival in corresponding wells averaged 33.6 ± 5.6%. Increasing the bortezomib concentration to 100 μM further reduced cell viability, as reflected by a relative absorption intensity of 26.6 ± 6.5% (not shown). While wells supplemented with 5-KF at a concentration of 1 mM showed cell viability comparable to the water control (98.8 ± 8.0%), higher 5-KF concentrations reduced the relative cell survival of HT-29 cells significantly ($p < 0.0001$). Cells treated with 10 mM 5-KF displayed a mean relative absorbance of 43.9 ± 5.6%. The inhibitory effect of 5-KF was further enhanced at 25 mM, as the relative cell survival was decreased to 23.6 ± 3.7% in respective assays. Thus, based

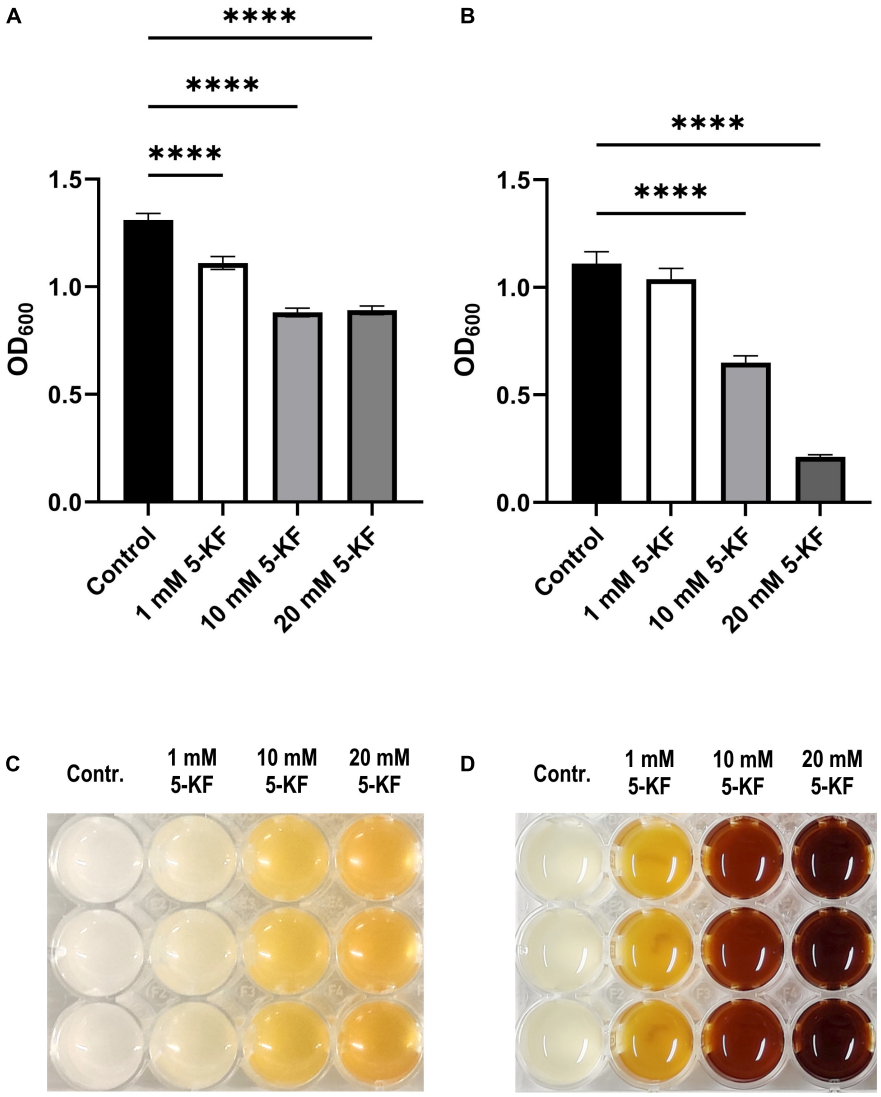

FIGURE 3 | OD_{600} values and browning of *B. subtilis* DSM 10 and *E. coli* DSM 498 cultures treated with and without 5-KF. *B. subtilis* DSM 10 was cultured in Spore minimal medium (Demain, 1958) at 30°C without and with different concentrations of 5-KF **(A,C)**. OD_{600}-values of *B. subtilis* DSM 10 cultures **(A)** were subjected to statistical analysis after 28.5 h of incubation when the control culture reached its maximum optical density. *B. subtilis* DSM 10 cultures were photographed at the end of the experiment after 45 h of incubation **(C)**. *E. coli* DSM 498 was grown in modified Wilms-MOPS-medium (Wilms et al., 2001) at 37°C without and with different concentrations of 5-KF **(B,D)**. Due to the intense browning, the biomass of *E. coli* DSM 498 was not accurately detected by the Tecan Infinite M200 plate reader (Tecan Group AG). After 45 h of incubation, *E. coli* DSM 498 cultures were photographed **(D)**, harvested, washed twice in buffer W, and subjected to final OD_{600} measurement **(B)**. Dunnett's multiple comparisons test was performed using GraphPad 9.3.1 (GraphPad Software, San Diego, US) to determine statistical significance; $^{****}p < 0.0001$. The experiment was performed as a biological triplicate.

on these measurements, cells were more restricted in viability in the presence of 25 mM 5-KF than in the presence of 100 μM bortezomib. In contrast, the D-fructose solution incubated with resting cells of *G. oxydans* 621H Δ*hsdR* showed no drastic effect on the viability of HT-29 cells.

Assessment of HT-29 Cell Viability in the Presence of 5-Keto-D-Fructose Using the RealTime-Glo™ MT Cell Viability Assay

To validate the inhibitory effect of 5-KF observed during the MTT assay, the RealTime-Glo™ MT Cell Viability assay (Promega Corp.) was performed. The assay enables real-time determination of luminescence units generated by a NanoLuc® luciferase upon conversion of a NanoLuc® Substrate. Said NanoLuc® Substrate must be generated beforehand by vital cells through reduction of the MT Cell Viability Substrate. Control wells supplemented with H_2O_{pure} displayed a linear increase in luminescence within the first 35 h of incubation (**Figure 5A**). Subsequently, the increase in luminescence flattened and reached a maximum of 831,533 ± 32,590 relative luminescence units (RLUs) after 52.5 h of incubation (**Figure 5B**). The addition of 1 μM bortezomib resulted in a significant decrease in luminescence in corresponding wells ($p < 0.0001$). After an initial moderate increase in luminescence in wells treated with bortezomib, the maximal RLU (242,633 ± 5,553 RLUs) of respective wells was measured after 30.5 h of incubation. Toward the end of the experiment, the luminescence signal in assays containing bortezomib decreased to 42,741 ± 3,889 RLUs. In the presence of 1 mM 5-KF the HT-29 cells produced 806,216 ± 16,376 RLUs, which is comparable to the water control. However, at concentrations ≥ 5 mM, the sugar derivative induced a significant decrease in generated luminescence in a dose-dependent manner ($p < 0.0001$). The luminescence levels of assays containing 20 and 30 mM 5-KF were even lower than the luminescence level of assays treated with bortezomib (**Figure 5A**). After 52.5 h of incubation, the lowest RLU count was observed for wells supplemented with 30 mM 5-KF (31,293 ± 1,690 RLUs). Control assays were carried out to exclude the possibility of 5-KF induced chemical reduction of the NanoLuc® Substrate (**Supplementary Figure 2**). No relevant luminescence signals were detected in the control assays, despite the presence or absence of 5-KF, indicating that 5-KF did not interfere with the assay components.

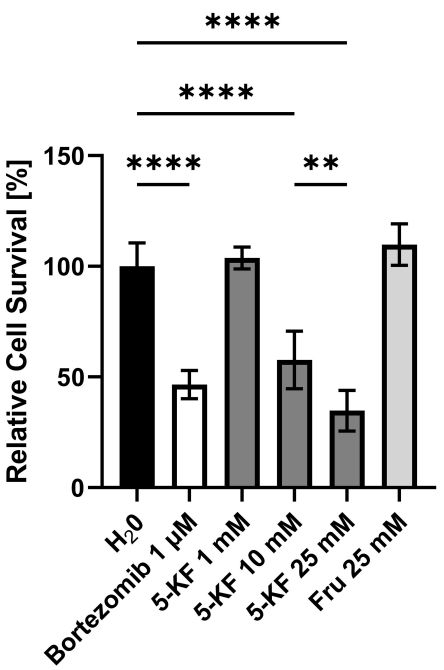

FIGURE 4 | Relative cell survival of HT-29 cells subjected to the MTT assay. The relative cell survival displayed is based on the absorbance caused by formazan crystals produced by HT-29 cells during the MTT assay. HT-29 cells (10,000 cells per well) were incubated in DMEM high glucose medium supplemented with 10% fetal bovine serum (FBS) and antibiotic–antimycotic at 37°C in a humidified 5% CO_2 atmosphere. Cells were supplemented either with H_2O_{pure} or various concentrations of bortezomib, 5-KF, or D-fructose. Once sufficient confluence was reached, the medium was removed from the 96-well plate and MTT was added to each well. The absorbance in each well, caused by redissolved formazan crystals, was measured at 570 nm using a Tecan Infinite 200 M Plex plate reader (Tecan Gr oup AG). Tukey's multiple comparison test was performed using GraphPad 9.3.1 (GraphPad Software, San Diego, US) to determine statistical significance; ****$p < 0.0001$; **$p = 0.023$. The experiment was performed using six biological replicates for each test compound.

Investigation of 5-Keto-D-Fructose Induced Maillard Reaction

The intense browning of *E. coli* DSM 498 cultures containing Wilms-MOPS medium and 5-KF indicated the formation of Maillard products (section "Effect of 5-KF on the Viability of Prokaryotic Microorganisms"). During prolonged storage of 5-KF under unfavorable conditions (e.g., non-purified crude preparations at room temperature) it was also observed that corresponding solutions changed color from colorless to yellow-brownish. To elucidate this effect in detail, 5-KF was incubated with varying concentrations of phosphate and ammonium chloride, which are known drivers of the Maillard reaction (Amrein et al., 2006; Moldoveanu, 2021). The effect of L-lysine on the browning reaction induced by 5-KF was investigated as well since the amino acid has been shown to promote a profound Maillard reaction in the presence of reducing sugars (Jing and Kitts, 2000; Ajandouz et al., 2001). The browning reaction was monitored at 360 nm as previous experiments showed that when 5-KF was incubated with the amines listed above, a strong absorbance change occurred at this wavelength (**Supplementary Figure 3**).

Overall, in the presence of 5-KF all three compounds favored the formation of brown-colored reaction products in a concentration-dependent manner (**Figures 6A,B**). It was noticeable that in the presence of lower phosphate concentrations, the increase in absorption favored by ammonium chloride was rather small (**Figure 6A**). However, this trend changed at higher phosphate concentrations (≥40 mM), as the change in absorbance per hour in the presence of ammonium chloride was greater than at equal concentrations of L-lysine. Unlike the experiments performed with ammonium chloride, incubation of L-lysine with 5-KF resulted in a visible

increase in absorbance already at low phosphate concentrations. Consecutively, a linear relationship was evident between phosphate concentration, L-lysine concentration, and observed absorbance change per hour.

It is worth noting that in control assays in which 5-KF was substituted with fructose, no change in absorption was observed at 360 nm during the observed reaction period (**Supplementary Figure 3**). In fact, the UV spectra of a reaction containing D-fructose, phosphate, and ammonium chloride were almost identical at the beginning of incubation and after 16 h of incubation at 37°C.

Since the Maillard reaction is accompanied by the formation of several fluorescent compounds (Adhikari and Tappel, 1973; Baker and Bradford, 1994; Leclère and Birlouez-Aragon, 2001), it was examined whether 5-KF promotes the formation of specific fluorophores. These studies were performed using the ammonium chloride/phosphate system due to the stronger brown coloration and absorption changes caused by 5-KF in previous experiments. The assays revealed that in the presence of ammonium chloride and phosphate, 5-KF triggered the formation of fluorescent compounds (**Figure 7**). In contrast, no increase in fluorescence was observed in control experiments in which 5-KF was replaced by water.

DISCUSSION

To assess the effect of the potential sugar substitute 5-keto-D-fructose on the viability of prokaryotic and eukaryotic cells,

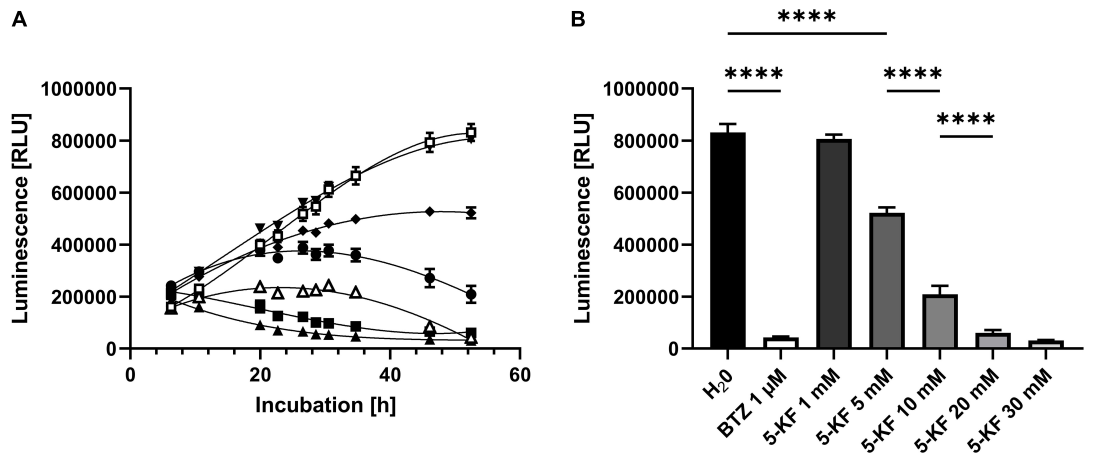

FIGURE 5 | Relative luminescence units (RLUs) produced by HT-29 cells during **(A)** and at the end **(B)** of Promega's RealTime-Glo™ MT Cell Viability assay. HT-29 cells (1,500 cells per well) were incubated in DMEM High glucose medium supplemented with 10% fetal bovine serum (FBS) and antibiotic–antimycotic at 37°C in a humidified 5% CO_2 atmosphere. Cells were supplemented either with H_2O_{pure} (□), bortezomib (△), or varying concentrations of 5-KF (▼1 mM, ♦ 5 mM, ● 10 mM, ■ 20 mM, ▲ 30 mM). Reagents of Promega's RealTime-Glo™ MT cell viability assay were added according to the manufacturer's instructions. At 10 individual time points, the relative luminescence units (RLUs) were assessed using a Promega Glomax® Discover System. Tukey's multiple comparison test was performed using GraphPad 9.3.1 (GraphPad Software, San Diego, US) to determine statistical significance; ****$p < 0.0001$. The experiment was performed using six biological replicates for each test compound.

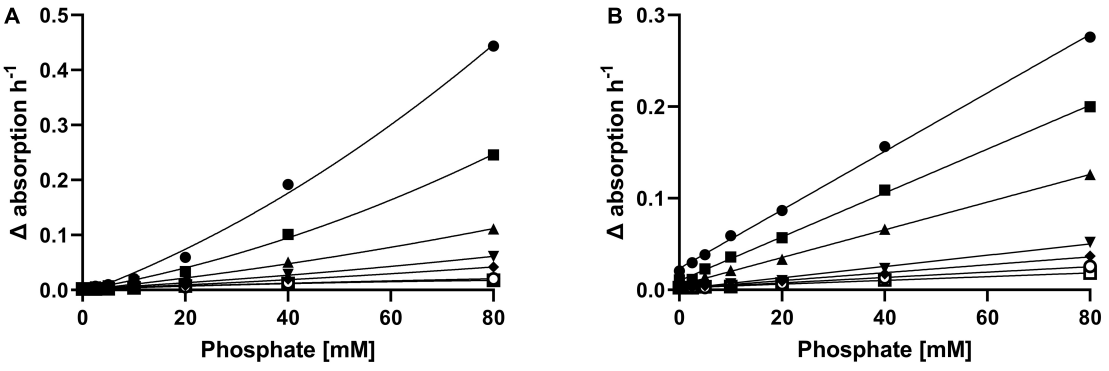

FIGURE 6 | Effect of ammonium chloride **(A)** and L-lysine **(B)** on the Maillard reaction induced by 5-KF and phosphate. Decreasing concentrations (● 80 mM, ■ 40 mM, ▲ 20 mM, ▼ 10 mM, ♦ 5 mM, ○ 2.5 mM, □ 0 mM) of ammonium chloride and L-lysine were incubated with 5-KF and phosphate at 37°C. Absorbance at 360 nm was measured every 15 min using a Tecan Infinite M200 plate reader (Tecan Group AG). Shown are the individual absorption changes per hour derived from the performed time-course measurement.

the diketone was produced, purified, and utilized for dedicated growth experiments and toxicological studies.

Oxidation of D-fructose by resting cells of *G. oxydans fdh* and subsequent downstream-processing granted access to a 5-KF solution with very high purity (> 98%). The dominant 5-KF peak in the corresponding HPLC chromatogram showed some minor front tailing and merged into a tiny preceding peak with a retention time of 8.5 min (**Figure 1A**). While in aqueous solution, 5-KF is present as a *gem*-diol hydrate, and the crystal structure of 5-KF has been reported to be a dimer of linked β-pyranose and β-furanose (Blanchard et al., 1982). This unusual spirane structure was also detected when 5-KF was solved in anhydrous Me_2SO-d_6, indicating that under anhydrous conditions, 5-KF turns into a dimer (Blanchard et al., 1982). Due to the size-exclusion character of the chromatography column used and the anhydrous character of the mobile phase acetonitrile, it can be suspected that the tiny leading peak was caused by dimerized 5-KF. Incubation of D-fructose with resting cells of the wild-type strain *G. oxydans* 621H was intended to generate a D-fructose solution that would serve as a control during toxicological studies. Since the fdh_{SCL} gene cluster, encoding the fructose-dehydrogenase complex, is not present in the genome of *G. oxydans* 621H, resting cells of the acetic acid bacterium should not be able to metabolize or oxidize D-fructose. Accordingly, D-fructose was not converted during bioconversion as indicated by the chromatographic HPLC analysis (**Figure 1A**). These results confirm the observation of Hoffmann et al. (2020), who did not detect measurable Fdh activity in resting cells of *G. oxydans* 621H.

During UV-Vis spectroscopy, two distinct peaks were observed for 5-KF with absorption maxima at 286 and 215 nm (**Figure 1B**). These peaks come very close to the UV-absorption of isolated keto groups, characterized by an $n \rightarrow \pi^*$ and a $\pi \rightarrow \pi^*$ transition. In the case of non-terminal keto groups, as present within 5-KF, the $n \rightarrow \pi^*$ transition exhibits a λ_{max} of 273, while the $\pi \rightarrow \pi^*$ transition features a λ_{max} of 187 nm (Bienz et al., 2016). Thus, according to the conducted UV-Vis spectroscopy, the investigated 5-KF preparation contained the expected keto groups. This finding, however, contradicts the observation, that in water 5-KF predominantly (> 95%) exists in a β-pyranose form, with the 5-keto group being hydrated to form a *gem*-diol (Blanchard et al., 1982). It could be hypothesized that the absorption in the longer wavelength region around 300 nm was caused by residues of the open-chain 5-KF form.

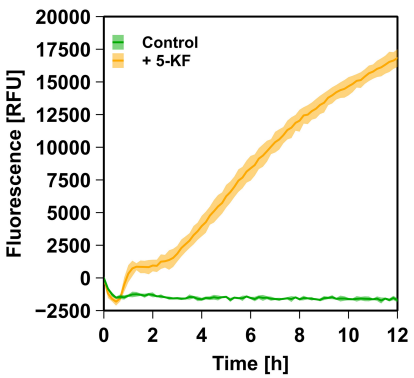

FIGURE 7 | Relative fluorescence units (RFUs) detected in assays containing 5-KF, ammonium chloride, and phosphate. Using 80 mM ammonium chloride, 80 mM phosphate, and 6.45 mM 5-KF fluorescence was measured using an excitation wavelength of 365 nm and an emission wavelength of 445 nm (orange line). In control assays, 5-KF was substituted with H_2O_{demin} (green line). Incubation of the biological triplicates at 37°C and simultaneous measurement was achieved using an Infinite M Plex plate reader (Tecan AG Group). The dark, central line of the data shown reflects the mean of each biological triplicate, while the lighter area above and below indicates the standard deviation.

Growth experiments involving the gram-positive and gram-negative bacteria *B. subtilis* DSM 10 and *E. coli* DSM 498 revealed that 5-KF significantly inhibited the growth of both prokaryotes at concentrations ≥ 5 mM ($p < 0.0001$). While this effect was rather moderate but still significant in the case of *B. subtilis* DSM 10 (**Figures 2**, **3A**), a drastic reduction in cell viability was observed for *E. coli* DSM 498 cultures supplemented with 5-KF (**Figure 3B**). The profound inhibition of *E. coli* DSM 498 correlated with an intense browning of the modified Wilms-MOPS medium (**Figure 3D**), which also occurred in non-inoculated medium (**Supplementary Figure 1**). Due to the reducing character of 5-KF, it was assumed that the observed browning was caused by the Maillard reaction. During this process, which is named after the French chemist Louis Maillard (1912), reducing sugars condense with compounds harboring free amino groups to give condensation products (N-substituted sugar-amines), which rearrange to form the so called Amadori rearrangement product (ARP) (Martins et al., 2000). Depending on the pH, this ARP further reacts into reductones, fission products, and Schiff's bases of hydroxymethylfurfural (HMF) or furfural. In the case of the glucose/glycine Maillard reaction a pH < 5 favors the formation of formic acid and various melanoidins, while at pH > 7 the ARP is mainly converted to flavor compounds (Tressl et al., 1995). Studies have shown that reducing sugars react not only with amino acids but also with ammonia to form a variety of Maillard products, including brown-colored polymers (Hodge, 1953; Van Soest and Mason, 1991). Therefore, it can be assumed that the intense browning observed during the cultivation of *E. coli* DSM 498 was caused by the high ammonium concentration of the Wilms-MOPS-medium and the increased incubation temperature of 37°C. The basic prerequisite for ammonium-based Maillard reaction is the deprotonation of ammonium, which takes place spontaneously at elevated temperatures and at neutral, preferably alkaline pH (Huang and Shang, 2006). The ammonia formed under these conditions is even more reactive than amino acids when reacting with reducing sugars (Moldoveanu, 2021). Maillard condensation products of glucose–ammonia systems were shown to occur even at mildly elevated temperatures, leading to the formation of 2,6-deoxyfructosazine and brown-colored polymers (Moldoveanu, 2021). It can be assumed that the much lower concentration of ammonium in the Spore minimal medium and the lower temperature during cultivation of *B. subtilis* DSM 10 were insufficient to promote the formation of ammonia and subsequent Maillard products. Accordingly, the

inhibition of *B. subtilis* DSM 10 was much weaker compared to *E. coli* DSM 498.

The inhibitory effect of 5-KF was not limited to prokaryotic cells as the diketone also reduced the viability of the eukaryotic cell line HT-29 in a concentration-dependent manner. At 5-KF concentrations $\geq$ 5 mM, this effect was significant ($p < 0.0001$) and evident in both the MTT assay (**Figure 4**) and the RealTime-Glo MT cell viability assay (**Figure 5**). D-Fructose solution incubated with wild-type *G. oxydans* 621H showed no effect on cell viability, suggesting that no toxic cellular components entered the sugar solutions during microbial bioconversion. Thus, the reduction in cell viability was selectively mediated by 5-KF and not by potentially toxic cell compartments.

Incubation with phosphate and ammonium chloride or L-lysine demonstrated that 5-KF triggered the formation of brown-colored reaction products, as confirmed by a substantial increase in absorbance at 360 nm (**Figure 6**). The accelerating effect of phosphate on Maillard browning is well-known but the exact mechanism for phosphate involvement is still not clear (Rizzi, 2004). The anion might act as a catalyst for the formation of reactive dicarbonyl derivatives as key intermediates of the Maillard reaction and facilitates the nucleophilic attack of amines on the keto groups of 5-KF. The observed increase in absorbance change at elevated concentrations of ammonium chloride or L-lysine is also consistent with observations in the literature (Amrein et al., 2006; Moldoveanu, 2021). The assumption that 5-KF favors the formation of Maillard products was supported by fluorescence measurements. Fluorescent products have been proposed as specific indicators for the Maillard reaction (Adhikari and Tappel, 1973; Baker and Bradford, 1994; Leclère and Birlouez-Aragon, 2001) and were also detected in assays containing 5-KF, phosphate, and ammonium chloride (**Figure 7**). Several studies reported on fluorescent compounds detected during the Maillard reaction, which had a maximum of excitation at wavelengths between 340 and 370 nm and showed maximum emission at wavelengths between 420 and 450 nm (Morales and Van Boekel, 1998; Leclère and Birlouez-Aragon, 2001; Rufian-Henares et al., 2002).

Based on the experiments conducted, it cannot be definitively elucidated whether the cytotoxic effect of 5-KF originates from the diketone itself or from the Maillard products formed in the presence of 5-KF. Since Maillard products have been shown to possess mutagenic and cytotoxic properties (Brands et al., 2000; Jing and Kitts, 2000), it is likely that the observed inhibition of *B. subtilis* DSM 10 and *E. coli* DSM 498 was induced by toxic Maillard products. Nonetheless, the rapid onset of inhibition observed during growth experiments with *B. subtilis* DSM 10 (**Figure 2**) and toxicological studies with HT-29 cells (**Figure 5**) indicate that 5-KF may also directly impact cellular processes in a detrimental way.

Due to the inhibitory effects of 5-KF toward prokaryotic and eukaryotic cells, we advise against using 5-KF in the food sector as a sugar substitute. Further studies are recommended to substantiate the effect shown here. Nevertheless, the high reactivity of the compound could be of great use in other branches of research, such as organic chemistry.

CONCLUSION

Due to the increasing number of sugar-associated diseases and the growing consumer awareness of the adverse effects of sugar, there is an urgent need for healthy sugar alternatives. A promising candidate with this regard is 5-keto-D-fructose, a natural diketone, which is produced in some acetic acid bacteria by oxidation of D-fructose, a process catalyzed primarily by the membrane-bound fructose dehydrogenase complex. In this work, the effect of 5-KF on prokaryotic and eukaryotic cells was investigated. It was shown that 5-KF significantly reduced the viability of *B. subtilis* DSM 10, *E. coli* DSM 498, and the epithelial cell line HT-29 at concentrations $\geq$ 5 mM. This effect might be related to the strong Maillard reaction favored by 5-KF in the presence of amines, which became apparent during this study. Due to the cytotoxic effects of the diketone, we hereby oppose the use of 5-KF in the food sector.

DATA AVAILABILITY STATEMENT

The raw data supporting the conclusions of this article will be made available by the authors, without undue reservation.

AUTHOR CONTRIBUTIONS

MH: conceptualization, validation, visualization, investigation, supervision, and writing—original draft. NG: investigation and methodology. SK, AK, JS, and TL: investigation. KK: conceptualization, writing—review and editing. UD: conceptualization, project administration, resources, funding acquisition, supervision, and writing—review and editing. All authors contributed to the article and approved the submitted version.

FUNDING

This work was supported by funds from the Federal Ministry of Education and Research (Germany) project IMPRES2 (FKZ 031B1054A).

ACKNOWLEDGMENTS

Great thanks are attributed to D. Winter from the Institute for Biochemistry and Molecular Biology (University of Bonn) for providing the HT-29 cell line. We want to thank Natalie Thum-Schmitz for technical assistance.

SUPPLEMENTARY MATERIAL

The Supplementary Material for this article can be found online at: https://www.frontiersin.org/articles/10.3389/fmicb.2022.935062/full#supplementary-material

REFERENCES

Adhikari, H. R., and Tappel, A. L. (1973). Fluorescent products in a glucose-glycine browning reaction. *J. Food Sci.* 38, 486–488. doi: 10.1111/j.1365-2621.1973.tb01462.x

Ajandouz, E. H., Tchiakpe, L. S., Ore, F. D., Benajiba, A., and Puigserver, A. (2001). Effects of pH on caramelization and Maillard reaction kinetics in fructose-lysine model systems. *J. Food Sci.* 66, 926–931. doi: 10.1111/j.1365-2621.2001.tb08213.x

Ameyama, M., Shinagawa, E., Matsushita, K., and Adachi, O. (1981). D-fructose dehydrogenase of *Gluconobacter industrius*: purification, characterization, and application to enzymatic microdetermination of D-fructose. *J. Bacteriol.* 145, 814–823. doi: 10.1128/jb.145.2.814-823.1981

Amrein, T. M., Andres, L., Manzardo, G. G., and Amadò, R. (2006). Investigations on the promoting effect of ammonium hydrogencarbonate on the formation of acrylamide in model systems. *J. Agric. Food Chem.* 54, 10253–10261. doi: 10.1021/jf0625860

Aragno, M., and Mastrocola, R. (2017). Dietary sugars and endogenous formation of advanced glycation endproducts: emerging mechanisms of disease. *Nutrients* 9:385. doi: 10.3390/nu9040385

Baker, E. H., and Bradford, K. J. (1994). The fluorescence assay for Maillard product accumulation does not correlate with seed viability. *Seed Sci. Res.* 4, 103–107. doi: 10.1017/S0960258500002087

Battling, S., Wohlers, K., Igwe, C., Kranz, A., Pesch, M., Wirtz, A., et al. (2020). Novel plasmid-free *Gluconobacter oxydans* strains for production of the natural sweetener 5-ketofructose. *Microb. Cell Fact.* 19:54. doi: 10.1186/s12934-020-01310-7

Bienz, S., Bigler, L., Fox, T., and Meier, H. (2016). *Spektroskopische Methoden In Der Organischen Chemie*. New York, NY: Georg Thieme Verlag, doi: 10.1055/b-004-129729

Blanchard, J. S., Brewer, C. F., Englard, S., and Avigad, G. (1982). Solution structure of 5-keto-D-fructose: relevance to the specificity of hexose kinases. *Biochemistry* 21, 75–81. doi: 10.1021/bi00530a014

Brands, C. M., Alink, G. M., van Boekel, M. A., and Jongen, W. M. (2000). Mutagenicity of heated sugar- casein systems: effect of the Maillard reaction. *J. Agric. Food Chem.* 48, 2271–2275. doi: 10.1021/jf9907586

Burroughs, L. F., and Sparks, A. H. (1973). Sulphite-binding power of wines and ciders. I. Equilibrium constants for the dissociation of carbonyl bisulphite compounds. *J. Sci. Food Agric.* 24, 187–198. doi: 10.1002/jsfa.2740240211

Chattopadhyay, S., Raychaudhuri, U., and Chakraborty, R. (2014). Artificial sweeteners–a review. *J. Food Sci. Technol.* 51, 611–621. doi: 10.1007/s13197-011-0571-1

Dekker, M. J., Su, Q., Baker, C., Rutledge, A. C., and Adeli, K. (2010). Fructose: a highly lipogenic nutrient implicated in insulin resistance, hepatic steatosis, and the metabolic syndrome. *Am. J. Physiol. Endocrinol. Metab.* 299, E685–E694. doi: 10.1152/ajpendo.00283.2010

Demain, A. L. (1958). Minimal media for quantitative studies with Bacillus subtilis. *J. Bacteriol.* 75, 517–522. doi: 10.1128/jb.75.5.517-522.1958

Englard, S., Berkower, I., and Avigad, G. (1972). 5-Keto-D-fructose VII. Phosphorylation by liver fructokinase and the monophosphate ester as an inhibitor of liver aldolase. *Biochim. Biophys. Acta Gen. Subj.* 279, 229–233. doi: 10.1016/0304-4165(72)90138-9

Grembecka, M. (2015). Sugar alcohols—their role in the modern world of sweeteners: a review. *Eur. Food Res. Technol.* 241, 1–14. doi: 10.1007/s00217-015-2437-7

Herweg, E., Schöpping, M., Rohr, K., Siemen, A., Frank, O., Hofmann, T., et al. (2018). Production of the potential sweetener 5-ketofructose from fructose in fed-batch cultivation with *Gluconobacter oxydans*. *Bioresour. Technol.* 259, 164–172. doi: 10.1016/j.biortech.2018.03.038

Herweg, E., Büchs, J., Bott, M., Kiefler, I., Deppenmeier, U., Kosciow, K., et al. (2020). *U.S. Patent Application No. 16/622,439*.

Hodge, J. E. (1953). Dehydrated foods, chemistry of browning reactions in model systems. *J. Agric. Food Chem.* 1, 928–943.

Hoffmann, J. J., Hövels, M., Kosciow, K., and Deppenmeier, U. (2020). Synthesis of the alternative sweetener 5-ketofructose from sucrose by fructose dehydrogenase and invertase producing *Gluconobacter* strains. *J. Biotechnol.* 307, 164–174. doi: 10.1016/j.jbiotec.2019.11.001

Hu, F. B., and Malik, V. S. (2010). Sugar-sweetened beverages and risk of obesity and type 2 diabetes: epidemiologic evidence. *Physiol. Behav.* 100, 47–54. doi: 10.1016/j.physbeh.2010.01.036

Huang, J. C., and Shang, C. (2006). "Air stripping," in *Advanced Physicochemical Treatment Processes*, eds L. K. Wang, Y. T. Hung, and N. K. Shammas (Totowa: Humana Press), 47–79. doi: 10.1007/978-1-59745-029-4_2

Jing, H., and Kitts, D. D. (2000). Comparison of the antioxidative and cytotoxic properties of glucose-lysine and fructose-lysine Maillard reaction products. *Food Res. Int.* 33, 509–516. doi: 10.1016/S0963-9969(00)00076-4

Johnson, R. J., Segal, M. S., Sautin, Y., Nakagawa, T., Feig, D. I., Kang, D. H., et al. (2007). Potential role of sugar (fructose) in the epidemic of hypertension, obesity and the metabolic syndrome, diabetes, kidney disease, and cardiovascular disease. *Am. J. Clin. Nutr.* 86, 899–906. doi: 10.1093/ajcn/86.4.899

Kawai, S., Goda-Tsutsumi, M., Yakushi, T., Kano, K., and Matsushita, K. (2013). Heterologous overexpression and characterization of a flavoprotein-cytochrome c complex fructose dehydrogenase of *Gluconobacter japonicus* NBRC3260. *Appl. Environ. Microbiol.* 79, 1654–1660. doi: 10.1128/AEM.03152-12

Kroger, M., Meister, K., and Kava, R. (2006). Low-calorie sweeteners and other sugar substitutes: a review of the safety issues. *Compr. Rev. Food Sci. Food Saf.* 5, 35–47. doi: 10.1111/j.1541-4337.2006.tb00081.x

Leclère, J., and Birlouez-Aragon, I. (2001). The fluorescence of advanced Maillard products is a good indicator of lysine damage during the Maillard reaction. *J. Agric. Food Chem.* 49, 4682–4687. doi: 10.1021/jf001433o

Maillard, L. C. (1912). Action des acides amines sur les sucres; formation des melanoidines par voie methodique. *C.R. Acad. Sci.* 154, 66–68.

Mäkinen, K. K. (2016). Gastrointestinal disturbances associated with the consumption of sugar alcohols with special consideration of xylitol: scientific review and instructions for dentists and other health-care professionals. *Int. J. Dent.* 2016:5967907. doi: 10.1155/2016/5967907

Malik, V. S., Popkin, B. M., Bray, G. A., Després, J. P., Willett, W. C., and Hu, F. B. (2010). Sugar-sweetened beverages and risk of metabolic syndrome and type 2 diabetes: a meta-analysis. *Diabetes Care* 33, 2477–2483. doi: 10.2337/dc10-1079

Martins, S. I., Jongen, W. M., and Van Boekel, M. A. (2000). A review of Maillard reaction in food and implications to kinetic modelling. *Trends Food Sci. Technol* 11, 364–373. doi: 10.1016/S0924-2244(01)00022-X

Moldoveanu, S. C. (2021). "Analytical pyrolysis of caramel colours and of Maillard browning polymers," in *Analytical Pyrolysis of Natural Organic Polymers*, (Amsterdam: Elsevier), 315-333. doi: 10.1016/b978-0-12-818571-1.00008-x

Morales, F. J., and Van Boekel, M. A. J. S. (1998). A study on advanced Maillard reaction in heated casein/sugar solutions: colour formation. *Int. Dairy J.* 8, 907–915.

Mosmann, T. (1983). Rapid colorimetric assay for cellular growth and survival: application to proliferation and cytotoxicity assays. *J. Immunol. Methods* 65, 55–63. doi: 10.1016/0022-1759(83)90303-4

Mowshowitz, S., Englard, S., and Avigad, G. (1974). Metabolic Consequences of a Block in the Synthesis of 5-Keto-D-Fructose in a Mutant of *Gluconobacter cerinus*. *J. Bacteriol.* 119, 363–370. doi: 10.1128/jb.119.2.363-370.1974

Riss, T. L., Moravec, R. A., Niles, A. L., Duellman, S., Benink, H. A., Worzella, T. J., et al. (2004). "Cell viability assays," in *Assay Guidance Manual*, eds S. Markossian, G. S. Sittampalam, A. Grossman, K. Brimacombe, M. Arkin, D. Auld, et al. (Bethesda, MD: Eli Lilly).

Rizzi, G. P. (2004). Role of phosphate and carboxylate ions in Maillard browning. *J. Agric. Food Chem.* 52, 953–957. doi: 10.1021/jf030691t

Rufian-Henares, J. A., Guerra-Hernandez, E., and Garcıìa-Villanova, B. (2002). Maillard reaction in enteral formula processing: furosine, loss of o-phthaldialdehyde reactivity, and fluorescence. *Food Res. Int.* 35, 527–533. doi: 10.1016/S0963-9969(01)00152-1

Sang, Z., Jiang, Y., Tsoi, Y. K., and Leung, K. S. Y. (2014). Evaluating the environmental impact of artificial sweeteners: a study of their distributions, photodegradation and toxicities. *Water Res.* 52, 260–274. doi: 10.1016/j.watres.2013.11.002

Schiessl, J., Kosciow, K., Garschagen, L. S., Hoffmann, J. J., Heymuth, J., Franke, T., et al. (2021). Degradation of the low-calorie sugar substitute 5-ketofructose by different bacteria. *Appl. Microbiol. Biotechnol.* 105, 2441–2453. doi: 10.1007/s00253-021-11168-3

Schiffman, S. S., Booth, B. J., Losee, M. L., Pecore, S. D., and Warwick, Z. S. (1995). Bitterness of sweeteners as a function of concentration. *Brain Res. Bull.* 36, 505–513. doi: 10.1016/0361-9230(94)00225-P

Siemen, A., Kosciow, K., Schweiger, P., and Deppenmeier, U. (2018). Production of 5-ketofructose from fructose or sucrose using genetically modified *Gluconobacter oxydans* strains. *Appl. Microbiol. Biotechnol.* 102, 1699–1710. doi: 10.1007/s00253-017-8699-1

Suez, J., Korem, T., Zeevi, D., Zilberman-Schapira, G., Thaiss, C. A., Maza, O., et al. (2014). Artificial sweeteners induce glucose intolerance by altering the gut microbiota. *Nature* 514, 181–186. doi: 10.1038/nature13793

Tappy, L., and Lê, K. A. (2010). Metabolic effects of fructose and the worldwide increase in obesity. *Physiol. Rev.* 90, 23–46. doi: 10.1152/physrev.00019.2009

Terada, O., Tomizawa, K., Suzuki, S., and Kinoshita, S. (1960). Formation of 5-dehydrofructose by members of Acetobacter. *J. Agric. Chem. Soc. Japan* 24, 535–536. doi: 10.1080/03758397.1960.10857706

Tressl, R., Nittka, C., Kersten, E., and Rewicki, D. (1995). Formation of isoleucine-specific Maillard products from [1-13C]-D-glucose and [1-13C]-D-fructose. *J. Agric. Food Chem.* 43, 1163–1169. doi: 10.1021/jf00053a009

Van Soest, P. J., and Mason, V. C. (1991). The influence of the Maillard reaction upon the nutritive value of fibrous feeds. *Anim. Feed Sci. Technol.* 32, 45–53. doi: 10.1016/0377-8401(91)90008-G

Wilms, B., Hauck, A., Reuss, M., Syldatk, C., Mattes, R., Siemann, M., et al. (2001). High-cell-density fermentation for production of L-N-carbamoylase using an expression system based on the *Escherichia coli rhaBAD* promoter. *Biotechnol. Bioeng.* 73, 95–103. doi: 10.1002/bit.1041

Conflict of Interest: The authors declare that the research was conducted in the absence of any commercial or financial relationships that could be construed as a potential conflict of interest.

frontiers | Frontiers in Microbiology

ORIGINAL RESEARCH
published: 19 July 2022
doi: 10.3389/fmicb.2022.897825

Selection of Acetic Acid Bacterial Strains and Vinegar Production From Local Maltese Food Sources

Joseph Mizzi[1], *Francesca Gaggìa*[2]*, *Nicole Bozzi Cionci*[2], *Diana Di Gioia*[2] and *Everaldo Attard*[1]

[1] Division of Rural Sciences and Food Systems, Institute of Earth Systems, University of Malta, Msida, Malta, [2] Department of Agricultural and Food Sciences, University of Bologna, Bologna, Italy

This study investigates the isolation, identification, and fermentation performance of autochthonous acetic acid bacteria (AAB) from local niche habitats on the Island of Gozo (Malta) and their further use for vinegar production, employing local raw materials. The bacteria were isolated from grapevine berries and vinegar produced in the cottage industry. Following phenotype and genotype identification, the AAB were ascribed to the genera *Acetobacter*, *Gluconobacter,* and *Komagataeibacter*. A mixture of selected AAB was tested as an inoculum for vinegar production in bench fermenters, under different conditions and substrates, namely, grapes, honey, figs, onions, prickly pear, and tomatoes. The bench fermenters were operated under semi-continuous fermentation where working volumes were maintained by discharging and subsequent recharging accordingly to maintain the acidity in fermenters by adding 30–50 g/l of acetic acid for optimal *Acetobacteraceae* performance. Finally, the vinegar products obtained from the different substrates were evaluated for their quality, including organoleptic properties, which showed the superior quality of wood-treated vinegar samples with respect to neat vinegar samples.

Keywords: *Acetobacteraceae*, vinegar, acetous fermentation, wood treatment, polyphenols

OPEN ACCESS

Edited by:
Maria Gullo,
University of Modena and Reggio Emilia, Italy

Reviewed by:
Ilkin Yucel Sengun,
Ege University, Turkey
Tiziana Nardi,
Council for Agricultural and Economics Research (CREA), Italy
Teresa Zotta,
University of Basilicata, Italy

***Correspondence:**
Francesca Gaggìa
francesca.gaggia@unibo.it

Specialty section:
This article was submitted to Food Microbiology, a section of the journal Frontiers in Microbiology

Received: *16 March 2022*
Accepted: *23 June 2022*
Published: *19 July 2022*

Citation:
Mizzi J, Gaggìa F, Bozzi Cionci N, Di Gioia D and Attard E (2022) Selection of Acetic Acid Bacterial Strains and Vinegar Production From Local Maltese Food Sources. Front. Microbiol. 13:897825. doi: 10.3389/fmicb.2022.897825

INTRODUCTION

Vinegar production is a millennia-old process. Vinegar is an acidic liquid resulting from a two-step fermentation process, in which a microbial consortium mainly consisting of *Saccharomyces cerevisiae* and acetic acid bacteria (AAB) transforms any edible carbohydrate-rich source into a liquid food rich in acetic acid (Garcia-Parrilla et al., 2017). Beyond its food preservative action, vinegar possesses some health properties (Ho et al., 2017). The acetic acid bacteria (AAB) are known as highly versatile microorganisms of great biotechnological relevance. They are Gram-negative or Gram-variable, ellipsoidal to rod-shaped cells, and have an obligate aerobic metabolism with oxygen as the terminal electron acceptor. In the first classification of AAB, two main genera were determined as *Acetobacter* and *Gluconobacter*, but currently, more than 12 genera are recognized and included within the family *Acetobacteraceae*. These microorganisms can produce high concentrations of acetic acid from ethanol, which makes them important to the vinegar industry (Sengun and Karabiyikli, 2011). The acetic acid produced by AAB during vinegar production is responsible for its characteristic aroma; AAB strongly influence the quality of vinegar, although the final quality is a result of a combination of factors, such as the raw material, technological process, and wood contact if vinegar undergoes aging step (Tesfaye et al., 2002). Two

standard systems are applied for vinegar brewing: solid-state fermentation, mostly used in Asian countries, and liquid fermentation, particularly developed in Western countries. Vinegar in Europe is mainly produced by the submerged system through an aerobic process by which the ethanol in liquids (spirits, wine, or cider) is oxidized to acetic acid by AAB, in controlled stirring conditions (Gullo et al., 2014). The most common vinegar on the EU market derives from the fermentation of white and/or red grapes and apples, but interest in other substrates is on the increase. The attention is mainly focused on surpluses of vegetables (second quality for size or shape) and waste of sugar-rich foods, which could be a potential source for vinegar production. Waste utilization in the fruit and vegetable processing industry is an important challenge for governments to address, in an attempt to sustain a natural balance in the future (Roda et al., 2017). Some successful attempts have been performed with strawberries (Ubeda et al., 2013), pepper leaves (Song et al., 2014), blueberry, pineapple (Roda et al., 2017), orange fruits (Davies et al., 2017), pomegranate (Kharchoufi et al., 2018), mango, and papaya (Bouatenin et al., 2021). Grapevine cultivation dates back to millennia in the Maltese Islands; the two main autochthonous grapevine varieties are Gellewza and Girgentina. The production of vinegar from grape wine is mainly used for the preservation of the Maltese cheeselet called "gbejna," which is pickled for around 24 h and then coated with coarsely ground black pepper (Morales et al., 2017). Typically, vinegar is produced from Maltese grapes. Substrates other than grapes were not very popular in the past, locally. The main objective of this study was to isolate new AAB strains from local niche habitats (berries from grape vines and locally produced vinegar) to exploit the local biodiversity within AAB in order to obtain strains that can be adapted to the fermentation of local substrates. The selected strains were utilized to develop an efficient reliable two-stage fermentation process to produce vinegar from locally available raw fruit and vegetable materials (e.g., figs, prickly pears, onions, tomatoes, and honey, apart from grapes). The island of Gozo, in fact, is rich in agri-food wastes; overproduction, damaged vegetables, and honey not suitable for human consumption can be recovered and used as substrates, limiting the amounts of waste.

MATERIALS AND METHODS

Grapes and Vinegar Samples

Mature grape berries and vinegar samples from the cottage industry were collected throughout the Island of Gozo (Malta) in sterile stomacher bags and 500 ml sterile jars, respectively. The grape samples were collected over two seasons, summer 2013 and summer 2014, while the vinegar samples were collected between these two harvests. Sampling sites and the number of samples are described in **Table 1**. The grape berries (500 g) were collected the week before harvest. In mono-varietal vineyards, sampling was carried throughout the field following the "W" shape collection method, whereas in multi-varietal fields, a random vine was chosen as the source of sampling. In the case of isolated indigenous vines at the boundaries of the field, whole grape bunches were collected from the same vine. Random vinegar samples were collected directly from the surface of the active fermenting containers with the slow traditional static method. The fermenting vat was topped up from time to time with wine usually left over at the bottom of the barrels (the last few centimeters), as this wine may contain some sediment. These collected samples bridged the cottage production of vinegar with laboratory-produced vinegar. The collected samples were stored in insulated containers with ample oxygen by transporting them in sample bottles with large headspace (350 ml sample in 500 ml jar) and induced agitation (hanging container) to favor a rich supply of dissolved oxygen.

TABLE 1 | Site of grape and vinegar sampling in the Island of Gozo, Malta.

Site of isolation		Year of sampling	Grape samples	Vinegar samples
North	Ghasri, Zebbug, Xaghra	2013–2014	/	7
East	Nadur, Qala, Ghajnsielem	2013–2014	13	4
South	Munxar, Sannat, Xewkija	2013–2014	3	3
West	Gharb, San Lawrenz, Kercem, Santa Lucija	2013–2014	13	14
Center	Rabat, Fontana	2013–2014	6	4

AAB Isolation and Culturing

Isolation From Grape Berries

To ∼50 g of berries, 47 ml of sterile distilled water and 3 ml of filtered absolute ethanol (99.8%; Sigma-Aldrich; Milan, Italy) were added. The suspension was mixed for 1 min, using the Seward Stomacher 400 (Seward Ltd, Technology Center, Worthing, West Sussex, UK) and incubated at room temperature for 7 days (Gullo et al., 2009). The obtained enrichment was inoculated on the surface of Glucose-Yeast-Extract-Calcium Carbonate Agar (GYC medium; glucose 5%, yeast extract 1%, CaCO3 1%, agar 1.5%, pH 6.8 ± 0.2; Scharlau Microbiology, Barcelona, Spain) supplemented with 100 mg/l of natamycin (Sigma-Aldrich, cod.: 32417) to inhibit fungal growth and incubated at 30°C for 5–10 days (Sengun and Karabiyikli, 2011). If no growth was noted, the enrichment broth was centrifuged, and inoculum from the sediment was streaked again on the GYC media plates. Where there was an overgrowth, a 1:10 dilution method up to five log reduction was applied. Tiny colonies with a clear halo were re-streaked onto WL nutrient agar (Oxoid, Ltd., Basingstoke, Hampshire, England), supplemented with cycloheximide (2 mg/l) (Sigma-Aldrich), and incubated at 25°C for 42–72 h. Colonies with a yellow halo were selected for further analysis and named with the prefix "G."

Isolation From Vinegar

About 10 ml of each vinegar sample was inoculated in 30 ml sterile nutrient broth (Sigma-Aldrich, Milan, Italy) with the addition of filtered absolute ethanol and acetic acid (Sigma-Aldrich, Milan, Italy) to obtain a final concentration of 2 and 1%, respectively. The broth suspension was then incubated for 7 days at room temperature, then sub-inoculated onto AE agar medium

(Entani et al., 1985) supplemented with natamycin (100 mg/l) and incubated at 30°C for 2–7 days. If no growth resulted on the sub-inoculated agar after 7 days, further AE medium plates were streaked and incubated for 7 days. This step was repeated three times at 7 days of interval before repeating the whole process on a fresh vinegar sample. When growth occurred, small colonies were re-streaked on WL nutrient agar (Scharlau Microbiology) supplemented with cycloheximide (2 mg/l) (Sigma-Aldrich) and incubated at 25°C for 48–72 h. Colonies were frozen for further analysis and named with the prefix "V."

Phenotypic and Genotypic Characterization of Isolated Strains

The fresh colonies were first characterized by Gram staining (Silva et al., 2006). The oxidase test was then performed using the Microbact Oxidase strips (Oxoid, Milan, Italy), and for the catalase test, colonies were placed onto a clean slide with a drop of a freshly prepared solution of 3% H_2O_2. Among all isolates, those being Gram-negative, oxidase-negative, and catalase-positive were purified by streak-plate technique and stored at 4°C on WL nutrient agar supplemented with cycloheximide (2 mg/l) and sub-inoculated every 6–8 weeks on the same medium. All isolates were also stored at −80°C. A single colony from an overnight culture (WL nutrient agar at 30°C) was picked up and suspended in 500 μl of sterile distilled water. The DNA extraction was carried out using the InstaGene Matrix kit (Bio-Rad, Milan, Italy) following the manufacturer's instructions. Extracted DNA was used for the amplification of the 16S rRNA gene with primers 27f (5′-GTGCCAGCAGCCGCGG-3′) and 1492r (5′-TACGGYTACCTTGTTACGACTT-3′), according to Gaggìa et al. (2013). The restriction analysis of amplified 16S rRNA (ARDRA) was performed according to Di Gioia et al. (2002). The reaction was performed by mixing 10 μl of PCR product, 17 μl of deionized water, 2 μl of 10X restriction buffer, and 1 μl of the enzyme (*Alu*I and *Hae*III; Thermos Fisher) and incubating at 37°C for 10 min. The enzymes were then inactivated by heating the reaction mixture to 65°C for 15 min. The reaction products were analyzed by agarose (2% w/v) gel electrophoresis and visualized with the gel acquisition system Gel DocTM XR (Bio-Rad). The purified PCR products of the representative strains obtained from the ARDRA analysis were delivered to Eurofins MWG Operon (Ebersberg, Germany) for sequencing. Sequence chromatograms were edited and analyzed using the software programs Finch TV version 1.4.0 (Geospiza Inc., Seattle, WA, USA). DNAMAN software (Version 6.0, Lynnon BioSoft. Inc., USA) was used to obtain consensus sequences that were processed for the species assignment through the GeneBank Database (NCBI), by using the nucleotide BLAST (Basic Local Alignment Search Tool; http://www.ncbi.nlm.nih.gov/BLAST/). The relatedness of the isolated strains within the Acetobactereaceae family was achieved with a phylogenetic tree reconstructed by sequence alignment, using the Neighbor-joining (NJ) algorithm (Saitou and Nei, 1987) and Mega version 5.0 (Tamura et al., 2011). The bootstrap values were calculated based on 1,000 replications in order to evaluate the confidence levels of the nodes.

The Raw Substrates for Vinegar Production

For this study, the choice of the raw materials (locally grown grapes, honey, onions, figs, prickly pears, and tomatoes) was based on their availability and their potential exploitation for vinegar production. On the island of Gozo, farmers grow a large number of international and local grape varieties. However, the indigenous varieties contain a low sugar content (15–19% brix) when mature (Theuma et al., 2015), compared to locally grown international varieties (21–25/26%) (Herrera et al., 2003; Fernández-Novales et al., 2009). The international variety chosen for this study was the Primitivo variety, which occupies 12 tumoli of land utilized for grapevine production (Monte, 2013). Another typical agricultural product, unique to the Maltese Islands is honey (Attard and Mizzi, 2013). Although honey is a sought-after product (Attard and Douglas, 2017), by-products of honey extraction and honey left over in hives for extended periods are not fit for direct human consumption and may be considered as a potential starting material for vinegar production. Hence, it can be diluted to obtain a brix content of 18% solution and fermented. One of the main crops that has made it to international markets is the onion. However, high quality for export has been achieved by grading onions by appearance and size. Over-sized onions, which may result due to abundant precipitation, may be crushed and used for vinegar production. The fig tree is renowned for its delicate fruit, which tends to spoil easily and reach maturity over a short period of time. Unless preserved at cool temperatures (Owino et al., 2004), this fruit perishes quickly, hence its potential use for vinegar production. Locally, the prickly pear is primarily used as a wind breaker at the boundaries of fields. Unlike its use as a crop in most Mediterranean countries, locally the prickly pear is an underutilized crop, which may be considered as a candidate for vinegar production. The island of Gozo is also renowned for its tomato industry, which is supported by financial grants or other forms of assistance to farmers. Being one of the major cash crops, its production, at times, is very abundant and hence its potential use as a fermentable substrate.

Fermentation Processes

The alcoholic and acetic acid fermentations proceeded separately according to the scheme shown in **Figure 1**. Locally grown grapes, figs, honey, onions, prickly pears, and tomatoes were chosen as substrates for the fermentation process. These raw materials were crushed, where applicable, using a traditional wine grape crusher. In order to standardize the sugar content of the substrates and obtain the desired brix value, either dilution with deionized water (as in the case of honey) or chaptalization (the addition of beetroot sugar and water) was performed. The resultant liquid ready for fermentation was denominated as wort (Grieson, 2009). The grape samples were processed immediately after collection to retain the highest level of the desired microorganisms present on the berries, without inducing any viable but non-culturable state.

Alcoholic Fermentation

Fifteen-liter food-grade plastic containers were used as bench fermenters. About 12 L of wort were prepared for each substrate, leaving ample headspace for any frotting or possible floating that

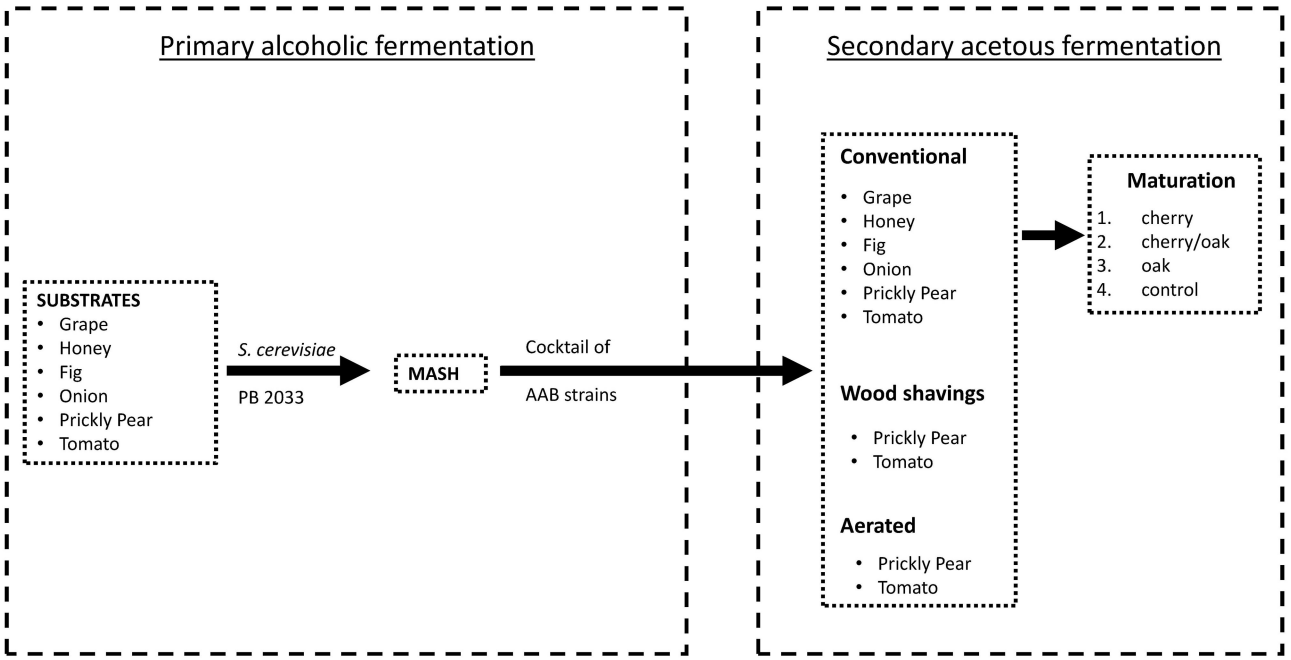

FIGURE 1 | Schematic representation of both alcoholic and acetous fermentations.

might take place. Nutriferm Vit (Supervit, Enartis, Novara, Italy) was added to guarantee the correct nitrogen supply at 0.1% (w/v), according to the manufacturer's instructions. Pectolytic enzymes (Endozym Cultivar, Pascal Biotech, Brescia, Italy) were also added at 2 g/hl. *Saccharomyces cerevisiae* PB 2033 (Collection de Levures d'Intérêt Biotechnologique, CLIB; INRA, Paris, France) was regenerated and inoculated into the substrate. The initial yeast inoculum was 2% (V/V) of a 0.5 McFarland suspension. The content of total soluble solids (TSS) of the raw material and wort was measured by using a refractometer (Brix %) (Atago 2363, Atago Co. Ltd., Japan). The fermentation progress was followed by reading the specific gravity (S.G.) using a hydrometer for rapid and easy estimation of the alcohol produced as the fermentation proceeded. When the S.G. value of about 1.020 was reached, the sugar to alcohol conversion was almost complete. At this point, this alcoholic liquid or mash was used for the acetous fermentation.

Acetous Fermentation

The secondary acetous fermentation was performed as described in **Figure 1**. The mash of grapes, honey, figs, onions, prickly pears, and tomatoes was inoculated with a consortium of selected AAB, following isolation and identification. The cocktail of AAB (*A. pasteurianus* V20, *K. saccharivorans* G1 and G10, *G. oxydans* G21, and *Gluconobacter japonicus/frauterii* G22) was prepared by sub-culturing the individual strains on a culture broth composed of yeast extract 1.0% (Sigma-Aldrich), K_2HPO_4 0.1% (Sigma-Aldrich), $MgSO_4.7H_2O$ 0.02% (Sigma-Aldrich), and ethanol 4% (Sigma-Aldrich) and incubated at room temperature for 48 h and then using an equal amount of each culture to inoculate the fermenters. The 3-L bench fermenters were filled with the mash substrate and covered with a cheese cloth to allow the fermentation, and the alcoholic degree was adjusted between 7 and 10% (Cirlini, 2008). A nutrient mixture (Acetozym DS plus2, Heinrich Frings GmbH & Co. KG, Rheinbach, Germany) was dissolved in the mash at a rate of 0.1%. Every fermentation was carried out in triplicates, having three cycles per treatment. The mash substrates of prickly pear and tomato were also subjected to two further acetous fermentation processes. (a) The use of wood shavings, where a fermenter with pre-sterilized beech wood shavings is utilized to carry out fermentation. The wood chips were placed in a pot, covered with ample water, brought to boil, and simmered for 2 h. When the wood shavings cooled to room temperature, they were added to the fermenter at a rate of 2% (w/v). (b) By aeration, where the fermenter was subjected to aeration using a regulated air pump at a constant rate of 0.25 l min^{-1}. Conventional, wood shavings, and aerated fermenters were allowed to ferment simultaneously. Acetic acid bacteria were adapted to the new substrate prior to the fermenters with discharging and recharging cycles, according to the methods described by Singh and Singh (2007) and Krusong and Vichitraka (2010). Each bench fermenter was monitored for temperature changes every 30 min using Nova 5000 MultiLogPRO data loggers (Fourier Systems Ltd., Illinois, USA), while the pH and the acidity values were recorded on a daily basis by titration against 0.5 N NaOH (Sigma-Aldrich Chemie GmbH, Steinheim, Germany) and using phenolphthalein as indicator. All bioreactors were repetitively batch fermented, initiated at 3% acidity and proceeded to about 5% acidity, discharged one-third

to half the volume, and replenished with more mash and nutrients to repeat the cycle.

Vinegar Maturation by Accelerated Aging

Four 700 mL samples of each vinegar produced from the conventional fermentation process were poured into 750 mL jars and were labeled according to the wood chips introduced: cherry, a mixture (1:1) of cherry and oak, oak, and neat (control). French oak and American cherry were used (I V Portelli & Sons Ltd, Rabat, Malta). The wood was first treated by submerging and stirring for 30 min in the respective vinegar, then drained off, and allowed to dry. The rate of application of wood chips was 2% (Tesfaye et al., 2004). After 15 days, the six vinegar samples from the conventional fermentation were transferred to new jars using a stainless steel colander to remove the wood chips and re-labeled according to the type of wood it has been matured in.

Physicochemical Analysis

Apart from the *in situ* tests like the total soluble solids (Brix %), acidity, pH, and specific gravity, the rest of the analyses were carried out on the mature batches. These analyses included the Folin-Ciocalteu method for total polyphenols as described by Attard (2013) and the anthocyanin content using UV-Vis spectrophotometric analysis at A420/A520 (Ivanova et al., 2010; Theuma et al., 2015). The samples collected at different stages of both fermentations and after maturation in wood were stored at 4 $\pm$1°C to be processed together. The acidification rate was calculated as described by Ndoye et al. (2007). The analysis was performed in triplicate.

Organoleptic Evaluation

The six panelists, who volunteered for the sensory analysis, had extensive expertise in vinegar-based sauce tasting. The participants were briefed on the specific sensorial parameters, which were pungency, winy character, ethyl acetate, wood, sweet aroma, and general impression. The panelists had to taste one set of vinegar samples (control and wood matured vinegar for each of the six substrates) at a time to evaluate the attributes, according to Tesfaye et al. (2010). The participants were instructed to judge the vinegar samples, and the data obtained from the sensory analysis were expressed numerically on a 10-point hedonic scale (one being the least acceptable and 10 being the most pleasant) and tabulated accordingly. Standard solutions for these attributes were also provided as reference points, to obtain a coherent evaluation of the sensory characteristics of the attributes (Chambers and Koppel, 2013). The results were grouped into five categories with outstanding for points 9–10, standard vinegar for 7–8.99, commercial for 5–6.99, below commercial for 3–4.99, and spoiled for 1–2.99, according to Kocher et al. (2012).

Data Collection and Analysis

The datasets generated from the fermentation monitoring analysis and batch analysis of samples were tabulated. The data collected from the questionnaire and from the organoleptic evaluation were expressed numerically and tabulated accordingly. The statistical analysis was performed by using the Statistical Package for Social Sciences (SPSS) V20 and XLSTAT version 2014.4.04 (Addinsoft). Analysis of variance (one-way ANOVA) and the Bonferroni *post-hoc* test were carried out to determine any significant differences between the mean values of the different treatments. The *p*-values obtained for correlations between the different variables were computed by the chi-square and the Friedman tests depending on the data type being analyzed. Principal component analysis with Pearson correlation statistics was carried out to determine any potential clustering of samples based on their characteristics. The level of significance was considered at $p \leq 0.05$.

RESULTS

Strain Isolation and Genotypic Identification

The colonies that were able to grow in the GYC plates and identified as Gram-negative, oxidase-negative, and catalase-positive were subcultured onto WL agar for further characterization. Overall, 32 presumptive AAB strains were isolated from grapes harvested in 2014 and grapes harvested in 2013 and vinegar samples. The fingerprinting analysis by ARDRA and the further 16S rRNA sequencing allowed for discrimination among the isolates. **Supplementary Figures 1**, **2** show electrophoretic gels of the restriction profiles of the 30 strains (two of the samples failed to grow when sub-inoculated) with *Alu*I and *Hae*III enzymes. The fingerprinting analysis evidenced that restriction enzymes produced three groups for *Alu*I and four groups for *Hae*III (**Supplementary Table 1**), with five representative strains to be sequenced (G2 restriction analysis with *Hae*III was repeated and the profile fell within cluster three). The sequencing led to species identification as presented in **Table 2**. All the bacteria were confirmed to belong to *Acetobacteraceae,* in particular to *Komagateibacter* spp. (strains G1 and G10), *Gluconobacter* spp. (strains G21 and G22), and *Acetobacter* spp. (strain V20). Species assignment was unique except for some strains. The sequences were then used to construct the phylogenetic tree (**Figure 2**) that clearly shows the different grouping of the samples and their relatedness within the *Acetobacteraceae* family. Most of the isolates (cluster 1) correspond to *Komagataeibacter* spp. In particular, all the investigated strains were found to belong to *Komagataeibacter saccharivorans*. Clusters 2 and 3 correspond to *Gluconobacter oxydans* and *Gluconobacter japonicus/frateurii*, respectively. The strain V20, whose profile with *Alu*I differs from the common pattern identified with *Hae*III, is 100% closely related to *Acetobacter pasteurianus*. These are all species commonly associated with vinegar production (Luzón-Quintana et al., 2021). *Komagataeibacter* spp., prior to the re-classification (Euzéby, 2013), formed part of the *Gluconacetobacter* and *Acetobacter* genera (Yamada et al., 2012) that were described as the major acetic acid producers in industrial vinegar fermenters with a propensity to tolerate relatively high (>6%) acetic acid concentrations (Schüller et al., 2000; Matsutani et al., 2011; Slapšak et al., 2013). Moreover, *K. saccharivorans,* together with *K. xylinus*, is reported as a major bacterial cellulose-producing species (La China et al., 2021). The isolates came from different

TABLE 2 | Best-match identification phylotypes of purified PCR products deriving from the 16S rRNA amplification of the isolated strains.

Strain ID	Location	Identification	Similarity (%)	Accession Number*
G1	Rabat	*Komagataeibacter saccharivorans*	99	OM984645
G10	Sannat	*Komagataeibacter saccharivorans*	100	OM984646
G21	Kercem	*Gluconobacter oxydans*	99.8	OM984648
G22	Qala	*Gluconobacter frateurii, japonicus*	99	OM984649
V20	Gharb	*Acetobacter pasteurianus*	100	OM984647

*Provided by GeneBank (https://www.ncbi.nlm.nih.gov/genbank/).

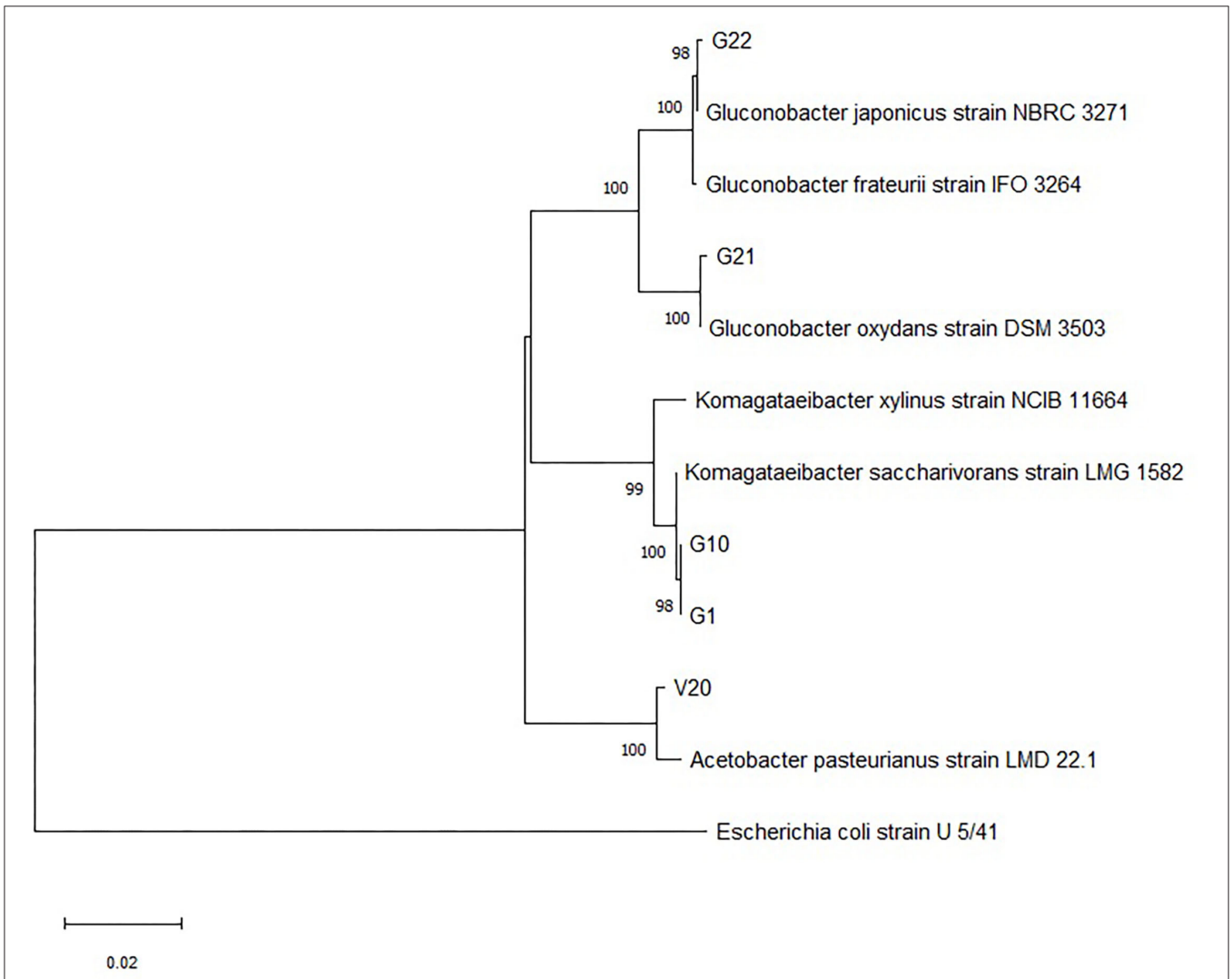

FIGURE 2 | Phylogenetic tree showing the location of the selected strains based on 16S rDNA gene sequences, using the neighbor-joining (NJ) algorithm and Mega version 5.0. The tree was rooted using sequences of *Acetobacteraceae* present in the NCBI database, and *Escherichia coli* U5/41 was used as an outgroup. Bar scale indicates phylogenetic distance. The numbers at the branches represent bootstrap values (100 bootstrap re-sampling).

samples of grape and vinegar. The grape samples were of a foreign origin, relatively recently imported vines, and isolations came from white table grapes and red wine grapes. Some samples were of an unknown local variety, one red table grape variety, and the other white wine/table grape variety, respectively. Their location varied from west to east of the island, showing that these *Acetobactereaceae* species are well-established and ubiquitous. The isolates from the vinegar samples came from the

village of Gharb on the west side of the island except for V21 whichoriginated from Munxar. The cluster associated with *G. oxidans* comprises strains from both healthy and spoiled grapes; *G. oxidans* G11 was sampled together with G12 and V2 (*K. saccharivorans*), and they all were sourced from the same farmer who has been cultivating his own grapes and producing vinegar for decades. There is a variation in species that demonstrates how the environmental conditions dictate the type of indigenous microbiota by which the local vinegar products are produced, in accordance with Solieri and Giudici (2009), Sengun (2015). *Gluconobacter* spp. show a weak resistance to acetic acid (Prust et al., 2005; Matsutani et al., 2011). The dehydrogenase enzyme in the cell membrane facilitates its survival in nutrient-rich environments and can metabolize sugars (Moonmangmee et al., 2000; Adachi et al., 2003) and sugar acids, which other organisms cannot assimilate. It can be also found in beverages like wines and beers, and also in soft drinks, causing spoilage and off-flavors (Prust et al., 2005). The last cluster is ascribed to *Gluconobacter japonicus*/*frauterii*; the identification score did not allow a clear assignment to a species. *G. japonicus* is able to metabolize a wide range of saccharides for the production of acid. Fructose, sorbitol, glycerol, sucrose, and ethanol are weakly metabolized into acid (Malimas et al., 2009). *G. frateurii* produces acids from saccharides including sucrose but not from fructose, lactose, dulcitol, and arabinose (Kommanee et al., 2012). This group of isolates came both from the western part and from the eastern side of the island. In this instance, grapes were of the white local varieties. *Acetobacter pasteurianus* V20 was isolated from a red wine vinegar sample collected from Gharb. Strains of *Acetobacter pasteurianus* species is a highly adaptable AAB (Azuma et al., 2009) and is a major protagonist in traditional vinegar productions with acetic acid concentrations up to 6% (Ilabaca et al., 2008; Matsutani et al., 2011; Vegas et al., 2013). Gullo et al. (2009) in their investigation of species shift during the acetification process, concluded that *A. pasteurianus* can tolerate high concentrations of alcohol and thus is more adapted to the startup of the acetous fermentation. Two less sought attributes for vinegar production for this organism are its ability to over-oxidize the acetic acid to carbon dioxide and water (Matsutani et al., 2011), and to synthesize bacterial cellulose (Azuma et al., 2009). A mixture of the strains *A. pasteurianus* V20, *K. saccharivorans* G1 and G10, *G. oxydans* G21, and *Gluconobacter japonicus*/*frauterii* G22 was used, considering the change of acetic acid concentration during the fermentation process. The inoculation of the mash with a co-culture of the selected strains is often performed in vinegar production, considering that the fermentation is carried on by a succession of strains and species, depending on the concentration of acetic acid (Vegas et al., 2010). At low concentrations of acetic acid, species of the genus *Acetobacter* predominate. When acetic acid concentrations exceed 5%, the species belonging to the *Komagataeibacter* or *Gluconacetobacter* genera predominate (Mas et al., 2014). Their individual fate and persistence, as well as their individual features, were not investigated in this study; the fermentation was simply stopped at the desired acidity level.

Fermentation Process

Alcoholic and Acetous Fermentation

The primary alcoholic fermentation of grape, fig, honey, onion, tomato, and prickly pear was performed with the chosen yeast culture, and the conversion of the sugars into alcohol lasted for a few days. There were no distinctive characteristics for the different fermentations that progressed quite uniformly for all the substrates. The TSS content of the raw substrates and the wort, and the specific gravity readings of the wort and the mash are listed in **Table 3**. The acetous fermentation process for the different mash treatments is shown in **Table 4**. The acidity and pH values were monitored for three cycles as the fermentation proceeded (**Supplementary Figures 3–5**). Honey and onion matrices required ∼9.6 days for complete fermentation, whereas grape, prickly pear, and tomato wines required 3–5 days. The honey, onions, and grapes were less acidic than the other two substrates, and this resulted in the final acidity obtained at the end of the fermentation process. Considering pH, there were no significant differences between the initial and final pH values obtained for all substrates (**Table 4**). This suggests that pH does not provide a good indication of the fermentation progress. Due to the weak acidic nature of most organic acids, this can only be determined by considering the total acidity. In fact, the percentage acidity at the beginning and the end of the fermentation process is highly significant for all the substrates ($p \leq 0.0001$). The acetification rate varied for the different substrates (**Table 4**). All substrates exhibited different fermentation kinetics rates in terms of rate of acidity conversion and days of fermentation. In spite of the variation between the fermentation kinetics of the different substrates, intra-fermentation kinetics was relatively similar with a very small standard deviation for each individual substrate and treatment. The onions had the slowest conversion rate of 0.18 $\pm$ 0.02% day^{-1} with a long fermentation cycle of 9.67 $\pm$ 0.88 days, whereas the fastest rate was observed in the aerated tomato being 0.64 $\pm$ 0.13% day^{-1} with a very short fermentation cycle of 3.00 $\pm$ 0.00 days. The mean rate was 0.42 $\pm$ 0.15% day^{-1} (**Table 4**). The initial acidity of 3% and the final acidity of 5% were chosen to maximize the performance of acetic acid bacteria, as also recommended by Gullo et al. (2014). The fermentation results showed a consistent reproducibility independent of the substrate used. Another noticeable trend is that with each consecutive fermentation cycle, a relatively shorter time than the previous cycle was recorded, indicating an increase in the acetification rate, as the acetic acid bacteria strains were able to adapt and acclimatize to the priming of the fermenter with a fresh mash sample (**Supplementary Figures 3–5**). The successively shorter lag phase is concordant with De Ory et al. (2004), who performed the fermentations using different immobilization techniques. Correlations between pH and acidity were computed using Pearson correlation, showing a degree of inverse linear dependence between the two variables (**Supplementary Table 2**). The only exception was the prickly pear wood-treated acetous fermentation. This can be explained by the potential heterogeneous fermentation with the wood chips.

TABLE 3 | List of the raw substrates used in the primary alcoholic fermentation and pre-treatment; TSS % and S.G. readings of the wort and mash.

Raw substrate	*TSS %	Pre-treatment	TSS % wort	*S.G. wort	S.G. mash
Grape	24	Crushed fruits	24	1,090	1,015
Fig	12	Crushed fruits and added sugar	18	1,055	1,010
Honey	75	Dilution to 18% brix by deionized water	16	1,060	1,010
Onion	12	Peeled, sliced and adjusted brix to 18% by addition of sugar	18	1,065	1,015
Tomato	5.5	Crushed and adjusted brix to 18% by addition of sugar	18	1,075	1,000
Prickly pear	12	Peeled, crushed and adjusted brix to 18% by addition of sugar	19	1,080	1,010

**TSS %, total soluble solid percentage; *S.G., specific gravity.*

TABLE 4 | Days of fermentation and acidic parameters (initial/final % acidity, rate of acidity, and pH) along the acetous fermentation; values are mean ± standard deviation.

	Days of fermentation	Initial acidity	Final acidity	Rate of acidity (% day^{-1})	Initial pH	Final pH
Figs	3.00 ± 0.00	2.59 ± 0.60	4.93 ± 0.13*	1.66 ± 0.03	3.14 ± 0.05	2.86 ± 0.06^{ns}
Honey	9.67 ± 0.67	3.18 ± 0.17	5.44 ± 0.36*	0.23 ± 0.02	2.69 ± 0.02	2.46 ± 0.01^{ns}
Onions	9.67 ± 0.88	3.04 ± 0.03	4.73 ± 0.06*	0.18 ± 0.02	3.08 ± 0.05	2.86 ± 0.06^{ns}
Grapes	5.00 ± 0.00	3.13 ± 0.23	4.76 ± 0.07*	0.33 ± 0.02	3.10 ± 0.05	2.77 ± 0.01^{ns}
Pickly pears C	4.33 ± 0.33	2.94 ± 0.16	5.00 ± 0.09*	0.48 ± 0.04	2.73 ± 0.04	2.61 ± 0.01^{ns}
Pickly pears W	4.33 ± 0.33	2.94 ± 0.22	5.10 ± 0.30*	0.50 ± 0.04	2.72 ± 0.01	2.61 ± 0.03^{ns}
Pickly pears A	3.33 ± 0.33	2.97 ± 0.18	4.96 ± 0.35*	0.60 ± 0.04	2.72 ± 0.01	2.61 ± 0.03^{ns}
Tomatoes C	5.00 ± 0.00	2.53 ± 0.38	4.84 ± 0.31*	0.46 ± 0.02	3.02 ± 0.02	2.78 ± 0.02^{ns}
Tomatoes W	5.00 ± 0.00	2.62 ± 0.67	5.04 ± 0.22*	0.48 ± 0.05	3.03 ± 0.06	2.75 ± 0.03^{ns}
Tomatoes A	3.00 ± 0.00	2.97 ± 0.23	4.50 ± 0.42*	0.65 ± 0.12	2.99 ± 0.02	2.82 ± 0.05^{ns}

*C, Control; W, Wood; A, Aerated. Statistical analysis has been performed using one-way ANOVA followed by Bonferroni post-hoc test for initial and final comparisons of acidity and pH; significance: ns, not significant, *$p < 0.0001$.*

Vinegar Maturation by Accelerated Aging

The vinegar products produced from the six matrices with the conventional method were induced to accelerated aging by the addition of wood chips to the vinegar. The aerated and wood-fermented vinegar samples for prickly pear and tomato were not subjected to this accelerated aging in order to limit the variables and identify the cause of potential differences between the control (neat) vinegar and the vinegar subjected to accelerated aging with wood. For this study, standard French oak chips were employed together with cherry, as the latter imparts a sweet flavor to counterbalance the acidity of the vinegar. Changes in the vinegar samples after 15 days of contact time were validated by both organoleptic and instrumental analysis. **Table 5** shows the main physicochemical characteristics of vinegar products produced from the six different substrates (grape, fig, tomato, honey, onion, and prickly pear) with different woods used for the maturation process (cherry, cherry/oak, oak, and control). For each substrate, all four treatments were compared statistically for any differences, and then in turn for each treatment. Finally, all substrates were compared for statistical differences. The tonality ratio represents the mixture of a color with white. Values ranged between 1.54 and 5.56 with no statistical significance. In principle, the absorbance values at 420 nm did not contribute to the variation between the matrices and treatments. On the other hand, parameters that depended on the 520 and 620, such as color intensity and anthocyanin content, were significantly affected. The color intensity represents the summation of the three prime colors at wavelengths 420, 520, and 620 nm. Although the color intensity values ranged between 0.52 and 18.29 A, the fig vinegar (14.07–18.29 A) and the prickly pear vinegar (5.86-5.94 A) products were significantly different from the other vinegar products (values < 2.53A) ($p \leq 0.01$). These vinegar samples had intensely darker colors than the other vinegar samples. This was also reflected in the anthocyanin content. Values ranged between 1.32 and 67.40 mg/l. The most prominent vinegar samples were the ones obtained from figs (47.40–67.40 mg/l) and prickly pears (27.36–28.48 mg/l) when compared to the other samples (values < 12.37 mg/l) ($p \leq 0.01$). Most of the wood-treated vinegar samples exhibited a low anthocyanin content when compared to the respective control, especially for the grape vinegar. This is consistent with Cerezo et al. (2010), concluding that the anthocyanins decrease with time, probably due to polymerization. The wood-treated samples had a consistently high content of phenols released by the wood with peak values resulting in the oak-treated samples (**Table 5**). The concentrations increased after 15 days of contact time with wood chips, except for the fig vinegar, whose phenolic content for the oak-treated vinegar was the lowest in value than the original mash. This can be attributed to the interaction between the bacterial cellulose and the phenolic content, as the latter is sequestrated by the cellulose fibers. This is concordant with Tang et al. (2003), who demonstrated the hydrophobic interaction between polyphenols and cellulose. Thus, the freshly produced vinegar has to be filtered to remove the cellulose fibers, and the

TABLE 5 | Tonality ratio, color intensity, anthocyanin (mg/l), and polyphenolic (μg/ml) contents for the accelerated wood-aged vinegar samples.

Vinegar	Treatment	Tonality ratio	Color intensity	Anthocyanins (mg/l)	Polyphenols GAE[a] (μg/ml)
Figs	Control	3.15 ± 0.05	18.29 ± 0.27*	67.40 ± 0.99*	901 ± 13.2*
	Cherry	3.64 ± 0.17	14.96 ± 0.69*	51.11 ± 2.35*	910 ± 41.8*
	Cherry/Oak	3.67 ± 0.07	14.07 ± 0.25*	47.40 ± 0.84*	898 ± 16.0*
	Oak	3.68 ± 0.10	14.80 ± 0.41*	49.71 ± 1.36*	849 ± 23.3*
Tomatoes	Control	2.41 ± 0.01	0.84 ± 0.00	3.42 ± 0.02	135 ± 0.6
	Cherry	2.54 ± 0.20	1.05 ± 0.08	4.18 ± 0.32	164 ± 12.6
	Cherry/Oak	5.56 ± 0.03	0.52 ± 0.00	1.32 ± 0.01	187 ± 0.9
	Oak	2.24 ± 0.02	1.26 ± 0.01	5.37 ± 0.05	204 ± 1.7
Honey	Control	2.08 ± 0.09	2.53 ± 0.11	11.82 ± 0.51	210 ± 9.1
	Cherry	2.61 ± 0.02	2.06 ± 0.02	8.72 ± 0.07	288 ± 2.3
	Cherry/Oak	2.37 ± 0.02	2.30 ± 0.02	10.05 ± 0.09	295 ± 2.5
	Oak	2.60 ± 0.17	1.77 ± 0.11	7.32 ± 0.46	297 ± 18.8
Onion	Control	1.93 ± 0.02	1.54 ± 0.01	7.24 ± 0.06	241 ± 2.0
	Cherry	2.46 ± 0.06	1.48 ± 0.03	6.11 ± 0.14	283 ± 6.4
	Cherry/Oak	2.43 ± 0.18	1.30 ± 0.10	5.76 ± 0.43	291 ± 21.5
	Oak	2.00 ± 0.04	1.74 ± 0.04	8.20 ± 0.18	301 ± 6.4
Prickly pear	Control	1.94 ± 0.59	5.86 ± 1.79*	27.97 ± 8.55*	1,346 ± 411.5**
	Cherry	1.86 ± 0.10	5.90 ± 0.31*	28.48 ± 1.48*	1,701 ± 88.1**
	Cherry/Oak	2.00 ± 0.23	5.94 ± 0.70*	27.95 ± 3.25*	1,704 ± 198.3**
	Oak	2.05 ± 0.11	5.87 ± 0.32*	27.36 ± 1.50*	1,794 ± 98.5**
Grapes	Control	1.54 ± 0.05	2.20 ± 0.08	12.37 ± 0.43	329 ± 11.4
	Cherry	1.93 ± 0.05	1.99 ± 0.05	10.18 ± 0.24	375 ± 8.7
	Cherry/Oak	2.16 ± 0.06	2.09 ± 0.06	9.97 ± 0.28	466 ± 12.9
	Oak	2.14 ± 0.17	2.39 ± 0.19	11.23 ± 0.89	528 ± 41.6

*GAE, Gallic acid equivalents. Statistical analysis has been performed using one-way ANOVA followed by Bonferroni post-hoc test for multiple mean comparisons; significance: *$p < 0.01$; **$p < 0.001$.*

microbial activity has to be deactivated through pasteurization to impede the polyphenol–cellulose fiber interaction. This step favors the retention of the maximum amount of phenolic content within the vinegar. However, fig vinegar (849–910 μg/ml) and prickly pear vinegar (1,346–1,794 μg/ml) exhibited significantly higher polyphenolic content than the other vinegar samples (values < 528 μg/ml) ($p \leq 0.01$ and $p \leq 0.001$). The correlation between matrices and treatments with respect to physicochemical content will be discussed later on. One of the major factors determining the quality of vinegar is the aging in wooden casks. The release of aromatic phenolic compounds from the wood, as it happens in the majority of the vinegar samples considered in this study, is higher in aged vinegar (Tesfaye et al., 2003, 2009; Callejón et al., 2010; Cerezo et al., 2010; Hidalgo et al., 2010). Moreover, the application of oak chips was found to accelerate the aging process, as reported by several authors (Tesfaye et al., 2003, 2009; Guerrero et al., 2011). Callejón et al. (2010) concluded that the preferred wood types for inducing aging in vinegar are oak and cherry for their rich, distinctive aromatic characteristics, particularly vanilla and wood correlated with oak, and red fruits and sweet with cherry (Mas, 2008). The presence of anthocyanins and other phenolic compounds in the finished product is directly related to the substrate type, maceration time, temperature, process method, sulfur dioxide presence, and alcohol content of wine among others, as confirmed by Dallas and Laureano (1994). Both these researchers and also Ivanova et al. (2010) concluded that the grape variety influences the level of the anthocyanins in the vinegar. The higher extractable anthocyanin portion is reflected in the chromatic characteristics of the final product. Thus, the level of anthocyanins in the finished product is not related to the high concentrations of anthocyanins in the berries but their extractability during the maceration process, as shown by Romero-Cascales et al. (2005). Most studies related to the anthocyanin content of vinegar are mostly based on the grape as substrate. There are very few studies showing this relationship with other substrates (Su and Silva, 2006; Wu et al., 2017; Chakraborty et al., 2018).

To further the investigation, correlation analysis was performed between phenolic compounds and the other parameters. Various cross-tab analyses were carried out to establish any correlation, both positive and negative, between the various datasets and establish any natural groups among the samples. The principal component analysis (PCA) was computed for the phenolic content, the anthocyanins, and the color intensity, as well as for the mean sensory evaluation of the vinegar sample. From the variables plot (**Figure 3A**), it can be assumed that there is a positive correlation between the color intensity and anthocyanin content ($r = 0.989$), as these all are clustered in one direction. For the principal components, F1 is represented by the physical properties of the non-flavonoids,

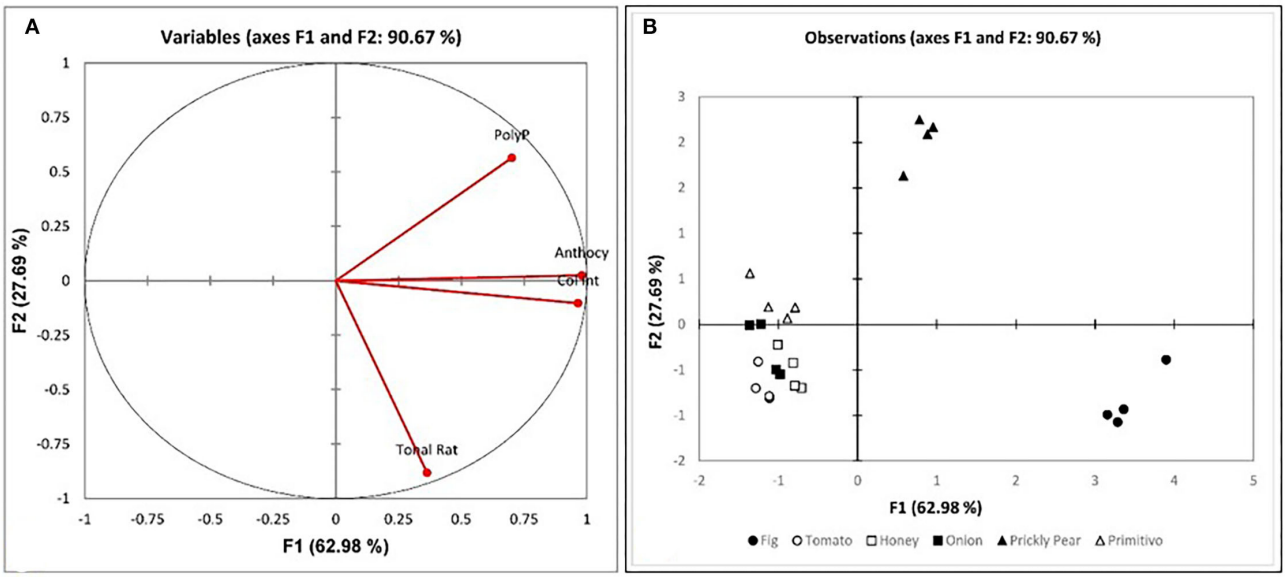

FIGURE 3 | PCA analysis of the physicochemical parameters by matrix; **(A)** Variables plot with percentages of data variability for different substrate ferments (the accelerated wood-aged vinegar samples) of 90.67% is accounted for; **(B)** Score plot of the physicochemical variables and the chemical components of the various substrates at the end of the fermentation.

including the phenolic acids and the flavonoids, i.e., the anthocyanins expressed as the color intensity and tonality. The F2 is represented by the chemical properties of the polyphenols. The clustering in the observations plot (**Figure 3B**) shows that while tomatoes, honey, grapes, and onions exhibited low values for anthocyanins (<12.37 mg/l), prickly pears and figs exhibited much higher values (>27.36 mg/l), and the honey correlated more strongly with the physicochemical tests, the acidity and pH. On the other hand, the prickly pear exhibited superior total polyphenolic content (>1,346.19%, w/w) when compared to all other matrices (<910.28% w/w). In addition to the physicochemical analyses, the organoleptic evaluation of the vinegar samples was performed. The results showed the distinction between the controls and the wood-treated vinegar samples, with the wood-treated vinegar being of a commercial grade, whereas all controls except for the fig were categorized as a domestic grade. The Pearson correlation coefficient (r) reveals a correlation between the wood and both the general impression and sweet aroma in **Figure 4A** ($r = 0.933$ and $r = 0.723$, respectively). This loading plot clearly demonstrated that the pungency is inversely correlated with the sweet aroma ($r = -0.502$). The reason behind this is that the wood-treated vinegar samples had the pungency masked by the mellower attributes the wood imparted into the vinegar, with the sweet aroma contributed by the wood, and the general impression giving the highest contrast. This is in accordance with Tesfaye et al.'s (2010) findings where the pungency correlated negatively with the sweet aroma sensation. The score plot in **Figure 4B** shows the position of the mean score obtained by the seven panelists for the neat and the accelerated wood-aged vinegar samples. The controls are clustered opposite the oak for the F1 axis. Apart from one cherry wood matured sample, all the other wood-treated vinegar samples give a higher score than the control or neat vinegar samples. Another distinctive clustering is observed in the neat vinegar samples and the cherry matured vinegar samples. However, the oak and cherry/oak treatments clearly exhibited a distinctive group. This confirms that the sweet cherry aroma and oak flavor released by the wood into the vinegar highly contrasts the pungent aroma and flavor of the neat vinegar samples.

CONCLUSION

This study aimed at describing the characteristics of vinegar produced from the available raw materials from local Maltese agricultural and food processing and retail facilities. The whole production process was considered step by step to identify the most efficient way forward. Autochthonous strains of AAB were isolated and used together as acetous fermentation starters. Finally, the qualities imparted by the wood maturation process were also investigated to complete the whole vinegar production process. Although the study did not rely on the appropriate selection of bacterial strains based on their functional and technological properties, it has demonstrated that all the substrates can be successfully employed in the production of vinegar, obtaining a product that is appreciated by consumers, complementing the vast list of condiments as part of the rich traditional Mediterranean culinary culture. The substrates can be both surpluses and/or by-products of a farm, food processing plants, food retail outlets, and food stores. Exploiting these materials and converting waste into a resource renders the

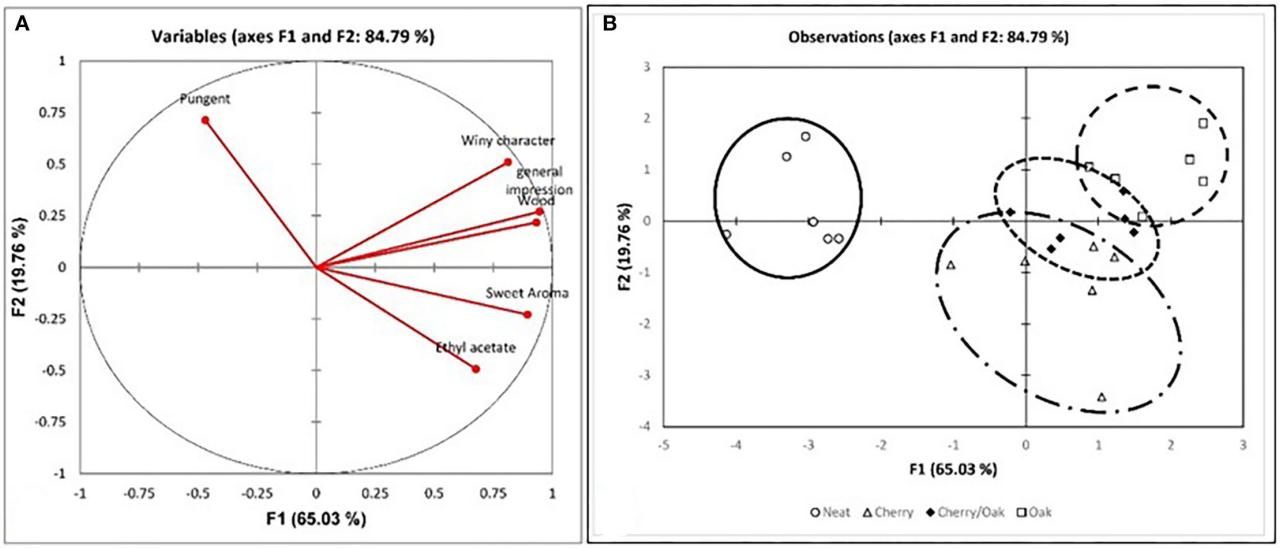

FIGURE 4 | PCA analysis for the sensorial parameters for the six matrices by treatment, i.e., control and three wood treatments. **(A)** Variables plot for the sensorial parameters with a total variance of 84.79%; **(B)** observations plot of the four vinegar samples (control and the accelerated wood-aged vinegar samples) for the six matrices.

system more sustainable not only for industry but also for the individual farmers, the cottage industry, and even a domestic application whereby the leftovers are utilized, reducing the load on the municipal refuse collection. Vinegar biotechnology is the result of environmental resources, culture, tradition, and science. The vast array of substrates from which vinegar can be produced leads the way for product diversification, based on the complex tasting habits of today's consumers, and it is the driving force for new product development with different organoleptic and sensorial characteristics. Although chaptalization can be somehow an added cost (when necessary), the use of different local raw materials, especially by-products of agro-industry, brand the local quality vinegar production as "zero kilometer" and sustainable, and the local vinegar production can be categorized as a low-carbon footprint niche industry with exponential growth potential.

DATA AVAILABILITY STATEMENT

The datasets presented in this study can be found in online repositories. The names of the repository/repositories and accession number(s) can be found at: NCBI GenBank–OM984645-OM984649.

AUTHOR CONTRIBUTIONS

JM and EA conceived the study, performed the chemical analysis, and prepared the statistical analysis. JM, FG, and NB carried out the microbiological analysis and sequence elaboration. JM, FG, NB, DD, and EA contributed to the writing of the paper. FG and DD critically revised the final manuscript. All authors contributed to the article and approved the submitted version.

ACKNOWLEDGMENTS

This paper is dedicated to Professor Bruno Biavati, microbiologist, who strongly believed in this work. He was affiliated with the University of Malta after retirement from the University of Bologna and was very keen on traditional Maltese food products and their transformation. This is a tribute to his research activity on fermented foods.

SUPPLEMENTARY MATERIAL

The Supplementary Material for this article can be found online at: https://www.frontiersin.org/articles/10.3389/fmicb.2022.897825/full#supplementary-material

Supplementary Figure 1 | Restriction profiles of isolated AAB strains with *Alu*I enzyme.

Supplementary Figure 2 | Restriction profiles of isolated AAB strains with *Hae*III enzyme.

Supplementary Figure 3 | Acidity and pH measures during three cycles of grape **(A)**, fig **(B)**, honey **(C)**, and onion **(D)** acetous fermentations.

Supplementary Figure 4 | Acidity and pH measures during three cycles of prickly pear (PP) acetous fermentations: control **(A)**, wood **(B)**, and aerated **(C)**.

Supplementary Figure 5 | Acidity and pH measures during three cycles of tomato (T) acetous fermentation: control **(A)**, wood **(B)**, and aerated **(C)**.

Supplementary Table 1 | Clustering of isolated strains based on ARDRA fingerprinting and restriction analysis with *Alu*I and *Hae*III.

Supplementary Table 2 | Pearson correlation values for the comparison between the pH and acidity at the beginning and end of the acetous fermentation.

REFERENCES

Adachi, O., Moonmangmee, D., Toyama, H., Yamada, M., Shinagawa, E., and Matsushita, K. (2003). New developments in oxidative fermentation. *Appl. Microbiol. Biotechnol.* 60, 643–653. doi: 10.1007/s00253-002-1155-9

Attard, E. (2013). A rapid Microtitre plate folin-ciocalteu method for the assessment of polyphenols. *Open Life Sci.* 8, 48–53. doi: 10.2478/s11535-012-0107-3

Attard, E., and Douglas, A. B. (2017). Physicochemical characterization of Maltese honey. *Honey Anal.* 8, 171–191. doi: 10.5772/66330

Attard, E., and Mizzi, J. (2013). Physicochemical characterization of gozitan honey. *Int. J. Food Stud.* 2, 180–187. doi: 10.7455/ijfs/2.2.2013.a5

Azuma, Y., Hosoyama, A., Matsutani, M., Furuya, N., Horikawa, H., Harada, T., et al. (2009). Whole-genome analyses reveal genetic instability of *Acetobacter pasteurianus*. *Nucleic Acids Res* 37, 5768–5783. doi: 10.1093/nar/gkp612

Bouatenin, K. M. J. P., Kouam,é, K. A., Gueu-Kehi, M. E., Djéni, N. T., and Djè, K. M. (2021). Organic production of vinegar from mango and papaya. *Food Sci. Nutr.* 9, 190–196. doi: 10.1002/fsn3.1981

Callejón, R. M., Torija, M. J., Mas, A., Morales, M. L., and Troncoso, A. M. (2010). Changes of volatile compounds in wine vinegars during their elaboration in barrels made from different woods. *Food Chem.* 120, 561–571. doi: 10.1016/j.foodchem.2009.10.026

Cerezo, A. B., Tesfaye, W., Soria-Díaz, M. E., Torija, J. M., Mateo, E. A., Garcia-Parrilla, M. C., et al. (2010). Effect of wood on the phenolic profile and sensory properties of wine vinegars during ageing. *J. Food Comp. Anal.* 23, 175–184. doi: 10.1016/j.jfca.2009.08.008

Chakraborty, K., Saha, S. K., Raychaudhuri, U., and Chakraborty, R. (2018). Vinegar from bael (*Aegle marmelos*): a mixed culture approach. *Ind. Chem. Eng.* 60, 384–395. doi: 10.1080/00194506.2017.1376601

Chambers, E., and Koppel, K. (2013). Associations of volatile compounds with sensory aroma and flavour: the complex flavour of nature. *Molecules* 18, 4887–4905. doi: 10.3390/molecules18054887

Cirlini, M. (2008). *Development of New Analytical Methods for the Characterization, Authentication and Quality Evaluation of Balsamic Vinegar of Modena*. [dissertation/PhD Thesis], Parma: University of Parma.

Dallas, C., and Laureano, O. (1994). Effect of SO_2 on the extraction of individual anthocyanins and coloured matter of three portugese varieties during winemaking. *Vitis* 33, 41–47.

Davies, C. V., Gerard, L. M., Ferreyra, M. M., Schvab, M. D. C., and Solda, C. A. (2017). Bioactive compounds and antioxidant activity analysis during orange vinegar production. *Food Sci. Technol.* 37, 449–455. doi: 10.1590/1678-457x.20816

De Ory, I., Romero, L. E., and Cantero, D. (2004). Optimization of immobilization conditions for vinegar production. Siran, wood chips and polyurethane foam as carriers for *Acetobacter aceti*. *Proc. Biochem.* 39, 547–555. doi: 10.1016/S0032-9592(03)00136-5

Di Gioia, D., Barberio, C., Spagnesi, S., Marchetti, L., and Fava, F. (2002). Characterization of four olive-mill-wastewater indigenous bacterial strains capable of aerobically degrading hydroxylated and methoxylated monocyclic aromatic compounds. *Arch. Microbiol.* 178, 208–217. doi: 10.1007/s00203-002-0445-z

Entani, E., Ohmori, S., Masai, H., and Suzuky, K. I. (1985). Acetobacter polyoxogenes sp. nov., a new species of an acetic acid bacterium useful for producing vinegar with high acidity. *J. Gen. App. Microbiol.* 31, 475–490. doi: 10.2323/jgam.31.475

Euzéby, J. (2013). List of new names and new combinations previously effectively, but not validly, published. Validation list no.149. *Int. J. System. Evol. Microbiol.* 63, 1–5. doi: 10.1099/ijs.0.049312-0

Fernández-Novales, J., L?pez, M. I., Sánchez, M. T., Morales, A. J., and González-Caballero, V. (2009). Shortwave-near infrared spectroscopy for determination of reducing sugar content during grape ripening, winemaking and aging of white and red wines. *Food Res. Int.* 42, 285–291. doi: 10.1016/j.foodres.2008.11.008

Gaggìa, F., Baffoni, L., Di Gioia, D., Accorsi, M., Bosi, S., Marotti, I., et al. (2013). Inoculation with microorganisms of *Lolium perenne* L.: evaluation of plant growth parameters and endophytic colonization of roots. *New Biotechnol.* 30, 695–704. doi: 10.1016/j.nbt.2013.04.006

Garcia-Parrilla, M. C., Torija, M. J., Mas, A., Cerezo, A. B., and Troncoso, A. M. (2017). "Vinegars and other fermented condiments," in *Fermented Foods in Health and Disease Prevention*, eds J. Frias, C. Martines-Villaluenga, and E. Peñas (Academic Press), 577–591. doi: 10.1016/B978-0-12-802309-9.00025-X

Grieson, B. (2009). "Malt and distilled malt vinegar," in *Vinegars of the World*, eds L. Solieri, and P. Giudici (Milano: Springer-Velag Italia), 135–143 doi: 10.1007/978-88-470-0866-3_8

Guerrero, E. D., Mejias, R. C., Marin, R. N., Bejarano, M. J. R., and Dodero, M. C. R. (2011). Accelerated aging of a sherry wine vinegar on an industrial scale employing microoxygenation and oak chips. *Eur. Food Res. Technol.* 232, 241–254. doi: 10.1007/s00217-010-1372-x

Gullo, M., De Vero, L., and Giudici, P. (2009). Succession of selected strains of *Acetobacter pasteurianus* and other acetic acid bacteria in traditional balsamic vinegar. *Appl. Environ. Microbiol.* 75, 2585–2589. doi: 10.1128/AEM.02249-08

Gullo, M., Verzelloni, E., and Canonico, M. (2014). Aerobic submerged fermentation by acetic acid bacteria for vinegar production: process and biotechnological aspects. *Proc. Biochem.* 49, 1571–1579. doi: 10.1016/j.procbio.2014.07.003

Herrera, J., Guesalaga, A., and Agosin, E. (2003). Shortwave-near infrared spectroscopy for non-destructive determination of maturity of wine grapes. *Meas. Sci. Technol.* 14, 689–697. doi: 10.1088/0957-0233/14/5/320

Hidalgo, C., Vegas, C., Mateo, E., Tesfaye, W., Cerezo, A. B., Callejón, R. M., et al. (2010). Effect of barrel design and the inoculation of *Acetobacter pasteurianus* in wine. *Int. J. Food Microbiol.* 141, 56–62. doi: 10.1016/j.ijfoodmicro.2010.04.018

Ho, C. W., Lazim, A. M., Fazry, S., Zaki, U. K. H. H., and Lim, S. J. (2017). Varieties, production, composition and health benefits of vinegars: a review. *Food Chem.* 221, 1621–1630. doi: 10.1016/j.foodchem.2016.10.128

Ilabaca, C., Navarrete, P., Mardones, P., Romero, J., and Mas, A. (2008). Application of culture culture-independent molecular biology based methods to evaluate acetic acid bacteria diversity during vinegar processing. *Int. J. Food Microbiol.* 126, 245–249. doi: 10.1016/j.ijfoodmicro.2008.05.001

Ivanova, V., Stefova, M., and Chinnici, F. (2010). Determination of the polyphenol content in macedonian grapes and wines by standardized spectrophotometric methods. *J. Serb. Chem. Soc.* 75, 45–59. doi: 10.2298/JSC1001045I

Kharchoufi, S.,Gomez, J., Lasanta, C., Castro, R., Sainz, F., and Hamadi, M. (2018). Benchmarking laboratory-scale pomegranate vinegar against commercial wine vinegars: antioxidant activity and chemical composition. *J. Sci. Food Agricul.* 98, 4749–4758. doi: 10.1002/jsfa.9011

Kocher, G. S., Dhillon, H. K., and Joshi, N. (2012). Scale Up of sugarcane vinegar production by recycling of successive fermentation batches and its organoleptic evaluation. *J. Food Process Preserv.* 38, 955–963. doi: 10.1111/jfpp.12050

Kommanee, J., Tanasupawat, S., Yukphan, P., Thongchul, N., Moonmangmee, D., and Yamada, Y. (2012). Identification of *Acetobacter* strains isolated in Thailand based on the phenotypic, chemotaxonomic and molecular characterisations. *Sci. Asia* 38, 44–53. doi: 10.2306/scienceasia1513-1874.2012.38.044

Krusong, W., and Vichitraka, A. (2010). An investigation of simultaneous pineapple vinegar fermentation interaction between acetic acid bacteria and yeast. *Asian J. Food Agro Ind.* 3, 192–203.

La China, S., Vero, L. D., Anguluri, K., Brugnoli, M., Mamlouk, D., and Gullo, M. (2021). Kombucha tea as a reservoir of cellulose producing bacteria: assessing diversity among komagataeibacter isolates. *Appl. Sci.* 11, 1595. doi: 10.3390/app11041595

Luzón-Quintana, L. M., Castro, R., and Durán-Guerrero, E. (2021). Biotechnological processes in fruit vinegar production. *Foods* 10, 945. doi: 10.3390/foods10050945

Malimas, T., Yukphan, P., Takahashi, M., Muramatsu, Y., Kaneyasu, M., Potacharoen, W., et al. (2009). *Gluconobacter japonicus* sp. nov., an acetic acid bacterium in the alphaproteobacteria. *Int. J. System. Evol. Microbiol.* 59, 466–471. doi: 10.1099/ijs.0.65740-0

Mas, A. (2008). *Wood Solutions to Excessive Acetification Length in Traditional Vinegar Production. Final Activity Report Winegar Project (Project Number 017269)*. Milano: Rovira Virgili University Spain. doi: 10.2147/IJWR.S4630

Mas, A., Torija, M. J., García-Parrilla, M. D. C., and Troncoso, A. M. (2014). Acetic acid bacteria and the production and quality of wine vinegar. *Sci. World J.* 2014, 394671. doi: 10.1155/2014/394671

Matsutani, M., Hirakawa, H., Yakushi, T., and Matsushita, K. (2011). Genome-Wide phylogenetic analysis of *Gluconobacter*, *Acetobacter*

and *Gluconacetobacter*. *FEMS Microbiol. Lett.* 315, 122–128. doi: 10.1111/j.1574-6968.2010.02180.x

Monte, L. G. (2013). *Winegrowing and Winemaking in Minor Islands of the Mediterranean*. Palermo: Priulla Printing Press. Available online at: www.progettopropmed.eu (accessed March 16, 2019).

Moonmangmee, D., Adachi, O., Ano, Y., Shinagawa, E., Toyama, H., Theeragool, G., et al. (2000). Isolation and characterisation of thermotolerant *Gluconobacter* strains catalyzing oxidative fermentation at higher temperatures. *Biosci. Biotechnol. Biochem*. 64, 2306–2315. doi: 10.1271/bbb.64.2306

Morales, M. B., Bintsis, T., Alichanidis, E., Herian, K., Jelen, P., Hynes, E. R., et al. (2017). "In global cheesemaking technology: cheese quality and characteristics," in *Chapter 4: Soft Cheeses (With Rennet)*, eds P. Papademas, and T. Bintsis (Ed: John Wiley and Sons) Part II, 301–321. doi: 10.1002/9781119046165.ch4

Ndoye, B., Lebecque, S., Destain, J., Guiro, A. T., and Thonart, P. (2007). A new pilot plant scale acetifier designed for vinegar production in Sub-Saharan Africa. *Proc. Biochem*. 42, 1561–1565. doi: 10.1016/j.procbio.2007.08.002

Owino, W. O., Nakano, R., Kubo, Y., and Inaba, A. (2004). Alterations in the cell wall polysaccharides during ripening in distinct anatomical tissue regions of the fig (*Ficus carica* L.) fruit. *Postharvest Biol. Technol.* 32, 67–77. doi: 10.1016/j.postharvbio.2003.10.003

Prust, C., Hoffmeister, M., Liesegang, H., Wiezer, A., Frike, W. F., Ehrenreich, A., et al. (2005). Complete genome sequence of the acetic acid bacterium *Gluconobacter oxydans*. *Nat. Biotechnol*. 23, 195–200. doi: 10.1038/nbt1062

Roda, A., Lucini, L., Torchio, F., Dordoni, R., De Faveri, D. M., and Lambri, M. (2017). Metabolite profiling and volatiles of pineapple wine and vinegar obtained from pineapple waste. *Food Chem*. 229, 734–742. doi: 10.1016/j.foodchem.2017.02.111

Romero-Cascales, I., Ortega-Regules, A., Lopez-Roca, J. M., Fernandez-fernandez, J. I., and Gomez-Plaza, E. (2005). Difference in anthocyanins extractability from grapes to wines aAccording to variety. *Am. J. Enol. Vitic*. 56, 212–219.

Saitou, N., and Nei, M. (1987). The neighbor-joining method: a new method for reconstructing phylogenetic trees. *Mol. Biol. Evol.* 4, 406–425.

Schüller, G., Hertel, C., and Hammes, W. P. (2000). *Gluconacetobacter entanii* sp. nov., isolated from submerged high-acid industrial vinegar fermentations. *Int. J. System. Evolut. Microbiol*. 50, 2013–2020. doi: 10.1099/00207713-50-6-2013

Sengun, I. K., and Karabiyikli, S. (2011). Importance of acetic acid bacteria in food industry. *Food Control* 22, 647–656. doi: 10.1016/j.foodcont.2010.11.008

Sengun, I. Y. (2015). "Acetic acid bacteria in food fermentations," in *Fermented Foods: Part 1. Biochemistry and Biotechnology*, eds D. Montet, and R. C. Ray (Boca Raton, FL: CRC Press), 91–111.

Silva, L. R., Cleenwerck, I., Rivas, R., Swings, J., Trujillo, M. E., Willems, A., et al. (2006). *Acetobacter oeni* sp.nov. isolated from spoiled red wine. *Int. J. System. Evolut. Microbiol.* 56, 21–24. doi: 10.1099/ijs.0.46000-0

Singh, R., and Singh, S. (2007). Design and development of batch type acetifier for wine-vinegar production. *Ind. J. Microbiol.* 47, 153–159. doi: 10.1007/s12088-007-0029-3

Slapšak, N., Cleenwerck, I., De Vos, P., and Trček, J. (2013). *Gluconacetobacter maltaceti* sp. nov., a novel vinegar producing acetic acid bacterium. *System. Appl. Microbiol*. 36, 17–21. doi: 10.1016/j.syapm.2012.11.001

Solieri, L., and Giudici, P. (2009). "Vinegars of the world," in *Vinegar of the World*, eds L. Solieri, and P. Giudici (Milan: Springer), 1–16. doi: 10.1007/978-88-470-0866-3_1

Song, Y. R., Shin, N. S., and Baik, S. H. (2014). Physicochemical properties, antioxidant activity and inhibition of α-glucosidase of a novel fermented pepper (*Capsiccum annuum* L.) leaves-based vinegar. *Int. J. Food Sci. Technol.* 49, 2491–2498. doi: 10.1111/ijfs.12573

Su, M. S., and Silva, J. L. (2006). Antioxidant activity, anthocyanins, and phenolics of rabbiteye blueberry (*Vaccinium ashei*) by-products as affected by fermentation. *Food Chem.* 97, 447–451. doi: 10.1016/j.foodchem.2005.05.023

Tamura, K., Peterson, D., Peterson, N., Stecher, G., Nei, M., and Kumar, S. (2011). MEGA5. Molecular evolutionary genetics analysis using maximum likelihood, evolutionary distance, and maximum parsimony. *Mol. Biol. Evol*. 28, 2731–2739. doi: 10.1093/molbev/msr121

Tang, H. R., Covington, A. D., and Hancock, R. A. (2003). Structure-activity relationships in the hydrophobic interactions of polyphenols with cellulose and collagen. *Biopolymers* 70, 403–413. doi: 10.1002/bip.10499

Tesfaye, W., Morales, M. L., Benitez, B., García-Parrilla, M. C., and Troncoso, A. M. (2004). Evolution of wine vinegar composition during accelerated aging with oak chips. *Anal. Chim. Acta* 513, 239–245. doi: 10.1016/j.aca.2003.11.079

Tesfaye, W., Morales, M. L., Callejon, R. M., Cerezo, A. B., Gonzalez, A. G., García-Parrilla, M. C., et al. (2010). Descriptive sensory analysis of wine vinegar: tasting procedure and reliability of new attributes. *J. Sens. Stud*. 25, 216–230. doi: 10.1111/j.1745-459X.2009.00253.x

Tesfaye, W., Morales, M. L., Garcia-Parrilla, M. C., and Troncoso, A. M. (2002). Wine vinegar: technology, authenticity and quality evaluation. *Trends Food Sci. Technol.* 13, 12–21. doi: 10.1016/S0924-2244(02)00023-7

Tesfaye, W., Morales, M. L., García-Parrilla, M. C., and Troncoso, A. M. (2003). Optimising wine vinegar production: fermentation and aging. *Appl. Biotechnol. Food Sci. Pol.* 1, 109–114.

Tesfaye, W., Morales, M. L., García-Parrilla, M. C., and Troncoso, A. M. (2009). Improvement of wine vinegar elaboration and quality analysis: iInstrumental and human sensory evaluation. *Food Rev. Int*. 25, 142–156. doi: 10.1080/87559120802682748

Theuma, M., Gambin, C., and Attard, E. (2015). Physicochemical characteristics of the Maltese grapevine varieties—gellewza and girgentina. *J. Agricul. Sci*. 7, 61. doi: 10.5539/jas.v7n4p61

Ubeda, C., Callejón, R. M., Hidalgo, C., Torija, M. J., Troncoso, A. M., and Morales, M. L. (2013). Employment of different processes for the production of strawberry vinegars: effects on antioxidant activity, total phenols and monomeric anthocyanins. *LWT Food Sci. Technol.* 52, 139–145. doi: 10.1016/j.lwt.2012.04.021

Vegas, C., González, A., Mateo, E., Mas, A., Poblet, M., and Torija, M. J. (2013). Evaluation of representativity of the acetic acid bacteria species identified by culture-dependent method during a traditional wine vinegar production. *Food Res. Int*. 51, 404–411. doi: 10.1016/j.foodres.2012.12.055

Vegas, C., Mateo, E., and González, A. (2010). Population dynamics of acetic acid bacteria during traditional wine vinegar production. *Int. J. Food Microbiol*. 138, 130–136. doi: 10.1016/j.ijfoodmicro.2010.01.006

Wu, X., Yao, H., Cao, X., Liu, Q., Cao, L., Mu, D., et al. (2017). Production of vinegar from purple sweet potato in a liquid fermentation process and investigation of its antioxidant activity. *3 Biotech* 7, 1–10. doi: 10.1007/s13205-017-0939-7

Yamada, Y., Yukphan, P., Lan Vu, H. T., Muramatsu, Y., Ochaikul, D., Tanasupawat, S., et al. (2012). Description of *Komagataeibacter* gen. nov., with proposals of new combinations (*Acetobacteraceae*). *J. Gen. Appl. Microbiol*. 58, 397–404. doi: 10.2323/jgam.58.397

Conflict of Interest: The authors declare that the research was conducted in the absence of any commercial or financial relationships that could be construed as a potential conflict of interest.

Publisher's Note: All claims expressed in this article are solely those of the authors and do not necessarily represent those of their affiliated organizations, or those of the publisher, the editors and the reviewers. Any product that may be evaluated in this article, or claim that may be made by its manufacturer, is not guaranteed or endorsed by the publisher.

frontiers | Frontiers in Microbiology

TYPE Original Research
PUBLISHED 02 August 2022
DOI 10.3389/fmicb.2022.951030

OPEN ACCESS

EDITED BY
Teresa Garcia-Martinez,
University of Cordoba, Spain

REVIEWED BY
Muhammad Kamruzzaman,
Westmead Institute for Medical Research, Australia
Xiaohui Zhou,
University of Connecticut, United States

*CORRESPONDENCE
Lei Zhang
zhanglei@zjgu.edu.cn
Xinle Liang
dbiot@mail.zjgsu.edu.cn

†These authors have contributed equally to this work and share first authorship

SPECIALTY SECTION
This article was submitted to Food Microbiology, a section of the journal Frontiers in Microbiology

RECEIVED 23 May 2022
ACCEPTED 07 July 2022
PUBLISHED 02 August 2022

CITATION
Qian C, Ma J, Liang J, Zhang L and Liang X (2022) Comprehensive deciphering prophages in genus *Acetobacter* on the ecology, genomic features, toxin–antitoxin system, and linkage with CRISPR-Cas system. *Front. Microbiol.* 13:951030. doi: 10.3389/fmicb.2022.951030

Comprehensive deciphering prophages in genus *Acetobacter* on the ecology, genomic features, toxin–antitoxin system, and linkage with CRISPR-Cas system

Chenggong Qian†, Jiawen Ma†, Jiale Liang, Lei Zhang* and Xinle Liang*

School of Food Science and Biotechnology, Zhejiang Gongshang University, Hangzhou, China

Acetobacter is the predominant microbe in vinegar production, particularly in those natural fermentations that are achieved by complex microbial communities. Co-evolution of prophages with *Acetobacter,* including integration, release, and dissemination, heavily affects the genome stability and production performance of industrial strains. However, little has been discussed yet about prophages in *Acetobacter.* Here, prophage prediction analysis using 148 available genomes from 34 *Acetobacter* species was carried out. In addition, the type II toxin–antitoxin systems (TAs) and CRISPR-Cas systems encoded by prophages or the chromosome were analyzed. Totally, 12,000 prophage fragments were found, of which 350 putatively active prophages were identified in 86.5% of the selected genomes. Most of the active prophages (83.4%) belonged to the order *Caudovirales* dominated by the families *Siphoviridae* and *Myroviridae* prophages (71.4%). Notably, *Acetobacter* strains survived in complex environments that frequently carried multiple prophages compared with that in restricted habits. *Acetobacter* prophages showed high genome diversity and horizontal gene transfer across different bacterial species by genomic feature characterization, average nucleotide identity (ANI), and gene structure visualization analyses. About 31.14% of prophages carry type II TAS, suggesting its important role in addiction, bacterial defense, and growth-associated bioprocesses to prophages and hosts. Intriguingly, the genes coding for Cse1, Cse2, Cse3, Cse4, and Cas5e involved in type I-E and Csy4 involved in type I-F CRISPR arrays were firstly found in two prophages. Type II-C CRISPR-Cas system existed only in *Acetobacter aceti*, while the other *Acetobacter* species harbored the intact or eroded type I CRISPR-Cas systems. Totally, the results of this study provide fundamental clues for future studies on the role of prophages in the cell physiology and environmental behavior of *Acetobacter*.

KEYWORDS

***Acetobacter*, prophage, co-evolution, vinegar, genomic analysis**

Introduction

Acetic acid bacteria (AAB), a group of Gram-negative and aerobic bacilli that can be isolated from flowers, fruits, soil, intestines, wine, and vinegar, are currently classified into 19 genera (Qiu et al., 2021). The *Acetobacter*, *Gluconobacter*, and *Komagataeibacter* species have been widely studied for their ability to efficiently oxidize ethanol to vinegar (Yang et al., 2022). However, abnormal vinegar fermentation is often observed, and the underlying mechanism remains unclear due to the complicated microbial community combined with uneven fermentation technology. The multi-omics studies on traditional food fermentations have indicated the impacts conferred by the bacterial community fluctuation and the environmental conditions on the fermentation process (Das and Tamang, 2021; Ma et al., 2022; Yang et al., 2022; Zotta et al., 2022). In parallel, the recent findings of virome contributions to the evolution of bacterial communities rely on the ocean, soil, and gut metagenome investigations, which suggest the potential of phages in shaping the architecture and development of fermented food communities (Roy et al., 2020; Chevallereau et al., 2022; Ge et al., 2022). Several phages have been adopted and engineered as alternative antimicrobials or therapeutic potency successfully (Bao et al., 2020; Ge et al., 2021, 2022; Grabowski et al., 2021). Phageomes in the cheese starters and fermented vegetables were determined, and virulent and temperate phages were isolated and sequenced. Recently, the analysis of historical and experimental samples from 82 years of Swiss hard cheese starter culture propagation showed that strains differ tremendously in their phage resistance capacity (Somerville et al., 2022). The co-evolution of phages and bacteria together has addressed the driver force of the community balance (Mancini et al., 2021; Harvey and Holmes, 2022).

Prophages are potential phages that integrate their genes into the host chromosomes after the invasion and replicate simultaneously with the host. Under physiological stress conditions, prophage can enter into the lytic stage, resulting in the death of a lysogenic host cell. This kind of switching helps to tune the dynamic balance of populations in the development of the bacterial community (Secor and Dandekar, 2020). For example, prophages co-evolved with *Lactobacillus plantarum* and helped the host to survive the acidic kimchi fermentation (Park et al., 2022). The temperate phage *Φ*AP1.1 exhibited a recurrent mechanism to counteract bacterial immunity by inserting itself into the CRISPR repeats and thus neutralizing the *Streptococcus pyogenes* immunity (Varble et al., 2021). In addition, prophages could promote horizontal gene transfer (HGT) among bacterial populations (Magaziner et al., 2019). The auxiliary gene modules confer the properties of virulence and antibiotic resistance through transduction pathways to the host (Naorem et al., 2021; Wendling et al., 2021). Meanwhile, several anti-CRISPR (Acr)-encoded genes in prophage have been found as a defense approach in the arms race with hosts (Wang et al., 2020), while genes encoding for hydrolysis enzymes were involved in the recycling of whole ocean materials. Currently, eight types of toxin–antitoxin systems (TAs) have been uncovered and annotated (Alvarez et al., 2020; Jurenas et al., 2022). Also, TAs on prophages are involved in prophage induction and regulation of the physiological state of cells (Li et al., 2020; Song and Wood, 2020; Jurenas et al., 2021). Previous studies suggested that diverse type II TAs are present in the active prophages of *Acetobacter* genomes (Omata et al., 2021; Xia et al., 2021b). Nevertheless, a full investigation of the distribution of prophages in the genus *Acetobacter* has not been performed yet.

Actually, several cases of contamination due to phages during the vinegar fermentation process were reported, and four phages were isolated (Schocher et al., 1979; Stamm et al., 1989; Kiesel and Wünsche, 1993; Kharina et al., 2015). In addition, a *Tectivirus*-infecting *Gluconobacter cerinus* was isolated from wine musts (Philippe et al., 2018), and six temperate phages were obtained from *Acetobacter pasteurianus* (Omata et al., 2021). Furthermore, the available genomic data exhibit plenty of putative prophage loci in *Acetobacter* genomes, as well as in transposons, insertion sequences (ISs), and phage-associated genes, which are associated with some evolutionary and genetic advantages but also contribute to unstable genome features in *Acetobacter* (Yang et al., 2022). Recently, the available genomic data provide us a chance to comprehensively decipher the profile of *Acetobacter* prophage and its important role in physiology, evolution, and genetic diversity of *Acetobacter*. In this study, we aimed to characterize the prophage profiles of *Acetobacter* based on 148 genomes obtained from 34 *Acetobacter* species, and tried to decipher the internal relations of ecology, genomic features, TA distribution, and CRISPR-Cas systems.

Materials and methods

Acetobacter genome collection

Acetobacter genomes (148) were obtained from the National Center for Biotechnology Information (NCBI) (https://www.ncbi.nlm.nih.gov/genome/?term=Acetobacter) database. These genomes represent 34 different species, including *Acetobacter aceti* (9), *Acetobacter ascendens* (3), *Acetobacter cerevisiae* (3), *Acetobacter cibinongensis* (3), *Acetobacter conturbans* (1), *Acetobacter estunensis* (2), *Acetobacter fabarum* (3), *Acetobacter fallax* (2), *Acetobacter farinalis* (1), *Acetobacter ghanensis* (2), *Acetobacter indonesiensis* (4), *Acetobacter lambici* (1), *Acetobacter lovaniensis* (2), *Acetobacter malorum* (7), *Acetobacter musti* (1), *Acetobacter nitrogenifige* (2), *Acetobacter oeni* (3), *Acetobacter okinawensis* (4), *Acetobacter orientalis* (7), *Acetobacter orleanensis* (4), *Acetobacter oryzifermentans* (2), *Acetobacter oryzoeni* (1), *Acetobacter papayae* (1), *Acetobacter pasteurianus* (32), *Acetobacter peroxydans* (3), *Acetobacter persici* (7), *Acetobacter pomorum* (8), *Acetobacter sacchari* (1),

Acetobacter senegalensis (4), *Acetobactersicerae* (1), *Acetobacter suratthaniensis* (1), *Acetobacter syzygii* (7), *Acetobacter thailandicus* (5), and *Acetobacter tropicalis* (11). The detailed information on these strains is listed in Supplementary Table S1.

Prophage prediction, ANI analysis, and genome annotation

Prophage Hunter was adopted as the guide for finding prophages. By measuring genomic similarity at the nucleotide level, the putative region with a score of more than or equal to 0.8 was defined as an active prophage, the region with a score between 0.8 and 0.5 as an unspecified prophage, and the region with a score of <0.5 as an inactive prophage (Song et al., 2019). The detailed information is listed in Supplementary Table S2. FastANI v1.3 was used to calculate the ANI value of prophages (Jain et al., 2018). Compared with prophage itself, the derived ANI value was recorded as 100%, and the default ANI value <70% was recorded as not accessible (NA). To annotate the prophage genome region precisely, the Rapid Annotation Using Subsystem Technology (RAST) software was applied (Aziz et al., 2008).

Prediction, analysis of type II toxin–antitoxin system, and CRISPR-Cas system

TAfinder tool on the TADB website (https://bioinfo-mml.sjtu.edu.cn/TADB2/tools.html) was used to search for type II TA loci (Xie et al., 2018). E-value for BLAST was set at 0.01, E-value for HMMer was set at 1, the maximum length of potential toxin/antitoxin was set at 300 amino acids, and the maximum distance (or overlap) between the potential toxin and antitoxin was set at - 20_ 150 nt. CRISPRCasFinder (https://crisprcas.i2bc.parissaclay.fr/CrisprCasFinder/Index) was then used to find CRISPR alignments, direct repeats, and spacers. According to the guidelines, only levels 3 and 4 CRISPR arrays were counted in this study. Spacer-prophage matching was performed using a local BLAST search, and the following parameters were adopted: blastn-short comparison, query-NA, E-value <1e-5, and outfmt at 6 (Abby et al., 2014; Couvin et al., 2018).

Data analysis and visualization

The Kruskal–Wallis test and the Mann–Whitney U-test were performed using SPSS PASW Statistics v18.0. Data aggregation and processing were done using Microsoft Office Excel 2016 with the assistance of Python. Point and line plots, bar graphs, box plots, violin plots, and pie charts were visualized using Origin 2021. Strain biogenesis geographic distribution maps and genomic CDS maps were visualized using R. Heatmap visualization and hierarchical clustering were done using HemI (Heatmap Illustrator v1.0) (Deng et al., 2014). The network relationship diagram was visualized using Cytoscape (Shannon et al., 2003). All figures were further embellished and retouched using Adobe Illustrator 2020.

Results

Ecological distribution of prophage diversity in *Acetobacter*

We performed a prophage search on the 148 genomes from 34 *Acetobacter* species and found 12,000 prophage fragments. Of which, most genomes contained more than 40 prophage fragments (Figure 1A). Specifically, *A. sacchari* TBRC 11175 (sac) isolated from flower showed the highest number of prophage fragments (119). Interestingly, no prophage fragments were predicted in the *A. syzygii* UBA5806 (syz) genome. Among the 12,000 prophage fragments, only 350 fragments were active and intact prophages. Moreover, 86.5% (128/148) of *Acetobacter* genomes harbored active prophages. The number of active prophages varied from 1 to 8 with a mean value of 2.7. Most *Acetobacter* strains contained 1–5 prophages, while a few strains like *A. oryzifermentans* SLV-7 (oryzi), *A. pomorum* SH (pom), and *A. sacchari* TBRC 11175 (sac) contained 7, 8, and 7 prophages, respectively (Figure 1B; Supplementary Table S1). The species *A. pasteurianus* is adopted universally by the food industry, and its active prophage number ranged from 0 to 7. The industrial species *A. pasteurianus* NBRC 3284 and *A. pasteurianus* Ab3 contained 1 and 5 active prophages, respectively, suggesting the evolutionary diversity of these strains. No active prophages were found in three species: *A. farinalis* (far), *A. papaya* (pap), and *A. suratthaniensis* (sur). These active prophages are embedded in the *Acetobacter* genome and are certainly expected to impact the host's physiological functions.

The fermented food biotopes like vinegar and wine production contribute to 16.2 % (24/148) and 20.3 % (30/148) distribution of *Acetobacter* strains recorded in NCBI genome data, respectively (Figure 1C; Supplementary Figure S1). Also, *Acetobacter* strains universally exist in variable habitats of flowers/fruits and relative stable habitats of the gut of flies (22.4 and 5.6 %, respectively). To investigate whether the number of active prophages of *Acetobacter* was related to the habitats, we divided 120 *Acetobacter* strains (except for 8 termed as NA) into fermented food habitat group (vinegar, wine, and tea, $n = 58$), insect gut habitat group (fly, gut, and culture, $n = 13$), and wild habitat group (flower, fruit, meat, mud,

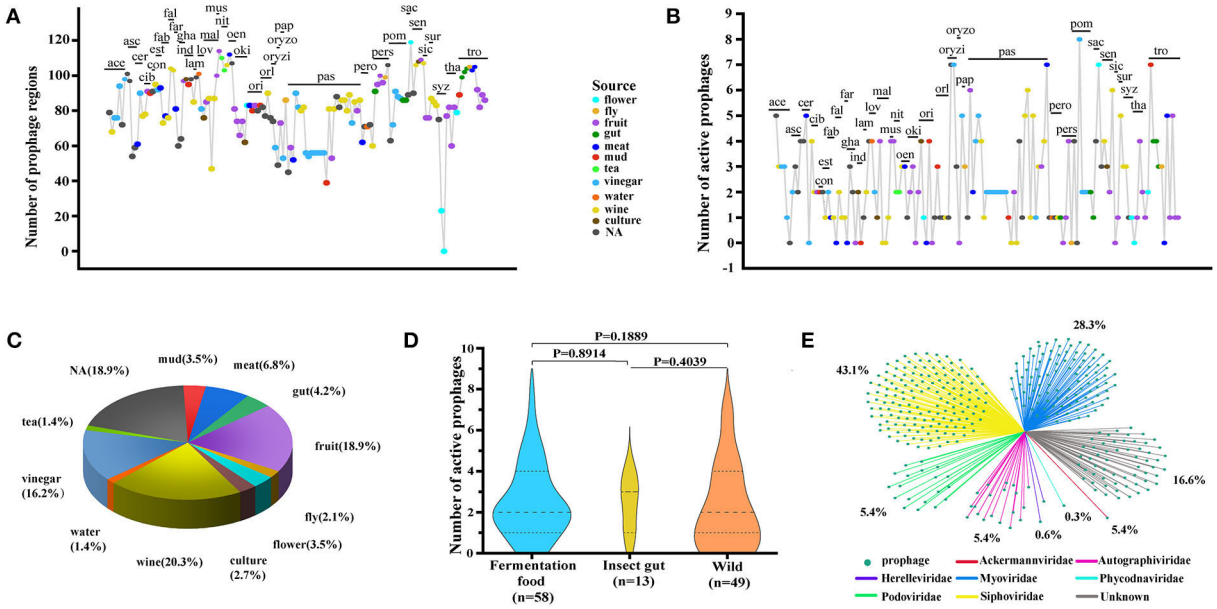

FIGURE 1
Depiction of prophages for 34 *Acetobacter* species. **(A)** All prophage fragments predicted in *Acetobacter*. **(B)** Active prophages predicted in *Acetobacter*. The above serial numbers are the classification of *Acetobacter* species (see Supplementary Table S1): *A. aceti* (ace); *A. ascendens* (asc); *A. cerevisiae* (cer); *A. cibinongensis* (cib); *A. conturbans* (con); *A. estunensis* (est); *A. fabarum* (fab); *A. fallax* (fal); *A. farinalis* (far); *A. ghanensis* (gha); *A. indonesiensis* (ind); *A. lambici* (lam); *A. lovaniensis* (lov); *A. malorum* (mal); *A. musti* (mus); *A. nitrogenifigens* (nit); *A. oeni* (oen); *A. okinawensis* (oki); *A. orientalis* (ori); *A. orleanensis* (orl); *A. oryzifermentans* (oryzi); A. oryzoeni (oryzo); *A. papaya* (pap); *A. pasteurianus* (pas); *A. peroxydans* (pero); *A. persici* (pers); *A. pomorum* (pom); *A. sacchari* (sac); *A. senegalensis* (sen); *A. sicerae* (sic); *A. suratthaniensis* (sur); *A. syzygii* (syz); *A. thailandicus* (tha); and *A. tropicalis* (tro). **(C)** Statistics of the source of *Acetobacter* isolates. **(D)** Comparison of predicted active prophages among the fermentation habitat group, the insect gut habitat group, and the variable habitat group. Statistical significance tests were performed using the nonparametric Mann–Whitney *U*-test, and two-tailed values of *p*-value were calculated. **(E)** Statistics of the family of prophages.

and water, $n = 49$) (Figure 1D). Unexpectedly, no significant difference in the number of prophages was observed among the three groups ($p > 0.05$). Nevertheless, we noticed that the strains possessing the active prophage counts of more than five mainly existed in the fermented food and wild habitat groups. For example, the aforementioned *A. pomorum* SH (pom) and *A. oryzifermentans* SLV-7 (oryzi) strains isolated from vinegar had seven and eight prophages, respectively, and *A. sacchari* TBRC 11175 (sac) strain isolated from flowers contained seven prophages. These findings suggested that a stressful and complex microbial community niche may prompt the integration of prophages into *Acetobacter* genome, which confer underlying advantages or disadvantages to the host evolution. Notably, except for the 16.6% of active prophages, the rest of the phages exclusively belonged to the order *Caudovirales* with reference to the NCBI virus database (Figure 1E). Of which, the families *Siphoviridae* and *Myroviridae* prophages yielded the higher distribution ratio of 43.1 and 28.3%, respectively, while the families *Herelleviridae* and *Phycodnaviridae* showed less distribution by 0.6 and 0.3%, respectively.

Genomic characteristics of *Acetobacter* prophages

The size of 350 active prophages varied from 10.074 kb (phiBCRC14145-4) to 66.17 kb (phiAb3-5) with an average of 21.01 ± 7.98 kb (median ± interquartile range), and a significant difference was found at the intraspecies level. Interestingly, the size of the active prophage genome was exactly the span of the prophage genome size of *A. pasteurianus* (pas) (Figure 2A; Supplementary Table S2). In line with the prophage genome size of *A. pasteurianus*, the prophage sizes of *A. aceti* (ace), *A. estunensis* (est), and *A. musti* (mus) showed a similar trend. Prophage genomes from *A. ascendens* (asc), *A. ghanensis* (gha), *A. orientalis* (ori), *A. pomorum* (pom), and *A. syzygii* (syz) had high or low outliers. In addition, no significant differences in the active prophage genome sizes were observed at the host interspecies level.

The variation in GC content is closely related to mutation, selection, and recombination of microbial genes (Lassalle et al., 2015; Hellweger et al., 2018). It was found that the GC content of *Acetobacter* prophages ranged from 32.73% (phiNBRC

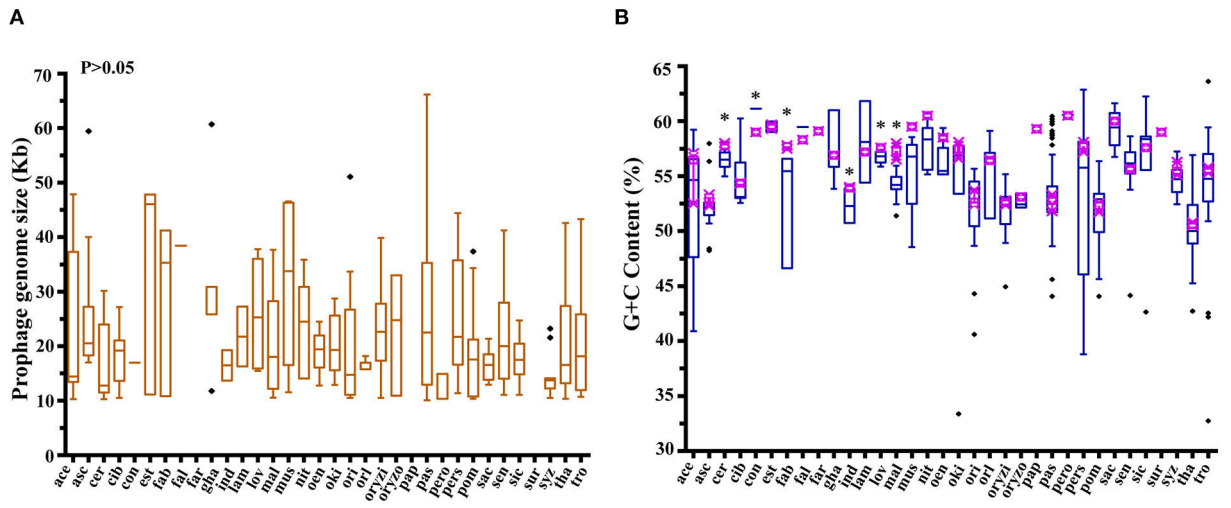

FIGURE 2
Characterization of 350 active prophage genomes. **(A)** Comparison of prophage genome size. A non-parametric test (Kruskal–Wallis) using multiple independent samples was performed. **(B)** Comparison of the GC content of the prophage genomes with their respective hosts. Blue boxes represent prophages and red boxes represent host strains. ♦, outliers. Non-parametric Mann–Whitney *U*-test and two-tailed method were used to check *p*-values comparing prophages and hosts in each group, $*p < 0.05$.

101654-2) to 63.62% (phiLMG 1663-2) at the interspecies level (Figure 2B; Supplementary Table S2). The phiNBRC 3277-4 and phiNBRC 3208-5 from *A. pasteurianus* (pas) NBRC 3277 and *A. pasteurianus* 3280, respectively, gave a low GC content of 44.07%, while phiBCRC 14145-1 from *A. pasteurianus* BCRC 14145 displayed a high GC content of 60.3%. The prophage genomes obtained from *A. aceti* (ace), *A. pasteurianus* (pas), *A. persici* (pers), and *A. tropicalis* (tro) exhibited a significant difference in the GC content. Interestingly, the prophages with the maximum and the minimum GC content appeared in the form of outliers in *A. tropicalis* (tro). Meanwhile, the GC content of prophage genomes also exhibited significant differences at the host intraspecies level, such as in *A. cerevisiae* (cer), *A. conturbans* (con), *A. fabarum* (fab), *A. indonesiensis* (ind), *A. lovaniensis* (lov), and *A. malorum* (mal) ($p < 0.05$). The prophages from *A. conturbans* showed a higher GC content of 61.13% than its host which showed 59%, while prophages from the other five species (*A. cerevisiae* (cer), *A. fabarum* (fab), *A. indonesiensis* (ind), *A. lovaniensis* (lov), and *A. malorum* (mal)) exhibited significantly lower GC content than their hosts (Supplementary Tables S1, S2). Nevertheless, the GC content of prophages was overall in line with their hosts, implying the biocompatibility of prophage–host and their co-evolution in the microbial community.

In order to uncover the prophage diversity at the nucleotide level, we calculated the average nucleotide identity (ANI) for the 350 active prophage genomes (Supplementary Table S3). The ANI analysis results were then arranged in pairs in a matrix. Notably, only 5.01% (6,138/122,500) of the modules were observed with matching values higher than 70% (Supplementary Table S3), illustrating the low identity and high diversity among *Acetobacter* prophage genomes. Subsequently, the matrix was clustered by using the mean linkage hierarchical clustering method based on Pearson distance, and then visualized in the form of a heat map with a gradual change from low (black) to high identity (red) (Figure 3A). Exception of nineteen prophages with the ANI value less than 70%, the remaining 331 prophages could be grouped into 8 large subclusters (termed as a, b, c, d, e, f, g, and h, where each subcluster contained $n > 10$ prophages) and 42 small subclusters (each subcluster contained the prophages at $2 \leq n \leq 8$, termed as i, j, k, …, and only the frontier i-s subclusters are labeled in the Figure 3A) based on the affinities. Specifically, the small subclusters i (*A. thailandicus*), j (*A. nitrogenifigens*), k (*A. lovaniensis*), l (*A. sacchari*), m (*A. nitrogenifigens*), n (*A. musti*), o (*A. fallax*), p (*A. sacchari*), q (*A. aceti*), r (*A. oeni*), and s (*A. thailandicus*) were predominantly composed of a single *Acetobacter* species, suggesting the host species are specific to the prophages. The remaining 31 small subclusters and 8 large subclusters of prophages divergently occurred in diverse *Acetobacter* species. Moreover, the prophages of each large subcluster were derived from different *Acetobacter* species with an average of 5.88 *Acetobacter* species per subcluster (Table 1). For example, the largest subcluster e contained 42 prophages derived from *A. aceti*, *A. pasteurianus*, *A. oryzifermentans*, *A. pomorum*, and *A. senegalensis*. The subclusters a and c contained 23 and 25 prophages from six and five host species, respectively. The prophages of subclusters b, f, and g were derived from seven different species each. There were many subclusters that contained only one prophage, implying their

separated evolution. Generally, an ANI value above 0.95 suggests the same species (Jain et al., 2018). In the large subclusters, the phiSRCM 101447-2 from *A. ascendens* SRCM 101447 in subcluster c showed 95% identity with phiAb3-2 from *A. pasteurianus* Ab3 in subcluster a, and the phiCICC 22518-1 from *A. pasteurianus* CICC 22518 in subcluster c showed 98.1% identity to the phiSRCM 101447-1 from *A. ascendens* SRCM 101447 in the subcluster a. Similarly, the phiLMG 1590-3 (96.8% identity), phiLMG 1591-1 (96.8%), phiBCRC 14118-1 (97.4%), phiBCRC 14118-2 (96.1%), and phiLMG 1590-2 (95.8%) in the subcluster c showed high identity to phiSRCM 101447-1 from *A. ascendens* SRCM 101447 in the subcluster a. Specifically, though the phiUBA 5402-1 shared a high identity of 98.8% with phiUBA 5402-2 of *A. orientalis* UBA 5402, they were separately clustered into different subclusters according to the ANI analysis.

In addition to the ANI analysis, to further investigate whether the prophage functional gene structures in each subcluster were continuous or segregated, we packaged the functional annotations of the prophage genomes of the eight large subclusters and selected the dominant prophage types from each subcluster for visualization (Figure 3B). Accordingly, 32 representative prophages were selected and 12 kinds of proteins were figured out, including phage (capsid, head protein, tail protein, and other structural proteins), cell lysis, DNA metabolism, hydrolase, integrase, mobile element protein, terminase, type II TAs, transcriptional regulator, and hypothetical protein. The composition and architecture of the prophage genomes displayed a high diversity within each subcluster, except for the g and h subclusters where the ANI and arrangement of prophage genomes shared a high identity. In subcluster a, the integrase showed a low identity below 83% among the four prophages, and the hydrolase was only found in phiIFO 3283-01-1. Notably, TAs located in multiple gene loci did not show any consistency, e.g., nearby the integrase genes in subcluster a, the transcriptional factors or cell lysis genes in the subcluster e, and the DNA metabolism genes in the subcluster h. The subclusters f and g did not have any TAs. Additionally, although prophages were clustered based on the ANI analysis, the genome size in each subcluster varied greatly, which was in line with the results of the distribution of prophage biodiversity.

Distribution of type II TAs in the *Acetobacter* prophages

Currently, TAs have been uncovered with a variety of physiological functions involved in multiple networks in the cellular metabolism and regulation process, specifically in the defense mechanisms and self-addictive evolution with the flanked genes (Kamruzzaman et al., 2021). Based on the TAfinder software analysis, 129 type II TA loci on 109 out of 350 active prophage genomes were predicted. Totally, 12 kinds of TAs were found, including *hicA-hicB*, *higB-higA*, *higA-mqsA*, *relE-relB*, *relE-RHH-Xre*, *mazF-mazE*, *ccdB-ccdA*, *vapC-vapB*, *ydaS-ydaR-NA*, *brnT-brnA*, NA-*vbhA*, and NA-*phd* (Figure 4; Supplementary Table S4). Moreover, only one copy of each type II TA existed in each prophage genome. The *hicA-hicB* showed an equally high distribution of 26.35% (34/129) in the nine *Acetobacter* species, while 34 *ydaS-ydaR-NA* was distributed more diversely in 12 species (Figure 4). *NA-phd* was found to exist only in phiDSM3508-1 of *A. aceti*. Similarly, the *ccdB-ccdA* was found in two prophages (phiDSM 23921-2 and phiNBRC 105050-2 of *A. nitrogenifigens*). Additionally, most prophage genomes (115/129) contained just one kind of TAs, while the phiJCM 20276-3 of *A. aceti*, phidm-6 of *A. oryzifermentans*, phiSH-3 of *A. pomorum*, and phi108B-2 of *A. senegalensis* contained three different TAs, respectively.

Acetobacter pasteurianus showed a relatively high abundance of TAs in their prophage genomes (Figure 4). Thirty-three out of eighty-nine prophage genomes contained TAs with a yield of 37.09%, consisting of the dominant species *hicB-hicA* (20/33), *ydaS-ydaT-NA* (5/33), *brnT-brnA* (3/33), and *relE-RHH/Xre* (3/33). *A. aceti* is another dominant species in fermented wine and vinegar, and 54.54% of its prophage genomes (12/22) contained TAs, and the dominant TAs included *higB-higA*, *hicA-hicB,* and *relE-relB*. The species *A. syzygii* can usually be isolated from wine and flower, and 7 out of the 13 prophage genomes had TA loci, such as *higB-higA*, *mazF-mazE*, and *ydaS-ydaT-NA*. A similar abundance of TAs existed in the prophage genomes of other *Acetobacter* species, including *A. oryzifermentans* (42.86%, 6/14), *A. persici* (45.45%, 5/11), *A. pomorum* (38.10%, 8/21), *A. sacchari* (42.86%, 3/7), *A. nitrogenifigens* (50%, 2/4), and *A. fabarum* (66.67%, 2/3). The loci of these type II TAs mainly belonged to six classical two-component families (*hicBA*, *relBE*, *mazEF*, *ccdBA*, *vapBC*, and *brnTA*), one three-component family *paaR-paaA-parE,* and other unknown families. The distribution and abundance of TAs harbored by the prophages appear to be strain-specific, which was consistent to the extensive transmission across the species of the prophage.

CRISPR-Cas system existence in *Acetobacter*

Even though *Acetobacter* has some interest in the co-existence with prophages, the host itself possesses the corresponding resistance systems to prevent the risk of prophage intrusion that may further limit the growth or cause a serious burden to hosts (Doron et al., 2018; Owen et al., 2021). Among the driver mechanisms responsible for bacterial defense against phage invasion, the CRISPR-Cas system is regarded as one of the classical approaches (Horvath and Barrangou, 2010). Based on the spacer sequences, we scanned the *Acetobacter*

10.3389/fmicb.2022.951030

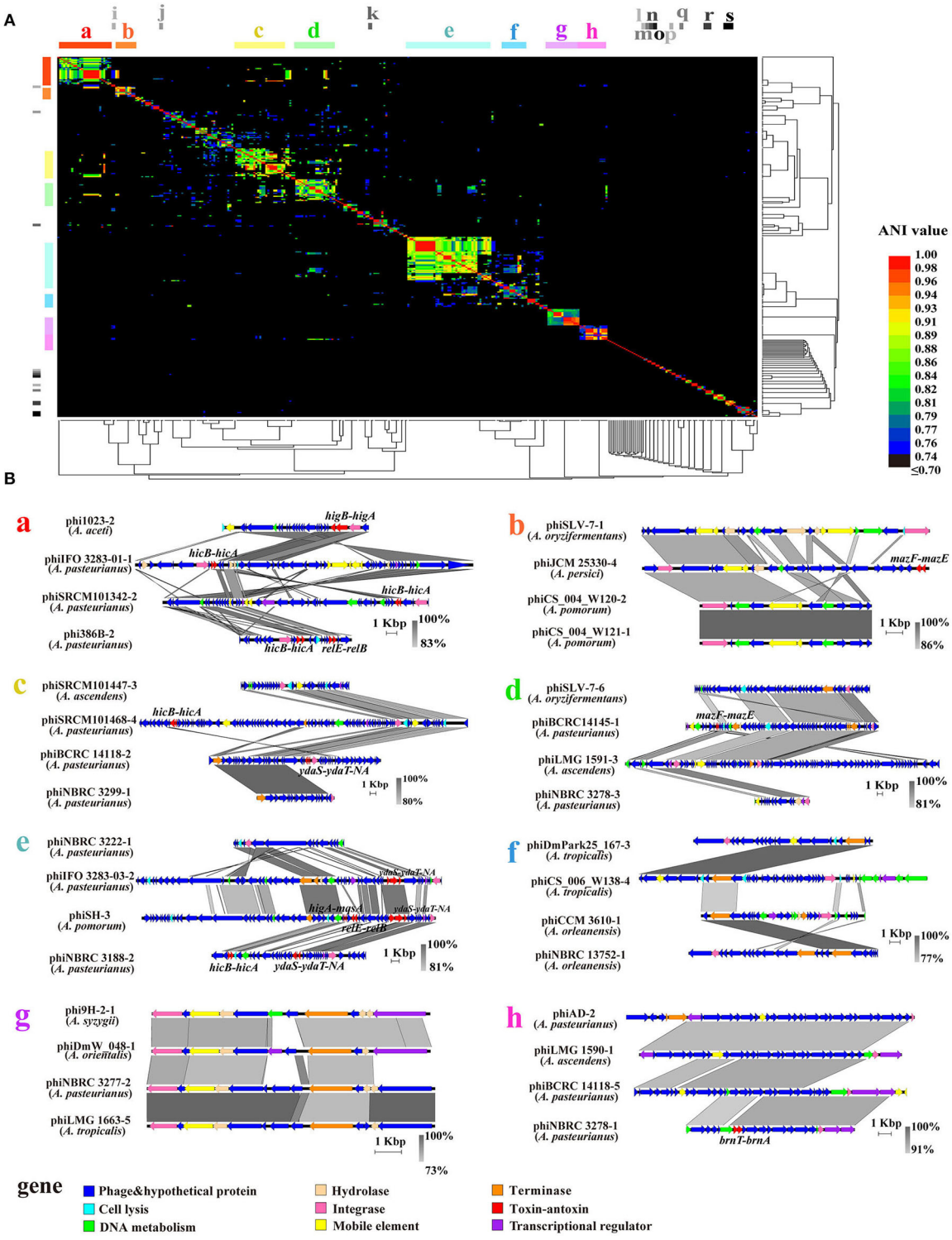

FIGURE 3
Analysis of 350 active prophage genomes. **(A)** The 350 prophage paired ANI values were clustered using a mean linkage hierarchical clustering method based on Pearson's distance for rows and columns in all clusters. The colors in the heat map represent different ANI values, gradually changing from blue (low identity) to red (high identity). a to h' represent the eight large subclusters and i to s' represent the small subclusters composed of prophages of a single Acetobacter species. The ANI values are shown in Supplementary Table S3. **(B)** Comparative genomics of prophages for each large subcluster 8 (a, b, c, d, e, f, g, and h). The gray area represents the similarity module and the similarity changes gradually from gray (low) to black (high).

10.3389/fmicb.2022.951030

TABLE 1 Distribution of prophages grouped in the eight large subclusters.

Subclusters	Total prophages	Prophages per host species		Host species	Host species classification
		min	max		
a	23	1	17	6	*A. aceti*; *A. ascendens*; *A. orientalis*; *A. pasteurianus*; *A. persici*; *A. pomorum*
b	10	1	3	7	*A. aceti*; *A. malorum*; *A. oryzifermentans*; *A. persici*; *A. pomorum*; *A. senegalensis*; *A. tropicalis*
c	25	2	10	5	*A. ascendens*; *A. oryzifermentans*; *A. oryzoeni*; *A. pasteurianus*; *A. pomorum*
d	20	1	15	4	*A. ascendens*; *A. oryzifermentans*; *A. pasteurianus*; *A. pomorum*
e	42	1	27	5	*A. aceti*; *A. oryzifermentans*; *A. pasteurianus*; *A. pomorum*; *A. senegalensis*
f	12	1	4	7	*A. indonesiensis*; *A. malorum*; *A. orleanensis*; *A. pasteurianus*; *A. persici*; *A. pomorum*; *A. tropicalis*
g	17	1	5	7	*A. orientalis*; *A. oryzifermentans*; *A. oryzoeni*; *A. pasteurianus*; *A. pomorum*; *A. syzygii*; *A. tropicalis*
h	14	1	9	6	*A. ascendens*; *A. cibinongensis*; *A. orientalis*; *A. pasteurianus*; *A. senegalensis*; *A. tropicalis*

genomes available currently. Of which, 44.6% (66/148) of *Acetobacter* genomes possessed CRISPR-Cas systems, and 23% had 2-3 loci. The main CRISPR-Cas systems in the *Acetobacter* belonged to the type I-A, I-C, I-E, I-F, and type II-C, respectively (Figure 5A; Supplementary Table S5). Specifically, we observed that type II-C CRISPR-Cas system existed only in *A. aceti* (ace) and type I-A only in *A. pasteurianus* UBA5418 compared to the prevalence of type I-E in the *Acetobacter* species. Additionally, the mean count of spacers of *Acetobacter* genome was up to 11 sequences. Thirty-five *Acetobacter* genomes harbored 43 putative or identified CRISPR-Cas arrays, and 82 genomes seemed not to contain any spacers or CRISPR-Cas systems, indicating the uneven distribution of CRISPR-Cas systems in *Acetobacter* (Supplementary Table S5). Specifically, *A. farinalis* LMG26772 (far) genome contained the highest spacer counts up to 82. However, 4 ambiguous and 77 inactive prophages were detected on its genome without any active prophages. Therefore, we determined the relationship between the active prophage number and their host's CRISPR-Cas systems (Figure 5B). No significant difference in the number of active prophages was demonstrated among each CRISPR-Cas type and the unknown groups ($p > 0.05$), while a similar phenomenon was observed for the number of prophages against the number of spacers in 1–10, 11–20, 21–30, 31–40, and 41–50 groups, respectively ($p > 0.05$). But when the host genome contained more than 50 spacers, the prophage numbers significantly reduced to <2 ($p < 0.05$) (Figure 5C).

When a total of 1,625 predicted spacers in the 148 *Acetobacter* genomes were mapped to all the active prophage genomes, only16.80% of the spacers were matched with 95% identity (Figure 5D), suggesting that most of the prophages were not recorded by their hosts. The spacers from 13 *Acetobacter* species presented the intricate information network with the prophages from 21 *Acetobacter* species (Supplementary Table S6). One host species contained spacers pairing with a few different prophages, while one prophage may infect multiple different hosts. Particularly, the spacers of *A. pomorum* matched with the most number of prophages from 12 *Acetobacter* species, and exhibited the highest number of prophage matching in *A. pasteurianus*. For instance, the match counts between the prophages of *A. pasteurianus* and the spacers of *A. pomorum* were found to be 250, between *A. pasteurianus* and *A. oryzifermentans* werein the range of 61- 87, between *A. pasteurianus* and *A. oryzoeni* were in the range of 22–46, and between *A. tropicalis* and *A. aceti* were in the range of 11–20. However, the match counts between the spacers of *A. pasteurianus* and the prophages of *A. pasteurianus* or *A. pomorum* ranged from 22 to 87, which is less than the abovementioned values. From the prophage standpoint, the prophages from *A. pasteurianus* could find much more counter-spacers from a variety of *Acetobacter* species. Therefore, the species matching analysis and ANI analysis together constructed a global model of host strain specificity to *Acetobacter* prophages.

Specifically, several genes encoding the CRISPR-related proteins were found, including *cse1*, *cse2*, *cse3*, *cse4*, and *cas5e* in the prophage phiLMG 1746-3 (hosted by *A. malorum* LMG 1746) and *csy4* in the prophage phiUBA 5402-3 (hosted by *A. orientalis* UBA 5402) (Figure 6A). Also, nine spacers were detected on phiUBA 5402-3 genome, while none were found

on phiLMG 1746-3 (Supplementary Table S7). The phiLMG 1746-3 showed 87% similarity to *Enterobacteria* phage-BP-4795 (temperate, *Siphoviridae*, GenBank accession number AJ556162) which consisted of 85 ORFs, including 2 IS 629 elements and 3 morons (Creuzburg et al., 2005). The host *A. malorum* LMG 1746 was isolated from fruit and predicted to harbor four active prophages and a total of 100 prophage fragments. Two CRISPR-Cas loci were found on the bacterial genome, where one was an eroded type I-F structure composed of *cas6*, *csy1*, *csy2,* and *csy3*, while the other loci only included *cas1*, *cas2,* and *cas3* (Figure 6B). The phiUBA5402-3 showed a 90% similarity with *Brucella* phage BK (lytic, *Podoviridae*, GenBank accession number KC556893) (Farlow et al., 2014). The host *A. orientalis* UBA 5402 was isolated from mud and harbored 3 active prophages and 83 prophage fragments, and three CRISPR-Cas system modules occurred on the bacterial genome, i.e., one intact type I-F CRISPR-Cas system and two unknown fragments which just contained adaption modules *cas1* and *cas2* or orphan effector element *cas3,* respectively (Figure 6B; Supplementary Table S5). In comparison to the canonical modular organization of CRISPR-Cas systems, *cse1-4* and *cas5e* usually exist in the Cse subtype I-E, while *csy4* does in the Csy subtype I-F. Meanwhile, lots of the truncated CRISPR-Cas modules that reside on the *Acetobacter* genomes, as well as those unidentified CRISPR-Cas loci, remained either adaption elements of *cas1*, cas2, *cas4*, and effector *cas3* or kinds of combination.

Discussion

Acetobacter is a predominant genus that occurs widely in a variety of artificial or wild environmental ecosystems, particularly several species, such as *A. pasteurianus,* are historically adopted for industry-of-interest. Since the first phage A-1 of *Acetobacter suboxydans* ATCC 621 (now reclassified as *Gluconobacter oxydans*) was reported in 1979 (Schocher et al., 1979), only five *Acetobacter*-specific phages (MO 1, Acm 1, phiAP1, phiAO1, and phiAX1) have been identified till 2021. Currently, a large amount of genomic data of *Acetobacter* is available on NCBI, which enables the *in silico* investigation of diversity, genome features, and ecological functions of *Acetobacter*-specific prophages and their potential relationship with hosts.

In parallel to the distribution of *Acetobacter* species, which shows high diversity in complexity and habitats in nature (De Roos et al., 2018), the 350 predicted active *Acetobacter*-specific prophages exhibited a similar diverse distribution and abundance at the levels of host species and strain. About 86.5% (128/148) of *Acetobacter* strains presented active prophages, and similar distribution yields were found in *Lactobacillus* (64.1%), *Pseudomonas* (46.7%), and *Klebsiella* (69.3%) (Marques et al., 2021; Pei et al., 2021; Johnson et al., 2022). Generally, increased environmental stresses may stimulate a bacterium to evolve a series of mechanisms against harsh environments. In this process, prophages are usually supposed to confer the host some advantages in competition. However, we did not find a significant difference between the prophage abundance and distribution specific to the habitat complexity of their *Acetobacter* hosts. This finding is not consistent with the investigation of the intact *Lactobacillus* prophages, where the prophage counts harbored by their host strains obtained from the fermented food group definitely displayed a difference from that obtained from the human/mammal group, i.e., a habit-associated pattern is observed (Pei et al., 2021). A more complex community may confer the host more options for co-survival with mobile genetic factors, including phages like that in *Lactococcus* (Matsutani et al., 2020). The investigation of 120 distinct phages from 303 *Lactobacillus helveticus* strains of natural whey starter cultures revealed that the high incidence of phage contamination cases can be recovered by high biodiversity of bacterial hosts and consequently maintaining a successful acidification capacity (Mancini et al., 2021). *A. pasteurianus* strains are adopted universally by food industries, while the active prophage numbers ranged from 0 to 7 whenever it occurs in wild or fermented foods, suggesting similar survival to the enteral genetic element challenges during the evolution process. Considering the fact that *Acetobacter* strains isolated from either industrial scenes or fly guts exactly and initially come from wild environmental niches and limited artificial domestications occur even for vinegar and wine production, we preferably suppose a unique strain-specific distribution for *Acetobacter*-specific prophages.

Also, the genome size, composition, and architecture of *Acetobacter*-specific prophages displayed a significant difference at the strain level but not at the species level of the host. A total of 350 active prophages exhibited the genome size varying from 10.074 to 66.17 kb with a significant difference, while a similar difference was not found at the species level. Furthermore, we observed that 32.73–63.62% GC content of prophages matched with that of their host *Acetobacter* strains (Figure 2B), highlighting the strong connection between a prophage and its cognate host strain. This observation was supported further by the ANI analysis, which exhibited a generally low identity and high diversity among *Acetobacter* prophage genomes (Figure 3A). Each large subcluster contained prophages derived from multiple *Acetobacter* species, suggesting that prophages can spread broadly across species. The same phenomenon was observed in *Lactobacillus* and *Oenococcus* prophages (Claisse et al., 2021; Pei et al., 2021; Qin et al., 2022). Based on the aforementioned findings, we conclude that most of the *Acetobacter*-specific prophages are strain-specific and can transmit across both intra- and interspecies levels. The co-evolution of prophage with its host bacterium often occurs at the strain level, which is in line with the significant difference observed in the functional gene organization of

10.3389/fmicb.2022.951030

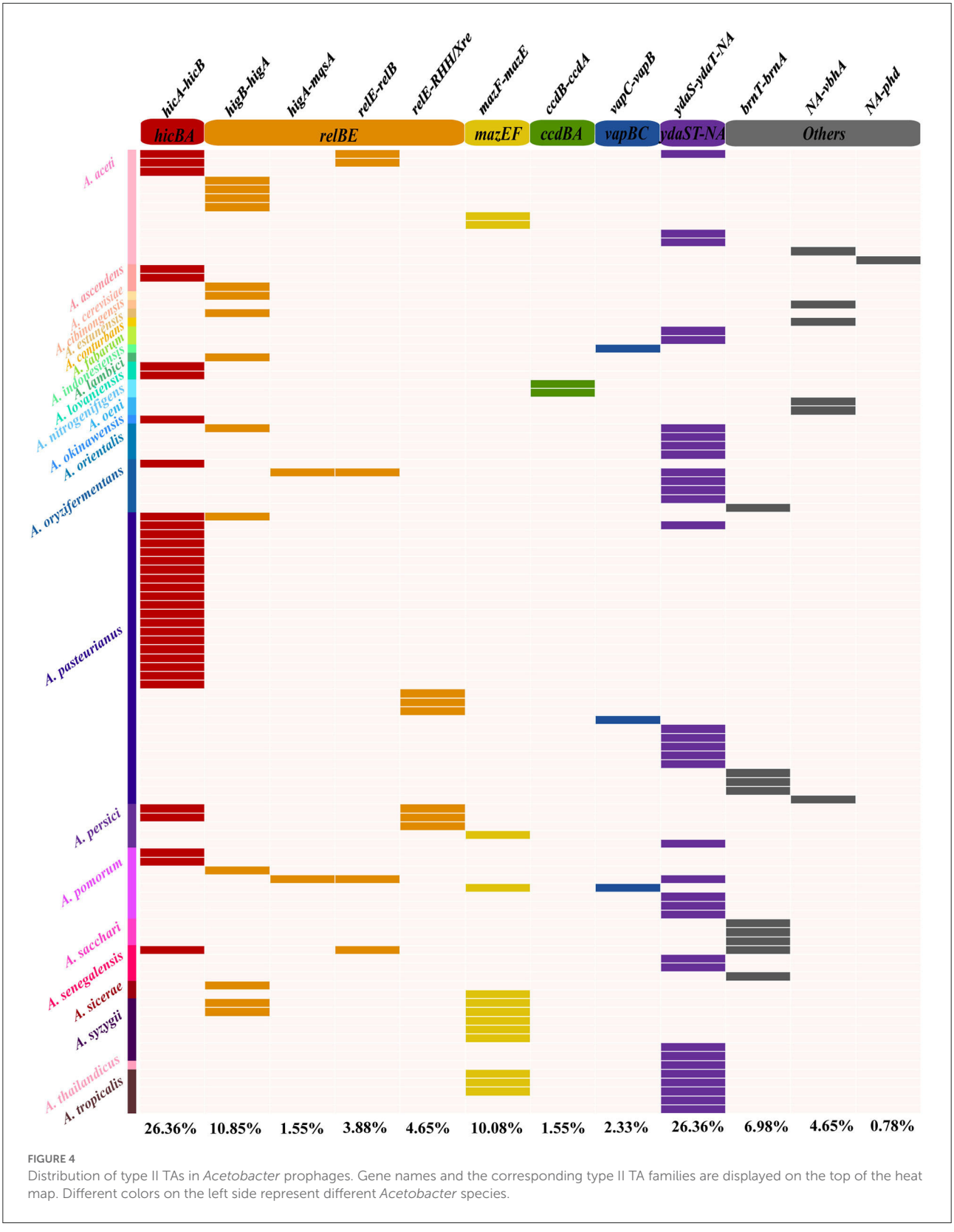

FIGURE 4
Distribution of type II TAs in *Acetobacter* prophages. Gene names and the corresponding type II TA families are displayed on the top of the heat map. Different colors on the left side represent different *Acetobacter* species.

10.3389/fmicb.2022.951030

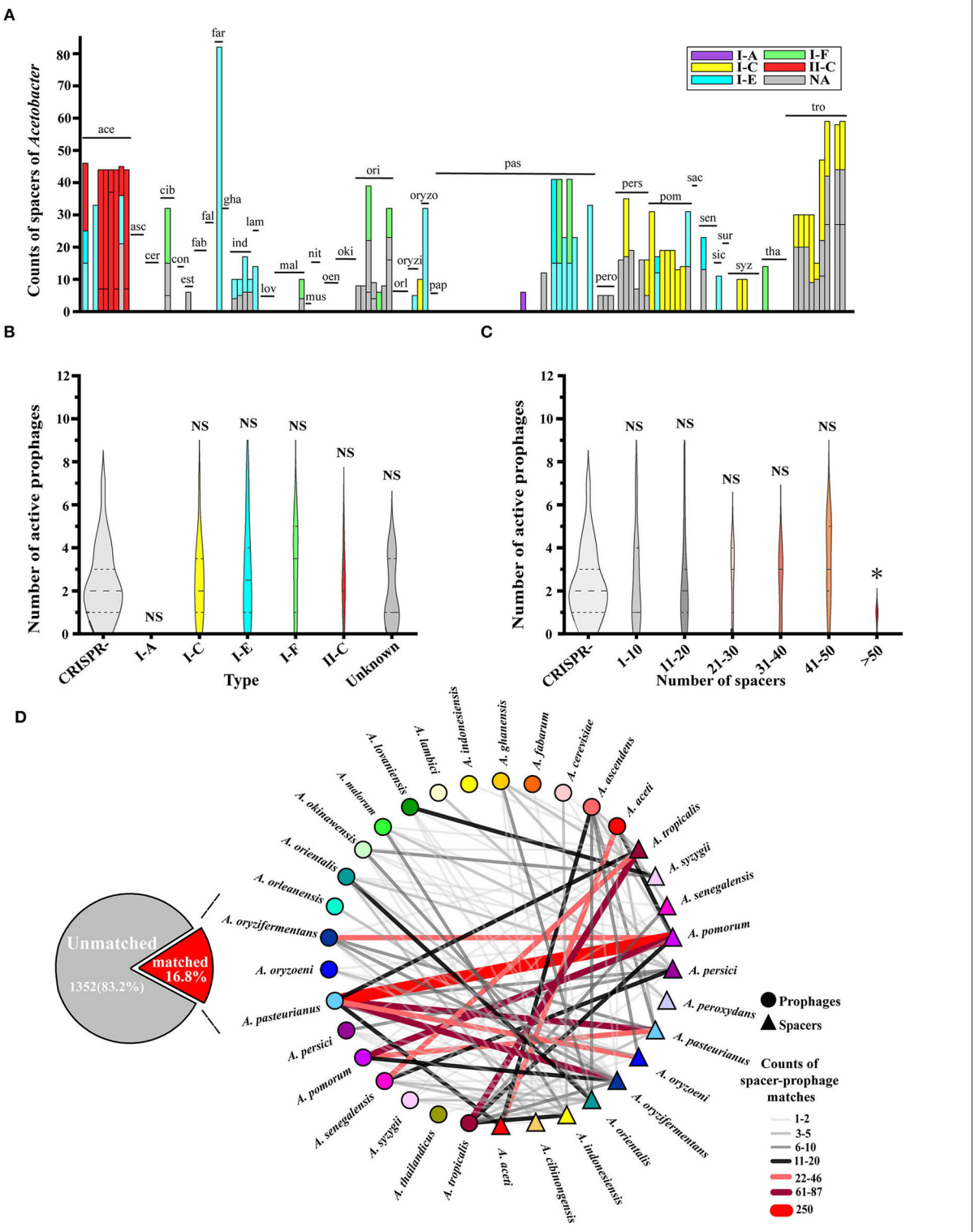

FIGURE 5
Analysis of CRISPR-Cas system spacers on the *Acetobacter* genome sequences. **(A)** The number of CRISPR-Cas system spacers counted for each *Acetobacter* species, and different colors represent different types of CRISPR-Cas systems. Purple I-A, yellow I-C, blue I-E, green I-F, red II-C, and black NA. **(B)** Relationship between CRISPR-Cas system types and prophage numbers. **(C)** Relationship between the genomic CRISPR-Cas system spacers and the number of prophages in *Acetobacter*. X-axis is the total number of CRISPR-Cas system spacers, and Y-axis is the number of prophages. Non-parametric Mann–Whitney U-test and two-tailed method were used to calculate *p*-values. **(D)** Spacer-prophage matching network.

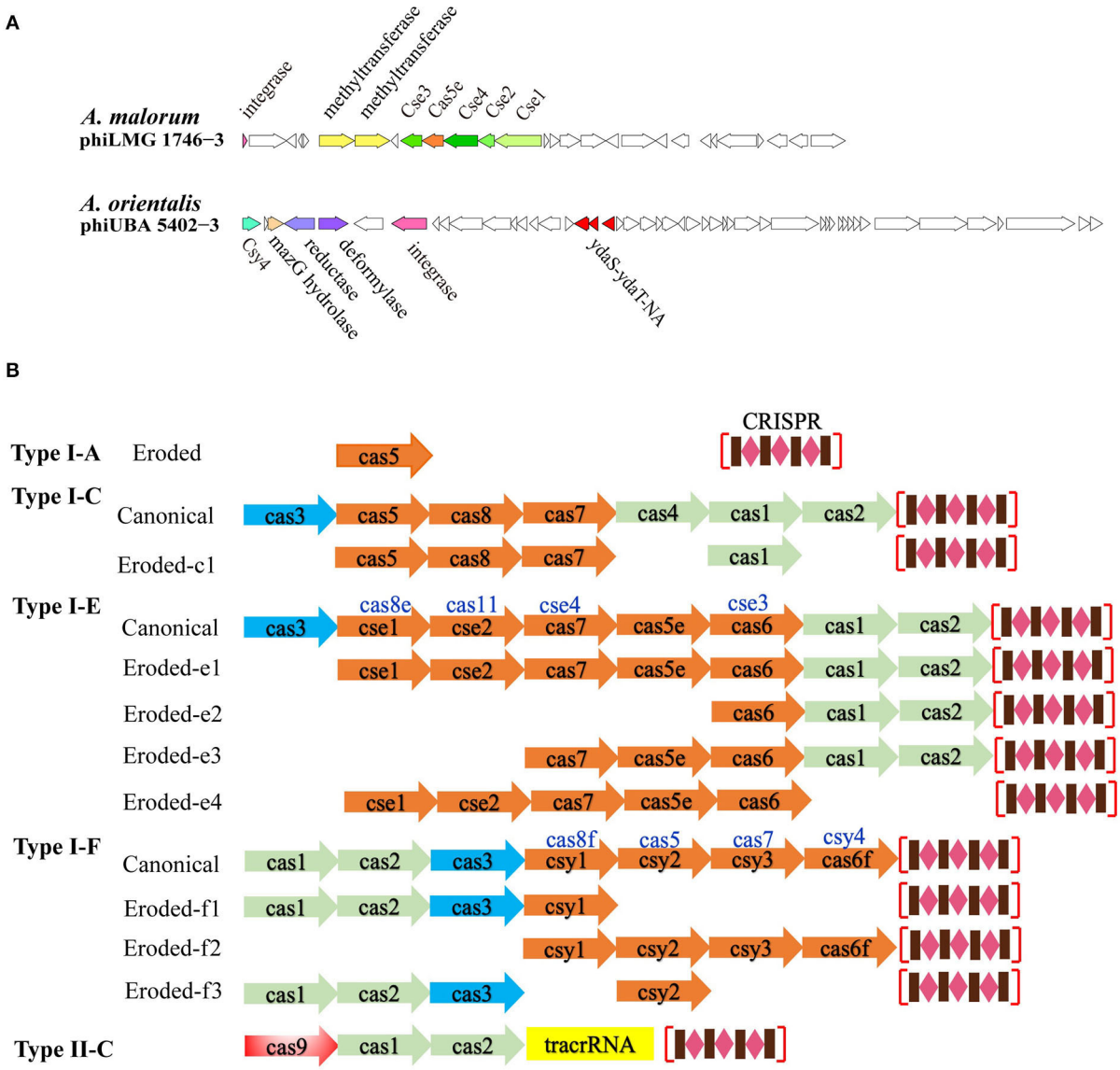

FIGURE 6
Architecture of prophage genomic loci for the subtypes of CRISPR-Cas systems. **(A)** Two unique genomes of the *Acetobacter*-specific prophages harbored the eroded type I-E and I-F CRISPR-Cas loci. **(B)** Diagrams of the intact or incomplete CRISPR-Cas loci representatives existed on *Acetobacter* genomes. Genes encoding the adaption, effector, and target cleavage module are colored in green, orange, and blue, respectively.

Acetobacter-specific prophages (Figure 3B). Bacterial genes may integrate into the prophage genome during replication and result in a longer genome or lose redundant genes from the prophage in order to facilitate its own replication, which results in the intermingling of host and prophage gene fragments and then changes the genome size of prophages from host species. This biodiversity in prophage genomes increases the host population-level diversity and drives the continuous host evolution (Nawel et al., 2022). It is rational that similar ecological functions can be mirrored by the *Acetobacter*-specific prophages, and the rich diversity and broad diffusivity of *Acetobacter* prophage populations drive the genetic plasticity of *Acetobacter*.

The arms race between phage and bacteria promotes co-evolution. Lysogeny offers great benefit through the auxiliary functional genes in the prophage genome that always confer additional immunity roles against phage infection by multiple mechanisms (Jurenas et al., 2022). TAs from plasmids and bacterial genomes have been extensively investigated with regard to their multiple biological functions. Recently, their

distribution and role in (pro)phages have become an attractive topic. However, only a few TAs on prophages have been identified (Jurenas et al., 2022). Previously, we have investigated the chromosomal *hicB-hicA* in *A. pasteurianus* Ab3 and annotated its functions (Xia et al., 2019, 2021a,b). The *hicB-hicA* was found on the phage phiS10 of *Streptococcus suis* and suggested a mechanism for the maintenance of the temperate phage (Tang et al., 2013). Considering the *hicB-hicA* ubiquity in the *Acetobacter* prophages, their roles remain to be investigated. The *ydaS-ydaT-NA* belongs to the family *paaR2-paarA2-parE2*; the latter occurs in CP933P prophage of *E. coli* O157:H7 and is regarded to stabilize this prophage (Jurenas et al., 2021). Notably, TAs of *higB-higA* and *hicB-hicA* are near integrase genes on prophage genomes (Figure 3B), and we speculate that the addiction of TAs benefits the stability of the latter, as what has been uncovered in *creT-creA* safeguarding *cas6* (Li et al., 2021). Till this study was presented, none of the *Acetobacter*-specific prophage-derived TAs has yet been identified, and the underlying functions, such as additional protection, host defense system, and lytic-to-lysogenic switch, deserve a comprehensive deciphering into the host–phage combat context. Whether the prophage-derived TA pair exerts a similar biological function as its counterpart derived from *Acetobacte*r chromosome and the plasmid is one open question.

Different from the bacterial defense mechanism at the population level by TAs acting in the Abi pattern in nature, the most intuitive patterns of phage defense should be CRISPR-Cas or restriction-modification systems at the single-cell level (Mohanraju et al., 2022). Our finding was in parallel to the previous study that the number of active prophages was necessarily neither correlated with CRISPR-Cas type number nor spacers number in the CRISPR arrays (Touchon et al., 2016). Considering that the *Acetobacter* species are not typical bacteria and efficient genetic tools are still lacking, our finding will benefit the development of novel CRISPR-Cas tools specific to *Acetobacter*. In this study, the type II-C CRISPR-Cas system was only found in *A. aceti*. The majority of *Acetobacter* genomes harbor either eroded unidentified CRISPR-Cas loci or no CRISPR-Cas loci (Supplementary Table S5), and in such cases, complex mechanisms led to the gradual elimination of a part or complete elements in the genome (Koonin and Makarova, 2017). The residual CRISPR modules varied in the composition of the adaptation, expression, or interference elements (Figure 6B), suggesting that each genome co-evolves differently in the same ecosystem and responds to divergent stress conditions. *Acetobacter*-specific type I-E organization seems a variant of the Cse type I-E derived from *Streptococcus thermophilus* DGCC7710, where *cse4* and *cas6* were replaced by *cas7* and *cas6*, respectively (Carte et al., 2014). The remaining four I-E loci occurred in the eroded organization for *Acetobacter* characterized without *cas3* interference function. Similarly, the *Acetobacter*-specific type I-F structure resembles the Csy subtype I-F derived from *Yersinia pestis* and *Pseudomonas aeruginosa* (Haft et al., 2005; Haurwitz et al., 2010). Intriguingly, we also observed that two specific prophages, phiLMG 1746-3 and phiUBA 5402-3, harbored the eroded genes encoding Cse1, Cse2, Cse3, Cse4, Cas5e, and Csy4, respectively (Figure 6A). The initial CRISPR repeat cleavage can be catalyzed by Cse3 (Cas6e) in the Cse type I-E and the Csy4 (Cas6f) of 'Cas6 superfamily' in the Csy type I-F system, and both Cse3 and Csy4 recognize and cleave downstream of a stem-loop structure in associated CRISPR repeats while retaining the repeat stem-loop at the 3'-end of the Cse type I-E and Csy type I-F crRNAs (Carte et al., 2014). Therefore, the prophage phiLMG 1746-3 appeared to retain the minor eroded expression elements (*cse1-cse2-cse3-cse4-cas5e*) to process pre-crRNAs and release crRNAs, while the phiLMG 1746-3 might retain the recognition and cleavage ability of pre-crRNAs, which may be employed to cope with host defense and phage–phage competition. Currently, studies of viromes from various environmental ecosystems indicate that more (pro)phages possess CRISPR arrays and/or *cas* genes (Mohanraju et al., 2022). Considering the bi-directional evolutionary connection between CRISPR arrays and mobile genetic elements, the uncovering of type I-F elements-contained Tn7-like transposons or virus as well as the Cas4-contained phages is growing (Faure et al., 2019). Consistently, a type I-F loci with adaptation and CRISPR array was inserted into the ICP1-related phages infecting *Vibrio cholerae* (Seed et al., 2013). Therefore, we hypothesize that the eroded type I-E CRISPR array in the phiLMG 1746-3 genome and Cys4 type I-F locus in the phiUBA 5402-3 may reversely be captured from the Cse type I-E and Csy type I-F CRISPR-Cas loci on the bacterial genomes, respectively. Specifically, it is notable that the eroded type I-E CRISPR-Cas loci on the phiLMG 1746-3 genome are greatly distinct from its host bacterial genome which harbors the type I-F CRISPR-Cas system, indicating the different evolutionary pathways between the prophage and its host CRISPR-Cas system. Against the context of a long-term complex phage–host arm races, it is rational that prophages can promise a universal of additional defense mechanisms that are yet to be uncovered.

In summary, this study displayed some cues to elucidate the ecological, genetic diversity, and evolutionary synergy of prophages and their host *Acetobacter*. The *Acetobacter*-specific prophages exhibited a significant difference in distribution, abundance, and genetic biodiversity at the strain level but not at the species level, and few prophages have been identified and annotated. In parallel to the existence of an intact or incomplete CRISPR-Cas system in the host genome dominated by type I, a unique prophage harboring the eroded Cse type I- E CRISPR-Cas array implies its different evolution. In addition to 350 active prophages, more than 11,650 putative predicted intact prophage fragments were not sorted out here, and the function of these phage fossils is still an open question. A comprehensive experimental study combined with *in silico* comparative

genomics will promote the understanding of the relationship between prophages and their *Acetobacter* hosts, and then afford the advantages to the fermented food industries in the future.

Data availability statement

The original contributions presented in the study are included in the article/Supplementary material, further inquiries can be directed to the corresponding authors.

Author contributions

CQ and JM designed and carried out the investigation, drafted the manuscript, and visualized the results. JL took part in the investigation. XL provided the general concept, supervised the work, and the writing of the manuscript. LZ provided the concept and reviewed the manuscript. All authors took part in the discussions and approved the final version.

Funding

This work was funded by the Natural Science Foundation of Zhejiang Province (LY19C200002) to XL.

Acknowledgments

The authors thank Kai Xia and Yudong Li for the Writing, Polishing, and Support of the Natural Science Foundation of Zhejiang Province.

Conflict of interest

The authors declare that the research was conducted in the absence of any commercial or financial relationships that could be construed as a potential conflict of interest.

Publisher's note

Supplementary material

The Supplementary Material for this article can be found online at: https://www.frontiersin.org/articles/10.3389/fmicb.2022.951030/full#supplementary-material

References

Abby, S. S., Neron, B., Menager, H., Touchon, M., and Rocha, E. P. (2014). MacSyFinder: a program to mine genomes for molecular systems with an application to CRISPR-Cas systems. *PLoS ONE* 9, e110726. doi: 10.1371/journal.pone.0110726

Alvarez, R., Ortega-Fuentes, C., Queralto, C., Inostroza, O., Diaz-Yanez, F., Gonzalez, R., et al. (2020). Evaluation of functionality of type II toxin-antitoxin systems of Clostridioides difficile R20291. *Microbiol. Res.* 239, 126539. doi: 10.1016/j.micres.2020.126539

Aziz, R. K., Bartels, D., Best, A. A., DeJongh, M., Disz, T., Edwards, R. A., et al. (2008). The RAST Server: rapid annotations using subsystems technology. *BMC Genomics* 9, 75. doi: 10.1186/1471-2164-9-75

Bao, H., Zhou, Y., Shahin, K., Zhang, H., Cao, F., Pang, M., et al. (2020). The complete genome of lytic Salmonella phage vB_SenM-PA13076 and therapeutic potency in the treatment of lethal Salmonella Enteritidis infections in mice. *Microbiol. Res.* 237, 126471. doi: 10.1016/j.micres.2020.126471

Carte, J., Christopher, R. T., Smith, J. T., Olson, S., Barrangou, R., Moineau, S., et al. (2014). The three major types of CRISPR-Cas systems function independently in CRISPR RNA biogenesis in Streptococcus thermophilus. *Mol. Microbiol.* 93, 98–112. doi: 10.1111/mmi.12644

Chevallereau, A., Pons, B. J., van Houte, S., and Westra, E. R. (2022). Interactions between bacterial and phage communities in natural environments. *Nat. Rev. Microbiol.* 20, 49–62. doi: 10.1038/s41579-021-00602-y

Claisse, O., Chaib, A., Jaomanjaka, F., Philippe, C., Barchi, Y., Lucas, P. M., et al. (2021). Distribution of prophages in the oenococcus oeni species. *Microorganisms* 9, 856. doi: 10.3390/microorganisms9040856

Couvin, D., Bernheim, A., Toffano-Nioche, C., Touchon, M., Michalik, J., Neron, B., et al. (2018). CRISPRCasFinder, an update of CRISRFinder, includes a portable version, enhanced performance and integrates search for Cas proteins. *Nucleic Acids Res.* 46, W246–W251. doi: 10.1093/nar/gky425

Creuzburg, K., Recktenwald, J., Kuhle, V., Herold, S., Hensel, M., and Schmidt, H. (2005). The Shiga toxin 1-converting bacteriophage BP-4795 encodes an NleA-like type III effector protein. *J. Bacteriol.* 187, 8494–8498. doi: 10.1128/JB.187.24.8494-8498.2005

Das, S., and Tamang, J. P. (2021). Changes in microbial communities and their predictive functionalities during fermentation of toddy, an alcoholic beverage of India. *Microbiol. Res.* 248, 126769. doi: 10.1016/j.micres.2021.126769

De Roos, J., Verce, M., Aerts, M., Vandamme, P., and De Vuyst, L. (2018). Temporal and spatial distribution of the acetic acid bacterium communities throughout the wooden casks used for the fermentation and maturation of lambic beer underlines their functional role. *Appl. Environ. Microbiol.* 84, e02846–17. doi: 10.1128/AEM.02846-17

Deng, W., Wang, Y., Liu, Z., Cheng, H., and Xue, Y. (2014). HemI: a toolkit for illustrating heatmaps. *PLoS ONE* 9, e111988. doi: 10.1371/journal.pone.0111988

Doron, S., Melamed, S., Ofir, G., Leavitt, A., Lopatina, A., Keren, M., et al. (2018). Systematic discovery of antiphage defense systems in the microbial pangenome. *Science* 359, eaar4120. doi: 10.1126/science.aar4120

Farlow, J., Filippov, A. A., Sergueev, K. V., Hang, J., Kotorashvili, A., and Nikolich, M. P. (2014). Comparative whole genome analysis of six diagnostic brucellaphages. *Gene* 541, 115–122. doi: 10.1016/j.gene.2014.01.018

Faure, G., Shmakov, S. A., Yan, W. X., Cheng, D. R., Scott, D. A., Peters, J. E., et al. (2019). CRISPR-Cas in mobile genetic elements: counter-defence and beyond. *Nat. Rev. Microbiol.* 17, 513–525. doi: 10.1038/s41579-019-0204-7

Ge, H., Lin, C., Xu, Y., Hu, M., Xu, Z., Geng, S., et al. (2022). A phage for the controlling of Salmonella in poultry and reducing biofilms. *Vet. Microbiol.* 269, 109432. doi: 10.1016/j.vetmic.2022.109432

Ge, H., Zhang, K., Gu, D., Chen, X., Wang, X., Li, G., et al. (2021). The rfbN gene of Salmonella Typhimurium mediates phage adsorption by modulating biosynthesis of lipopolysaccharide. *Microbiol. Res.* 250, 126803. doi: 10.1016/j.micres.2021.126803

Grabowski, L., Lepek, K., Stasilojc, M., Kosznik-Kwasnicka, K., Zdrojewska, K., Maciag-Dorszynska, M., et al. (2021). Bacteriophage-encoded enzymes destroying bacterial cell membranes and walls, and their potential use as antimicrobial agents. *Microbiol. Res.* 248, 126746. doi: 10.1016/j.micres.2021.126746

Haft, D. H., Selengut, J., Mongodin, E. F., and Nelson, K. E. (2005). A guild of 45 CRISPR-associated (Cas) protein families and multiple CRISPR/Cas subtypes exist in prokaryotic genomes. *PLoS Comput. Biol.* 1, e60. doi: 10.1371/journal.pcbi.0010060

Harvey, E., and Holmes, E. C. (2022). Diversity and evolution of the animal virome. *Nat. Rev. Microbiol.* 20, 321–34. doi: 10.1038/s41579-021-00665-x

Haurwitz, R. E., Jinek, M., Wiedenheft, B., Zhou, K., and Doudna, J. A. (2010). Sequence- and structure-specific RNA processing by a CRISPR endonuclease. *Science* 329, 1355–1358. doi: 10.1126/science.1192272

Hellweger, F. L., Huang, Y., and Luo, H. (2018). Carbon limitation drives GC content evolution of a marine bacterium in an individual-based genome-scale model. *ISME J.* 12, 1180–1187. doi: 10.1038/s41396-017-0023-7

Horvath, P., and Barrangou, R. (2010). CRISPR/Cas, the immune system of bacteria and archaea. *Science* 327, 167–170. doi: 10.1126/science.1179555

Jain, C., Rodriguez, R. L., Phillippy, A. M., Konstantinidis, K. T., and Aluru, S. (2018). High throughput ANI analysis of 90K prokaryotic genomes reveals clear species boundaries. *Nat. Commun.* 9, 5114. doi: 10.1038/s41467-018-07641-9

Johnson, G., Banerjee, S., and Putonti, C. (2022). Diversity of Pseudomonas aeruginosa Temperate Phages. *mSphere* 7, e0101521. doi: 10.1128/msphere.01015-21

Jurenas, D., Fraikin, N., Goormaghtigh, F., De Bruyn, P., Vandervelde, A. and Zedek, S., et al. (2021). Bistable expression of a toxin-antitoxin system located in a cryptic prophage of escherichia coli O157:H7. *mBio* 12, e0294721. doi: 10.1128/mBio.02947-21

Jurenas, D., Fraikin, N., Goormaghtigh, F., and Van Melderen, L. (2022). Biology and evolution of bacterial toxin-antitoxin systems. *Nat. Rev. Microbiol.* 20, 335–350. doi: 10.1038/s41579-021-00661-1

Kamruzzaman, M., Wu, A. Y., and Iredell, J. R. (2021). Biological functions of type ii toxin-antitoxin systems in bacteria. *Microorganisms* 9, 1276. doi: 10.3390/microorganisms9061276

Kharina, A., Podolich, O., Faidiuk, I., Zaika, S., Haidak, A., Kukharenko, O., et al. (2015). Temperate bacteriophages collected by outer membrane vesicles in Komagataeibacter intermedius. *J. Basic Microbiol.* 55, 509–513. doi: 10.1002/jobm.201400711

Kiesel, B., and Wünsche, L. (1993). Phage Acm1-mediated transduction in the facultatively methanol-utilizing Acetobacter methanolicus MB 58/4. *J. Gen. Virol.* 74 (Pt 9), 1741–1745. doi: 10.1099/0022-1317-74-9-1741

Koonin, E. V., and Makarova, K. S. (2017). Mobile genetic elements and evolution of CRISPR-cas systems: all the way there and back. *Genome Biol. Evol.* 9, 2812–2825. doi: 10.1093/gbe/evx192

Lassalle, F., Perian, S., Bataillon, T., Nesme, X., Duret, L., and Daubin, V. (2015). GC-Content evolution in bacterial genomes: the biased gene conversion hypothesis expands. *PLoS Genet.* 11, e1004941. doi: 10.1371/journal.pgen.1004941

Li, M., Gong, L., Cheng, F., Yu, H., Zhao, D., Wang, R., et al. (2021). Toxin-antitoxin RNA pairs safeguard CRISPR-Cas systems. *Science* 372, eabe5601. doi: 10.1126/science.abe5601

Li, Y., Liu, X., Tang, K., Wang, W., Guo, Y., and Wang, X. (2020). Prophage encoding toxin/antitoxin system PfiT/PfiA inhibits Pf4 production in *Pseudomonas aeruginosa*. *Microb. Biotechnol.* 13, 1132–1144. doi: 10.1111/1751-7915.13570

Ma, S., Luo, H., Zhao, D., Qiao, Z., Zheng, J., An, M., et al. (2022). Environmental factors and interactions among microorganisms drive microbial community succession during fermentation of Nongxiangxing daqu. *Bioresour. Technol.* 345, 126549. doi: 10.1016/j.biortech.2021.126549

Magaziner, S. J., Zeng, Z., Chen, B., and Salmond, G. P. C. (2019). The prophages of citrobacter rodentium represent a conserved family of horizontally acquired mobile genetic elements associated with enteric evolution towards pathogenicity. *J. Bacteriol.* 201, e00638–18. doi: 10.1128/JB.00638-18

Mancini, A., Rodriguez, M. C., Zago, M., Cologna, N., Goss, A., Carafa, I., et al. (2021). Massive survey on bacterial-bacteriophages biodiversity and quality of natural whey starter cultures in trentingrana cheese production. *Front. Microbiol.* 12, 678012. doi: 10.3389/fmicb.2021.678012

Marques, A. T., Tanoeiro, L., Duarte, A., Gonçalves, L., Vítor, J. M. B., and Vale, F. F. (2021). Genomic analysis of prophages from klebsiella pneumoniae clinical isolates. *Microorganisms* 9, 2252. doi: 10.3390/microorganisms9112252

Matsutani, M., Matsumoto, N., Hirakawa, H., Shiwa, Y., Yoshikawa, H., Okamoto-Kainuma, A., et al. (2020). Comparative genomic analysis of closely related *Acetobacter pasteurianus* strains provides evidence of horizontal gene transfer and reveals factors necessary for thermotolerance. *J. Bacteriol.* 202, e00553–19. doi: 10.1128/JB.00553-19

Mohanraju, P., Saha, C., van Baarlen, P., Louwen, R., Staals, R. H. J., and van der Oost, J. (2022). Alternative functions of CRISPR-Cas systems in the evolutionary arms race. *Nat. Rev. Microbiol.* 20, 351–364. doi: 10.1038/s41579-021-00663-z

Naorem, R. S., Goswami, G., Gyorgy, S., and Fekete, C. (2021). Comparative analysis of prophages carried by human and animal-associated Staphylococcus aureus strains spreading across the European regions. *Sci. Rep.* 11, 18994. doi: 10.1038/s41598-021-98432-8

Nawel, Z., Rima, O., and Amira, B. (2022). An overview on Vibrio temperate phages: Integration mechanisms, pathogenicity, and lysogeny regulation. *Microb. Pathog.* 165, 105490. doi: 10.1016/j.micpath.2022.105490

Omata, K., Hibi, N., Nakano, S., Komoto, S., Sato, K., Nunokawa, K., et al. (2021). Distribution and genome structures of temperate phages in acetic acid bacteria. *Sci. Rep.* 11, 21567. doi: 10.1038/s41598-021-00998-w

Owen, S. V., Wenner, N., Dulberger, C. L., Rodwell, E. V., Bowers-Barnard, A., Quinones-Olvera, N., et al. (2021). Prophages encode phage-defense systems with cognate self-immunity. *Cell Host. Microbe* 29, 1620–1633 e1628. doi: 10.1016/j.chom.2021.09.002

Park, D. W., Kim, S. H., and Park, J. H. (2022). Distribution and characterization of prophages in Lactobacillus plantarum derived from kimchi. *Food Microbiol.* 102, 103913. doi: 10.1016/j.fm.2021.103913

Pei, Z., Sadiq, F. A., Han, X., Zhao, J., Zhang, H., Ross, R. P., et al. (2021). Comprehensive scanning of prophages in lactobacillus: distribution, diversity, antibiotic resistance genes, and linkages with CRISPR-Cas systems. *mSystems* 6, e0121120. doi: 10.1128/mSystems.01211-20

Philippe, C., Krupovic, M., Jaomanjaka, F., Claisse, O., Petrel, M., and le Marrec, C. (2018). Bacteriophage GC1, a novel Tectivirus infecting *Gluconobacter cerinus*, an acetic acid bacterium associated with wine-making. *Viruses* 10, 39. doi: 10.3390/v10010039

Qin, Z., Yu, S., Chen, J., and Zhou, J. (2022). Dehydrogenases of acetic acid bacteria. *Biotechnol. Adv.* 54, 107863. doi: 10.1016/j.biotechadv.2021.107863

Qiu, X., Zhang, Y., and Hong, H. (2021). Classification of acetic acid bacteria and their acid resistant mechanism. *AMB Express* 11, 29. doi: 10.1186/s13568-021-01189-6

Roy, K., Ghosh, D., DeBruyn, J. M., Dasgupta, T., Wommack, K. E., Liang, X., et al. (2020). Temporal dynamics of soil virus and bacterial populations in agricultural and early plant successional soils. *Front. Microbiol.* 11, 1494. doi: 10.3389/fmicb.2020.01494

Schocher, A. J., Kuhn, H., Schindler, B., Palleroni, N. J., Despreaux, C. W., Boubblik, M., et al. (1979). Acetobacter bacteriophage A-1. *Arch. Microbiol.* 121, 193–197. doi: 10.1007/BF00689986

Secor, P. R., and Dandekar, A. A. (2020). More than simple parasites: the sociobiology of bacteriophages and their bacterial hosts. *mBio* 11, e00041–20. doi: 10.1128/mBio.00041-20

Seed, K. D., Lazinski, D. W., Calderwood, S. B., and Camilli, A. (2013). A bacteriophage encodes its own CRISPR/Cas adaptive response to evade host innate immunity. *Nature* 494, 489–491. doi: 10.1038/nature11927

Shannon, P., Markiel, A., Ozier, O., Baliga, N. S., Wang, J. T., Ramage, D., et al. (2003). Cytoscape: a software environment for integrated models of biomolecular interaction networks. *Genome Res.* 13, 2498–2504. doi: 10.1101/gr.1239303

Somerville, V., Berthoud, H., Schmidt, R. S., Bachmann, H. P., Meng, Y. H., Fuchsmann, P., et al. (2022). Functional strain redundancy and persistent phage infection in Swiss hard cheese starter cultures. *Isme J* 16, 388–399. doi: 10.1038/s41396-021-01071-0

Song, S., and Wood, T. K. (2020). A primary physiological role of toxin/antitoxin systems Is phage inhibition. *Front. Microbiol.* 11, 1895. doi: 10.3389/fmicb.2020.01895

Song, W., Sun, H. X., Zhang, C., Cheng, L., Peng, Y., Deng, Z., et al. (2019). Prophage Hunter: an integrative hunting tool for active prophages. *Nucleic Acids Res.* 47, W74–W80. doi: 10.1093/nar/gkz380

Stamm, W. W., Kittelmann, M., Follmann, H., and Truper, H. G. (1989). The occurrence of bacteriophages in spirit vinegar fermentation. *Appl. Microbiol. Biotechnol.* 30, 41–46. doi: 10.1007/BF00255994

Tang, F., Bossers, A., Harders, F., Lu, C., and Smith, H. (2013). Comparative genomic analysis of twelve Streptococcus suis (pro)phages. *Genomics* 101, 336–344. doi: 10.1016/j.ygeno.2013.04.005

Touchon, M., Bernheim, A., and Rocha, E. P. (2016). Genetic and life-history traits associated with the distribution of prophages in bacteria. *ISME J.* 10, 2744–2754. doi: 10.1038/ismej.2016.47

Varble, A., Campisi, E., Euler, C. W., Maguin, P., Kozlova, A., Fyodorova, J., et al. (2021). Prophage integration into CRISPR loci enables evasion of antiviral immunity in Streptococcus pyogenes. *Nat. Microbiol.* 6, 1516–1525. doi: 10.1038/s41564-021-00996-8

Wang, G., Liu, Q., Pei, Z., Wang, L., Tian, P., Liu, Z., et al. (2020). The diversity of the CRISPR-Cas system and prophages present in the genome reveals the co-evolution of bifidobacterium pseudocatenulatum and phages. *Front. Microbiol.* 11, 1088. doi: 10.3389/fmicb.2020.01088

Wendling, C. C., Refardt, D., and Hall, A. R. (2021). Fitness benefits to bacteria of carrying prophages and prophage-encoded antibiotic-resistance genes peak in different environments. *Evolution* 75, 515–528. doi: 10.1111/evo.14153

Xia, K., Bao, H., Zhang, F., Linhardt, R. J., and Liang, X. (2019). Characterization and comparative analysis of toxin-antitoxin systems in Acetobacter pasteurianus. *J. Ind. Microbiol. Biotechnol.* 46, 869–882. doi: 10.1007/s10295-019-02144-y

Xia, K., Han, C., Xu, J., and Liang, X. (2021a). Toxin-antitoxin HicAB regulates the formation of persister cells responsible for the acid stress resistance in Acetobacter pasteurianus. *Appl. Microbiol. Biotechnol.* 105, 725–739. doi: 10.1007/s00253-020-11078-w

Xia, K., Ma, J., and Liang, X. (2021b). Impacts of type II toxin-antitoxin systems on cell physiology and environmental behavior in acetic acid bacteria. *Appl. Microbiol. Biotechnol.* 105, 4357–4367. doi: 10.1007/s00253-021-11357-0

Xie, Y., Wei, Y., Shen, Y., Li, X., Zhou, H., Tai, C., et al. (2018). TADB 2.0: an updated database of bacterial type II toxin-antitoxin loci. *Nucleic Acids Res.* 46, D749–D753. doi: 10.1093/nar/gkx1033

Yang, H., Chen, T., Wang, M., Zhou, J., Liebl, W., Barja, F., et al. (2022). Molecular biology: Fantastic toolkits to improve knowledge and application of acetic acid bacteria. *Biotechnol. Adv.* 58, 107911. doi: 10.1016/j.biotechadv.2022.107911

Zotta, T., Ricciardi, A., Condelli, N., and Parente, E. (2022). Metataxonomic and metagenomic approaches for the study of undefined strain starters for cheese manufacture. *Crit. Rev. Food Sci. Nutr.* 62, 3898–912. doi: 10.1080/10408398.2020.1870927

frontiers | Frontiers in Microbiology

MINI REVIEW
published: 04 August 2022
doi: 10.3389/fmicb.2022.957167

Acetic Acid Bacteria in Sour Beer Production: Friend or Foe?

*Arne Bouchez and Luc De Vuyst**

Research Group of Industrial Microbiology and Food Biotechnology, Faculty of Sciences and Bioengineering Sciences, Vrije Universiteit Brussel, Brussels, Belgium

Beer is the result of a multistep brewing process, including a fermentation step using in general one specific yeast strain. Bacterial presence during beer production (or presence in the beer itself) is considered as bad, since bacteria cause spoilage, produce off-flavors, and/or turbidity. Although most problems in the past related to lack of hygiene and/or cleaning, bacteria do still cause problems nowadays. Despite this negative imago, certain bacteria play an irreplaceable role during fermentation and/or maturation of more unique, funky, and especially refreshing sour beers. The term *sour beers* or *sours* is not restricted to one definition but covers a wide variety of beers produced *via* different techniques. This review proposes an uncluttered sour beer classification scheme, which includes all sour beer production techniques and pays special attention to the functional role of acetic acid bacteria. Whereas their oxidation of ethanol and lactate into acetic acid and acetoin usually spoils beer, including sour beers, organoleptically, a controlled growth leads to a desirable acidic flavor in sour beers, such as lambic-style, lambic-based, and red-brown acidic ales.

Keywords: sour beer, beer classification, lambic beer, *Acetobacter*, *Brettanomyces*, acetic acid bacteria

OPEN ACCESS

Edited by:
Isidoro García-García, University of Cordoba, Spain

Reviewed by:
Shao Quan Liu, National University of Singapore, Singapore
Diego Bonatto, Departamento de Biologia Molecular e Biotecnologia da UFRGS, Brazil

***Correspondence:**
Luc De Vuyst
luc.de.vuyst@vub.be

Specialty section:
This article was submitted to Food Microbiology, a section of the journal Frontiers in Microbiology

Received: *30 May 2022*
Accepted: *15 June 2022*
Published: *04 August 2022*

Citation:
Bouchez A and De Vuyst L (2022) Acetic Acid Bacteria in Sour Beer Production: Friend or Foe? Front. Microbiol. 13:957167. doi: 10.3389/fmicb.2022.957167

INTRODUCTION

Food fermentations have been done by humans for thousands of years as means of preservation of raw materials from agricultural and husbandry origin (Hutkins, 2019). Other desirable attributes of fermented food products, such as unique flavors, textures, appearances, or other functionalities were recognized rapidly as well (Leroy and De Vuyst, 2004). With the development of other preservation techniques, a lot of fermentation processes have been replaced, and the main goal of the production of fermented foods has shifted from preservation to flavor production and health promotion (Marco et al., 2021). Also, food fermentations are associated with cultural connotations, gastronomic qualities, artisan characteristics, and natural appeal. In several food fermentation processes, not only yeasts and lactic acid bacteria (LAB) but also acetic acid bacteria (AAB) are involved, such as in the production of cocoa, kombucha, lambic beer, vinegar, and water kefir (Gullo et al., 2016; Pothakos et al., 2016; Cousin et al., 2017; De Roos and De Vuyst, 2018; Gomes et al., 2018; Villareal-Soto et al., 2018; De Vuyst and Leroy, 2020; Bongaerts et al., 2021; Lynch et al., 2021).

Fermented foods and drinks play a major role in the human diet and human nutrition worldwide (Marco et al., 2017, 2021). Beer, the end-product of the brewing process, including a fermentation and maturation step, is the most consumed fermented beverage by humans worldwide (Neves et al., 2011; Colen and Swinnen, 2015). Whereas, originally, beer was fermented

in a spontaneous way, due to lack of knowledge and starter cultures, all beers were at least slightly acidic (Hornsey, 2003). This acidity contributed to a safe water supply for beer drinkers, as hop and spice antimicrobial compounds do for non-sour beers. Nowadays, for almost all beers produced the fermentation relies on specific yeast strains and the presence of bacteria is completely undesirable due to their spoilage potential (Briggs et al., 2004; Vriesekoop et al., 2012). However, although their spoilage capacity, some specific beers do require LAB and/or AAB to introduce characteristic beer flavors (Van Oevelen et al., 1977; De Keersmaecker, 1996; Tonsmeire, 2014; De Roos and De Vuyst, 2019; Bongaerts et al., 2021; Kubizniaková et al., 2021). Sour beers, with their typical refreshing and (slightly) acidic flavor because of high organic acid concentrations are an example of such beers, during the production process of some LAB or even both LAB and AAB are part of the core microbiota and hence contribute to their flavor formation (Van Oevelen et al., 1976; Snauwaert et al., 2016; De Roos and De Vuyst, 2019; Bongaerts et al., 2021). Today, the production of sour beers or sours knows an increasing trend.

BEER SPOILAGE BY AAB

AAB are traditionally well known for their beer-spoiling capacity. Beer spoilage has been a problem since multiple decades (Sakamoto and Konings, 2003). The combination of multiple inhibitory factors or hurdles, such as the presence of ethanol (up to 10%, v/v), hop antimicrobial compounds, a low pH, relatively high carbon dioxide concentrations, low oxygen concentrations, and the lack of nutritive compounds makes beer hard to spoil (Kourtis and Arvanitoyannis, 2001; Sakamoto and Konings, 2003; Briggs et al., 2004; Menz et al., 2009; Dysvik et al., 2020c). Despite this harsh environment, some Gram-positive bacteria, Gram-negative bacteria, and so-called wild yeasts are capable of spoiling beer (Van Vuuren et al., 1979; Vriesekoop et al., 2012; Schneiderbanger et al., 2020; Suiker and Wösten, 2021). The Gram-negative bacteria capable of beer spoilage include enterobacteria (such as *Citrobacter*, *Klebsiella*, *Rahnella*, and *Obesumbacterium*), *Zymomonas* spp., *Pectinatus* spp., *Megasphaera* spp., *Selenomonas* spp., *Zymophilus* spp., and AAB, whereof *Acetobacter* and *Gluconobacter* have been mainly reported (Sakamoto and Konings, 2003; Van Vuuren and Priest, 2003). Even though AAB species are strict aerobic, some strains have been detected and identified from beer and have been reported as micro-aerotolerant (Harper, 1980; Briggs et al., 2004; Jeon et al., 2014). Today, aerobic AAB species do not form a big problem of beer spoilage anymore thanks to the development of improved brewing technology and beer storage, capable of lowering oxygen levels drastically (Sakamoto and Konings, 2003).

As AAB are in particular acid- and ethanol-tolerant and not inhibited by hop compounds, they may grow in beer. Beer spoilage by AAB species is characterized by a sour taste and vinegary aroma, caused by ethanol oxidation into acetic acid (Ingledew, 1979; Magnus et al., 1986). Besides off-flavor formation, AAB species, such as *Acetobacter aceti, Acetobacter liquefaciens*, *Acetobacter pasteurianus, Acetobacter hansenii* and *Gluconobacter oxydans*, can cause haziness and ropiness in the beer or form pellicles on the beer surface (Van Vuuren, 1999; Van Vuuren and Priest, 2003; Briggs et al., 2004; Hill, 2015; Paradh, 2015).

Since most spoilage incidents with AAB are related to oxygen, the key to prevent spoilage by AAB is to limit oxygen ingress as much as possible and apply good hygiene regimes. Additional care should be applied during bottling in the brewery and cleaning of beer lines, taps, and dispense systems in pubs (Briggs et al., 2004; Vriesekoop et al., 2012). Alternatively, when AAB belong to the desired fermentation microbiota, key will be to have their growth under control.

GENERAL BEER CLASSIFICATION

Beers are generally classified within four different beer production types, being bottom-fermented beers, top-fermented beers, spontaneously fermented beers, and mixed-fermented beers (Briggs et al., 2004; De Roos and De Vuyst, 2019; Bongaerts et al., 2021). This classification is made according to the fermentation step and which microorganisms are involved, in particular related to their origin. The use of specific strain(s) of the yeast species *Saccharomyces bayanus* or *Saccharomyces pastorianus* for bottom fermentation and *Saccharomyces cerevisiae* for top fermentation characterizes these yeast-based fermentation processes, which are carried out in stainless-steel vessels. In stark contrast to these very controlled fermentation processes stands a spontaneous one, for which a diverse multistage fermentation and maturation process in horizontal wooden barrels results in a unique sour beer, thanks to the successive activities of different microbial groups, in particular yeasts, LAB, and AAB (Bokulich et al., 2012; Spitaels et al., 2014a, 2015b; De Roos et al., 2018a,b, 2020; De Roos and De Vuyst, 2019; Bongaerts et al., 2021). Mixed fermentation is a combination of top and spontaneous fermentation techniques, for which process an in-house starter culture, a yeast slurry also containing LAB from previous fermentations, is added, and maturation in vertical wooden barrels (potentially involving AAB) or stainless-steel vessels (Tonsmeire, 2014; Snauwaert et al., 2016; Spitaels et al., 2017; De Roos and De Vuyst, 2019).

EXTENDED CLASSIFICATION SYSTEM

The traditional classification into four different beer production types does not cover all beers on the market nowadays, especially more experimental beers, craft beers, or beers produced by microbreweries, which are known to experiment more in the search for new flavor profiles. The craft beer industry, growing since the 1970s, is characterized not only by reusing traditional techniques and brewing with traditional ingredients but also by their diverging application regarding ingredients used, yeasts applied, alcohol content, aging, isotonic claims, and/or packaging (Donadini and Porretta, 2017; Li et al., 2017; Baiano, 2020; Lattici et al., 2020).

The traditional four-type classification system hence only includes three added *Saccharomyces* species, namely *S. cerevisiae* for top fermentation and *S. bayanus* or S. *pastorianus* for bottom fermentation. Therefore, beers produced using other, non-*Saccharomyces* yeast species, such as *Brettanomyces* spp., *Torulaspora* spp., *Pichia* spp., etc., cannot be classified unambiguously. Consequently, an extended classification system is suggested in this review, taking into account the fermentation type (distinguishing five production processes), the microorganisms involved (not only yeasts but also LAB and AAB), and the acidification principle (**Figure 1**). A separate beer production type, indicated as non-conventional fermented beers, covers all beers fermented solely using yeasts, except for *S. cerevisiae*, *S. pastorianus* and *S. bayanus* (Type C in **Figure 1**). This beer production type likely makes the transition from yeast-based fermentation processes to sour beer production types.

Whereas non-sour beers rely on fermentation and/or maturation steps done using an axenic *Saccharomyces* yeast strain, the story differs for sour beers (Bokulich and Bamforth, 2013; Tonsmeire, 2014; Bossaert et al., 2019; Dysvik et al., 2020c).

Spontaneously Fermented Sour Beers

One of the, if not the, most traditional sour beer production processes is based on spontaneous inoculation, thus without initiation of the fermentation of the wort by addition of a starter culture (Type D in **Figure 1**). It mainly concerns Belgian lambic beer and American coolship ale (ACA) productions, two of the most popular spontaneously fermented beers worldwide. Generally, the boiled and sterile wort is inoculated *via* multiple ways with a so-called wild microbiota, consisting of both wanted and unwanted yeasts and bacteria (De Keersmaecker, 1996; Spitaels et al., 2014a, 2015b; De Roos and De Vuyst, 2019; Bongaerts et al., 2021). Inoculation takes place when the environmental air gets into contact with the wort during an overnight cooling step using a metallic open vessel or coolship, when the wort gets into contact with the surfaces of the brewery equipment, and especially by contact of the fermenting wort and maturing beer with the interior surfaces of the horizontal, wooden barrels during the long-lasting fermentation and maturation steps (De Keersmaecker, 1996; De Roos and De Vuyst, 2019; Bongaerts et al., 2021). Therefore, spontaneously fermented beers are produced during the winter period to cool down the boiled wort fast enough, and so limit enterobacterial growth, in particular when the wort is not acidified manually, and in temperature-controlled cellars to achieve an optimal microbial succession (Bokulich et al., 2012; De Roos et al., 2018a; De Roos and De Vuyst, 2019; Bongaerts et al., 2021).

Specifically for bacteria, a broad range of species, including enterobacteria, LAB, and AAB have been isolated and identified from spontaneously fermenting lambic beer and ACA worts (Bokulich et al., 2012; De Roos and De Vuyst, 2019; Bongaerts et al., 2021; De Roos et al., unpublished results). Bacteria are typically present from the start of the lambic beer wort fermentation till the end of the extended barrel maturation process, which can last up to 3 years (Van Oevelen et al., 1977; Verachtert and Iserentant, 1995; De Roos et al., 2018b; Bongaerts et al., 2021). They are also present in lambic-based beers, such as gueuze, a bottle-refermented blend of young and old lambic beers (Spitaels et al., 2015a; De Roos et al., 2018a,b, 2020;

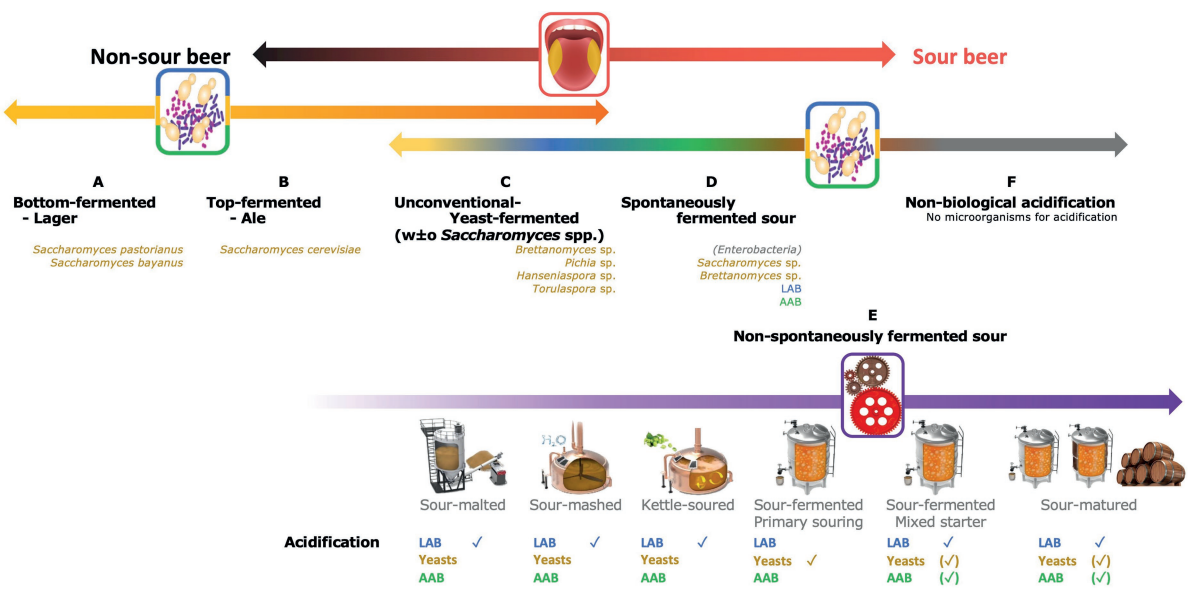

FIGURE 1 | Schematic representation of an extended beer classification. On top, a first subdivision is made based on taste [from left to right non-sour (black) to sour (red)]; in the middle, distinction is made based on the fermentation technology applied and the microorganisms involved [yeasts (yellow-orange); lactic acid bacteria (LAB, blue); acetic acid bacteria (AAB, green); and no microorganisms (gray)]. Category E is further subdivided according to the acidification technique applied and the microorganisms responsible for the acidification are indicated.

Bongaerts et al., 2021; Piraine et al., 2021). More specifically, AAB are encountered during nearly the whole fermentation and maturation process of lambic beers but are mainly active during the first weeks, called the wild or enterobacterial and thus initial fermentation phase, during the acidification phase (two up to 12 months), and during maturation (up to 3 years; Bokulich et al., 2012; Spitaels et al., 2014a; De Roos and De Vuyst, 2019; Bongaerts et al., 2021). Next to gueuze, different types of lambic-based sour beers are produced in a traditional way, in particular fruit beers, such as *Oude Kriek* [additional fermentation in barrels of young (around 1 year old) lambic beer blended with fresh sour cherries], *Framboise* (young lambic beer blended with raspberries), and *Pecheresse* (young lambic beer blended with peaches), as well as Faro (young lambic beer blended with rock sugar; De Keersmaecker, 1996; Briggs et al., 2004; Tonsmeire, 2014; Verachtert and Derdelinckx, 2014; Pothakos et al., 2016; Dysvik et al., 2020c).

Culture-dependently, AAB species belonging to only two genera (*Acetobacter* and *Gluconobacter*) have been isolated and identified from spontaneously fermented sour beers (Bokulich et al., 2012; Spitaels et al., 2014a,b,c, 2015a,b; Snauwaert et al., 2016; De Roos et al., 2018a,b; **Table 1**). Culture-independent methods, such as metagenetics (targeting a part of or the whole 16S rRNA marker gene) and shotgun metagenomics, have led to the identification of not only *Acetobacter* spp. and *Gluconobacter* spp. but also *Gluconacetobacter* spp. and *Komagataeibacter* spp. (Bokulich et al., 2012; Snauwaert et al., 2016; De Roos et al., 2018a, 2020; Piraine et al., 2021; Tyakht et al., 2021; De Roos et al., unpublished results; **Table 2**).

Non-spontaneously Fermented Sour Beers

Multiple techniques of sour beer production fall in this category, differing according to the acidification method and especially where and when the acidification takes place (Bossaert et al., 2019; Dysvik et al., 2020a,b,c; Type E in **Figure 1**).

Sour-Malted and Sour-Mashed Beers

Malt, barley grains processed during the malting process, is used for almost all beers produced worldwide (Briggs et al., 2004). In the case of sour malting and sour mashing, acidification takes place during malting or mashing, respectively (Bossaert et al., 2019; Dysvik et al., 2019, 2020b,c). The acidification is achieved by the growth and metabolic activity of LAB, such as *Lactiplantibacillus plantarum* or *Pediococcus pentosaceus* (Laitila et al., 2006; Vriesekoop et al., 2012; Peyer et al., 2017). Carbohydrates present on the surfaces of the malted grains or in the mash are converted into lactic acid and in the case of sour malting, this lactic acid is retained on the grain surfaces (Lowe and Arendt, 2004; Vriesekoop et al., 2012). Lactic acid typically lowers the pH value around 0.15 to 0.25 units and therefore only 3–10% of the total grist will be acidified malt (Lowe et al., 2004; Lowe and Arendt, 2004). The resulting wort using acidified malts has a pH value around 5.2, in contrast with a pH of around 5.5 for non-acidified malt-based wort (Back, 2005; Vriesekoop et al., 2012). Whereas the influence of LAB starter cultures seems marginally, it results in an improved malting process, by suppressing rootlet growth of the germinating grain kernels, which has been shown to outperform chemical rootlet inhibitors (Vriesekoop et al., 2012). LAB starter culture application during the malting process results in an increased malt yield, an improved filterability, and lower wort viscosity (Vriesekoop et al., 2012). Additionally, LAB show certain antifungal and antibacterial activities, lowering the growth of fungi, such as *Fusarium*, which are involved in gushing and potential mycotoxin production (Batish et al., 1997; Lowe and Arendt, 2004; Shetty and Jespersen, 2006; Rouse et al., 2008; Vriesekoop et al., 2012).

Kettle-Soured Beers

During kettle souring, LAB acidify the wort in the brewing kettle. Sometimes, wort is boiled (without hops) prior to LAB pitching or the LAB inoculation can happen straight after mashing, without boiling (Cantwell and Bouckaert, 2016; Bossaert et al., 2019; Dysvik et al., 2020c). Kettle souring, also called quick souring, is a modern technique with the biggest advantage that the desired acidification typically takes place after one to 3 days (Bossaert et al., 2019). Acidification can be stopped either by boiling or by the addition of (heavily) hopped wort. LAB are then inactivated due to their sensitivity to hop-related compounds, such as α-acids (humulones), β-acids (lupulones), or their isomerized forms (iso-α-acids or iso-humulones and iso-β-acids or iso-lupulones, respectively; Almaguer et al., 2014). Further, addition of heavily hopped wort limits the loss of flavor compounds, which can happen during boiling (Tonsmeire, 2014; Bossaert et al., 2019; Dysvik et al., 2020c). Yet, when a less complex sour beer is wanted, boiling after acidification can be desired (Tonsmeire, 2014; Admassie, 2018).

Sour-Fermented Beers

Sour-fermented beers comprise all techniques for which ethanol production and acidification take place at the same moment. Sour-fermented beers can be divided into two large categories, based on the fact if there are bacteria present or not. For both, wort is prepared as usual, and the fermentation takes place in stainless-steel vessels (Tonsmeire, 2014).

Primary Souring

Sour-fermented beers produced in the total absence of any bacteria must be produced through fermentation with yeast species capable of degradation of carbohydrates into lactic acid, ethanol, and carbon dioxide (Osburn et al., 2016, 2018). *Hanseniaspora vineae, Lachancea fermentati, Lachancea thermotolerans, Schizosaccharomyces japonicus,* and *Wickerhamomyces anomalus* species have been tested before and most strains examined are able to completely ferment the wort within 4 weeks (Domizio et al., 2016; Osburn et al.,

TABLE 1 | Overview of acetic acid bacterial species identified culture-dependently from sour beers.

Taxon	Production phase				Isolation medium	Reference
	Initial fermentation phase	Alcoholic fermentation phase	Acidification phase	Maturation phase		
Belgian lambic beer						
Acetobacter cerevisiae	Inside cask				AAM	Spitaels et al., 2014a
	✓				mDMS	De Roos et al., 2018b
	✓				mDMS	De Roos et al., unpublished results
Acetobacter orientalis	✓				mMRS	De Roos et al., 2018a
	✓				mDMS	De Roos et al., 2018b
	✓	✓	✓		AAM	Spitaels et al., 2015a
Acetobacter lambici			✓	✓	mDMS	De Roos et al., 2018b
				✓	mMRS	De Roos et al., 2018a
	✓	✓			AAM	Spitaels et al., 2015a
			✓		AAM	Spitaels et al., 2014c
				✓	AAM	Spitaels et al., 2015b
				✓	mDMS	De Roos et al., unpublished results
Acetobacter pasteurianus			✓	✓	mDMS	De Roos et al., 2018b
Acetobacter aceti	✓				mDMS	De Roos et al., 2018b
Acetobacter lovaniensis	✓				mDMS	De Roos et al., 2018b
Acetobacter indonesiensis	✓				mDMS	De Roos et al., 2018b
Acetobacter fabarum	✓	✓	✓	✓	AAM	Spitaels et al., 2015a
	✓				mDMS	De Roos et al., unpublished results
Gluconobacter cerevisiae	✓				mDMS	De Roos et al., 2018b
	✓	✓	✓		AAM	Spitaels et al., 2014b, 2015a
Gluconobacter wancherniae	✓				mDMS	De Roos et al., 2018b
Gluconobacter cerinus	✓	✓			AAM	Spitaels et al., 2015a
American coolship ales						
A. fabarum		✓	✓	✓	WLD	Bokulich et al., 2012
Acetobacter lovanesiensis	✓	✓	✓	✓	WLD	Bokulich et al., 2012
Belgian red-brown acidic ales						
A. pasteurianus				✓	mDMS	Snauwaert et al., 2016

AAM, acetic acid medium; mDMS, modified deoxycholate-mannitol-sorbitol medium; mMRS, modified de Man-Rogosa-Sharpe medium; and WLD, Wallerstein differential medium.

2018; Bossaert et al., 2019). Whereas these yeast species have mainly been reported as members of mixed-starter cultures for beer wort and wine must fermentations, generally combined with *Saccharomyces* yeast species, they are able to attenuate beer wort sufficiently when used as the sole yeast starter, and they are capable of producing L-lactic acid in sufficient concentrations to produce sour beers (Banilas et al., 2016; Domizio et al., 2016; Benito, 2018; Osburn et al., 2018; Larroque et al., 2021; Vicente et al., 2022). Strain selection is of major importance, since large within-species and -strain variations occur, which greatly influences the final products (Osburn et al., 2018; Gatto et al., 2020). A high variability has been reported regarding lactic acid and ester production, flavor formation, sourness perception, and final pH (Domizio et al., 2016; Gamero et al., 2016; Osburn et al., 2018; Gatto et al., 2020; Vicente et al., 2021). Brewing primary-soured beers has the additional advantage of being produced without blocking the brewing kettle for days. It results in better sensory profiles compared to kettle-soured beers, without a long barrel aging process as is the case for spontaneously fermented sour beers (Osburn et al., 2018). The absence of acidifying bacteria in the brewing apparatus and brewery eliminates the risk of contaminating non-sour beers, especially when both sour and non-sour beers are brewed on the same site and/or using

TABLE 2 | Overview of acetic acid bacterial species identified culture-independently from sour beers.

Taxon	Production phase				Technique	Reference
	Initial fermentation phase	Alcoholic fermentation phase	Acidification phase	Maturation phase		
Belgian lambic beer						
Acetobacter spp.	✓	✓	✓	✓	Metagenetics (V4 region of 16S rRNA gene)	De Roos et al., 2018a
			✓	✓	Shotgun metagenomics	De Roos et al., 2020
	✓		✓	✓	Shotgun metagenomics	De Roos et al., unpublished results
Acetobacter cerevisiae	✓				Shotgun metagenomics	De Roos et al., unpublished results
Acetobacter fabarum	✓				Shotgun metagenomics	De Roos et al., unpublished results
Acetobacter indonesiensis	✓				Shotgun metagenomics	De Roos et al., unpublished results
Acetobacter lambici				✓	Shotgun metagenomics	De Roos et al., unpublished results
Acetobacter malorum	✓				Shotgun metagenomics	De Roos et al., unpublished results
Acetobacter pasteurianus			✓		Shotgun metagenomics	De Roos et al., 2020
Acetobacter pomorum			✓		Shotgun metagenomics	De Roos et al., 2020
Gluconobacter spp.			✓	✓	Shotgun metagenomics	De Roos et al., 2020
	✓				Shotgun metagenomics	De Roos et al., unpublished results
	✓				Shotgun metagenomics	De Roos et al., 2018a
Gluconobacter japonicus	✓				Shotgun metagenomics	De Roos et al., unpublished results
Gluconacetobacter spp.			✓	✓	Shotgun metagenomics	De Roos et al., 2020
Gluconacetobacter liquefaciens	✓				Shotgun metagenomics	De Roos et al., unpublished results
Komagataeibacter spp.			✓	✓	Shotgun metagenomics	De Roos et al., 2020
American Coolship Ales (ACAs)						
Acetobacteraceae		✓		✓	16S-Terminal Restriction Fragment Length Polymorphism (TRFLP)	Bokulich et al., 2012
Belgian red-brown acidic ales						
Acetobacteraceae		Bottled red-brown acidic ale			Metagenetics (V4 region of 16S rRNA gene)	Tyakht et al., 2021
A. pasteurianus				✓	Metagenetics (V1-V3 region of 16S rRNA gene)	Snauwaert et al., 2016
Spontaneously fermented beer						
Acetobacter spp.		Finished beer, beer slurry			Metagenetics (V3-V4 region of 16S rRNA gene)	Piraine et al., 2021
Gluconobacter oxydans		Finished beer			Metagenetics (V3-V4 region of 16S rRNA gene)	Piraine et al., 2021

the same brewing equipment (Osburn et al., 2018; Bossaert et al., 2019). Additionally, yeast growth is very limited or completely not impacted by the hop dosing and release of iso-α-acids into the wort. Consequently, higher hop dosages can be applied during primary souring brewing, since acidification does not rely on bacteria, which are generally more sensitive to iso-α-acids, in particular Gram-positive LAB (Hazelwood et al., 2010; Almaguer et al., 2014; Domizio et al., 2016; Osburn et al., 2018).

Mixed-Culture Fermented Sour Beers

The term mixed culture is used when more than one specific microbial strain and/or species is present during fermentation. The application of a mixed-starter culture differs from spontaneously fermented beers, such as lambic beer, in that in the latter case all yeasts and bacteria originate from the environment and/or brewing tools (De Keersmaecker, 1996; De Roos et al., 2018b; Bongaerts et al., 2021). Both traditional, red/brown (Flanders red ales) and old-brown (Flanders brown ales) acidic (Flemish) ales, and modern mixed-culture sour beers (Flanders-style sour ales) exist on industrial scale nowadays (Tonsmeire, 2014; Snauwaert et al., 2016; Bossaert et al., 2019; Dysvik et al., 2020c). During red/brown acidic ale production, a yeast slurry from previous fermentation processes is added to the cooled wort to perform the fermentation. Although the yeast slurry typically undergoes an acid wash, it still contains LAB (Martens et al., 1997). Initially, AAB have not been detected in the slurry or during primary fermentation (Martens et al., 1997). However, making use of appropriate selective agar media and incubation conditions, AAB have been isolated from beers at the end of the maturation phase, in particular *A. pasteurianus* (Snauwaert et al., 2016). Notice that the final beers representing Flanders red ales are also blends of two-year barrel-matured beers and young, non-matured beers, whereby different blend ratios give different red-brown sours (such as Rodenbach Classic, Grand Cru, and Vintage). During modern mixed fermentation processes, a mixture of yeasts (*Saccharomyces* and/or non-*Saccharomyces* spp.) and bacteria (LAB and/or AAB) is added as starter culture after wort production, either all at the same time, or spread over time (Peyer et al., 2017; Ciosek et al., 2019; Dysvik et al., 2019, 2020a,b,c).

Sour-Matured Beers

When acidification happens during the maturation phase, either solely during maturation or as further souring during maturation, the beers can be classified as sour-matured. Sour maturation can take place in both stainless-steel vessels or wooden barrels, but maturation differs according to the container used (Tonsmeire, 2014; Snauwaert et al., 2016).

Sour Maturation in Wooden Barrels

Wooden barrels were historically by far the most applied beer transport and storage tool, but have later disappeared due to practical reasons and the unpredictability of the quality of the resulting beers (Twede, 2005; Tonsmeire, 2014; Bossaert et al., 2019, 2020, 2022b). Yet, wooden barrels are nowadays gaining interest again, either for production or maturation, to introduce additional flavors and hence achieve more complex flavor profiles and/or sour beers (Garcia et al., 2012; Tonsmeire, 2014; Cantwell and Bouckaert, 2016; Bossaert et al., 2019, 2020; Shayevitz et al., 2020). Although introducing wood-associated flavors seems to be the most obvious reason, wooden barrel maturation does more. Flavors from previous uses of the barrels, such as for the production of port wine, wine or spirits, or for storage, can be introduced in the maturing beer (De Rosso et al., 2009; Fernandez de Simon et al., 2014; Cantwell and Bouckaert, 2016; Shayevitz et al., 2020). Also, microbial activity during barrel maturation can lead to new flavors, including a sour taste and acidic notes (Tonsmeire, 2014; Cantwell and Bouckaert, 2016; Bossaert et al., 2019, 2022a). Wooden barrels are generally made of oak, chestnut, cherry, and/or acacia wood (Cantwell and Bouckaert, 2016; Bossaert et al., 2019, 2020, 2022c). Due to the porous nature of the wood, wooden barrels are slightly permeable for oxygen gas and thus create a microaerobic environment, which may allow the growth of AAB (Cantwell and Bouckaert, 2016; De Roos et al., 2019; Bongaerts et al., 2021). Also linked with their porosity, wooden barrels harbor microorganisms up to 1.2 cm deep and act so as inoculation source for the fermenting wort and/or maturing beer (De Roos et al., 2019; Shayevitz et al., 2020; Bongaerts et al., 2021). The typical wooden barrel-associated microbiota consists of *Brettanomyces* yeasts, LAB and AAB, which have been isolated numerously from barrel-aged beers, including barrel-aged ales (Bokulich et al., 2012; Spitaels et al., 2014a; De Roos et al., 2018b, 2019; Shayevitz et al., 2020). In combination with a microaerobic environment, ethanol can be oxidized to acetic acid easily, which in turn impacts the beer flavor significantly and causes acidification of the beer (Cantwell and Bouckaert, 2016; De Roos et al., 2019; Shayevitz et al., 2020). Despite widespread use of wooden barrels, barrel maturation is generally a long-lasting process, and it remains trial and error concerning the flavor of the final beer, since the outcome relies on many factors including barrel characteristics, such as barrel history, barrel cleaning methods applied, barrel condition, and barrel wood, intrinsic beer characteristics such as alcohol level and pH, duration of the maturation, temperature, and humidity (Garcia et al., 2012; Sterckx et al., 2012; Cantwell and Bouckaert, 2016; Bossaert et al., 2022a,c).

Sour Maturation in Metallic Vessels

In contrast with wooden barrels, stainless-steel vessels are not permeable for oxygen gas and do not harbor microorganisms. Consequently, acidification in metallic vessels can take place if the beer itself contains acidifying microorganisms, such as LAB, or acidifying microorganisms can be added (Tonsmeire, 2014). One of the most known beers produced through acidification in metallic vessels are old-brown acidic ales (Flanders brown ales; Tonsmeire, 2014; De Roos and De Vuyst, 2019). Old-brown acidic ales are produced as red/red-brown acidic ales but differ in the usage of metallic vessels for old-brown acidic ales and wooden barrels for red/red-brown acidic ales, and have been described as more malty and less acidic (Verachtert and Iserentant, 1995; Martens et al., 1997; Preedy, 2008; Tonsmeire, 2014; Snauwaert et al., 2016; De Roos and De Vuyst, 2019). The sour taste and acidic notes of old-brown acidic ales mainly comes from LAB activity during fermentation, prior to the metallic vessel maturation, but these beers do not acidify by acetic acid formation during maturation (Tonsmeire, 2014; Snauwaert et al., 2016). This must be ascribed to the lack of inoculation of barrel-associated AAB and the anaerobic environment inside stainless-steel vessels.

Non-biological Acidification

Whereas all beers of Types D and E are acidified by bacteria and/or yeasts, sour beers can also be acidified without microbial interference (Tonsmeire, 2014; Dysvik et al., 2019; Tan et al., 2021; Type F in **Figure 1**). Non-biologically acidified beers, also called chemically acidified beers, are produced by adding food-grade organic acids, such as lactic acid, fresh fruits, fruit juices, or lemonades (Franz et al., 2009; Tonsmeire, 2014; Dysvik et al., 2019; Tan et al., 2021). The main advantage linked with this production technique is the ability to experiment extensively with juice/beer ratios or the kinds of fruits used (Tonsmeire, 2014). In general, the most used fruits are berries, such as blueberries and raspberries, and cherries, but many more have been used, such as citrus fruits, peaches, mangoes, etc. (Tonsmeire, 2014; Tan et al., 2021). Beers produced by blending fruit juices with finished (eventually pasteurized) beers should not be confused with traditional fruit lambic beers, as the latter still evolve over time by the presence of metabolically active microorganisms, whereas non-biological acidified beers do not evolve anymore.

FUNCTIONAL ROLE OF AAB DURING SOUR BEER PRODUCTION

AAB, and bacteria in general, are completely unwanted during non-sour beer production, mainly due to their acetic

acid production turning the beer into vinegar (Bokulich and Bamforth, 2013). Despite their bad reputation, AAB do contribute unambiguously to desired flavor formation during the fermentation and/or maturation of certain sour beer types (Vriesekoop et al., 2012; De Roos and De Vuyst, 2019; Bongaerts et al., 2021; **Figure 1**). As mentioned above, the best studied example of AAB in beers is their appearance and functionality during fermentation and maturation of spontaneously fermented beers, such as lambic beer, and to a lesser extent the ACA analogue (Martens et al., 1997; Bokulich et al., 2012; Spitaels et al., 2014a, 2015b, 2017; Tonsmeire, 2014; Snauwaert et al., 2016; De Roos and De Vuyst, 2019; Bongaerts et al., 2021). Historically, the functional role of AAB in spontaneously fermented beers was considered limited and solely restricted to the oxidation of ethanol to acetic acid. Although this is their most impacting and characterizing feature, more functionalities and contributions during fermentation and maturation have been described in the last decade. Limited literature is available about AAB presence in sour beers, except for red-brown acidic ales, ACAs and especially lambic beer, and so is the following writing mainly based on findings during spontaneously fermented beers, and to a lesser extent on findings originating from research applied on red-brown acidic ales.

Acetic Acid Production

Acetic acid bacteria occurrence in beers is mainly linked with their most characterizing feature, being the aerobic, incomplete oxidation of ethanol, carbohydrates, or sugar alcohols by dehydrogenase activities into the corresponding organic acids, sometimes referred to as oxidative fermentation (Cleenwerck et al., 2002; Ashtavinayak and Elizabeth, 2016; De Roos and De Vuyst, 2018; De Roos et al., 2018a). The two-step catalytic oxidation of ethanol comprises first oxidation of ethanol by membrane-bound pyrroloquinoline quinone (PQQ)-dependent alcohol dehydrogenase (ADH) activity to acetaldehyde and the further oxidation of the latter compound by a membrane-bound aldehyde dehydrogenase (ALDH) to acetic acid (Yakushi and Matsushita, 2010; Gomes et al., 2018). Since both enzymes, ADH and ALDH, form a multienzyme complex, acetaldehyde is not released (Gomes et al., 2018). Acetic acid influences the beer flavor in a drastic way, since it is described as harsh, and it thus contributes a sharp sourness and vinegary notes if present above the threshold concentration of around 200 mg/l (Van Oevelen et al., 1976; De Roos et al., 2019). Although acetic acid possibly causes problems in non-sour beers or when it is present in excessively high concentrations in sour beers, it is crucial to get the unique flavor profile and refreshing character of most sour beers (Van Oevelen et al., 1976; De Roos et al., 2019; Bongaerts et al., 2021).

Maltooligosaccharide Degradation

Maltooligosaccharides (MOS) is the overarching term of linearly α-1-4 glycosidically bound glucopyranosyl units, covering chain lengths of two up to 10 glucose molecules. MOS are formed from starch due to a breakdown by heat and endogenous amylase activity, mainly during the mashing process (Fangel et al., 2018). During beer production with pitching of an axenic yeast culture of *S. cerevisiae*, *S. pastorianus* or *S. bayanus*, MOS remain untouched, due to the lack of the expression of the degrading enzymes (Sheih et al., 1979). Other yeast species, such as *Saccharomyces kudriavzevii* but especially *Brettanomyces/Dekkera* spp., are known to express α-glucosidases, which allows the metabolism of MOS (Kumara et al., 1993; De Roos et al., 2020). Especially *Brettanomyces/Dekkera* spp. can metabolize this additional substrate when all mono- and disaccharides are depleted and hence explaining their growth and activity during the maturation phase of lambic beer production (De Roos and De Vuyst, 2019; Bongaerts et al., 2021). Besides MOS breakdown by yeasts, shotgun metagenomic research of fermenting lambic beer wort has shown that two genes for MOS breakdown, encoding maltooligosyl trehalose synthase and maltooligosyl trehalose, are associated mainly with *A. pasteurianus* as well as with *Acetobacter pomorum* and an unknown *Acetobacter* species, most likely *A. lambici* (De Roos et al., 2020). Shotgun metagenomic research of fermenting lambic beer wort has additionally demonstrated that *A. cerevisiae* and *Acetobacter malorum* contain these two genes, encoding maltooligosyl trehalose synthase and maltooligosyl trehalose, as well (De Roos et al., unpublished results). These two enzymes allow the degradation of MOS by their conversion into maltooligosyl trehalose, followed by the release of trehalose (disaccharide of α-1-1 glycosidically bound glucopyranosyl molecules) by maltooligosyl trehalose activity, to protect the cells against osmotic stress (Zhang et al., 2015; De Roos et al., 2020). Although these two genes are present, it still has to be confirmed if MOS degradation indeed takes place by the latter two species, since high acetic acid concentrations inhibit the biosynthesis of trehalose (Yang et al., 2019). Surprisingly, examining the whole genome of one of the most encountered AAB species, *A. lambici*, it is not one of the species possessing the latter two enzymes for MOS degradation *via* trehalose, although it is very well adapted to the harsh late stages of the lambic beer production process when all mono- and disaccharides are depleted (De Roos et al., 2020; De Roos et al., unpublished results).

Ester Formation

Esters are extremely important for flavor formation of fermented beverages, including beer, among which ethyl acetate, isoamyl acetate, ethyl hexanoate and ethyl octanoate are the most desired ones produced by yeasts (Engan, 1974; Verstrepen et al., 2003; He et al., 2014). The ester profile of sour beers covers two main types, namely ethyl esters (the condensation products of ethanol and fatty acids) and acetate esters (the condensation products of acetic acid and higher alcohols; Pires et al., 2014; Bongaerts et al., 2021). The ester profile of sour beers differs from top-fermented and bottom-fermented beers, as AAB species contribute to

not only acetic acid formation but also ester formation by their expression of esterases (Kashima et al., 2000; De Roos et al., 2020). AAB, more specifically *Acetobacter* spp., possess the intracellular esterases EST1 and EST2 and are thus able to catalyze the condensation of ethanol and acetic acid into ethyl acetate, the most abundant ester in lambic beers (Van Oevelen et al., 1976; Kashima et al., 1998, 2000; Tonsmeire, 2014; Witrick et al., 2017; De Roos and De Vuyst, 2019; De Roos et al., 2020; Bongaerts et al., 2021). Ethyl acetate is of indisputable importance for the lambic beer flavor, and by extension sour beer flavor, due to its high odor activity value and high concentrations. Its formation is ascribed to not only the activities of *Brettanomyces* yeasts and AAB but also chemical esterification of ethanol and acetate (Van Oevelen et al., 1976; Verstrepen et al., 2003; De Roos et al., 2018a). Besides with the formation of ethyl acetate, esterase EST1 is also linked with the formation of isoamyl acetate, an abundantly formed ester by *S. cerevisiae* (Kashima et al., 2000).

Acetoin Production

Acetoin or 3-hydroxy-2-butanone is a flavor-active compound associated with yoghurt flavor, cream odor, and buttery taste (Xiao and Lu, 2014; De Roos and De Vuyst, 2018, 2019; Bongaerts et al., 2021). Acetoin can be produced by yeasts, LAB (such as *P. damnosus*) and AAB, since they all possess the necessary genes. *Acetobacter* spp. are most likely the main producers of acetoin in sour beers, as has been shown during lambic beer productions and cocoa fermentation processes (Adler et al., 2014; Moens et al., 2014; De Roos et al., 2018a,b, 2020). The acetoin concentrations increase when AAB appear and acetoin is produced more at the air/liquid interface of fermenting lambic beer wort in wooden barrels, where typically AAB are present in higher numbers (De Roos et al., 2018a,b, 2020). Indeed, lactic acid can be used as carbon source and oxidized into pyruvate, further converted by acetolactate synthase and/or acetolactate decarboxylase into α-acetolactate and finally by diacetyl reductase into acetoin (Adler et al., 2014; Moens et al., 2014; De Roos et al., 2020; Pelicaen et al., 2020). These features have been supported by metagenomic identification of the appropriate genes and phenotypically in both lambic beer productions and cocoa fermentation processes (Moens et al., 2014; De Roos et al., 2020). Acetoin, in combination with acetic acid, contributes to sour beer flavors. However, excessive concentrations should be avoided, since high acetoin levels can cause undesirable buttery notes (De Roos et al., 2018a; Bongaerts et al., 2021). AAB growth should always be controlled by using well-sealed wooden barrels, which do allow microaerobic conditions through the pores of the wood and the formation of a yeast pellicle at the surface of the liquor to limit oxygen inlet from the headspace into the beer. Volume adjustments over time compensate volume losses by evaporation, decrease headspace volumes containing oxygen, and decrease the contact surface between the maturing beer and the barrel headspace, all limiting oxygen entering the beer, and so preventing AAB to grow too extensively (Tonsmeire, 2014; De Roos et al., 2018b, 2019). Finally, the temperature should always be controlled and kept stable, typically below 20°C, again to prevent excessive AAB growth (Van den Steen, 2012; Tonsmeire, 2014).

HEALTH-PROMOTING PROPERTIES

Sour beers, especially the ones produced by a spontaneous fermentation process, can be linked with health benefits (De Roos and De Vuyst, 2022). First, sour beers containing living LAB and/or AAB cells may contribute to a good microbial balance inside the human gut (Marco et al., 2017, 2021; De Roos and De Vuyst, 2022). Regarding this feature, sour beers have been produced using probiotic LAB strains, for instance with *Lacticaseibacillus paracasei* L26 and DTA-81, and sour beers have been evaluated regarding their suitability as probiotic delivery matrix, which has been demonstrated successfully if produced using a semi-separated co-culture system (Chan et al., 2019; Silva et al., 2020). Further, the occurrence of high-molecular-mass pentosans and ß-glucans, produced by LAB, in sour beer can provide this beer with a natural source of prebiotics (Peyer et al., 2017; Silva et al., 2020).

Regarding caloric values, sour beers can be a helping hand. Whereas non-sour beers are rich in calories, mainly caused by the ethanol content in combination with the presence of residual unfermentable carbohydrates, most sour beers are almost carbohydrate-free, thanks to their complete MOS degradation by interference of non-conventional yeasts, LAB, and/or AAB (De Cort et al., 1994; Briggs et al., 2004; Tonsmeire, 2014; Bossaert et al., 2019; De Roos et al., 2020; De Roos et al., unpublished results). Indeed, if sour beers are produced using *Brettanomyces* yeast species, intentionally added or not, the fraction of unfermentable carbohydrates decreases because of extracellular and intracellular α-glucosidase activities, causing the breakdown of MOS with chain lengths of at least up to eight glucose molecules (Kumara et al., 1993; De Roos and De Vuyst, 2019; De Roos et al., 2020; Bongaerts et al., 2021).

Finally, regarding antioxidant properties, especially those provided by polyphenolic compounds, sour beers produced by the addition of fresh fruits contain significantly high concentrations of these compounds (Cho et al., 2018; Kawa-Rygielska et al., 2019; Zapata et al., 2019; Nardini and Garaguso, 2020). Fruit addition acts as additional source of antioxidant compounds (e.g., carotenoids, tocopherols, and/or ascorbic acid), besides those provided by barley and hops (Nardini and Garaguso, 2020). Beer antioxidant activities and polyphenolic contents are influenced by the raw materials used, the quantity and quality of the fruits added, and the brewing process applied (Kawa-Rygielska et al., 2019; Nardini and Garaguso, 2020). Dietary intake of antioxidants counters negative effects of oxidative stress, which is caused by the overproduction of reactive oxygen species or reactive nitrogen species (Martinez-Gomes et al., 2020).

CONCLUSION

Historically, the role of AAB in beers was underestimated and limited to solely oxidation of ethanol into acetic acid, causing a sharp sour taste and pungent smell, impacting the flavor of most beers negatively. Despite their negative imago, research has extended the knowledge about AAB, exposing new features of AAB in sour beers. Sour beer production involving AAB can possibly result in more complex and funky beers. To achieve a positive contribution of AAB to the beer flavor, controlled growth should always be aimed for. Despite an increased understanding of AAB and their functional role during sour beer production, controlled growth of AAB with sufficient but not excessive production of flavor compounds, such as acetic acid and acetoin, requires skills only experienced brewers do master.

AUTHOR CONTRIBUTIONS

AB drafted the manuscript. AB and LDV revised and edited the manuscript. All authors contributed to the article and approved the submitted version.

FUNDING

This work was supported by the Research Council of the Vrije Universiteit Brussel (SRP7 and IOF3017 projects).

REFERENCES

Adler, P., Frey, L. J., Berger, A., Bolten, C. J., Hansen, C. E., and Wittmann, C. (2014). The key to acetate: metabolic fluxes of acetic acid bacteria under cocoa pulp fermentation-simulating conditions. *Appl. Environ. Microbiol.* 80, 4702–4716. doi: 10.1128/AEM.01048-14

Admassie, M. (2018). A review on food fermentation and the biotechnology of lactic acid bacteria. *World J. Food Sci. Technol.* 2, 19–24. doi: 10.11648/j.wjfst.20180201.13

Almaguer, C., Schönenberger, C., Gastl, M., Arendt, E. K., and Becker, T. (2014). *Humulus lupulus* - a story that begs to be told. *A review. J. Inst. Brew.* 120, 289–314. doi: 10.1002/jib.160

Ashtavinayak, P., and Elizabeth, H. A. (2016). Review: gram negative bacteria in brewing. *Adv. Microbiol.* 6, 195–209. doi: 10.4236/aim.2016.63020

Back, W. (2005). *Ausgewählte Kapitel der Brauereitechnologie*. Nürnberg: Fachverlag Hans Carl.

Baiano, A. (2020). Craft beer: an overview. *Compr. Rev. Food Sci. Food Saf.* 20, 1829–1856. doi: 10.1111/1541-4337.12693

Banilas, G., Sgouros, G., and Nisiotou, A. (2016). Development of microsatellite markers for *Lachancea thermotolerans* typing and population structure of wine-associated isolates. *Microbiol. Res.* 193, 1–10. doi: 10.1016/j.micres.2016.08.010

Batish, V. K., Roy, U., Lal, R., and Grower, S. (1997). Antifungal attributes of lactic acid bacteria - A review. *Crit. Rev. Biotechnol.* 17, 209–225. doi: 10.3109/07388559709146614

Benito, S. (2018). The impacts of *Lachancea thermotolerans* yeast strains on winemaking. *Appl. Microbiol. Biotechnol.* 102, 6775–6790. doi: 10.1007/s00253-018-9117-z

Bokulich, N. A., and Bamforth, C. W. (2013). The microbiology of malting and brewing. *Microbiol. Mol. Biol. Rev.* 77, 157–172. doi: 10.1128/MMBR.00060-12

Bokulich, N. A., Bamforth, C. W., and Mills, D. A. (2012). Brewhouse-resident microbiota are responsible for multi-stage fermentation of American coolship ale. *PLoS One* 7:e35507. doi: 10.1371/journal.pone.0035507

Bongaerts, D., De Roos, J., and De Vuyst, L. (2021). Technological and environmental features determine the uniqueness of the lambic beer microbiota and production process. *Appl. Environ. Microbiol.* 87, e00612–e00621. doi: 10.1128/AEM.00612-21

Bossaert, S., Crauwels, S., De Rouck, G., and Lievens, B. (2019). The power of sour - a review: old traditions, new opportunities. *BrewSci.* 72, 78–88. doi: 10.23763/BrSc19-10bossaert

Bossaert, S., Kocijan, T., Winne, V., Schlich, J., Herrera-Malaver, B., Verstrepen, K. J., et al. (2022a). Beer ethanol and iso-α-acid level affect microbial community establishment and beer chemistry throughout wood maturation of beer. BioRxiv [Preprint]. Available at: https://www.biorxiv.org/content/10.1101/2022.03.07.483260v1.full.pdf (Accessed May 03, 2022).

Bossaert, S., Kocijan, T., Winne, V., Van Opstaele, F., Schlich, J., Herrera-Malaver, B., et al. (2022b). Development of a tractable model system to mimic wood-ageing of beer on a lab scale. BioRxiv [Preprint]. Available at: https://www.biorxiv.org/content/10.1101/2022.03.11.483928v1 (Accessed May 26, 2022).

Bossaert, S., Winne, V., Van Opstaele, F., Buyse, J., Verreth, C., Herrera-Malaver, B., et al. (2020). Description of the temporal dynamics in microbial community composition and beer chemistry in sour beer production via barrel ageing of finished beers. *Int. J. Food Microbiol.* 339:109030. doi: 10.1016/j.ijfoodmicro.2020.109030

Bossaert, S., Winne, V., Van Opstaele, F., Buyse, J., Verreth, C., Herrera-Malaver, B., et al. (2022c). Impact of wood species on microbial community composition, beer chemistry and sensory characteristics during barrel-ageing of beer. *Int. J. Food Sci. Technol.* 57, 1122–1136. doi: 10.1111/ijfs.15479

Briggs, D. E., Boulton, C., Brookes, P., and Stevens, R. (2004). *Brewing Science and Practice*. Cambridge: Woodhead Publishing Limited.

Cantwell, D., and Bouckaert, P. (2016). *Wood & Beer: A Brewer's Guide*. Boulder: Brewers Publications.

Chan, M. Z. A., Chua, J. Y., Toh, M., and Liu, S.-Q. (2019). Survival of probiotic strain *Lactobacillus paracasei* L26 during co-fermentation with *S. cerevisiae* for the development of a novel beer beverage. *Food Microbiol.* 82, 541–550. doi: 10.1016/j.fm.2019.04.001

Cho, J.-H., Kim, I.-D., Dhungana, S. K., Do, H.-M., and Shin, D.-H. (2018). Persimmon fruit enhanced quality characteristics and antioxidant potential of beer. *Food Sci. Biotechnol.* 27, 1067–1073. doi: 10.1007/s10068-018-0340-2

Ciosek, A., Rusiecka, I., and Poreda, A. (2019). Sour beer production: impact of pitching sequence of yeast and lactic acid bacteria. *J. Inst. Brew.* 126, 53–58. doi: 10.1002/jib.590

Cleenwerck, I., Vandemeulebroecke, K., Janssens, D., and Swings, J. (2002). Re-examination of the genus *Acetobacter*, with descriptions of *Acetobacter cerevisiae* sp. nov. and *Acetobacter malorum* sp. nov. *Int. J. Syst. Evol. Microbiol.* 52, 1551–1558. doi: 10.1099/00207713-52-5-1551

Colen, L., and Swinnen, J. (2015). Economic growth, globalisation and beer consumption. *J. Agric. Econ.* 67, 186–207. doi: 10.1111/1477-9552.12128

Cousin, F. J., Le Guellec, R., Schlusselhuber, M., Dalmasso, M., Laplace, J.-M., and Cretenet, M. (2017). Microorganisms in fermented apple beverages: current knowledge and future directions. *Microorg.* 5:39. doi: 10.3390/microorganisms5030039

De Cort, S., Kumara, H. S., and Verachtert, H. (1994). Localization and characterization of α-glucosidase activity in *Lactobacillus brevis*. *Appl. Environ. Microbiol.* 60, 3074–3078. doi: 10.1128/aem.60.9.3074-3078.1994

De Keersmaecker, J. (1996). The mystery of lambic beer. *SciAm* 275, 74–80. doi: 10.1038/scientificamerican0896-74

De Roos, J., and De Vuyst, L. (2018). Acetic acid bacteria in fermented foods and beverages. *Curr. Opin. Biotechnol.* 49, 115–119. doi: 10.1016/j.copbio.2017.08.007

De Roos, J., and De Vuyst, L. (2019). Microbial acidification, alcoholization, and aroma production during spontaneous lambic beer production. *J. Sci. Food Agric.* 99, 25–38. doi: 10.1002/jsfa.9291

De Roos, J., and De Vuyst, L. (2022). "Lambic beer, a unique blend of tradition and good microorganisms," in *Good Microbes in Medicine, Food Production, Biotechnology, Bioremediation, and Agriculture*, eds. F. J. de Bruijn, H. Smidt, L. Cocolin, M. Sauer, D. Dowling and L. Thomashow (Hoboken: John Wiley & Sons), 219–229. doi: 10.1128/AEM.02226-18

De Roos, J., Vandamme, P., and De Vuyst, L. (2018a). Wort substrate consumption and metabolite production during lambic beer fermentation and maturation explain the successive growth of specific bacterial and yeast species. *Front. Microbiol.* 9:2763. doi: 10.3389/fmicb.2018.02763

De Roos, J., Van der Veken, D., and De Vuyst, L. (2019). The interior surfaces of wooden barrels are an additional microbial inoculation source for lambic beer production. *Appl. Environ. Microbiol.* 85, e02226–e02218.

De Roos, J., Verce, M., Aerts, M., Vandamme, P., and De Vuyst, L. (2018b). Temporal and spatial distribution of the acetic acid bacterium communities throughout the wooden casks used for the fermentation and maturation of lambic beer underlines their functional role. *Appl. Environ. Microbiol.* 84, e02846–e02817. doi: 10.1128/AEM.02846-17

De Roos, J., Verce, M., Weckx, S., and De Vuyst, L. (2020). Temporal shotgun metagenomics revealed the potential metabolic capabilities of specific microorganisms during lambic beer production. *Front. Microbiol.* 11:1692. doi: 10.3389/fmicb.2020.01692

De Rosso, M., Panighel, A., Dalla Vedova, A., Stella, L., and Flamini, R. (2009). Changes in chemical composition of a red wine aged in acacia, cherry, chestnut, mulberry, and oak wood barrels. *J. Agric. Food Chem.* 57, 1915–1920. doi: 10.1021/jf803161r

De Vuyst, L., and Leroy, F. (2020). Functional role of yeasts, lactic acid bacteria and acetic acid bacteria in cocoa fermentation processes. *FEMS Microbiol. Rev.* 44, 432–453. doi: 10.1093/femsre/fuaa014

Domizio, P., House, J. F., Joseph, C. M. L., Bisson, L. F., and Bamforth, C. W. (2016). *Lachancea thermotolerans* as an alternative yeast for the production of beer. *J. Inst. Brew.* 122, 599–604. doi: 10.1002/jib.362

Donadini, G., and Porretta, S. (2017). Uncovering patterns of consumers' interest for beer: a case study with craft beers. *Food Res. Int.* 91, 183–198. doi: 10.1016/j.foodres.2016.11.043

Dysvik, A., La Rosa, S. L., Buffetto, F., Liland, K. H., Myhrer, K. S., Rukke, E. O., et al. (2020a). Secondary lactic acid bacteria fermentation with wood-derived xylooligosaccharides as a tool to expedite sour beer production. *J. Agric. Food Chem.* 68, 301–314. doi: 10.1021/acs.jafc.9b05459

Dysvik, A., La Rosa, S. L., De Rouck, G., Rukke, E.-O., Westereng, B., and Wicklund, T. (2020c). Microbial dynamics in traditional and modern sour beer production. *Appl. Environ. Microbiol.* 86, e00566–e00520. doi: 10.1128/AEM.00566-20

Dysvik, A., La Rosa, S. L., Liland, K. H., Myhrer, K. S., Østlie, H. M., De Rouck, G., et al. (2020b). Co-fermentation involving *Saccharomyces cerevisiae* and *Lactobacillus* species tolerant to brewing-related stress factors for controlled and rapid production of sour beer. *Front. Microbiol.* 11:279. doi: 10.3389/fmicb.2020.00279

Dysvik, A., Liland, K. H., Myhrer, K. S., Westereng, B., Rukke, E.-O., De Rouck, G., et al. (2019). Pre-fermentation with lactic acid bacteria in sour beer production. *J. Inst. Brew.* 125, 342–356. doi: 10.1002/jib.569

Engan, S. (1974). Esters in beer. *J. Inst. Brew.* 49, 40–48.

Fangel, J. U., Eiken, J., Sierksma, A., Schols, H. A., Willats, W. G. T., and Harholt, J. (2018). Tracking polysaccharides through the brewing process. *Carbohydr. Polym.* 196, 465–473. doi: 10.1016/j.carbpol.2018.05.053

Fernandez de Simon, B., Martinez, J., Sanz, M., Cadahaia, E., Esteruelas, E., and Muñoz, A. M. (2014). Volatile compounds and sensorial characterisation of red wine aged in cherry, chestnut, false acacia, ash and oak wood barrels. *Food Chem.* 147, 346–356. doi: 10.1016/j.foodchem.2013.09.158

Franz, O., Gastl, M., and Back, W. (2009). "Beer-based mixed drinks," in *Handbook of Brewing: Processes, Technology, Markets.* ed. H. M. Esslinger (Wiley-VCH Verlag GmbH, Weinheim, Germany), 257–273.

Gamero, A., Quintilla, R., Groenewald, M., Alkema, W., Boekhout, T., and Hazelwood, L. (2016). High-throughput screening of a large collection of non-conventional yeasts reveals their potential for aroma formation in food fermentation. *Food Microbiol.* 60, 147–159. doi: 10.1016/j.fm.2016.07.006

Garcia, R., Soares, B., Dias, C. B., Freitas, A. M. C., and Cabrita, M. J. (2012). Phenolic and furanic compounds of Portuguese chestnut and French, American and Portuguese oak wood chips. *Eur. Food Res. Technol.* 235, 457–467. doi: 10.1007/s00217-012-1771-2

Gatto, V., Binati, R. L., Lemos Junior, W. J. F., Basile, A., Treu, L., de Almeida, O. G. G., et al. (2020). New insights into the variability of lactic acid production in *Lachancea thermotolerans* at the phenotypic and genomic level. *Microbiol. Res.* 238:126525. doi: 10.1016/j.micres.2020.126525

Gomes, R. J., Borges, M. D. F., Rosa, M. F., Castro-Gómez, R. J. H., and Spinosa, W. M. (2018). Acetic acid bacteria in the food industry: systematics, characteristics and applications. *Food Technol. Biotechnol.* 56, 139–151. doi: 10.17113/ftb.56.02.18.5593

Gullo, M., Verzelloni, E., and Canonico, M. (2016). Aerobic submerged fermentation by acetic acid bacteria for vinegar production: process and biotechnological aspects. *Process Biochem.* 49, 1571–1579. doi: 10.1016/j.procbio.2014.07.003

Harper, D. R. (1980). Microbial contamination of draught beer in public houses. *Process Biochem.* 16, 2–7.

Hazelwood, L. A., Walsh, M. C., Pronk, J. T., and Daran, J.-M. (2010). Involvement of vacuolar sequestration and active transport in tolerance of *Saccharomyces cerevisiae* to hop iso-a-acids. *Appl. Environ. Microbiol.* 76, 318–328. doi: 10.1128/AEM.01457-09

He, Y., Dong, J., Yin, H., Zhao, Y., Chen, R., Wan, X., et al. (2014). Wort composition and its impact on the flavour-active higher alcohol and ester formation of beer – a review. *J. Inst. Brew.* 120, 157–163. doi: 10.1002/jib.145

Hill, A. (2015). "Gram-negative spoilage bacteria in brewing," in *Brewing Microbiology: Managing Microbes, Ensuring Quality and Valorising Waste*. ed. A. D. Paradh (Amsterdam: Elsevier Science & Technology), 175–194.

Hornsey, I. S. (2003). *A History of Beer and Brewing*. Cambridge: The Royal Society of Chemistry.

Hutkins, R. W. (2019). *Microbiology and Technology of Fermented Foods*. Ames: Wiley-Blackwell Publishing.

Ingledew, M. W. (1979). Effect of bacterial contaminants on beer. A review. *J. Am. Soc. Brew. Chem.* 37, 145–150.

Jeon, S. H., Kim, N. H., Shim, M. B., Jeon, Y. W., Ahn, J. H., Lee, S. H., et al. (2014). Microbiological diversity and prevalence of spoilage and pathogenic bacteria in commercial fermented alcoholic beverages (beer, fruit wine, refined rice wine, and yakju). *J. Food Prot.* 78, 812–818. doi: 10.4315/0362-028X.JFP-14-431

Kashima, Y., Iijima, M., Nakano, T., Tayama, K. A., Koizumi, Y., Udaka, S., et al. (2000). Role of intracellular esterases in the production of esters by *Acetobacter pasteurianus*. *J. Biosci. Bioeng.* 89, 81–83. doi: 10.1016/S1389-1723(00)88055-X

Kashima, Y., Iijima, M., Okamoto, A., Koizumi, Y., Udaka, S., and Yanagida, F. (1998). Purification and characterization of intracellular esterases related to ethyl acetate formation in *Acetobacter pasteurianus*. *J. Ferm. Bioeng.* 85, 584–588. doi: 10.1016/S0922-338X(98)80009-3

Kawa-Rygielska, J., Adamenko, K., Kucharska, A. Z., Prorok, P., and Piórecki, N. (2019). Physicochemical and antioxidative properties of cornelian cherry beer. *Food Chem.* 281, 147–153. doi: 10.1016/j.foodchem.2018.12.093

Kourtis, L., and Arvanitoyannis, I. (2001). Implementation of hazard analysis critical control point (HACCP) system to the alcoholic beverages industry. *Food Rev. Int.* 17, 1–44. doi: 10.1081/FRI-100000514

Kubizniaková, P., Kyselová, L., Brožová, M., Hanzalíková, K., and Matoulková, D. (2021). The role of acetic acid bacteria in brewing and their detection in operation. *Kvasny Prumysl* 67, 511–522. doi: 10.18832/kp2021.67.511

Kumara, H. M., De Cort, S., and Verachtert, H. (1993). Localization and characterization of α-glucosidase activity in *Brettanomyces lambicus*. *Appl. Environ. Microbiol.* 59, 2352–2358. doi: 10.1128/aem.59.8.2352-2358.1993

Laitila, A., Sweins, H., Vilpola, A., Kotaviita, E., Olkku, J., Home, S., et al. (2006). *Lactobacillus plantarum* and *Pediococcus pentosaceus* starter cultures as a tool for microflora management in malting and for enhancement of malt processability. *J. Agric. Food Chem.* 54, 3840–3851. doi: 10.1021/jf052979j

Larroque, M. N., Carrau, F., Fariña, L., Boido, E., Dellacassa, E., and Medina, K. (2021). Effect of *Saccharomyces* and non-*Saccharomyces* native yeasts on beer aroma compounds. *Int. J. Food Microbiol.* 337:108953. doi: 10.1016/j.ijfoodmicro.2020.108953

Lattici, F., Catallo, M., and Solieri, L. (2020). Designing new yeasts for craft brewing: when natural biodiversity meets biotechnology. *Beverages* 6:3. doi: 10.3390/beverages6010003

Leroy, F., and De Vuyst, L. (2004). Lactic acid bacteria as functional starter cultures for the food fermentation industry. *Trends Food Sci. Technol.* 15, 67–78. doi: 10.1016/j.tifs.2003.09.004

Li, F., Shi, Y., Boswell, M., and Rozelle, C. (2017). "Craft beer in China," in *Economic Perspectives on Craft Beer: A Revolution in the Global Beer Industry*. eds. C. Garavaglia and J. Swinnen (London: Palgrave Macmillan), 457–484.

Lowe, D. P., and Arendt, E. K. (2004). The use and effects of lactic acid bacteria in malting and brewing with their relationships to antifungal activity, mycotoxins and gushing: a review. *J. Inst. Brew.* 110, 163–180. doi: 10.1002/j.2050-0416.2004.tb00199.x

Lowe, D. P., Ulmer, H. M., van Sinderen, D., and Arendt, E. K. (2004). Application of biological acidification to improve the quality and processability of wort produced from 50% raw barley. *J. Inst. Brew.* 110, 133–140. doi: 10.1002/j.2050-0416.2004.tb00192.x

Lynch, K. M., Wilkinson, S., Daenen, L., and Arendt, A. K. (2021). An update on water kefir: microbiology, composition and production. *Int. J. Food Microbiol.* 345:109128. doi: 10.1016/j.ijfoodmicro.2021.109128

Magnus, C. A., Ingledew, M. W., and Casey, G. (1986). High-gravity brewing: influence of high-ethanol beer on the viability of contaminating brewery bacteria. *J. Am. Soc. Brew. Chem.* 44, 158–161. doi: 10.1094/ASBCJ-44-0158

Marco, M. L., Heeney, D., Binda, S., Cifelli, C. J., Cotter, P. D., Foligné, B., et al. (2017). Health benefits of fermented foods: microbiota and beyond. *Curr. Opin. Biotechnol.* 44, 94–102. doi: 10.1016/j.copbio.2016.11.010

Marco, M. L., Sanders, M. E., Gänzle, M., Arrieta, M. C., Cotter, P. D., De Vuyst, L., et al. (2021). The international scientific Association for Probiotics and Prebiotics (ISAPP) consensus statement on fermented foods. *Nat. Rev. Gastroenterol. Hepatol.* 18, 196–208. doi: 10.1038/s41575-020-00390-5

Martens, H., Iserentant, D., and Verachtert, H. (1997). Microbiological aspects of a mixed yeast-bacterial fermentation in the production of a special Belgian acidic ale. *J. Inst. Brew.* 103, 85–91. doi: 10.1002/j.2050-0416.1997.tb00939.x

Martinez-Gomes, A., Caballero, I., and Blanco, C. A. (2020). Phenols and Melanoidins as Natural Antioxidants in Beer. Structure, Reactivity and Antioxidant Activity. *Biomolecules* 10:400. doi: 10.3390/biom10030400

Menz, G., Aldred, P., and Vriesekoop, F. (2009). "Pathogens in beer," in *Beer in Health and Disease Prevention*. ed. V. R. Preedy (Amsterdam: Academic Press), 403–413.

Moens, F., Lefeber, T., and De Vuyst, L. (2014). Oxidation of metabolites highlights the microbial interactions and role of *Acetobacter pasteurianus* during cocoa bean fermentation. *Appl. Environ. Microbiol.* 80, 1848–1857. doi: 10.1128/AEM.03344-13

Nardini, M., and Garaguso, I. (2020). Characterization of bioactive compounds and antioxidant activity of fruit beers. *Food Chem.* 305:125437. doi: 10.1016/j.foodchem.2019.125437

Neves, M. F., Trombin, V. G., Lopes, F. F., Kalaki, R., and Milan, P. (2011). *The Orange Juice Business*. (Wageningen: Wageningen Academic Publishers).

Osburn, K., Ahmadd, N. N., and Bochman, M. L. (2016). Bio-prospecting, selection, and analysis of wild yeasts for ethanol fermentation. *Zymurgy* 39, 81–88. doi: 10.13140/RG.2.2.16952.14080

Osburn, K., Amaral, J., Metcalf, S. R., Nickens, D. M., Rogers, C. M., Sausen, C., et al. (2018). Primary souring: a novel bacteria-free method for sour beer production. *Food Microbiol.* 70, 76–84. doi: 10.1016/j.fm.2017.09.007

Paradh, A. D. (2015). "Gram-negative spoilage bacteria in brewing," in *Brewing Microbiology Managing Microbes, Ensuring Quality and Valorising Waste*. ed. A. E. Hill (Sawston: Woodhead Publishing), 175–194.

Pelicaen, R., Gonze, D., De Vuyst, L., and Weckx, S. (2020). Genome-scale metabolic modeling of *Acetobacter pasteurianus* 386B reveals its metabolic adaptation to cocoa fermentation conditions. *Food Microbiol.* 92:103597. doi: 10.1016/j.fm.2020.103597

Peyer, L. C., Zarnkow, M., Jacob, F., De Schutter, D. P., and Arendt, E. K. (2017). Sour brewing: impact of *Lactobacillus amylovorus* FST2.11 on technological and quality attributes of acid beers. *J. Am. Soc. Brew. Chem.* 75, 207–216. doi: 10.1094/ASBCJ-2017-3861-01

Piraine, R. E. A., Leite, F. P. L., and Bochman, M. L. (2021). Mixed-culture metagenomics of the microbes making sour beer. *Fermentation* 7:174. doi: 10.3390/fermentation7030174

Pires, E. J., Teixeira, J. A., Brányik, T., and Vicente, A. A. (2014). Yeast: the soul of beer's aroma - A review of flavour-active esters and higher alcohols produced by the brewing yeast. *Appl. Microbiol. Biotechnol.* 98, 1937–1949. doi: 10.1007/s00253-013-5470-0

Pothakos, V., Illeghems, K., Laureys, D., Spitaels, F., Vandamme, P., and De Vuyst, L. (2016). "Acetic acid bacteria in fermented food and beverage ecosystems," in *Acetic Acid Bacteria: Ecology and Physiology*. eds. K. Matsushita, H. Toyama, N. Tonouchi and A. Okamoto-Kainuma (Tokyo: Springer), 73–100.

Preedy, V. (2008). *Beer in Health and Disease Prevention*. Amsterdam: Academic Press.

Rouse, S., Harnett, D., Vaughan, A., and van Sinderen, D. (2008). Lactic acid bacteria with potential to eliminate fungal spoilage in foods. *J. Appl. Microbiol.* 104, 915–923. doi: 10.1111/j.1365-2672.2007.03619.x

Sakamoto, K., and Konings, W. N. (2003). Beer spoilage bacteria and hop resistance. *Int. J. Food Microbiol.* 89, 105–124. doi: 10.1016/S0168-1605(03)00153-3

Schneiderbanger, J., Jacob, F., and Hutzler, M. (2020). Mini-review: The current role of lactic acid bacteria in beer spoilage. *BrewSci.* 73, 19–28. doi: 10.23763/BrSc19-28schneiderbanger

Shayevitz, A., Harrison, K., and Curtin, C. D. (2020). Barrel-induced variation in the microbiome and mycobiome of aged sour ale and imperial porter beer. *J. Am. Soc. Brew. Chem.* 79, 33–40. doi: 10.1080/03610470.2020.1795607

Sheih, K. K., Donnely, B. J., and Scallet, B. L. (1979). Reactions of oligosaccharides. IV. Fermentability by yeasts. *Cereal Chem* 50, 169–175.

Shetty, P. H., and Jespersen, L. (2006). *Saccharomyces cerevisiae* and lactic acid bacteria as potential mycotoxin decontaminating agents. *Trends Food Sci. Technol.* 17, 48–55. doi: 10.1016/j.tifs.2005.10.004

Silva, L. C., Schmidt, G. B., Alves, L. G. O., Oliveira, V. S., Laureano-Melo, R., Stutz, E., et al. (2020). Use of probiotic strains to produce beers by axenic or semi-separated co-culture system. *Food Bioprod. Process.* 124, 408–418. doi: 10.1016/j.fbp.2020.10.001

Snauwaert, I., Roels, S. P., Van Nieuwerburg, F., Van Landschoot, A., De Vuyst, L., and Vandamme, P. (2016). Microbial diversity and metabolite composition of Belgian red-brown acidic ales. *Int. J. Food Microbiol.* 221, 1–11. doi: 10.1016/j.ijfoodmicro.2015.12.009

Spitaels, F., Li, L., Wieme, A., Balzarini, T., Cleenwerck, I., Van Landschoot, A., et al. (2014c). *Acetobacter lambici* sp. nov., isolated from fermenting lambic beer. *Int. J. Syst. Evol. Microbiol.* 64, 1083–1089. doi: 10.1099/ijs.0.057315-0

Spitaels, F., Van Kerrebroeck, S., Wieme, A. D., Snauwaert, I., Aerts, M., Van Landschoot, A., et al. (2015a). Microbiota and metabolites of aged bottled gueuze beers converge to the same composition. *Food Microbiol.* 47, 1–11. doi: 10.1016/j.fm.2014.10.004

Spitaels, F., Wieme, A. D., Balzarini, T., Cleenwerck, I., Van Landschoot, A., De Vuyst, L., et al. (2014b). *Gluconobacter cerevisiae* sp. nov., isolated from the brewery environment. *Int. J. Syst. Evol. Microbiol.* 64, 1134–1141. doi: 10.1099/ijs.0.059311-0

Spitaels, F., Wieme, A. D., Janssens, M., Aerts, M., Daniel, H.-M., Van Landschoot, A., et al. (2014a). The microbial diversity of traditional spontaneously fermented lambic beer. *PLoS One* 9:e95384. doi: 10.1371/journal.pone.0095384

Spitaels, F., Wieme, A. D., Janssens, M., Aerts, M., Van Landschoot, A., De Vuyst, L., et al. (2015b). The microbial diversity of an industrially produced lambic beer shares members of a traditionally produced one and reveals a core microbiota for lambic beer fermentation. *Food Microbiol.* 49, 23–32. doi: 10.1016/j.fm.2015.01.008

Spitaels, F., Wieme, A. D., Snauwaert, I., De Vuyst, L., and Vandamme, P. (2017). "Microbial ecology of traditional beer fermentations," in *Brewing Microbiology: Current Research, Omics and Microbial Ecology*. eds. N. Bokulich and C. Bamforth (Poole: Caister Academic Press), 179–196.

Sterckx, F. L., Saison, D., and Delvaux, F. R. (2012). Wood aging of beer. Part II: influence of wood aging parameters on monophenol concentrations. *J. Am. Soc. Brew. Chem.* 70, 62–69. doi: 10.1094/ASBCJ-2011-1201-02

Suiker, I. M., and Wösten, H. A. B. (2021). Spoilage yeasts in beer and beer products. *Curr. Opin. Food Sci.* 44:100815. doi: 10.1016/j.cofs.2022.100815

Tan, Z., Hou, C., Jiang, X., Li, Y., Song, Y., and Dong, X. (2021). "The Brewing process of the Schisandra sour beer," in *3rd World Congress on Chemistry, Biotechnology and Medicine (WCCBM 2021)*, (Cambridge: Francis Academic Press); July 2-4, 2021; 52–58.

Tonsmeire, M. (2014). *American Sour Beers: Innovative Techniques For Mixed Fermentations*, Colorado: Brewers Publications.

Twede, D. (2005). The cask age: the technology and history of wooden barrels. *Pack. Technol. Sci.* 18, 253–264. doi: 10.1002/pts.696

Tyakht, A., Kopeliovich, A., Klimenko, N., Efimova, D., Dovidchenko, N., Odintsova, V., et al. (2021). Characteristics of bacterial and yeast microbiomes

in spontaneous and mixed-fermentation beer and cider. *Food Microbiol.* 94:103658. doi: 10.1016/j.fm.2020.103658

Van den Steen, J. (2012). *Geuze & Kriek: The Secret of Lambic*. Tielt: Uitgeverij Lannoo.

Van Oevelen, D., Delescaille, F., and Verachtert, H. (1976). Synthesis of aroma components during spontaneous fermentation of lambic and gueuze. *J. Inst. Brew.* 82, 322–326. doi: 10.1002/j.2050-0416.1975.tb06953.x

Van Oevelen, D., Spaepen, M., Timmermans, P., and Verachtert, H. (1977). Microbiological aspects of spontaneous wort fermentation in the production of lambic and gueuze. *J. Inst. Brew.* 83, 356–360. doi: 10.1002/j.2050-0416.1977.tb03825.x

Van Vuuren, H. J. J. (1999). "Gram negative spoilage bacteria," in *Brewing Microbiology*. eds. F. Priest and I. Campbell (Gaithersburg: Aspen Publishers Inc.), 163–191.

Van Vuuren, H. J. J., Loos, M. A., Louw, H. A., and Meisel, R. (1979). Distribution of bacterial contaminants in a south African lager brewery. *J. Appl. Bacteriol.* 47, 421–424. doi: 10.1111/j.1365-2672.1979.tb01202.x

Van Vuuren, H. J. J., and Priest, F. G. (2003). "Gram-negative brewery bacteria," in *Brewing Microbiology*. eds. F. G. Priest and I. Campbell (New York: Kluwer Academic/Plenum Publishers), 219–245.

Verachtert, H., and Derdelinckx, G. (2014). Belgian acidic beers daily reminiscences of the past. *Cerevisia* 38, 121–128. doi: 10.1016/j.cervis.2014.04.002

Verachtert, H., and Iserentant, D. (1995). Properties of Belgian acidic beers and their microflora. I. The production of gueuze and related refreshing acid beers. *Cerevisia* 20, 37–41.

Verstrepen, K. J., Derdelinckx, G., Dufour, J.-P., Winderickx, J., Thevelein, J. M., Pretorius, I. S., et al. (2003). Flavor-active esters: adding fruitiness to beer. *J. Biosci. Bioeng.* 96, 110–118. doi: 10.1016/S1389-1723(03)90112-5

Vicente, J., Baran, Y., Navascués, E., Santos, A., Caldéron, F., Marquina, D., et al. (2022). Biological management of acidity in wine industry: a review. *Int. J. Food Microbiol.* 375:109726. doi: 10.1016/j.ijfoodmicro.2022.109726

Vicente, J., Navascués, E., Calderón, F., Santos, A., Marquina, D., and Benito, S. (2021). An integrative view of the role of *Lachancea thermotolerans* in wine technology. *Foods* 10:2878. doi: 10.3390/foods10112878

Villareal-Soto, S. A., Beaufort, S., Bouajila, J., Souchard, J.-P., and Taillandier, P. (2018). Understanding kombucha tea fermentation: a review. *J. Food Sci.* 83, 580–588. doi: 10.1111/1750-3841.14068

Vriesekoop, F., Krahl, M., Hucker, B., and Menz, G. (2012). 125th anniversary review: Bacteria in brewing: the good, the bad and the ugly. *J. Inst. Brew.* 118, 335–345. doi: 10.1002/jib.49

Witrick, K. T., Duncan, S. E., Hurley, K. E., and O'Keefe, S. F. (2017). Acid and volatiles of commercially available lambic beers. *Beverages* 3:51. doi: 10.3390/beverages3040051

Xiao, Z., and Lu, J. R. (2014). Generation of acetoin and its derivatives in foods. *J. Agric. Food Chem.* 62, 6487–6497. doi: 10.1021/jf5013902

Yakushi, T., and Matsushita, K. (2010). Alcohol dehydrogenase of acetic acid bacteria: structure, mode of action, and applications in biotechnology. *Appl. Microbiol. Biotechnol.* 86, 1257–1265. doi: 10.1007/s00253-010-2529-z

Yang, H., Yu, Y., Fu, C., and Chen, F. (2019). Bacterial acid resistance toward organic weak acid revealed by RNA-seq transcriptomic analysis in *Acetobacter pasteurianus*. *Front. Microbiol.* 10:1616. doi: 10.3389/fmicb.2019.01616

Zapata, P. J., Martínez-Esplá, A., Gironés-Vilaplana, A., Santos-Lax, D., Noguera-Artiaga, L., and Carbonell-Barrachina, Á. A. (2019). Phenolic, volatile, and sensory profiles of beer enriched by macerating quince fruits. *Food Sci. Technol.* 103, 139–146. doi: 10.1016/j.lwt.2019.01.002

Zhang, Z., Ma, H., Yang, Y., Dai, L., and Chen, K. (2015). Protein profile of *Acetobacter pasteurianus* HSZ3-21. *Curr. Microbiol.* 70, 724–729. doi: 10.1007/s00284-015-0777-y

Conflict of Interest: The authors declare that the research was conducted in the absence of any commercial or financial relationships that could be construed as a potential conflict of interest.

frontiers | Frontiers in Microbiology

TYPE Original Research
PUBLISHED 16 August 2022
DOI 10.3389/fmicb.2022.981767

OPEN ACCESS

EDITED BY
Isidoro García-García,
University of Cordoba, Spain

REVIEWED BY
Uwe Deppenmeier,
University of Bonn, Germany
Paul Schweiger,
University of Wisconsin–La Crosse, United States

*CORRESPONDENCE
Tino Polen
t.polen@fz-juelich.de

SPECIALTY SECTION
This article was submitted to Food Microbiology, a section of the journal Frontiers in Microbiology

RECEIVED 29 June 2022
ACCEPTED 13 July 2022
PUBLISHED 16 August 2022

CITATION
Fricke PM, Gries ML, Mürköster M, Höninger M, Gätgens J, Bott M and Polen T (2022) The L-rhamnose-dependent regulator RhaS and its target promoters from *Escherichia coli* expand the genetic toolkit for regulatable gene expression in the acetic acid bacterium *Gluconobacter oxydans*. *Front. Microbiol.* 13:981767. doi: 10.3389/fmicb.2022.981767

The L-rhamnose-dependent regulator RhaS and its target promoters from *Escherichia coli* expand the genetic toolkit for regulatable gene expression in the acetic acid bacterium *Gluconobacter oxydans*

Philipp Moritz Fricke, Mandy Lynn Gries, Maurice Mürköster, Marvin Höninger, Jochem Gätgens, Michael Bott and Tino Polen*

Institute of Bio- and Geosciences, IBG-1: Biotechnology, Forschungszentrum Jülich GmbH, Jülich, Germany

For regulatable target gene expression in the acetic acid bacterium (AAB) *Gluconobacter oxydans* only recently the first plasmids became available. These systems solely enable AraC- and TetR-dependent induction. In this study we showed that the L-rhamnose-dependent regulator RhaS from *Escherichia coli* and its target promoters P_{rhaBAD}, P_{rhaT}, and P_{rhaSR} could also be used in *G. oxydans* for regulatable target gene expression. Interestingly, in contrast to the responsiveness in *E. coli*, in *G. oxydans* RhaS increased the expression from P_{rhaBAD} in the absence of L-rhamnose and repressed P_{rhaBAD} in the presence of L-rhamnose. Inserting an additional RhaS binding site directly downstream from the –10 region generating promoter variant $P_{rhaBAD(+RhaS\text{-}BS)}$ almost doubled the apparent RhaS-dependent promoter strength. Plasmid-based P_{rhaBAD} and $P_{rhaBAD(+RhaS\text{-}BS)}$ activity could be reduced up to 90% by RhaS and L-rhamnose, while a genomic copy of $P_{rhaBAD(+RhaS\text{-}BS)}$ appeared fully repressed. The RhaS-dependent repression was largely tunable by L-rhamnose concentrations between 0% and only 0.3% (w/v). The RhaS-P_{rhaBAD} and the RhaS-$P_{rhaBAD(+RhaS\text{-}BS)}$ systems represent the first heterologous repressible expression systems for *G. oxydans*. In contrast to P_{rhaBAD}, the *E. coli* promoter P_{rhaT} was almost inactive in the absence of RhaS. In the presence of RhaS, the P_{rhaT} activity in the absence of L-rhamnose was weak, but could be induced up to 10-fold by addition of L-rhamnose, resulting in a moderate expression level. Therefore, the RhaS-P_{rhaT} system could be suitable for tunable low-level expression of difficult enzymes or membrane proteins in *G. oxydans*. The insertion of an additional RhaS binding site directly downstream from the *E. coli* P_{rhaT} –10 region increased the non-induced expression strength and reversed the regulation by RhaS and L-rhamnose from inducible to repressible. The P_{rhaSR} promoter appeared to be positively auto-regulated by RhaS and this activation was increased by L-rhamnose. In summary, the interplay of the L-rhamnose-

binding RhaS transcriptional regulator from *E. coli* with its target promoters P_{rhaBAD}, P_{rhaT}, P_{rhaSR} and variants thereof provide new opportunities for regulatable gene expression in *G. oxydans* and possibly also for simultaneous L-rhamnose-triggered repression and activation of target genes, which is a highly interesting possibility in metabolic engineering approaches requiring redirection of carbon fluxes.

KEYWORDS

***Gluconobacter*, rhamnose, regulation, transcription, promoter, activation, repression, acetic acid bacteria**

Introduction

The acetic acid bacterium (AAB) *Gluconobacter oxydans* harbors the beneficial ability of regio- and stereoselective incomplete oxidation of a variety of sugars, sugar alcohols and other substrates in the periplasm by membrane-bound dehydrogenases (mDHs) and release of resulting products into the cultivation medium (Mamlouk and Gullo, 2013; Pappenberger and Hohmann, 2014; Mientus et al., 2017). Therefore, *G. oxydans* is industrially used for oxidative biotransformations of carbohydrates to produce, *e.g.*, the tanning lotion additive dihydroxyacetone, the vitamin C precursor L-sorbose, and 6-amino-L-sorbose used for production of the antidiabetic drug miglitol (Ameyama et al., 1981; Saito et al., 1997; Gupta et al., 2001; Tkac et al., 2001; Hekmat et al., 2003; Wang et al., 2016). The industrial versatility of *G. oxydans*, current applications and future perspectives have been reviewed recently (da Silva et al., 2022).

For target gene expression in *G. oxydans*, only constitutive promoters were used in the past due to the lack of a regulatable promoter. For expression, derivatives of the pBBR1MCS plasmid family obtained from the endogenous plasmid pBBR1 from *Bordetella bronchiseptica* were the most successful shuttle and expression vectors used (reviewed in Fricke et al., 2021a). Since pBBR1MCS-2 conferring kanamycine resistance typically results in an abnormal cell morphology of *G. oxydans* in the presence of kanamycin and potentially also in reduced expression performance, pBBR1MCS-5 and the use of gentamicin is advantageous (Fricke et al., 2021b). However, both plasmid backbones recently enabled high functionality of transferred heterologous expression systems for regulatable target gene expression in *G. oxydans* for the first time. Firstly, the L-arabinose-dependent AraC-P_{araBAD} system from *Escherichia coli* MC4100, which exhibits a better *araC* codon usage in *G. oxydans* than *araC* from *E. coli* MG1655, was tunable and inducible up to 480-fold (Fricke et al., 2020). Interestingly, in *G. oxydans* the AraC target promoter P_{araBAD} from *E. coli* was not active in the absence of AraC. This indicated that P_{araBAD} alone is not recognized by the *G. oxydans* RNA polymerase. Therefore, the typical repression of P_{araBAD} by AraC in the absence of the inducer L-arabinose was not required to ensure non-induced tightness of P_{araBAD} in *G. oxydans*. Secondly, the TetR-P_{tet} system in its native divergent organization as present in the *E. coli* transposon Tn*10* exhibited extremely low basal expression in *G. oxydans* and achieved more than 3,500-fold induction according to reporter assays using the fluorescence protein mNeonGreen (Fricke et al., 2021b). In contrast to P_{araBAD} and AraC, P_{tet} highly required the repression by its regulator TetR for tightness of the system, otherwise the expression from P_{tet} was very strong in *G. oxydans* without TetR. Moreover, in cases where the native divergent organization *tetR*-P_{tetR}-P_{tet}-gene-of-interest is leaky, modifying the genetic organization that the target gene and *tetR* expression both are under control of P_{tet} and therefore expressed as an operon and auto-regulated by TetR, can improve the non-induced tightness and the resulting inducibility of P_{tet} in *G. oxydans* (Bertucci et al., 2022).

In this study, to expand the still very limited genetic toolbox for regulatable target gene expression in *G. oxydans* we chose to test the L-rhamnose-dependent RhaSR system from *E. coli* (Baldoma et al., 1990; Egan and Schleif, 1993, 1994; Vía et al., 1996; Bhende and Egan, 1999; Wickstrum et al., 2010). Compared to the AraC-, TetR-, and LacI-based systems from *E. coli*, the RhaRS system offers special features that could be particularly interesting and useful for applications in *G. oxydans* or AAB in general (Supplementary Figure S1). Firstly, the system comprises not only one, but two transcriptional regulators, RhaR and RhaS, both responding to L-rhamnose. They are encoded by the *rhaSR* operon and are expressed from the promoter P_{rhaSR}. In *E. coli*, basal expression from P_{rhaSR} is positively auto-regulated by RhaR in the presence of L-rhamnose, resulting in increased expression of the *rhaSR* operon and in turn P_{rhaSR} is negatively auto-regulated by RhaS since RhaS is also able to bind to the RhaR binding site at P_{rhaSR}, competing with RhaR and blocking *rhaSR* expression. Secondly, the major target promoters of RhaS are P_{rhaBAD} and P_{rhaT}. P_{rhaBAD} drives transcription of the structural *rhaBAD* genes encoding the L-rhamnose catabolic enzymes L-rhamnulose kinase, L-rhamnose isomerase and L-rhamnulose-1-phosphate aldolase. P_{rhaT} drives transcription of *rhaT* encoding an L-rhamnose transport system. In *E. coli*, RhaS activates transcription from P_{rhaBAD} and P_{rhaT} in the presence of L-rhamnose. Furthermore, in *E. coli* the L-rhamnose metabolism is under catabolite repression by glucose, which is overcome by the binding

of the cAMP receptor protein (CRP) to consensus recognition sequences found in all three P_{rha} promoters and interaction of CRP with the RNA polymerase, which depends on the bending of the promoter DNA by RhaS or RhaR. In *G. oxydans* CRP is absent since the predicted CRP gene (GOX0974/GOX_RS06010) was shown to encode an iron–sulfur cluster protein termed GoxR, an FNR-type transcriptional regulator of genes involved in respiration and redox metabolism (Schweikert et al., 2021). Overall, it seemed very interesting to analyze how RhaS, RhaR, and the promoters P_{rhaBAD}, P_{rhaT}, and P_{rhaSR} perform in *G. oxydans* and if they could be useful for regulatable gene expression in this AAB.

We found that in *G. oxydans* the RhaS-dependent regulation of P_{rhaBAD} surprisingly was reversed compared to *E. coli*. In the absence of L-rhamnose, RhaS increased expression from P_{rhaBAD} and in the presence of L-rhamnose RhaS repressed P_{rhaBAD} enabling complete repression of a genomically encoded P_{rhaBAD} promoter variant, thereby potentially providing a dynamic knock-down system for genes in *G. oxydans*. The effects and properties of the L-rhamnose-binding RhaS regulator and the promoters P_{rhaBAD}, P_{rhaT}, and P_{rhaSR} from *E. coli* exhibit very interesting characteristics in *G. oxydans* and provide new opportunities for regulatable gene expression, both in fundamental research and metabolic engineering approaches.

Materials and methods

Bacterial strains, plasmids, media and growth conditions

Bacterial strains and plasmids used in this study and their relevant characteristics are listed in Table 1. *G. oxydans* cells were routinely cultivated in D-mannitol complex medium containing 40 g L^{-1} D-mannitol, 5 g L^{-1} yeast extract, 1 g L^{-1} KH_2PO_4, 1 g L^{-1} $(NH_4)_2SO_4$, and 2.5 g L^{-1} $MgSO_4 \times 7\ H_2O$ at 30°C. The initial pH of the medium was set to 6 by the addition of KOH (5 M stock). Because *G. oxydans* possesses a natural resistance toward cefoxitin, 50 µg ml^{-1} of the antibiotic was routinely added to the medium as a precaution to prevent bacterial contaminations. Stock solutions of cefoxitin (50 mg ml^{-1}) and D-mannitol (200 g L^{-1}) were sterile-filtered and added to autoclaved medium. Unless stated otherwise, for shake flask cultivations cells from 10 ml overnight pre-cultures were used to inoculate 50 ml D-mannitol medium in 500 ml shaking flasks with three baffles to an initial optical density at 600 nm (OD_{600}) of 0.3 (UV-1800, Shimadzu). All shake flasks cultures were grown on a rotary shaker at an agitation speed of 180 rpm. *G. oxydans* cells harboring pBBR1MCS-5-based plasmids were supplemented with 10 µg ml^{-1} gentamicin (Kovach et al., 1994). *Escherichia coli* strains were cultivated at 37°C and 160 rpm in lysogeny broth (LB) medium. Medium of *E. coli* carrying pBBR1MCS-5-based plasmids was supplemented with 10 µg ml^{-1} gentamicin. *Escherichia coli* S17-1 was used as donor strain to transform *G. oxydans* by conjugation (Kiefler et al., 2017). Competent *E. coli* S17-1 were prepared and transformed by $CaCl_2$ procedure as described (Hanahan, 1983).

Recombinant DNA work

All DNA oligonucleotides used in this study were obtained from Eurofins Genomics and are listed in Supplementary Table S1. All enzymes required for recombinant DNA work were purchased from Thermo Scientific. Polymerase chain reactions (PCR) used for DNA manipulation and plasmid verification followed standard protocols as described (Sambrook et al., 1989). For amplification of DNA fragments Q5 DNA polymerases was utilized as recommended by the manufacturer (New England Biolabs). All reporter plasmids were constructed in a one-step isothermal Gibson assembly (50°C, 1 h) by integrating amplified DNA fragments into the restricted broad-host vector derivative pBBR1MCS-5-T_{gdhM}-MCS-$T_{GOX0028}$ (Gibson et al., 2009). All DNA modifications to create the desired plasmids were conducted in *E. coli* S17-1. For plasmid isolation a QIAprep spin miniprep kit (Qiagen) was used according to the manufacturer's protocol. The correctness of the plasmid inserts was checked by DNA sequencing (Eurofins MWG).

Construction of plasmids

In this study, all plasmids were constructed using the vector pBBR1MCS-5-T_{gdhM}-MCS-$T_{GOX0028}$ that we created previously for the TetR-P_{tet} system (Fricke et al., 2021b). The terminator sequences of GOX0265 (T_{gdhM}) and GOX0028 ($T_{GOX0028}$) flank the multiple cloning site (MCS) to reduce potential interferences caused by genetic elements on the plasmid backbone. Unless stated otherwise, pBBR1MCS-5-T_{gdhM}-MCS-$T_{GOX0028}$ was restricted for insert integration with the restriction endonucleases *Xba*I and *Eco*RI. Furthermore, in all constructs using the promoters P_{rhaBAD}, P_{rhaSR}, P_{rhaT}, $P_{GOX0264}$, or $P_{GOX0452}$ to express the reporter gene *mNeonGreen* (*mNG*), the ribosome binding site (RBS) AGGAGA was placed upstream from *mNG* and downstream from the naturally occurring RBS of the respective promoter region.

For construction of plasmid pBBR1MCS-5-*rhaSR*-P_{rhaSR}-P_{rhaBAD}-*mNG*, two DNA fragments were inserted in pBBR1MCS-5-T_{gdhM}-MCS-$T_{GOX0028}$: DNA fragment with *rhaSR*-P_{rhaSR}-P_{rhaBAD}-RBS amplified with the primer pair PF1/PF2 from the genome of *E. coli* LJ110 and DNA fragment with *mNG*-T_{BBa_B1002} amplified with the primer pair PF3/PF4 from pBBR1MCS-5-*araC*-P_{BAD}-*mNG* (Fricke et al., 2020). The latter DNA fragment included the terminator BBa_B1002 from the iGEM parts library directly downstream from the reporter gene *mNG*.

The plasmid pBBR1MCS-5-*rhaS*-P_{rhaSR}-P_{rhaBAD}-*mNG* lacking *rhaR* was constructed with a DNA fragment amplified with the primer pair PF5/PF4 from pBBR1MCS-5-*rhaSR*-P_{rhaSR}-P_{rhaBAD}-*mNG* resulting in fragment *rhaS*-P_{rhaSR}-P_{rhaBAD}-RBS-*mNG*-T_{BBa_B1002} and subsequent integration of this fragment into pBBR1MCS-5-T_{gdhM}-MCS-$T_{GOX0028}$.

The plasmid pBBR1MCS-5-*rhaR*-P_{rhaSR}-P_{rhaBAD}-*mNG* lacking *rhaS* was constructed with a DNA fragment containing *rhaR* and a DNA fragment containing P_{rhaSR}-P_{rhaBAD}-RBS-*mNG*-T_{BBa_B1002}

TABLE 1 Strains and plasmids used or constructed in this study.

Strain	Relevant characteristics	Reference/ Source
E. coli S17-1	Δ*recA*, *endA1*, *hsdR17*, *supE44*, *thi*-1, *tra*$^{+}$	Simon et al. (1983)
Gluconobacter oxydans 621H	DSM 2343	DSMZ
G. oxydans mNG	Derivative of *G. oxydans* 621H with reporter gene *mNG* under control of $P_{rhaBAD(+RhaS\text{-}BS)}$ integrated into the intergenic region igr3 (GOX0038/GOX_RS01330–GOX0039/GOX_RS01335)	This work
G. oxydans mNG igr2::$P_{GOX0264}$-*rhaS*	Derivative of *G. oxydans mNG* with *rhaS* under control of $P_{GOX0264}$ integrated into igr2 (GOX0028/GOX_RS01280 - GOX0029/GOX_RS01285)	This work
G. oxydans mNG igr2::P_{rhaSR}-*rhaS*	Derivative of *G. oxydans mNG* with *rhaS* under control of P_{rhaSR} integrated into igr2 (GOX0028/GOX_RS01280–GOX0029/GOX_RS01285)	This work
G. oxydans mNG igr1::$P_{GOX0264}$-*rhaS* igr2::*rhaS*	Derivative of *G. oxydans mNG* igr2::$P_{GOX0264}$-*rhaS* with a second copy of *rhaS* under control of $P_{GOX0264}$ integrated into igr1 (GOX0013/GOX_RS01200–GOX0014/GOX_RS01205)	This work
G. oxydans mNG igr1::P_{rhaSR}-*rhaS* igr2::*rhaS*	Derivative of *G. oxydans mNG* igr2::$P_{GOX0264}$-*rhaS* with a second copy of *rhaS* under control of P_{rhaSR} integrated into igr1 (GOX0013/GOX_RS01200–GOX0014/GOX_RS01205)	This work
Plasmid		
pBBR1MCS-5	Derivative of pBBR1MCS; Gm^{R}	Kovach et al. (1995)
pBBR1MCS-5-T_{gdhM}-MCS-$T_{GOX0028}$	Derivative of pBBR1MCS-5 with terminator sequences of GOX0265 (T_{gdhM}) and GOX0028 ($T_{GOX0028}$) flanking the multiple cloning site	Fricke et al. (2021b)
pBBR1MCS-5-*rhaSR*-P_{rhaSR}-P_{rhaBAD}-*mNG*	Derivative of pBBR1MCS-5-T_{gdhM}-MCS-$T_{GOX0028}$ with DNA fragment *rhaSR*-P_{rhaSR}-P_{rhaBAD} from *E. coli* with L-rhamnose-regulated promoter P_{rhaBAD} controlling expression of the fluorescent reporter gene *mNG*	This work
pBBR1MCS-5-*rhaS*-P_{rhaSR}-P_{rhaBAD}-*mNG*	Derivative of pBBR1MCS-5-*rhaSR*-P_{rhaSR}-P_{rhaBAD}-*mNG* lacking the regulator gene *rhaR*	This work
pBBR1MCS-5-*rhaR*-P_{rhaSR}-P_{rhaBAD}-*mNG*	Derivative of pBBR1MCS-5-*rhaSR*-P_{rhaSR}-P_{rhaBAD}-*mNG* lacking the regulator gene *rhaS*	This work
pBBR1MCS-5-P_{rhaSR}-P_{rhaBAD}-*mNG*	Derivative of pBBR1MCS-5-*rhaSR*-P_{rhaSR}-P_{rhaBAD}-*mNG* lacking the *rhaSR* operon	This work
pBBR1MCS-5-*rhaS*-$P_{GOX0264}$-P_{rhaBAD}-*mNG*	Derivative of pBBR1MCS-5-*rhaS*-P_{rhaSR}-P_{rhaBAD}-*mNG* with *rhaS* constitutively expressed from strong promoter $P_{GOX0264}$	This work
pBBR1MCS-5-*rhaS*-$P_{GOX0452}$-P_{rhaBAD}-*mNG*	Derivative of pBBR1MCS-5-*rhaS*-P_{rhaSR}-P_{rhaBAD}-*mNG* with *rhaS* constitutively expressed from moderate promoter $P_{GOX0452}$	This work
pBBR1MCS-5-*mNG*-P_{rhaSR}-$P_{GOX0264}$-*rhaS*	Derivative of pBBR1MCS-5-*rhaS*-P_{rhaSR}-P_{rhaBAD}-*mNG* with *mNG* expressed from P_{rhaSR} and, in opposite direction, *rhaS* constitutively expressed from strong promoter $P_{GOX0264}$	This work
pBBR1MCS-5-*mNG*-P_{rhaSR}-$P_{GOX0452}$-*rhaS*	Derivative of pBBR1MCS-5-*rhaS*-P_{rhaSR}-P_{rhaBAD}-*mNG* with *mNG* expressed from P_{rhaSR} and, in opposite direction, *rhaS* constitutively expressed from moderate promoter $P_{GOX0452}$	This work
pBBR1MCS-5-*mNG*-P_{rhaSR}	Derivative of pBBR1MCS-5-*mNG*-P_{rhaSR}-$P_{GOX0264}$-*rhaS* lacking $P_{GOX0264}$-*rhaS*	This work
pBBR1MCS-5-*rhaS*-P_{rhaSR}-$P_{rhaBAD(+RhaS\text{-}BS)}$-*mNG*	Derivative of pBBR1MCS-5-*rhaS*-P_{rhaSR}-P_{rhaBAD}-*mNG* with an additional copy of the RhaS binding site (+RhaS-BS) in P_{rhaBAD} directly downstream from the −10 region	This work
pBBR1MCS-5-P_{rhaSR}-*rhaS*	Derivative of pBBR1MCS-5 to expresses *rhaS* under control of P_{rhaSR} (pBBR1MCS-5-T_{gdhM}-P_{rhaSR}-*rhaS*-$T_{GOX0028}$)	This work
pBBR1MCS-5-*rhaS*-P_{rhaSR}-P_{rhaT}-*mNG*	Derivative of pBBR1MCS-5-*rhaS*-P_{rhaSR}-P_{rhaBAD}-*mNG* with P_{rhaT} controlling *mNG* expression	This work
pBBR1MCS-5-P_{rhaT}-*mNG*	Derivative of pBBR1MCS-5-*rhaS*-P_{rhaSR}-P_{rhaT}-*mNG* lacking regulator gene *rhaS*	This work
pBBR1MCS-5-*rhaS*-$P_{GOX0264}$-P_{rhaT}-*mNG*	Derivative of pBBR1MCS-5-*rhaS*-P_{rhaSR}-P_{rhaT}-*mNG* with $P_{GOX0264}$ controlling *rhaS* expression	This work
pBBR1MCS-5-*rhaS*-$P_{GOX0452}$-P_{rhaT}-*mNG*	Derivative of pBBR1MCS-5-*rhaS*-P_{rhaSR}-P_{rhaT}-*mNG* with $P_{GOX0452}$ controlling *rhaS* expression	This work
pBBR1MCS-5-*rhaS*-$P_{GOX0264}$-$P_{rhaT(-10\text{-}RhaS\text{-}BS)}$-*mNG*	Derivative of pBBR1MCS-5-*rhaS*-$P_{GOX0264}$-P_{rhaT}-*mNG* with additional RhaS binding site in P_{rhaT} directly downstream from the −10 region	This work
pBBR1MCS-5-*rhaS*-$P_{GOX0452}$-$P_{rhaT(-10\text{-}RhaS\text{-}BS)}$-*mNG*	Derivative of pBBR1MCS-5-*rhaS*-$P_{GOX0452}$-P_{rhaT}-*mNG* with additional RhaS binding site in P_{rhaT} directly downstream from the −10 region	This work
pBBR1MCS-5-*rhaS*-$P_{GOX0264}$-$P_{rhaT(TSS\text{-}RhaS\text{-}BS)}$-*mNG*	Derivative of pBBR1MCS-5-*rhaS*-$P_{GOX0264}$-P_{rhaT}-*mNG* with additional RhaS binding site in P_{rhaT} directly downstream from the *E. coli* transcriptional start	This work
pBBR1MCS-5-*rhaS*-$P_{GOX0452}$-$P_{rhaT(TSS\text{-}RhaS\text{-}BS)}$-*mNG*	Derivative of pBBR1MCS-5-*rhaS*-$P_{GOX0452}$-P_{rhaT}-*mNG* with additional RhaS binding site in P_{rhaT} directly downstream from the *E. coli* transcriptional start	This work
pKOS6b	Derivative of pAJ63a, *upp* removed, *codBA* integrated, Km^{R}, confers 5-fluorocytosine sensitivity (FC^{S})	Kostner et al. (2013)

(Continued)

TABLE 1 Continued

Strain	Relevant characteristics	Reference/ Source
pKOS6b-igr3::*mNG*	Derivative of pKOS6b for genomic integration of $P_{rhaBAD(+RhaS-BS)}$-RBS-*mNG*-T_{BBa_B1002}-$T_{GOX0028}$ into igr3 (GOX0038/GOX_RS01330–GOX0039/GOX_RS01335)	This work
pKOS6b-igr2::$P_{GOX0264}$-*rhaS*	Derivative of pKOS6b for genomic integration of $P_{GOX0264}$-*rhaS*-T_{gdhM} into igr2 (GOX0028/GOX_RS01280–GOX0029/GOX_RS01285)	This work
pKOS6b-igr2::P_{rhaSR}-*rhaS*	Derivative of pKOS6b for genomic integration of P_{rhaSR}-*rhaS*-T_{gdhM} into igr2 (GOX0028/GOX_RS01280–GOX0029/GOX_RS01285)	This work
pKOS6b-igr1::$P_{GOX0264}$-*rhaS*	Derivative of pKOS6b for genomic integration of $P_{GOX0264}$-*rhaS*-T_{gdhM} into igr1 (GOX0013/GOX_RS01200–GOX0014/GOX_RS01205)	This work
pKOS6b-igr1::P_{rhaSR}-*rhaS*	Derivative of pKOS6b for genomic integration of P_{rhaSR}-*rhaS*-T_{gdhM} into igr1 (GOX0013/GOX_RS01200–GOX0014/GOX_RS01205)	This work

amplified with the primer pairs PF1/PF6 and PF7/PF4 from template pBBR1MCS-5-*rhaSR*-P_{rhaSR}-P_{rhaBAD}-*mNG*. Due to the design of the primers, *rhaS*, being the first gene of the *rhaSR* operon, was deleted in such a way that the first and last three codons of *rhaS* remained *in frame* in the plasmid, thereby in principle maintaining the original operon structure.

The plasmid pBBR1MCS-5-P_{rhaSR}-P_{rhaBAD}-*mNG* lacking the whole *rhaSR* operon was constructed with a DNA fragment comprising P_{rhaSR}-P_{rhaBAD}-RBS-*mNG*-T_{BBa_B1002} generated with the primer pair PF8/PF4 from pBBR1MCS-5-*rhaSR*-P_{rhaSR}-P_{rhaBAD}-*mNG* by inserting it into pBBR1MCS-5-T_{gdhM}-MCS-$T_{GOX0028}$.

The plasmid pBBR1MCS-5-*rhaS*-$P_{GOX0264}$-P_{rhaBAD}-*mNG* was constructed using three DNA fragments: The first fragment contained *rhaS* and was amplified with the primer pair PF5/PF9 from pBBR1MCS-5-*rhaS*-P_{rhaSR}-P_{rhaBAD}-*mNG*. The second fragment contained RBS-$P_{GOX0264}$ and was amplified with primer pair PF10/PF11 from the genome of *G. oxydans* 621H. The third fragment contained P_{rhaBAD}-RBS-*mNG*-T_{BBa_B1002} and was amplified with primer pair PF12/PF4 from pBBR1MCS-5-*rhaS*-P_{rhaSR}-P_{rhaBAD}-*mNG*.

Similarly, plasmid pBBR1MCS-5-*rhaS*-$P_{GOX0452}$-P_{rhaBAD}-*mNG* was constructed from three DNA fragments: Again, the first fragment contained *rhaS* and was amplified with the primer pair PF5/PF9 from pBBR1MCS-5-*rhaS*-P_{rhaSR}-P_{rhaBAD}-*mNG*. The second fragment contained RBS-$P_{GOX0452}$ and was amplified with the primer pair PF13/PF14 from the genome of *G. oxydans* 621H. The third fragment contained P_{rhaBAD}-RBS-*mNG*-T_{BBa_B1002} and was amplified with the primer pair PF15/PF4 from pBBR1MCS-5-*rhaS*-P_{rhaSR}-P_{rhaBAD}-*mNG*.

The plasmid pBBR1MCS-5-*mNG*-P_{rhaSR}-$P_{GOX0264}$-*rhaS* was created with the DNA fragment T_{BBa_B1002}-*mNG*-RBS-P_{rhaBAD} amplified with the primer pair PF16/PF17 from pBBR1MCS-5-*rhaS*-P_{rhaSR}-P_{rhaBAD}-*mNG* and with fragment $P_{GOX0264}$-RBS-*rhaS* amplified with the primer pair PF18/PF19 from pBBR1MCS-5-*rhaS*-$P_{GOX0264}$-P_{rhaBAD}-*mNG*.

Similarly, plasmid pBBR1MCS-5-*mNG*-P_{rhaSR}-$P_{GOX0452}$-*rhaS* was generated from DNA fragment T_{BBa_B1002}-*mNG*-RBS-P_{rhaBAD} amplified with the primer pair PF16/PF20 from template pBBR1MCS-5-*rhaS*-P_{rhaSR}-P_{rhaBAD}-*mNG* and from DNA fragment $P_{GOX0452}$-RBS-*rhaS* amplified with the primer pair PF21/PF19 from template pBBR1MCS-5-*rhaS*-$P_{GOX0452}$-P_{rhaBAD}-*mNG*.

The plasmid pBBR1MCS-5-*mNG*-P_{rhaSR} was constructed with DNA fragment T_{BBa_B1002}-*mNG* amplified with the primer pair PF16/PF22 and DNA fragment RBS-P_{rhaSR}-P_{rhaBAD} amplified with the primer pair PF23/PF24, both fragments generated from plasmid pBBR1MCS-5-*rhaS*-P_{rhaSR}-P_{rhaBAD}-*mNG* as PCR template. In the resulting construct pBBR1MCS-5-*mNG*-P_{rhaSR}, the P_{rhaBAD} region next to P_{rhaSR} was included to retain the native P_{rhaSR} upstream region.

For construction of plasmid pBBR1MCS-5-*rhaS*-P_{rhaSR}-$P_{rhaBAD(+RhaS-BS)}$-*mNG* containing an additional RhaS binding site (+RhaS-BS) directly downstream from the −10 region of P_{rhaBAD}, a DNA fragment consisting of $_{(+RhaS-BS)}$-RBS-*mNG*-T_{BBa_B1002} was amplified with the primer pair PF25/PF4 from pBBR1MCS-5-*rhaS*-P_{rhaSR}-P_{rhaBAD}-*mNG* and integrated into the *Eco*RI-restricted plasmid pBBR1MCS-5-*rhaS*-P_{rhaSR}-P_{rhaBAD}-*mNG*. The additional RhaS binding site was introduced by primer PF25.

The plasmid pBBR1MCS-5-P_{rhaSR}-*rhaS* was constructed from plasmid pBBR1MCS-5-*rhaS*-P_{rhaSR}-P_{rhaBAD}-*mNG* by *Eco*RI digestion and religation. Two *Eco*RI sites were located perfectly to remove *mNG* without the need of further cloning steps.

The plasmid pBBR1MCS-5-P_{rhaT}-*mNG* lacking *rhaS* was constructed with the DNA fragments P_{rhaT}-RBS generated with the primer pair PF26/PF27 from the genome of *E. coli* LJ110 and the fragment *mNG*-T_{BBa_B1002} generated with the primer pair PF28/PF4 from plasmid pBBR1MCS-5-*rhaS*-P_{rhaSR}-P_{rhaBAD}-*mNG*.

The plasmid pBBR1MCS-5-*rhaS*-P_{rhaSR}-P_{rhaT}-*mNG* was created with two DNA fragments. The first DNA fragment contained *rhaS*-P_{rhaSR} amplified with the primer pair PF5/PF29 from pBBR1MCS-5-*rhaS*-P_{rhaSR}-P_{rhaBAD}-*mNG*. The second DNA fragment contained P_{rhaT}-RBS-*mNG*-T_{BBa_B1002} amplified with the primer pair PF30/PF4 from pBBR1MCS-5-P_{rhaT}-*mNG*.

The plasmid pBBR1MCS-5-*rhaS*-$P_{GOX0264}$-P_{rhaT}-mNG was constructed using two fragments. The fragment containing *rhaS*-$P_{GOX0264}$ was amplified from template pBBR1MCS-5-*rhaS*-$P_{GOX0264}$-P_{rhaBAD}-*mNG* with the primer pair PF5/PF34. The fragment

containing P_{rhaT}-*mNG* was amplified from template pBBR1MCS-5-*rhaS*-P_{rhaSR}-P_{rhaT}-*mNG* with the primer pair PF4/PF37.

The plasmid pBBR1MCS-5-*rhaS*-$P_{GOX0452}$-P_{rhaT}-mNG was constructed using two fragments. The fragment containing *rhaS*-$P_{GOX0452}$ was amplified from template pBBR1MCS-5-*rhaS*-$P_{GOX0452}$-P_{rhaBAD}-*mNG* with the primer pair PF5/PF38. The fragment containing P_{rhaT}-*mNG* was amplified from template pBBR1MCS-5-*rhaS*-P_{rhaSR}-P_{rhaT}-*mNG* with the primer pair PF4/PF39.

The plasmid pBBR1MCS-5-*rhaS*-$P_{GOX0264}$-$P_{rhaT(-10\text{-RhaS-BS})}$-*mNG* was constructed using two fragments. The fragment containing *rhaS*-$P_{GOX0264}$ and the 5′ part of P_{rhaT} was amplified from template pBBR1MCS-5-*rhaS*-$P_{GOX0264}$-P_{rhaT}-*mNG* with the primer pair MM14/PF5. The fragment containing the remaining 3′ part of P_{rhaT} followed by *mNG* was amplified from template pBBR1MCS-5-*rhaS*-$P_{GOX0264}$-P_{rhaT}-*mNG* with the primer pair MM13/PF4. The additional RhaS binding site directly downstream from the −10 region of P_{rhaT} was created and introduced by the primers MM13 and MM14.

The plasmid pBBR1MCS-5-*rhaS*-$P_{GOX0452}$-$P_{rhaT(-10\text{-RhaS-BS})}$-*mNG* was constructed using two fragments. The fragment containing *rhaS*-$P_{GOX0452}$ and the 5′ part of P_{rhaT} was amplified from template pBBR1MCS-5-*rhaS*-$P_{GOX0452}$-P_{rhaT}-*mNG* with the primer pair MM14/PF5. The fragment containing the remaining 3′ part of P_{rhaT} followed by *mNG* was amplified from template pBBR1MCS-5-*rhaS*-$P_{GOX0452}$-P_{rhaT}-*mNG* with the primer pair MM13/PF4. The additional RhaS binding site directly downstream from the −10 region of P_{rhaT} was created and introduced by the primers MM13 and MM14.

The plasmid pBBR1MCS-5-*rhaS*-$P_{GOX0264}$-$P_{rhaT(TSS\text{-RhaS-BS})}$-*mNG* was constructed using two fragments. The fragment containing *rhaS*-$P_{GOX0264}$ and the 5′ part of P_{rhaT} was amplified from template pBBR1MCS-5-*rhaS*-$P_{GOX0264}$-P_{rhaT}-*mNG* with the primer pair MM16/PF5. The fragment containing the remaining 3′ part of P_{rhaT} followed by *mNG* was amplified from template pBBR1MCS-5-*rhaS*-$P_{GOX0264}$-P_{rhaT}-*mNG* with the primer pair MM15/PF4. The additional RhaS binding site directly downstream from the *E. coli* transcriptional start of P_{rhaT} was created and introduced by the primers MM15 and MM16.

The plasmid pBBR1MCS-5-*rhaS*-$P_{GOX0452}$-$P_{rhaT(TSS\text{-RhaS-BS})}$-*mNG* was constructed using two fragments. The fragment containing *rhaS*-$P_{GOX0452}$ and the 5′ part of P_{rhaT} was amplified from template pBBR1MCS-5-*rhaS*-$P_{GOX0452}$-P_{rhaT}-*mNG* with the primer pair MM16/PF5. The fragment containing the remaining 3′ part of P_{rhaT} followed by *mNG* was amplified from template pBBR1MCS-5-*rhaS*-$P_{GOX0452}$-P_{rhaT}-*mNG* with the primer pair MM15/PF4. The additional RhaS binding site directly downstream from the *E. coli* transcriptional start of P_{rhaT} was created and introduced by the primers MM15 and MM16.

The plasmid pKOS6b-igr3::*mNG* for genomic labelling of *G. oxydans* 621H by *mNG* under control of $P_{rhaBAD(+\text{RhaS-BS})}$ in igr3 was constructed with three fragments. The upstream and downstream flanking regions of igr3 were amplified from genomic DNA of *G. oxydans* 621H with the primer pairs PF31/PF32 and PF33/PF34, respectively. The fragment containing $P_{rhaBAD(+\text{RhaS-BS})}$-*mNG* was amplified from plasmid pBBR1MCS-5-*rhaS*-P_{rhaSR}-$P_{rhaBAD(+\text{RhaS-BS})}$-*mNG* with the primer pair PF35/PF36.

The plasmid pKOS6b-igr2::$P_{GOX0264}$-*rhaS* for genomic integration of a $P_{GOX0264}$-*rhaS* copy into igr2 of *G. oxydans mNG* was constructed with three fragments. The upstream and downstream flanking regions of igr2 were amplified from genomic DNA of *G. oxydans* 621H with the primer pairs PF40/PF41 and PF42/PF43, respectively. The fragment containing $P_{GOX0264}$-*rhaS* was amplified from plasmid pBBR1MCS-5-*rhaS*-$P_{GOX0264}$-P_{rhaBAD}-*mNG* with the primer pair PF44/PF45.

The plasmid pKOS6b-igr2::P_{rhaSR}-*rhaS* for genomic integration of a P_{rhaSR}-*rhaS* copy into igr2 of *G. oxydans mNG* was constructed with three fragments. The upstream and downstream flanking regions of igr2 were amplified from genomic DNA of *G. oxydans* 621H with the primer pairs PF40/PF46 and PF42/PF43, respectively. The fragment containing P_{rhaSR}-*rhaS* was amplified from plasmid pBBR1MCS-5-*rhaS*-P_{rhaSR}-P_{rhaBAD}-*mNG* with the primer pair PF44/PF47.

The plasmid pKOS6b-igr1::$P_{GOX0264}$-*rhaS* for genomic integration of a $P_{GOX0264}$-*rhaS* copy into igr1 of *G. oxydans mNG* igr2::$P_{GOX0264}$-*rhaS* was constructed with three fragments. The upstream and downstream flanking regions of igr1 were amplified from genomic DNA of *G. oxydans* 621H with the primer pairs MH3/MH10 and MH6/MH9, respectively. The fragment containing $P_{GOX0264}$-*rhaS* was amplified from plasmid pBBR1MCS-5-*rhaS*-$P_{GOX0264}$-P_{rhaBAD}-*mNG* with the primer pair MH4/MH5.

The plasmid pKOS6b-igr1::P_{rhaSR}-*rhaS* for genomic integration of a P_{rhaSR}-*rhaS* copy into igr1 of *G. oxydans mNG* igr2::$P_{GOX0264}$-*rhaS* was constructed with three fragments. The upstream and downstream flanking regions of igr1 were amplified from genomic DNA of *G. oxydans* 621H with the primer pairs MH7/MH10 and MH6/MH9, respectively. The fragment containing P_{rhaSR}-*rhaS* was amplified from plasmid pBBR1MCS-5-*rhaS*-P_{rhaSR}-P_{rhaBAD}-*mNG* with the primer pair MH5/MH8.

Construction and selection of genomically modified *Gluconobacter oxydans* strains

Integrations of expression cassettes into the genome of *G. oxydans* 621H and selection of excised plasmid backbones were carried out using pKOS6b plasmid derivatives and counterselection by cytosine deaminase, encoded by *codA* from *E. coli*, in the presence of the fluorinated pyrimidine analogue 5-fluorocytosine (FC). The cytosine deaminase converts nontoxic FC to toxic 5-fluorouracil, which is channeled into the metabolism by the uracil phosphoribosyltransferase, encoded by the chromosomal *upp* gene of *Gluconobacter*. The details of the method are described elsewhere (Kostner et al., 2013). According to this method, strain *G. oxydans mNG* was constructed and selected from *G. oxydans* 621H using the plasmid pKOS6b-igr3::*mNG*. The *G. oxydans* strains *mNG* igr2::$P_{GOX0264}$-*rhaS* and *mNG* igr2::P_{rhaSR}-*rhaS* were constructed and selected from *G. oxydans mNG* using the plasmids pKOS6b-igr2::$P_{GOX0264}$-*rhaS* and pKOS6b-igr2::P_{rhaSR}-*rhaS*, respectively. The *G. oxydans* strains *mNG* igr1::$P_{GOX0264}$-*rhaS* igr2::*rhaS* and *mNG* igr1::P_{rhaSR}-*rhaS* igr2::*rhaS* were constructed and selected from

G. oxydans mNG igr2::$P_{GOX0264}$-*rhaS* using the plasmids pKOS6b-igr1::$P_{GOX0264}$-*rhaS* and pKOS6b-igr1::P_{rhaSR}-*rhaS*, respectively.

Measurements of fluorescence protein

The regulation and relative strength of the promoters on constructed plasmids was monitored in *G. oxydans* by means of expressing *mNG* encoding the fluorescent reporter protein mNG (Shaner et al., 2013). For analysis of *mNG* expression with various promoters by mNG signals, *G. oxydans* cultures were supplemented with L-rhamnose at the indicated concentrations (w/v) using a 40% (w/v) stock solution. Equal volumes of medium were added to non-supplemented reference cultures. Throughout the cultivation, growth (OD_{600}) and fluorescence emission were monitored in intervals using a spectrophotometer (UV-1800, Shimadzu) and an Infinite M1000 PRO Tecan reader (λ_{ex} 504 nm/λ_{em} 517 nm, ex/em bandwidth 5 nm, infinite M1000 PRO Tecan). For microscale BioLector cultivations, overnight starter cultures were used to inoculate 800 µl batches of D-mannitol medium in 48-well Flowerplates® (m2p-labs) to an initial OD_{600} of 0.3. Sealed with disposable foil (m2p-labs), plates were cultivated for 24 h at 1,200 rpm, 85% humidity and 30°C. Growth was monitored in each well as backscattered light at 620 nm ($A_{620\ nm}$) and protein fluorescence was monitored as emission (λ_{ex} 510 nm/λ_{em} 532 nm). For backscatter signal amplification, gain 20 was applied. Signal amplification of fluorescence emission varied (gain 40–70) and is indicated in the figure legends. All BioLector data shown in a diagram were measured in the same run of a growth experiment.

Cell flow cytometer analysis

For single cell analysis, a FACSAria™ cell sorter controlled by FACSDiva 8.0.3 software (BD Biosciences) was used to analyze the mNG reporter protein signals in *G. oxydans* 621H harboring either plasmid pBBR1MCS-5-*rhaS*-P_{rhaSR}-P_{rhaBAD}-*mNG* or pBBR1MCS-5-*rhaS*-P_{rhaSR}-P_{rhaT}-*mNG*. The FACS was operated with a 70 µm nozzle and run with a sheath pressure of 70 psi. The forward scatter (FSC) and side scatter (SSC) were recorded as small-angle scatter and orthogonal scatter, respectively, by means of a 488 nm solid blue laser beam. For analysis, only particles/events above 200 a.u. for FSC-H and above 300 a.u. for SSC-H as the thresholds were considered. The mNG fluorescence emission was detected from the SSC through the combination of a 502 nm long-pass and 530/30 nm band-pass filter. Prior to data acquisition, the FSC-A vs. SSC-A plot was employed to gate the population and to exclude signals originating from cell debris or electronic noise. In a second and third gating step, from the resulting population, the SSC-H signal was plotted against the SSC-W signal and this population was subsequently gated in a FSC-H vs. FSC-W plot to exclude doublets. From this resulting singlet population, 100,000 events were recorded at a rate of <10,000 events/s for fluorescence data acquisition. For data analysis and visualization of all gated events (n = 100,000) FlowJo 10.7.2 for Windows (FlowJo, LLC) was applied.

L-Rhamnose biotransformation test assay and GC-TOF-MS analysis

G. oxydans cells were grown to an OD_{600} of 1.3, centrifuged (4,000 × *g*, 5 min) and washed twice with 50 mM phosphate buffer (pH 6). After the second washing step, cells were resuspended in biotransformation buffer (6.6 g L^{-1} Na_2HPO_4, 3 g L^{-1} KH_2PO_4, 1 g L^{-1} NH_4Cl, 0.5 g L^{-1} NaCl, 0.49 g L^{-1} $MgSO_4$, 0.02 g L^{-1} $CaCl_2$) supplemented with 2% (w/v) L-rhamnose and incubated for 24 h at 30°C and 200 rpm. Then, the cells were removed from the buffer (4,000 × *g*, 5 min) and the supernatant was used for analysis by gas chromatography (Agilent 6,890 N, Agilent Technologies) coupled to a Waters Micromass GCT Premier high-resolution time-of-flight mass spectrometer (Waters). Sample handling for derivatization, GC-TOF-MS operation, and peak identification were carried out as described (Paczia et al., 2012). As a control, samples from biotransformation buffer with L-rhamnose and without cells as well as biotransformation buffer without L-rhamnose yet with cells were prepared.

Total DNA extraction, library preparation, illumina sequencing, and data analysis

Total DNA was purified from a culture aliquot using a NucleoSpin Microbial DNA Mini kit (MACHEREY–NAGEL). DNA concentrations were measured using a Qubit 2.0 fluorometer (Thermo Fisher Scientific). Illumina sequencing and data analysis of the indicated P_{rhaBAD} DNA sample was carried out as described (Fricke et al., 2021b). For the read mapping, the improved genome sequence from *G. oxydans* 621H and the indicated P_{rhaBAD} plasmid sequence were used (Kranz et al., 2017).

Determination of transcriptional starts

G. oxydans cells carrying plasmid pBBR1MCS-5-*rhaS*-P_{rhaSR}-$P_{rhaBAD(+RhaS\text{-}BS)}$-*mNG* were cultivated in shake flasks with 50 ml complex D-mannitol medium. Cells were harvested at OD_{600} of 1.5 in the mid-exponential phase and total RNA was extracted as described (Kranz et al., 2018). The RNA sample was sent to the company Vertis Biotechnology AG (Germany) for further sample processing and data generation. For Cappable-seq RNA, the RNA sample was enriched by capping of the 5′ triphosphorylated RNA with 3′-desthiobiotin-TEG-guanosine 5′ triphosphate (DTBGTP; NEB) using the vaccinia capping enzyme (VCE; NEB) for reversible binding of biotinylated RNA species to streptavidin. Then, streptavidin beads were used to capture biotinylated RNA species followed by elution to obtain highly enriched 5′ fragment of the

primary transcripts. The Cappable enriched RNA sample was poly(A)-tailed using poly(A) polymerase. In order to remove residual 5'-P-ends, the RNA was treated with Antarctic Phosphatase (NEB). Then, the 5'-PPP cap structures were converted to 5'-P using the RppH enzyme (NEB). Afterwards, an RNA adapter was ligated to the newly formed 5′-monophosphate structures. First-strand cDNA synthesis was performed using an oligo(dT)-adapter primer and the MMLV reverse transcriptase. The resulting cDNA was PCR-amplified to about 10–20 ng/μl using a high fidelity DNA polymerase. For Illumina sequencing, 100–300 bp long 5′ fragments were isolated from the full-length cDNA. For this purpose the cDNA preparation was fragmented and the 5'-cDNA fragments were then bound to streptavidin magnetic beads. The bound cDNAs were blunted and the 3' Illumina sequencing adapter was ligated to the 3′ ends of the cDNA fragments. The bead-bound cDNAs were finally PCR-amplified. The library was sequenced on an Illumina NextSeq 500 system using 75 bp read length. The fastq file output was used for data analysis with CLC Genomics Workbench (v21.0.3). Imported reads were trimmed and quality filtered. Passed reads were used for strand-specific mapping to the *G. oxydans* genome and the pBBR1MCS-5-*rhaS*-P_{rhaSR}-$P_{rhaBAD(+RhaS\text{-}BS)}$-*mNG* plasmid sequence using the RNA-seq analysis tool implemented in the CLC software. Read mapping settings used were 80% length fraction and 80% similarity fraction. The starts of mapped reads and total nucleotide coverage according to the mappings were used to assess transcriptional starts on the expression plasmid with the promoters P_{rhaSR} and $P_{rhaBAD(+RhaS\text{-}BS)}$.

Results

L-Rhamnose does not affect growth and is not oxidized by *Gluconobacter oxydans* 621H

The RhaSR-P_{rhaBAD} system from *E. coli* responds to the monosaccharide rhamnose in the uncommon L conformation, which is similar to the AraC-P_{araBAD} system and its effector L-arabinose. Like L-arabinose, the inducer L-rhamnose needs to enter the cell to interact with its targeted regulators RhaR and RhaS (Tobin and Schleif, 1987). In contrast to L-arabinose, which is readily oxidized by *Gluconobacter* already in the periplasm (Peters et al., 2013; Fricke et al., 2022), for more than 90% of the strains of the genus *Gluconobacter* no acid formation from L-rhamnose has been reported (Kersters et al., 1990). *G. oxydans* 621H whole-cell enzyme activity assays using the artificial electron acceptor DCPIP also revealed no detectable activity with L-rhamnose as substrate (Peters et al., 2013). To exclude a hitherto unrecognized consumption or oxidation of the inducer L-rhamnose by *G. oxydans* 621H, we carried out biotransformation assays followed by GC-TOF-MS analysis, and a growth experiment.

The results confirmed that *G. oxydans* does not consume or oxidize L-rhamnose. In the GC-TOF-MS analysis, no new peaks were detected in 24 h samples, and the areas of the GC-TOF peaks assigned to L-rhamnose were very similar for the samples at 0 h and after 24 h (Supplementary Table S2; Supplementary Figure S2). Hence, if at all, L-rhamnose is degraded or converted by strain 621H so slowly that this effector is hardly diminished during potential applications. To check if L-rhamnose somehow affects the growth of *G. oxydans* 621H, we added L-rhamnose to the complex medium. With 1% (w/v) L-rhamnose instead of D-mannitol, there was no growth of *G. oxydans* 621H and the initial start OD_{600} of 0.04 did not change within 24 h (Supplementary Figure S3). In 4% (w/v) D-mannitol medium supplemented with 1% (w/v) L-rhamnose, the strain 621H grew very similar and without a significant difference compared to the growth in the D-mannitol complex medium without L-rhamnose supplement. Furthermore, with and without L-rhamnose the initial pH 6 of the growth medium was acidified to pH 4.3 after 24 h, suggesting no relevant oxidation of L-rhamnose to a corresponding acid. Therefore, there was no negative or supportive effect of L-rhamnose on the growth of *G. oxydans* 621H up to 1% (w/v).

In *Gluconobacter oxydans*, P_{rhaBAD} from *Escherichia coli* is repressed in the presence of L-rhamnose

First, we tested the inducibility of P_{rhaBAD} in *G. oxydans* by constructing a pBBR1MCS-5-based plasmid placing all the genetic elements in the same order as in *E. coli*. The *rhaSR* operon was under the control of its native promoter P_{rhaSR} in divergent orientation to P_{rhaBAD}. The fluorescent reporter mNeonGreen (mNG) was used to measure the P_{rhaBAD}-controlled expression by placing the *mNG* gene downstream from P_{rhaBAD}. On the plasmid, the elements *rhaSR*-P_{rhaSR}-P_{rhaBAD}-*mNG* were flanked by three terminators, T_{gdhM} downstream from *rhaR*, and T_{BBa_B1002} and $T_{GOX0028}$ downstream from *mNG* (Figure 1A). Furthermore, downstream from the native ribosome binding site (RBS) present in P_{rhaBAD} the RBS 5′-AGGAGA was inserted upstream from *mNG*. This RBS appeared strong in *G. oxydans* and was also used in the regulatable AraC-P_{araBAD} and TetR-P_{tet} expression systems (Fricke et al., 2020, 2021b). The inducibility of the resulting plasmid pBBR1MCS-5-*rhaSR*-P_{rhaSR}-P_{rhaBAD}-*mNG* was tested in *G. oxydans* 621H with 1% (w/v) L-rhamnose. Overnight pre-cultures were split to inoculate main cultures in D-mannitol medium with and without L-rhamnose. Growth and mNG fluorescence was monitored in a BioLector.

As expected from the previous growth tests in shake flasks, all BioLector microscale cultures exhibited very similar growth regardless of L-rhamnose supplementation (Figure 1B). However, surprisingly and contrary to our expectation, the mNG fluorescence of the cultures without L-rhamnose strongly increased during growth and peaked ~6 h after inoculation when cells entered the stationary phase, while in cultures with L-rhamnose a much lower level of mNG fluorescence (~28%) was

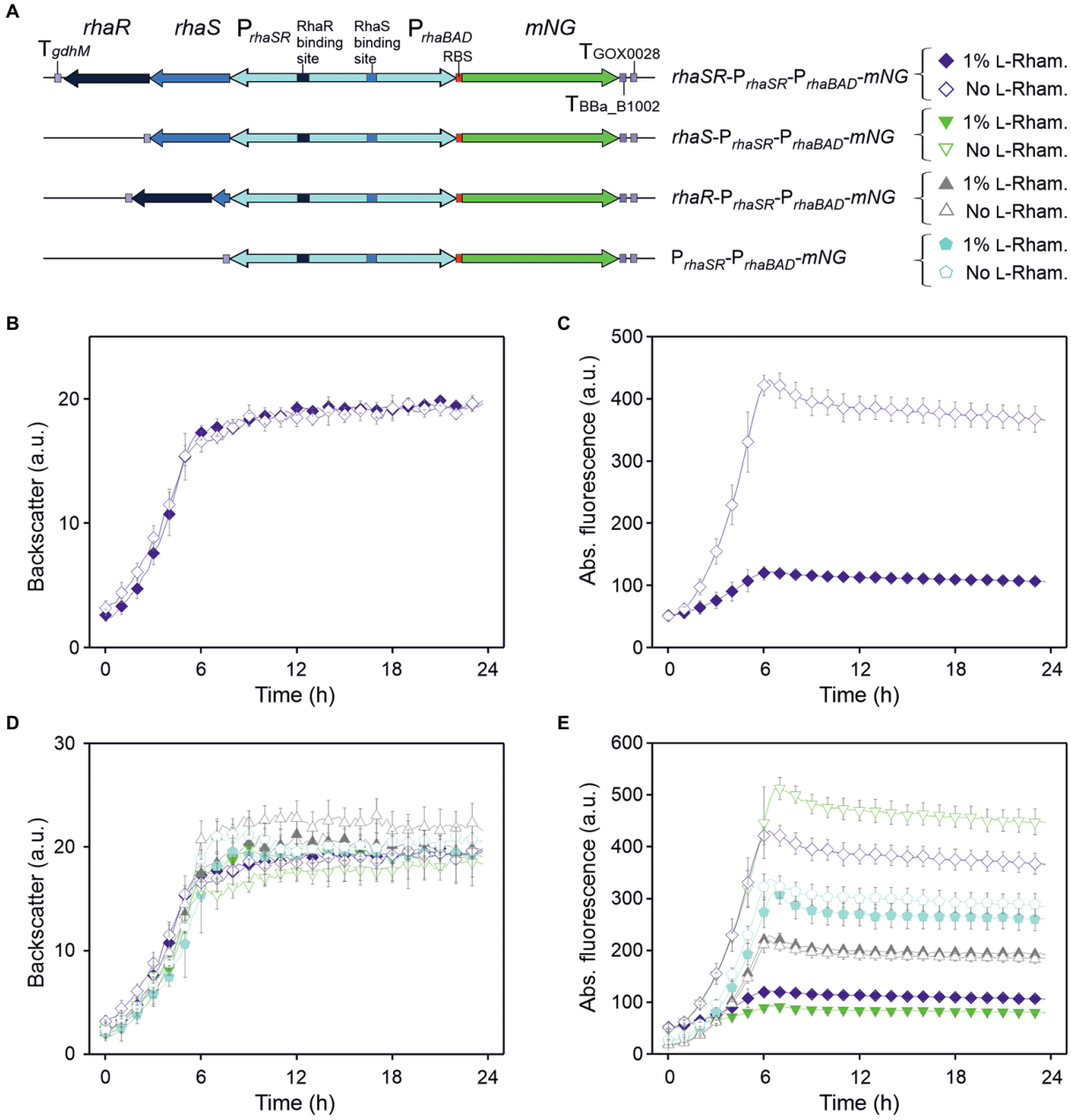

FIGURE 1
pBBR1MCS-5-based expression plasmids and analysis of the regulation of the RhaSR-P_{rhaBAD} system from *Escherichia coli* in *G. oxydans* 621H. **(A)** Schematic illustration of the plasmid variants with reporter gene *mNG* used to test L-rhamnose-dependent regulation of P_{rhaBAD}-derived expression in the presence and absence of RhaS and RhaR. T_{gdhM}: terminator sequence of *gdhM* (GOX0265); $T_{GOX0028}$: terminator sequence of GOX0028. The RBS 5′-AGGAGA was inserted in the 3′ region of P_{rhaBAD} upstream from *mNG*. **(B)** Growth according to backscatter and **(C)** absolute mNG fluorescence in *G. oxydans* carrying plasmid pBBR1MCS-5-*rhaSR*-P_{rhaSR}-P_{rhaBAD}-*mNG* grown in D-mannitol medium without and with 1% (w/v) L-rhamnose in BioLector microscale. **(D)** Growth according to backscatter and **(E)** absolute mNG fluorescence of *G. oxydans* carrying either plasmid pBBR1MCS-5-*rhaSR*-P_{rhaSR}-P_{rhaBAD}-*mNG*, or a plasmid lacking either *rhaR*, or *rhaS*, or both *rhaSR*. Cells were grown in microscale (BioLector) in D-mannitol medium without and with 1% (w/v) L-rhamnose. All data represent mean values and standard deviation from two biological replicates (clones) with three technical replicates each. BioLector settings: backscatter gain 20, fluorescence gain 50.

observed (Figure 1C). Thus, *mNG* expression from P_{rhaBAD} appeared to be strongly repressed in the presence of L-rhamnose, suggesting that in *G. oxydans* the responsiveness of the RhaSR-P_{rhaBAD} system is inverted compared to *E. coli*. Furthermore, according to the absolute mNG fluorescence in the absence of L-rhamnose, the promoter P_{rhaBAD} appeared to be very strong in *G. oxydans* compared to P_{araBAD} and P_{tet} (Fricke et al., 2020, 2021b).

To test whether the *rhaSR*-P_{rhaBAD}-*mNG* expression plasmid shows L-rhamnose-inducibility in *E. coli*, the plasmid-carrying *E. coli* S17-1 used for transformation of *G. oxydans* was tested. As

expected, in LB medium supplemented with 1% (w/v) L-rhamnose, the mNG fluorescence was ~2,200-fold higher compared to the mNG fluorescence in cultures without L-rhamnose (data not shown). To verify that the reversed responsiveness of RhaSR-P_{rhaBAD} indeed was observed in *G. oxydans* 621H carrying the intended plasmid without mutations possibly acquired later during growth, *G. oxydans* cells of an induced culture were harvested at the end of the cultivation (24 h) for isolation of total DNA and Illumina sequencing. The read data analysis excluded unexpected contamination of the culture, since 99.48% of 1,402,738 trimmed and quality-filtered reads mapped to the updated reference sequences of the *G. oxydans* 621H genome (88-fold coverage), the 5 endogenous plasmids, and the *mNG* expression plasmid with *rhaSR*-P_{rhaSR}-P_{rhaBAD}-*mNG* (1,011-fold coverage; Kranz et al., 2017). Besides, the sequencing results corroborated three DNA point mutations in *rhaSR* already observed before by Sanger sequencing when checking the insert of the plasmid after cloning in *E. coli*. In *rhaR* there was the silent mutation of CGC to CGT (Arg56). In *rhaS* there was the silent mutation of CTG to CTT (Leu166) and the mutation of GGG to TGG resulting in the exchange Gly136Trp in RhaS. All three mutations were present already on the plasmid when it was cloned in *E. coli*. To exclude an effect of these mutations on the reversed responsiveness only in *G. oxydans*, the plasmid was cloned again using a new *rhaS* DNA template from *E. coli* MG1655. This plasmid lacked the two point mutations in *rhaS* and also showed the reversed responsiveness in *G. oxydans* 621H with the same extent of repression (data not shown). Thus, the DNA point mutations in *rhaS* did not affect the regulatory properties of the system in *G. oxydans*. In summary, these results showed that in contrast to *E. coli* the P_{rhaBAD} promoter is repressed in *G. oxydans* in the presence of L-rhamnose.

RhaS is responsible for L-rhamnose-dependent repression of P_{rhaBAD} in *Gluconobacter oxydans*

To analyze whether RhaS and/or RhaR, or an interfering endogenous *G. oxydans* protein is responsible for the reversed responsiveness of the RhaSR-P_{rhaBAD} system, we constructed derivatives of the expression plasmid either lacking in-frame a substantial part of *rhaS*, or lacking *rhaR*, or lacking both genes, yet keeping all the elements upstream and downstream from *rhaS* and *rhaR* (Figure 1A). *G. oxydans* clones carrying one of these plasmid derivatives were grown in D-mannitol medium without and with 1% (w/v) L-rhamnose and cultivated in a BioLector to monitor growth and mNG fluorescence. Regardless of the plasmid used, all *G. oxydans* cultures exhibited very similar growth with and without L-rhamnose (Figure 1D). The differences in mNG fluorescence with and without L-rhamnose clearly indicated that RhaS alone is either directly or indirectly responsible for the regulation of P_{rhaBAD}. All clones with the plasmid lacking only *rhaS* exhibited a moderate maximal mNG fluorescence after ~6 h (220–228 a.u.), regardless of L-rhamnose supplementation (Figure 1E). The clones with the plasmid lacking both *rhaS* and *rhaR* also showed no response of the mNG fluorescence to L-rhamnose, yet the maximal mNG fluorescence was 50% higher compared to the plasmid still containing *rhaR*. Without *rhaSR*, the mNG signals of all clones peaked at 6 h and reached a higher intensity (314–338 a.u.), suggesting a general negative effect of RhaR on the P_{rhaBAD} activity regardless of the presence or absence of L-rhamnose. This is in line with the observation that with the plasmid lacking only *rhaR*, expression from P_{rhaBAD} increased in the absence of L-rhamnose by ~20% (513 a.u.) compared to the plasmid with both regulator genes (431 a.u.). Furthermore, with 1% (w/v) L-rhamnose the *mNG* expression from P_{rhaBAD} was more reduced with the *rhaS*-P_{rhaBAD} construct (94 a.u.) than with the *rhaSR*-P_{rhaBAD} construct (122 a.u.).

In summary, these data indicated that RhaS activates the P_{rhaBAD} promoter in the absence of L-rhamnose and represses P_{rhaBAD} in the presence of L-rhamnose, and thus is exerting a dual role in *G. oxydans* (Figure 1E).

In the absence of L-rhamnose P_{rhaBAD} activity is stimulated by RhaS

The clear differences in the mNG fluorescence observed with the previous plasmid derivatives with or without *rhaS* suggested that RhaS activates P_{rhaBAD} in the absence of L-rhamnose in *G. oxydans*. If so, the apparent strength of P_{rhaBAD} in the absence of L-rhamnose could partially be tuned by the strength of *rhaS* expression. To test this and the resulting down-regulation of P_{rhaBAD}-derived *mNG* expression in the presence of L-rhamnose starting then from different initial expression levels, we constructed derivatives of pBBR1MCS-5-*rhaS*-P_{rhaSR}-P_{rhaBAD}-*mNG* expressing *rhaS* constitutively either from the *G. oxydans* promoter $P_{GOX0264}$ or $P_{GOX0452}$ (Figure 2A). $P_{GOX0264}$ and $P_{GOX0452}$ have been shown to be strong and moderate promoters in *G. oxydans*, respectively (Kallnik et al., 2010). With the resulting plasmids pBBR1MCS-5-*rhaS*-$P_{GOX0264}$-P_{rhaBAD}-*mNG* and pBBR1MCS-5-*rhaS*-$P_{GOX0452}$-P_{rhaBAD}-*mNG*, the *mNG* expression was compared to that with pBBR1MCS-5-*rhaS*-P_{rhaSR}-P_{rhaBAD}-*mNG* in microscale BioLector cultivations (Figure 2B). Without L-rhamnose, constitutive expression of *rhaS* from $P_{GOX0264}$ reduced P_{rhaBAD}-derived *mNG* expression by more than half and from this latter level the *mNG* expression was reduced by half when expressing *rhaS* from $P_{GOX0452}$ (Figure 2C). Thus, expression of *rhaS* from its native promoter P_{rhaSR} led to the highest P_{rhaBAD}-derived mNG signals (514 a.u. after ~7 h) in the absence of L-rhamnose. These results suggested that P_{rhaSR} is a very strong promoter *per se*, or because it is positively auto-regulated by RhaS. However, the RhaS protein was reported to severely aggregate when overexpressed (Wickstrum et al., 2010), and biochemical analysis of RhaS binding to the promoter DNA had

10.3389/fmicb.2022.981767

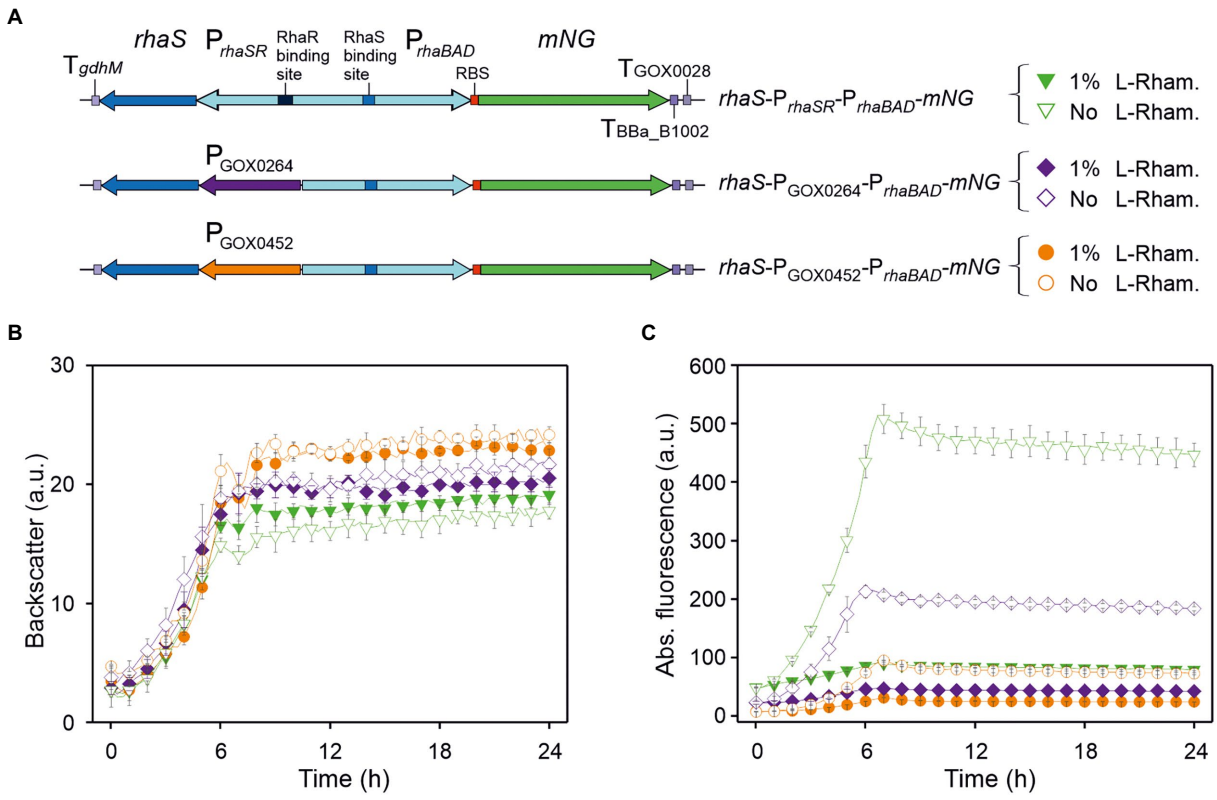

FIGURE 2
Performance of P_{rhaBAD}-derived *mNG* expression in dependence of *rhaS* expression and presence of L-rhamnose. **(A)** Schematic illustration of the plasmid variants for constitutive expression of *rhaS* from the strong and moderate *G. oxydans* promoters $P_{GOX0264}$ and $P_{GOX0452}$. T_{gdhM}: terminator sequence of *gdhM* (GOX0265); $T_{GOX0028}$: terminator sequence of GOX0028. RBS: 5′-AGGAGA inserted in the 3′ region of P_{rhaBAD} upstream from *mNG*. **(B)** Growth in D-mannitol medium according to backscatter and **(C)** absolute mNG fluorescence of *G. oxydans* 621H carrying either plasmid pBBR1MCS-5-*rhaS*-P_{rhaSR}-P_{rhaBAD}-*mNG*, or pBBR1MCS-5-*rhaS*-$P_{GOX0264}$-P_{rhaBAD}-*mNG*, or pBBR1MCS-5-*rhaS*-$P_{GOX0452}$-P_{rhaBAD}-*mNG*. Repression of *mNG* expression from P_{rhaBAD} was tested with 1% (w/v) L-rhamnose. Data represent mean values and standard deviation from two biological replicates (clones) with three technical replicates each. BioLector settings: backscatter gain 20, fluorescence gain 50.

not been possible due to the extreme insolubility of the overproduced RhaS protein (Egan and Schleif, 1994). Therefore, it appears more likely that P_{rhaSR} is a weak promoter also in *G. oxydans* resulting in sufficient levels of functional RhaS protein activating P_{rhaBAD}, while stronger *rhaS* expression *via* $P_{GOX0264}$ and $P_{GOX0452}$ likely resulted in aggregated non-functional RhaS protein.

In the presence of 1% (w/v) L-rhamnose, the strong *mNG* expression obtained with *rhaS*-P_{rhaSR}-P_{rhaBAD}-*mNG* was reduced by ~82% (from 514 to 90 a.u.). The *mNG* expression obtained with *rhaS*-$P_{GOX0264}$-P_{rhaBAD}-*mNG* and with *rhaS*-$P_{GOX0452}$-P_{rhaBAD}-*mNG* was reduced by 77% (from 212 to 48 a.u.) and by 68% (from 95 to 30 a.u.), respectively (Figure 2C).

P_{rhaSR} is weak in *Gluconobacter oxydans*, stimulated by RhaS and further stimulated by L-rhamnose

To check the strength of P_{rhaSR} in *G. oxydans* and the influence of RhaS on P_{rhaSR} activity, we created plasmids with *mNG* under the control of P_{rhaSR} and with *rhaS* under the control of the constitutive promoters $P_{GOX0452}$ or $P_{GOX0264}$, or lacking *rhaS* (Supplementary Figure S4A). The respective *G. oxydans* strains were cultivated in a BioLector and showed similar growth (Supplementary Figure S4B). In the absence of L-rhamnose, moderate $P_{GOX0452}$-derived *rhaS* expression resulted in a similar low *mNG* expression from P_{rhaSR} as without *rhaS*, while the stronger $P_{GOX0264}$-derived *rhaS* expression resulted in a two-fold higher *mNG* expression from P_{rhaSR}, suggesting a positive effect of the RhaS level on P_{rhaSR} activity (Supplementary Figures S4C,D). In the presence of L-rhamnose, *mNG* expression from P_{rhaSR} was always increased with *rhaS*, while there was no effect by L-rhamnose when *rhaS* was absent. With moderate *rhaS* expression in *G. oxydans* harboring pBBR1MCS -5-*mNG*-P_{rhaSR}-$P_{GOX0452}$-*rhaS*, the mNG fluorescence increased ~2.5-fold from 74 to 189 a.u. with 1% (w/v) L-rhamnose. This L-rhamnose-dependent increase was less pronounced with *rhaS* under control of the stronger $P_{GOX0264}$ where the RhaS level was expected to be higher. Here, the mNG fluorescence increased only 1.3-fold from 144 to 187 a.u. (Supplementary Figure S4C). Together, P_{rhaSR} is also

stimulated by RhaS in the absence of L-rhamnose, yet in contrast to the repressed P_{rhaBAD} promoter, P_{rhaSR} is further activated by RhaS in the presence of L-rhamnose.

Repression of P_{rhaBAD} is sensitive to low L-rhamnose levels and is homogeneous

Since from all tested plasmid variants the one lacking *rhaR* and containing *rhaS* under the control of its native auto-regulated P_{rhaSR} promoter exhibited the highest P_{rhaBAD} activity in the absence of L-rhamnose and the highest grade of repression in the presence of L-rhamnose, the construct pBBR1MCS-5-*rhaS*-P_{rhaSR}-P_{rhaBAD}-*mNG* was analyzed further. The sensitivity of repression and residual *mNG* expression was tested in D-mannitol medium with 0.3%, 1% and 3% (w/v) L-rhamnose in a BioLector (Figures 3A,B). Already 0.3% (w/v) L-rhamnose strongly reduced the mNG fluorescence after ~7 h by 75% (225 vs. 55 a.u.). This indicated that the RhaS-P_{rhaBAD} system is quite sensitive and already low L-rhamnose concentrations should enable a tuning of target gene repression. Supplementation with 1% and 3% (w/v) L-rhamnose reduced mNG fluorescence by 83% (38 a.u.) and 85% (34 a.u.), respectively. This suggested that already 1% (w/v) L-rhamnose was sufficient to reach almost maximal possible repression of plasmid-based P_{rhaBAD} copies in *G. oxydans*.

This responsiveness of P_{rhaBAD}-based expression toward relatively low L-rhamnose concentrations was also observed in shake flask cultivations. When grown in 50 ml D-mannitol medium supplemented with 0.25% L-rhamnose, the mNG fluorescence was reduced to 24% (from 3,267 to 783 a.u.) after 9 h (Figures 3C,D). In shake flask cultures with 1% (w/v) L-rhamnose, the mNG fluorescence was reduced to 17% (from 3,267 to 553 a.u.).

Flow cytometry was used to analyze the repression of P_{rhaBAD}-derived *mNG* expression on the single cell level. In the absence of L-rhamnose, 7 h after inoculation 95.5% of the analyzed cells showed strong mNG fluorescence (~100,000 a.u.), while when grown with 1% (w/v) L-rhamnose, 96.4% of the analyzed cells showed a 89% reduced fluorescence (~11,000 a.u.; Figure 3E). Thus, the results of this FACS analysis are in line with the results of the BioLector and Tecan reader (shake flasks) measurements. Additionally, the FACS analysis demonstrated a high population homogeneity in both conditions.

An additional RhaS binding site directly downstream from the −10 region doubled the P_{rhaBAD}-derived expression strength and the dynamic range of repression

In an attempt to reduce the residual expression from P_{rhaBAD} in the presence of L-rhamnose and achieve complete repression, and to possibly lower the L-rhamnose concentrations required, we constructed and tested a plasmid with an additional RhaS binding site (+RhaS-BS) directly downstream from the annotated *E. coli* −10 region of P_{rhaBAD}. Additional binding of the RhaS-L-rhamnose complex downstream from the −10 region should potentially contribute to the repression of P_{rhaBAD}. Also, it was interesting to see the general impact of this additional RhaS BS on the P_{rhaBAD} activity in the absence of L-rhamnose.

We used plasmid pBBR1MCS-5-*rhaS*-P_{rhaSR}-P_{rhaBAD}-*mNG* as template and created a copy of the 50 bp region comprising the native RhaS-BS present in P_{rhaBAD}. This copy was inserted directly downstream from the −10 region of P_{rhaBAD}. The resulting plasmid was termed pBBR1MCS-5-*rhaS*-P_{rhaSR}-$P_{rhaBAD(+RhaS\text{-}BS)}$-*mNG* and its expression performance was compared with that of the template plasmid (Figure 4). In D-mannitol medium without and with 1% (w/v) L-rhamnose, both strains showed similar growth independent of the plasmids or L-rhamnose supplementation (Figure 4D). Interestingly, in the absence of L-rhamnose, the maximal mNG fluorescence observed for the plasmid carrying +RhaS-BS was almost twice (405 a.u.) that of the parental plasmid (225 a.u.), suggesting additional activation of P_{rhaBAD} by RhaS in the absence of L-rhamnose or a new transcriptional start increasing the *mNG* expression (Figure 4E). In the presence of 1% (w/v) L-rhamnose, the absolute residual *mNG* expression were similarly low for both constructs according to the mNG fluorescence. Therefore, the relative residual plasmid-based mNG expression was decreased to 11% by +RhaS-BS due to the doubled absolute expression strength in the absence of L-rhamnose (11% for +RhaS-BS: 405 a.u. reduced to 45 a.u.; 17% for parental: 225 a.u. reduced to 38 a.u.).

The tunability of $P_{rhaBAD(+RhaS\text{-}BS)}$ repression was tested with 0.05%, 0.1%, 0.2%, 0.3%, 1%, and 3% (w/v) L-rhamnose (Figures 5A–D). With 1% and 3% (w/v), the reduction of the mNG fluorescence was similarly high (from 405 a.u. to 43 and 41 a.u., respectively), indicating that like P_{rhaBAD}, plasmid-based $P_{rhaBAD(+RhaS\text{-}BS)}$ is also almost maximally repressed by 1% (w/v) L-rhamnose. The calculated residual *mNG* expression from $P_{rhaBAD(+RhaS\text{-}BS)}$ was 11% and 10%, respectively. With 0.3% (w/v) L-rhamnose, the residual mNG fluorescence was 17% (405 vs. 69 a.u.). With only 0.05% (w/v) L-rhamnose, the mNG fluorescence was reduced approximately by half (from 406 to 197 a.u.), showing the sensitivity and tunability of the system. In shake flask cultivations with 0.25% and 1% (w/v) L-rhamnose, $P_{rhaBAD(+RhaS\text{-}BS)}$ showed a similar repression performance as in microscale BioLector conditions. After 9 h of growth in shake flasks, the maximal mNG fluorescence without L-rhamnose (5,833 a.u.) was reduced to 1,060 and 600 a.u. in the presence of 0.25% and 1% (w/v) L-rhamnose (Figures 5E,F), representing 18% and 10% residual *mNG* expression.

Plotting the relative maximal P_{rhaBAD}- and $P_{rhaBAD(+RhaS\text{-}BS)}$-derived mNG fluorescence vs. the L-rhamnose concentrations

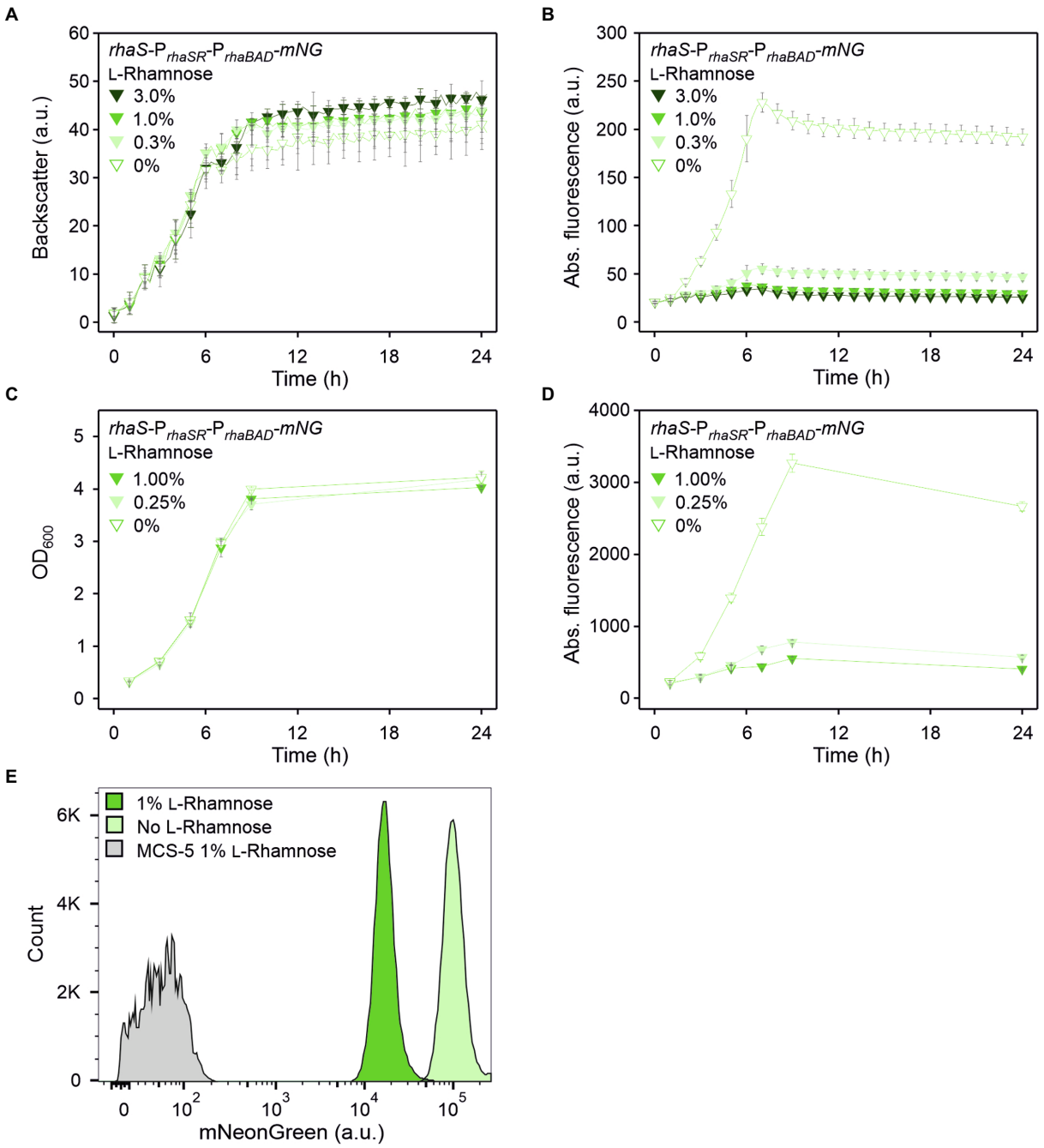

FIGURE 3
RhaS-dependent repression of P_{rhaBAD} in *G. oxydans* in the presence of L-rhamnose. **(A)** Growth according to backscatter and **(B)** absolute mNG fluorescence in *G. oxydans* 621H with plasmid pBBR1MCS-5-*rhaS*-P_{rhaSR}-P_{rhaBAD}-*mNG* in microscale BioLector cultivations without or with L-rhamnose (w/v) as indicated. BioLector settings: backscatter gain 20, fluorescence gain 40. **(C)** Growth (OD_{600}) and **(D)** absolute mNG fluorescence in *G. oxydans* 621H with plasmid pBBR1MCS-5-*rhaS*-P_{rhaSR}-P_{rhaBAD}-*mNG* in shake flask cultivations without and with L-rhamnose (w/v) as indicated. mNG fluorescence was measured in a Tecan reader (gain 60). Data represent mean values and standard deviation from two biological replicates (clones) with three technical replicates each. **(E)** FACS analysis of *G. oxydans* 621H with plasmid pBBR1MCS-5-*rhaS*-P_{rhaSR}-P_{rhaBAD}-*mNG* or empty vector pBBR1MCS-5 as a control (MCS-5). Cells were grown in shake flasks with D-mannitol medium without and with 1% (w/v) L-rhamnose. FACS analysis was performed 7h after inoculation (induction). Total counts per sample represent 100,000 events.

illustrates the responsiveness of both promoters toward low L-rhamnose concentrations (Figure 6). While the absolute repression of both promoters was similar and down to 10% of the maximal individual expression strength, non-repressed $P_{rhaBAD(+RhaS\text{-}BS)}$ was two-fold stronger than P_{rhaBAD} and therefore offers a wider dynamic range of expression.

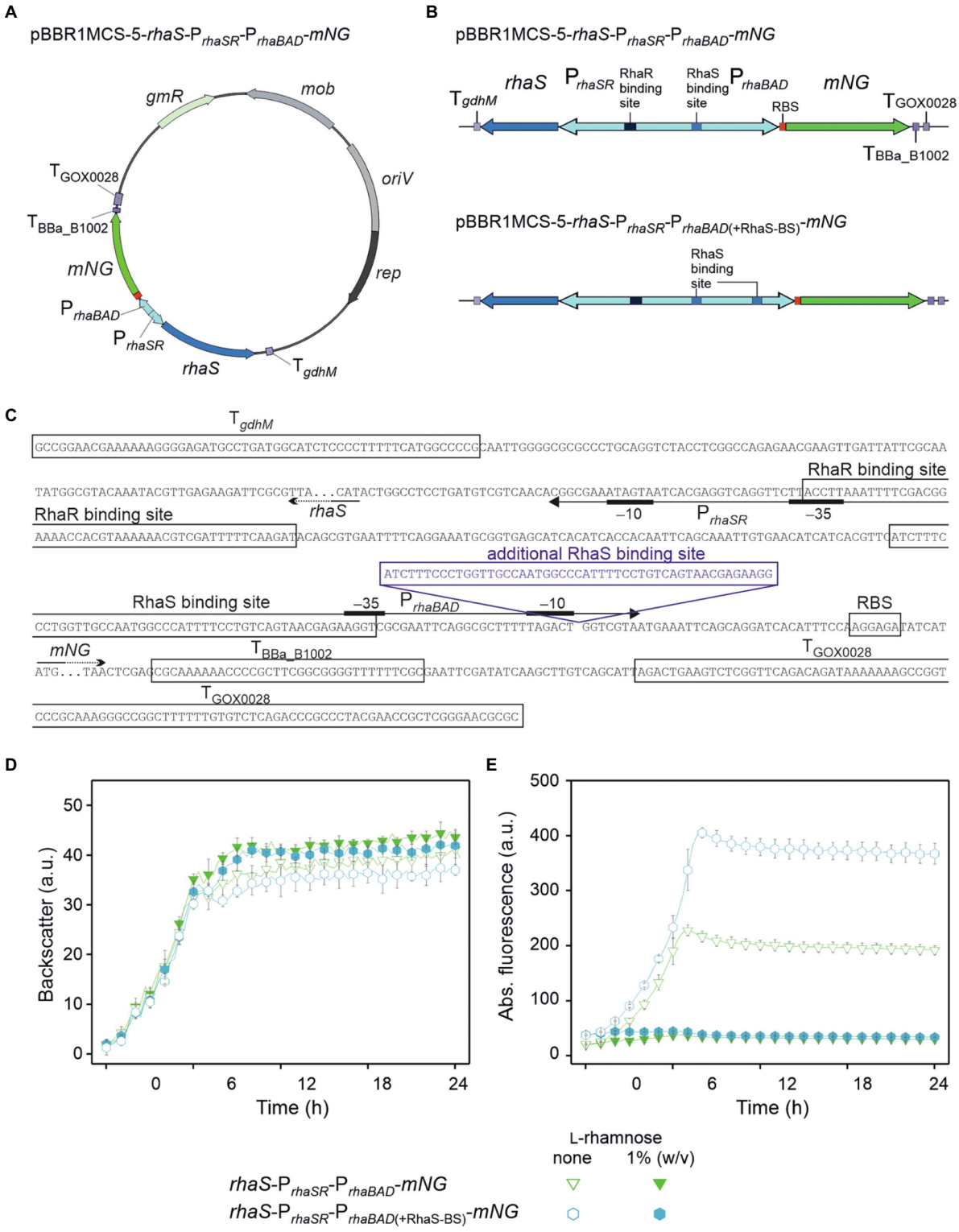

FIGURE 4
Insertion of an additional RhaS binding site downstream from the –10 region doubled the expression strength of P_{rhaBAD} and the range of repression. **(A)** Map of plasmid pBBR1MCS-5-*rhaS*-P_{rhaSR}-P_{rhaBAD}-*mNG*. **(B)** Schematic illustration of the pBBR1MCS-5 inserts *rhaS*-P_{rhaSR}-P_{rhaBAD}-*mNG* and its variant *rhaS*-P_{rhaSR}-$P_{rhaBAD(+RhaS-BS)}$-*mNG* harboring an additional RhaS binding site directly downstream from the –10 region, all flanked by terminators. **(C)** DNA sequence details of the fragment *rhaS*-P_{rhaSR}-$P_{rhaBAD(+RhaS-BS)}$-*mNG* with RhaS and RhaR binding sites as well as terminator sequences adjacent to *rhaS* and *mNG*. The promoter elements are given according to Egan and Schleif (1993). **(D)** Growth according to backscatter and **(E)** absolute mNG fluorescence of *G. oxydans* 621H carrying either plasmid pBBR1MCS-5-*rhaS*-P_{rhaSR}-P_{rhaBAD}-*mNG* or pBBR1MCS-5-*rhaS*-P_{rhaSR}-$P_{rhaBAD(+RhaS-BS)}$-*mNG* in microscale BioLector cultivations in D-mannitol medium without and with 1% (w/v) L-rhamnose. Data represent mean values and standard deviation from two biological replicates (clones) with three technical replicates each. BioLector settings: backscatter gain 20, fluorescence gain 40.

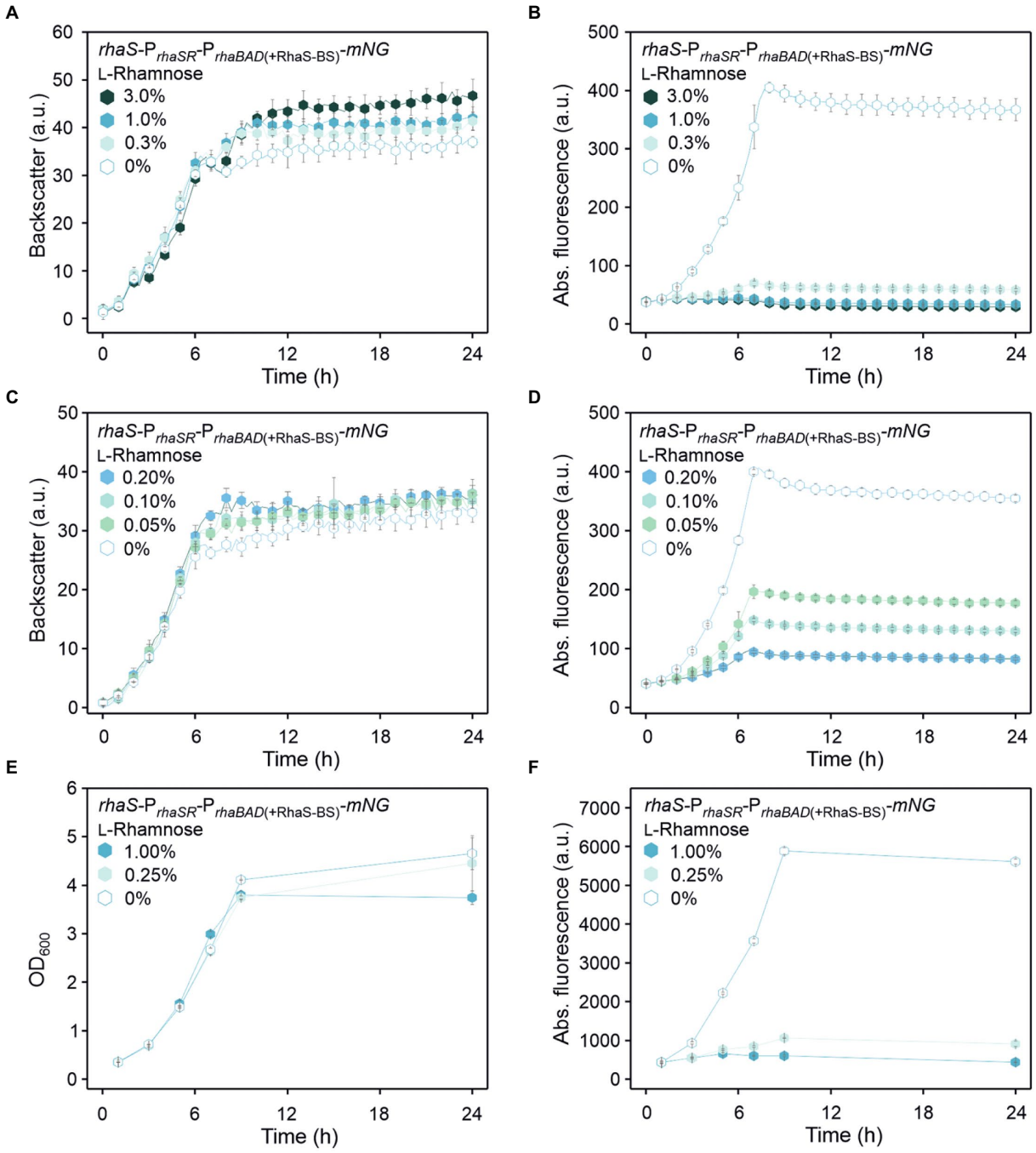

FIGURE 5
Tunability of the RhaS-$P_{rhaBAD(+RhaS-BS)}$ system in *G. oxydans* 621H carrying plasmid pBBR1MCS-5-*rhaS*-P_{rhaSR}-$P_{rhaBAD(+RhaS-BS)}$-*mNG*. **(A,C)** Growth in D-mannitol medium according to backscatter and **(B,D)** absolute mNG fluorescence in BioLector cultivations. L-Rhamnose was supplemented in concentrations ranging from 0.05 to 3% (w/v). All data represent mean values and standard deviation from two biological replicates (clones) with three technical replicates each. BioLector settings: backscatter gain 20, fluorescence gain 40. **(E)** Growth in D-mannitol medium and **(F)** absolute mNG fluorescence in shake flasks. The mNG fluorescence was measured in a Tecan reader (gain 60).

A genomic single copy of $P_{rhaBAD(+RhaS-BS)}$ can be tuned and completely repressed by RhaS and L-rhamnose

We then analyzed if the stronger P_{rhaBAD} variant can be completely repressed in a plasmid-free strain when this modified target promoter and *rhaS* are genomically integrated and present as a single copy instead of being present on a plasmid with medium copy number (Figure 7A). Therefore, we integrated the reporter gene *mNG* under control of $P_{rhaBAD(+RhaS-BS)}$ into the intergenic region igr3 (GOX0038/GOX_RS01330–GOX0039/GOX_RS01335). The resulting strain was

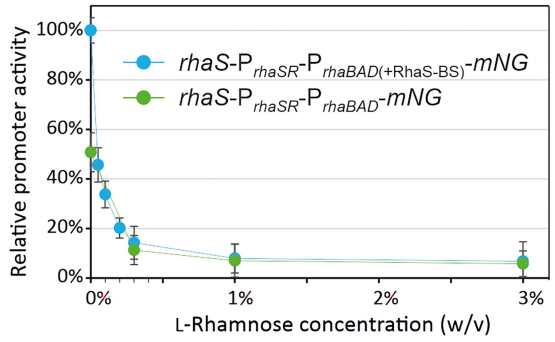

FIGURE 6
Responsiveness of P_{rhaBAD} and $P_{rhaBAD(+RhaS\text{-}BS)}$ towards L-rhamnose. The maximal mNG fluorescence of *G. oxydans* 621H carrying either plasmid pBBR1MCS-5-*rhaS*-P_{rhaSR}-P_{rhaBAD}-*mNG* or pBBR1MCS-5-*rhaS*-P_{rhaSR}-$P_{rhaBAD(+RhaS\text{-}BS)}$-*mNG* in response to different L-rhamnose concentrations was used to calculate relative % promoter activities compared to the maximal $P_{rhaBAD(+RhaS\text{-}BS)}$ activity in the absence of L-rhamnose (100%).

termed *G. oxydans mNG*. For single-copy *rhaS* expression, we tested the promoters P_{rhaSR} and $P_{GOX0264}$ and integrated both *rhaS* constructs in *G. oxydans mNG* separately into igr2 (GOX0028/GOX_RS01280–GOX0029/GOX_RS01285). The resulting *G. oxydans* strains *mNG* igr2::$P_{GOX0264}$-*rhaS* and *mNG* igr2::P_{rhaSR}-*rhaS* were cultivated and analyzed in a BioLector (Figures 7B,C). As observed before with the plasmid-based approach, in the absence of L-rhamnose expression of single-copy *rhaS* under control of P_{rhaSR} resulted in higher activity of $P_{rhaBAD(+RhaS\text{-}BS)}$ than with $P_{GOX0264}$-*rhaS*. However, with *rhaS* under control of $P_{GOX0264}$ a much higher extent of repression was observed with 1% (w/v) L-rhamnose. Here, the maximal mNG signals were reduced by 64% from 217 to 78 a.u. (Figure 7C). These results indicated that single-copy *rhaS* expression is not sufficient to completely repress $P_{rhaBAD(+RhaS\text{-}BS)}$. We then tested if a second genomic *rhaS* copy could be sufficient and integrated both $P_{GOX0264}$-*rhaS* and P_{rhaSR}-*rhaS* into strain *mNG* igr2::$P_{GOX0264}$-*rhaS* separately into igr1 (GOX0013/GOX_RS01200–GOX0014/GOX_RS01205). The two resulting *G. oxydans* strains *mNG* igr1::$P_{GOX0264}$-*rhaS* igr2::*rhaS* and *mNG* igr1::P_{rhaSR}-*rhaS* igr2::*rhaS* were cultivated and analyzed in a BioLector (Figures 7D,E). The extent of repression in the presence of L-rhamnose was higher with two *rhaS* copies compared to only one copy and again $P_{GOX0264}$-*rhaS* performed better in repression than P_{rhaSR}-*rhaS*, yet two genomic *rhaS* copies were still not sufficient to completely repress $P_{rhaBAD(+RhaS\text{-}BS)}$. With one copy of P_{rhaSR}-*rhaS* and one copy of $P_{GOX0264}$-*rhaS* the maximal mNG signals were reduced by 78% from 435 to 96 a.u. With two genomic copies of $P_{GOX0264}$-*rhaS*, the maximal mNG signals were reduced by 84% from 444 to 73 a.u. (Figure 7E).

To test if a genomic single-copy $P_{rhaBAD(+RhaS\text{-}BS)}$ can be completely repressed at all, we constructed the *rhaS* expression plasmid pBBR1MCS-5-P_{rhaSR}-*rhaS* and introduced it into the single-copy *rhaS* strain *G. oxydans mNG* igr2::$P_{GOX0264}$-*rhaS* already showing 64% promoter repression (Figure 8A). The resulting plasmid-carrying strain was cultivated and analyzed in a BioLector (Figures 8B,C). According to the mNG signals, the genomic single-copy $P_{rhaBAD(+RhaS\text{-}BS)}$ appeared completely repressed by 3% and possibly also by 1% (w/v) L-rhamnose. To test the tunability of this repression with plasmid-based expression of *rhaS*, we also tested lower L-rhamnose concentrations (Supplementary Figure S5). In the presence of 0.1% (w/v) L-rhamnose, the maximal mNG signals were reduced by 64% from 216 to 78 a.u.. In the presence of 0.2% (w/v) L-rhamnose, the maximal mNG signals were reduced by 78% from 216 to 47 a.u.. These results indicated a relatively high sensitivity of the system toward lower L-rhamnose concentrations and that a genomic copy of the RhaS target promoter variant can be tuned.

The *Escherichia coli* promoter P_{rhaT} is weak, inducible and tunable in *Gluconobacter oxydans*

As mentioned above, in *E. coli* RhaS also activates the promoter P_{rhaT} of the L-rhamnose transporter gene *rhaT*. Similar to P_{rhaBAD}, P_{rhaT} contains two regulatory elements, one for RhaS and one for CRP binding. Contrary to P_{rhaBAD}, the RhaS binding site on P_{rhaT} is differently composed and slightly shifted, so that the binding site does not overlap with the −35 element of P_{rhaT} (Vía et al., 1996; Wickstrum et al., 2010). To analyze the regulation and performance of P_{rhaT} by RhaS in *G. oxydans*, we constructed reporter plasmid pBBR1MCS-5-*rhaS*-P_{rhaSR}-P_{rhaT}-*mNG*. As a control, plasmid pBBR1MCS-5-P_{rhaT}-*mNG* lacking *rhaS* was constructed (Figure 9).

In BioLector cultivations, *G. oxydans* cells with pBBR1MCS-5-*rhaS*-P_{rhaSR}-P_{rhaT}-*mNG* or pBBR1MCS-5-P_{rhaT}-*mNG* showed very similar growth independent of the presence or absence of L-rhamnose (Figure 10A). Interestingly and in contrast to P_{rhaBAD}, *mNG* expression controlled by P_{rhaT} was induced by L-rhamnose. Addition of 1% (w/v) L-rhamnose increased mNG fluorescence ~7.5-fold (from 36 to 266 a.u.) within 8 h. The values indicated a weak or moderate strength of P_{rhaT} in *G. oxydans* (Figure 10B). Almost no mNG fluorescence was observed in the strain with plasmid pBBR1MCS-5-P_{rhaT}-*mNG* without *rhaS*. Thus, on the one hand P_{rhaT} was almost not active in *G. oxydans* without RhaS and an endogenous *G. oxydans* protein did not interfere. On the other hand, RhaS apparently weakly activated P_{rhaT} already in the absence of L-rhamnose since with plasmid pBBR1MCS-5-*rhaS*-P_{rhaSR}-P_{rhaT}-*mNG* a low basal mNG fluorescence was observed also in the absence of L-rhamnose exceeding the extremely low mNG signals when *rhaS* was absent (Figure 10B). Alternatively, a low level of L-rhamnose could be present in the complex medium resulting in a basal RhaS-dependent induction of the system. It should be noted that due to the relatively weak expression from P_{rhaT} compared to P_{rhaBAD}, in these BioLector cultivations the fluorescence signals were monitored with gain 70 instead of gain 40 or 50.

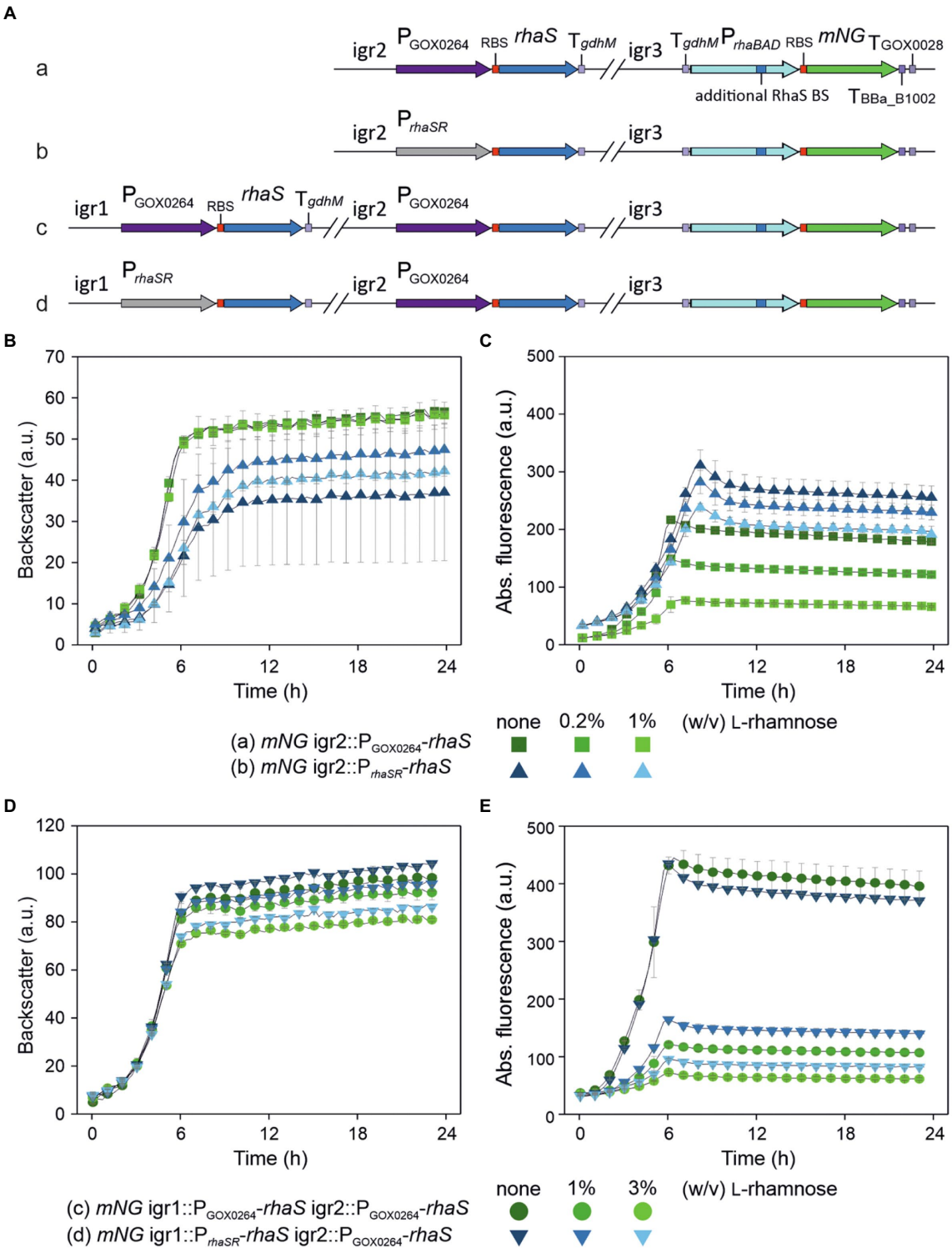

FIGURE 7
Partial repression of genomic single-copy $P_{rhaBAD(+RhaS\text{-}BS)}$-*mNG* using genomically integrated copies of *rhaS*. **(A)** Schematic illustration of the genomic backgrounds of the *G. oxydans* 621H strains. The expression cassette $P_{rhaBAD(+RhaS\text{-}BS)}$-*mNG* of the reporter gene was genomically integrated into the intergenic region igr3 (GOX0038/GOX_RS01330–GOX0039/GOX_RS01335). The resulting strain was termed *G. oxydans mNG*. For single-copy *rhaS* expression, a *rhaS* expression cassette either under control of $P_{GOX0264}$ (a) or P_{rhaSR} (b) was genomically integrated in *G. oxydans mNG* into igr2 (GOX0028/GOX_RS01280 - GOX0029/GOX_RS01285). A second *rhaS* expression cassette again either under control of $P_{GOX0264}$ (c) or P_{rhaSR} (d) was genomically integrated into igr1 (GOX0013/GOX_RS01200 - GOX0014/GOX_RS01205) in strain A with $P_{GOX0264}$-*rhaS* in igr2. **(B,D)** Growth of the strains in D-mannitol medium according to backscatter and **(C,E)** absolute mNG fluorescence in BioLector cultivations. L-Rhamnose was supplemented as indicated. All data represent mean values and standard deviation from two biological replicates (clones) with three technical replicates each. BioLector settings: backscatter gain 20, fluorescence gain 70.

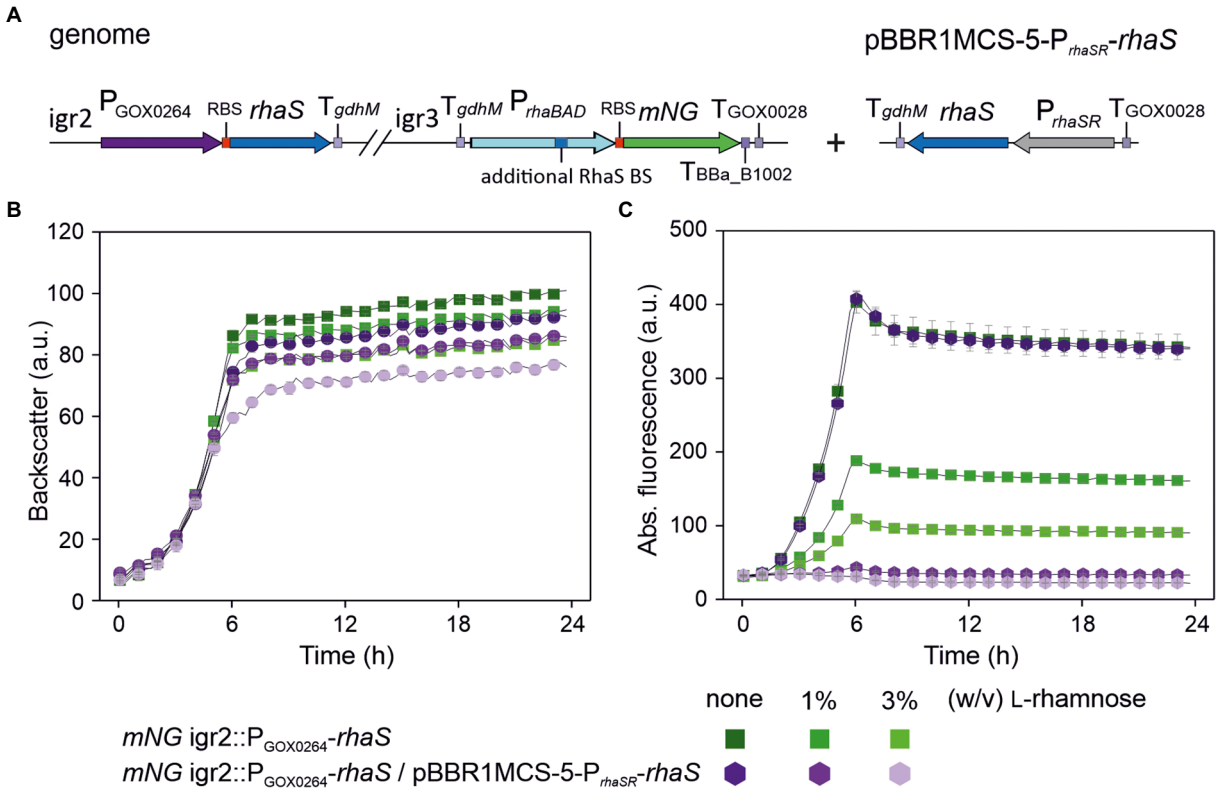

FIGURE 8
Complete repression of genomic single-copy $P_{rhaBAD(+RhaS\text{-}BS)}$-*mNG* by plasmid-based expression of *rhaS* and L-rhamnose. **(A)** Schematic illustration of the genomic background as described in Figure 7A (variant a) of the plasmid-carrying *G. oxydans mNG* igr2::$P_{GOX0264}$-*rhaS* strain. **(B)** Growth in D-mannitol medium according to backscatter and **(C)** absolute mNG fluorescence in BioLector cultivations. For comparison, the plasmid-free strain with only the single-copy *rhaS* in igr2 was included in the BioLector run. L-Rhamnose was supplemented as indicated. Data represent mean values and standard deviation from three technical replicates of one clone (*mNG* igr2::$P_{GOX0264}$-*rhaS*/pBBR1-MCS-5-P_{rhaSR}-*rhaS*) and two clones (*mNG* igr2::$P_{GOX0264}$-*rhaS*). BioLector settings: backscatter gain 20, fluorescence gain 70.

The tunability of P_{rhaT} induction was tested with L-rhamnose concentrations ranging from 0.25% to 4% (w/v). Again, growth of *G. oxydans* cells with pBBR1MCS-5-*rhaS*-P_{rhaSR}-P_{rhaT}-*mNG* was largely unaffected by up to 2% (w/v) L-rhamnose (Figure 10C). With 4% (w/v) L-rhamnose, the backscatter data suggested a biphasic growth. The P_{rhaT}-derived *mNG* expression increased gradually in an inducer-dependent manner (Figure 10D). The maximal induction observed was 9.2-fold (36 vs. 330 a.u.) and required 4% (w/v) L-rhamnose. With 0.25% (w/v) L-rhamnose already half of the maximal induction was reached showing that the weak to moderate P_{rhaT}-derived *mNG* expression could be nicely tuned by low L-rhamnose concentrations (Figure 10E). The low expression strength of P_{rhaT} and its tunability could be of particular interest for the synthesis of proteins forming inclusion bodies when expressed at higher levels.

The homogeneity of P_{rhaT} induction was analyzed by FACS using cells harvested after 7 h of growth in D-mannitol medium without or with 1% (w/v) L-rhamnose (Figure 10F). In the absence of L-rhamnose, 97.4% of the analyzed cells with pBBR1MCS-5-*rhaS*-P_{rhaSR}-P_{rhaT}-*mNG* showed relatively low fluorescence signals (~1,000 a.u.). In the presence of 1% (w/v) L-rhamnose, 96.9% of the population showed approximately 9-fold higher mNG fluorescence signals (~9,000 a.u.). We also tested the inducible P_{rhaT}-derived *mNG* expression in shake flask cultures with 0.3% and 1% (w/v) L-rhamnose. Under these conditions, all cultures with pBBR1MCS-5-*rhaS*-P_{rhaSR}-P_{rhaT}-*mNG* exhibited very similar growth (Figure 10G). The *mNG* expression was similarly induced as in the BioLector cultivations (Figure 10H). The maximal mNG fluorescence was reached after 9 h of growth and represented 4-fold and 6-fold induction with 0.3% (50 vs. 210 a.u.) and 1% (w/v) L-rhamnose (50 vs. 297 a.u.), respectively.

To test the influence of *rhaS* expression strength from different promoters on the performance of the RhaS-P_{rhaT} system, we replaced P_{rhaSR} and constructed plasmid variants with $P_{GOX0264}$-*rhaS* and $P_{GOX0452}$-*rhaS* (Figure 11A). The *G. oxydans* strains with either of the reporter plasmids were cultivated and analyzed in a BioLector to compare the basal expression level and the induction performance with that of cells expressing *rhaS* under the control of P_{rhaSR} (Figures 11B–E). For both tested *G. oxydans* promoters the maximal mNG signals with 4% (w/v) L-rhamnose were ~25% lower compared to that obtained with P_{rhaSR}-*rhaS*. Since the non-induced maximal mNG signals obtained with P_{rhaT} were somewhat

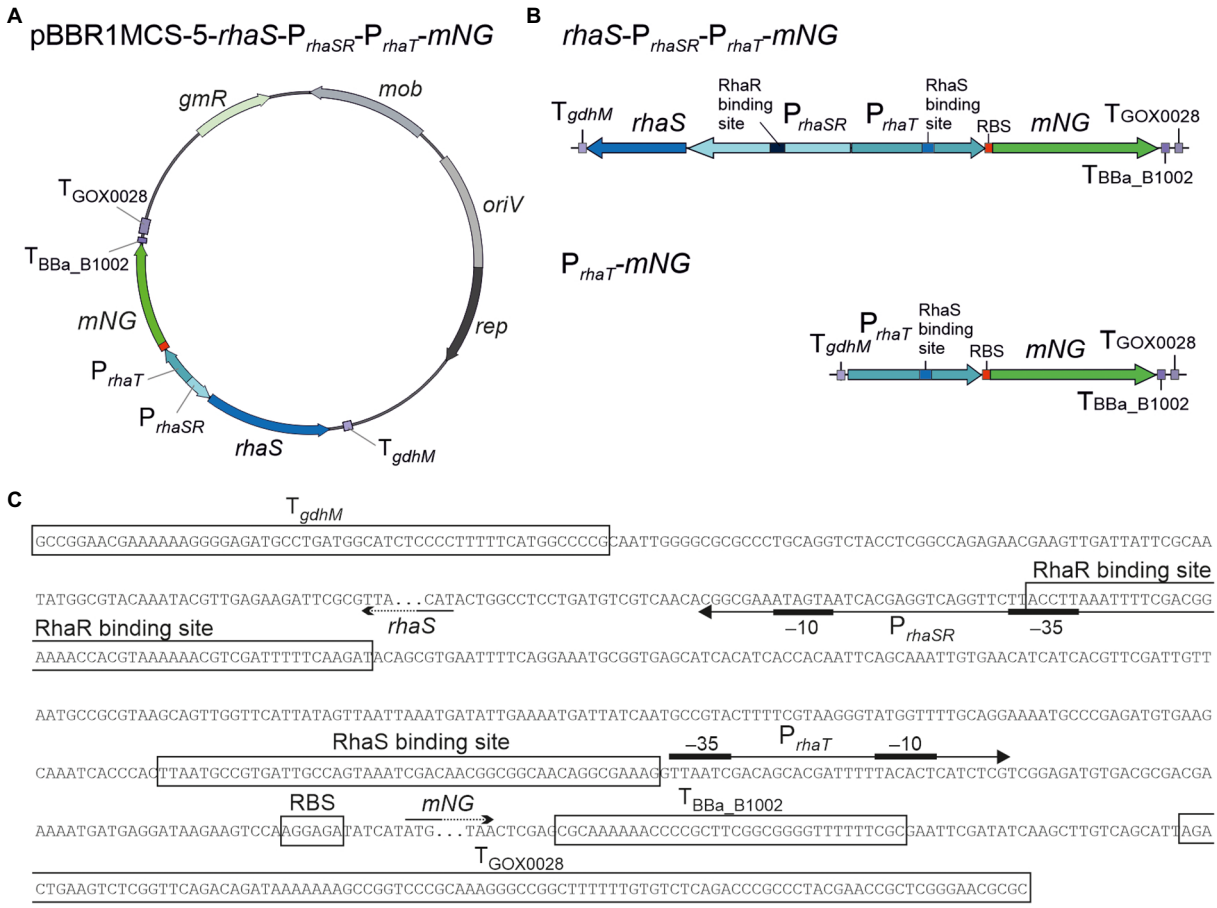

FIGURE 9
Reporter plasmids with P_{rhaT} and sequence details. **(A)** Map of plasmid pBBR1MCS-5-*rhaS*-P_{rhaSR}-P_{rhaT}-*mNG* with the fluorescence reporter gene *mNeonGreen* (*mNG*) under control of the promoter P_{rhaT} from the L-rhamnose transporter gene *rhaT* with the adjacent *rhaS* gene under control of P_{rhaSR}, all flanked by the terminators T_{gdhM}, T_{BBa_B1002} and $T_{GOX0028}$. **(B)** Schematic illustration of the pBBR1MCS-5 inserts *rhaS*-P_{rhaSR}-P_{rhaT}-*mNG* and its variant P_{rhaT}-*mNG* lacking *rhaS*-P_{rhaSR}. **(C)** DNA sequence details with RhaS and RhaR binding sites and terminator sequences downstream from *rhaS* and *mNG*. P_{rhaT} promoter elements are given according to Vía et al. (1996).

higher with $P_{GOX0264}$-*rhaS* (46 a.u.) and were approximately 3-fold higher with $P_{GOX0452}$-*rhaS* (104 a.u.) compared to P_{rhaSR}-*rhaS* (36 a.u.), the maximal induction fold changes with 4% (w/v) L-rhamnose were only 5-fold with $P_{GOX0264}$-*rhaS* and 2.4-fold with $P_{GOX0452}$-*rhaS*. Thus, compared to P_{rhaSR}-*rhaS* the non-induced basal expression level was not lowered and the induction fold changes of the RhaS-P_{rhaT} system were not improved by using $P_{GOX0264}$ or $P_{GOX0452}$ for *rhaS* expression.

Insertion of an additional RhaS binding site can reverse the regulation making P_{rhaT} repressible by RhaS and L-rhamnose

To test the influence of an additional RhaS binding site on the expression performance of P_{rhaT}, we inserted the RhaS binding site sequence from P_{rhaBAD} on the one hand directly downstream from the *E. coli* −10 region (−10-RhaS-BS) and on the other hand downstream from the *E. coli* TSS (TSS-RhaS-BS), and constructed for both P_{rhaT} variants expression plasmids with *rhaS* under control of either $P_{GOX0264}$ or $P_{GOX0452}$ (Figures 12A,B). In case of the −10-RhaS-BS, the regulation was reversed and $P_{rhaT(-10\text{-RhaS-BS})}$ was repressible. The maximal mNG signals in the absence of L-rhamnose for both *rhaS* constructs $P_{GOX0264}$-*rhaS* (250 a.u.) and $P_{GOX0452}$-*rhaS* (214 a.u.) were reduced by 65% (87 and 77 a.u.; Figures 12C,D). In contrast, the variant $P_{rhaT(TSS\text{-RhaS-BS})}$ was still inducible, yet showed increased and relatively high non-induced mNG signals in the absence of L-rhamnose, which could maximally only be doubled by induction with 4% (w/v) L-rhamnose (Figures 12E,F).

Discussion

In this study, we found that the promoters P_{rhaBAD} and P_{rhaT} together with the transcriptional regulator RhaS, all derived from *E. coli*, exhibit interesting characteristics for the control of gene expression in the AAB *G. oxydans*. These characteristics are affected by the *rhaS* expression strength and additional RhaS

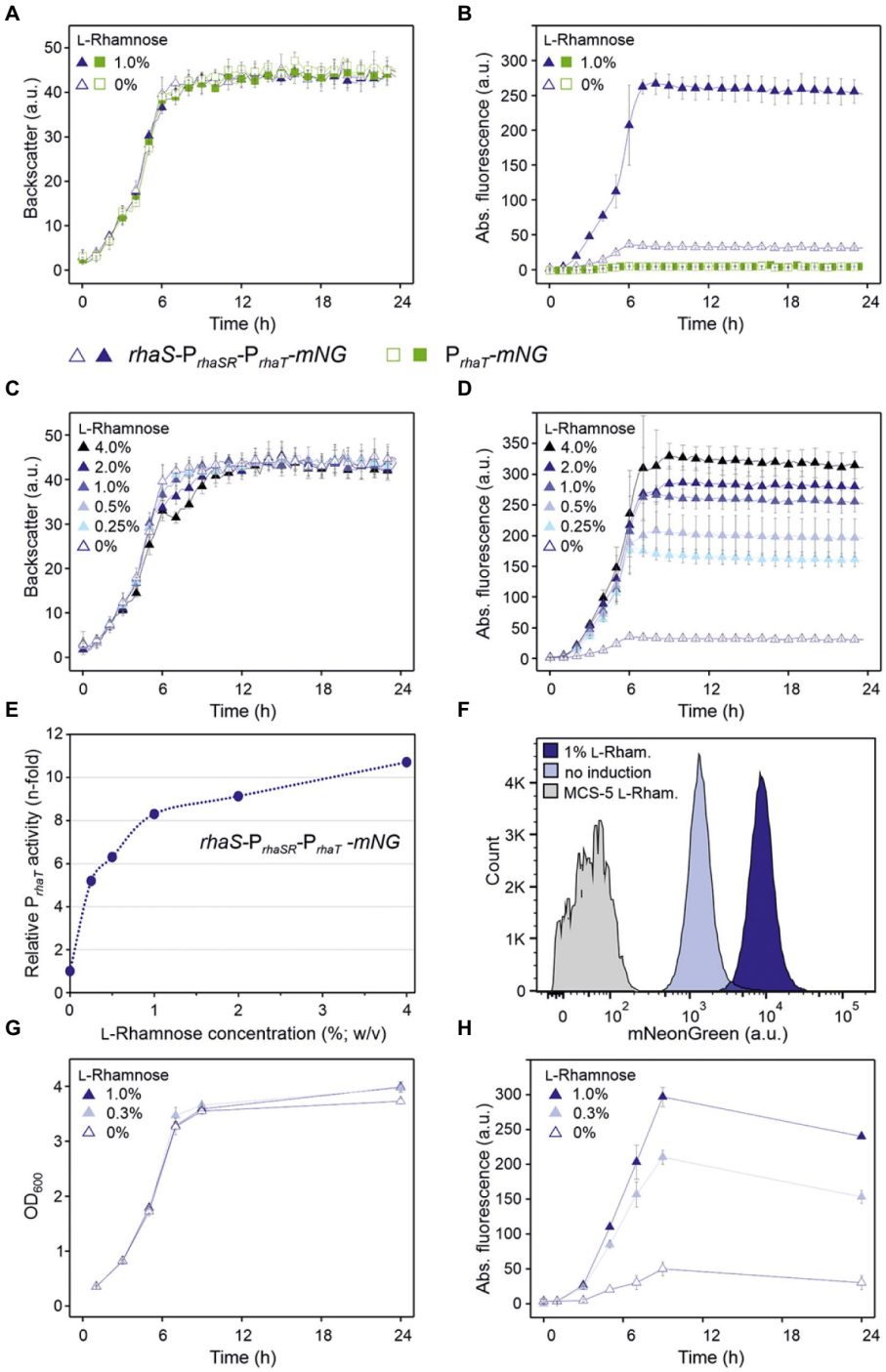

FIGURE 10
Performance of the RhaS-P_{rhaT} system in *G. oxydans* 621H. **(A)** Growth according to backscatter and **(B)** absolute mNG fluorescence of *G. oxydans* 621H carrying plasmid pBBR1MCS-5-*rhaS*-P_{rhaSR}-P_{rhaT}-*mNG* or pBBR1MCS-5-P_{rhaT}-*mNG* lacking *rhaS* in microscale BioLector cultivations without and with 1% (w/v) L-rhamnose. **(C)** Growth (backscatter) and **(D)** absolute mNG fluorescence of *G. oxydans* 621H carrying plasmid pBBR1MCS-5-*rhaS*-P_{rhaSR}-P_{rhaT}-*mNG* in microscale BioLector cultivations with L-rhamnose concentrations from 0.25% to 4% (w/v) as indicated. BioLector settings: backscatter gain 20, fluorescence gain 70. **(E)** Correlation between the relative n-fold P_{rhaT} activity in *G. oxydans* 621H carrying plasmid pBBR1MCS-5-*rhaS*-P_{rhaSR}-P_{rhaT}-*mNG* and the L-rhamnose concentrations. For the calculation, the maximal mNG fluorescence in the absence of L-rhamnose was set to 1. **(F)** FACS analysis of *G. oxydans* 621H carrying plasmid pBBR1MCS-5-*rhaS*-P_{rhaSR}-P_{rhaT}-*mNG* or empty vector pBBR1MCS-5 (MCS-5) as a control. Cells were grown in shake flasks with D-mannitol medium without and with 1% (w/v) L-rhamnose. FACS analysis was performed 7h after inoculation (induction). Total counts per sample represent 100,000 events. **(G)** Growth (OD_{600}) and **(H)** L-Rhamnose-induced mNG fluorescence of *G. oxydans* 621H carrying plasmid pBBR1MCS-5-*rhaS*-P_{rhaSR}-P_{rhaT}-*mNG* in shake flask cultivations with D-mannitol medium. The mNG fluorescence was measured in a Tecan reader (gain 60). All data represent mean values and standard deviation from two biological replicates (clones) with three technical replicates each.

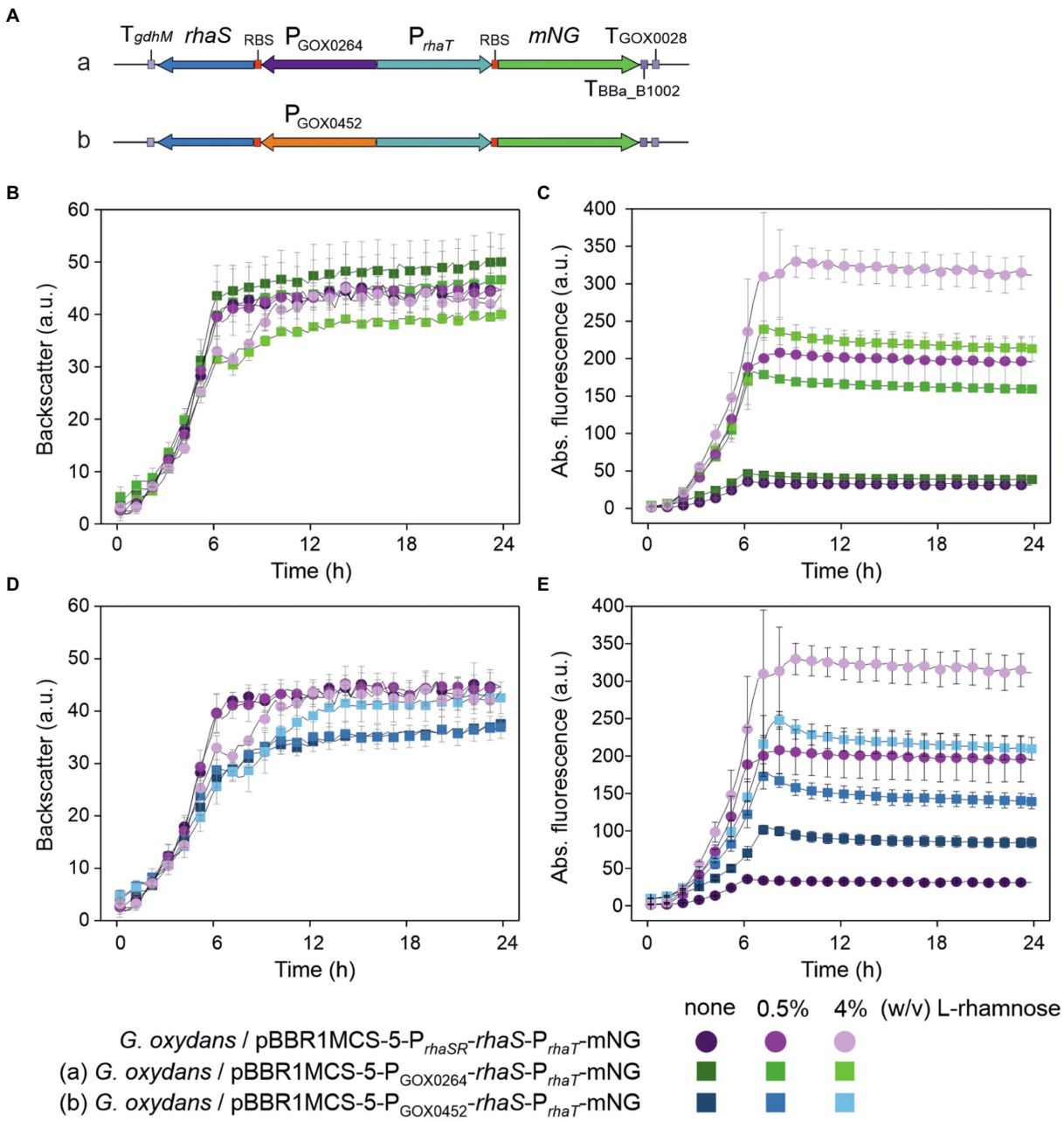

FIGURE 11
Performance of P_{rhaT}-derived induction of *mNG* expression in dependence of *rhaS* expression and presence of L-rhamnose. **(A)** Schematic illustration of the pBBR1MCS-5 plasmid inserts to test the effects of *rhaS* expression. **(B,D)** Growth of the *G. oxydans* 621H strains with *rhaS* expression plasmid in D-mannitol medium according to backscatter and **(C,E)** absolute mNG fluorescence in BioLector cultivations. L-Rhamnose was supplemented as indicated. All data represent mean values and standard deviation from two biological replicates (clones) with three technical replicates each. BioLector settings: backscatter gain 20, fluorescence gain 70.

binding sites in P_{rhaBAD} and P_{rhaT}. With RhaS-P_{rhaBAD} we found the first system for *G. oxydans* that permits controlled down-regulation in an effector-dependent manner exhibiting tunability and enabling complete repression of a genomically encoded target gene. Furthermore, the regulation of P_{rhaT} could be reversed from inducible to repressible by inserting an additional RhaS binding site. Altogether, these features provide novel opportunities expanding the genetic toolbox for regulatable gene expression in *G. oxydans* and are possibly also interesting for other AAB.

In *E. coli* the L-rhamnose-induced regulation of P_{rhaBAD} requires both RhaR and RhaS (Egan and Schleif, 1993, 1994; Kelly et al., 2016). In *G. oxydans*, only RhaS played an effective role for the regulation of the system. In *E. coli*, first RhaR activates expression of the *rhaSR* operon in the presence of L-rhamnose, which is a prerequisite to provide sufficient RhaS levels for the induction of

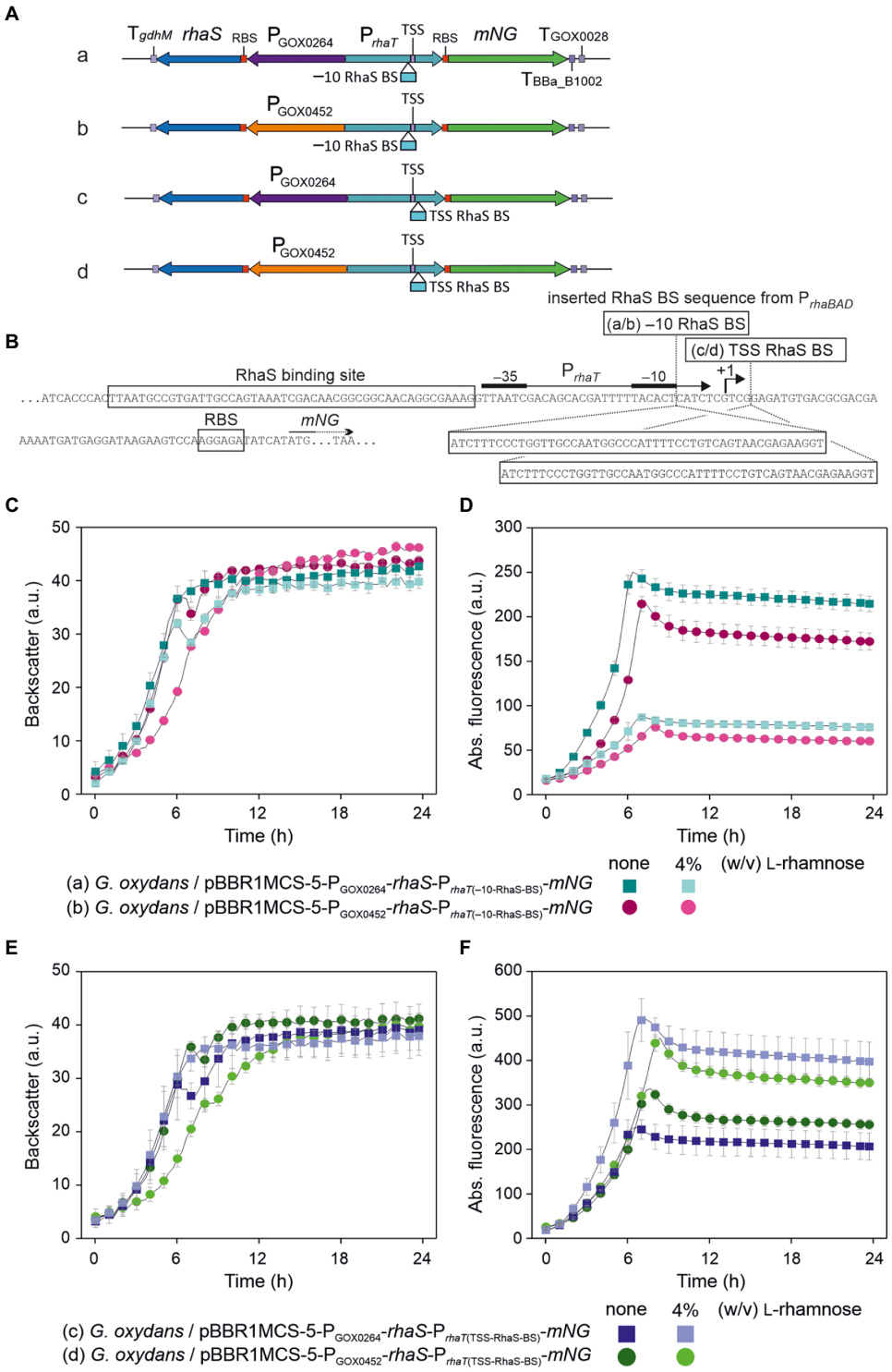

FIGURE 12
Insertion of an additional RhaS binding site directly downstream from the *E. coli* −10 region of P_{rhaT} reversed the regulation in *G. oxydans* making the modified RhaS-P_{rhaT} system repressible in the presence of L-rhamnose. **(A)** Schematic illustration of the pBBR1MCS-5 plasmid inserts to test the effects of an additional RhaS binding site (RhaS BS) in P_{rhaT} directly downstream from the *E. coli* −10 region (−10 RhaS BS) or downstream from the *E. coli* P_{rhaT} transcriptional start site (TSS RhaS BS) together with *rhaS* expression from $P_{GOX0264}$ or $P_{GOX0452}$. **(B)** Sequence details of P_{rhaT} with the positions and RhaS binding site sequence from P_{rhaBAD} inserted either directly downstream from the *E. coli* −10 region or downstream from the *E. coli* transcriptional start site (TSS +1) according to Vía et al. (1996). **(C,E)** Growth of the *G. oxydans* 621H strains with *rhaS* expression plasmid and modified P_{rhaT} in D-mannitol medium according to backscatter and **(D,F)** absolute mNG fluorescence in BioLector cultivations. L-Rhamnose was supplemented as indicated. All data represent mean values and standard deviation from two biological replicates (clones) with three technical replicates each. BioLector settings: **(C,E)** backscatter gain 20, **(D)** fluorescence gain 60, **(F)** fluorescence gain 70.

P_{rhaBAD} by RhaS. This stimulation of *rhaSR* expression by RhaR is proposed to be achieved by bending the P_{rhaSR} promoter DNA so that P_{rhaSR}-bound cAMP receptor protein (CRP) can interact with the RNA polymerase (RNAP) and thereby activates transcription of *rhaSR* (Wickstrum et al., 2010). Activation of P_{rhaSR} by RhaR in such a manner is not possible in *G. oxydans* since CRP is absent. The protein showing the highest similarity to CRP was shown to function as an iron–sulfur cluster-containing FNR-type transcriptional regulator (GOX0974/GOX_RS06010) of genes involved in respiration and redox metabolism (Schweikert et al., 2021). In *G. oxydans*, the presence of RhaR even decreased the RhaS-dependent P_{rhaBAD} activity (Figure 1). This might be caused by a decreased expression of *rhaSR*, resulting in a lower RhaS level. In *E. coli*, L-rhamnose only affects the RhaR-dependent DNA bending and thereby activates transcription from P_{rhaSR}, yet the binding of RhaR to its target DNA *per se* was not affected by L-rhamnose (Kolin et al., 2008). RhaS can also bind to the RhaR binding site of P_{rhaSR} leading to lowered expression of the *rhaSR* operon in *E. coli*, thereby providing a negative feedback loop since the RhaS-dependent DNA bending of P_{rhaSR} is different from the bending by RhaR and prevents CRP-dependent activation of *rhaSR* expression (Wickstrum et al., 2010). In *G. oxydans*, RhaS alone activated P_{rhaSR} already in the absence of L-rhamnose and L-rhamnose further stimulated this effect (Supplementary Figures S4A,C). Therefore, in *G. oxydans* RhaR likely binds to P_{rhaSR} and competes with RhaS, causing an inhibition of P_{rhaSR} activation by RhaS and consequently lowered the RhaS level, resulting in the lower P_{rhaBAD} activity. Alternatively, or partially, the data obtained with the constructs omitting only *rhaS* and both *rhaSR* suggested that in *G. oxydans* RhaR could also bind to P_{rhaBAD} and competes with RhaS in binding to P_{rhaBAD}, resulting in the lowered reporter signals in the absence of L-rhamnose (Figure 1). Hence, omitting *rhaR* and using only *rhaS* provides advantages when using these regulatable *E. coli* promoters for gene expression in *G. oxydans*.

A surprising outcome of this study was the reversed regulation of P_{rhaBAD} by RhaS in *G. oxydans*, while P_{rhaT} was still inducible as in *E. coli*. RhaS belongs to the AraC/XylS family of transcriptional regulators (Tobin and Schleif, 1987). Within this protein family most members interact with the C-terminal domain (CTD) of the α-subunit of the RNAP to activate transcription (reviewed in Ebright and Busby, 1995). It was shown that deletion of the RNAP α-CTD reduced expression 180-fold, suggesting a direct interaction of RhaS and the α-CTD of the *E. coli* RNAP (Holcroft and Egan, 2000). Nevertheless, some members of the AraC/XylS family may also activate transcription through interaction with the sigma 70 factor (σ^{70}) subunit RpoD of the RNAP. This mode of activation is often indicated by regulator binding sites overlapping with the −35 element of the target promoter (Lonetto et al., 1998; Bhende and Egan, 2000). Within P_{rhaBAD}, 4 bp of the RhaS binding site overlap with the −35 hexamer of this promoter (Figure 4), while within P_{rhaT} the RhaS binding site does not overlap and ends 1 bp upstream from the −35 element (Figure 9). Among the family of σ^{70} transcription factors, the C-terminus is highly conserved as it contains DNA-binding domains and well-defined functional regions (Hakimi et al., 2000; Paget, 2015). In alanine substitution experiments, it was shown that D241 and D250 of RhaS and K593 and R599 of σ^{70} are likely interacting residues required for RhaS-dependent activation of P_{rhaBAD} in *E. coli* (Bhende and Egan, 2000; Wickstrum and Egan, 2004). While the entire σ^{70} amino acid sequences from *G. oxydans* and from *E. coli* K12 exhibit only 49% identity, primarily due to little similarities in the N-terminal part, the C-terminal regions share 84% identity. In the two regions likely involved in −10 and −35 recognition, only two residues are different (Supplementary Figure S6). R448 and R599 in σ^{70} from *E. coli* correspond to K486 and K637 in σ^{70} from *G. oxydans*. R599 is involved in the recognition of the −35 hexamer and in interaction with RhaS in *E. coli* (Bhende and Egan, 2000; Wickstrum and Egan, 2004). Although the exchange is conservative, K637 might contribute to the reversed responsiveness in *G. oxydans*.

As mentioned above, in P_{rhaBAD} the RhaS binding site overlaps with most of the −35 region by 4 bp while in P_{rhaT} the RhaS binding site does not overlap with the −35 region and ends 1 bp upstream (Vía et al., 1996). These different distances in DNA binding positions result in different radial orientations of RhaS toward σ^{70}-RNAP along the longitudinal DNA axis. Theoretically, with a turn of 36° per bp, a distance of 5 bp turns the radial orientation by 180°, putting RhaS (or σ^{70}-RNAP) to the other side of the DNA strand when comparing the theoretical binding of RhaS and σ^{70}-RNAP to P_{rhaBAD} with the binding to P_{rhaT}. Because of this theoretical difference in the orientation of RhaS toward σ^{70}-RNAP, RhaS possibly interacts with the α-CTD of the RNAP in the case of P_{rhaT} and with σ^{70} in the case of P_{rhaBAD}. Since the α-CTD and σ^{70} from *G. oxydans* and *E. coli* differ to some extent, the conformational changes of RhaS induced by the binding of L-rhamnose may affect the interactions of RhaS with the α-CTD and with σ^{70} from *G. oxydans* differently compared to the interactions with the α-CTD and with σ^{70} from *E. coli*, finally resulting in the different modes of the regulation of P_{rhaBAD} and P_{rhaT} in *G. oxydans*. Interestingly, in the case of P_{rhaSR}, the RhaR binding site also overlaps with the −35 region as the RhaS binding site in P_{rhaBAD}. Moreover, one of the major groove regions of each RhaR half site on P_{rhaSR} is nearly identical to the corresponding half site for RhaS binding on P_{rhaBAD} and RhaS can also bind to the RhaR binding site in P_{rhaSR} as mentioned above (Egan and Schleif, 1994). Despite these similarities between P_{rhaSR} and P_{rhaBAD}, in contrast to P_{rhaBAD}, P_{rhaSR} was still inducible by RhaS and L-rhamnose in *G. oxydans*. These differences in *G. oxydans* cannot be explained without further experimental data. For example, the recognition by and the affinity of σ^{70} to potential −35 and −10 regions in the absence and in the presence of RhaS and therefore the positional binding of the host RNAP to the *E. coli* promoter DNA relative to the RhaS binding position might differ in *G. oxydans* because of different DNA sequence specificities of σ^{70}. Therefore, knowledge about the transcriptional starts sites (TSSs) within the three *E. coli* promoter regions P_{rhaBAD}, P_{rhaT}, and P_{rhaSR} in *G. oxydans* is required to better explain the effects, including the activation of P_{rhaBAD} by RhaS in the absence of L-rhamnose, the repression, and the effects of the additional RhaS binding site inserted into P_{rhaBAD} and P_{rhaT}.

In a first and preliminary attempt to obtain such TSS data, we prepared a total RNA sample from *G. oxydans* 621H with plasmid pBBR1MCS-5-*rhaS*-P_{rhaSR}-$P_{rhaBAD(+RhaS\text{-}BS)}$-*mNG* cultivated in the complex medium with D-mannitol in the absence of L-rhamnose and harvested in the mid-exponential phase. The RNA sample was sent to Vertis Biotechnologie AG for sample processing and Illumina sequencing to obtain high-quality TSS data (see Materials and Methods). The resulting fastq file comprised 10,255,084 reads (75 bp). After reads trimming and quality filtering, 1,023,259 reads mapped to the sequence of pBBR1MCS-5-*rhaS*-P_{rhaSR}-$P_{rhaBAD(+RhaS\text{-}BS)}$-*mNG*. The overall reads mapping showed three prominent reads stacks indicating the three most active transcriptional starts on the plasmid (Supplementary Figure S7). The by far highest stack (~560,000 coverage) corresponded to the annotated promoter region of *gmR* (*aacC1*) conferring gentamycin resistance and was oriented toward *gmR*. The second-highest stack (~175,000 coverage) was upstream from *rhaS* and oriented toward *rhaS*. In contrast to the expectation for *rhaS*, the start position of this stack was not within P_{rhaSR}, but upstream from P_{rhaSR} within the P_{rhaBAD} region between its −35 and −10 regions from *E. coli*. The third-highest stack (~65,000 coverage) was found within the coding region of *rhaS* and oriented toward the 3′ end of *rhaS*. For P_{rhaBAD}, the insertion of an additional RhaS binding site could possibly generate an additional transcriptional start site in *G. oxydans* enabling the two-fold increased mNG signals described above for $P_{rhaBAD(+RhaS\text{-}BS)}$. However, in contrast to the expectations, no one or two major TSSs with high coverage toward *mNG* corresponding to the reported *E. coli* TSS and a potential new TSS could be seen. Instead, the detailed reads mapping showed several reads stacks of only medium coverage, partially with scattering start positions, in the $P_{rhaBAD(+RhaS\text{-}BS)}$ region and the 5′ region of *mNG* (Supplementary Figure S8). Therefore, the mapping data surprisingly suggested several TSSs in this promoter region oriented toward the 3′ end of the reporter gene: 2 or more potential TSSs upstream from *mNG* and 3 or more potential TSSs in the 5′ region of *mNG*. The most upstream potential TSS for *mNG* was very close to the *E. coli* −35 region of P_{rhaBAD}. These unexpected preliminary results require further and more detailed analysis as well as some comparisons, including the analysis of RNA samples from *G. oxydans* grown in the presence of L-rhamnose, from cells without *rhaS*, and with the other promoters P_{rhaSR} and P_{rhaT}.

Summing up and looking ahead, in *G. oxydans* the RhaS-dependent regulation of the *E. coli* RhaS target promoters and variants thereof provide new modes for regulatable gene expression in this AAB and possibly also in other AAB species. Inducible and repressible gene expression in response to L-rhamnose could be achieved simultaneously, which may be especially advantageous for combinatorial engineering. Tunability and complete repression of a genomic promoter copy was tested and shown only with the variant $P_{rhaBAD(+RhaS\text{-}BS)}$, yet it is likely that also with P_{rhaBAD} and $P_{rhaT(-10\text{-}RhaS\text{-}BS)}$ complete repression of a genomic copy could be achieved. These promoters cover different ranges of expression strength, which could be selected according to the requirements of the genomic target gene. Tunable and complete promoter repression is also useful for the functional study of essential genes that cannot be deleted. Optimizing genomic *rhaS* expression or further increasing the genomic *rhaS* copy number beyond two to achieve a sufficient RhaS level may finally overcome the necessity of plasmid-based *rhaS* expression to achieve complete chromosomal promoter repression. Furthermore, more TSS data sets and deeper analysis are required to better understand the regulations of the target promoters by RhaS in *G. oxydans*. The TSS results also suggested to analyze the TSSs of heterologous promoters when they are transferred and used in *G. oxydans* or AAB in general. It can be expected that TSS data sets will help to better understand and overcome the difficulties in getting transferred heterologous regulatable expression systems functional and high-performant in AAB.

Data availability statement

The raw data supporting the conclusions of this article will be made available by the authors, without undue reservation. The Illumina sequencing data are available in the NCBI sequence read archive via the accession numbers PRJNA854345 and PRJNA854679.

Author contributions

TP and PF designed and supervised the study. PF, MLG, MM, and MH carried out cloning and experiments. JG performed the GC-TOF analysis. PF, MLG, MM, MH, and TP performed data analysis. PF and TP wrote the manuscript. All authors contributed to the article and approved the submitted version.

Funding

We are grateful to the Federal Ministry of Education and Research (BMBF) for financial support of the project IMPRES (031B0370B). The funding organization did not influence the design of the study or collection, analysis, and interpretation of data, or writing the manuscript.

Acknowledgments

We thank Christiane Sonntag and Ulli Degner for their technical assistance with FACS analysis and laboratory work. We thank Armin Ehrenreich for helpful discussion.

Conflict of interest

The authors declare that the research was conducted in the absence of any commercial or financial relationships that could be construed as a potential conflict of interest.

Publisher's note

All claims expressed in this article are solely those of the authors and do not necessarily represent those of their affiliated organizations, or those of the publisher, the editors and the reviewers. Any product that may be evaluated in this article, or claim that may be made by its manufacturer, is not guaranteed or endorsed by the publisher.

Supplementary material

The supplementary material for this article can be found online at: https://www.frontiersin.org/articles/10.3389/fmicb.2022.981767/full#supplementary-material

References

Ameyama, M., Shinagawa, E., Matsushita, K., and Adachi, O. (1981). D-fructose dehydrogenase of *Gluconobacter industrius*: purification, characterization, and application to enzymatic microdetermination of D-fructose. *J. Bacteriol.* 145, 814–823. doi: 10.1128/jb.145.2.814-823.1981

Baldoma, L., Badia, J., Sweet, G., and Aguilar, J. (1990). Cloning, mapping and gene product identification of *rhaT* from *Escherichia coli K12*. *FEMS Microbiol. Lett.* 60, 103–107. doi: 10.1111/j.1574-6968.1990.tb03870.x

Bertucci, M., Ariano, K., Zumsteg, M., and Schweiger, P. (2022). Engineering a tunable bicistronic TetR autoregulation expression system in *Gluconobacter oxydans*. *Peer J.* 10:e13639. doi: 10.7717/peerj.13639

Bhende, P. M., and Egan, S. M. (1999). Amino acid-DNA contacts by RhaS: an AraC family transcription activator. *J. Bacteriol.* 181, 5185–5192. doi: 10.1128/JB.181.17.5185-5192.1999

Bhende, P. M., and Egan, S. M. (2000). Genetic evidence that transcription activation by RhaS involves specific amino acid contacts with sigma 70. *J. Bacteriol.* 182, 4959–4969. doi: 10.1128/JB.182.17.4959-4969.2000

da Silva, G. A. R., Oliveira, S. S. S., Lima, S. F., do Nascimento, R. P., Baptista, A. R. S., and Fiaux, S. B. (2022). The industrial versatility of *Gluconobacter oxydans*: current applications and future perspectives. *World J. Microbiol. Biotechnol.* 38:134. doi: 10.1007/s11274-022-03310-8

Ebright, R. H., and Busby, S. (1995). The *Escherichia coli* RNA polymerase alpha subunit: structure and function. *Curr. Opin. Genet. Dev.* 5, 197–203. doi: 10.1016/0959-437X(95)80008-5

Egan, S. M., and Schleif, R. F. (1993). A regulatory cascade in the induction of *rhaBAD*. *J. Mol. Biol.* 234, 87–98. doi: 10.1006/jmbi.1993.1565

Egan, S. M., and Schleif, R. F. (1994). DNA-dependent renaturation of an insoluble DNA binding protein. Identification of the RhaS binding site at *rhaBAD*. *J. Mol. Biol.* 243, 821–829. doi: 10.1006/jmbi.1994.1684

Fricke, P. M., Hartmann, R., Wirtz, A., Bott, M., and Polen, T. (2022). Production of L-arabinonic acid from L-arabinose by the acetic acid bacterium *Gluconobacter oxydans*. *Bioresour. Technol.* 17:100965. doi: 10.1016/j.biteb.2022.100965

Fricke, P. M., Klemm, A., Bott, M., and Polen, T. (2021a). On the way toward regulatable expression systems in acetic acid bacteria: target gene expression and use cases. *Appl. Microbiol. Biotechnol.* 105, 3423–3456. doi: 10.1007/s00253-021-11269-z

Fricke, P. M., Link, T., Gätgens, J., Sonntag, C., Otto, M., Bott, M., et al. (2020). A tunable L-arabinose-inducible expression plasmid for the acetic acid bacterium *Gluconobacter oxydans*. *Appl. Microbiol. Biotechnol.* 104, 9267–9282. doi: 10.1007/s00253-020-10905-4

Fricke, P. M., Lürkens, M., Hunnefeld, M., Sonntag, C. K., Bott, M., Davari, M. D., et al. (2021b). Highly tunable TetR-dependent target gene expression in the acetic acid bacterium *Gluconobacter oxydans*. *Appl. Microbiol. Biotechnol.* 105, 6835–6852. doi: 10.1007/s00253-021-11473-x

Gibson, D. G., Young, L., Chuang, R. Y., Venter, J. C., Hutchison, C. A., and Smith, H. O. (2009). Enzymatic assembly of DNA molecules up to several hundred kilobases. *Nat. Methods* 6, 343–345. doi: 10.1038/nmeth.1318

Gupta, A., Singh, V. K., Qazi, G. N., and Kumar, A. (2001). *Gluconobacter oxydans*: its biotechnological applications. *J. Mol. Microb. Biotech.* 3, 445–456.

Hakimi, M. A., Privat, I., Valay, J. G., and Lerbs-Mache, S. (2000). Evolutionary conservation of C-terminal domains of primary sigma(70)-type transcription factors between plants and bacteria. *J. Biol. Chem.* 275, 9215–9221. doi: 10.1074/jbc.275.13.9215

Hanahan, D. (1983). Studies on transformation of *Escherichia coli* with plasmids. *J. Mol. Biol.* 166, 557–580. doi: 10.1016/S0022-2836(83)80284-8

Hekmat, D., Bauer, R., and Fricke, J. (2003). Optimization of the microbial synthesis of dihydroxyacetone from glycerol with *Gluconobacter oxydans*. *Bioprocess Biosyst. Eng.* 26, 109–116. doi: 10.1007/s00449-003-0338-9

Holcroft, C. C., and Egan, S. M. (2000). Interdependence of activation at *rhaSR* by cyclic AMP receptor protein, the RNA polymerase alpha subunit C-terminal domain, and RhaR. *J. Bacteriol.* 182, 6774–6782. doi: 10.1128/JB.182.23.6774-6782.2000

Kallnik, V., Meyer, M., Deppenmeier, U., and Schweiger, P. (2010). Construction of expression vectors for protein production in *Gluconobacter oxydans*. *J. Biotechnol.* 150, 460–465. doi: 10.1016/j.jbiotec.2010.10.069

Kelly, C. L., Liu, Z., Yoshihara, A., Jenkinson, S. F., Wormald, M. R., Otero, J., et al. (2016). Synthetic chemical inducers and genetic decoupling enable orthogonal control of the *rhaBAD* promoter. *ACS Synth. Biol.* 5, 1136–1145. doi: 10.1021/acssynbio.6b00030

Kersters, K., Lisdiyanti, P., Komagata, K., and Swings, J. (1990). "The family Acetobacteraceae: the genera Acetobacter, Acidomonas, Asaia, Gluconacetobacter, Gluconobacter, and Kozakia," in *The Prokaryotes*. eds. M. Dworkin, S. Falkow, E. Rosenberg, K. H. Schleifer and E. Stackebrandt (New York, NY: Springer).

Kiefler, I., Bringer, S., and Bott, M. (2017). Metabolic engineering of *Gluconobacter oxydans* 621H for increased biomass yield. *Appl. Microbiol. Biotechnol.* 101, 5453–5467. doi: 10.1007/s00253-017-8308-3

Kolin, A., Balasubramaniam, V., Skredenske, J. M., Wickstrum, J. R., and Egan, S. M. (2008). Differences in the mechanism of the allosteric L-rhamnose responses of the AraC/XylS family transcription activators RhaS and RhaR. *Mol. Microbiol.* 68, 448–461. doi: 10.1111/j.1365-2958.2008.06164.x

Kostner, D., Peters, B., Mientus, M., Liebl, W., and Ehrenreich, A. (2013). Importance of *codB* for new *codA*-based markerless gene deletion in *Gluconobacter* strains. *Appl. Microbiol. Biotechnol.* 97, 8341–8349. doi: 10.1007/s00253-013-5164-7

Kovach, M. E., Elzer, P. H., Hill, D. S., Robertson, G. T., Farris, M. A., Roop, R. M. 2nd, et al. (1995). Four new derivatives of the broad-host-range cloning vector pBBR1MCS, carrying different antibiotic-resistance cassettes. *Gene* 166, 175–176. doi: 10.1016/0378-1119(95)00584-1

Kovach, M. E., Phillips, R. W., Elzer, P. H., Roop, R. M. 2nd, and Peterson, K. M. (1994). pBBR1MCS: a broad-host-range cloning vector. *BioTechniques* 16, 800–802. PMID: 8068328

Kranz, A., Steinmann, A., Degner, U., Mengus-Kaya, A., Matamouros, S., Bott, M., et al. (2018). Global mRNA decay and 23S rRNA fragmentation in *Gluconobacter oxydans* 621H. *BMC Genomics* 19, 753. doi: 10.1186/s12864-018-5111-1

Kranz, A., Vogel, A., Degner, U., Kiefler, I., Bott, M., Usadel, B., et al. (2017). High precision genome sequencing of engineered *Gluconobacter oxydans* 621H by combining long nanopore and short accurate Illumina reads. *J. Biotechnol.* 258, 197–205. doi: 10.1016/j.jbiotec.2017.04.016

Lonetto, M. A., Rhodius, V., Lamberg, K., Kiley, P., Busby, S., and Gross, C. (1998). Identification of a contact site for different transcription activators in region 4 of the *Escherichia coli* RNA polymerase sigma(70) subunit. *J. Mol. Biol.* 284, 1353–1365. doi: 10.1006/jmbi.1998.2268

Mamlouk, D., and Gullo, M. (2013). Acetic acid bacteria: physiology and carbon sources oxidation. *Indian J. Microbiol.* 53, 377–384. doi: 10.1007/s12088-013-0414-z

Mientus, M., Kostner, D., Peters, B., Liebl, W., and Ehrenreich, A. (2017). Characterization of membrane-bound dehydrogenases of *Gluconobacter oxydans* 621H using a new system for their functional expression. *Appl. Microbiol. Biotechnol.* 101, 3189–3200. doi: 10.1007/s00253-016-8069-4

Paczia, N., Nilgen, A., Lehmann, T., Gatgens, J., Wiechert, W., and Noack, S. (2012). Extensive exometabolome analysis reveals extended overflow metabolism in various microorganisms. *Microb. Cell Factories* 11:122. doi: 10.1186/1475-2859-11-122

Paget, M. S. (2015). Bacterial sigma factors and anti-sigma factors: structure, function and distribution. *Biomol. Ther.* 5, 1245–1265. doi: 10.3390/biom5031245

Pappenberger, G., and Hohmann, H. P. (2014). Industrial production of L-ascorbic acid (vitamin C) and D-isoascorbic acid. *Adv. Biochem. Eng. Biotechnol.* 143, 143–188. doi: 10.1007/10_2013_243

Peters, B., Mientus, M., Kostner, D., Junker, A., Liebl, W., and Ehrenreich, A. (2013). Characterization of membrane-bound dehydrogenases from *Gluconobacter oxydans* 621H *via* whole-cell activity assays using multideletion strains. *Appl. Microbiol. Biotechnol.* 97, 6397–6412. doi: 10.1007/s00253-013-4824-y

Saito, Y., Ishii, Y., Hayashi, H., Imao, Y., Akashi, T., Yoshikawa, K., et al. (1997). Cloning of genes coding for L-sorbose and L-sorbosone dehydrogenases from *Gluconobacter oxydans* and microbial production of 2-keto-L-gulonate, a precursor of L-ascorbic acid, in a recombinant *G. oxydans* strain. *Appl. Environ. Microb.* 63, 454–460. doi: 10.1128/aem.63.2.454-460.1997

Sambrook, J., Fritsch, E. F., and Maniatis, T. (1989). *Molecular Cloning: A Laboratory Manual*. Cold Spring Harbor, NY: Cold Spring Harbor Laboratory Press.

Schweikert, S., Kranz, A., Yakushi, T., Filipchyk, A., Polen, T., Etterich, H., et al. (2021). FNR-type regulator GoxR of the obligatorily aerobic acetic acid bacterium *Gluconobacter oxydans* affects expression of genes involved in respiration and redox metabolism. *Appl. Environ. Microbiol.* 87, 87. doi: 10.1128/AEM.00195-21

Shaner, N. C., Lambert, G. G., Chammas, A., Ni, Y., Cranfill, P. J., Baird, M. A., et al. (2013). A bright monomeric green fluorescent protein derived from *Branchiostoma lanceolatum*. *Nat. Methods* 10, 407–409. doi: 10.1038/nmeth.2413

Simon, R., Priefer, U., and Pühler, A. (1983). A broad host range mobilization system for *in vivo* genetic-engineering – transposon mutagenesis in gram-negative bacteria. *Nature Biotechnology* 1, 784–791. doi: 10.1038/nbt1183-784

Tkac, J., Navratil, M., Sturdik, E., and Gemeiner, P. (2001). Monitoring of dihydroxyacetone production during oxidation of glycerol by immobilized *Gluconobacter oxydans* cells with an enzyme biosensor. *Enzyme Microb. Technol.* 28, 383–388. doi: 10.1016/S0141-0229(00)00328-8

Tobin, J. F., and Schleif, R. F. (1987). Positive regulation of the *Escherichia coli* L-rhamnose operon is mediated by the products of tandemly repeated regulatory genes. *J. Mol. Biol.* 196, 789–799. doi: 10.1016/0022-2836(87)90405-0

Vía, P., Badia, J., Baldoma, L., Obradors, N., and Aguilar, J. (1996). Transcriptional regulation of the *Escherichia coli rhaT* gene. *Microbiology* 142, 1833–1840. doi: 10.1099/13500872-142-7-1833

Wang, E. X., Ding, M. Z., Ma, Q., Dong, X. T., and Yuan, Y. J. (2016). Reorganization of a synthetic microbial consortium for one-step vitamin C fermentation. *Microb. Cell Factories* 15, 21. doi: 10.1186/s12934-016-0418-6

Wickstrum, J. R., and Egan, S. M. (2004). Amino acid contacts between sigma 70 domain 4 and the transcription activators RhaS and RhaR. *J. Bacteriol.* 186, 6277–6285. doi: 10.1128/JB.186.18.6277-6285.2004

Wickstrum, J. R., Skredenske, J. M., Balasubramaniam, V., Jones, K., and Egan, S. M. (2010). The AraC/XylS family activator RhaS negatively autoregulates *rhaSR* expression by preventing cyclic AMP receptor protein activation. *J. Bacteriol.* 192, 225–232. doi: 10.1128/JB.00829-08

frontiers | Frontiers in Microbiology

TYPE Original Research
PUBLISHED 29 September 2022
DOI 10.3389/fmicb.2022.964855

OPEN ACCESS

EDITED BY
Lisa Solieri,
University of Modena and Reggio Emilia,
Italy

REVIEWED BY
Li Li,
South China University of Technology,
China
Benedetta Bottari,
University of Parma,
Italy

*CORRESPONDENCE
Yu Zheng
yuzheng@tust.edu.cn
Min Wang
minw@tust.edu.cn

†These authors have contributed equally to this work and share first authorship

SPECIALTY SECTION
This article was submitted to
Food Microbiology,
a section of the journal
Frontiers in Microbiology

RECEIVED 09 June 2022
ACCEPTED 12 September 2022
PUBLISHED 29 September 2022

CITATION
Xia M, Zhang X, Xiao Y, Sheng Q, Tu L, Chen F, Yan Y, Zheng Y and Wang M (2022) Interaction of acetic acid bacteria and lactic acid bacteria in multispecies solid-state fermentation of traditional Chinese cereal vinegar.
Front. Microbiol. 13:964855.
doi: 10.3389/fmicb.2022.964855

Interaction of acetic acid bacteria and lactic acid bacteria in multispecies solid-state fermentation of traditional Chinese cereal vinegar

Menglei Xia[1†], Xiaofeng Zhang[1†], Yun Xiao[1], Qing Sheng[1], Linna Tu[1], Fusheng Chen[2], Yufeng Yan[3], Yu Zheng[1*] and Min Wang[1*]

[1]State Key Laboratory of Food Nutrition and Safety, Key Laboratory of Industrial Fermentation Microbiology, Ministry of Education, College of Biotechnology, Tianjin University of Science and Technology, Tianjin, China, [2]Hubei International Scientific and Technological Cooperation Base of Traditional Fermented Foods, Huazhong Agricultural University, Wuhan, China, [3]Shanxi Zilin Vinegar Industry Co., Ltd., Shanxi Province Key Laboratory of Vinegar Fermentation Science and Engineering, Taiyuan, China

The microbial community plays an important role on the solid-state fermentation (SSF) of Chinese cereal vinegar, where acetic acid bacteria (AAB) and lactic acid bacteria (LAB) are the dominant bacteria. In this study, the top-down (*in situ*) and bottom-up (*in vitro*) approaches were employed to reveal the interaction of AAB and LAB in SSF of Shanxi aged vinegar (SAV). The results of high-throughput sequencing indicates that *Acetobacter pasteurianus* and *Lactobacillus helveticus* are the predominant species of AAB and LAB, respectively, and they showed negative interrelationship during the fermentation. *A. pasteurianus* CGMCC 3089 and *L. helveticus* CGMCC 12062, both of which were isolated from fermentation of SAV, showed no nutritional competition when they were co-cultured *in vitro*. However, the growth and metabolism of *L. helveticus* CGMCC 12062 were inhibited during SSF due to the presence of *A. pasteurianus* CGMCC 3089, indicating an amensalism phenomenon between these two species. The transcriptomic results shows that there are 831 differentially expressed genes (|log2 (Fold Change)|>1 and, $p \leq 0.05$) in *L. helveticus* CGMCC 12062 under co-culture condition comparing to its mono-culture, which are mainly classified into Gene Ontology classification of molecular function, biological process, and cell composition. Of those 831 differentially expressed genes, 202 genes are up-regulated and 629 genes are down-regulated. The down-regulated genes were enriched in KEGG pathways of sugar, amino acid, purine, and pyrimidine metabolism. The transcriptomic results for *A. pasteurianus* CGMCC 3089 under co-culture condition reveals 529 differentially expressed genes with 393 up-regulated and 136 down-regulated, and the genes within KEGG pathways of sugar, amino acid, purine, and pyrimidine metabolism are up-regulated. Results indicate an amensalism relationship in co-culture of *A. pasteurianus* and *L. helveticus*. Therefore, this work gives a whole insight on the interaction between the predominant species in SSF of cereal vinegar from

nutrient utilization, endogenous factors inhibition and the regulation of gene transcription.

KEYWORDS

Chinese cereal vinegar, acetic acid bacteria, lactic acid bacteria, microbial interaction, amensalism, *Acetobacter pasteurianus*, *Lactobacillus helveticus*

Introduction

Fermentation is one of the oldest technologies for food preservation, moreover, it allows foods to achieve better flavor and functions (Tamang et al., 2016). Many traditionally fermented foods are typically produced by a naturally enriched microbiota, such as sourdough, sausages, cheese and vinegar (Kleerebezem and van Loosdrecht, 2007; Smid and Lacroix, 2013). Regardless of the raw materials, these consortia microbes contribute to the desired characteristics of the final product through biological processes (Papalexandratou et al., 2011; Lu et al., 2018; Yunita and Dodd, 2018). Compared with mono-culture, co-culture is more conducive to the production of complex metabolites. Under co-cultivation conditions, the yeasts provide various nutrients such as amino acids, unsaturated fatty acids and vitamins for the growth of lactic acid bacteria (LAB; Furukawa et al., 2013). In general, the fermentation process conducted by natural microbial consortia is more flexible and robust than that with single microorganism, even providing greater resistance to bacteriophage attack (Smid and Lacroix, 2013).

In China, many famous vinegars are produced with a spontaneous solid-state fermentation (SSF) technology with cereals as the main raw material, including Shanxi aged vinegar (SAV), Sichuan bran vinegar, Zhenjiang aroma vinegar, and Duliu mature vinegar, which have a history of thousands of years. Due to the open fermentation technology, multiple microorganisms including molds, yeasts, and bacteria co-exist in the SSF process (Wu et al., 2021a). Studies have shown that LAB and acetic acid bacteria (AAB) are the two dominant bacteria in the SSF process (Nie et al., 2013; Wu et al., 2021b; Huang et al., 2022a). Lactic acid and acetic acid are the most important organic acids in vinegar, accounting for more than 90% of the total acid, which are produced by LAB and AAB (Wu et al., 2021b). The most common LAB and AAB in cereal vinegar fermentation are *Lactobacillus helveticus* and *Acetobacter pasteurianus* (Huang et al., 2022b).

Microbe-microbe interactions are widespread in the multispecies food fermentation. The coexistence of microorganisms in the same ecological niche can lead to positive or negative interactions, affecting their growth patterns, adaptation, and ability to synthesize proteins and metabolites (Bertrand et al., 2014; Feng et al., 2018; Nai and Meyer, 2018). During the fermentation process of Fukuyama pot vinegar (liquid-state fermentation), LAB and yeasts are mutually beneficial (Furukawa et al., 2013). Due to the aerobic growth characteristic, AAB generally grow in the upper medium with rich oxygen content, providing a suitable low-oxygen environment for yeast and LAB (Furukawa et al., 2013). In cocoa pulp fermentation lactic acid that will inhibit the growth of LAB in high concentration can be utilized by AAB to produce acetoin (Adler et al., 2014). Different from some liquid-state fermentation, in SSF system the mass (e.g., oxygen and water) and bio-heat transfer is poor, resulting the growth inhibition due to the endogenous environmental factors (Zhang et al., 2020). Moreover, these solid substrates (including wheat bran, sorghum and rice hull) can serve as supports (carriers) for the microbial cells, and the immobilized microorganism might be help to improve the survival of microorganism under stress conditions (Oleinikova et al., 2020). The high niche overlap, nutritional deficiency and optimal redox potential of microorganisms are important factors affecting the symbiosis of microorganisms (Edwardson and Hollibaugh, 2018). However, the interaction mechanism of the predominant microorganism in SSF of Chinese cereal vinegar is not clear yet. Due to the significant complementarity, the top-down microbiomics method and the bottom-up rational analysis are usually adopted to study the interactions between microorganisms (Wolfe et al., 2014; Liang et al., 2016; Lu et al., 2016; Zheng et al., 2018). In this study, top-down (*in situ*) and bottom-up (*in vitro*) approaches were applied to reveal the interaction between LAB and AAB in SSF of cereal vinegar.

Materials and methods

Samples

Samples of *Cupei* (brewing mash of Chinese cereal vinegar with solid-state fermentation technology) used in this study were collected from a SAV factory (Qingxu, China) on day 0, 1, 3, 5 and 7 during the fermentation process. A five-point sampling method was used to collect the samples. They were parallelly collected from three fermenter. These samples were analyzed according to previous methods (Nie et al., 2013).

Strains and media

Strains *A. pasteurianus* CGMCC 3089 and *L. helveticus* CGMCC 12062 were used in this study, which were isolated from

the SAV fermentation of the same factory and were registered in Chinese General Microbiological Culture Collection Center. GY and MRS media were applied for *A. pasteurianus* and *L. helveticus* culture, respectively. SSF medium (Solid-state fermentation medium, SSFM) was used for *in vitro* solid-state fermentation, which consists of the following ingredients: wheat bran, 30 g/100 g; rice husk, 10 g/100 g; MRS (de Man, Rogosa, Sharp) medium, 55 g/100 g, ethanol, 4 g/100 g; acetic acid, 0.5 g/100; and lactic acid, 0.5 g/100. The *in vitro* SSF was performed in a 5,000 ml ceramic pot containing 3,000 g of SSFM.

In situ analysis of LAB and AAB communities

The metagenomic DNA of *Cupei* was extracted in accordance with a previously described method (Nie et al., 2013). The V3-V4 region of 16S rDNA was amplified with the metagenome as template. The result fragment was sent to GENEWIZ Company (Suzhou, China) for sequencing analysis using the Illumina MiSeq platform. Sequencing reads were sorted to specific samples on the basis of unique barcodes, which were subsequently trimmed. Sequencing reads were removed if the reads were <200 or >1,000 bp, had a non-exact barcode match, exceeded two ambiguous bases, exceeded eight consecutive identical bases, or had average quality scores <25. A nearest alignment space termination-based sequence aligner was used to align sequences to a custom reference based on SILVA alignment. Chimeric sequences were identified and filtered by quality. Chimera-free sequences were clustered in operational taxonomic units (OTUs) defined by 97% similarity by using a complete-linkage clustering tool (Gan et al., 2017). Representative sequences per OTU were classified in accordance with previously described methods, and the LAB and AAB communities were obtained.

CCA (Canonical Correspondence Analysis) was performed to determine the species-species relationship between LAB and AAB community and fermentation parameters (pH, total acid, reducing sugar, and temperature, and metabolites ethanol, lactic acid, and acetic acid). The analysis was conducted using Canoco for Windows v4.51 and Canodraw (Wageningen UR, Netherlands). The interaction network of the microorganisms *Lactobacillus* and *Acetobacter* was inferred using Metagenomic Microbial Interaction Simulator (MetaMIS) software (Shaw et al., 2016). The dynamic abundance of OTUs that were identified as *Acetobacter* and *Lactobacillus* were used for MetaMIS analysis. The website address for obtaining MetaMIS software is.[1] Data standardization was performed using IBM SPSS 19.0.[2]

In vitro solid-state fermentation of *Acetobacter pasteurianus* and *Lactobacillus helveticus*

Acetobacter pasteurianus CGMCC 3089 was inoculated into GY medium (100 ml) and incubated aerobically at 30°C for 24 h in a rotary shaker (180 r/min). *L. helveticus* CGMCC 12062 was statically incubated in MRS medium (100 ml) at 37°C for 24 h. The *in vitro* SSF was performed by inoculating them individually (mono-culture) or together (co-culture) into the SSFM with the initial count of 10^7 CFU/g, which was the same as their initial count in the SSF of SAV (Zheng et al., 2022). The *in vitro* SSF was performed at 35°C, and the medium was stirred every 12 h to improve the mass transfer. Therefore, the time curves in mono-culture and co-culture of *L. helveticus* and *A. pasteurianus* were produced.

Samples of mono-culture at 24 h and co-culture at 24 h with SSFM were collected for transcriptomic analysis. In brief, 5.0 g of SSFM sample was added into 95 ml of DEPC water and shaken for 5 min. The samples were filtered with two layers of sterile cheesecloth, and the filtrate was centrifuged at 8,000× *g* for 10 min at 4°C. The pellet was then subjected to RNA extraction using the RNA plus Kit (Takara Biotechnology, Dalian, China) following manufacturer's procedure. Transcriptome sequencing was performed by Novogene Co., Ltd. (Tianjin). The transcriptome sequencing data has been uploaded to NCBI Short Read Archive and the accession number is PRJNA833267. The genomes of strain *A. pasteurianus* IFO3283-01 (PRJDA31129) and *L. helveticus* CGMCC 1.1877 (PRJNA34619) were used as the references to identify the genes of transcriptome. Gene expression level was calculated by fragment per kilo bases per million reads (FPKM) using RSEM software (v1.2.6) with 0.1 as the rounding threshold for gene expression. The GI numbers of the selected genes were imported into the Kyoto Encyclopedia of Genes and Genomes (KEGG) database[3] for biological pathway analysis. A differential metabolic network was constructed based on transcriptomic analysis, mainly involving glycolytic pathway, TCA cycle, ABC transport system, amino acid metabolism, purine and pyrimidine metabolism, and two-component system.

Several representative genes were selected to analyze the potential interaction mechanism by using the method of qRT-PCR. Software of Primer 5 was used for primers design, which is listed in Table 1. The total RNA was isolated using RNA Plus Kit as mentioned above. To remove residual DNA, total RNA was treated with DNase I for 30 min at 37°C. RNA samples were reverse transcribed with Revert Aid™ First Strand cDNA Synthesis Kit (Takara Biotechnology, Dalian, China) in accordance with the manufacturer's instructions. The quantity analysis of RNA was performed with ABI Step one system (Applied Biosystems, United States). The results were expressed by using $2^{-\triangle\triangle Ct}$ with the 16S rRNA as the internal standard

1 https://sourceforge.net/projects/metamis/

2 http://www.spss.com.hk/

3 http://www.genome.jp/kegg/

TABLE 1 Primer used for qRT-PCR analysis of genes transcription in *Lactobacillus helveticus*.

Primer	Sequence (5′-3′)	Corresponding genes
LAF_RS00730_F	TTTAAGGTCCATGGCTTTGC	Aspartate aminotransferase
LAF_RS00730_R	CTCGTCGTCTTGTTCCAGGT	
LAF_RS09565_F	GTAACATGGTCGGGAACTGG	ABC transporter ATP-binding protein
LAF_RS09565_R	GGGGTCGGTAAGTCAACCTT	
LAF_RS04525_F	GGTGAAGGAAGTGGTCATCG	3-Phosphoglycerate dehydrogenase
LAF_RS04525_R	GTAGCCAATCACGTCCATCC	
LAF_RS07750_F	ATCAGGCAGCAGTTGGTTTC	Succinate-semialdehyde dehydrogenase
LAF_RS07750_R	AAGGTCTTCAACACCCAACG	
LAF_RS10410_F	TTAACGATCGCCTTGGAAAC	Alcohol dehydrogenase
LAF_RS10410_R	CCTTCATCAACCCGTACACC	
LAF_RS04455_F	GCCGACCAGTTTGAGTTCAT	ATP phosphoribosyl transferase
LAF_RS04455_R	GGGTCAAAGTCTTCGGTTGA	
16S F	AGCGAGCAGAACCAGCAGATT	16S rRNA
16S R	TGCACCGCGGGGCCATCCCA	

gene. For each gene, the relative transcription of mono-culture was defined as the expression level of 1.0, and the result was expressed as the fold increased in mRNA compared with the control sample (log2).

The effects of endogenous factors on cell growth in co-culture

To analyze the effects of endogenous factors on cell growth, the SSF medium without ethanol and acids was prepared. And then the initial concentrations of ethanol, lactic acid, and acetic acid were set as 0, 1.5, 3.0, 4.5 g/100 g, 0, 1.0, 2.0, 3.0 g/100 g, and 0, 1.0, 2.0, 3.0 g/100 g, respectively. The fermentation was performed at 35°C. In particular, to compare the effect of temperature on cell growth the SSF medium without ethanol and acids was used, and the fermentation was conducted at temperatures of 30°C, 37°C, and 45°C. Those endogenous factors were set according to their change in the SSF process of SAV. The effects of endogenous factors on microbial growth in co-culture condition were analyzed by comparing their CFU (Colony-Forming Unit) changes after 24 h co-culture. The colon of *L. helveticus* and *A. pasteurianus* on same plate can be distinguished by the transparent.

Analytical methods

For the analysis of physicochemical property, 5.0 g of *Cupei* and 95.0 ml of double distilled water were mixed for 1 h in 60°C water bath. The mixture was then centrifuged for 10 min at 8,000× *g*, and the supernatant was collected for analysis. Contents of ethanol and glucose were detected by a biosensor (SBA, Shandong, China). Lactic acid and acetic acid were determined through high-performance liquid chromatography (HPLC), as described previously (Wolfe et al., 2014).

Statistical analysis

All experiments were conducted in triplicate unless otherwise indicated. Origin 2018 and Excel were used for data analysis. Spearman coefficient (p) was calculated with Origin software by paired-sample two-tailed t-test.

Results

Prediction of the interaction between the dominant microorganisms during *in situ* fermentation

High-throughput sequencing was used to investigate the composition and succession of bacterial communities during SSF of SAV. As shown in Figure 1A, *Lactobacillus* and *Acetobacter* are the dominant genera, accounting for more than 95% of all the bacteria. The relative abundance of *Lactobacillus* (mainly *L. helveticus* and *Lactobacillus acetotolerans*) on day 1 was 87.6%, and then gradually decreased to 46.0% on the last day of fermentation. The relative abundance of *Acetobacter* increased from 2.2 to 50.9% from day 1 to day 7. During the fermentation process the OTU with the highest relative abundance (more than 55%) was *L. helveticus*, followed with *L. acetotolerans*, *Limosilactobacillus fermentun* (*L. fermentun*), *Lacticaseibacillus casei* (*L. casei*), *Lactiplantibacillus plantarum*(*L. plantarum*; Zheng et al., 2020). 12 OTUs were classified as *Acetobacter*, including *A. pasteurianus*, *Acetobacter aceti*, *Acetobacter cerevisiae*, *Acetobacter ghanensis*, *Acetobacter indonesiensis*, *Acetobacter malorum*, *Acetobacter orleanensis*, *Acetobacter pomorum*, *Acetobacter senegalensis*, *Acetobacter senegalensis*, *Acetobacter senegalensis*, *Acetobacter* spp., among which the most dominant OTU was *A. pasteurianus* (more than 70%). LAB and AAB are the main microorganisms in SSF of SAV, however, their succession patterns differentiated. OTU of *L. plantarum* (4.34% at day 0) disappeared since day 3. The relative abundances of *L. casei* and *L. acetotolerans* decreased, while those of *L. helveticus*,

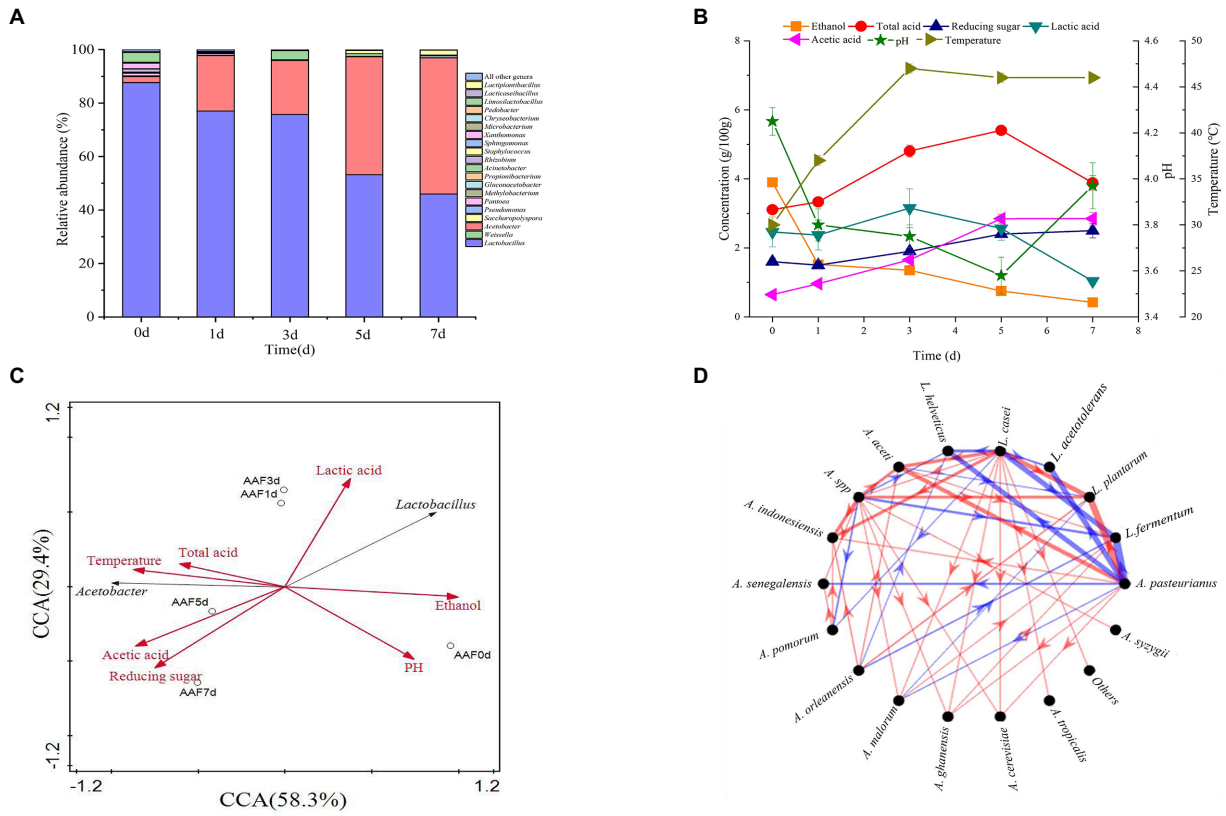

FIGURE 1
Time curves and the microbial correlations in SAV fermentation. **(A)** The composition of bacterial communities; **(B)** The physicochemical indicators; **(C)** CCA analysis; **(D)** Interaction networks of *Lactobacillus* and *Acetobacter*: Edge thickness represents the correlation value, and edge color represents the positive (red) or negative (blue) correlation.

L. fermentum increased. The relative abundance of *Acetobacter* increased. Throughout the fermentation *Lactobacillus* and *Acetobacter* were the dominant bacteria, the most OTUs were identified as *L. helveticus* and *A. pasteurianus*. Though the relative abundance of *L. helveticus* increased, its absolute number decreased due to the various stress factors (Zheng et al., 2022), indicating the growth inhibition in SSF of SAV. While, the absolute number of *A. pasteurianus* increased. Ethanol, reducing sugar, total acid, temperature, acetic acid, and lactic acid are the key physical and chemical indicators for monitoring SSF of SAV, and they also affect the cell growth and succession of microbial communities (Chen et al., 2017). As shown in Figure 1B, the ethanol content decreased from 3.89 to 0.40 g/100 g *Cupei* from day 0 to day 7. Generally, the fermentation is stopped when the total acidity no longer increases and the ethanol concentration is less than 0.5 g/100 g *Cupei*. Lactic acid increased from 2.461 to 3.152 g/100 g *Cupei* from day 0 to day 3, and then decreased to 1.039 g/100 g *Cupei* at the end of fermentation (day 7). Acetic acid accumulated from 0.646 to 2.847 g/100 g *Cupei* throughout the fermentation process. As described in Figure 1C, the abundance of *Lactobacillus* and *Acetobacter* are positively related to the content of lactic acid and acetic acid, respectively, indicating that they were the main acid producers. The temperature was highly positively related to content of *Acetobacter*, total acid, and acetic acid, and negatively related to ethanol. Those results indicated that the oxidation of ethanol to acetic acid by *Acetobacter* was the main source of bio-heat, particularly in the middle stage of fermentation (day 5 and day 7; Zhang et al., 2020). Therefore, the dynamic of dominant genera was highly related to the endogenous factors of acetic acid, ethanol, lactic acid, and temperature. This result was in agreement with previous reports that analyzed the correlations between environmental factors and the microbial community in SSF of cereal vinegar (Lu et al., 2018; Zheng et al., 2018; Fang et al., 2021).

The interaction between microorganisms plays an important role on regulating the succession of bacterial community (Wu et al., 2021a). The MetaMIS method was used to predict the interaction network among the dominant species of *Acetobacter* and *Lactobacillus* based on the high-throughput sequencing (as shown in Figure 1D). The high negative correlations are observed between *A. pasteurianus* and *L. fermentum*, *A. pasteurianus* and *L. helveticus*, and *A. pasteurianus* and *L. acetotolerans*. The high positive correlations are between *A. pasteurianus* and *L. aceti*, *A. pasteurianus* and *L. plantarum*, and *L. plantarum* and *L. case*. The negative interactions between LAB and AAB are well known (Hutchinson et al., 2019; Chai et al., 2020) and analyzed with

kinetic models (Lefeber et al., 2010; Zheng et al., 2022). In particular, the most thick edges are observed on *A. pasteurianus*, representing it plays the most important role in the succession of bacterial community. Interestingly, *L. helveticus* is the other predominant species, however only one thick edge is observed, indication less effect on the succession of bacterial community. *L. helveticus* and *A. pasteurianus* are the two dominant species in SAV fermentation, and also the most abundant microorganisms in the other cereal vinegars, such as Zhenjiang aroma vinegar and Sichuan bran vinegar (Ai et al., 2019; Huang et al., 2022b). They are responsible for the formation of organics acids, acetoin, and the other flavor compounds such as esters and phenols, and are important for the fermentation and product flavor of vinegar (Fang et al., 2021). The related research of Zhenjiang aroma vinegar shows that adding *A. pasteurianus* during the acetic acid fermentation can speed up the fermentation process and increase the content of amino acids, glutamic acid, 2, 3-butanediol, and ligustrazine and other flavor substances (Wang et al., 2016). Considering their import role in the SAV fermentation, their potential interaction mechanism was studied with the bottom-up approach.

The interaction between two dominant species during *in vitro* fermentation

To reveal the interaction between the two dominant species of *L. helveticus* and *A. pasteurianus* in SSF of SAV, *in vitro* SSF was performed with SSFM containing 4 g/100 g ethanol, 0.5 g/100 acetic acid, and 0.5 g/100 lactic acid, which are according to those in the initial SSF of SAV (Figure 1B). The cell growth of *A. pasteurianus* under co-culture condition was the same than in mono-culture, however, the growth of *L. helveticus* under co-culture condition was inhibited compared to that of mono-culture (Figure 2A). As described in Figure 2, under mono-culture condition ethanol was utilized as carbon sources for cell growth of *A. pasteurianus*, and the content of acetic acid increased. Glucose was utilized as carbon sources for *L. helveticus*, and the content of lactic acid increased. Those results indicate there was no nutritional competition between *A. pasteurianus* and *L. helveticus* when they were co-cultured. However, the glucose utilization and lactic acid production decreased in mono-culture (Figures 2B,D) due to the present of *A. pasteurianus*. While, the ethanol utilization, acetic acid production, and the biomass of *A. pasteurianus* were not affected by *L. helveticus* (Figures 2C,E). Adler et al. (2014) investigated the specialized metabolism of *A. pasteurianus* under cocoa pulp fermentation-simulating conditions, and found lactate was served for the biomass building blocks to maximize the cell growth and ethanol conversion.

As shown in Figure 1C, the content of *Acetobacter* and *Lactobacillus* were highly related with the endogenous factors, ethanol, acetic acid, lactic acid, and temperature. Therefore, the effect of the endogenous factors on the cell growth was compared. As shown in Figure 3, all those endogenous factors showed an inhibitory effect on the growth of both of *A. pasteurianus* and *L. helveticus*. However, the intensity of the influence on two species was different. The cell growth of *L. helveticus* became negative when the endogenous factors, ethanol, acetic acid, lactic acid, were above 2 g/100 g acetic acid (Figure 3A), 3 g/100 g ethanol (Figure 3B), and 2 g/100 g lactic acid. While, *A. pasteurianus* was more tolerant against acetic acid (Figure 3A), ethanol (Figure 3B), and lactic acid (Figure 3C) than *L. helveticus*. Those results indicate acids were the main stress factors for *L. helveticus* growth, and *A. pasteurianus* would affect *L. helveticus* growth by producing acetic acid from ethanol and utilizing lactic acid (Adler et al., 2014). The temperature would be more than 45°C in the middle stage of SAV fermentation (Figure 1B), and *A. pasteurianus* grew better at 30°C than 37°C and 45°C 45°C (Figure 3D). The microorganism requires appropriate temperature for growth (the optimal temperature for AAB is about 30°C, and for LAB is 30–40°C). Due to the poor heat transfer efficiency in SSF systems, the temperature may influence the growth and metabolism of the microorganisms. When the temperature was above 37°C, a sharp reduction of cell growth rate was observed in *A. pasteurianus*. *L helveticus* grow better at 35–40°C than 30°C under mono-culture condition (Zhang et al., 2020). However, under 45°C its growth was inhibited (Figure 3D). Those explain how the endogenous factors affect the succession of *Acetobacter* and *Lactobacillus* during SSF of SAV. Coincidentally, all those endogenous factors are the metabolites of LAB and AAB in SAV fermentation. Thus, the *in vitro* SSF of co-culture presented an amensalism relationship between *A. pasteurianus* and *L. helveticus*. However, the interaction mechanism was not clear yet.

Transcriptomic analysis to reveal the mechanism of interaction between *Lactobacillus helveticus* and *Acetobacter pasteurianus*

To reveal the potential mechanism of interaction between *L. helveticus* and *A. pasteurianus*, the transcriptomes of *L. helveticus* and *A. pasteurianus* under mono-culture and co-culture conditions were sequenced and compared. DEseq software was used to screen out statistically significant differentially expressed genes ($|\log2 \text{ (Fold Change)}| > 1$ and p value <0.05). The result shows that the number of differentially expressed genes in *L. helveticus* CGMCC 12062 and *A. pasteurianus* CGMCC 3089 under co-culture condition are 831 and 529, respectively, comparing to their corresponding mono-cultures (Figures 4A,B). For *L. helveticus* CGMCC 12062, 202 differentially expressed genes were up-regulated and 629 genes were down-regulated (Figure 4A), and those differentially expressed genes are mainly classified into Gene Ontology classification of molecular function, biological process, and cell composition (Figure 4C). The down-regulated genes in *L. helveticus* CGMCC 12062 were enriched in KEGG pathways of

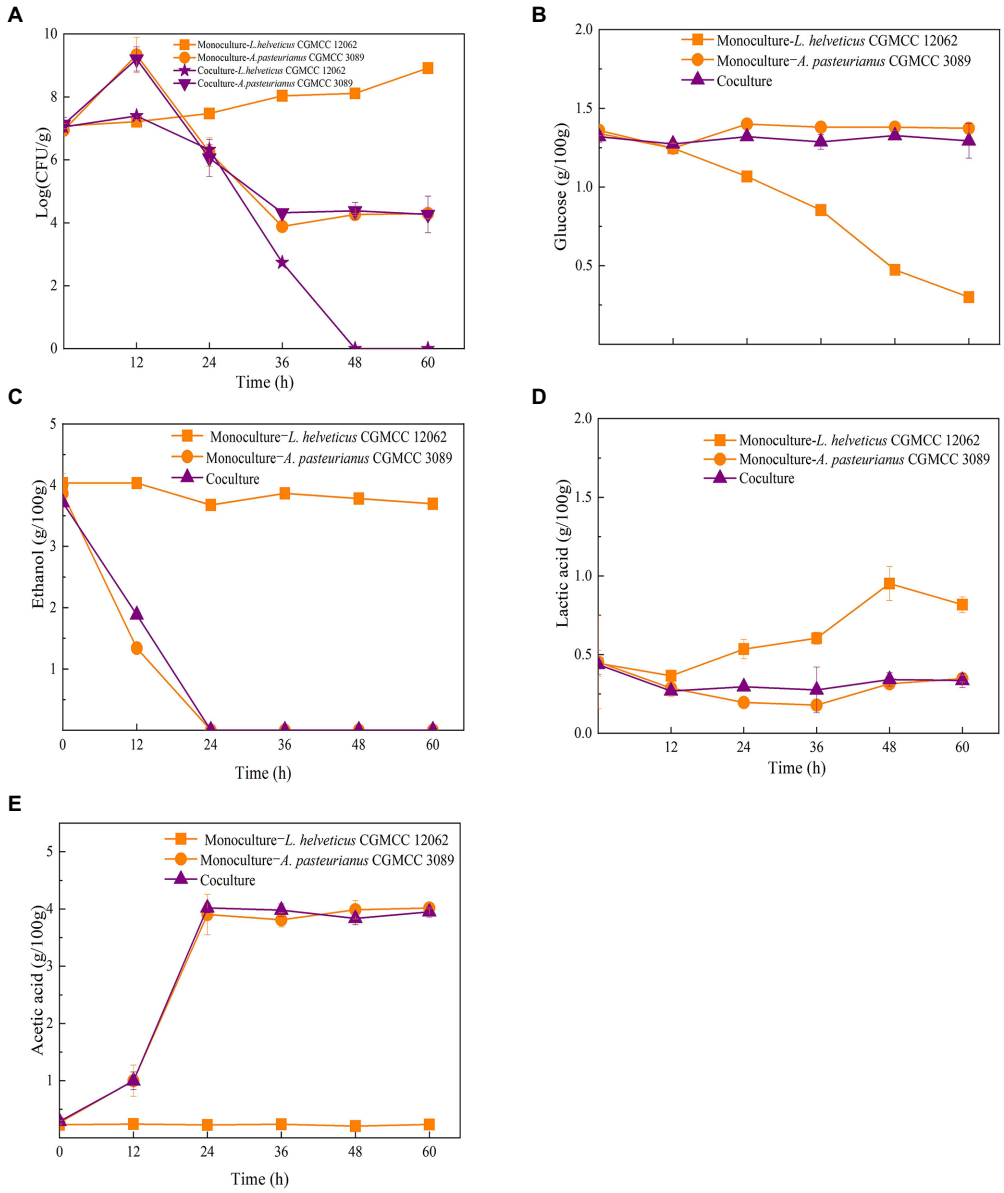

FIGURE 2
Time curves in mono-culture and co-culture of *L. helveticus* and *A. pasteurianus*. **(A)** Cell growth; **(B)** Glucose consumption; **(C)** Ethanol consumption; **(D)** Lactic acid production; **(E)** Acetic acid production.

sugar, amino acid, purine, and pyrimidine metabolism. For *A. pasteurianus* CGMCC 3089, 393 differentially expressed genes were up-regulated and 136 genes were down-regulated (Figure 4B), and the genes for KEGG pathways of sugar, amino acid, purine, and pyrimidine metabolism were up-regulated (Figure 4D). There were more differentially expressed genes in *L. helveticus* under co-culture condition than those in *A. pasteurianus*. In *L. helveticus* the more genes related to cellular constituents and less genes related to molecular function were regulated than those in *A. pasteurianus*. Those results were agreed with the amensalism phenomenon between *A. pasteurianus* and *L. helveticus*.

The KEGG metabolic pathway analysis was performed for the enrichment genes. As shown in Figure 5A, under co-culture condition the up-regulated genes in *L. helveticus* CGMCC 12062 were mainly categorized in metabolic pathway of pyrimidine, purine, amino acids (lysine, glycine, serine, cysteine, alanine, aspartate and glycine), glycerophospholipid, and energy (ABC transporters) comparing to its mono-culture condition. The genes in starch and sucrose, propanonate, amino acids (tyrosine, phenylalanine, tryptophan, histidine), galactose, and fatty acid metabolic pathways were down-regulated (Figure 5B). For *A. pasteurianus* CGMCC 3089, due to the existence of *L. helveticus* CGMCC 12062, the genes in the pathways of terpenoids, protein

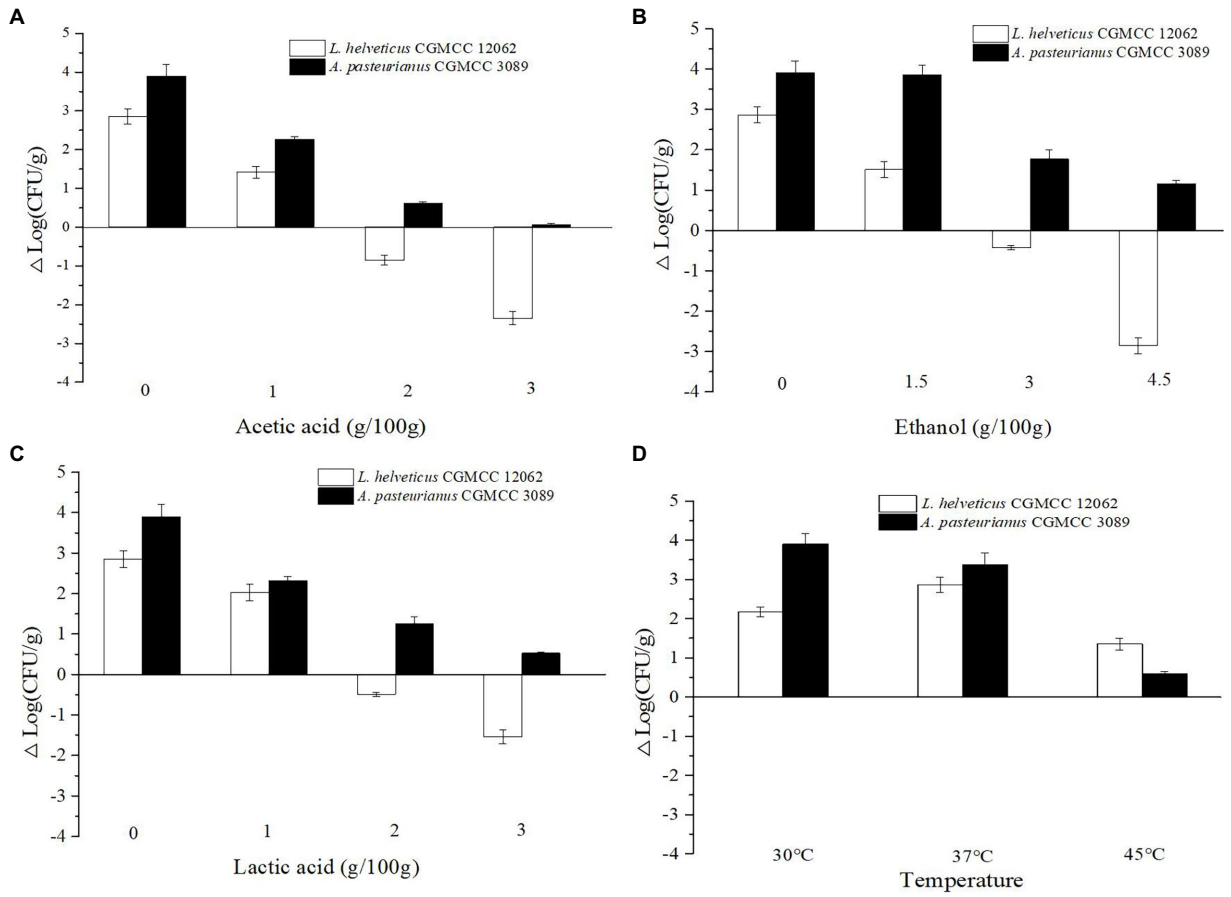

FIGURE 3
Effects of endogenous factors on microbial growth in co-culture condition. **(A)** Acetic acid; **(B)** Ethanol; **(C)** Lactic acid; **(D)** Temperature.

transport, amino acids (valine, leucine, isoleucine, lysine, cysteine, methionine), glycerophospholipids, metabolism of monocyclic β-lactams, fatty acids, aromatic compounds, hydrocarbons, sugars, and sulfur were up-regulated (Figure 5C), and those in pyruvate, glyoxylic acid, fructose and mannose pathways were down-regulated (Figure 5D).

To verify the effect of *A. pasteurianus* CGMCC 3089 on the metabolic pathways of *L. helveticus* CGMCC 12062, the transcription of several most significantly different genes, including 3-phosphoglycerate dehydrogenase, succinate-semialdehyde dehydrogenase, aspartate aminotransferase, alcohol dehydrogenase, ABC transporter ATP-binding protein, and ATP phosphoribosyl transferase, were assayed using the method of qRT-PCR. They were the important genes in pathways of EMP, TCA cycle, amino acid metabolism, acid stress tolerance, transmembrane transport, and histidine formation, respectively, and were significant differently ($|\log2 \text{ (Fold Change)}| > 1$ and $p \leq 0.05$) descripted under mono-culture and co-culture conditions. As listed in Table 2, all those genes in *L. helveticus* CGMCC 12062 were down-regulated under co-culture condition comparing with those under mono-culture due to the presence of *A. pasteurianus* CGMCC 3089. Results from qPCR analysis were in agreement with those of transcriptomics.

Discussion

A lot of traditionally fermented foods are produced with a spontaneous fermentation. The dynamics of microbial community is affected by the endogenous factors, which results in the desired characteristics of the final products (Singh and Ramesh, 2008; Houngbédji et al., 2019; Zhao et al., 2020). However, the endogenous factors are complex, such as nutrients, metabolic product and environmental factors. Besides, the interrelationship among microorganisms is unavoidable in these ecosystems. Several studies have reported the interactions between microorganisms in fermentation of cereal vinegars. For example, *L. casei* and *A. pasteurianus* in Zhenjiang aromatic vinegar have synergistic effects in the synthesis of acetoin (Chai et al., 2020). In addition, other studies have shown that during the fermentation of Zhenjiang aromatic vinegar, *L. buchneri* and *L. brevis* are positively correlated, while *A. pasteurianus* and *Lactobacillus* are negatively correlated (Chai et al., 2020; Zheng et al., 2022).

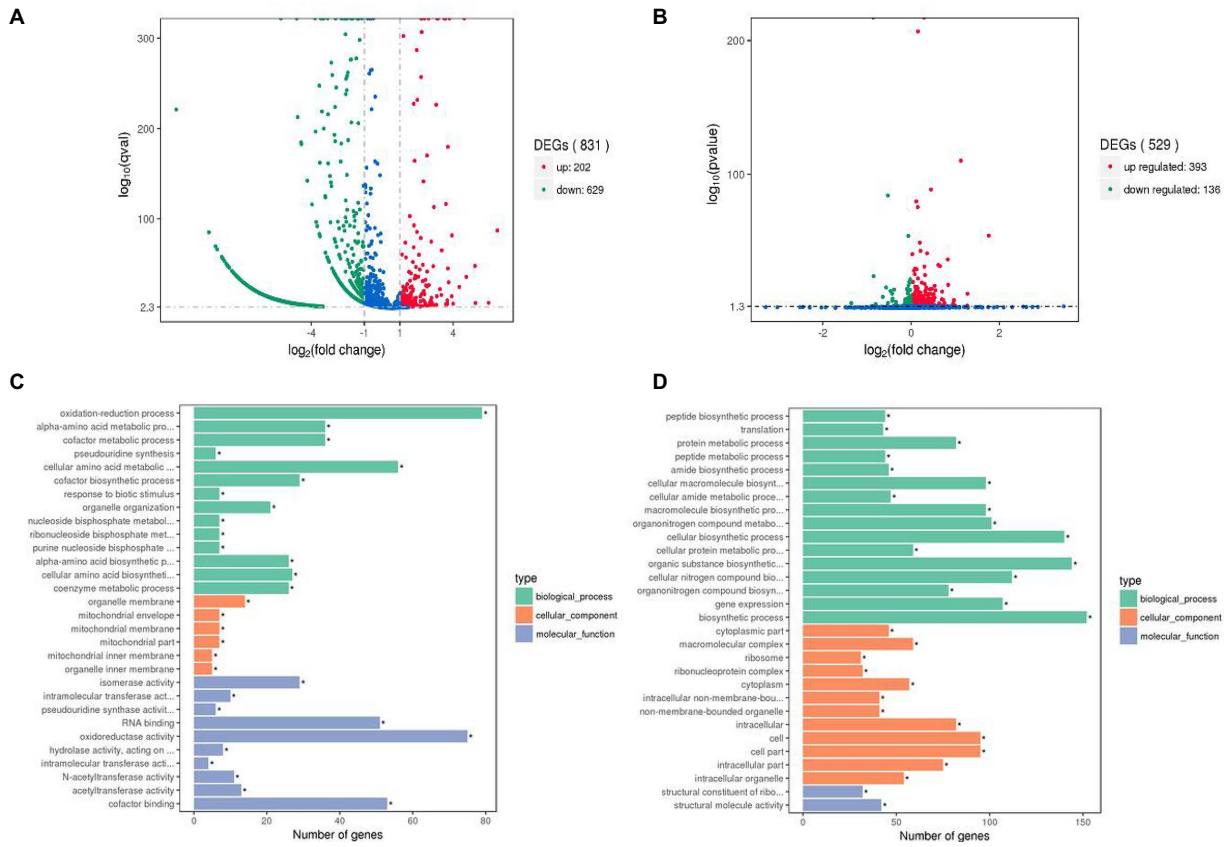

FIGURE 4
Gene expression profiles volcano map and the most enriched GO terms of differential genes. **(A)** Gene expression profiles volcano map of *L. helveticus* CGMCC 12062; **(B)** and *A. pasteurianus* CGMCC 3089; **(C)** Differential gene GO terms of *L. helveticus* CGMCC 12062; **(D)** and *A. pasteurianus* CGMCC 3089. |log2 (Fold Change)|>1 and p value ≤0.05 was the criteria for transcriptome differential genes.

However, the potential mechanism of the interactions is still unclear.

In this study, the interaction of dominant microorganisms in SSF of SAV was revealed by employing top-down (*in situ*) and bottom-up (*in vitro*) approaches. Firstly, important physical and chemical indicators during *in situ* culture were monitored. Ethanol and reducing sugars are important carbon sources for AAB fermentation (Wang et al., 2015). Acetic acid and lactic acid are the most important organic acids in vinegar (Xu et al., 2011; Hen et al., 2013). The content of lactic acid increases at first and then decreases during fermentation, which is mainly due to the fact that lactic acid is used as a carbon source by other microorganisms at the later stage of fermentation (Chai et al., 2020). Temperature is the most intuitive indicator for evaluating the fermentation process of vinegar, which can reflect the metabolic activities of microorganisms (Adler et al., 2014; Li et al., 2016). Secondly, correlation analysis was performed for *Lactobacillus* and *Acetobacter* with physical and chemical indicators. In the initial stage of AAF, ethanol (the carbon source of AAB) is the main factor affecting fermentation. The main influencing factors in the middle stage of fermentation are temperature and lactic acid. In the late stage of fermentation, acetic acid become an important inhibitor of the growth of LAB, affecting the fermentation process. Thirdly, the result of MetaMIS prediction showed that *A. pasteurianus* and *L. helveticus* are inversely correlated in the SSF of SAV. Interestingly, though *L. helveticus* is the most predominant species, a few high correlations are observed from it, besides a high negative correlation with *A. pasteurianus*. Those result implies *L. helveticus* might be used for bioaugmentation of SSF of SAV to modulate the lactic acid formation without affecting the other microorganisms. Little difference was observed on growth and ethanol oxidation between mono- and co-culture of *A. pasteurianus* CGMCC 3089, while the growth and metabolism of *L. helveticus* CGMCC 12062 was significantly inhibited due to the existence of *A. pasteurianus* CGMCC 3089. In the transcriptomic analysis, the number of differentially expressed genes of *L. helveticus* CGMCC 12062 was higher than that of *A. pasteurianus* CGMCC 3089 under co-culture condition. The down-regulated genes in *L. helveticus* CGMCC 12062 were enriched in KEGG pathways of sugar, amino acid, purine, and pyrimidine metabolism, which are related to biological processes and cell compositions. These results suggest an amensalism phenomenon in co-culture of *A. pasteurianus* and *L. helveticus*.

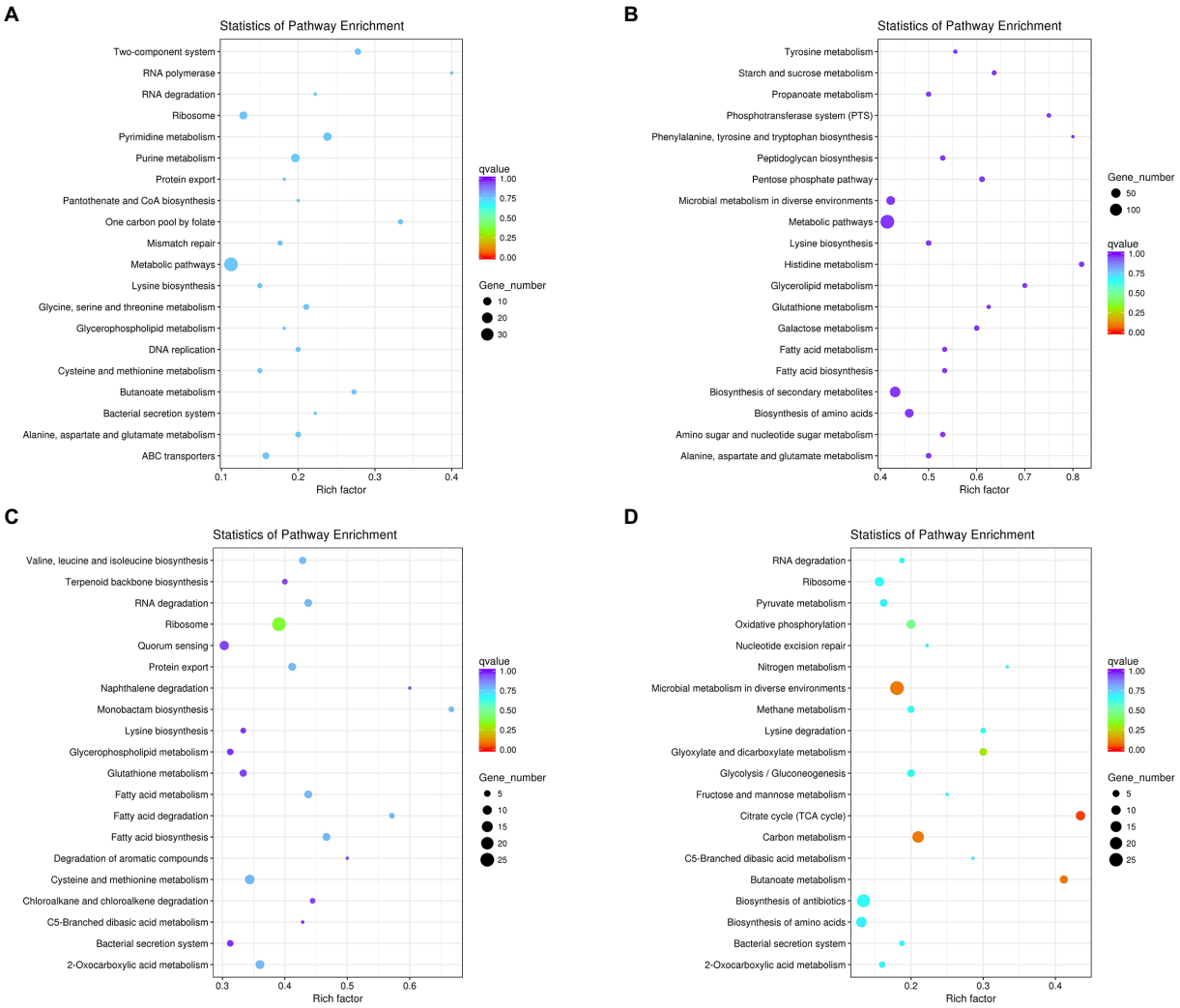

FIGURE 5
The KEGG metabolic pathway analysis of differential genes under coculture condition compared with those of mono-culture. **(A)** Pathway of up-regulated in *L. helveticus* CGMCC 12062; **(B)** and down-regulated; **(C)** Pathway of up-regulated in *A. pasteurianus* CGMCC 3089; **(D)** and down-regulated.

TABLE 2 Assay of the transcription of genes by the method of qRT-PCR.

Genes description	$\log_2$ (qRT-PCR analysis)	$\log_2$ (RNA-seq analysis)
Aspartate aminotransferase	−8.189 ± 0.12	−8.680
ABC transporter ATP-binding protein	−6.750 ± 0.08	−7.669
3-phosphoglycerate dehydrogenase	−3.211 ± 0.13	−6.793
Succinate-semialdehyde dehydrogenase	−3.031 ± 0.04	−5.763
Alcohol dehydrogenase	−2.816 ± 0.07	−5.711
ATP phosphoribosyl transferase	−2.130 ± 0.05	−4.361

The enzyme of 3-phosphoglycerate dehydrogenase (PGDH) catalyzes the oxidation (dehydrogenation) and phosphorylation of 3-phosphoglyceraldehyde to generate 1,3-diphosphoglycerate. PGDH is an important enzyme in the glycolysis pathway and is also involved in the synthesis of serine (Zhang et al., 2017). When glucose is the sole carbon source in *Escherichia coli*, 15% of the absorbed carbon is synthesized by PGDH and other related enzymes in glycolysis, and the L-serine is then converted into other products (Pizer and Potochny, 1964). Therefore, down-regulation of PGDH may lead to decreased glucose metabolism. Succinate semialdehyde dehydrogenase oxidizes succinate semialdehyde to form succinate that then enters the tricarboxylic acid cycle. The down-regulation of succinate semialdehyde dehydrogenase indicates the decreased energy metabolism in

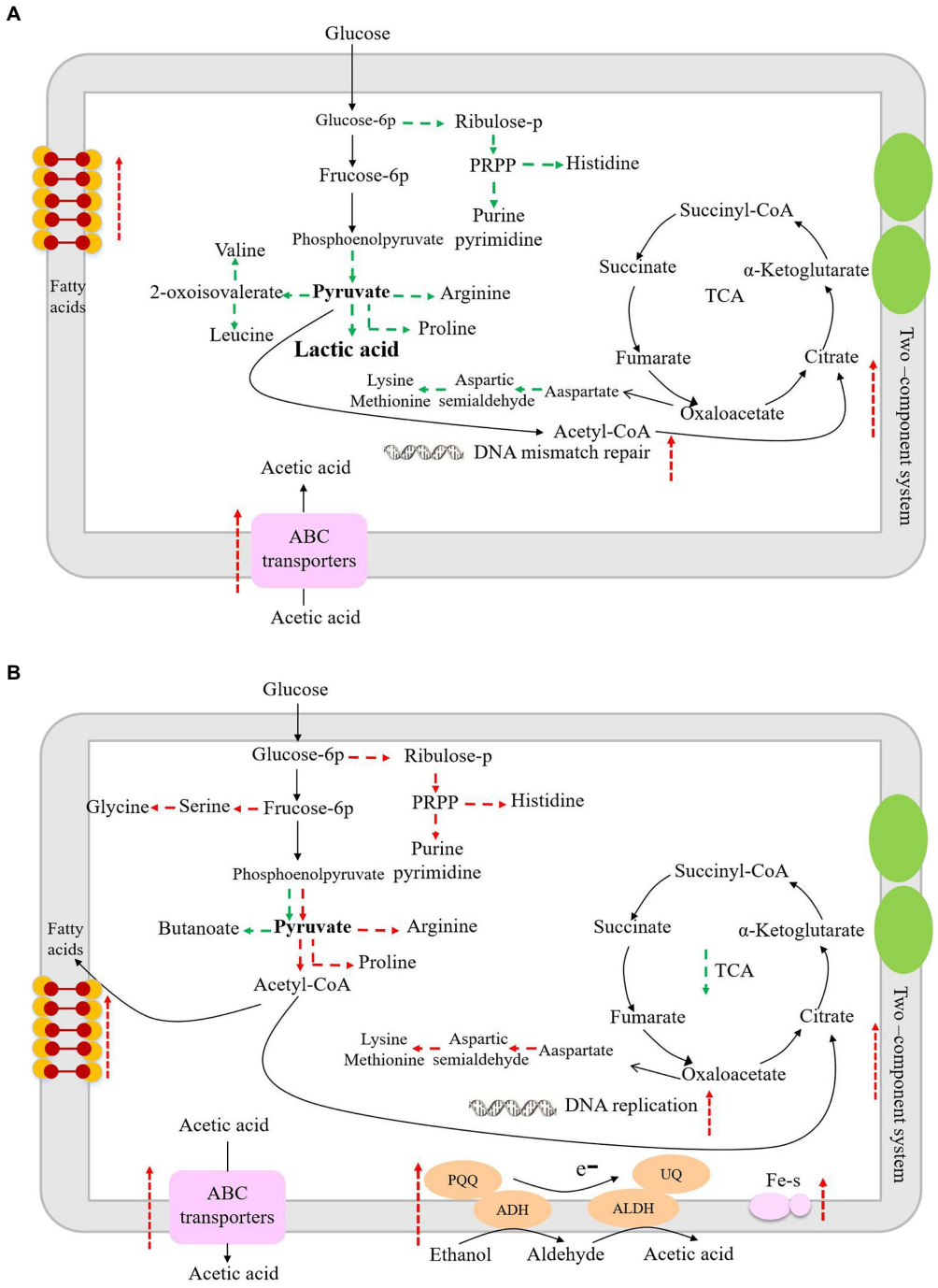

FIGURE 6
The sketch map of metabolism changes in *L. helveticus* CGMCC 12062 **(A)** and *A. pasteurianus* CGMCC 3089 **(B)** under coculture condition compared with that of mono-culture. Red represents up-regulation of metabolic pathway or gene transcription, and green represents down-regulation.

L. helveticus (Legendre et al., 2020). Aspartate aminotransferase catalyzes the conversion of aspartate into oxaloacetate and glutamate, which further participate in the tricarboxylic acid cycle and glutamate decarboxylase metabolic pathways. Another study has shown that aspartate aminotransferase plays an important role in nitrogen metabolism in *Mycobacterium tuberculosis* (Jansen et al., 2020). In co-culture condition the down-regulated aspartate aminotransferase would result in the decrease of nitrogen metabolism. ABC transporters are associated with the transport of proteoglycans,

amino acids, metal ions, polypeptides, proteins, and cellular metabolites (Locher, 2016). Studies have shown that LAB can change the expression of ABC transporters under acetic acid stress, which is important for bacteria to adapt to environmental stress (Kang et al., 2022). Therefore, due to the down-regulation of those enzymes, the biomass of *L. helveticus* decreased under co-cultivation condition, as shown in Figure 2. According to the main differentially expressed genes and related pathways, the speculated sketch map of metabolic changes in *L. helveticus* CGMCC 12062 (Figure 6A) and *A. pasteurianus* CGMCC 3089 (Figure 6B) under co-culture condition comparing to their corresponding mono-cultures were proposed.

SSF is one of the most features of Chinese cereal vinegar. The solid auxiliary materials, including wheat bran, rice hull, not only serve as solid supports for the cells but also provide a slow mass transfer environment. Moreover, wheat bran contains additional nutrients. In this research SSFM containing wheat bran, rice hull, MRS, and the main metabolites of predominant microorganism was used to simulate the SSF of SAV. The correlation between *A. pasteurianus* and *L. helveticus* from *in vitro* fermentation were agreement with that *in situ* fermentation. However, comparing to the real SSF process, a lot of substrates are missed, e.g., some sugars, esters, which might affect the cell growth. To simulate the real SSF of cereal vinegar assembling wheat bran, rice hull and the sterilized leach liquor of *Cupei* might be a potential candidate medium.

Conclusion

In this study, top-down (*in situ*) and bottom-up (*in vitro*) approaches were employed to reveal the mechanism of interaction between *A. pasteurianus* and *L. helveticus*, which are the two dominant bacteria in SSF of SAV. Their growth is negatively correlated to each other both *in situ* and *in vitro*, and there is no nutritional competition between them. The growth and metabolism of *L. helveticus* were inhibited due to the presence of *A. pasteurianus*, indicating an amensalism relationship between them. Ethanol, acetic acid, and lactic acid were proved the most important endogenous factors that regulate the growth profiles of *A. pasteurianus* and *L. helveticus*. Transcriptomic analysis results showed that in *L. helveticus* the genes in metabolic pathways of starch and sucrose, galactose, fatty acids and some amino acids were down-regulated under co-culture condition comparing to its mono-culture condition, while the genes in metabolic pathways of glycerophospholipid, energy (ABC transporters), pyrimidine and purine were up-regulated. The number of transcriptionally regulated genes was less in *A. pasteurianus* than in *L. helveticus*. The genes for KEGG pathways of sugar, amino acid, purine, and pyrimidine metabolism were up-regulated in *A. pasteurianus* under co-culture condition, and metabolic pathways of pyruvate, glyoxylate, fructose and mannose were down-regulated comparing to its mono-culture condition. These results prove the amensalism between *A. pasterurinaus* and *L. helveticus*. This work gives a whole insight on the interaction between the predominant species in SSF of cereal vinegar from nutrient utilization, endogenous factors inhibition and the regulation of gene transcription.

Data availability statement

The datasets presented in this study can be found in online repositories. The names of the repository/repositories and accession number(s) can be found in the article/supplementary material.

Author contributions

MX and XZ performed the experiments and substantially contributed to the acquisition, analysis, and interpretation of data. YX and QS were involved in the experiments and revised and discussed the manuscript. LT and FC were involved in revising the manuscript. YY was involved in the experiments. YZ and MW designed the study and were involved in drafting and revising the manuscript. All authors contributed to the article and approved the submitted version.

Funding

This work was supported by the National Natural Science Foundation of China (32072203), the Tianjin Synthetic Biotechnology Innovation Capacity Improvement Project (TSBICIP-KJGG-016-03), the Tianjin Science and Technology Commission (21ZYJDJC00030), Key Research and Development Program of Ningxia (2022BBF02010), and the Shanxi Science and Technology Department (2022D10019405131901445045921 7).

Conflict of interest

YY is employed by Shanxi Zilin Vinegar Industry Co., Ltd.

The remaining authors declare that the research was conducted in the absence of any commercial or financial relationships that could be construed as a potential conflict of interest.

Publisher's note

References

Adler, P., Frey, L. J., Berger, A., Bolten, C. J., Hansen, C. E., and Wittmann, C. (2014). The key to acetate: metabolic fluxes of acetic acid bacteria under cocoa pulp fermentation simulating conditions. *Appl. Environ. Microbiol.* 80, 4702–4716. doi: 10.1128/AEM.01048-14

Ai, M., Qiu, X., Huang, J., Wu, C., Jin, Y., and Zhou, R. (2019). Characterizing the microbial diversity and major metabolites of Sichuan bran vinegar augmented by *Monascus purpureus*. *Int. J. Food Microbiol.* 292, 83–90. doi: 10.1016/j.ijfoodmicro.2018.12.008

Bertrand, S., Bohni, N., Schnee, S., Schumpp, O., Gindro, K., and Wolfender, J. L. (2014). Metabolite induction via microorganism co-culture: a potential way to enhance chemical diversity for drug discovery. *Biotechnol. Adv.* 32, 1180–1204. doi: 10.1016/j.biotechadv.2014.03.001

Chai, L. J., Qiu, T., Lu, Z. M., Deng, Y. J., Zhang, X. J., Shi, J. S., et al. (2020). Modulating microbiota metabolism via bioaugmentation with *Lactobacillus casei* and *Acetobacter pasteurianus* to enhance acetoin accumulation during cereal vinegar fermentation. *Food Res. Int.* 138:109737. doi: 10.1016/j.foodres.2020.109737

Chen, Y., Huang, Y., Bai, Y., Fu, C., Zhou, M., and Gao, B. (2017). Effects of mixed cultures of *Saccharomyces cerevisiae* and *Lactobacillus plantarum* in alcoholic fermentation on the physicochemical and sensory properties of citrus vinegar. *LWT* 84, 753–763. doi: 10.1016/j.lwt.2017.06.032

Edwardson, C. F., and Hollibaugh, J. T. (2018). Composition and activity of microbial communities along the redox gradient of an alkaline, hypersaline, lake. *Front. Microbiol.* 9:14. doi: 10.3389/fmicb.2018.00014.eCollection 2018

Fang, G. Y., Chai, L. J., Zhong, X. Z., and Jiang, Y. J. (2021). Deciphering the succession patterns of bacterial community and their correlations with environmental factors and flavor compounds during the fermentation of Zhejiang rosy vinegar. *Int. J. Food Microbiol.* 341:109070. doi: 10.1016/j.ijfoodmicro.2021.109070

Feng, R., Chen, L., and Chen, K. (2018). Fermentation trip: amazing microbes, amazing metabolisms. *Ann. Microbiol.* 68, 717–729. doi: 10.1007/s13213-018-1384-5

Furukawa, S., Watanabe, T., Toyama, H., and Morinaga, Y. (2013). Significance of microbial symbiotic coexistence in traditional fermentation. *J. Biosci. Bioeng.* 116, 533–539. doi: 10.1016/j.jbiosc.2013.05.017

Gan, X., Tang, H., Ye, D., Li, P., Luo, L., and Lin, W. (2017). Diversity and dynamics stability of bacterial community in traditional solid-state fermentation of Qishan vinegar. *Ann. Microbiol.* 67, 703–713. doi: 10.1007/s13213-017-1299-6

Hen, T., Gui, Q., Shi, J. J., Zhang, X. Y., and Chen, F. S. (2013). Analysis of variation of main components during aging process of Shanxi Aged Vinegar. *Acetic Acid Bacteria* 2:6. doi: 10.4081/aab.2013.s1.e6

Houngbédji, M., Johansen, P., Padonou, S. W., Hounhouigan, D. J., Siegumfeldt, H., and Jespersen, L. (2019). Effects of intrinsic microbial stress factors on viability and physiological condition of yeasts isolated from spontaneously fermented cereal doughs. *Int. J. Food Microbiol.* 304, 75–88. doi: 10.1016/j.ijfoodmicro.2019.05.018

Huang, T., Lu, Z. M., Peng, M. Y., Chai, L. J., Zhang, X. J., Shi, J. S., et al. (2022b). Constructing a defined starter for multispecies vinegar fermentation via evaluation of the vitality and dominance of functional microbes in an autochthonous starter. *Appl. Environ. Microbiol.* 88:e0217521. doi: 10.1128/AEM.02175-21

Huang, T., Lu, Z. M., Peng, M. Y., Liu, Z. F., Chai, L. J., Zhang, X. J., et al. (2022a). Combined effects of fermentation starters and environmental factors on the microbial community assembly and flavor formation of Zhenjiang aromatic vinegar. *Food Res. Int.* 152:110900. doi: 10.1016/j.foodres.2021.110900

Hutchinson, U. F., Ntwampe, S., Ngongang, M. M., Chidi, B. S., Hoff, J. W., and Jolly, N. P. (2019). Product and microbial population kinetics during balsamic-styled vinegar production. *J. Food Sci.* 84, 572–579. doi: 10.1111/1750-3841.14429

Jansen, R. S., Mandyoli, L., Hughes, R., Wakabayashi, S., Pinkham, J. T., Selbach, B., et al. (2020). Aspartate aminotransferase Rv3722c governs aspartate-dependent nitrogen metabolism in *Mycobacterium tuberculosis*. *Nat. Commun.* 11:1960. doi: 10.1038/s41467-020-15876-8

Kang, J., Zhou, X., Zhang, W., Pei, F., and Ge, J. (2022). Transcriptomic analysis of bacteriocin synthesis and stress response in *Lactobacillus paracasei* HD1. 7 under acetic acid stress. *LWT* 154:112897. doi: 10.1016/j.lwt.2021.112897

Kleerebezem, R., and van Loosdrecht, M. C. (2007). Mixed culture biotechnology for bioenergy production. *Curr. Opin. Biotechnol.* 18, 207–212. doi: 10.1016/j.copbio.2007.05.001

Lefeber, T., Janssens, M., Camu, N., and Vuyst, L. D. (2010). Kinetic analysis of strains of lactic acid bacteria and acetic acid bacteria in cocoa pulp simulation media toward development of a starter culture for cocoa bean fermentation. *Appl. Environ. Microbiol.* 76, 7708–7716. doi: 10.1128/AEM.01206-10

Legendre, F., MacLean, A., Appanna, V. P., and Appanna, V. D. (2020). Biochemical pathways to α-ketoglutarate, a multi-faceted metabolite. *World J. Microbiol. Biotechnol.* 36:123. doi: 10.1007/s11274-020-02900-8

Li, S., Li, P., Liu, X., Luo, L., and Lin, W. (2016). Bacterial dynamics and metabolite changes in solid-state acetic acid fermentation of Shanxi aged vinegar. *Appl. Microbiol. Biotechnol.* 100, 4395–4411. doi: 10.1007/s00253-016-7284-3

Liang, J., Xie, J., Hou, L., Zhao, M., Zhao, J., Cheng, J., et al. (2016). Aroma constituents in Shanxi aged vinegar before and after aging. *J. Agric. Food Chem.* 64, 7597–7605. doi: 10.1021/acs.jafc.6b03019

Locher, K. P. (2016). Mechanistic diversity in ATP-binding cassette (ABC) transporters. *Nat. Struct. Mol. Biol.* 23, 487–493. doi: 10.1038/nsmb.3216

Lu, Z. M., Liu, N., Wang, L. J., Wu, L. H., Gong, J. S., Yu, Y. J., et al. (2016). Elucidating and regulating the acetoin production role of microbial functional groups in multispecies acetic acid fermentation. *Appl. Environ. Microbiol.* 82, 5860–5868. doi: 10.1128/AEM.01331-16

Lu, Z. M., Wang, Z. M., Zhang, X. J., Mao, J., Shi, J. S., and Xu, Z. H. (2018). Microbial ecology of cereal vinegar fermentation: insights for driving the ecosystem function. *Curr. Opin. Biotechnol.* 49, 88–93. doi: 10.1016/j.copbio.2017.07.006

Nai, C., and Meyer, V. (2018). From axenic to mixed cultures: technological advances accelerating a paradigm shift in microbiology. *Trends Microbiol.* 26, 538–554. doi: 10.1016/j.tim.2017.11.004

Nie, Z., Zheng, Y., Wang, M., Han, Y., Wang, Y., Luo, J., et al. (2013). Exploring microbial succession and diversity during solid-state fermentation of Tianjin duliu mature vinegar. *Bioresour. Technol.* 148, 325–333. doi: 10.1016/j.biortech.2013.08.152

Oleinikova, Y., Amangeldi, A., Yelubaeva, M., Alybaeva, A., Amankeldy, S., Saubenova, M., et al. (2020). Immobilization effects of wheat bran on enhanced viability of dairy starters under acid and bile salts stresses. *Appl. Food Biotechnol.* 7, 215–223. doi: 10.22037/afb.v7i4.29723

Papalexandratou, Z., Vrancken, G., De Bruyne, K., Vandamme, P., and De Vuyst, L. (2011). Spontaneous organic cocoa bean box fermentations in Brazil are characterized by a restricted species diversity of lactic acid bacteria and acetic acid bacteria. *Food Microbiol.* 28, 1326–1338. doi: 10.1016/j.fm.2011.06.003

Pizer, L. I., and Potochny, M. L. (1964). Nutritional and regulatory aspects of serine metabolism in *Escherichia coli*. *J. Bacteriol.* 88, 611–619. doi: 10.1128/jb.88.3.611-619.1964

Singh, A. K., and Ramesh, A. (2008). Succession of dominant and antagonistic lactic acid bacteria in fermented cucumber: insights from a PCR-based approach. *Food Microbiol.* 25, 278–287. doi: 10.1016/j.fm.2007.10.010

Smid, E. J., and Lacroix, C. (2013). Microbe-microbe interactions in mixed culture food fermentations. *Curr. Opin. Biotechnol.* 24, 148–154. doi: 10.1016/j.copbio.2012.11.007

Tamang, J. P., Watanabe, K., and Holzapfel, W. H. (2016). Review: diversity of microorganisms in global fermented foods and beverages. *Front. Microbiol.* 7:377. doi: 10.3389/fmicb.2016.00377

Wang, Z. M., Lu, Z. M., Shi, J. S., and Xu, Z. H. (2016). Exploring flavour-producing core microbiota in multispecies solid-state fermentation of traditional Chinese vinegar. *Sci. Rep.* 6:26818. doi: 10.1038/srep26818

Wang, Z. M., Lu, Z. M., Yu, Y. J., Li, G. Q., Shi, J.-S., and Xu, Z.-H. (2015). Batch-to-batch uniformity of bacterial community succession and flavor formation in the fermentation of Zhenjiang aromatic vinegar. *Food Microbiol.* 50, 64–69. doi: 10.1016/j.fm.2015.03.012

Wolfe, B. E., Button, J. E., Santarelli, M., and Dutton, R. J. (2014). Cheese rind communities provide tractable systems for *in situ* and *in vitro* studies of microbial diversity. *Cells* 158, 422–433. doi: 10.1016/j.cell.2014.05.041

Wu, Y., Xia, M., Zhang, X., Li, X., Zhang, R., Yan, Y., et al. (2021b). Unraveling the metabolic network of organic acids in solid-state fermentation of Chinese cereal vinegar. *Food Sci. Nutr.* 9, 4375–4384. doi: 10.1002/fsn3.2409

Wu, Y., Xia, M., Zhao, N., Tu, L., Xue, D., Zhang, X., et al. (2021a). Metabolic profile of main organic acids and its regulatory mechanism in solid-state fermentation of Chinese cereal vinegar. *Food Res. Int.* 145:110400. doi: 10.1016/j.foodres.2021.110400

Xu, W., Huang, Z., Zhang, X., Li, Q., Lu, Z., Shi, J., et al. (2011). Monitoring the microbial community during solid-state acetic acid fermentation of Zhenjiang aromatic vinegar. *Food Microbiol.* 28, 1175–1181. doi: 10.1016/j.fm.2011.03.011

Yunita, D., and Dodd, C. E. R. (2018). Microbial community dynamics of a blue-veined raw milk cheese from the United Kingdom. *J. Dairy Sci.* 101, 4923–4935. doi: 10.3168/jds.2017-14104

Zhang, Q., Fu, C., Zhao, C., Yang, S., Zheng, Y. U., Xia, M., et al. (2020). Monitoring microbial succession and metabolic activity during manual and mechanical solid-state fermentation of Chinese cereal vinegar. *LWT* 133:109868. doi: 10.1016/j.lwt.2020.109868

Zhang, W., Zhang, M., Gao, C., Zhang, Y., Ge, Y., Guo, S., et al. (2017). Coupling between d-3-phosphoglycerate dehydrogenase and d-2-hydroxyglutarate dehydrogenase drives bacterial l-serine synthesis. *Proc. Natl. Acad. Sci. U. S. A.* 114, E7574–E7582. doi: 10.1073/pnas.1619034114

Zhao, N., Yang, B., Lu, W., Liu, X., Zhao, J., and Zhang, H. (2020). Divergent role of abiotic factors in shaping microbial community assembly of paocai brine during aging process. *Food Res. Int.* 137:109559. doi: 10.1016/j.foodres.2020.109559

Zheng, Y., Mou, J., Niu, J., Yang, S., Chen, L., Xia, M., et al. (2018). Succession sequence of lactic acid bacteria driven by environmental factors and substrates throughout the brewing process of Shanxi aged vinegar. *Appl. Microbiol. Biotechnol.* 102, 2645–2658. doi: 10.1007/s00253-017-8733-3

Zheng, J., Wittouck, S., Salvetti, E., Franz, C. M., Harris, H. M., Mattarelli, P., et al. (2020). A taxonomic note on the genus *Lactobacillus*: description of 23 novel genera, emended description of the genus *Lactobacillus* Beijerinck 1901, and union of *Lactobacillaceae* and *Leuconostocaceae*. *Int. J. Syst. Evol. Microbiol.* 70, 2782–2858. doi: 10.1099/ijsem.0.004107

Zheng, Y., Zhao, C., Li, X., Xia, M., Wang, X., Zhang, Q., et al. (2022). Kinetics of predominant microorganisms in the multi-microorganism solid-state fermentation of cereal vinegar. *LWT* 159:113209. doi: 10.1016/j.lwt.2022.113209

frontiers | Frontiers in Microbiology

TYPE Original Research
PUBLISHED 29 September 2022
DOI 10.3389/fmicb.2022.956729

OPEN ACCESS

EDITED BY
Giovanna Suzzi,
University of Teramo,
Italy

REVIEWED BY
Yu Zheng,
Tianjin University of Science and Technology, China
Salvatore La China,
University of Modena and Reggio Emilia, Italy

*CORRESPONDENCE
Fusheng Chen
chenfs@mail.hzau.edu.cn

SPECIALTY SECTION
This article was submitted to Food Microbiology, a section of the journal Frontiers in Microbiology

RECEIVED 30 May 2022
ACCEPTED 06 September 2022
PUBLISHED 29 September 2022

CITATION
Yang H, He Y, Liao J, Li X, Zhang J, Liebl W and Chen F (2022) RNA-Seq transcriptomic analysis reveals gene expression profiles of acetic acid bacteria under high-acidity submerged industrial fermentation process.
Front. Microbiol. 13:956729.
doi: 10.3389/fmicb.2022.956729

RNA-Seq transcriptomic analysis reveals gene expression profiles of acetic acid bacteria under high-acidity submerged industrial fermentation process

Haoran Yang[1,2,3], Yating He[1,2], Jing Liao[1,2], Xin Li[4], Junhong Zhang[4], Wolfgang Liebl[3] and Fusheng Chen[1,2]*

[1]Hubei International Scientific and Technological Cooperation Base of Traditional Fermented Foods, Huazhong Agricultural University, Wuhan, Hubei, China, [2]College of Food Science and Technology, Huazhong Agricultural University, Wuhan, Hubei, China, [3]Chair of Microbiology, Technical University of Munich, Freising, Germany, [4]Jiangsu Hengshun Vinegar Industry Co., Ltd, Zhenjiang, Jiangsu, China

Acetic acid bacteria (AAB) are Gram-negative obligate aerobics in Acetobacteraceae family. Producing acetic acid and brewing vinegars are one of the most important industrial applications of AAB, attributed to their outstanding ability to tolerate the corresponding stresses. Several unique acid resistance (AR) mechanisms in AAB have been revealed previously. However, their overall AR strategies are still less-comprehensively clarified. Consequently, omics analysis was widely performed for a better understanding of this field. Among them, transcriptome has recently obtained more and more attention. However, most currently reported transcriptomic studies were conducted under lab conditions and even in low-acidity environment, which may be unable to completely reflect the conditions that AAB confront under industrialized vinegar-brewing processes. In this study, we performed an RNA-Seq transcriptomic analysis concerning AAB's AR mechanisms during a continuous and periodical industrial submerged vinegar fermentation process, where a single AAB strain performed the fermentation and the acetic acid concentration fluctuated between ~8% and ~12%, the highest acidity as far we know for transcriptomic studies. Samples were directly taken from the initial (CK), mid, and final stages of the same period of the on-going fermentation. 16S rRNA sequence analysis indicated the participation of *Komagataeibacter europaeus* in the fermentation. Transcriptomic results demonstrated that more genes were downregulated than upregulated at both mid and final stages. Kyoto Encyclopedia of Genes and Genomes (KEGG) enrich analysis reflected that the upregulated genes mainly carried out tricarboxylic acid cycle and oxidative phosphorylation processes, probably implying a considerable role of acetic acid overoxidation in AR during fermentation. Besides, upregulation of riboflavin biosynthesis pathway and two NAD^+-dependent succinate-semialdehyde dehydrogenase-coding genes suggested a critical role of succinate oxidation in AR. Meanwhile, downregulated genes were mainly ribosomal protein-coding ones, reflecting that the adverse impact on ribosomes initiates at the transcription level. However, it is ambiguous

whether the downregulation is good for stress responding or it actually reflects the stress. Furthermore, we also assumed that the fermentation stages may have a greater effect on gene expression than acidity. Additionally, it is possible that some physiological alterations would affect the AR to a larger extent than changes in gene expression, which suggests the combination of molecular biology and physiology research will provide deeper insight into the AR mechanisms in AAB.

KEYWORDS

acetic acid bacteria, industrial submerged fermentation, high acidity, RNA-seq transcriptome, acid resistance mechanisms

Introduction

Acetic acid bacteria (AAB) are Gram-negative obligate aerobics in the family of Acetobacteraceae (Saichana et al., 2015). Their multiple membrane-bound dehydrogenases are capable of incompletely oxidizing a series of alcohols, sugars, and sugar alcohols to the corresponding aldehydes, ketones, and carboxylic acids, which is named as oxidative fermentation and has been extensively applied in industries (Adachi et al., 2003; Matsushita and Matsutani, 2016; Qin et al., 2022). Of these, the production of acetic acid from incomplete oxidation of ethanol is one of the most important features of AAB and has been used for vinegar production around the world (Gullo et al., 2014; Yang et al., 2022). Strains within species of *Acetobacter pasteurianus* and *Komagataeibacter europaeus* are most commonly used for vinegar brewing, attributed to their remarkable ability to produce as well as tolerate acetic acid (Gullo et al., 2014; Wang et al., 2015a). Under certain conditions, AAB strains are able to produce as high as 20% of acetic acid (Sokollek et al., 1998). However, acetic acid will cause the stress from several aspects (Trcek et al., 2015), while only 0.5% of acetic acid is sufficient to impose a lethal effect on many other microorganisms (Conner and Kotrola, 1995). Therefore, knowledge on the acid resistance (AR) mechanisms of AAB might be critical to reduce the harmful effect of acetic acid on the cells during the fermentation process and further to promote the relevant productivity. In addition, such extraordinary AR mechanisms of AAB that are able to tolerate high acidity are also attracting interests from researchers.

In recent decades, several unique mechanisms that contribute to AR in AAB have been revealed, which have been comprehensively reviewed and elucidated in details (Trcek et al., 2015; Wang et al., 2015a; Nakano and Ebisuya, 2016; Xia et al., 2017; Qiu et al., 2021; Yang et al., 2022). In brief, these mainly include the involvement of pyrroloquinoline quinone (PQQ)-dependent alcohol dehydrogenase (ADH) that also plays an indispensable role in producing acetic acid (Chinnawirotpisan et al., 2003; Trcek et al., 2006), overoxidation of acetic acid through a specialized tricarboxylic acid (TCA) cycle where succinyl-CoA:acetate CoA transferase (also known as AarC) functions as succinyl-CoA synthetase (Mullins et al., 2008), two acetic acid pumping-out systems that are either depended on ATP (Nakano et al., 2006) or proton motive force (PMF; Matsushita et al., 2005), contribution of molecular chaperons (Okamoto-Kainuma and Ishikawa, 2016), and alterations in the compositions of cell membrane (Trcek et al., 2007; Li et al., 2019). These AR-conferring mechanisms are most discussed and accepted by scientists at present (Yang et al., 2022). Recently, some new mechanisms that might be involved in AAB's AR have also been proposed, such as repair of DNA damages under high concentration of acetic acid by protein UrvA (Zheng et al., 2018), 2-methylcitrate cycle (Yang et al., 2019), contribution of two-component signal transduction systems (Xia et al., 2016b, 2020), as well as toxin-antitoxin systems (Xia et al., 2019, 2021).

Unfortunately, the overall AR mechanisms in AAB are still yet to be clarified. It is unclear whether the acetic acid tolerance is resulted from the combination of different biological activities or only benefits from one or few critical but individual and specific processes. In order to obtain a whole view as well as a relatively better understanding of the AR mechanisms in AAB, scientists have carried out omics studies within this field. As a result, several genomes of AAB strains participating acetic acid fermentation were sequenced and analyzed (Azuma et al., 2009; Wang et al., 2015b; Xia et al., 2016a), while proteomic approaches were extensively exploited and have provided a number of important findings regarding AAB's AR mechanisms, which have been reviewed and summarized previously (Nakano and Fukaya, 2008; Xia et al., 2017; Yang et al., 2022). Nowadays, being considered as the important bond linking genome and proteome, transcriptome has been obtaining more and more attentions from the researchers, leading to the reports of many relevant studies. For example, Sakurai et al. (2012) conducted a DNA microarray transcriptomic study which analyzed the gene expression patterns of *A. aceti* NBRC 14818 when the cells were oxidizing ethanol; Okamoto-Kainuma and Ishikawa (2016) carried out an RNA-Seq transcriptomic analysis of AR mechanisms in *A. pasteurianus* NBRC 3283, with special attention to the contribution of molecular chaperons; Yang et al. (2019) reported a transcriptome study concerning AR mechanisms in *A. pasteurianus* CGMCC

1.41 under acetic acid fermentation conditions, which proposed 2-methylcitrate cycle as a potential AR-conferring pathway; Xia et al. (2020) compared the gene expression profiles under high (7%) and low concentration (1%) of acetic acid conditions, focusing on the involvement of two-component signal transduction systems and toxin-antitoxin systems in AR of *A. pasteurianus* Ab3. Recently, Wang et al. (2021) performed a transcriptomic study concerning *K. europaeus* CGMCC 20445 in ethanol-oxidating environment, elucidating the contribution of several different AR mechanisms in *K. europaeus* at different stages of acetic acid fermentation.

However, these studies were all implemented under lab conditions, while some of these studies were even carried out in extremely low-acidity environment (around 1%). As AAB strains are commonly used for industrialized vinegar brewing process, inhabiting in the environment with much higher acidity than the lab conditions can provide, we believe that these studies may not be able to sufficiently reflect the genuine adversities that AAB strains have to deal with and therefore cannot provide the most valuable information for the industrial fermentation process. In this context, we intended to perform this RNA-Seq transcriptomic study within industrial background, collecting samples directly from an on-going continuous and periodical submerged liquid-state acetic acid fermentation process for the production of spirit vinegar in a Chinese vinegar factory, in which a single AAB strain performed the fermentation and the concentration of acetic acid fluctuated between ~8% and ~12% (Figure 1).

Here with this study, the analysis of gene expression patterns of AAB under this industrial fermentation as well as high acidity conditions will be presented, with a special focus on AAB's AR mechanism. We took samples at the initial, mid, and final stages of the same fermentation period (Figure 1) and extracted total RNA for RNA-Seq transcriptome analysis. In parallel, a 16S rRNA sequence analysis together with the corresponding phylogenic analysis was also conducted in order to identify the AAB species executing the submerged fermentation and therefore select a proper reference genome for transcriptome analysis. Finally, a detailed elucidation of the transcriptome results based on Kyoto Encyclopedia of Genes and Genomes (KEGG) enrichment analysis would also be performed.

Materials and methods

Submerged fermentation, sample collection, and preparation

The submerged acetic acid fermentation was conducted uninterruptedly and periodically in the industrialized fermentor (Frings Co., Bonn, Germany). Bacterial strain used to execute the fermentation was provided by the fermentor manufacturer as part of the fermentation equipment. However, at the time of carrying out this study, the taxonomy background of this strain was unknown. Clarified and sterilized rice wine was constantly supplied in order to maintain the ethanol concentration around 3%. The fermentation was carried out at 30°C. When the acidity in the fermentor reached around 12%, which took about 17 h since a new fermentation period started, 1/3 volume of the fermentation broth was discharged for further processes of the spirit vinegar production. Subsequently, an equal volume of fresh medium prepared with Angel® Vinegar Fermentation Nutrient Salt (Angel Yeast Co., Ltd., Yichang, China) according to the instruction of the manufacturer was supplied to initiate a new period of

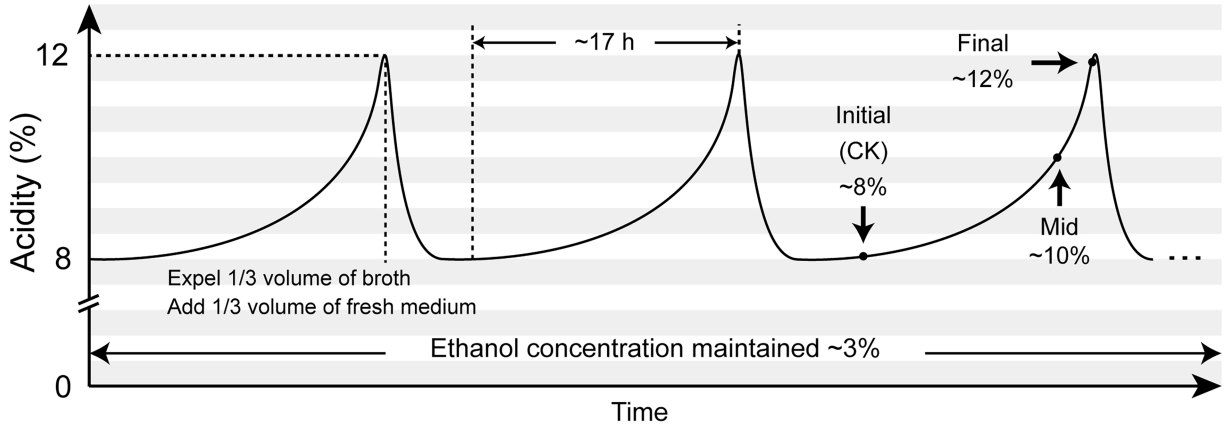

FIGURE 1
Illustration of the submerged liquid state fermentation process for sprit vinegar production and sampling plan. The submerged acetic acid fermentation was carried out uninterruptedly and periodically in a Chinese vinegar factory. Each fermentation period lasted for around 17h, with the maximum acidity reaching around 12%. The concentration of ethanol was kept around 3% at all times. A fermentation period was terminated by discharging one-third volume of the fermentation broth, while a new period was initiated by adding another equal volume of the fresh medium. In this way, the acidity within the fermentor fluctuated between ~8% and ~12%. Samples for this transcriptomic study were collected at the initial, mid, and final stages within the same fermentation period.

TABLE 1 Sample information of the transcriptomic analysis.

Sample name	Acidity (%)	Time since the start of the fermentation period (h)
Initial (CK)	8.1	0.5
Mid	10.5	12.5
Final	11.7	16.5

fermentation, which simultaneously reduced the acidity in the fermentor to ~8% (Figure 1).

Samples were directly collected from the fermentor without disturbing the fermentation. At each scheduled sampling time point, that is, initial, mid, and final stages within the same fermentation period (Figure 1; Table 1), 50 ml of the sample was collected in a sterilized 50 ml centrifuge tube and was quickly put in ice, prior to which, 1 ml of the collected sample was pipetted out for determination of acidity by titration with 0.1 M NaOH solution. Cells in the remaining 49 ml sample were pelleted followed by washing twice with 25 ml ice-cold 1 M sodium acetate (pH 5.2). Finally, the washed cell pellets were suspended in 500 µl 1 M sodium acetate (pH 5.2) and stored under −80°C for 12 ~ 24 h prior to RNA extraction. The centrifuge was all carried out under 5,000 rpm for 10 min and 4°C for the above-mentioned manipulation. Two replicate samples were independently collected for each scheduled sampling point. Extraction of total RNA was performed as described by Yang et al. (2019).

16S rRNA sequence analysis

In order to identify the AAB species performing the fermentation, 16S rRNA fragment was amplified followed by sequence comparison and phylogenic analysis. This was carried out as described by Yang and Zhou (2014) with modification. 1 ml of the fermentation broth collected separately from the samples for RNA-Seq was centrifuged at 11,000 rpm for 2 min. The obtained pellet was then resuspended with 50 µl lysis buffer (Leagene Biotechnology Co., Beijing, China) and was put in a water bath of 95°C for 20 min, followed by centrifugation at 12,000 rpm for 2 min. The obtained supernatant was diluted by 10× with sterilized ddH_2O and then was used as the template of PCR. PCR was conducted with Phanta Max Master Mix (Vazyme Biotechnology Co., Nanjing, China) in the volume of 25 µl and with primer pair P0 (5′-GAGAGTTTGATCCTGGCTCAG-3′) and P6 (5′-CTACGGCTACCTTGTTACGA-3′). PCR program was set according to the manual of PCR master mix. PCR products were then cleaned up with EasyPure PCR Purification Kit (TransGen Biotech Co., Beijing, China). Cleaned PCR products were subsequently the subjects for Sanger DNA sequencing, which was carried out by Sangon Biotech Co., Ltd. (Shanghai, China). The obtained sequence then acted as the query for conducting an online BLASTn search. The 16S rRNA sequence generated in this study now can be found at GeneBank[1] with accession number OP164709.

For providing a clearer view of the taxonomy relationship, a phylogenic analysis based on 16S rRNA sequences was further conducted. Sequences from type strains of the relevant species were used to indicate the species position within the phylogenic tree. The information of species type strains was obtained from List of Prokaryotic names with Standing in Nomenclature.[2] All 16S rRNA sequences except the one generated in this study were downloaded from NCBI Nucleotide database.[3] Phylogenic tree was constructed by MEGA 7.0 software with the Neighbor-Joining method. Bootstrap method was used for phylogeny test with 1000 times of the bootstrap replications.

Transcriptomic sequencing and data analysis

The purity and quality of the extracted RNA samples were evaluated by NanoDrop and Agilent 2100 Bioanalyzer, respectively. Upon good quality, rRNA was removed followed by the fragmentation of the samples. cDNA library was constructed with Illumina TruSeq Stranded Kit. Sequencing was then conducted with the HiSeq sequencing platform. The obtained raw reads were subsequently undergone a series of quality control processes including the removal of reads containing adaptor contamination as well as those containing more than 5% of the unknown bases (N) for downstream analysis. Reads with accepted quality were then mapped to the reference genome and reference genes with HISAT (2.0.1-beta; Kim et al., 2015) and Bowtie2 (2.2.5; Langmead and Salzberg, 2012) software, respectively. Based on the mapping data, RSEM (Li and Dewey, 2011) software was used to calculate the expression value of each gene, which was presented with Fragments Per Kilobase Million (FPKM) value. Based on the comparison scheme, differently expressed genes (DEGs) were identified by DESeq2 algorithm (Love et al., 2014) with the criteria of fold change ≥2 together with Bonferroni-corrected p value ≤0.05. The screened up- and downregulated genes of each treatment sample then separately acted as the subjects of KEGG enrichment analysis, which was carried out on OmicShare platform.[4] KEGG terms with false discovery rate-corrected value of $p \leq 0.05$ were regarded as the enriched terms of the up- or downregulated genes within a treatment sample. Expression data were visualized as heatmaps using TBtools software (Chen et al., 2020). The transcriptomic data now can be found at Gene Expression Omnibus database[5] with accession number GSE210697.

1 https://www.ncbi.nlm.nih.gov/genbank/
2 https://lpsn.dsmz.de/
3 https://www.ncbi.nlm.nih.gov/nuccore/
4 http://www.omicshare.com/tools/
5 https://www.ncbi.nlm.nih.gov/geo/

Results

Microorganism identification, reference genome selection, and transcriptomic data overview

Since *K. europaeus* is regarded as the participator of submerged acetic acid fermentation (Gullo et al., 2014; Wang et al., 2015a), the strain inhabiting within the fermentor and conducting the fermentation in this study was expected to belong to this species. In order to verify this and therefore select a proper reference genome for transcriptome analysis, a 16S rRNA gene comparison was carried out prior to any other analysis. Online BLAST analysis results are listed in Table 2, which showed many hits to *Komagataeibacter* strains. Even though *Bacillus amyloliquefaciens* is also present in Table 2, we believe that this was an error in the information of the relevant sequence (MH824159), as the BLAST search using this sequence as the query only resulted in hit to *Komagataeibacter* 16S rRNA sequences instead of any other sequences from *Bacillus*, while currently there is also no report presenting the involvement of *Bacillus* species in submerged acetic acid fermentation. Meanwhile, *K. xylinus* and *K. swingsii* are also shown in Table 2. According to a phylogenic tree of 16S rRNA sequence from type strains of all AAB species reported by July 2021 (Yang et al., 2022), 16S rRNA sequence of *K. europaeus* and *K. swingsii* were identical, which explains the presence of *K. swingsii* in Table 2. In contrast, distance exists between *K. europaeus* and *K. xylinus*. On the other hand, *K. xylinus* strains shown in Table 2 were reported to possess the outstanding cellulose-producing ability (Ryngajłło et al., 2019; Du et al., 2020; Lu et al., 2020), which is the prominent feature of species *K. xylinus* acting as the model organism for studying bacterial cellulose production (Gullo et al., 2018). However, the production of bacterial cellulose is common among *Komagataeibacter* strains (Ryngajłło et al., 2019), including *K. europaeus*, in which cellulose-producing ability was also reported (Dubey et al., 2017). Thus, we assume that the *K. xylinus* strains listed in Table 2 may actually belong to *K. europaeus*.

TABLE 2 Top 10 hits of online BLASTn search using the sequence of 16S rRNA PCR product amplified from the samples in this study as the query.

Strain name	*E* value	Identity	Accession	Sequence type
Komagataeibacter europaeus DHBR3702	0	100%	MH845618.1	16S rRNA
Bacillus amyloliquefaciens BH072-1	0	100%	MH824159.1	16S rRNA
Komagataeibacter xylinus TJU-D2	0	100%	MH588135.1	16S rRNA
Komagataeibacter europaeus SRCM101446	0	100%	CP021467.1	complete genome
Komagataeibacter xylinus E25	0	100%	CP004360.1	complete genome
Komagataeibacter europaeus KGMA0119	0	100%	AB818453.1	16S rRNA
Komagataeibacter xylinus DSM 46603	0	100%	MZ435949.1	16S rRNA
Komagataeibacter swingsii JCM 17123	0	100%	NR_113400.1	16S rRNA
Komagataeibacter europaeus NBRC 3261	0	100%	AB680040.1	16S rRNA
Komagataeibacter xylinus OTG001	0	100%	MT730006.1	16S rRNA

In order to further provide evidence for the hypotheses above, while given the fact that Table 2 could not provide a clear view of the taxonomy relationship, a Neighbor-Joining phylogenic tree was constructed using 16S rRNA sequences of the relevant strains, in which the sequences from the type strains of *K. xylinus*, *K. europaeus*, and *B. amyloliquefaciens* were set as the indicator of species position (Figure 2). It was demonstrated that the type strains of *B. amyloliquefaciens* and other *Komagataeibacter* species reside in two distinct clusters of the tree, while *B. amyloliquefaciens* BH072-1 stays with *K. europaeus* type strains, reflecting the error in taxonomy information about the sequence with accession number MH824159 on NCBI. Additionally, *K. xylinus* DSM 46603, OTG001, and TJU-D2, as well as 16S rRNA sequence generated in this study, were found present within the same subcluster as *K. europaeus* type strains, which indicated that these claimed *K. xylinus* strains may be more likely to belong to *K. europaeus* from this point of view, and that the genome of a *K. europaeus* strain can be a suitable reference genome for this study. As the fact that the complete genome of *K. europaeus* SRCM101446, which is also shown in Table 2 with 100% identity, was available at NCBI Genome data base (Bioproject No. PRJNA386757) at the time when this study was conducted, we therefore chose it as the reference genome for this transcriptome analysis.

Samples for this transcriptomic study were taken from the initial (acidity: 8.1%), mid (acidity: 10.5%), and final (acidity: 11.7%) stages of the same fermentation period of the continuous submerged liquid state fermentation process, in which the fermentation period had initiated for 0.5, 12.5, and 16.5 h, respectively (Figure 1; Table 1). Prior to cDNA library construction, the integrity of the extracted RNA was checked by Agilent 2100 Bioanalyzer and was regarded as qualified for further manipulation. In addition, reads obtained from RNA-Seq transcriptomic sequencing also passed the quality control, while more than 70% of the reads from each sample were mapped to the reference genome, which indicated that choosing the genome of *K. europaeus* SRCM101446 was feasible for this study and that the alignment results were sufficient to carry out subsequent expression qualification analysis. The sample group collected from the initial fermentation stage was set as the control group (CK) for the

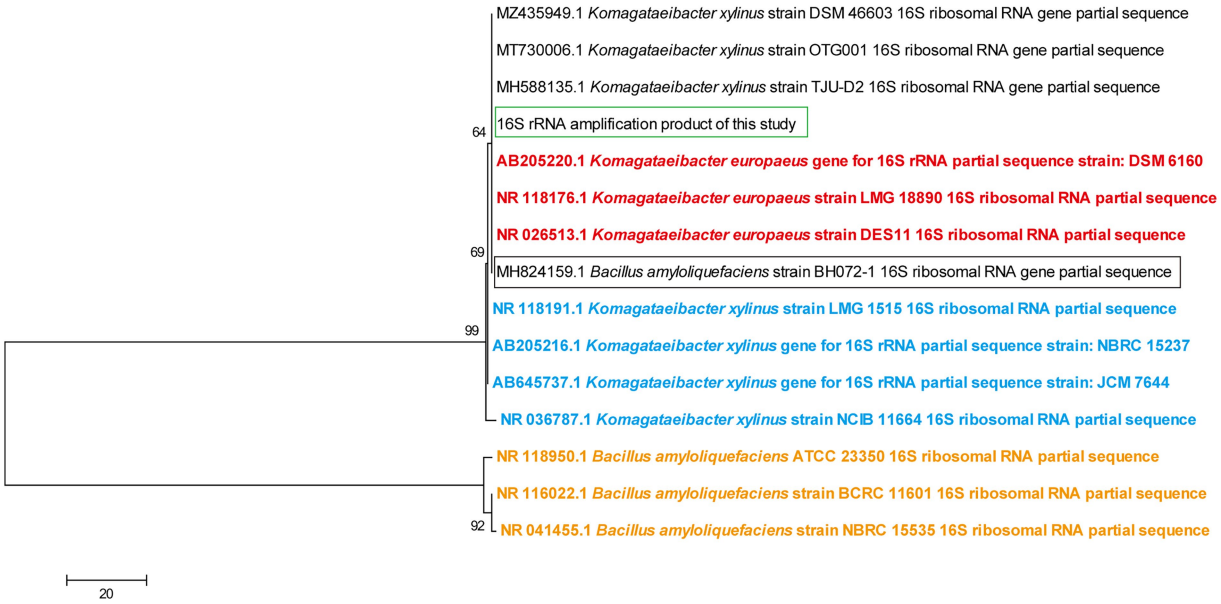

FIGURE 2
Neighbor-Joining phylogenic tree based on 16S rRNA sequences of relavant strains. Sequences from type strains of *Komagataeibacter europaeus*, *Komagataeibacter xylinus*, and *Bacillus amyloliquefaciens* were shown in red, blue, and orange font, respectively. 16S rRNA sequence that was amplified in this study and was from *B. amyloliquefaciens* BH072-1 was marked with a green and black box, respectively. Numbers next to the corresponding nodes indicate the bootstrap value (%) after 1,000 times of replication.

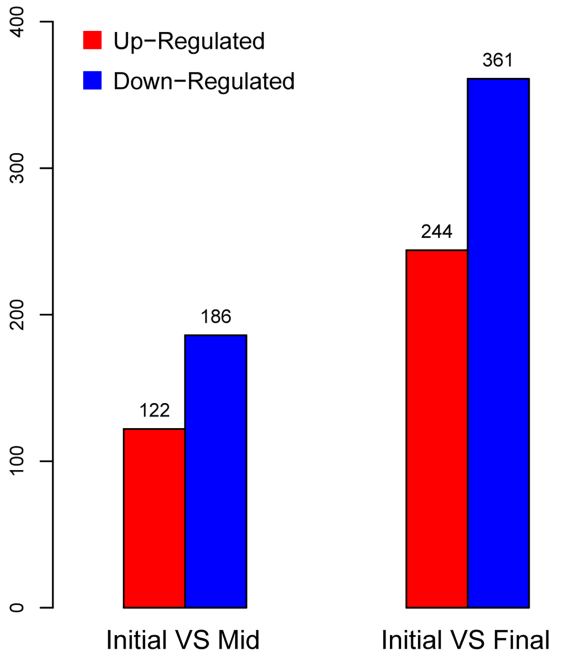

FIGURE 3
Statics of differently expressed genes (DEGs) within treatment samples.

analysis regarding DEGs. Based on this, it was found that more genes were downregulated than upregulated when the fermentation entered mid and final stages, that is, 186, 361 genes were downregulated, while only 122,244 genes were upregulated at the mid and final stage of fermentation, respectively (Figure 3). In addition, it is also worth noting that the number of DEGs in the final stage was around twice as many as that in the mid stage, suggesting that cells were undergone more changes in biological activities in respond to the increasing amount of acetic acid.

In order to further elucidate the transcriptomic data and obtain more insight into the gene expression profile, the following paragraphs will present a detailed analysis based on KEGG enrichment analysis, of which the detailed results are shown in Supplementary Table S1.

Detailed transcriptomic data analysis based on KEGG enrichment

TCA cycle and oxidative phosphorylation

Tricarboxylic acid cycle and oxidative phosphorylation both play critical roles in energy metabolism, in which, a large amount of NADH is produced by TCA cycle and will be further oxidated through oxidative phosphorylation, that is, respiratory chain, to generate PMF for ATP synthesis. In the context of AAB's acetic acid production and AR mechanisms, both of these processes have gained much attention, as TCA cycle plays a dominate part in acetic acid overoxidation, while enzymes that produce acetic acid from incomplete ethanol oxidation, that is, PQQ-ADH and PQQ-aldehyde dehydrogenase (ALDH; Saichana et al., 2015), also form a special ethanol respiratory chain (Yakushi and Matsushita,

2010; Yang et al., 2019, 2022; Figure 4). It was found that KEGG terms of "TCA cycle" and "oxidative phosphorylation" were significantly enriched within the upregulated genes in both mid and final stages of fermentation (Supplementary Table S1). As TCA cycle is regarded as the major pathway responsible for acetic acid overoxidation, while the subsequently generated NADH and succinate can participate in electron transfer process that yields a large amount of ATP, the significant upregulation of almost all the genes involved in both metabolic processes and the enrichment of relevant KEGG terms may reflect that acetic acid overoxidation probably still contributes considerably to AR in AAB under acetic acid fermentation conditions, especially in terms of the energy metabolism, even though previously it was not regarded as the main AR-conferring mechanism during ethanol oxidation (Kanchanarach et al., 2010; Yang et al., 2019). In addition, it was also demonstrated that *acs* (RS16030, RS02790), *ackA* (RS13330), and *pta* (RS14395), of which the product convert acetic acid into acetyl-CoA, were all upregulated during the fermentation process, while significant changes in the expression of these genes was not observed in a previous transcriptomic study regarding *A. pasteurianus* (Yang et al., 2019). Moreover, *K. europaeus* simultaneously harbors genes encoding common succinyl-CoA synthetase complex (RS00155 and RS00160) and AarC (RS05360), where the former were downregulated and the latter was upregulated (Figure 4; Supplementary Table S2). These together might indicate that *K. europaeus*, especially under industrial submerged fermentation conditions, can overoxidize acetic acid in a more effective way, which is therefore in line with the fact that *K. europaeus* is able to tolerate more acetic acid than *A. pasteurianus* (Wang et al., 2015a; Barja et al., 2016). However, both in mid and final stages, changes in the expression of almost all of the genes encoding the components of ethanol respiratory chain, that is, PQQ-ADH and PQQ-ALDH, did not meet the set criteria of DEGs (fold change ≥2, Figure 4; Supplementary Table S2), probably due to the constant concentration of ethanol (around 3%) throughout the fermentation process. On the other hand, the fold change of PQQ-ADH genes, including *adhB* (RS14865), *adhA* (RS14870), and its two paralogs (RS07925 and RS01330), was higher than those of PQQ-ALDH, with RS14870 was even found upregulated more than 2-fold at the final stage of the fermentation (Supplementary Table S2), which may again emphasize the contribution of PQQ-ADH to the AR when cells are facing high concentration of acetic acid. In addition, genes encoding ATP synthetase complex were found downregulated under higher acidity conditions (Figure 4; Supplementary Table S2), which was more likely to be resulted from the stress of a large amount of acetic acid that was imposed on the cells.

Riboflavin biosynthesis pathway and succinate-semialdehyde dehydrogenase

"Riboflavin metabolism" is another KEGG term that was significantly enriched within the upregulated genes (Supplementary Table S1). Subsequently, we discovered that all the genes responsible for riboflavin biosynthesis were upregulated at both mid and final stages of fermentation (Figure 5). Riboflavin can act as the backbone of a variety of relevant derivatives (such as FMN and FAD) that consist of several flavoproteins, which are mainly involved in a series of redox biochemical reactions and photosensitization (García-Angulo, 2017). To our knowledge, currently, there is no report concerning the effect of light on *K. europaeus* and other AAB species. Hence, it is reasonable to assume that the upregulation of riboflavin biosynthesis pathway mainly contributed to redox processes, especially those related to energy metabolism, which might be a very important biological activity during later stages of acetic acid fermentation. Besides, KEGG term of "Butanoate metabolism" was also present in the enriched list within upregulated genes (Supplementary Table S1), where only genes coding for enzymes related to succinate metabolism were upregulated, including succinate dehydrogenase complex, AarC, and two NAD^+-dependent succinate-semialdehyde dehydrogenases. Succinate-semialdehyde dehydrogenase catalyzes the oxidation of succinate-semialdehyde, which yields succinate and is involved in glutamate metabolism (Fuhrer et al., 2007). As it is well-known that succinate dehydrogenase complex, of which the relevant genes were also found upregulated in this study, operates in an FAD-dependent manner and therefore requires the support of riboflavin supply, these findings here together may suggest a critical role of succinate when AAB cells have to deal with the relatively high amount of acetic acid, in particular, under the context of succinate oxidation within the field of energy metabolism.

Downregulated ribosome-related protein-coding genes

Among downregulated genes, there were almost no KEGG terms that were significantly enriched, except for "Ribosome" (Supplementary Table S1). Many ribosomal protein-coding genes were significantly downregulated during the mid and final stages of the fermentation (Figure 6). Previously, proteomic analysis indicated that ribosomal proteins would be downregulated as the concentration of acetic acid increases (Andrés-Barrao et al., 2012; Xia et al., 2016b). In addition, a recent transcriptomic study regarding *K. europaeus* also demonstrated that genes encoding ribosomal proteins were downregulated during the fermentation process (Wang et al., 2021). Hence, our results here once again suggest that the downregulation of the expression of ribosomal proteins may initiate at the transcription level. As their critical role in protein biosynthesis, ribosomes are always essential for all kinds of biological activities. Therefore, the downregulation of ribosome-related genes might actually reflect the stress from high concentration of acetic acid. However, at present, more evidence is still required to clarify the actual relationship between the downregulated ribosome-related genes and high acetic acid concentration.

Other downregulated genes were expected to involve in a wider range of different metabolic processes, as the fact that

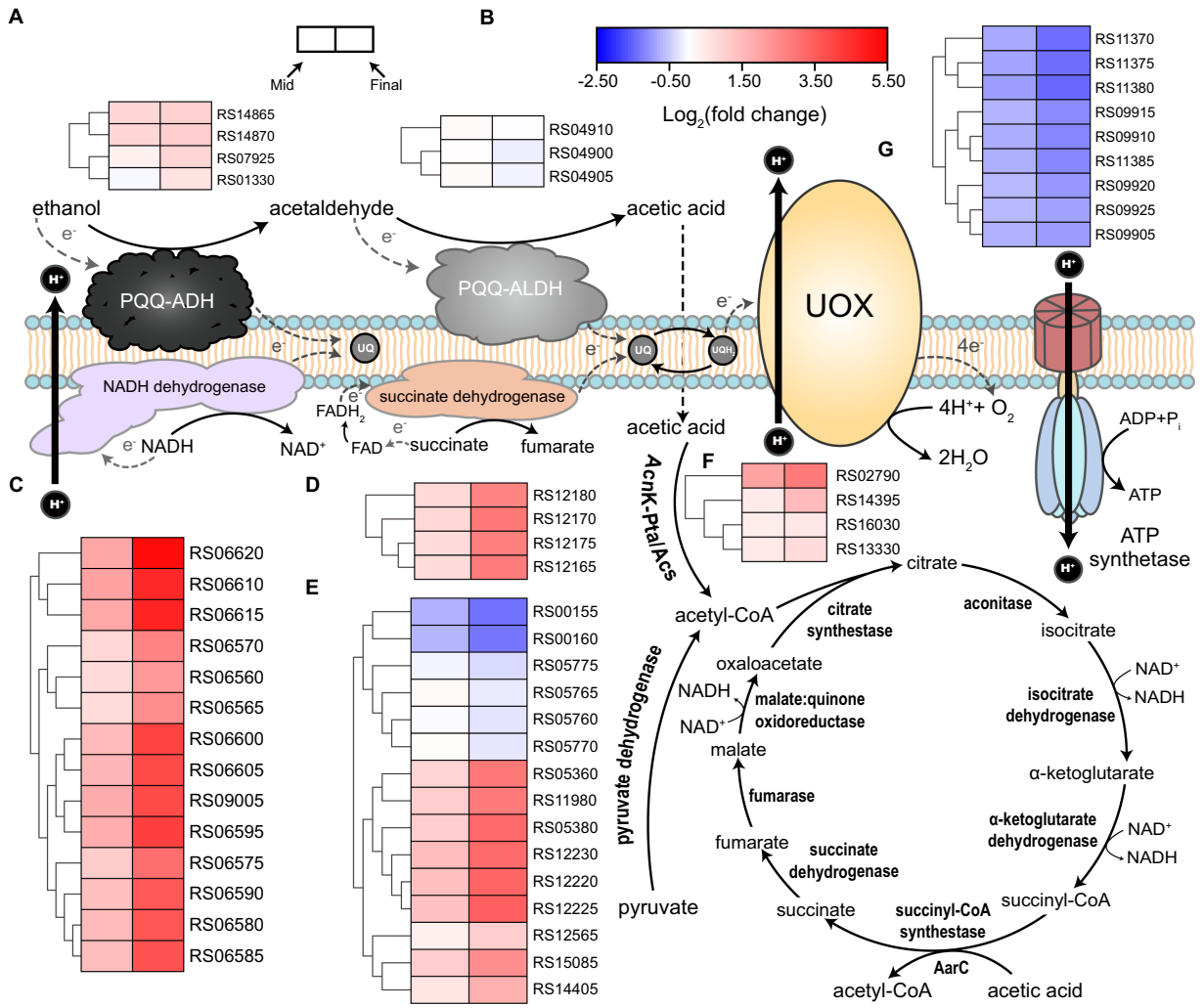

FIGURE 4
Illustration of respiratory chain and tricarboxylic acid (TCA) cycle together with the expression patterns of related genes. Acetic acid bacteria (AAB) cells possess both ethanol respiratory chain, which consists of PQQ-ADH and PQQ-ALDH, and common respiratory chain based on NADH and succinate dehydrogenase. Both respiratory chains deprive electrons from corresponding substrates and transfer them to ubiquinone (UQ), which is consequently reduced to ubiquinol (UQH_2). UQH_2 then transfers the electrons to ubiquinol oxidase (UOX) so that to be oxidized back to UQ. Finally, oxygen gains electrons from UOX, and then water is formed. NADH dehydrogenase and UOX are able to utilize the energy released from relevant redox reactions to expel protons out of the cells, generating proton motive force that can be used to yield ATP by ATP synthetase. Acetic acid produced by the ethanol respiratory chain from the incomplete oxidation of ethanol can penetrate into the cells and then is transferred to acetyl-CoA, which can be conducted either by the combination of acetate kinase (AckA) and phosphotransacetylase (Pta), or acetyl-CoA synthetase (Acs), or AarC. These processes enable acetic acid to enter TCA cycle and therefore act as a carbon source. Gene expression patterns (heatmap) together with the corresponding gene ID are present besides the relevant components or metabolic pathways, in which, **(A)** PQQ-ADH; **(B)** PQQ-ALDH; **(C)** NADH dehydrogenase; **(D)** succinate dehydrogenase; **(E)** TCA cycle; **(F)** AckA, Pta, and Acs; and **(G)** ATP synthetase. Detailed gene annotations and expression data are shown in Supplementary Table S2.

they accounted for the majority of DEGs but were rarely enriched to certain KEGG terms. Meanwhile, although more KEGG terms were enriched within the upregulated genes, it was hard to obtain clear clues from most of the enriched terms, as many upregulated genes within these terms cannot form intact presently known and curated metabolic pathways. Therefore, it is difficult to clarify the relationship between these genes and biological activities under acetic acid fermentation conditions at present, which requires further comprehensive and detailed studies.

Discussion

In this study, we reported an RNA-Seq transcriptomic analysis of AAB concerning their AR mechanisms under acidity between ~8% and ~12%, the highest acidity as far we know for transcriptomic studies. Besides, our samples were directly taken from the production line of an industrial submerged acetic acid fermentation process, revealing gene expression patterns under realistic application background. Therefore, we believe the results presented in this study are of more practical value, which

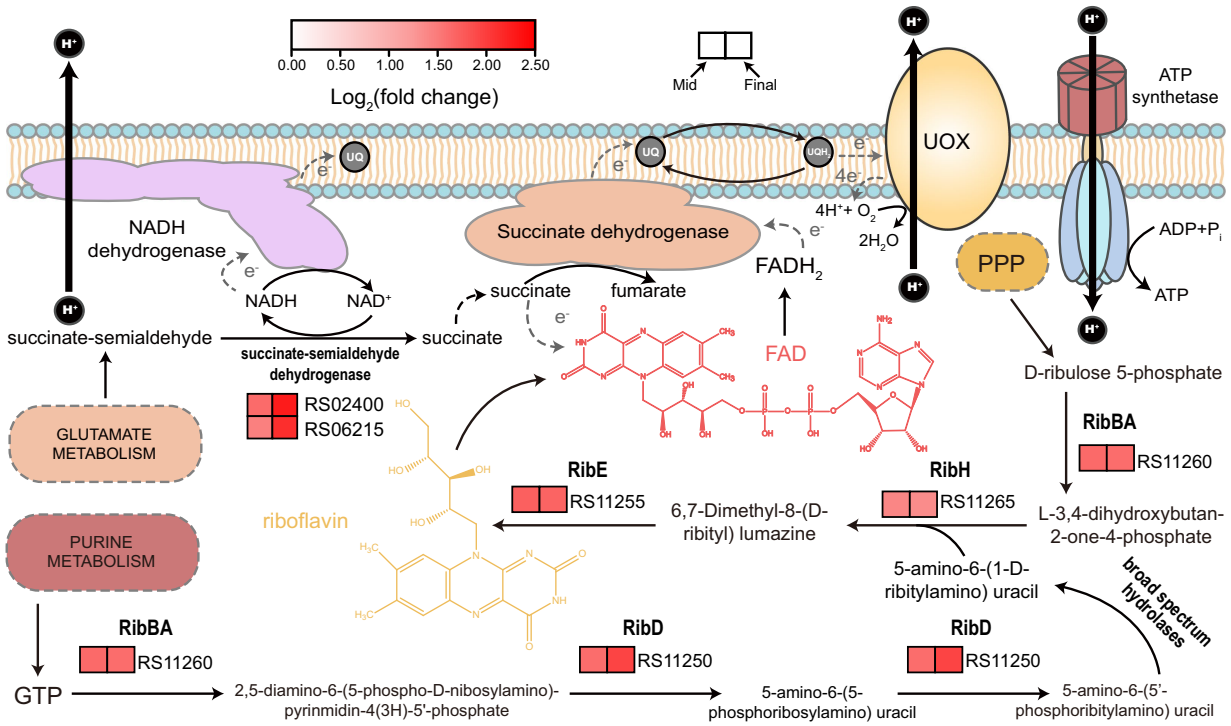

FIGURE 5
Illustration of riboflavin biosynthesis and its relationship to succinate oxidation together with relevant gene expression patterns. GTP from purine metabolism and D-ribulose 5-phosphate from pentose phosphate pathway (PPP) act as the start point of riboflavin biosynthesis. FAD is one of the derivatives of riboflavin and is related to succinate oxidation, which is a part of respiratory chain, as demonstrated in Figure 4. Succinate can be also obtained from oxidation of succinate-semialdehyde in an NAD^+-dependent manner, which is also related to glutamate metabolism. Expression patterns (heatmap) with relevant gene ID are shown besides the biochemical reactions catalyzed by the corresponding gene products. Detailed expression data and gene annotations are listed in Supplementary Table S2. RibBA, 3,4-dihydroxy-2-butanone-4-phosphate synthase; RibD, bifunctional diaminohydroxyphosphoribosylaminopyrimidine deaminase; RibE, riboflavin synthase; and RibH, 6,7-dimethyl-8-ribityllumazine synthase.

simultaneously can provide important evidence to support AR mechanisms that were proposed previously.

Our analysis reflected that the contribution of overoxidation of acetic acid to AR during fermentation may not be ignored, although the catabolism of acetic acid has been regarded as undesired and suppressed to some extent during acetic acid fermentation, since it is contradictory to the aim and the fact of the accumulation of a large amount of acetic acid (Kanchanarach et al., 2010; Yang et al., 2019). Besides, in a previous transcriptomic analysis, the shift of the main means of energy supply from ethanol oxidation to acetic acid overoxidation was presented, in which the degree of downregulation (compared to non-ethanol-oxidating conditions) of both TCA cycle and oxidative phosphorylation process based on NADH and succinate dehydrogenases was alleviated as the fermentation went by (Yang et al., 2019), a finding that was actually in accordance with the upregulation of both of these processes shown in this study. The trade-off between the common respiratory chain and the special respiratory chains for oxidative fermentation may extensively exist among more AAB species (Kostner et al., 2015). Unfortunately, here, we could not provide more direct evidence supporting this shift. This might be due to the reasons from two aspects. Firstly, in the aforementioned transcriptomic study, the control sample was collected from the culture without producing acetic acid, which was unable to be performed under industrial submerged fermentation conditions in this study, and consequently, we could not show the expression patterns of relevant genes that are exactly similar with previous one, in particular, drastic downregulation of TCA cycle and common respiratory chain at the initial stage of fermentation was absent. Secondly, significant downregulation of genes coding for ethanol respiratory chain was also not observed in this study (Figure 4). As the concentration of ethanol was always kept around 3% throughout the fermentation process, cells might use ethanol respiratory chain to constantly oxidize ethanol for energy generation. From this point of view, the balance effect between the two different respiratory chains and different means of energy metabolism may not be as obvious and necessary as under the conditions of previous studies. Furthermore, the expression of genes encoding the PQQ-ADH complex retained at a relatively high level during the whole fermentation period, while gene *adhA* was even up-regulated about 2-fold at the final stage (Figure 4; Supplementary Table S2), which probably suggested again the importance of PQQ-ADH in AR.

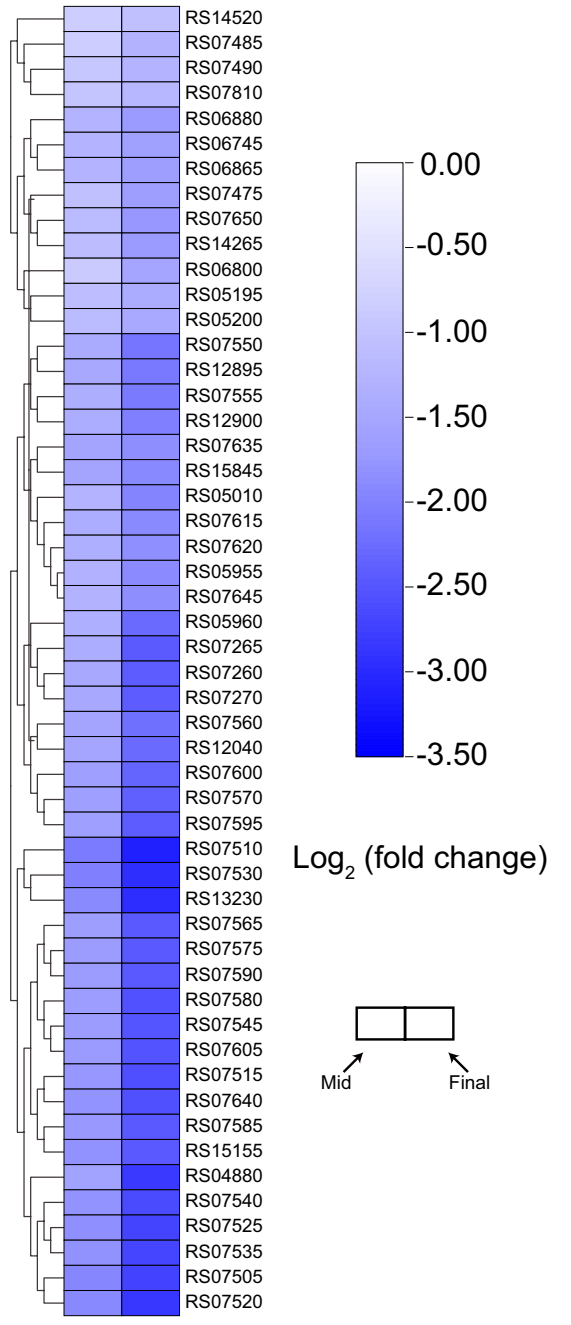

FIGURE 6
Expression pattern of genes encoding ribosome component. Detailed gene annotation and expression data are listed in Supplementary Table S2.

Succinate, the compound itself and/or the related metabolisms, may also play a considerable part in stress respond during acetic acid fermentation. In this study, genes coding for enzymes that participate in several processes with regard to succinate were found upregulated, including succinate-semialdehyde dehydrogenases (Figure 5), AarC, and succinate dehydrogenase complex (Figure 4). Both succinate-semialdehyde dehydrogenases and AarC catalyze reactions generating succinate, while succinate dehydrogenase is responsible for its oxidation. It is worth noting that succinate-semialdehyde dehydrogenases may also be associated with glutamate metabolism, while adding glutamate was found positively related to AR in *A. pasteurianus* (Yin et al., 2017). Hence, it is possible that the additional glutamate in the culture strengthened the AR partially by means of the enhanced succinate supply. In addition, adding succinate has been proven to be able to enhance acetic acid fermentation (Qi et al., 2013) while two previously proposed potential AR-conferring metabolic pathways in *Acetobacter* strains, that is, 2-methylcitrate cycle (Yang et al., 2019) and glyoxylate pathway (Sakurai et al., 2013), can also result in an additional supply of succinate. These findings altogether may further demonstrate the relationship between succinate and AR. Moreover, genes within the riboflavin biosynthesis pathway were significantly upregulated as well (Figure 5), which was assumed to link with succinate oxidation to some extent. Under such context, it is suggested that the involvement of succinate in AR of AAB may particularly lie in the contribution to the common respiratory chain, which was also found upregulated (Figure 4) and discussed above. Therefore, we believe that the further investigation into the relationship between succinate, perhaps also together with its oxidation metabolism, and AR may lead to more novel findings.

Although downregulated genes accounted for a large fraction of DEGs (Figure 3), almost all of their KEGG terms did not show significant enrichment, with the exception of "Ribosome" (Figure 6; Supplementary Table S1). The downregulation of ribosome-related genes under higher acidity conditions, both on transcription (Wang et al., 2021) and translation level (Andrés-Barrao et al., 2012; Xia et al., 2016b), was also demonstrated previously. Besides, genes coding for ATP synthetase complex were as well downregulated at the mid and final stages of fermentation (Figure 4), despite that the related KEGG terms were not significantly enriched within downregulated genes. The degree of downregulation of genes related to ATP synthetase and ribosome, which are both well-known to be vital to the basic biological activities of the cells, even increased at the final stage of fermentation (Figures 4, 6). However, it is incredible to draw such a conclusion that the downregulation of the essential genes is beneficial to the cells, or, these genes are harmful to the cells under stressful environment. On the other hand, since here we are quite in short of more compelling evidence, it is as well not easy to confirm that the downregulation itself actually reflected the stress, that is, the adverse conditions inhibit the expression of these genes, resulting in a number of negative effects on cells' living activities, even though we would tend to accept this explanation. Do cells need actively downregulate these genes to cope with the stress, or, they are just unable to maintain the normal expression when encountering the stress? This is the question that all omics studies may need to handle, which, however, we pessimistically believe that none of the relevant omics studies can properly answer at the moment. In addition, although it is more rational to presume that cells would upregulate some genes and choose corresponding mechanisms to effectively deal with the stress, the upregulation may also instead act as the reflection of how the cells struggle within the stress, trying to seize the little opportunity for

their survival. From this point of view, the relationship between DEGs and the stress might be more ambiguous and complicated than we expected and is hard to be clearly and objectively elucidated without further investigation. Consequently, we believe that researchers may need to be more cautious when discussing the effect of DEGs on stress responses, especially in the case of down-regulated genes. Besides, more comprehensive investigations are required to be involved to provide more experimental evidence for clarifying the relevant mechanisms in detail.

In this transcriptomic analysis, we obtained the expression patterns of many genes that were similar with the previous studies (Yang et al., 2019; Wang et al., 2021), even though the acidity we presented here was much higher. Nevertheless, it is worth noting that our sampling scheme was also similar with the previous ones, that is, we all planned to collect the samples at different stages of the fermentation. Thus, the combined changes of various factors within the environments of different fermentation stages are expected to have a greater impact on gene expression than acetic acid concentration alone. On the other hand, it is reasonable to expect that upon the survival of the cells, AR mechanisms of AAB work in a more effective way in high acidity environment than under low-acidity conditions. To this end, some physiological changes would be likely to affect the AR to a larger extent than alterations in gene expression, perhaps, such as the previously proposed but yet to be characterized PMF-dependent acetic acid pumping-out system (Matsushita et al., 2005). Additionally, AatA, an ATP-binding cassette transporter for acetic acid, was proved to be involved in AR in AAB (Nakano et al., 2006; Nakano and Fukaya, 2008). However, the transcription of gene *aatA* did not show a significant change as the acidity increased during fermentation (Sakurai et al., 2012; Yang et al., 2019), indicating that the contribution of AatA may not be reflected on the transcription level. In fact, the AR and acetic acid productivity of AAB has been regarded as unstable, as the relevant abilities might be immediately lost without genetical changes if the cells are grown in a acetic acid-free or non-ethanol-oxidating environment (Azuma et al., 2009), which may suggest that maintaining a specific physiological status is crucial to the capabilities of defending the stress from acetic acid. In this case, omics studies focusing on gene expression may have less chance to find out the key factor in AR mechanisms. As a result, researchers probably have to pay more attention to the investigation on physiological activities in terms of AAB's AR mechanisms.

In general, we believe that something other than gene expression could make a more considerable difference in the AR mechanisms of AAB. Therefore, physiological analysis with regard to this field deserves more efforts from the scientists. Additionally, molecular biological research concentrating on the relevant genetic background is still one of the indispensable parts in terms of clarifying the underlying mechanisms. Hence, the combination of molecular biology and physiology research would be a better choice for related studies. Overall, we expect that by carrying out more well-designed and comprehensive studies, a deeper understanding and knowledge of the overall AR mechanism of AAB will be gained in the further.

Data availability statement

The datasets presented in this study can be found in online repositories. The names of the repository/repositories and accession number(s) can be found in the article/Supplementary material.

Author contributions

FC supervised the entire work and planned the experiments. HY carried out the majority of experiments, performed the analysis, and wrote the manuscript. YH and JL participated in the preparation of the figures. XL is in charge of the submerged fermentation and revised the manuscript. JZ contributed to 16S rRNA analysis. WL and FC revised the manuscript. All authors contributed to the article and approved the submitted version.

Funding

This work was funded by Major Special Projects of Technological Innovation of Hubei Province, China (No. 2018ABA075), Programs of International S&T Cooperation, Ministry of Science and Technology, China (No. 2014DFG32380), and China Scholarship Council (202006760070).

Conflict of interest

XL and JZ are employed by the company Jiangsu Hengshun Vinegar Industry Co., Ltd.

The remaining authors declare that the research was conducted in the absence of any commercial or financial relationships that could be construed as a potential conflict of interest.

Publisher's note

Supplementary material

The Supplementary material for this article can be found online at: https://www.frontiersin.org/articles/10.3389/fmicb.2022.956729/full#supplementary-material

References

Adachi, O., Moonmangmee, D., Toyama, H., Yamada, M., Shinagawa, E., and Matsushita, K. (2003). New developments in oxidative fermentation. *Appl. Microbiol. Biotechnol.* 60, 643–653. doi: 10.1007/s00253-002-1155-9

Andrés-Barrao, C., Saad, M. M., Chappuis, M.-L., Boffa, M., Perret, X., Ortega Pérez, R., et al. (2012). Proteome analysis of *Acetobacter pasteurianus* during acetic acid fermentation. *J. Proteome* 75, 1701–1717. doi: 10.1016/j.jprot.2011.11.027

Azuma, Y., Hosoyama, A., Matsutani, M., Furuya, N., Horikawa, H., Harada, T., et al. (2009). Whole-genome analyses reveal genetic instability of *Acetobacter pasteurianus*. *Nucleic Acids Res.* 37, 5768–5783. doi: 10.1093/nar/gkp612

Barja, F., Andrés-Barrao, C., Ortega Pérez, R., Cabello, E. M., and Chappuis, M.-L. (2016). "Physiology of *Komagataeibacter* spp. during acetic acid fermentation," in *Acetic Acid Bacteria: Ecology and Physiology*. eds. K. Matsushita, H. Toyama, N. Tonouchi and A. Okamoto-Kainuma (Tokyo: Springer Japan), 201–221.

Chen, C., Chen, H., Zhang, Y., Thomas, H. R., Frank, M. H., He, Y., et al. (2020). TBtools: an integrative toolkit developed for interactive analyses of big biological data. *Mol. Plant* 13, 1194–1202. doi: 10.1016/j.molp.2020.06.009

Chinnawirotpisan, P., Theeragool, G., Limtong, S., Toyama, H., Adachi, O. O., and Matsushita, K. (2003). Quinoprotein alcohol dehydrogenase is involved in catabolic acetate production, while NAD-dependent alcohol dehydrogenase in ethanol assimilation in *Acetobacter pasteurianus* SKU1108. *J. Biosci. Bioeng.* 96, 564–571. doi: 10.1016/S1389-1723(04)70150-4

Conner, D. E., and Kotrola, J. S. (1995). Growth and survival of *Escherichia coli* O157:H7 under acidic conditions. *Appl. Environ. Microbiol.* 61, 382–385. doi: 10.1128/aem.61.1.382-385.1995

Du, R., Wang, Y., Zhao, F., Qiao, X., Song, Q., Li, S., et al. (2020). Production, optimization and partial characterization of bacterial cellulose from *Gluconacetobacter xylinus* TJU-D2. *Waste Biomass Valoriz.* 11, 1681–1690. doi: 10.1007/s12649-018-0440-5

Dubey, S., Sharma, R. K., Agarwal, P., Singh, J., Sinha, N., and Singh, R. P. (2017). From rotten grapes to industrial exploitation: *Komagataeibacter europaeus* SGP37, a micro-factory for macroscale production of bacterial nanocellulose. *Int. J. Biol. Macromol.* 96, 52–60. doi: 10.1016/j.ijbiomac.2016.12.016

Fuhrer, T., Chen, L., Sauer, U., and Vitkup, D. (2007). Computational prediction and experimental verification of the gene encoding the NAD^+/$NADP^+$-dependent succinate semialdehyde dehydrogenase in *Escherichia coli*. *J. Bacteriol.* 189, 8073–8078. doi: 10.1128/JB.01027-07

García-Angulo, V. A. (2017). Overlapping riboflavin supply pathways in bacteria. *Crit. Rev. Microbiol.* 43, 196–209. doi: 10.1080/1040841X.2016.1192578

Gullo, M., La China, S., Falcone, P. M., and Giudici, P. (2018). Biotechnological production of cellulose by acetic acid bacteria: current state and perspectives. *Appl. Microbiol. Biotechnol.* 102, 6885–6898. doi: 10.1007/s00253-018-9164-5

Gullo, M., Verzelloni, E., and Canonico, M. (2014). Aerobic submerged fermentation by acetic acid bacteria for vinegar production: process and biotechnological aspects. *Process Biochem.* 49, 1571–1579. doi: 10.1016/j.procbio.2014.07.003

Kanchanarach, W., Theeragool, G., Inoue, T., Yakushi, T., Adachi, O., and Matsushita, K. (2010). Acetic acid fermentation of *Acetobacter pasteurianus*: relationship between acetic acid resistance and pellicle polysaccharide formation. *Biosci. Biotechnol. Biochem.* 74, 1591–1597. doi: 10.1271/bbb.100183

Kim, D., Langmead, B., and Salzberg, S. L. (2015). HISAT: a fast spliced aligner with low memory requirements. *Nat. Methods* 12, 357–360. doi: 10.1038/nmeth.3317

Kostner, D., Luchterhand, B., Junker, A., Volland, S., Daniel, R., Büchs, J., et al. (2015). The consequence of an additional NADH dehydrogenase paralog on the growth of *Gluconobacter oxydans* DSM3504. *Appl. Microbiol. Biotechnol.* 99, 375–386. doi: 10.1007/s00253-014-6069-9

Langmead, B., and Salzberg, S. L. (2012). Fast gapped-read alignment with bowtie 2. *Nat. Methods* 9, 357–359. doi: 10.1038/nmeth.1923

Li, B., and Dewey, C. N. (2011). RSEM: accurate transcript quantification from RNA-Seq data with or without a reference genome. *BMC Bioinformatics* 12:323. doi: 10.1186/1471-2105-12-323

Li, Y., Yan, P., Lei, Q., Li, B., Sun, Y., Li, S., et al. (2019). Metabolic adaptability shifts of cell membrane fatty acids of *Komagataeibacter hansenii* HDM1-3 improve acid stress resistance and survival in acidic environments. *J. Ind. Microbiol. Biotechnol.* 46, 1491–1503. doi: 10.1007/s10295-019-02225-y

Love, M. I., Huber, W., and Anders, S. (2014). Moderated estimation of fold change and dispersion for RNA-seq data with DESeq2. *Genome Biol.* 15:550. doi: 10.1186/s13059-014-0550-8

Lu, T., Gao, H., Liao, B., Wu, J., Zhang, W., Huang, J., et al. (2020). Characterization and optimization of production of bacterial cellulose from strain CGMCC 17276 based on whole-genome analysis. *Carbohydr. Polym.* 232:115788. doi: 10.1016/j.carbpol.2019.115788

Matsushita, K., Inoue, T., Adachi, O., and Toyama, H. (2005). *Acetobacter aceti* possesses a proton motive force-dependent efflux system for acetic acid. *J. Bacteriol.* 187, 4346–4352. doi: 10.1128/JB.187.13.4346-4352.2005

Matsushita, K., and Matsutani, M. (2016). "Distribution, evolution, and physiology of oxidative fermentation" in *Acetic acid bacteria: Ecology and physiology*. eds. K. Matsushita, H. Toyama, N. Tonouchi and A. Okamoto-Kainuma (Tokyo: Springer Japan), 159–178.

Mullins, E. A., Francois, J. A., and Kappock, T. J. (2008). A specialized citric acid cycle requiring succinyl-coenzyme a (CoA):acetate CoA-transferase (AarC) confers acetic acid resistance on the acidophile *Acetobacter aceti*. *J. Bacteriol.* 190, 4933–4940. doi: 10.1128/JB.00405-08

Nakano, S., and Ebisuya, H. (2016). "Physiology of *Acetobacter* and *Komagataeibacter* spp.: acetic acid resistance mechanism in acetic acid fermentation," in *Acetic Acid Bacteria: Ecology and Physiology*. eds. K. Matsushita, H. Toyama, N. Tonouchi and A. Okamoto-Kainuma (Tokyo: Springer Japan), 223–234.

Nakano, S., and Fukaya, M. (2008). Analysis of proteins responsive to acetic acid in *Acetobacter*: molecular mechanisms conferring acetic acid resistance in acetic acid bacteria. *Int. J. Food Microbiol.* 125, 54–59. doi: 10.1016/j.ijfoodmicro.2007.05.015

Nakano, S., Fukaya, M., and Horinouchi, S. (2006). Putative ABC transporter responsible for acetic acid resistance in *Acetobacter aceti*. *Appl. Environ. Microbiol.* 72, 497–505. doi: 10.1128/AEM.72.1.497-505.2006

Okamoto-Kainuma, A., and Ishikawa, M. (2016). "Physiology of *Acetobacter* spp.: involvement of molecular chaperones during acetic acid fermentation," in *Acetic Acid Bacteria: Ecology and Physiology*. eds. K. Matsushita, H. Toyama, N. Tonouchi and A. Okamoto-Kainuma (Tokyo: Springer Japan), 179–199.

Qi, Z., Yang, H., Xia, X., Wang, W., and Yu, X. (2013). Analysis of energetic metabolism of *Acetobacter pasteurianus* during high acidic vinegar fermentation. *Microbiol. China* 40, 2171–2181. doi: 10.13344/j.microbiol.china.2013.12.002

Qin, Z., Yu, S., Chen, J., and Zhou, J. (2022). Dehydrogenases of acetic acid bacteria. *Biotechnol. Adv.* 54:107863. doi: 10.1016/j.biotechadv.2021.107863

Qiu, X., Zhang, Y., and Hong, H. (2021). Classification of acetic acid bacteria and their acid resistant mechanism. *AMB Express* 11:29. doi: 10.1186/s13568-021-01189-6

Ryngajłło, M., Kubiak, K., Jędrzejczak-Krzepkowska, M., Jacek, P., and Bielecki, S. (2019). Comparative genomics of the *Komagataeibacter* strains—efficient bionanocellulose producers. *MicrobiologyOpen* 8:e00731. doi: 10.1002/mbo3.731

Saichana, N., Matsushita, K., Adachi, O., Frébort, I., and Frebortova, J. (2015). Acetic acid bacteria: a group of bacteria with versatile biotechnological applications. *Biotechnol. Adv.* 33, 1260–1271. doi: 10.1016/j.biotechadv.2014.12.001

Sakurai, K., Arai, H., Ishii, M., and Igarashi, Y. (2012). Changes in the gene expression profile of *Acetobacter aceti* during growth on ethanol. *J. Biosci. Bioeng.* 113, 343–348. doi: 10.1016/j.jbiosc.2011.11.005

Sakurai, K., Yamazaki, S., Ishii, M., Igarashi, Y., and Arai, H. (2013). Role of the glyoxylate pathway in acetic acid production by *Acetobacter aceti*. *J. Biosci. Bioeng.* 115, 32–36. doi: 10.1016/j.jbiosc.2012.07.017

Sokollek, S. J., Hertel, C., and Hammes, W. P. (1998). Description of *Acetobacter oboediens* sp. nov. and *Acetobacter pomorum* sp. nov., two new species isolated from industrial vinegar fermentations. *Int. J. Syst. Evol. Microbiol.* 48, 935–940.

Trcek, J., Jernejc, K., and Matsushita, K. (2007). The highly tolerant acetic acid bacterium *Gluconacetobacter europaeus* adapts to the presence of acetic acid by changes in lipid composition, morphological properties and PQQ-dependent ADH expression. *Extremophiles* 11, 627–635. doi: 10.1007/s00792-007-0077-y

Trcek, J., Mira, N. P., and Jarboe, L. R. (2015). Adaptation and tolerance of bacteria against acetic acid. *Appl. Microbiol. Biotechnol.* 99, 6215–6229. doi: 10.1007/s00253-015-6762-3

Trcek, J., Toyama, H., Czuba, J., Misiewicz, A., and Matsushita, K. (2006). Correlation between acetic acid resistance and characteristics of PQQ-dependent ADH in acetic acid bacteria. *Appl. Microbiol. Biotechnol.* 70, 366–373. doi: 10.1007/s00253-005-0073-z

Wang, L., Hong, H., Zhang, C., Huang, Z., and Guo, H. (2021). Transcriptome analysis of *Komagataeibacter europaeus* CGMCC 20445 responses to different acidity levels during acetic acid fermentation. *Pol. J. Microbiol.* 70, 305–313. doi: 10.33073/pjm-2021-027

Wang, B., Shao, Y., and Chen, F. (2015a). Overview on mechanisms of acetic acid resistance in acetic acid bacteria. *World J. Microbiol. Biotechnol.* 31, 255–263. doi: 10.1007/s11274-015-1799-0

Wang, B., Shao, Y., Chen, T., Chen, W., and Chen, F. (2015b). Global insights into acetic acid resistance mechanisms and genetic stability of *Acetobacter pasteurianus* strains by comparative genomics. *Sci. Rep.* 5:18330. doi: 10.1038/srep18330

Xia, K., Bao, H., Zhang, F., Linhardt, R., and Liang, X. (2019). Characterization and comparative analysis of toxin-antitoxin systems in *Acetobacter pasteurianus*. *J. Ind. Microbiol. Biotechnol.* 46, 869–882. doi: 10.1007/s10295-019-02144-y

Xia, K., Han, C., Xu, J., and Liang, X. (2020). Transcriptome response of *Acetobacter pasteurianus* Ab3 to high acetic acid stress during vinegar production. *Appl. Microbiol. Biotechnol.* 104, 10585–10599. doi: 10.1007/s00253-020-10995-0

Xia, K., Han, C., Xu, J., and Liang, X. (2021). Toxin-antitoxin HicAB regulates the formation of persister cells responsible for the acid stress resistance in *Acetobacter pasteurianus*. *Appl. Microbiol. Biotechnol.* 105, 725–739. doi: 10.1007/s00253-020-11078-w

Xia, K., Li, Y., Sun, J., and Liang, X. (2016a). Comparative genomics of *Acetobacter pasteurianus* Ab3, an acetic acid producing strain isolated from chinese traditional rice vinegar Meiguichu. *PLoS One* 11:e0162172. doi: 10.1371/journal.pone.0162172

Xia, K., Zang, N., Zhang, J., Zhang, H., Li, Y., Liu, Y., et al. (2016b). New insights into the mechanisms of acetic acid resistance in *Acetobacter pasteurianus* using iTRAQ-dependent quantitative proteomic analysis. *Int. J. Food Microbiol.* 238, 241–251. doi: 10.1016/j.ijfoodmicro.2016.09.016

Xia, K., Zhu, J., and Liang, X. (2017). Advances in acid resistant mechanism of acetic acid bacteria and related quorum sensing system. *Acta Microbiol Sin.* 57, 321–332. doi: 10.13343/j.cnki.wsxb.20160233

Yakushi, T., and Matsushita, K. (2010). Alcohol dehydrogenase of acetic acid bacteria: structure, mode of action, and applications in biotechnology. *Appl. Microbiol. Biotechnol.* 86, 1257–1265. doi: 10.1007/s00253-010-2529-z

Yang, H., Chen, T., Wang, M., Zhou, J., Liebl, W., Barja, F., et al. (2022). Molecular biology: fantastic toolkits to improve knowledge and application of acetic acid bacteria. *Biotechnol. Adv.* 58:107911. doi: 10.1016/j.biotechadv.2022.107911

Yang, H., Yu, Y., Fu, C., and Chen, F. (2019). Bacterial acid resistance toward organic weak acid revealed by RNA-Seq transcriptomic analysis in Acetobacter pasteurianus. *Front. Microbiol.* 10:1616. doi: 10.3389/fmicb.2019.01616

Yang, G., and Zhou, S. (2014). *Sinibacillus* soli gen. Nov., sp. nov., a moderately thermotolerant member of the family *Bacillaceae*. *Int. J. Syst. Evol. Microbiol.* 64, 1647–1653. doi: 10.1099/ijs.0.055608-0

Yin, H., Zhang, R., Xia, M., Bai, X., Mou, J., Zheng, Y., et al. (2017). Effect of aspartic acid and glutamate on metabolism and acid stress resistance of Acetobacter pasteurianus. *Microb. Cell Factories* 16:109. doi: 10.1186/s12934-017-0717-6

Zheng, Y., Wang, J., Bai, X., Chang, Y., Mou, J., Song, J., et al. (2018). Improving the acetic acid tolerance and fermentation of Acetobacter pasteurianus by nucleotide excision repair protein UvrA. *Appl. Microbiol. Biotechnol.* 102, 6493–6502. doi: 10.1007/s00253-018-9066-6

frontiers | Frontiers in Microbiology

TYPE Original Research
PUBLISHED 12 October 2022
DOI 10.3389/fmicb.2022.994097

OPEN ACCESS

EDITED BY
Viviana Corich,
University of Padua,
Italy

REVIEWED BY
Muhammad Wajid Ullah,
Jiangsu University,
China
Wilson José Fernandes Lemos Junior,
Austrian Institute of Technology (AIT),
Austria

*CORRESPONDENCE
Salvatore La China
salvatore.lachina@unimore.it

SPECIALTY SECTION
This article was submitted to
Food Microbiology,
a section of the journal
Frontiers in Microbiology

RECEIVED 14 July 2022
ACCEPTED 26 September 2022
PUBLISHED 12 October 2022

CITATION
Anguluri K, La China S, Brugnoli M, Cassanelli S and Gullo M (2022) Better under stress: Improving bacterial cellulose production by *Komagataeibacter xylinus* K2G30 (UMCC 2756) using adaptive laboratory evolution.
Front. Microbiol. 13:994097.
doi: 10.3389/fmicb.2022.994097

Better under stress: Improving bacterial cellulose production by *Komagataeibacter xylinus* K2G30 (UMCC 2756) using adaptive laboratory evolution

Kavitha Anguluri, Salvatore La China*, Marcello Brugnoli, Stefano Cassanelli and Maria Gullo

Department of Life Sciences, University of Modena and Reggio Emilia, Reggio Emilia, Italy

Among naturally produced polymers, bacterial cellulose is receiving enormous attention due to remarkable properties, making it suitable for a wide range of industrial applications. However, the low yield, the instability of microbial strains and the limited knowledge of the mechanisms regulating the metabolism of producer strains, limit the large-scale production of bacterial cellulose. In this study, *Komagataeibacter xylinus* K2G30 was adapted in mannitol based medium, a carbon source that is also available in agri-food wastes. *K. xylinus* K2G30 was continuously cultured by replacing glucose with mannitol (2% w/v) for 210days. After a starting lag-phase, in which no changes were observed in the utilization of mannitol and in bacterial cellulose production (cycles 1–25), a constant improvement of the phenotypic performances was observed from cycle 26 to cycle 30, accompanied by an increase in mannitol consumption. At cycle 30, the end-point of the experiment, bacterial cellulose yield increased by 38% in comparision compared to cycle 1. Furthermore, considering the mannitol metabolic pathway, D-fructose is an intermediate in the bioconversion of mannitol to glucose. Based on this consideration, *K. xylinus* K2G30 was tested in fructose-based medium, obtaining the same trend of bacterial cellulose production observed in mannitol medium. The adaptive laboratory evolution approach used in this study was suitable for the phenotypic improvement of *K. xylinus* K2G30 in bacterial cellulose production. Metabolic versatility of the strain was confirmed by the increase in bacterial cellulose production from D-fructose-based medium. Moreover, the adaptation on mannitol did not occur at the expense of glucose, confirming the versatility of K2G30 in producing bacterial cellulose from different carbon sources. Results of this study contribute to the knowledge for designing new strategies, as an alternative to the genetic engineering approach, for bacterial cellulose production.

KEYWORDS

bacterial cellulose, *Komagataeibacter xylinus*, adaptive laboratory evolution, phenotypic improvement, alternative carbon sources

Introduction

Naturally produced polymers are characterized by impressive traits. They are produced by living organisms, converting suitable raw materials into large and complex polymeric structures. Biopolymers are produced both by the biggest living organisms, such as plants, and by the smallest living cells, as bacteria (Kaplan, 1998). Referring to the bacterial life cycle, one of the main mechanisms adopted by bacteria to resist to environmental stressors is by biofilm formation, a biomass consisting of microbial cells immersed in an exopolysaccharidic matrix (Moradali and Rehm, 2020). Among biofilm exopolysaccharides, bacterial cellulose (BC) was massively studied in the last decades, due to its natural properties of interest for many industrial applications (La China et al., 2021; Manan et al., 2022). Unlike plant cellulose, BC is an ultrapure biopolymer based on glucose monomers linked by β-1,4 glycosidic bond. BC is synthetized by a membrane protein complex, named cellulose synthase (CS), constituted by four main subunits (BcsA, BcsB, BcsC, BcsD). The glucan chain is synthetized by the catalytic core of CS (BcsA and BcsB), in which activated glucose monomers (UDP-glucose) are linked to the native glucan chain (Gullo et al., 2018). The glucan chain is extruded *via* structural proteins of CS (BcsC and BcsD), which form a channel in the periplasmic space and outer membrane. The extrusion point of the native glucan chain in the environmental space is called terminal complex and it is a distinct site on the surface of the outer membrane (Manan et al., 2022). The final structure of BC is the result of assembling events occurring in the extracellular space of cells. Briefly, the first assembly event occur between glucan chains forming protofibrils of about 2–20 nm in diameter. Subsequent events involve the protofibril assembly, by forming the ribbon shaped microfibrils *via* the formation of hydrogen bonds and Van der Waals forces, and finally the 3D hierarchical network of bundles (Gullo et al., 2018; Kim et al., 2019). The hierarchical polymerization of the glucan chains confers to BC unique properties, such as high crystallinity and high tensile strength (Singhania et al., 2021). Such properties make BC suitable for a wide range of applications, spanning from food (Vigentini et al., 2019), biomedical (Brugnoli et al., 2021; Manan et al., 2022) and cosmetics fields (Ullah et al., 2015). The most performant BC producers are found within the *Acetobacteraceae* family. This bacterial family includes species that are able to oxidize carbon substrates resulting in the production of a wide range of carboxylic acids (La China et al., 2018; Stasiak-Różańska and Płoska, 2018). Industrial processes in which *Acetobacteraceae* members of the acetic acid bacteria (AAB) group are exploited, include fermented beverages production, where BC is an undesired compound (Giudici et al., 2009; Gullo et al., 2016). Within AAB, strains belonging to the *Komagataeibacter* genus are not only interesting for fermentation processes because of their high aptitude in producing organic acids (Wang et al., 2015), but are widely studied for their ability in producing BC (Gullo et al., 2018; La China et al., 2021; Vadanan et al., 2022). At least six species of *Komagataeibacter* were described as BC producers, namely *K. europaeus, K. hansenii, K. rhaeticus, K. medellinensis, K. melomenusus,* and *K. xylinus*. The above-mentioned species were described to achieve variable and considerable BC yield and be able to metabolize different carbon sources for BC production (Masaoka et al., 1993; Keshk and Sameshima, 2005). Among the described species of *Komagataeibacter,* high intra and inter-species variability in term of BC yield was observed (Brugnoli et al., 2021; La China et al., 2021). However, *K. xylinus* species is considered as the model organism for BC production and the highest producer in different conditions (Wang et al., 2018; Zhong, 2020). Indeed, many efforts for scaling-up BC production are directed to the strain selection, especially considering the intra-species variability within *K. xylinus* (Gullo et al., 2017; Sharma and Bhardwaj, 2019; Andriani et al., 2020; Ryngajłło et al., 2020). Different approaches were assayed, mainly by replacing the carbon source with alternative substrates, also derived from wastes, such as agro-food, contributing to the development of more sustainable bioprocesses (Islam et al., 2017, 2020; Machado et al., 2018; Wang et al., 2018; Raiszadeh-Jahromi et al., 2020; Li et al., 2021a). Using cell-free system, an improved yield was observed compared to BC produced by microbial cells, consuming less carbon source and, consequently, reducing production costs (Ullah et al., 2015). Other approaches were assessed by developing synthetic biology tools, modifying metabolic pathways involved in BC synthesis (Ryngajłło et al., 2020; Singh et al., 2020). An alternative approach to genetic engineering strategy is the exploitation of adaptation mechanisms, developed by bacteria under predefined environmental conditions (Lee and Palsson, 2010; Barve and Wagner, 2013; Matsutani et al., 2013; Zorraquino et al., 2016). The activation of programs that regulate the cell physiology to the new environmental condition, is provided by metabolite concentration, energy levels or physical stressors, tuning the gene expression with the physiological needs (López-Maury et al., 2008). The modulation plasticity of the adaptation programs is depending both on the environmental changes and on the bacterial species (Hindré et al., 2012).

Here we have assayed the adaptation ability of *K. xylinus* K2G30 to mannitol as an alternative carbon source by applying the adaptive laboratory evolution (ALE) approach. Glucose, conventionally known as the main building block for BC production, was replaced by mannitol, already tested in *K. xylinus* K2G30, achieving an improvement of BC yield (Gullo et al., 2019). In addition, the choice of mannitol as carbon source to test the adaptation abilities in *K. xylinus* lies in the metabolic pathway, by which mannitol is converted into glucose for BC production. *K. xylinus* K2G30 was repeatedly cultivated using mannitol as sole carbon source along 210 days. The carbon sources consumption and the production of organic acids were evaluated. Structural changes over adaptation cycles, including X-ray diffraction (XRD), network frame variation, crystallinity, and fiber size, were evaluated by using scanning electron microscopy (SEM).

Materials and methods

Strain and culture conditions

The parental strain *K. xylinus* K2G30 used in this study had previously been isolated from kombucha tea (Mamlouk, 2012). The strain was deposited in UMCC (Unimore Microbial Culture Collection) under the collection code UMCC 2756 (Gullo et al., 2019). All the experiments were carried out in Hestrin–Schramm (HS) medium, which consists of yeast extract 1% w/v, polypeptone 0.5% w/v, disodium phosphate anhydrous 0.27% w/v, citric acid monohydrate 0.115% w/v, supplemented with D-glucose (standard) or D-mannitol (alternative), at the final concentration of 2% w/v (Hestrin and Schramm, 1954). A subculture of K2G30 was generated by rehydrating a glycerol (50% v/v) stock from −80°C preservation condition. From this subculture a total of 60 new glycerol stocks were prepared as control for the experiment of adaption cycles (Figure 1).

Adaptive laboratory evolution

ALE was carried out as per the experimental design referring to Figure 1. To establish the evolutionary experiment, the parental *K. xylinus* K2G30 strain was revitalized in 5 ml of HS-Glucose (HS-G) medium and cultivated for 4 days at 28°C, under static conditions. Preculture was prepared by inoculating the refreshed culture into 10 ml of fresh HS-G medium, the incubation was performed at 28°C for 7 days. This preculture was used to initiate the adaptation in mannitol, where the spent medium was removed by centrifugation at 8000 g for 5 min at 4°C. Cells were washed twice and refreshed with the HS-mannitol (HS-M) medium, and this inoculum was assayed at OD_{600}. With the known absorbance value (0.01), 0.5 ml (5% v/v) of the inoculum (HS-M) was inoculated into three test tubes, each containing 10 ml of fresh HS-M medium and incubated at 28°C for 7 days. Continuous adaptation of the strain to the new carbon source was performed by transferring the culture to a fresh medium every 7 days, washing the cells as described before, and transferring 0.5 ml (5% v/v) of the inoculum. The refreshing step is referred to as "cycles of adaptation," in this study. Adaptation was carried out up to

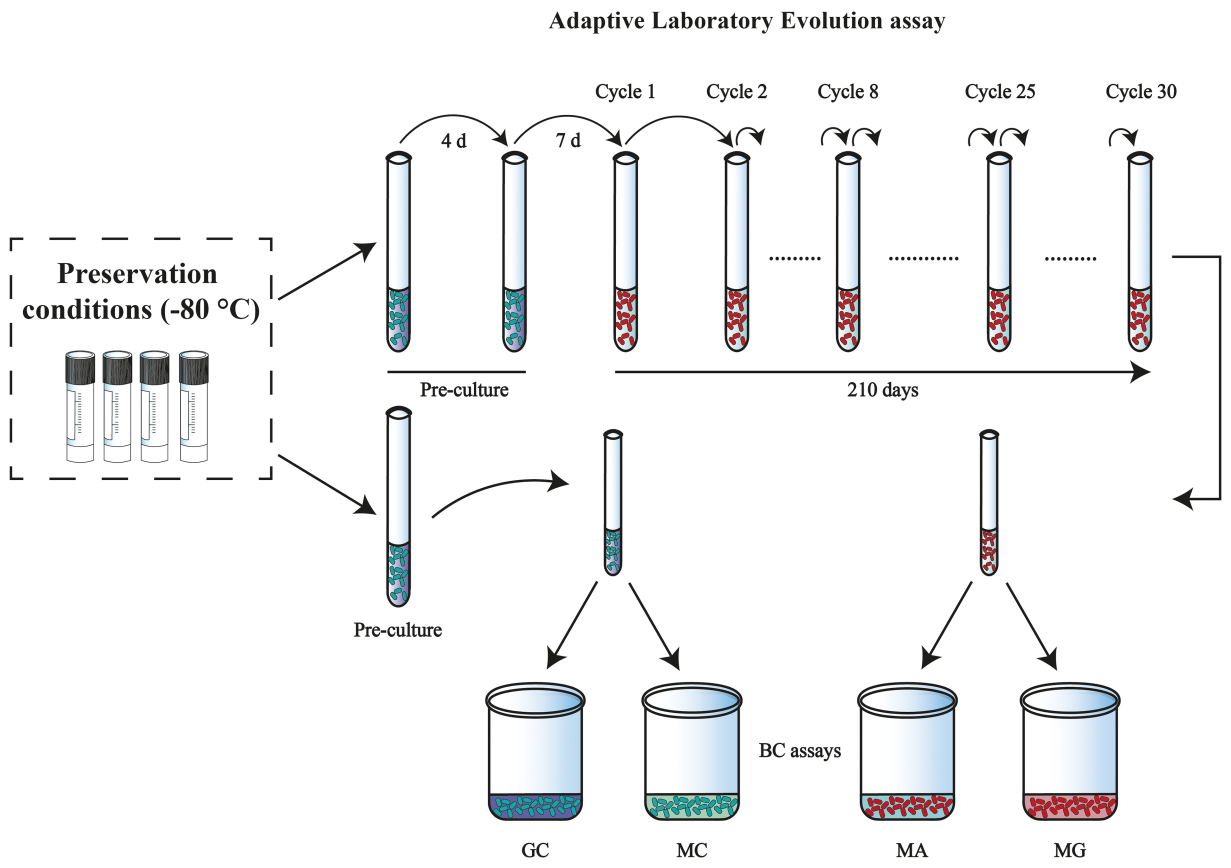

FIGURE 1
Overview of the experimental design: adaptation induction of *Komagataeibacter xylinus* K2G30 in mannitol medium. Preculture was maintained in HS-G and adaptation of the strain in mannitol medium begins from cycle 1. Both the adapted and the parental strain were tested for BC quantification and each color represents a different condition: MA (adapted in mannitol medium), MG (adapted strain in glucose medium), GC (parental strain in glucose medium), and MC (parental strain in mannitol medium).

30 cycles, with 1 to 8 cycles considered for short-term adaptation, and 25 and 30 cycles were tested for long-term adaptation. Control conditions were maintained constant for every cycle and performed using subcultures generated, as previously described.

Bacterial cellulose production

BC production assay was performed in four individual conditions as illustrated in Figure 1, by removing the spent culture medium by centrifugation at 8000 g for 5 min. Pellets were washed twice, refreshed in the representative medium (HS-G, HS-M) and OD_{600} was taken before the culture strains were inoculated. A total of 3 ml of these cultures was inoculated in 60 ml of the carbon source (glucose or mannitol) medium and incubated at 28°C for 5 days, under static conditions. All the experiments were performed with three biological replicates.

Bacterial cellulose harvesting, purification, and quantification

Native BC pellicles were separated from the culture broth, washed with distilled water to remove the medium components, and treated with 1 M NaOH, for 30 min at 80°C. Further, the pellicles were washed with distilled water until neutral pH and dried at 20°C with air flow, until the constant weight of cellulose layer was reached. Dried BC layers were weighed and analyzed as described by Gullo et al., 2017. The residual culture medium was collected immediately and stored at −20°C for further analysis.

Evaluation of carbon source consumption and gluconic acid production over the adaptation cycles

Residual concentration of mannitol and glucose in the culture medium were quantified by using K-MANOL and K-SUCGL assay kits (Megazyme Ltd. Bray, Ireland), respectively. Furthermore, gluconic acid was determined by the enzymatic kit from K-GATE, Megazyme Ltd. Bray, Ireland. Analyses were performed according to the manufacturer instructions and calculated using MEGA-CALC. The pH of the medium was determined by using an automatic titrator (TitroLine EASY SCHOTT Instruments GmbH. Mainz, Germany). All the data were expressed as gram per liter (mean ± standard deviation).

Bacterial cellulose production using D-fructose as carbon source in the adapted strain

K. xylinus K2G30 strain adapted in mannitol for 30 cycles was tested in HS medium supplemented with D-fructose (HS-F) instead of D-Mannitol and compared with the parental strain. Quantification of BC was performed as described above. Residual D-Fructose was quantified by using the Megazyme kit (K-SUFRG, Megazyme Ltd. Bray, Ireland) according to manufacturer instructions and calculated using MEGA-CALC. Genes and proteins sequences were obtained by downloading the already sequenced *K. xylinus* K2G30 genome from NCBI database (assembly id GCA_004302915.1) and performed the structural and functional annotation using Prodigal v2.6.3 (Hyatt et al., 2010) and Prokka v1.13.4 (Seemann, 2014), respectively. The pathway reconstruction was performed using KEGG database.

Structural characterization of bacterial cellulose layers

The surface morphology of dried BC layers were observed by SEM (NovaNano SEM 450, FEI, United States), as described by Mohammadkazemi et al. (2015) with some modifications. Briefly, SEM was performed in high vacuum mode with an acceleration voltage of 10 kV. All the samples were coated with a layer of gold to improve conductivity. Fiber dimension was estimated by randomly measuring the diameter of 100 fibers using ImageJ software (ImageJ 1.53 k version) (Schneider et al., 2012).

Dried BC layers were X-rayed using a film diffractometer (X'Pert PRO, Marvel Panalytical, United Kingdom). XRD patterns of the samples were recorded using CuKα radiation (λ = 1.54 Å), at a voltage of 40 kV and a filament emission of 40 mA. Samples were scanned with ramping at 1° min^{-1}, analyzing the range of 10°–30° (2θ). A zero-background holder was used to avoid the detection of any peak not related/associated to the sample. The crystallinity index was calculated using the following formula:

$$cr(\%) = \frac{sc}{st} * 100 \qquad \text{Equation 1}$$

Where s_c is the sum of net area and s_t is the sum of total area (Mohammadkazemi et al., 2015).

Results and discussion

Adaptive laboratory evolution to increase the bacterial cellulose yield in *Komagataeibacter xylinus* K2G30

To optimize BC production, different approaches have been implemented in the past, by using alternative carbon sources, also deriving from wastes, with the aim of reducing the production cost (Jozala et al., 2015; Kadier et al., 2021). In this context, it is possible to depict main features that a rapresentative carbon source should possess: fits the metabolic needs of the bacterial strain; guarantees high yield; be available in wastes.

Mannitol was previously tested in *Komagataeibacter* strains, obtaining an increasing of BC yield (Oikawa et al., 1995; Mohammadkazemi et al., 2015). In our previous studies on *K. xylinus* K2G30 and K1G4 strains, we observed an increase of BC production of about 42 and 21%, respectively, compared to glucose, highlighting the suitability of mannitol for BC production (Gullo et al., 2019; La China et al., 2020). Furthermore, *K. xylinus* K2G30 was previously tested in mannitol-based medium under shaking conditions. Cultivation conditions were different respect to that of the present study; however, BC was formed as spheres and a low yield was obtained (Gullo et al., 2019). This evidence is confirmed by previous studies aimed at evaluating the effect of dissolved oxygen on BC yield in agitated culture. The decrease of BC production in agitated conditions was correlated to the genetic instability of strains and the overgrowth of non-cellulose producers. Moreover, the increase of viscosity, proportional to BC production in agitated system, seems responsible for the non-homogeneous air bubbles dispersion, affecting the oxygen availability (Hwang et al., 1999).

Based on these considerations, mannitol was chosen as selective carbon source to adapt *K. xylinus* K2G30 by using ALE approach, in static regime. The strain was propagated in mannitol medium (condition MA) for 30 cycles (210 days). The evaluation of the strain adaptability to the new condition was assayed by measuring the BC produced during each cycle of adaptation. To monitor the ALE condition and the efficacy of the experimental design, two control conditions were used, by the cultivation of parental strain in standard conditions, using glucose as primary carbon source (GC condition), and mannitol medium (MC condition), both for every cycle (Figure 1). To evaluate if the parental phenotype persisted, the adapted strain was cultured in standard medium, using glucose as carbon source (MG condition).

In mannitol (MA condition), the amount of BC produced during the first adaptation cycles (cycles from 1 to 8) remained unchaged (Figure 2A). This condition persisted until cycle 25. Starting from this cycle, we observed a constant increase of produced BC. At cycle 28, BC yield was 3.04 ± 0.17 g/l, reaching 3.43 ± 0.09 g/l of BC at cycle 30. Regarding glucose control (GC condition) no significant changes were observed over the cycles (Figure 2B). The BC produced in this condition ranged between 1.71 ± 0.08 g/l (at cycle 25) to 2.30 ± 0.15 g/l (at cycle 2), corresponding to the minimum and maximum among all the tested cycles, respectively. Also in the case of mannitol control (MC) no significant differences in BC production were observed over the cycle (Figure 2C). We tested also the condition in which *K. xylinus* K2G30 in MA condition, was cultured back in glucose medium (MG condition). The BC yield obtained over the cycles does not show significant differences (Figure 2D). Furthermore, in MG condition, a low yield of BC production was observed, compared to glucose control (GC condition), producing 1.45 ± 0.18 g/l on average in over all cycles, while 1.99 ± 0.17 g/l of BC were observed in GC condition. The low yield observed in MG, corresponded to a loss of 27.13% of BC compared to the parental strain. Bacterial cellulose layers obtained during the adaptation cycles were illustrated in Figure 2E, highlighting the differences described. This behaviour could be explained considering the bet-hedging strategy that bacteria adopt to optimize their fitness in the environment (Solopova et al., 2014). The bet-hedging describes the strategies adopted by individuals in a population to optimize their fitness in a specific environment (Olofsson et al., 2009). The idea behind the bet-hedging theory is that individuals tend to reduce their variance in fitness to increase their fitness in long-term (Monod, 1949; Slatkin, 1974; Olofsson et al., 2009). When bacteria are cultivated in a different condition than stardard (glucose is considered the standard carbon source for most of bacteria), their metabolism is modulated in order to increase their survival rate. If multiple carbon sources are supplied in the medium, a growth transition usually occur, characterized

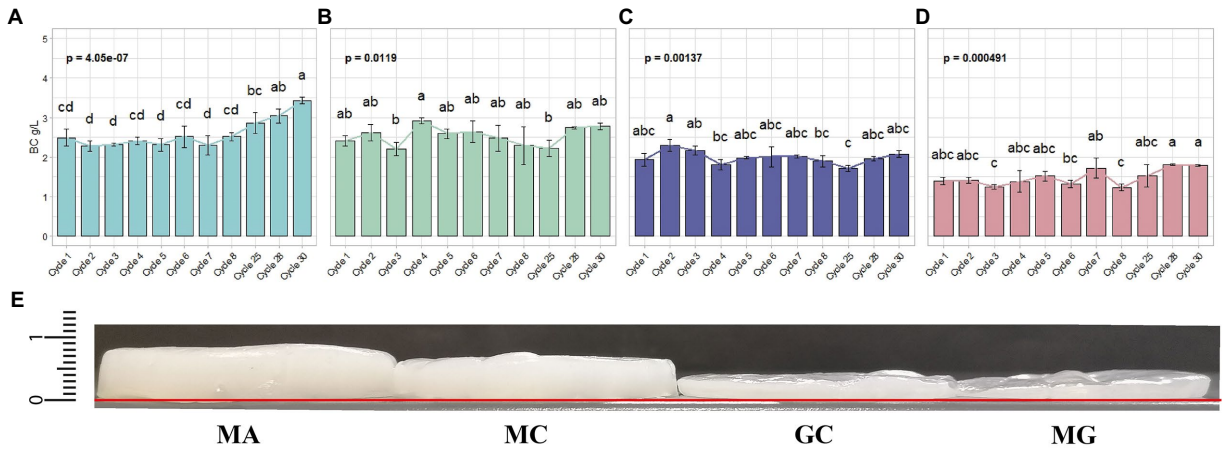

FIGURE 2
Quantification of BC yield in the four conditions tested **(A)** MA **(B)** MC **(C)** GC **(D)** MG. Each bar indicating the mean±SD of BC yield in the representative cycles. Significant difference among the BC yield was represented by letters. **(E)** Layers thickness of native BC pellicles at cycle 30: MA=0.85mm; MC=0.70; GC=0.40; MG=0.40. The baseline was marked in red.

by the growth interruption. This step is followed by a growth recovery in which bacterial cells switch to the less "attractive" carbon source. The interruption of cell growth (known as diauxic lag-phase) represents the period in which bacteria apply changes in their enzimatic sets, shifting to the metabolic pathways related to the new carbon source (Stanier, 1951). The diauxic and bet-hedging were widely studied in *Escherichia coli* (Wang et al., 2019) and *Lactobacillus lactis* (Solopova et al., 2014). In this study, by repeated culturing *K. xylinus* K2G30 in mannitol, we can speculate that its metabolism was reprogrammed to use mannitol as main carbon source. By re-cultivating the adapted *K. xylinus* K2G30 strain in glucose, we observed a reduction of the BC yield, highlighting a metabolic shift. Previous works related to ALE approach to improve BC production in *Komagataeibacter* strains were focused on the description of genetic mutation related to the metabolic shift. *K. medellinensis* NBRC 3288 was repeatedly cultured to increase the BC production. The genomic analysis revealed mutations involving 11 proteins involved in BC biosynthesis (Matsutani et al., 2015). In a recent work, performed on *K. xylinus* MSKU12, the ALE approach was used to increase the BC yield using different modified media. In coconut water-based medium, an increase of BC starting from 140 days and which further improvement until the end of the tested period (i.e. 210 days) (Naloka et al., 2020). Our results are in accordance with the adaptation time of *K. xylinus* MSKU12, showing a slow and steady improvement of BC production using an alternative carbon source. These data highlight the time frame required for the metabolic shift in *K. xylinus* strain.

Substrate uptake rates and production of byproduct in the adapted *Komagataeibacter xylinus* K2G30

The BC production occurs through the consumption of carbon sources supplemented in the medium. *Komagataeibacter* strains are able to use a wide range of sugars or sugar-alcohol for BC production (Mikkelsen et al., 2009; Mohammadkazemi et al., 2015; Gullo et al., 2019). The efficiency of the carbon source utilization for BC production is strictly influenced by the metabolic status of bacterial cells and the availability of dedicated metabolic pathways (Nguyen et al., 2021a). The utilization of mannitol as carbon source for BC biosynthesis varies among *Komagataeibacter* species. Ours previous work on *K. xylinus* K2G30 and K1G4 strains highlighted the highest BC production in mannitol-based medium (Gullo et al., 2019; La China et al., 2020). In contrast, a recent work on *K. uvaceti* reported a low BC synthesis in mannitol media (Nascimento et al., 2021). In this study, consumption of carbon sources during the adaptation cycles were monitored for the four conditions (MA, MG, MC, and GC) and were represented in Figure 3. A comparison between cycle 1 and cycle 30, based on BC produced and carbon source consumed, was reported in Table 1. When *K. xylinus* K2G30 was repeatedly cultivated in mannitol-based medium, the initial cycles were characterized by low consumption of the carbon source (cycle 1, 12.22 ± 0.42 g/l; Figure 3B). An increased mannitol utilization was observed between cycle 1 and cycle 2 (14.23 ± 0.68 g/l), remaining unchanged until cycle 25. A further increase of mannitol consumption has been observed in cycle 28 (15.31 ± 1.28 g/l) and cycle 30 (15.35 ± 0.18 g/l). The carbon source consumption in MA condition follows the same trend of BC production. This increase in the carbon source utilization could be explained considering the diauxic shift occurring in bacteria when they are cultivated in a multiple carbon source media. The metabolic shift is a time-consuming process, occurring during the continuous exposure to a carbon source by the modulation of the enzymatic set (Solopova et al., 2014; Bajic and Sanchez, 2020). This phenotype is highly visible considering the MC condition, in which high variability in mannitol consumption was observed (Figure 3E). Indeed, the consumption of the carbon source in the parental strain varied between 12.57 ± 3.82 g/l at cycle 1 to 13.46 ± 0.68 g/l at cycle 30, characterized by fluctuations in every cycle (Figure 3C). Such fluctuations, reflecting the BC production trend described in the previous section, could be the results of the adaptation process at early stage. A study conducted on *Lactococcus lactis* highlighted a heterogenicity in the cell population when cultivated in a multiple carbon source medium (glucose and cellobiose; Solopova et al., 2014): a cell fraction was able to utilize the favorable carbon source, while the remaining fraction utilized the new carbon source. This heterogeneity is the result of the dynamic mechanisms of the adaptation process occurring during the adaptation period, in which is possible to distinguish adaptive "driver" events (as genetic mutations) and non-adaptive events (mutation not involved in the adaptation response; Numata et al., 2019). Based on this consideration, we can speculate that regulatory mechanisms act in the metabolic shifting from glucose to mannitol, determining heterogenicity in *K. xylinus* K2G30 population.

While the parental strain cultivated in glucose-based medium (GC condition) showed the same consumption rate of the carbon sources (15.95 ± 0.69 g/l) among cycles (Figure 3A), an increase of the consumption rate has been observed when the adapted strain was cultivated in glucose (MG condition), resulting in average consumption of 16.51 ± 0.45 g/l of glucose (Figure 3E). A reduction in glucose consumption has been observed between cycle 1 and cycle 2, remaining stable for the successive cycles (Figure 3D). The increased consumed carbon source does not reflect the BC production, for which MG resulted to be the lower BC yield condition (Table 1). The reduction of the carbon source utilization in the BC biosynthetic pathway could be explained by considering the survival strategies adopted by bacteria under stress condition. The exposure to an environmental change induces in bacteria physiological and translational events to tune the molecular machinery to the new environmental condition (Nguyen et al., 2021b). Two possible scenarios are possible based on the environmental conditions. The exposure to a fluctuating environment, for example rapid changes (in minutes timescale) in nutrient concentrations, causes the activation of extremely rapid responses to the nutrient fluctuations. In contrast, the exposure to a steady environment, as a nutrient shift, lead to a

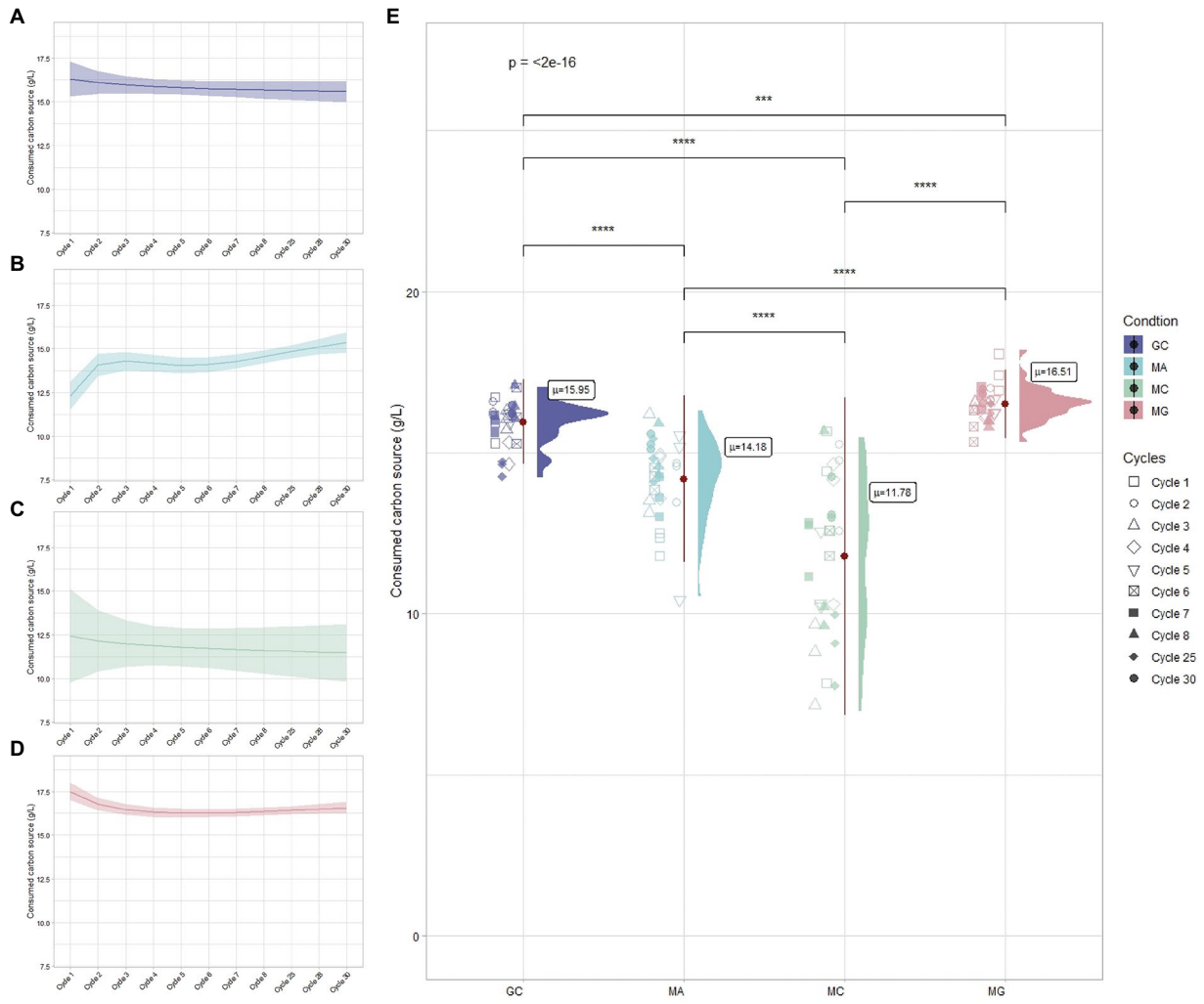

FIGURE 3
Carbon source utilization during the ALE cycles for **(A)** GC, **(B)** MA, **(C)** MC, and **(D)** MG conditions. **(E)** Overall carbon source consumption among conditions: each points represents the carbon source replicates related to the cycle and "μ" indicates the average consumption of carbon source among tested cycles.

TABLE 1 Comparison between 1 and 30cycles in term of BC produced, consumed carbon source, gluconic acid, and pH.

SAMPLES	BC yield (g/L)		Consumed CS (g/L)		Gluconic acid		pH	
	1 cycle	30 cycle	1 cycle	30 cycle	1 cycle	30 cycle	1 cycle	30 cycle
MA	2.49 ± 0.22	3.43 ± 0.09	12.22 ± 0.42	15.35 ± 0.18	0.04 ± 0.02	0.08 ± 0.02	6.25 ± 0.01	6.37 ± 0.05
MC	2.41 ± 0.14	2.77 ± 0.08	12.57 ± 3.82	13.46 ± 0.68	0.09 ± 0.01	0.01 ± 0.05	6.32 ± 0.04	6.27 ± 0.02
GC	1.94 ± 0.17	2.08 ± 0.09	16.02 ± 0.58	16.3 ± 0.16	8.33 ± 0.65	7.65 ± 0.77	3.6 ± 0.06	3.49 ± 0.02
MG	1.4 ± 0.1	1.8 ± 0.02	17.55 ± 0.6	16.78 ± 0.19	7.43 ± 1.79	4.87 ± 0.45	3.55 ± 0.04	3.39 ± 0.01

Data were reported as mean ± standard deviation.

new steady growth state (Nguyen et al., 2021a). The second scenario may explain the MG condition, in which *K. xylinus* K2G30 cells, repeatedly exposed to a nutrient shift (glucose to mannitol), reached the steady growth state in mannitol-based medium but not in glucose-based medium. We can hypothesize that the amount of carbon source consumed was not used for BC production but was consumed to adjust the cell physiology to the new shift in carbon source (mannitol to glucose).

In this study, also the byproduct formation was evaluated, mainly represented by gluconic acid formation (Supplementary Table S1). Formation of organic acids is a peculiar trait of AAB during the oxidative fermentation (Gullo et al., 2018). A massive

production of organic acids leads to a reduction of environmental pH, representing a stressor for the bacterial culture and affecting the BC production (Li et al., 2021b). By using mannitol (condition MA and MC), no production of gluconic acid was detected. When glucose was used as carbon source (GC and MG) a high production of gluconic acid was observed, particularly in GC condition. In this condition, *K. xylinus* K2G30 cells are exposed to stress condition, due to the acidification of the environment. Furthermore, since gluconic acid is produced starting from glucose by the membrane-bound glucose dehydrogenase EC 1.1.5.2, the availability of the carbon source resulted limited (Gullo et al., 2018). It is important to highlight the production of gluconic acid in MG condition. At cycle 1, the production was similar to GC, but focusing on cycle 30 a reduced amount of gluconic acid was produced. This could be attributed to the adaptation mechanism, valorizing our hypothesis that a metabolic shift occurred in the late stages of the adaptation. Furthermore, the reduction of gluconic acid observed at cycle 30 in MG was not accompanied by an increase of pH (Table 1).

Bacterial cellulose production in D-fructose-based medium improved by adaptive laboratory evolution

So far, we described the phenotypic improvement of *K. xylinus* K2G30 by applying the ALE approach. At this stage we focused on mannitol pathway to deeply understand the metabolic reactions involved in the conversion of mannitol to UDP-glucose, the activated substrate utilized for BC biosynthesis. A schematic representation of the pathway is illustrated in Figure 4A. Enzymes involved in the catabolism of mannitol and production of BC are listed in Table 2.

Based on the pathway reconstruction on the previous analysis on *K. xylinus* K2G30 genome and the reconstruction using KEGG, mannitol is the substrate of mannitol-2-dehydrogenase (MTLDH), converting the D-mannitol in to D-fructose. It will be converted in fructose-6-phosphate by the activity of a fructokinase (FK) and in glucose-6-phosphate by the phosphoglucose isomerase (PGI). The reaction that provides glucose monomers to BC biosynthesis is the isomerization of the glucose-6-phosphate to glucose-1-phosphate by the phosphoglucomutase (PGM). This pathway was also described previously (Zikmanis et al., 2021).

Based on this description, it is reasonable to hypothesize that if *K. xylinus* K2G30 was adapted in mannitol, possibly, the adaptation effect should be visible also supplementing fructose as carbon source. We tested the *K. xylinus* K2G30 from cycle 30 in MA condition in D-fructose based medium (MF condition) and the parental strain, comparing the BC yield with MA and GC at cycle 1 and cycle 30 (Figure 4B). As expected, at cycle 1 the only appreciable difference was related to the comparison MA versus GC. Considering cycle 30, MF showed the same improvement described for MA in the previous section, producing 3.46 ± 0.1 g/l (MF) and 3.43 ± 0.09 g/l (MA). No changes in gluconic acid production and pH were observed in MF and MA conditions (Supplementary Table S2). The observed increase of production in MF condition could reflect an up-regulation of the fructose-mannose metabolic pathway caused by the continuous cultivation in mannitol. By looking at the structural annotation of *K. xylinus K2G30 genome*, the *pgi* gene are deprived of a ribosomal binding site (rbs) (gene coordinates 150,700–151,629), suggesting that the regulation of the transcription mechanism of this gene is depending

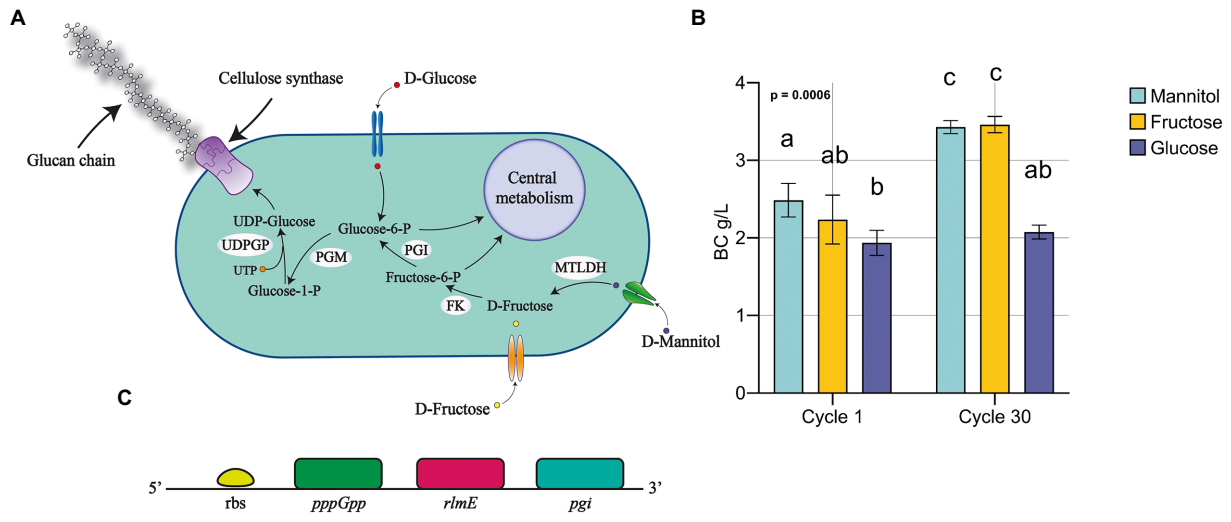

FIGURE 4
Fructose utilization as carbon source for BC production: **(A)** schematic illustration of fructose and mannose metabolic pathway, focusing on the bioconversion of mannitol for BC production; **(B)** BC production using fructose and comparison among MA, MF and GC. Data were represented as mean±standard deviation. Tukey test was used to assess multiple comparison among conditions. Different letters indicate statistical differences among conditions (p <0.05); **(C)** schematic representation of *pgi* related gene disposition in *K. xylinus* K2G30 genome.

TABLE 2 Metabolic pathway of mannitol metabolism for the biosynthesis of BC.

Enzyme	Gene	Enzyme	EC	Pathway	Gene coordinate (bp) (strand)
MTLDH	*mtlK*	Mannitol 2-dehydrogenase	1.1.1.67	Fructose and mannose metabolism	84,394–85,875 (+)
FK	*srcK*	Fructokinase	2.7.1.4	Fructose and mannose metabolism	150,700–151,629 (−)
PGI	*pgi*	Phosphoglucose isomerase	5.3.1.9	Starch and sucrose metabolism	53,428–56,292 (+)
					3,784–6,642(−)
PGM	*pgm*	Phosphoglucomutase	5.4.2.2	Starch and sucrose metabolism	12,962–14,620 (−)
UDPGP	*galU*	UTP--glucose-1-phosphate uridylyltransferase	2.7.7.9	Starch and sucrose metabolism	51,546–52,415 (+)
BcsI	*bglB_2*	Cellulose synthase (operon I)	3.2.1.21	Starch and sucrose metabolism	256,838–259,045 (−)
	bcsD		–		259,263–259,733 (−)
	bcsC		–		259,733–263,695 (−)
	bcsB		–		263,698–266,121 (−)
	bcsA		2.4.1.12		266,108–268,372 (−)
	ccpax		–		268,550–269,545 (−)
	cmcax		3.2.1.4		269,542–270,633 (−)
BcsII	*bcsAB*	Cellulose synthase (operon II)	–	Starch and sucrose metabolism	5,579–10,150 (+)
	bcsX		–		10,265–10,936 (+)
	bcsY		2.3.1.-		11,023–12,183 (+)
	bcsC		–		12,266–16,126 (+)
BcsIII	*bcsAB*	Cellulose synthase (operon III)	–	Starch and sucrose metabolism	28,895–33,346 (+)
	bcsC		–		33,349–37,149 (+)
bcsAB	*bcsAB*	Cellulose synthase	–	Starch and sucrose metabolism	83,990–88,687 (+)

The enzymatic set was retrieved analyzing the *K. xylinus* K2G30 previously reported (Gullo et al., 2019). The table reports the enzymes and relative genes involved in the bioconversion of mannitol until the formation of the activated glucose monomer (UDP-Glucose). The number of BC operons described in the *K. xylinus* K2G30 genome were reported as well. Furthermore, the gene coordinates were specified.

on the rbs of another genes. The first available rbs has been found two genes upstream and is related to the gene coding for the guanosine-5′-triphosphate 3′-diphosphate pyrophosphatase (pppGpp) (Figure 4C). This enzyme was identified as one of the key enzymes in the modulation of to growing-limiting conditions adopted by bacteria (Steinchen et al., 2020). High level of pppGpp induce a process recognized as "stringent response," a major cellular reprogramming in which the rRNA and tRNA synthesis is down regulated, stress-related genes upregulated and the limiting resource allocation is optimized (Atkinson et al., 2011; Gaca et al., 2013). Depending on the pppGpp rbs, an upregulation of the *pgi* gene is possible, increasing the conversion rate of fructose-6-phosphate in to glucose-6-phosphate from fructose-6-phosphate. When microbial cells are transferred into an environment with harmful pressure, they evolve the target metabolic pathway to enhance the growth condition, by exploiting the most abundant resources (Tan et al., 2019). As an example, in *E. coli* an increase in the β-lactamase metabolic pathway by continuous exposure to β-lactam was obtained (Abraham and Chain, 1940; Fevre et al., 2005). The up-regulation of target metabolic pathways as adaptation mechanisms were also reported in yeast (Hong et al., 2011). Nevertheless, in bacteria, the adaptation mechanisms when they are exposed to specific environmental condition have been described highly complex, in which genetic mutations, up-regulation processes, and metabolic arrangements are finely tuned (Connolly et al., 2021).

Structural and optical changes in bacterial cellulose layers during the adaptation cycles

Mechanical properties of the BC are mostly dependent on the ultrafine structure and arrangement of the nanofibers (Mohammadkazemi et al., 2015). BC structure rearrangements, especially in fiber diameter, were reported in previous work as a consequence of changes in the culture conditions (Li et al., 2021a). For this reason, we evaluated the morphology of BC layers during the adaptation cycles using SEM. A set of comparisons between cycle 1 and 30 for the conditions MA (Figures 5A–E), MG (Figures 5B–F) and MF (Figures 5C–G) was conducted. Fibrous networks were compared with GC (Figure 5D) and MC (Figure 5H). From Figure 5, it is possible to observe the presence of bacterial cells entrapped in the cellulose layer (Figures 5A,B,H). This is an eventuality that can occur as previously reported by Hult et al. (2003) and Yim et al. (2017), which observed that the treatment with 1 M NaOH solution guarantees the death/disruption of bacterial cells but in some cases, not the total removal. In this study,

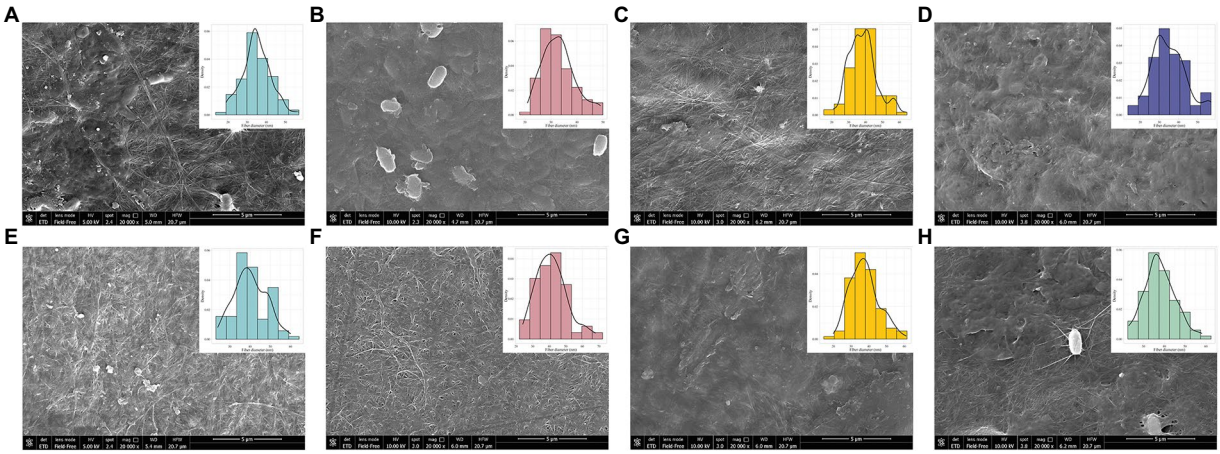

FIGURE 5
BC morphology characterization among conditions by using SEM. The characterization was performed considering cycle 1 and cycle 30 for **(A–E)** MA, **(B–F)** MG and **(C–G)** MF conditions. Only sample from the cycle 1 were assayed for **(D)** GC and **(H)** MC conditions.

SEM imaging revealed a heterogenous rod shaped nanofibrillar structure in all the samples and, in some cases, noticeable fibers agglomerates. However, a more compact fiber arrangement could be attributable to fibers random assembling (Sheykhnazari et al., 2011; Mohammadkazemi et al., 2015) or even to a failed integration of the microfibrils to the nascent BC sheet (Nicolas et al., 2011). At cycle 1, comparing the diameter of the fibers among the conditions, no differences were observed among them by using the three carbon sources, except when the adapted strain was tested back in glucose, showing thinnest fibers among all. The slight change in the fiber diameter could be due to changes in culture condition, which interfere with the formation of microfibers, resulting in smaller diameters, as observed by Li et al. (2021b). At cycle 30, a general increase in width of fiber dimension in all the conditions was detected, ranging from 34–54, 28–52, and 26–44 nm in 30MA, 30MG, and 30MF, respectively. Increasing in fiber dimension are correlated with an improvement of the mechanical properties. In BC produced by *Komagataeibacter* strains, an improvement in the G'and G" modules was observed (Numata et al., 2019).

The XRD diffraction was applied to assess crystallinity changes during the ALE. The X-ray diffractograms of the BC in all conditions showed the characteristic peaks at the angle of 14.5, 16.5, and 22.5 (Supplementary Figure S1) with slight differences in intensity. The least crystallinity index was observed in GC condition (79.35%), whereas MF and MG in the cycle 1 showed the highest crystallinity (95.69 and 91.75%, respectively). Among the adaptation cycles, no differences were observed in the crystallinity terms. Only when the adapted strain was cultivated in a different carbon source than mannitol (MG and MF conditions at cycle 30), a decrease in the crystallinity (84.81 and 89.20%, respectively) was observed. This result is in agreement with a previous study, in which similar decreasing pattern was observed when the *K. xylinus* MSKU12 adapted in coconut water was cultured in standard HS medium (Naloka et al., 2020).

Conclusion

Different approaches have been applied to improve BC production. The strain selection and the utilization of the proper carbon source are the crucial points to set-up new processes for BC production. The greatest efforts to improve the BC yield are focused on testing alternative carbon sources, often exploiting waste materials, mainly to make the process more sustainable. In this study we adopted the ALE approach to improve the BC production by repeatedly cultivating *K. xylinus* K2G30 supplementing a different carbon source (D-mannitol) than glucose. We observed an improvement in BC of about 38% in the adapted strain compared to the parental one, followed by an increase in mannitol utilization for BC production.

These results show that the use of mannitol was considerable increased respect to glucose. This evidence is relevant considering the production of BC from waste containing mannitol. Moreover, the adaptation on mannitol did not strongly affect the ability of the strain to use glucose, since the BC yield resulted slightly decreased. Based on these considerations, the adaptation on mannitol did not occur at the expense of glucose, highlighting the versatility of K2G30 in producing BC from different carbon sources.

Furthermore, according to the metabolic pathway of mannitol, we assayed a second carbon source (fructose) and observed a substantial increase in the BC production. The improvements obtained for the tested carbon sources increase considerably the use of *K. xylinus* K2G30 for BC production, allowing the design of new complex media, including multiple carbon sources and/or waste as feedstock. The adaptation mechanism is a highly complex process, involving remodulation of the metabolic pathways, genetic mutations and translational events. Previous studies highlighted time-lapse of the adaptation events occurring during the early stage and in long-term evolutionary experiments. The *K. xylinus*

K2G30 adaptation presented here is an ongoing experiment and will be used in the future to analyze short- and long-term adaptation events occurring in the shift of the carbon source. To this aim, the transcriptome analysis of the adapted strain will be performed. Furthermore, the genome sequencing of the adapted strain and the comparison with the parental one, can clarify if the observed phenotype changes are due to genetic alteration or to a transient phenotypic shift.

Integrating the ALE approach with the development of genetic engineering tools could provide the resources necessary to tune the adaptation mechanisms existing in bacteria with the need to obtain high cellulose producer strain.

Data availability statement

The original contributions presented in the study are included in the article/Supplementary material, further inquiries can be directed to the corresponding author.

Author contributions

KA: methodology, formal analysis, writing the original draft and data curation. SLC: conceptualization, investigation, validation, data visualization and analysis, supervision and writing—review and editing. MB: structural analysis and writing the original draft. SC: supervision and review and editing. MG: conceptualization, investigation, resources, review and editing, supervision, project administration, and funding acquisition. All authors contributed to the article and approved the submitted version.

Funding

This research was supported by FAR Fondo di Ateneo per la Ricerca UNIMORE 2020 and EU Project "Implementation and Sustainability of Microbial Resource Research Infrastructure for the 21st Century" (IS_MIRRI21, Grant Agreement Number 871129).

Acknowledgments

The Research Doctorate School in Food and Agricultural Science, Technology and Biotechnology (STEBA) is acknowledged for assigning the "Michela Stanca" award to KA. The kind help of Luciana De Vero, as curator of Unimore Microbial Culture collection (UMCC) is acknowledged for the management and maintenance of bacterial strains.

Conflict of interest

The authors declare that the research was conducted in the absence of any commercial or financial relationships that could be construed as a potential conflict of interest.

Publisher's note

Supplementary material

The Supplementary material for this article can be found online at: https://www.frontiersin.org/articles/10.3389/fmicb.2022.994097/full#supplementary-material

References

Abraham, E. P., and Chain, E. (1940). An enzyme from bacteria able to destroy penicillin. *Nature* 146:837. doi: 10.1038/146837a0

Andriani, D., Apriyana, A. Y., and Karina, M. (2020). The optimization of bacterial cellulose production and its applications: a review. *Cellulose* 27, 6747–6766. doi: 10.1007/s10570-020-03273-9

Atkinson, G. C., Tenson, T., and Hauryliuk, V. (2011). The RelA/SpoT homolog (RSH) superfamily: distribution and functional evolution of ppGpp synthetases and hydrolases across the tree of life. *PLoS One* 6:e23479. doi: 10.1371/journal.pone.0023479

Bajic, D., and Sanchez, A. (2020). The ecology and evolution of microbial metabolic strategies. *Curr. Opin. Biotechnol.* 62, 123–128. doi: 10.1016/j.copbio.2019.09.003

Barve, A., and Wagner, A. (2013). A latent capacity for evolutionary innovation through exaptation in metabolic systems. *Nature* 500, 203–206. doi: 10.1038/nature12301

Brugnoli, M., Robotti, F., La China, S., Anguluri, K., Haghighi, H., Bottan, S., et al. (2021). Assessing effectiveness of Komagataeibacter strains for producing surface-microstructured cellulose via guided assembly-based biolithography. *Sci. Rep.* 11:19311. doi: 10.1038/s41598-021-98705-2

Connolly, J. P. R., Roe, A. J., and O'Boyle, N. (2021). Prokaryotic life finds a way: insights from evolutionary experimentation in bacteria. *Crit. Rev. Microbiol.* 47, 126–140. doi: 10.1080/1040841X.2020.1854172

Fevre, C., Jbel, M., Passet, V., Weill, F. X., Grimont, P. A. D., and Brisse, S. (2005). Six groups of the OXY β-lactamase evolved over millions of years in Klebsiella *oxytoca*. *Antimicrob. Agents Chemother.* 49, 3453–3462. doi: 10.1128/AAC.49.8.3453-3462.2005

Gaca, A. O., Kajfasz, J. K., Miller, J. H., Liu, K., Wang, J. D., Abranches, J., et al. (2013). Basal levels of (p)ppGpp in enterococcus faecalis: the magic beyond the stringent response. *mBio* 4, e00646–e00613. doi: 10.1128/mBio.00646-13

Giudici, P., Gullo, M., and Solieri, L. (2009). "Traditional balsamic vinegar," in *Vinegars of the world* (Springer, Milan), 157–177.

Gullo, M., La China, S., Falcone, P. M., and Giudici, P. (2018). Biotechnological production of cellulose by acetic acid bacteria: current state and perspectives. *Appl. Microbiol. Biotechnol.* 102, 6885–6898. doi: 10.1007/s00253-018-9164-5

Gullo, M., La China, S., Petroni, G., Di Gregorio, S., and Giudici, P. (2019). Exploring K2G30 genome: a high bacterial cellulose producing strain in glucose and mannitol based media. *Front. Microbiol.* 10, 1–12. doi: 10.3389/fmicb.2019.00058

Gullo, M., Sola, A., Zanichelli, G., Montorsi, M., Messori, M., and Giudici, P. (2017). Increased production of bacterial cellulose as starting point for scaled-up applications. *Appl. Microbiol. Biotechnol.* 101, 8115–8127. doi: 10.1007/s00253-017-8539-3

Gullo, M., Zanichelli, G., Verzelloni, E., Lemmetti, F., and Giudici, P. (2016). Feasible acetic acid fermentations of alcoholic and sugary substrates in combined operation mode. *Process Biochem.* 51, 1129–1139. doi: 10.1016/j.procbio.2016.05.018

Hestrin, S., and Schramm, M. (1954). Synthesis of cellulose by *Acetobacter xylinum*. 2. Preparation of freeze-dried cells capable of polymerizing glucose to cellulose. *Biochem. J.* 58, 345–352. doi: 10.1042/bj0580345

Hindré, T., Knibbe, C., Beslon, G., and Schneider, D. (2012). New insights into bacterial adaptation through in vivo and in silico experimental evolution. *Nat. Rev. Microbiol.* 10, 352–365. doi: 10.1038/nrmicro2750

Hong, K. K., Vongsangnak, W., Vemuri, G. N., and Nielsen, J. (2011). Unravelling evolutionary strategies of yeast for improving galactose utilization through integrated systems level analysis. *Proc. Natl. Acad. Sci.* 108, 12179–12184. doi: 10.1073/pnas.1103219108

Hult, E. L., Yamanaka, S., Ishihara, M., and Sugiyama, J. (2003). Aggregation of ribbons in bacterial cellulose induced by high pressure incubation. *Carbohydr. Polym.* 53, 9–14. doi: 10.1016/S0144-8617(02)00297-7

Hwang, J. W., Yang, Y. K., Hwang, J. K., Pyun, Y. R., and Kim, Y. S. (1999). Effects of pH and dissolved oxygen on cellulose production by *Acetobacter xylinum* BRC5 in agitated culture. *J. Biosci. Bioeng.* 88, 183–188. doi: 10.1016/S1389-1723(99)80199-6

Hyatt, D., Chen, G. L., Locascio, P. F., Land, M. L., Larimer, F. W., and Hauser, L. J. (2010). Prodigal: prokaryotic gene recognition and translation initiation site identification. *BMC Bioinform.* 11:119. doi: 10.1186/1471-2105-11-119

Islam, M. U., Ullah, M. W., Khan, S., and Park, J. K. (2020). Production of bacterial cellulose from alternative cheap and waste resources: a step for cost reduction with positive environmental aspects. *Korean J. Chem. Eng.* 37, 925–937. doi: 10.1007/s11814-020-0524-3

Islam, M. U., Ullah, M. W., Khan, S., Shah, N., and Park, J. K. (2017). Strategies for cost-effective and enhanced production of bacterial cellulose. *Int. J. Biol. Macromol.* 102, 1166–1173. doi: 10.1016/j.ijbiomac.2017.04.110

Jozala, A. F., Pértile, R. A. N., dos Santos, C. A., de Carvalho Santos-Ebinuma, V., Seckler, M. M., Gama, F. M., et al. (2015). Bacterial cellulose production by *Gluconacetobacter xylinus* by employing alternative culture media. *Appl. Microbiol. Biotechnol.* 99, 1181–1190. doi: 10.1007/s00253-014-6232-3

Kadier, A., Ilyas, R. A., Huzaifah, M. R. M., Harihastuti, N., Sapuan, S. M., Harussani, M. M., et al. (2021). Use of industrial wastes as sustainable nutrient sources for bacterial cellulose (BC) production: mechanism, advances, and future perspectives. *Polymers (Basel)* 13:3365. doi: 10.3390/polym13193365

Kaplan, D. L. (1998). "Introduction to biopolymers from renewable resources," in *Biopolymers from renewable resources* (Berlin, Heidelberg: Berlin, Germany: Springer Verlag), 1–29.

Keshk, S. M. A. S., and Sameshima, K. (2005). Evaluation of different carbon sources for bacterial cellulose production. *African J. Biotechnol.* 4, 478–482. doi: 10.4314/ajb.v4i6.15125

Kim, Y., Ullah, M. W., Islam, M. U., Khan, S., Jang, J. H., and Park, J. K. (2019). Self-assembly of bio-cellulose nanofibrils through intermediate phase in a cell-free enzyme system. *Biochem. Eng. J.* 142, 135–144. doi: 10.1016/j.bej.2018.11.017

La China, S., Bezzecchi, A., Moya, F., Petroni, G., Di Gregorio, S., and Gullo, M. (2020). Genome sequencing and phylogenetic analysis of K1G4: a new *Komagataeibacter* strain producing bacterial cellulose from different carbon sources. *Biotechnol. Lett.* 42, 807–818. doi: 10.1007/s10529-020-02811-6

La China, S., De Vero, L., Anguluri, K., Brugnoli, M., Mamlouk, D., and Gullo, M. (2021). Kombucha tea as a reservoir of cellulose producing bacteria: assessing diversity among *Komagataeibacter* isolates. *Appl. Sci.* 11:1595. doi: 10.3390/app11041595

La China, S., Zanichelli, G., De Vero, L., and Gullo, M. (2018). Oxidative fermentations and exopolysaccharides production by acetic acid bacteria: a mini review. *Biotechnol. Lett.* 40, 1289–1302. doi: 10.1007/s10529-018-2591-7

Lee, D. H., and Palsson, B. O. (2010). Adaptive evolution of *Escherichia coli* K-12 MG1655 during growth on a nonnative carbon source, L-l,2-propanediol. *Appl. Environ. Microbiol.* 76, 4158–4168. doi: 10.1128/AEM.00373-10

Li, Z. Y., Azi, F., Ge, Z. W., Liu, Y. F., Yin, X. T., and Dong, M. S. (2021a). Bio-conversion of kitchen waste into bacterial cellulose using a new multiple carbon utilizing *Komagataeibacter rhaeticus*: fermentation profiles and genome-wide analysis. *Int. J. Biol. Macromol.* 191, 211–221. doi: 10.1016/j.ijbiomac.2021.09.077

Li, Z., Chen, S. Q., Cao, X., Li, L., Zhu, J., and Yu, H. (2021b). Effect of pH buffer and carbon metabolism on the yield and mechanical properties of bacterial cellulose produced by *Komagataeibacter hansenii* ATCC 53582. *J. Microbiol. Biotechnol.* 31, 429–438. doi: 10.4014/JMB.2010.10054

López-Maury, L., Marguerat, S., and Bähler, J. (2008). Tuning gene expression to changing environments: from rapid responses to evolutionary adaptation. *Nat. Rev. Genet.* 9, 583–593. doi: 10.1038/nrg2398

Machado, R. T. A., Meneguin, A. B., Sábio, R. M., Franco, D. F., Antonio, S. G., Gutierrez, J., et al. (2018). *Komagataeibacter rhaeticus* grown in sugarcane molasses-supplemented culture medium as a strategy for enhancing bacterial cellulose production. *Ind. Crop. Prod.* 122, 637–646. doi: 10.1016/j.indcrop.2018.06.048

Mamlouk, D. (2012). *Insight into physiology and functionality of acetic acid bacteria through a multiphasic approach*. Dissertation, University of Modena and Reggio Emilia, Modena.

Manan, S., Ullah, M. W., Ul-Islam, M., Shi, Z., Gauthier, M., and Yang, G. (2022). Bacterial cellulose: molecular regulation of biosynthesis, supramolecular assembly, and tailored structural and functional properties. *Prog. Mater. Sci.* 129:100972. doi: 10.1016/j.pmatsci.2022.100972

Masaoka, S., Ohe, T., and Sakota, N. (1993). Production of cellulose from glucose by *Acetobacter xylinum*. *J. Ferment. Bioeng.* 75, 18–22. doi: 10.1016/0922-338X(93)90171-4

Matsutani, M., Ito, K., Azuma, Y., Ogino, H., Shirai, M., Yakushi, T., et al. (2015). Adaptive mutation related to cellulose producibility in *Komagataeibacter medellinensis* (*Gluconacetobacter xylinus*) NBRC 3288. *Appl. Microbiol. Biotechnol.* 99, 7229–7240. doi: 10.1007/s00253-015-6598-x

Matsutani, M., Nishikura, M., Saichana, N., Hatano, T., Masud-Tippayasak, U., Theergool, G., et al. (2013). Adaptive mutation of *Acetobacter pasteurianus* SKU1108 enhances acetic acid fermentation ability at high temperature. *J. Biotechnol.* 165, 109–119. doi: 10.1016/j.jbiotec.2013.03.006

Mikkelsen, D., Flanagan, B. M., Dykes, G. A., and Gidley, M. J. (2009). Influence of different carbon sources on bacterial cellulose production by *Gluconacetobacter xylinus* strain ATCC 53524. *J. Appl. Microbiol.* 107, 576–583. doi: 10.1111/j.1365-2672.2009.04226.x

Mohammadkazemi, F., Azin, M., and Ashori, A. (2015). Production of bacterial cellulose using different carbon sources and culture media. *Carbohydr. Polym.* 117, 518–523. doi: 10.1016/j.carbpol.2014.10.008

Monod, J. (1949). The growth of bacterial cultures. *Annu. Rev. Microbiol.* 3, 371–394. doi: 10.1146/annurev.mi.03.100149.002103

Moradali, M. F., and Rehm, B. H. A. (2020). Bacterial biopolymers: from pathogenesis to advanced materials. *Nat. Rev. Microbiol.* 18, 195–210. doi: 10.1038/s41579-019-0313-3

Naloka, K., Matsushita, K., and Theeragool, G. (2020). Enhanced ultrafine nanofibril biosynthesis of bacterial nanocellulose using a low-cost material by the adapted strain of *Komagataeibacter* xylinus MSKU 12. *Int. J. Biol. Macromol.* 150, 1113–1120. doi: 10.1016/j.ijbiomac.2019.10.117

Nascimento, F. X., Torres, C. A. V., Freitas, F., Reis, M. A. M., and Crespo, M. T. B. (2021). Functional and genomic characterization of *Komagataeibacter uvaceti* FXV3, a multiple stress resistant bacterium producing increased levels of cellulose. *Biotechnol. Rep.* 30:e00606. doi: 10.1016/j.btre.2021.e00606

Nguyen, J., Fernandez, V., Pontrelli, S., Sauer, U., Ackermann, M., and Stocker, R. (2021a). A distinct growth physiology enhances bacterial growth under rapid nutrient fluctuations. *Nat. Commun.* 12:3662. doi: 10.1038/s41467-021-23439-8

Nguyen, J., Lara-Gutiérrez, J., and Stocker, R. (2021b). Environmental fluctuations and their effects on microbial communities, populations and individuals. *FEMS Microbiol. Rev.* 45, 1–16. doi: 10.1093/femsre/fuaa068

Nicolas, W. J., Ghosal, D., Tocheva, E. I., Meyerowitz, E. M., and Jensen, G. J. (2011). Structure of the bacterial cellulose ribbon and its assembly-guiding cytoskeleton by electron cryotomography. *J. Bacteriol.* 203, e00371–e00320. doi: 10.1128/JB.00371-20

Numata, Y., Kono, H., Mori, A., Kishimoto, R., and Tajima, K. (2019). Structural and rheological characterization of bacterial cellulose gels obtained from *Gluconacetobacter genus*. *Food Hydrocoll.* 92, 233–239. doi: 10.1016/j.foodhyd.2019.01.060

Oikawa, T., Ohtori, T., and Ameyama, M. (1995). Production of cellulose from D-mannitol by *Acetobacter xylinum* KU-1. *Biosci. Biotechnol. Biochem.* 59, 331–332. doi: 10.1271/bbb.59.331

Olofsson, H., Ripa, J., and Jonzén, N. (2009). Bet-hedging as an evolutionary game: the trade-off between egg size and number. *Proc. R. Soc. B Biol. Sci.* 276, 2963–2969. doi: 10.1098/rspb.2009.0500

Raiszadeh-Jahromi, Y., Rezazadeh-Bari, M., Almasi, H., and Amiri, S. (2020). Optimization of bacterial cellulose production by *Komagataeibacter xylinus* PTCC 1734 in a low-cost medium using optimal combined design. *J. Food Sci. Technol.* 57, 2524–2533. doi: 10.1007/s13197-020-04289-6

Ryngajłło, M., Jędrzejczak-Krzepkowska, M., Kubiak, K., Ludwicka, K., and Bielecki, S. (2020). Towards control of cellulose biosynthesis by *Komagataeibacter*

using systems-level and strain engineering strategies: current progress and perspectives. *Appl. Microbiol. Biotechnol.* 104, 6565–6585. doi: 10.1007/s00253-020-10671-3

Schneider, C., Rasband, W., and Eliceiri, K. (2012). NIH image to ImageJ: 25 years of image analysis. *Nat. Methods* 9, 671–675. doi: 10.1038/nmeth.2089

Seemann, T. (2014). Prokka: rapid prokaryotic genome annotation. *Bioinformatics* 30, 2068–2069. doi: 10.1093/bioinformatics/btu153

Sharma, C., and Bhardwaj, N. K. (2019). Bacterial nanocellulose: present status, biomedical applications and future perspectives. *Mater. Sci. Eng. C* 104:109963. doi: 10.1016/j.msec.2019.109963

Sheykhnazari, S., Tabarsa, T., Ashori, A., Shakeri, A., and Golalipour, M. (2011). Bacterial synthesized cellulose nanofibers; effects of growth times and culture mediums on the structural characteristics. *Carbohydr. Polym.* 86, 1187–1191. doi: 10.1016/j.carbpol.2011.06.011

Singh, A., Walker, K. T., Ledesma-Amaro, R., and Ellis, T. (2020). Engineering bacterial cellulose by synthetic biology. *Int. J. Mol. Sci.* 21, 1–13. doi: 10.3390/ijms21239185

Singhania, R. R., Patel, A. K., Tsai, M. L., Chen, C. W., and Di Dong, C. (2021). Genetic modification for enhancing bacterial cellulose production and its applications. *Bioengineered* 12, 6793–6807. doi: 10.1080/21655979.2021.1968989

Slatkin, M. (1974). Hedging one's evolutionary bets. *Nature* 250, 704–705. doi: 10.1038/250704b0

Solopova, A., Van Gestel, J., Weissing, F. J., Bachmann, H., Teusink, B., Kok, J., et al. (2014). Bet-hedging during bacterial diauxic shift. *Proc. Natl. Acad. Sci. U. S. A.* 111, 7427–7432. doi: 10.1073/pnas.1320063111

Stanier, R. Y. (1951). Enzymatic adaptation in bacteria. *Annu. Rev. Microbiol.* 5, 35–56. doi: 10.1146/annurev.mi.05.100151.000343

Stasiak-Różańska, L., and Płoska, J. (2018). Study on the use of microbial cellulose as a biocarrier for 1,3-dihydroxy-2-propanone and its potential application in industry. *Polymers* 10:438. doi: 10.3390/polym10040438

Steinchen, W., Zegarra, V., and Bange, G. (2020). (p)ppGpp: magic modulators of bacterial physiology and metabolism. *Front. Microbiol.* 11:2072. doi: 10.3389/fmicb.2020.02072

Tan, Z. L., Zheng, X., Wu, Y., Jian, X., Xing, X., and Zhang, C. (2019). In vivo continuous evolution of metabolic pathways for chemical production. *Microb. Cell Factories* 18:82. doi: 10.1186/s12934-019-1132-y

Ullah, M. W., Islam, M. U., Khan, S., Kim, Y., and Park, J. K. (2015). Innovative production of bio-cellulose using a cell-free system derived from a single cell line. *Carbohyd. Polym.* 132, 286–294. doi: 10.1016/j.carbpol.2015.06.037

Vadanan, S. V., Basu, A., and Lim, S. (2022). Bacterial cellulose production, functionalization, and development of hybrid materials using synthetic biology. *Polym. J.* 54, 481–492. doi: 10.1038/s41428-021-00606-8

Vigentini, I., Fabrizio, V., Dellacà, F., Rossi, S., Azario, I., Mondin, C., et al. (2019). Set-up of bacterial cellulose production from the genus Komagataeibacter and its use in a gluten-free bakery product as a case study. *Front. Microbiol.* 10:1953. doi: 10.3389/fmicb.2019.01953

Wang, S. S., Han, Y. H., Chen, J. L., Zhang, D. C., Shi, X. X., Ye, Y. X., et al. (2018). Insights into bacterial cellulose biosynthesis from different carbon sources and the associated biochemical transformation pathways in *Komagataeibacter* sp. W1. *Polymers (Basel)* 10:963. doi: 10.3390/polym10090963

Wang, B., Shao, Y., Chen, T., Chen, W., and Chen, F. (2015). Global insights into acetic acid resistance mechanisms and genetic stability of *Acetobacter pasteurianus* strains by comparative genomics. *Sci. Rep.* 5, 1–14. doi: 10.1038/srep18330

Wang, X., Xia, K., Yang, X., and Tang, C. (2019). Growth strategy of microbes on mixed carbon sources. *Nat. Commun.* 10, 1279–1277. doi: 10.1038/s41467-019-09261-3

Yim, S. M., Song, J. E., and Kim, H. R. (2017). Production and characterization of bacterial cellulose fabrics by nitrogen sources of tea and carbon sources of sugar. *Process Biochem.* 59, 26–36. doi: 10.1016/j.procbio.2016.07.001

Zhong, C. (2020). Industrial-scale production and applications of bacterial cellulose. *Front. Bioeng. Biotechnol.* 8, 1–19. doi: 10.3389/fbioe.2020.605374

Zikmanis, P., Kolesovs, S., Ruklisha, M., and Semjonovs, P. (2021). Production of bacterial cellulose from glycerol: the current state and perspectives. *Bioresour. Bioprocess* 8:116. doi: 10.1186/s40643-021-00468-1

Zorraquino, V., Kim, M., Rai, N., and Tagkopoulos, I. (2016). The genetic and transcriptional basis of short and long term adaptation across multiple stresses in *Escherichia coli*. *Mol. Biol. Evol.* 34:msw269. doi: 10.1093/molbev/msw269

frontiers | Frontiers in Microbiology

TYPE Original Research
PUBLISHED 17 November 2022
DOI 10.3389/fmicb.2022.991688

OPEN ACCESS

EDITED BY
Janja Trcek,
University of Maribor,
Slovenia

REVIEWED BY
Xuefeng Wu,
Hefei University of Technology,
China
Weizhu Zeng,
Jiangnan University,
China

*CORRESPONDENCE
Warawut Krusong
warawut.kr@kmitl.ac.th

SPECIALTY SECTION
This article was submitted to Food Microbiology, a section of the journal Frontiers in Microbiology

RECEIVED 11 July 2022
ACCEPTED 19 October 2022
PUBLISHED 17 November 2022

CITATION
Krusong W, La China S, Pothimon R and Gullo M (2022) Defining *Paenibacillus azoreducens* (P8) and *Acetobacter pasteurianus* (UMCC 2951) strains performances in producing acetic acid. *Front. Microbiol.* 13:991688. doi: 10.3389/fmicb.2022.991688

Defining *Paenibacillus azoreducens* (P8) and *Acetobacter pasteurianus* (UMCC 2951) strains performances in producing acetic acid

Warawut Krusong[1]*, Salvatore La China[2], Ruttipron Pothimon[1] and Maria Gullo[2]

[1]Laboratory of Fermentation Technology, Division of Food Industrial Fermentation, School of Food Industry, King Mongkut's Institute of Technology Ladkrabang, Bangkok, Thailand, [2]Department of Life Sciences, University of Modena and Reggio Emilia, Reggio Emilia, Italy

In this study, spore-forming bacteria isolated from saccharified rice were selected for producing acetic acid. From the screening of 15 strains, P8 strain was chosen as a candidate. The strain was identified as *Paenibacillus azoreducens* by 16S rRNA analysis (99.85% similarity with *P. azoreducens* CM1^T). Acetic acid is the main component of vinegar but also an industrial commodity produced by chemical synthesis. Sustainable routes for obtaining acetic acid are of great interest for decreasing the environmental impact generated by chemical syntheses. Biological acetic acid production is effective for vinegar production by acetic acid bacteria, but it cannot economically compete with the chemical synthesis for producing it as a pure commodity. Considering the need to improve the yield of pure acetic acid produced by microbial conversions, in this study, P8 strain was chosen for designing processes in different fermentation conditions. Tests were conducted in single and semi-continuous systems, using rice wine as substrate. Acetic acid produced by P8 strain was compared with that of *Acetobacter pasteurianus* (UMCC 2951), a strain known for producing acetic acid from rice wine. Even though the fermentation performances of *P. azoreducens* P8 were slightly lower than those of acetic acid bacteria usually used for vinegar production, results highlight its suitability for producing acetic acid. The final acetic acid produced by *P. azoreducens* P8 was 73g/L, in a single stage fermentation, without losses. In nine cycles of semi-continuous regime the average of acetification rate was 0.814 (g/L/days). Two main attributes of *P. azoreducens* P8 are of relevance for producing acetic acid, namely the ability to grow at temperature higher (+ 37°C), than mesophilic acetic acid bacteria, and the absence of cytoplasmic assimilation of acetic acid. These features allow to design multiple strains cultures, in which *P. azoreducens* can acts as a helper strain. Based on our results, the new isolate *P. azoreducens* P8 can be propagated in fermenting broths for boosting acetic acid production, under the selected conditions, and used in combination with acetic acid bacteria to produce biological acetic acid, as a non-food grade commodity.

KEYWORDS

spore-forming bacteria, acetic acid bacteria, *Paenibacillus azoreducens*, *Acetobacter pasteurianus*, acetic acid, saccharified rice

Introduction

Spore-forming bacteria are receiving great attention for their biotechnological potential in different industrial areas and sustainable productions. Their ability to survive in different environments at high physiological stresses, make them suitable for several bioprocesses, leading to high production of useful bio-compounds (Lal and Tabacchioni, 2009; Grady et al., 2016; Kaziūnienė et al., 2022).

Spore-forming bacteria were longed classified into two orders represented by *Bacillales* and *Clostridiales* (Abecasis et al., 2013). More recently, the new order *Thermoanaerobacterales* was proposed (Wiegel, 2015). Food spoilage *Bacillales* members belong to the genera of *Bacillus*, *Geobacillus*, *Anoxybacillus*, *Alicyclobacillus* and *Paenibacillus* (Mcclure, 2006).

Among these genera, *Paenibacillus* includes Gram-positive or variable, spore-forming bacteria, rod-shaped, aerobic or facultative anaerobic. Species belonging to *Paenibacillus* were reported to be ubiquitous, widely isolated from various environment, as cow feces (Velazquez et al., 2004), plant roots and food (Berge et al., 2002), warm springs (Chou et al., 2007), raw and heat-treated milk (Scheldeman et al., 2004), paper mill white water (Chiellini et al., 2014), blood cultures (Roux and Raoult, 2004) and traditional Chinese vinegar produced from cereals (Li et al., 2016). Many species of *Paenibacillus* produce antimicrobial compounds that are useful in medicine or as pesticides, and many yield enzymes that could be utilized for bioremediation or to produce valuable chemicals (Grady et al., 2016; da Costa et al., 2022). Due to their antibacterial activity, *Paenibacillus* species were also reported to be suitable for foods and beverages production (Marwoto et al., 2004; Grady et al., 2016; Li et al., 2016). Among recognized species, *Paenibacillus azoreducens*, a facultative anaerobic bacterium able to decolorize azo dyes, grows in a temperature range between 10°C and 50°C, with optimal growth at 37°C and can produces acids from sugars (Meehan et al., 2001).

Chemically synthesized acetic acid and its derivates are commodities that have become a major feedstock for the United States and worldwide chemical industry. Petrochemically produced acetic acid reached a level of 4.68 × 109 lbs./year in the United States by 1995 and was ranked 35th in abundance of all chemicals produced (Kirschner, 1996). Worldwide production in 1998 was estimated at 11.9 × 109 lbs./year (Layman, 1998). From more recent data, the global demand for virgin acetic acid is estimated to be 16.1 million tons in 2020, and it is expected to reach 19.6 million tons by 2027 (Martín-Espejo et al., 2022). Although many research efforts, bioderived acetic acid does not compete economically with acetic acid produced by chemical synthesis. The chemical process, although is expensive and depends on non-renewable petroleum for raw materials, takes advantage of an initially high acetic acid concentration (35%–45%) and high production yield. Instead, acetic acid produced by microbial processes, *via* ethanol oxidation by acetic acid bacteria (AAB) or by anaerobic fermentation, can be obtained from a number of renewable raw materials, but the major disadvantage is the cost of recovery of low concentrations of acetic acid (4%–12%) from the fermentation broths. Moreover, during AAB fermentation other compounds, such as bacterial cellulose and gluconic acid can be formed, which could affect the final acetic acid content (La China et al., 2021; He et al., 2022). On the other hands, considering the use of vinegar in non-food productions, for instance, it can be added to correct pH in detergents preparations, together with its derivatives, acetic acid is applied in pharmaceuticals, plasticizers, solvents, textiles, heat transfer liquids, neutralizer, fungicide and de-icers productions (Kersters et al., 2006). Considering the need of the biotechnology industry in producing compounds, such as organic acid by microbial conversions, the production of acetic acid, traditionally associated to vinegar production by AAB (La China et al., 2018), could be improved in terms of yield. Moreover, due to the global demand for acetic acid, sustainable routes for obtaining it are an open challenge, as an alternative to the chemical synthesis.

In this study, we present a new strain (P8) belonging to the genus *Paenibacillus* isolated from upland rice during the saccharification process, identified as *P. azoreducens* species. Given the continuous increasing interest in members belonging to this genus, the phenotypic traits of this new strain were studied, including the ability to produce acetic acid and other volatile organic compounds (VOCs). The acetic acid production by *P. azoreducens* (P8 strain) was compared with that of *Acetobacter pasteurianus* UMCC 2951, an AAB strain previously isolated from rotten pineapple pomace and studied for its attitude in performing ethanol oxidation into acetic acid. The output of this study can be further exploited for design a multiple microbial culture composed by the two strains aimed at producing bioderived acetic acid.

Materials and methods

Strains isolation and cultivation conditions

Isolation of spore-forming bacteria was conducted from 30 samples of contaminated or rotten saccharified rice. Samples were diluted in peptone water (1% w/v) and aliquots (1 ml) were plated in sterile *Paenibacillus*-basal agar medium consisting of (g/L of water) glucose 20, yeast extract 5, tryptone 5, $(NH_4)_2HPO_4$ 0.5, $MgSO_4.7H_2O$ 0.25, $CaCO_3$ 10 and agar 15 (modified from Nakashimada et al., 1998). Plates were incubated at 37°C for 3–5 days, under aerobic conditions. Then, single colonies were selected based on the clear halo formed on the agar medium due to acid production. Selected colonies were picked up and sub-cultured on the isolation medium until pure cultures were obtained. All isolates were checked for spore production by spore staining test, according to the procedure reported by Oktari et al. (2017). Briefly, samples of cell culture were stained by using Malachite Green solution of 5 and 0.5% Safranin. After first staining with Malachite Green by a moist heating process for 10 min, the cell culture was washed with water and then covered with paint Safranin which

results in the green coloring on the spores, as well as red in the vegetative cells. The spore former-acid producing strains were named as "P" followed by a progressive number and preserved in *Paenibacillus*-basal medium agar slant, at 4°C.

Selection of spore former-acid producing bacteria and acetic acid production tests

Upland rice vinegar, containing 80 g/L of acetic acid was obtained from the Laboratory of Fermentation Technology, King Mongkut's Institute of Technology Ladkrabang, Thailand. It was used as a substrate in acetification medium. Meanwhile, upland rice wine with an ethanol content of 90 ± 0.2 g/L and titratable acidity of 1.8 ± 0.2 g/L was also used in the adjustment of ethanol in acetification medium. All spore former-acid producing strains were cultivated in acetification medium consisting of (g/L of water) glucose 50, yeast extract 5, $MgSO_4.7H_2O$ 0.2 and $(NH_4)_2HPO_4$ 0.5 which was adjusted to a total concentration (TC; a parameter which expresses the maximal concentration of acetic acid that can be obtained in a complete fermentation) of 80 g/L by using upland rice wine and vinegar in a 1 l Duran bottle (working volume 500 ml), as described by Krusong et al. (2014, 2015). The aeration was controlled at a constant rate of 4 l/min.

Upland rice vinegar and wine were used for adjustment of acetic acid and ethanol contents in the medium of acetification process by P8 and *A. pasteurianus* UMCC 2951 strains, respectively. *A. pasteurianus* UMCC 2951 strain was previously adapted to high acetic acid concentration at 30 ± 1°C by stepwise scaling up, starting from 10 g/L to 65 ± 1 g/L of acetic acid, over a six-year period (Krusong and Tantratian, 2014; Pothimon et al., 2020). The broth culture from *A. pasteurianus* UMCC 2951 strain was prepared by using the following medium (g/L of water): glucose 50, yeast extract 5, $MgSO_4.7H_2O$ 0.2 and $(NH_4)_2HPO_4$ 0.5, under aeration (4.5 L/min), for 7 days at 30 ± 1°C (Krusong et al., 2007). According to the high initial acetic acid concentration (HAA_i) process previously set up (Krusong et al., 2014), the acetification medium (g/L of water: glucose 50, yeast extract 5, $MgSO_4.7H_2O$ 0.2 and $(NH_4)_2HPO_4$ 0.5) was standardized to a total concentration of 80 g/L, by adjusting the ethanol and acetic acid contents to 35 ± 1 g/L and 45 ± 1 g/L, respectively.

16S rRNA gene sequencing and phylogenetic analysis

Strain identity was determined by 16S rRNA gene sequencing. Genomic DNA extraction, amplification and sequencing of 16S rRNA gene was performed by Macrogen Inc. company, according to their protocols. Then, the sequence was trimmed, removing low quality bases, using Phred v 0.071220.c and assembled using Pharp v 1.090518 (Ewing and Green, 1998). The dataset was structured by downloading a total of 20 16S rRNA sequences of *Paenibacillus* strains from NCBI 16S rRNA database, selecting sequencing of strains isolated from food matrices. The 16S rRNA sequences were aligned using Muscle v3.8.31 (Edgar, 2004). Resulting alignment was imported in MegaX (Kumar et al., 2018) and trimmed in to obtain sequences with the same length. Trimmed alignment was used to generate a maximum-likelihood (ML) phylogenetic tree, applying the Tamura-Nei evolutionary model (Tamura and Nei, 1993), setting a discrete gamma distribution to model evolutionary rate differences among sites. The ML phylogenetic tree was computed using 1,000 replicates. The alignment was also used to calculate the phylogenetic distant matrix. In addition, the nucleotide sequence of 16S rRNA gene is available at GenBank, under the accession number OP353700.1.

Acetification performance by single and semi-continuous processes

The acetification conditions (single stage) for both P8 and *A. pasteurianus* UMCC 2951 strains were setup in a 100 L internal Venturi injector bioreactor (as reported in our previous study; Krusong et al., 2015), which comprised a stainless-steel tank 1.00 m high and 0.40 m internal diameter that had a maximum working volume of 75 l. The medium (consisting of (g/L of water): glucose 50, yeast extract 5, $MgSO_4.7H_2O$ 0.2 and $(NH_4)_2HPO_4$ 0.5 which was adjusted to a TC of 80 g/L by using upland rice wine and vinegar) was recycled using a centrifugal pump (Grundfos Ltd., Bangkok, Thailand), filtered and entrained. Well-compressed air was introduced into the medium at the injector nozzle (Mazzei Injector Com., LLC, Bakersfield, CA, USA) at 7.25–14.5 psi creating a plentiful amount of fine air bubbles in the bioreactor. The temperature of the medium was controlled at 30°C by cooling unit with Thermocouple Resistance Temperature Detector (RTD) PT100 RTD (Omega Engineering Inc., Connecticut, USA).

The startup phase was conducted with 25 L of working volume of the bioreactor at 7.25 psi of air (Krusong et al., 2015). The end of this phase occurred when the ethanol content reached 5 g/L or less (Fregapane et al., 2001; de Ory et al., 2004). Then, the fermentation phase was started by adding a volume of fresh medium to make up the medium volume to 75 L at 14.5 psi of air (Krusong et al., 2015), fixing TC at 80 ± 1 g/L. The overoxidation of acetic acid was tested after the ethanol content reached 0 g/L, by extending acetification period under the same rate of aeration supply. Samples were collected at the end of the operational phase.

The semi-continuous acetification by P8 strain under HAA_i conditions was conducted fixing TC at 80 g/L (consisting of 45 g/L acetic acid and 35 g/L ethanol) in the 100 l internal Venturi injector bioreactor. The temperature was controlled at 30°C. Acetification rate (ETA), which measures the rate of acetic acid production (difference between the final and initial acidity during each acetification cycle) and biotransformation yield (percentage of ethanol that is converted to acetic acid; Fregapane et al., 2001; de Ory et al., 2004; Krusong et al., 2015) were used as indicators of process effectiveness. The means of the calculated values of these

two parameters were recorded for each cycle, along with the cell biomass in forms of cell dried weight (CDW) values.

Analytical determinations

Acetic acid and ethanol content during acetification was measured using GC–MS (Thermo Scientific Trace GC Ultra coupled to an ISQ Single Quadrupole Mass Spectrometer, Thermo Fisher Scientific Inc., Waltham, Massachusetts, USA). The DB-wax column (length 30 m, Pressure 6.76 psi, Flow 1.0 ml/min) was used with an inlet temperature of 250°C and with splitless injection of 75 ml/min. Helium gas was employed as the carrier at 1.2 ml/min. Samples were introduced and maintained at 40°C for 5 min. The temperature increment was 5°C/min to 120°C for acetic acid or 5°C/min to 90°C for ethanol, and this was then held constant for 10 min and 3 min, respectively. Identification of acetic acid or ethanol was based on retention times compared with the Wiley, 275.L data library for the GC–MS system. Standard curve of acetic acid and ethanol was carried out and used for concentration evaluation. The cell biomass in terms of CDW in each acetification cycle was measured from the absorbance at 660 nm with a spectrophotometer (GENESYS 10VIS). The sample was diluted to an OD660nm value between 0.3 and 0.8 and converted to CDW through a linear correlation standard curve of *P. azoreducens,* one DO660 was almost equivalent to 0.3 g/L. The resulting CDW was determined in the same way as that in the fermentation medium (Krusong and Tantratian, 2014).

The volatile compounds (VOCs) produced by P8 and *A. pasteurianus* UMCC 2951 strains were removed by solid phase micro-extraction (SPME; modified from Vas and Vékey, 2004) and measured using GC–MS. First, 5 ml of the sample was placed in a 25 ml glass bottle leaving a 20 ml headspace volume. Then, 3 g of solid NaCl was added and the bottle was sealed with a septum cap (Stableflex PDMS/DVB for SPME fiber size 60 µm; Supelco Inc., Bellefonte, PA, USA). After 60 min at 37°C, to allow for extraction, the components were analyzed using GC–MS (as above). Samples were introduced and maintained at 40°C for 5 min. The temperature increment was 5°C/min to 230°C and was then held constant for 5 min. For MS determination, an electron ionization mode was employed with ion source temperature of 230°C, scan mass range of 35–300 amu, and MS transfer line at 240°C with 0 min solvent delay time. Identification of the volatile components was based on retention times and mass spectra fragmentation patterns and qualitatively compared with the Wiley, 275.L data library for the GC–MS system.

Statistical analyses

Measurements were replicated three times and their means are reported together with appropriate standard deviations (±standard deviation). The statistical significance was determined using one-way ANOVA and differences among samples were assessed using Tukey *post-hoc* test, when required. All statistical tests were performed using R, Version 4.1.0.

Results and discussion

Isolation and selection of spore former-acid producing bacteria from saccharified rice

In this study, 60 isolates were collected from a total of 30 samples of contaminated saccharified rice. Fifteen strains (labeled from P1 to P15) produced both spores and a clear halo area around the colony on *Paenibacillus*-basal agar medium supplemented with $CaCO_3$, indicating that they were acid producers. To evaluate the acetic acid ability of the spore forming strains, tests were conducted in Duran bottles for 30 days, at 30 ± 2°C; TC: 80 g/L (45 g/L acetic acid and 35 g/L ethanol, respectively), and aeration at 4 l/min, according to the method described by Krusong et al., 2015. All the strains produced acetic acid in the range between 45–55 g/L, except for strain P8, which produced a higher acetic acid amount (56 g/L; Figure 1). Given the highest amount of acetic acid by P8 strain, it was selected for further investigation.

Species level identification of P8 strain

An almost complete 16S rRNA gene sequence (1,515 bp) from gDNA of P8 strain was determined. Sequences, from the multiple alignment of the 20 sequences retrieved from NCBI and P8 16S rRNA sequence were trimmed to the same length, reducing the total sequence length to 1,354. The ML phylogenetic tree obtained (Figure 2) showed the presence of three major clades. 16S rRNA sequence of P8 strain had highest similarity (99.85%) with *P. azoreducens* CM1^T. The bootstrap value of 100, highlights the strength of the analysis. The distant matrix (Supplementary material) computed, excluding the outgroup represented by *Lactobacillus*

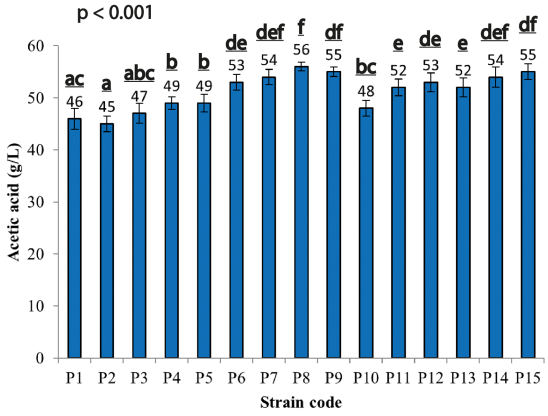

FIGURE 1
Acetic acid production by spore former-acid producing strains at 30±2°C during 30days of cultivation. Each value is the mean of three parallel replicates ± standard deviation. Significant differences among the samples in acetic acid production were represented by different letters.

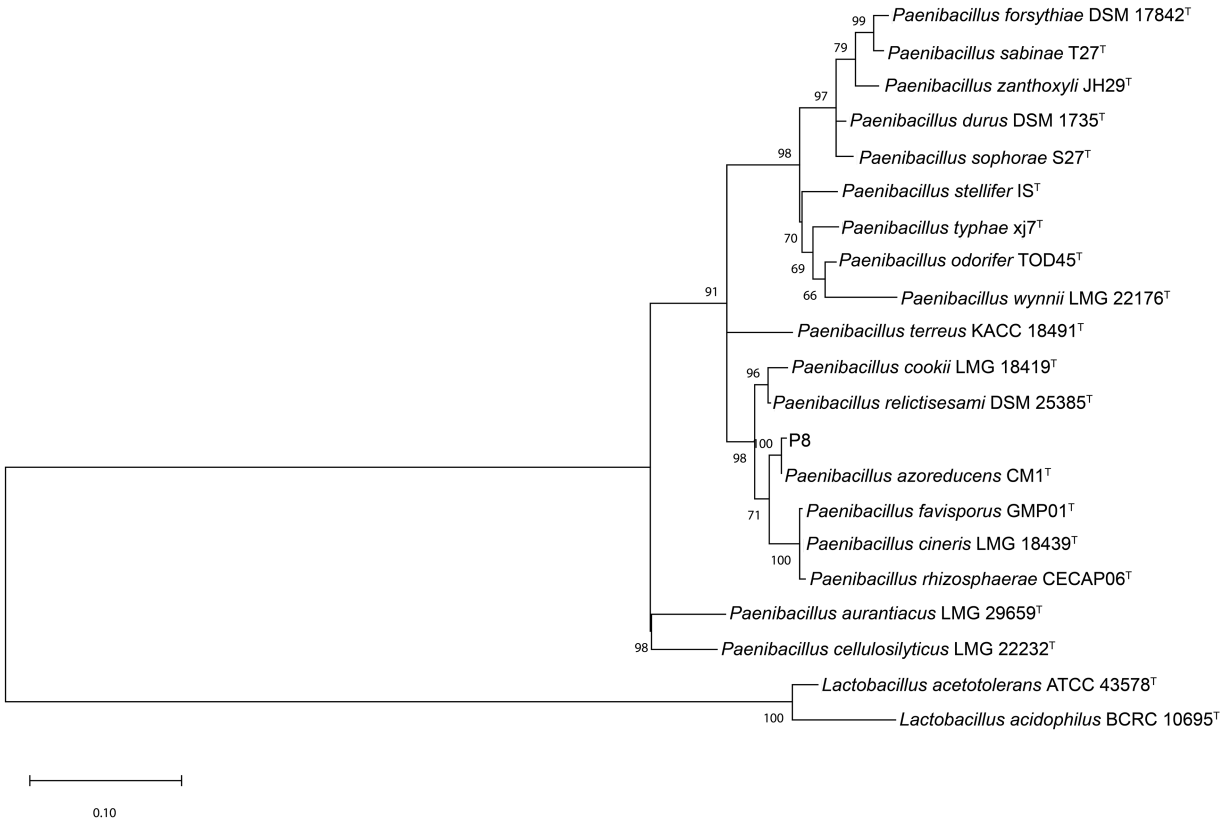

FIGURE 2
Phylogenetic tree of based on the 16S rRNA gene sequence of strain P8 and representative strains from NCBI.

strains, showed that the distant index of both P8 and *P. azoreducens* CM1^T was 0.145%, meaning the sequence similarity was 99.85%. The average distant values among overall strains were calculated resulting in 5.44%. Given the high similarity percentage compared with the average distance calculated for all 21 strains, it can be assumed that P8 is a new strain of *P. azoreducens* species. Bacteria belonging to *Paenibacillus* are widely distributed in natural matrices, especially in soil and plant roots (Grady et al., 2016). *P. azoreduncens* strains were isolated from textile wastewater and were recognized as synthetic azo dye producers (Meehan et al., 2001).

Performance of *Paenibacillus azoreducens* P8 and *Acetobacter pasteurianus* UMCC 2951 in producing acetic acid

The production of acetic acid of *P. azoreducens* P8 strain in scaling up conditions was first tested in Venturi injector bioreactor and results compared with those obtained from *A. pasteurianus* UMCC 2951, which is a well described strain for its aptitude to produce acetic acid under environmental stressors, like high temperature and HAA_i (Krusong and Tantratian, 2014; Pothimon et al., 2020). The results obtained showed that *P. azoreducens* P8 strain was able to start ethanol oxidization after 2 weeks of cultivation (Figure 3A). During the second cycle, at 6 weeks, the ethanol oxidation started after 1 week of the fermentation process. Finally, after 12 days of fermentation, the ethanol was completely oxidized, reaching a final acetic acid content of 73 g/L. Considering *A. pasteurianus* UMCC 2951, our data highlighted that the trends were almost the same comparing to P8 strain (Figure 3B). About the fermentation process for *A. pasteurianus* UMCC 2951, the start-up period was shorter. Indeed, the ethanol fermentation started after 1 day of cultivation and the first cycle finished at day 6. The second cycle was started on day 6 and after 4 days the ethanol was completely oxidized into acetic acid. However, it could be noticed that the same characteristics of acetification profile consisting of start-up and operational phases of both cultures were similar, but only difference in acetification period was observed. The difference in acetic acid production by *P. azoreducens* P8 and *A. pasteurianus* UMCC 2951 can be explained considering the different cultivation history of the two strains. *A. pasteurianus* UMCC 2951 was subjected to a selective pressure along 6 years of adaptation at high acetic acid content and high temperature (Pothimon et al., 2020). Instead, P8 is a new isolated strain. The propagation of microbial cultures under selective pressure, is well known in the case of AAB generally used for industrial vinegar production, where cultures acquire resistance to environmental stressors if continuously

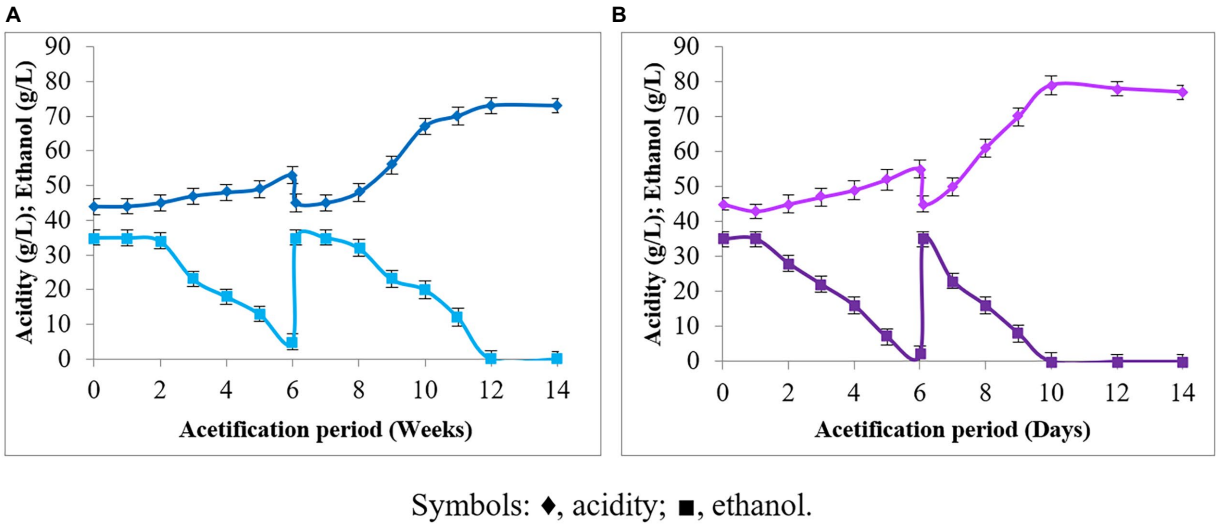

FIGURE 3
Acetification under HAA$_i$ conditions: **(A)** *Paenibacillus azoreducens* P8; **(B)** *A. pasteurianus* (UMCC 2951). Acetic acid and ethanol concentrations were adjusted constantly at 45 and 35g/L, respectively. Symbols: ♦, acidity (in terms of acetic acid); ■, ethanol. Each value is the mean of three parallel replicates ± standard deviation.

TABLE 1 Semi-continuous acetification under HAA$_i$ conditions by *Paenibacillus azoreducens* P8: 45+1g/L acetic acid with constant 35+1g/L ethanol concentration at 30+1°C (TC 80g/L).

	Experiment time (week)	Total acidity[a]		Aceti acid produced (g/L)	ETA (g/L/d)	Ethanol[a]		Ethanol oxidized[a] (g/L)	Transformation yield (%)	CDW (g/L)
		Initial (g/L)	Final (g/L)			Initial (g/L)	Final (g/L)			
Start up	6	44 ± 0.2	53 ± 0.1	9 ± 0.1	0.214	35 ± 0.1	4.9 ± 0.1	30.1 ± 0.1	29.9	0.026
Cycle 1	6	45 ± 0.3	73 ± 0.3	28 ± 0.3	0.671	35 ± 0.3	3 ± 0.2	32 ± 0.2	87.5	0.029
Cycle 2	5	45 ± 0.2	75 ± 0.2	30 ± 0.2	0.857	35 ± 0.4	1 ± 0.1	34 ± 0.2	88.2	0.043
Cycle 3	5	45 ± 0.3	78 ± 0.2	33 ± 0.2	0.943	35 ± 0.1	1 ± 0.1	34 ± 0.1	97.1	0.045
Cycle 4	5	45 ± 0.2	76 ± 0.3	31 ± 0.2	0.886	35 ± 0.3	2 ± 0.3	33 ± 0.3	93.9	0.04
Cycle 5	5	45 ± 0.5	78 ± 0.4	33 ± 0.4	0.943	35 ± 0.3	1 ± 0.2	34 ± 0.2	97.1	0.048
Cycle 6	6	45 ± 0.2	69 ± 0.5	24 ± 0.3	0.571	35 ± 0.1	3 ± 0.1	32 ± 0.1	75	0.027
Cycle 7	6	45 ± 0.4	70 ± 0.2	25 ± 0.3	0.6	35 ± 0.1	3 ± 0.1	32 ± 0.1	78.1	0.031
Cycle 8	5	45 ± 0.5	78 ± 0.2	34 ± 0.3	0.971	35 ± 0.3	0	35 ± 0.3	97.1	0.042
Cycle 9	5	45 ± 0.3	78 ± 0.5	33 ± 0.4	0.943	35 ± 0.2	1 ± 0.1	34 ± 0.1	97.1	0.048
Average[b]					**0.814**				**90.1**	

[a]Values represent the mean ± standard deviation of triplicate.
[b]Average ETA and transformation yield (values in bold) were calculated among nine semi-continuous cycles, not including start-up phase.
ETA, acetification rate; CDW, cell dried weight.

maintained under stringent physiological conditions (Azuma et al., 2009; Gullo et al., 2012).

Semi-continuous acetification by *Paenibacillus azoreducens* P8

To evaluate large scale production of acetic acid by *P. azoreducens* P8, a semi-continuous process, in a 100 L internal Venturi injector bioreactor, was developed. As reported by many studies the biological process of vinegar fermentation can be considered completed when the amount of residual ethanol is around or below 5 g/L (Ebner et al., 1996; Ndoye et al., 2007; Gullo et al., 2014; Krusong et al., 2015). In this study, between each cycle, a 40% of the total volume was replaced by fresh medium and, subsequently, the new cycle was started. A total of nine cycles were performed in which *P. azoreducens* P8 was continuously under stressors, like high acetic acid and ethanol. Full data are reported in Table 1. In the startup phase and the first cycle, the ETA values (0.214 g/L/d and 0.671 g/L/d, respectively) were low, showing an initial adaptation stage of the culture to fermentation. This consideration is supported by the

CDW values, showing that the weight of the dried cell was 0.026 at the start-up phase and 0.029 at cycle 1. However, during the first cycle, the ETA value reached 0.671 g/L/d, indicating the fermentation start. From cycle 2 until the end of the process, the amount of acetic acid produced was considerable (about 30 g/L for each cycle) except for cycles 6 and 7 in which a slight decrease was observed (24 ± 0.3 g/L and 25 ± 0.3 g/L, respectively). This reduction can be due to the oscillation of the cell viability (CDW 0.027 in the cycle 6 and 0.031 in the cycle 7), that generally might occur (Maestre et al., 2008) considering the toxic effect of acetic acid on cells (Saeki et al., 1997; Lu et al., 1999; Baena-Ruano et al., 2010; Song et al., 2022). The ETA and the CDW values were consistently with the acetic acid production trend. The biotransformation percentage, excluding the startup phase, ranged from 75% up to 97% (90.1% as average). Comparing *P. azoreducens* P8 with *A. pasteurianus* UMCC 2951, previously tested (Pothimon et al., 2020), the average of acetic acid production was slightly reduced (30.11 g/L on average of acetic acid produced by P8; 52 g/L on average of *A. pasteurianus* UMCC 2951). Compared to others AAB used in semi-continuous processes, the ETA values resulted to be low, such as 2.2 + 0.06 g/L/d by an industrial culture of vinegar (Fregapane et al., 2001); 12 g/L/d by *A. senegalensis* (CWBI-B418^T) (Ndoye et al., 2007) and 5 g/L/h *A. pasteurianus* (Mounir et al., 2018). These differences can be correlated to the handling of cultures, especially to the different cultivation time under selective pressure, as previously discussed (Paragraph 3.3). Thus, the new isolate *P. azoreducens* P8, which showed appreciable aptitude to produce acetic acid, can be considered a suitable candidate for industrial acetic acid production. It is reasonable to suppose that longer adaptation cycles to fermentation conditions could further enhance the amount of acetic acid produced.

At current this strategy is not aimed at producing food grade acetic acid because the absence of deep information on the use of *Paenibacillus* strains in food, but it can be of great relevance to produce biological acetic acid for non-food uses.

Main advantages of the strategy proposed in this study arise at least from two technological traits that can affect the biological production of acetic acid. AAB have optimal temperature growth of 28–30°C and in absence of thermotolerant strains, the oxidation of ethanol into acetic acid could be stopped because of the exergonic nature of the reaction (Ebner et al., 1996; Gullo et al., 2016). Moreover, AAB could oxidize acetic acid when ethanol is depleted and can produce bacterial cellulose, which is undesired during organic acid production (La China et al., 2018). If the process is aimed at producing acetic acid at higher rate than vinegar, a multiple culture of AAB and other bacteria, which can growth at higher temperature and that do not oxidize acetic acid could be an innovative introduction for the biological production of acetic acid. Based on these considerations *P. azoreducens* P8 can be considered a helper strain in producing acetic acid in a multiple starter, as a booster of the fermentation, contributing to maintain the acetic acid level, avoiding losses during processes.

Volatile compounds produced by *Paenibacillus azoreducens* P8 and *Acetobacter pasteurianus* UMCC 2951 strains, under HAA_i conditions

In this study, to have more knowledge on microbial compounds of industrial interest from *P. azoreducens* P8 and *A. pasteurianus* UMCC 2951, VOCs composition was determined. The VOCs composition of rice wine, which was the alcoholic substrate used to produce acetic acid, is highly complex and depends on many factors, including the microbial composition of the starter and the fermentation practices. Main VOCs categories, previously described, belong to esters, alcohols, amino acids, and organic acids (Zhang et al., 2022).

The VOCs distribution in terms of chemical families was found to be different among the fermented products obtained by *P. azoreducens* P8 and *A. pasteurianus* UMCC 2951, respectively (Figure 4A). A total of 40 and 37 VOCs were found in *P. azoreducens* P8 and *A. pasteurianus* UMCC 2951 fermented products, respectively. Among all the identified VOCs, 20 were produced by both culture (Table 2). The most abundant VOCs belonged to esters (29.46% for P8 and 14.62% for UMCC 2951) and acids (15.54% for P8 and 12.14 for UMCC 2951; Figure 4B). VOCs in these chemical families were represented by products or intermediates of the oxidation of ethanol into acetic acid. In the case of esters, the most abundant VOC was ethyl acetate for both culture strains, whereas for acids, the most abundant VOC was acetic acid. Other VOCs species belong to these chemical families were intermediates of the fermentation process (e.g., 2-methyl propanoic acid or pentanoic acid) detected in different amount and different chemical species. Regarding other abundant chemical families, alcohols and aldehydes were the most abundant. In detail, we observed the same number of species of alcohols in both cultures (6 per each sample), but considering the total percentage, alcohols were most abundant in *A. pasteurianus* UMCC 2951 (8.41%) culture compared to *P. azoreducens* P8 (3.72%). In the case of aldehydes, the number of VOCs were different (3 for P8 and 5 for *A. pasteurianus* UMCC 2951, while the total percentage was higher in P8 culture (8.1%) compared to *A. pasteurianus* UMCC 2951 (4.46%). Among these chemical families, the two samples were characterized by a different amount of VOCs belonging to acids and esters. In particular, in *P. azoreducens* P8 culture the number of acids and esters was higher than in *A. pasteurianus* UMCC 2951 culture. Also, ethers were found to be abundant in both samples, (9.8% of the total in P8 and 2.98% in UMCC 2951; Figure 4B). In addition to the chemical families discussed, other VOCs belong to different chemical families were detected in small amount. Phenols and benzene derivatives were detected in both samples (Figure 4A). Some chemical species were detected just in one sample. For example, one amide (3-amino-4,5,6-trimethyl-thieno[2,3-b]pyridine-2-carboxylic acid tert-butylamide) and one pyrazine (methyl-pyrazine) were produced by *P. azoreducens* P8. The VOC analysis performed in this study

10.3389/fmicb.2022.991688

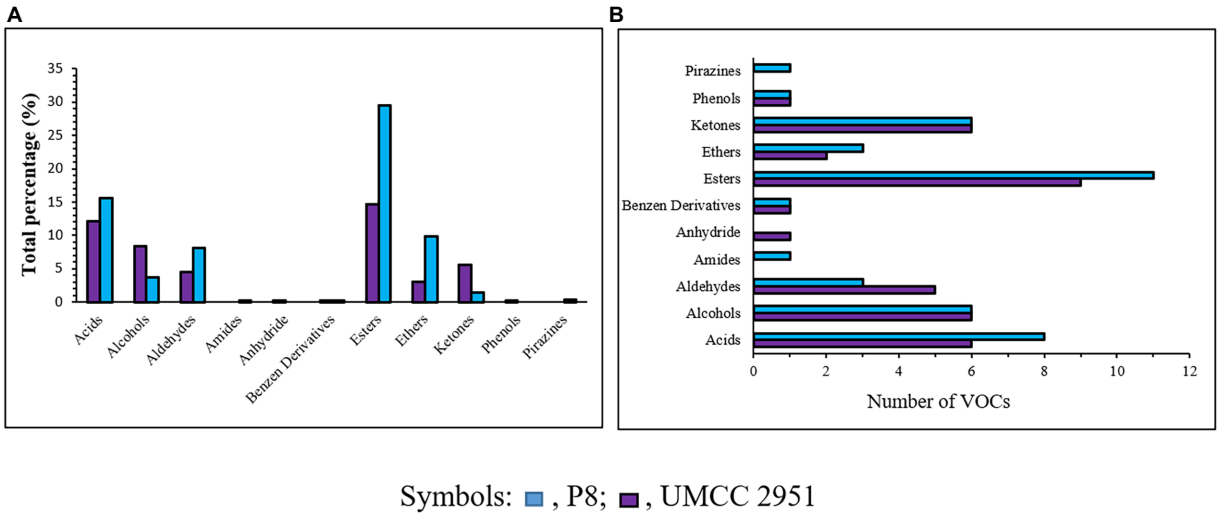

FIGURE 4
VOCs classification in the fermentation process using both *P. azoreducens* P8 and *Acetobacter pasteurianus* (UMCC 2951). **(A)** Number of compounds grouped in chemical families. **(B)** Total percentages for each chemical family detected.

TABLE 2 VOCs composition in samples obtained from *P. azoreducens* P8 and *A. aceti* WK acetification.

CAS#	Chemical family	Formula	*P. azoreducens* P8			*Acetobacter pasteurianus* UMCC 2951		
			% of total	Component area	Component RT	% of Total	Component area	Component RT
	Acids							
3,724-65-0	2-Butenoic acid	$C_4H_6O_2$	-	-	-	0.04	5065418.9	25.3566
64-19-7	*Acetic acid*	$C_2H_4O_2$	7.21	5,789,197,422	18.3692	7.89	7,142,863,733	18.2338
65-85-0	Benzoic acid	$C_7H_6O_2$	0.05	7,451,135.9	33.8314	-	-	-
107-92-6	*Butanoic acid*	$C_4H_8O_2$	0.45	67,991,028.8	22.9552	0.21	25,357,116.2	22.9643
334-48-5	Decanoic acid	$C_{10}H_{20}O_2$	0.01	1,056,726.4	31.8485	-	-	-
142-62-1	*Hexanoic acid*	$C_6H_{12}O_2$	0.53	79,128,285.9	26.3835	0.08	9,829,193	26.3913
124-07-2	Octanoic acid	$C_8H_{16}O_2$	0.26	39,195,729.5	29.2712	-	-	-
109-52-4	*Pentanoic acid*	$C_5H_{10}O_2$	5.02	752,384,101	23.6423	1.8	216,205,301	23.6736
79-31-2	*Propanoic acid, 2-methyl-*	$C_4H_8O_2$	2.01	301,178,116	21.8405	2.12	253,806,031	21.8385
	Alcohols							
24,629-25-2	(S)-(+)-Isoleucinol	$C_6H_{15}NO$	0.11	16,888,981.6	25.3551	-	-	-
60-12-8	*Benzeneethanol*	$C_8H_{10}O$	2.32	348,606,611	27.436	-	-	-
100-51-6	Benzyl alcohol	C_7H_8O	-	-	-	0.06	7,094,432.2	26.9161
913,176-41-7	Caryophyllenyl alcohol	$C_{15}H_{26}O$	0.02	2,530,766.1	29.4892	-	-	-
123-51-3	*Isoamylalcohol*	$C_5H_{12}O$	1.24	185,441,662	13.3035	2.91	348,946,524	13.4474
78-83-1	*Isobutylalcohol*	$C_4H_{10}O$	0.02	2,559,288.9	9.6436	0.07	8,118,441.1	9.6442
10,482-56-1	L-.alpha.-Terpineol	$C_{10}H_{18}O$	-	-	-	0.03	3,331,502.1	24.2235
108-95-2	Phenol	C_6H_6O	0.01	1,694,766.4	28.6518	-	-	-
	Aldehydes							
98-01-1	2-furan-carboxaldehyde	$C_5H_4O_2$	4.47	670,371,399	19.8976	-	-	-
620-02-0	2-Furancarboxaldehyde, 5-methyl-	$C_6H_6O_2$	-	-	-	0.46	55,092,770.7	22.1427
67-47-0	5-Hydroxymethylfurfural	$C_6H_6O_3$	-	-	-	0.01	1,561,246.1	34.651
75-07-0	*Acetaldehyde*	C_2H_4O	0.03	4,828,477.5	3.4066	0.06	6,999,246.9	3.4061
100-52-7	*Benzaldehyde*	C_7H_6O	3.6	540,672,024	21.2164	3.86	463,180,656	21.2608
122-78-1	Phenyleacetaldehyde	C_8H_8O	-	-	-	0.07	8,709,543.5	23.4808
	Esters							
2,000,696-25-7	.beta.-1,5-O-Dibenzoyl-ribofuranose	$C_{19}H_{18}O_7$	-	-	-	0.03	3,794,906.6	33.8524

(Continued)

TABLE 2 (Continued)

CAS#	Chemical family	Formula	*P. azoreducens* P8			*Acetobacter pasteurianus* UMCC 2951		
			% of total	Component area	Component RT	% of Total	Component area	Component RT
108-64-5	1-Butanol, 3-methyl-, acetate	$C_7H_{14}O_2$	0.16	24,353,399.3	9.0075	-	-	-
123-92-2	*1-Butanol, 3-methyl-, acetate*	$C_7H_{14}O_2$	0.23	34,999,276.3	10.7144	0.83	98,998,845.5	10.8224
96-48-0	2(3H)-Furanone, dihydro-	$C_4H_6O_2$	-	-	-	0.07	7,850,092.2	23.235
7,779-72-8	3-methylbutyl 2-oxopropanoate	$C_8H_{14}O_3$	-	-	-	0.22	25,893,946.9	10.5573
2,000,224-92-1	5,6,7,8-Tetrahydro-8,8-dimethyl-2-indolizinecarboxylic acid methyl ester	$C_{12}H_{17}NO_2$	11	1,650,383,131	32.2686	-	-	-
110-19-0	Acetic acid, 2-methylpropyl ester	$C_6H_{12}O_2$	0.93	139,127,424	7.5917	-	-	-
103-45-7	*Acetic acid, 2-phenylethyl ester*	$C_{10}H_{12}O_2$	0.41	61,756,862.5	26.1146	0.82	98,203,150.3	26.1187
101-97-3	Acetic acid, phenyl-, ethyl ester	$C_{10}H_{12}O_2$	0.16	23,761,288.8	25.6463	-	-	-
140-11-4	Acetic acid, phenylmethyl ester	$C_9H_{10}O_2$	-	-	-	0.03	3,705,089	24.7854
2,000,532-52-8	Adipic acid, 2,4-dimethylpent-3-yl isobutyl ester	$C_{17}H_{32}O_4$	0.02	3,406,092.8	27.0345	-	-	-
105-54-4	Butanoic acid, ethyl ester	$C_6H_{12}O_2$	0.63	94,570,465.9	8.1925	-	-	-
141-78-6	*Ethyl Acetate*	$C_4H_8O_2$	15.69	2,353,245,444	5.0955	10.91	1,308,584,233	5.0465
110-19-0	Isobutyl acetate	$C_6H_{12}O_2$	-	-	-	1.02	122,616,009	7.5834
166,273-38-7	Pentanoic acid, 5-hydroxy-, 2,4-di-t-butylphenyl esters	$C_{19}H_{30}O_3$	0.01	892,790.9	28.7834	-	-	-
97-64-3	*Propanoic acid, 2-hydroxy-, ethyl ester*	$C_5H_{10}O_3$	0.22	33,654,169.2	17.04	0.69	82,300,126.9	17.0678
	Ketones							
2,000,008-43-4	1 - cyclopentene - 3,4 - di - one	$C_5H_4O_2$	-	-	-	0.29	35,233,139.8	22.3792
56,599-61-2	1,3-Dioxolane, 4,5-dimethyl-2-pentadecyl-	$C_{20}H_{40}O_2$	0.01	793,322.3	11.5766	-	-	-
431-03-8	2,3-Butanedione	$C_4H_6O_2$	-	-	-	2.26	271,480,012	6.803
513-86-0	*2-Butanone, 3-hydroxy-*	$C_4H_8O_2$	1.13	168,997,873	15.5356	2.39	286,712,291	15.6043
10,150-87-5	*2-Butanone, 4-(acetyloxy)-*	$C_6H_{10}O_3$	0.17	25,995,012.6	21.7543	0.49	12,569,367.4	21.7532
4,906-24-5	*3-(Acetyloxy)-2-butanone*	$C_6H_{10}O_3$	0.14	20,934,458.3	18.0772	0.11	13,094,275.1	18.0929
127-51-5	3-Buten-2-one, 3-methyl-4-(2,6,6-trimethyl-2-cyclohexen-1-yl)-	$C_{14}H_{22}O$	0.01	1,576,299.6	26.7035	-	-	-
98,419-10-4	4,4-Dimethyl-3-(3-methylbut-2-enylidene)octane-2,7-dione	$C_{15}H_{24}O_2$	-	-	-	0.01	1,016,732.5	30.6742
2,715-54-0	Acetophenone, 2,4,5-triethyl-	$C_{14}H_{20}O$	0.01	2,027,351.4	25.8559	-	-	-
	Ethers							
624-92-0	*Disulfide, dimethyl*	$C_2H_6S_2$	0.02	3,128,137.3	9.1197	0.09	11,247,301.7	9.1324
115-10-6	*Methane, oxybis-*	C_2H_6O	9.64	1,446,391,003	5.8865	2.89	347,279,203	5.8372
20,662-83-3	Oxazole, 4,5-dimethyl-	C_5H_7NO	0.14	20,468,078.4	11.9103	-	-	-
	Benzene derivatives							
91-20-3	*Naphthalene*	$C_{10}H_8$	0.02	3,087,984.8	25.1307	0.07	8,544,835.9	25.1377
	Anhydrides							
108-24-7	Acetic acid, anhydride	$C_4H_6O_3$	-	-	-	0.09	10,738,673.1	14.2065
	Amides							
2,000,501-84-7	3-amino-4,5,6-trimethyl-thieno[2,3-B]pyridine-2-carboxylic acid tert-butylamide	$C_{15}H_{21}N_3OS$	0.11	16,468,136.4	36.1808	-	-	-
	Phenol							
54,063-14-8	1,3-Dioxan-5-ol, 4,4,5-trimethyl-	$C_7H_{14}O_3$	-	-	-	0.04	4,713,875.2	17.5423
	Pirazines							
109-08-0	Pyrazine, methyl-	$C_5H_6N_2$	0.32	48,512,571.6	15.1769	-	-	-

VOCs retrieved were grouped based on chemical families.

provided data of interest for further studies aimed at building up a coculture fermentation for evaluating the amount of acetic acid and other microbial products of industrial interest.

Conclusion

In study we screened and characterized a new spore-former acid producing bacterium, identified as *P. azoreducens*, strain P8. The strain was tested for the ability of producing acetic acid following industrial vinegar technology. The results obtained testing *P. azoreducens* P8 highlight the abilities of the strain in acetification process, even though the fermentation performances were slightly lower than the AAB usually used at industrial scale. *P. azoreducens* P8 possessed ethanol and acidity tolerances, developed during the early stages of HAA_i process (start up and the cycle 1). Comparing the fermentation activities of *P. azoreducens* P8 with *A. pasteurianus* UMCC 2951, the amount of acetic acid obtained was relatively high. Regarding the VOCs analysis, some of them were shared among the fermented broth by the *P. azoreducens* P8 and *A. pasteurianus* UMCC 2951. Given the advantages of the application in the fermentation processes at industrial of spore-forming bacteria, we can confirm that *P. azoreducens* P8, after future analysis to better clarify its genomic and phenotypic features, could be suitable for fermentation processes. Based on the output of this study, it is reasonable to suppose its use in single or multiple cultures to improve the stability and the production yield of acetic acid by biological processes.

Data availability statement

The data presented in the study are deposited in the Genebank repository, accession number OP353700.1.

Author contributions

WK: conceptualization, funding acquisition, project administration, validation, and writing—original draft. MG: conceptualization, validation, review and editing, and funding acquisition. RP: methodology, formal analysis, and investigation. SL: conceptualization, validation, and writing—review. All authors contributed to the article and approved the submitted version.

Funding

The authors gratefully acknowledge two funding sources of this research consisting of School of Food Industry Research Fund (2562–01-07001), King Mongkut's Institute of Technology Ladkrabang, Thailand and Thailand Toray Science Foundation: Science and Technology Research Grant (Year 2018).

Conflict of interest

The authors declare that the research was conducted in the absence of any commercial or financial relationships that could be construed as a potential conflict of interest.

Publisher's note

References

Abecasis, A. B., Serrano, M., Alves, R., Quintais, L., Pereira-Leal, J. B., and Henriques, A. O. (2013). A genomic signature and the identification of new sporulation genes. *J. Bacteriol.* 195, 2101–2115. doi: 10.1128/jb.02110-12

Azuma, Y., Hosoyama, A., Matsutani, M., Furuya, N., Horikawa, H., Harada, T., et al. (2009). Whole-genome analyses reveal genetic instability of *Acetobacter pasteurianus*. *Nucleic Acids Res.* 37, 5768–5783. doi: 10.1093/nar/gkp612

Baena-Ruano, S., Jiménez-Ot, C., Santos-Dueñas, I. M., Jiménez-Hornero, J. E., Bonilla-Venceslada, J. L., Álvarez-Cáliz, C., et al. (2010). Influence of the final ethanol concentration on the acetification and production rate in the wine vinegar process. *J. Chem. Technol. Biotechnol.* 85, 908–912. doi: 10.1002/jctb.2368

Berge, O., Guinebretière, M. H., Achouak, W., Normand, P., and Heulin, T. (2002). *Paenibacillus graminis* sp. nov. and *Paenibacillus odorifer* sp. nov., isolated from plant roots, soil and food. *Int. J. Syst. Evol. Microbiol.* 52, 607–616. doi: 10.1099/00207713-52-2-607

Chiellini, C., Iannelli, R., Lena, R., Gullo, M., and Petroni, G. (2014). Bacterial community characterization in paper mill white water. *Bioresources* 9, 2541–2559. doi: 10.15376/biores.9.2.2541-2559

Chou, J. H., Chou, Y. J., Lin, K. Y., Sheu, S. Y., Sheu, D. S., Arun, A. B., et al. (2007). *Paenibacillus fonticola* sp. nov., isolated from a warm spring. *Int. J. Syst. Evol. Microbiol.* 57, 1346–1350. doi: 10.1099/ijs.0.64872-0

da Costa, R. A., Andrade, I. E. P. C., Pinto, O. H. B., de Souza, B. B. P., Fulgêncio, D. L. A., Mendonca, M. L., et al. (2022). A novel family of non-secreted tridecaptin lipopeptide produced by *Paenibacillus elgii*. *Amino Acids*. doi: 10.1007/s00726-022-03187-9

De Ory, I., Romero, L. E., and Cantero, D. (2004). Operation in semi-continuous with a closed pilot plant scale acetifier for vinegar production. *J. Food Eng.* 63, 39–45. doi: 10.1016/S0260-8774(03)00280-2

Ebner, H., Sellmer, S., and Follmann, H. (1996). "Acetic acid" in *Biotechnology: A Multi-Volume Comprehensive Treatise. 2nd Edn*. H. J. Rehm and G. Reed (Weinheim, Germany: Wiley-VCH), 381–401.

Edgar, R. C. (2004). MUSCLE: multiple sequence alignment with high accuracy and high throughput. *Nucleic Acids Res.* 32, 1792–1797. doi: 10.1093/nar/gkh340

Ewing, B., and Green, P. (1998). Base-calling of automated sequencer traces using Phred. II. Error probabilities. *Genome Res.* 8, 186–194. doi: 10.1101/gr.8.3.186

Fregapane, G., Rubio-Fernández, H., and Salvador, M. D. (2001). Influence of fermentation temperature on semi-continuous acetification for wine vinegar production. *Eur. Food Res. Technol.* 213, 62–66. doi: 10.1007/S002170100348

Grady, E. N., MacDonald, J., Liu, L., Richman, A., and Yuan, Z. C. (2016). Current knowledge and perspectives of *Paenibacillus*: a review. *Microb. Cell Factories* 15, 1–18. doi: 10.1186/s12934-016-0603-7

Gullo, M., Mamlouk, D., De Vero, L., and Giudici, P. (2012). *Acetobacter pasteurianus* strain AB0220: cultivability and phenotypic stability over 9 years of preservation. *Curr. Microbiol* 64, 576–580. doi: 10.1007/s00284-012-0112-9

Gullo, M., Verzelloni, E., and Canonico, M. (2014). Aerobic submerged fermentation by acetic acid bacteria for vinegar production: process and biotechnological aspects. *Process Biochem.* 49, 1571–1579. doi: 10.1016/j.procbio.2014.07.003

Gullo, M., Zanichelli, G., Verzelloni, E., Lemmetti, F., and Giudici, P. (2016). Feasible acetic acid fermentations of alcoholic and sugary substrates in combined operation mode. *Process Biochem.* 51, 1129–1139. doi: 10.1016/j.procbio.2016.05.018

He, Y., Xie, Z., Zhang, H., Liebl, W., Toyama, H., and Chen, F. (2022). Oxidative fermentation of acetic acid bacteria and its products. *Front. Microbiol.* 13:879246. doi: 10.3389/fmicb.2022.879246

Kaziūnienė, J., Mažylytė, R., Krasauskas, A., Toleikienė, M., and Gegeckas, A. (2022). Optimizing the growth conditions of the selected plant-growth-promoting Rhizobacteria *Paenibacillus* sp. MVY-024 for industrial scale production. *Biology* 11:745. doi: 10.3390/biology11050745

Kersters, K., Lisdiyanti, P., Komagata, K., and Swings, J. (2006). "The family Acetobacteraceae: The Genera *Acetobacter*, *Acidomonas*, *Asaia*, *Gluconacetobacter*, *Gluconobacter*, and *Kozakia*," in *The Prokaryotes*. eds. M. Dworkin, S. Falkow, E. Rosenberg, K. H. Schleifer and E. Stackebrandt (New York, NY: Springer), 163–200.

Kirschner, E. M. (1996). Growth of top 50 chemicals slowed in 1995 from very high 1994 rate. *Chem. Eng. News* 74, 16–22. doi: 10.1021/cen-v074n015.p016

Krusong, W., Pornpukdeewatana, S., Kerdpiboon, S., and Tantratian, S. (2014). Prediction of influence of stepwise increment of initial acetic acid concentration in charging medium on acetification rate of semi-continuous process by artificial neural network. *LWT-Food Sci. Technol.* 56, 383–389. doi: 10.1016/j.lwt.2013.11.026

Krusong, W., and Tantratian, S. (2014). Acetification of rice wine by *Acetobacter aceti* using loofa sponge in a low-cost reciprocating shaker. *J. Appl. Microbiol.* 117, 1348–1357. doi: 10.1111/jam.12634

Krusong, W., Vichitraka, A., and Pornpakdeewattana, S. (2007). Luffa sponge as supporting material of *Acetobacter aceti* WK for corn vinegar production in semi-continuous process. *KMITL Sci. J.* 7, 63–68.

Krusong, W., Yaiyen, S., and Pornpukdeewatana, S. (2015). Impact of high initial concentrations of acetic acid and ethanol on acetification rate in an internal Venturi injector bioreactor. *J. Appl. Microbiol.* 118, 629–640. doi: 10.1111/jam.12715

Kumar, S., Stecher, G., Li, M., Knyaz, C., and Tamura, K. (2018). MEGA X: molecular evolutionary genetics analysis across computing platforms. *Mol. Biol. Evol.* 35, 1547–1549. doi: 10.1093/molbev/msy096

La China, S., De Vero, L., Anguluri, K., Brugnoli, M., Mamlouk, D., and Gullo, M. (2021). Kombucha tea as a reservoir of cellulose producing bacteria: assessing diversity among Komagataeibacter isolates. *Appl. Sci.* 11:1595. doi: 10.3390/app11041595

La China, S., Zanichelli, G., De Vero, L., and Gullo, M. (2018). Oxidative fermentations and exopolysaccharides production by acetic acid bacteria: a mini review. *Biotechnol. Lett.* 40, 1289–1302. doi: 10.1007/s10529-018-2591-7

Lal, S., and Tabacchioni, S. (2009). Ecology and biotechnological potential of *Paenibacillus polymyxa*: a minireview. *Indian J. Microbiol.* 49, 2–10. doi: 10.1007/s12088-009-0008-y

Layman, P. (1998). Acetic acid industry gears up for possible building boom. *Chem. Eng. News Arch.* 76, 17–18. doi: 10.1021/cen-v076n031.p017

Li, P., Lin, W., Liu, X., Li, S., Luo, L., and Lin, W. T. (2016). *Paenibacillus aceti* sp. nov., isolated from the traditional solid-state acetic acid fermentation culture of Chinese cereal vinegar. *Int. J. Syst. Evol. Microbiol.* 66, 3426–3431. doi: 10.1099/ijsem.0.001214

Lu, S. F., Lee, F. L., and Chen, H. K. (1999). A thermotolerant and high acetic acid-producing bacterium *Acetobacter* sp. I14–2. *J. Appl. Microbiol.* 86, 55–62. doi: 10.1046/j.1365-2672.1999.00633.x

Maestre, O., Santos-Dueñas, I. M., Peinado, R., Jiménez-Ot, C., García-García, I., and Mauricio, J. C. (2008). Changes in amino acid composition during wine vinegar production in a fully automatic pilot acetator. *Process Biochem.* 43, 803–807. doi: 10.1016/j.procbio.2008.03.007

Martín-Espejo, J. L., Gandara-Loe, J., Odriozola, J. A., Reina, T. R., and Pastor-Pérez, L. (2022). Sustainable routes for acetic acid production: traditional processes vs a low-carbon, biogas-based strategy. *Sci. Total Environ.* 840:156663. doi: 10.1016/j.scitotenv.2022.156663

Marwoto, B., Nakashimada, Y., Kakizono, T., and Nishio, N. (2004). Metabolic analysis of acetate accumulation during xylose consumption by *Paenibacillus polymyxa*. *Appl. Microbiol. Biotechnol.* 64, 112–119. doi: 10.1007/s00253-003-1435-z

Mcclure, P. J. (2006). Spore-forming bacteria. *Food Spoilage Microorg.* 579–623. doi: 10.1533/9781845691417.5.579

Meehan, C., Bjourson, A. J., and McMullan, G. (2001). *Paenibacillus azoreducens* sp. nov., a synthetic azo dye decolorizing bacterium from industrial wastewater. *Int. J. Syst. Evol. Microbiol.* 51, 1681–1685. doi: 10.1099/00207713-51-5-1681

Mounir, M., Fauconnier, M. L., Afechtal, M., Thonart, P., Alaoui, M. I., and Delvigne, F. (2018). Aroma profile of pilot plant-scale produced fruit vinegar using a thermotolerant *Acetobacter pasteurianus* strain isolated from *Moroccan cactus*. *Acetic Acid Bact.* 7:7312. doi: 10.4081/aab.2018.7312

Nakashimada, Y., Kanai, K., and Nishio, N. (1998). Optimization of dilution rate, pH and oxygen supply on optical purity of 2, 3-butanediol produced by *Paenibacillus polymyxa* in chemostat culture. *Biotechnol. Lett.* 20, 1133–1138. doi: 10.1023/a:1005324403186

Ndoye, B., Lebecque, S., Destain, J., Guiro, A. T., and Thonart, P. (2007). A new pilot plant scale acetifier designed for vinegar production in sub-Saharan Africa. *Process Biochem.* 42, 1561–1565. doi: 10.1016/j.procbio.2007.08.002

Oktari, A., Supriatin, Y., Kamal, M., and Syafrullah, H. (2017). The bacterial endospore stain on schaeffer fulton using variation of methylene blue solution. *J. Phys. Conf. Ser.* 812:012066.

Pothimon, R., Gullo, M., La China, S., Thompson, A. K., and Krusong, W. (2020). Conducting high acetic acid and temperature acetification processes by *Acetobacter pasteurianus* UMCC 2951. *Process Biochem.* 98, 41–50. doi: 10.1016/j.procbio.2020.07.022

Roux, V., and Raoult, D. (2004). *Paenibacillus massiliensis* sp. nov. *Paenibacillus sanguinis* sp. nov. and *Paenibacillus timonensis* sp. nov., isolated from blood cultures. *Int. J. Syst. Evol. Microbiol.* 54, 1049–1054. doi: 10.1099/ijs.0.02954-0

Saeki, A., Theeragool, G., Matsushita, K., Toyama, H., Lotong, N., and Adachi, O. (1997). Development of thermotolerant acetic acid bacteria useful for vinegar fermentation at higher temperatures. *Biosci. Biotechnol. Biochem.* 61, 138–145. doi: 10.1271/bbb.61.138

Scheldeman, P., Goossens, K., Rodriguez-Diaz, M., Pil, A., Goris, J., Herman, L., et al. (2004). *Paenibacillus lactis* sp. nov., isolated from raw and heat-treated milk. *Int. J. Syst. Evol. Microbiol.* 54, 885–891. doi: 10.1099/ijs.0.02822-0/

Song, J., Wang, J., Wang, X., Zhao, H., Hu, T., Feng, Z., et al. (2022). Improving the acetic acid fermentation of *Acetobacter pasteurianus* by enhancing the energy metabolism. *Front. Bioeng. Biotechnol.* 10:815614. doi: 10.3389/fbioe.2022.815614

Tamura, K., and Nei, M. (1993). Estimation of the number of nucleotide substitutions in the control region of mitochondrial DNA in humans and chimpanzees. *Mol. Biol. Evol.* 10, 512–526. doi: 10.1093/oxfordjournals.molbev.a040023

Vas, G., and Vékey, K. (2004). Solid-phase microextraction: a powerful sample preparation tool prior to mass spectrometric analysis. *J. Mass Spectrom.* 39, 233–254. doi: 10.1002/jms.606

Velazquez, E., De Miguel, T., Poza, M., Rivas, R., Rosselló-Mora, R., and Villa, T. G. (2004). *Paenibacillus favisporus* sp. nov., a xylanolytic bacterium isolated from cow faeces. *Int. J. Syst. Evol. Microbiol.* 54, 59–64. doi: 10.1099/ijs.0.02709-0

Wiegel, J. (2015). "Thermoanaerobacter," in *Bergey's Manual of Systematics of Archaea and Bacteria*. eds. R. U. Onyenwoke and J. Wiegel (New York: John Wiley & Sons, Inc., in association with Bergey's Manual Trust), 1–29.

Zhang, H., Wang, Y., Feng, X., Iftikhar, M., Meng, X., and Wang, J. (2022). The analysis of changes in nutritional components and flavor characteristics of Wazu rice wine during fermentation process. *Food Anal. Methods* 15, 1132–1142. doi: 10.1007/s12161-021-02188-w

frontiers | Frontiers in Microbiology

TYPE Original Research
PUBLISHED 24 November 2022
DOI 10.3389/fmicb.2022.1060160

OPEN ACCESS

EDITED BY
Maria Gullo,
University of Modena and Reggio Emilia, Italy

REVIEWED BY
Salvatore La China,
University of Modena and Reggio Emilia, Italy
Uwe Deppenmeier,
University of Bonn, Germany

*CORRESPONDENCE
Luc De Vuyst
luc.de.vuyst@vub.be

SPECIALTY SECTION
This article was submitted to Food Microbiology, a section of the journal Frontiers in Microbiology

RECEIVED 02 October 2022
ACCEPTED 04 November 2022
PUBLISHED 24 November 2022

CITATION
Pelicaen R, Weckx S, Gonze D and De Vuyst L (2022) Application of comparative genomics of *Acetobacter* species facilitates genome-scale metabolic reconstruction of the *Acetobacter ghanensis* LMG 23848^T and *Acetobacter senegalensis* 108B cocoa strains.
Front. Microbiol. 13:1060160.
doi: 10.3389/fmicb.2022.1060160

Application of comparative genomics of *Acetobacter* species facilitates genome-scale metabolic reconstruction of the *Acetobacter ghanensis* LMG 23848^T and *Acetobacter senegalensis* 108B cocoa strains

Rudy Pelicaen[1,2], Stefan Weckx[1,2], Didier Gonze[2,3] and Luc De Vuyst[1]*

[1]Research Group of Industrial Microbiology and Food Biotechnology, Faculty of Sciences and Bioengineering Sciences, Vrije Universiteit Brussel, Brussels, Belgium, [2]ULB-VUB Interuniversity Institute of Bioinformatics in Brussels, Brussels, Belgium, [3]Unité de Chronobiologie Théorique, Service de Chimie Physique, Faculté des Sciences, Université libre de Bruxelles, Brussels, Belgium

Acetobacter species play an import role during cocoa fermentation. However, *Acetobacter ghanensis* and *Acetobacter senegalensis* are outcompeted during fermentation of the cocoa pulp-bean mass, whereas *Acetobacter pasteurianus* prevails. In this paper, an *in silico* approach aimed at delivering some insights into the possible metabolic adaptations of *A. ghanensis* LMG 23848^T and *A. senegalensis* 108B, two candidate starter culture strains for cocoa fermentation processes, by reconstructing genome-scale metabolic models (GEMs). Therefore, genome sequence data of a selection of strains of *Acetobacter* species were used to perform a comparative genomic analysis. Combining the predicted orthologous groups of protein-encoding genes from the *Acetobacter* genomes with gene-reaction rules of GEMs from two reference bacteria, namely a previously manually curated model of *A. pasteurianus* 386B (iAp386B454) and two manually curated models of *Escherichia coli* (EcoCyc and iJO1366), allowed to predict the set of reactions present in *A. ghanensis* LMG 23848^T and *A. senegalensis* 108B. The predicted metabolic network was manually curated using genome re-annotation data, followed by the reconstruction of species-specific GEMs. This approach additionally revealed possible differences concerning the carbon core metabolism and redox metabolism among *Acetobacter* species, pointing to a hitherto unexplored metabolic diversity. More specifically, the presence or absence of reactions related to citrate catabolism and the glyoxylate cycle for assimilation of C2 compounds provided not only new insights into cocoa fermentation but also interesting guidelines for future research. In general, the *A. ghanensis* LMG 23848^T and *A. senegalensis* 108B GEMs, reconstructed in a semi-automated way, provided a proof-of-concept toward accelerated formation of GEMs of candidate functional starter cultures for food fermentation processes.

10.3389/fmicb.2022.1060160

KEYWORDS

cocoa fermentation, *Acetobacter* metabolism, comparative genomics, genome-scale metabolic modelling, flux balance analysis

Introduction

Acetic acid bacteria (AAB) are Gram-negative, obligately aerobic bacteria that incompletely oxidize a range of alcohols and reducing sugars for energy production. The region-and stereo-selectivity of these oxidation reactions has led to numerous biotechnological applications, most notably the conversion of *D*-sorbitol into *L*-sorbose (Shinjoh and Toyama, 2016). The genus *Acetobacter* comprises tens of species and is common to food fermentation processes, among which traditional vinegar production, kombucha fermentation, and cocoa fermentation (De Vuyst and Weckx, 2016; Yamada, 2016; Coton et al., 2017; Lu et al., 2018; De Vuyst and Leroy, 2020). For the latter fermentation process, several *Acetobacter* species have been isolated and selected as candidate functional starter cultures, including *Acetobacter ghanensis* LMG 23848^T and *Acetobacter senegalensis* 108B (Camu et al., 2007; Moens et al., 2014; Illeghems et al., 2016). To gain more insights into their contribution to cocoa fermentation processes, their genomes have been sequenced and functionally annotated, revealing a possible role in citrate assimilation during fermentation of the cocoa pulp-bean mass (Illeghems et al., 2016). However, *A. ghanensis* and *A. senegalensis* are outcompeted during cocoa fermentation, whereas *Acetobacter pasteurianus* prevails (Lefeber et al., 2010, 2011, 2012; Papalexandratou et al., 2013; Díaz-Muñoz et al., 2021).

The gold standard in the taxonomic analysis of AAB are polyphasic approaches, combining phenotypic, chemotaxonomic, and genotypic data (Cleenwerck and De Vos, 2008; De Vuyst et al., 2008; Papalexandratou et al., 2009; Li et al., 2017). One specific metabolic feature that is typically tested for differentiating *Acetobacter* species is growth on ethanol as the sole carbon source. Therefore, a defined medium containing ethanol as the sole carbon source and ammonium as the sole nitrogen source is often used (Cleenwerck et al., 2002). However, carbon source usage may also be deduced through genomic analysis, since carbon assimilation pathways consist of a defined sequence of biochemical reactions, for which the respective enzyme-encoding genes must be present in the genome (Serres and Riley, 2006).

Growth of *Acetobacter* species on C2 compounds, such as ethanol and acetate, has so far been related to the presence of the glyoxylate cycle enzymes (Saeki et al., 1997; Sakurai et al., 2013). The glyoxylate cycle is a shunt of the tricarboxylic acid (TCA) cycle and involves only two enzymes, namely isocitrate lyase (EC 4.1.3.1), which converts isocitrate into glyoxylate and succinate, and malate synthase (EC 2.3.3.9), which binds acetyl-CoA onto glyoxylate to form malate. The glyoxylate cycle circumvents the carbon dioxide-producing reactions of the TCA cycle, thus leading to a net succinate production. The presence of genes encoding the glyoxylate cycle enzymes in *Acetobacter* species genomes and their relationship to the growth of these species in a medium containing ethanol as the sole carbon source has not been thoroughly investigated.

A genome-scale metabolic model (GEM) provides a well-defined data structure of the metabolic network inferred from a bacterial genome (Thiele and Palsson, 2010). Next to the use of a GEM as knowledge base of the biochemical reaction potential of a microbial strain, a GEM is also useful to perform simulations of the metabolism of a microbial strain, for instance using constraint-based modeling methods. GEMs have been used to compare the reaction potential of different microorganisms, and led to the concept of a pan-reactome (Prigent et al., 2018; Seif et al., 2018; Gu et al., 2019). In this case, the GEM reconstruction process is performed for different strains in parallel using different metabolic resources, for instance GEMs of reference species and metabolic databases.

In the present study, the approach mentioned above was applied to reconstruct GEMs for *A. ghanensis* LMG 23848^T and *A. senegalensis* 108B, taking advantage of a comparative genomic analysis that encompassed a selection of 36 strains belonging to 27 species of the *Acetobacter* genus and a previously reconstructed and manually curated GEM of *A. pasteurianus* 386B (Pelicaen et al., 2019, 2020). These GEMs will be useful to gain more insights into the metabolism and hence metabolic adaptations of *A. ghanensis* LMG 23848^T and *A. senegalensis* 108B to cocoa fermentation conditions by applying *in silico* flux balance analysis.

Materials and methods

Strains

Three strains of *Acetobacter* species, originating from spontaneous cocoa fermentation processes carried out in heaps in Ghana in 2004, namely *A. pasteurianus* 386B, *A. ghanensis* LMG 23848^T, and *A. senegalensis* 108B, were used throughout this study (Camu et al., 2007; Illeghems et al., 2013, 2016; Moens et al., 2014).

Growth experiments

Growth experiments were performed in a modified defined medium (Verduyn et al., 1992). This medium contained: $(NH_4)_2SO_4$, 5.0 g/l; KH_2PO_4, 1.375 g/l; $MgSO_4.7H_2O$, 0.5 g/l; ethylenediaminetetraacetic acid (EDTA), 15.0 mg/l;

$ZnSO_4.7H_2O$, 4.5 mg/l; $CoSO_4.7H_2O$, 0.35 mg/l; $MnCl_2.4H_2O$, 1.0 mg/l; $CuSO_4.5H_2O$, 0.3 mg/l; $CaCl_2.2H_2O$, 4.5 mg/l; $FeSO_4.7H_2O$, 3.0 mg/l; MoO_3, 0.24 mg/l; H_3BO_3, 1.0 mg/l; and KI, 0.1 mg/l, dissolved in 30 mM citrate buffer (pH 6.0). The final pH of the medium was adjusted to 5.0 with 0.1 M NaOH. A filter-sterilised vitamin mixture was added after heat sterilisation of the medium at 121°C for 20 min. The final vitamin concentrations were: biotin, 0.0005 mg/l; calcium pantothenate, 0.01 mg/l; nicotinic acid, 0.01 mg/l; *myo*-inositol, 0.25 mg/l; thiamine-HCl, 0.01 mg/l; pyridoxine-HCl, 0.01 mg/l; and *para*-aminobenzoic acid, 0.002 mg/l. Eight different carbon sources, namely glucose, fructose, mannitol, citric acid, glycerol, lactic acid, ethanol, and acetic acid (as sodium acetate), were used at a final concentration of 30 mM to assess if they could sustain growth of the three *Acetobacter* strains investigated. The pH of the citric acid, lactic acid, and sodium acetate stock solutions was set to 5.0.

For inoculum build-up, the three *Acetobacter* strains were grown overnight at 30°C in a standard incubator (160 rpm) in a modified yeast extract-glucose-mannitol (mYGM) medium (Lefeber et al., 2012), which contained: *D*-glucose, 20.0 g/l; *D*-mannitol, 20.0 g/l; lactic acid, 10.0 g/l; granulated yeast extract, 10.0 g/l; soy peptone, 5.0 g/l; $MgSO_4.7H_2O$, 1.0 g/l; $(NH_4)_2HPO_4$, 1.0 g/l; KH_2PO_4, 1.0 g/l; and $Na_3C_6H_5O_7$, 1.0 g/l. The final pH of the medium was adjusted to 5.5 with 0.1 M NaOH. The overnight culture was centrifuged (4,000 x *g*, 20 min, 4°C) and washed with a filter-sterilized saline solution (0.85%, m/v, NaCl). Then, the cells were resuspended in sterile saline solution and inoculated in 2 ml of the defined medium mentioned above at an optical density at 600 nm (OD_{600}) of 0.01, in duplicate, in test tubes with a total volume of 20 ml. The three *Acetobacter* strains were allowed to grow at 30°C for 48 h and 120 h. A threshold value for the OD_{600} of 0.1 was used to identify whether or not the strains had grown.

A similar growth experiment was performed in a modified defined medium with 30 mM phosphate buffer (pH 6.0) in triplicate. In this case, for inoculum build-up, the three *Acetobacter* strains were grown overnight at 30°C in a semi-defined medium (pH 5.5), which contained: lactic acid, 5.0 g/l; sodium acetate, 10.0 g/l; granulated yeast extract, 5.0 g/l; $MgSO_4.7H_2O$, 1.0 g/l; $NH_4H_2PO_4$, 20.0 g/l; and K_2HPO_4, 10.0 g/l (Pelicaen et al., 2019). A threshold value for the OD_{600} of 0.1 was used to identify whether or not the strains had grown.

Re-annotation of the *Acetobacter ghanensis* LMG 23848^T and *Acetobacter senegalensis* 108B genomes

The protein-encoding genes of the *A. ghanensis* LMG 23848^T and *A. senegalensis* 108B genomes were originally annotated using the bacterial genome annotation system GenDB v2.2 (Meyer, 2003; Illeghems et al., 2016). In the present study, these genomes were re-annotated using a previously in-house developed bioinformatics workflow (Pelicaen et al., 2019). The National Center for Biotechnology Information (NCBI, Bethesda, Madison, United States) RefSeq genome annotation version was taken as a basis for re-annotation of the genome of *A. ghanensis* LMG 23848^T (accessed in April 2017; 2,454 protein-encoding genes) and *A. senegalensis* 108B (accessed in October 2017; 3,444 protein-encoding genes). The amino acid sequences of each set of protein-encoding genes were annotated using a combination of tools, namely BlastKOALA from the KEGG database (Kanehisa et al., 2016, 2017), the TransAAP tool to predict transport proteins (Elbourne et al., 2017), the subcellular localization predictor CELLO (Yu et al., 2004), eggNOG-mapper (Huerta-Cepas et al., 2017), the enzyme annotation tool PRIAM (Claudel-Renard et al., 2003), the RAST annotation pipeline from the KBase software (Overbeek et al., 2014; Arkin et al., 2018), and the tools embedded in InterProScan 5.22–61.0 (Jones et al., 2014). Furthermore, since the publication of the genome sequences of *A. ghanensis* LMG 23848^T and *A. senegalensis* 108B (Illeghems et al., 2016), these genomes have been re-annotated by several annotation pipelines and the functional annotation data known at the time of analysis were stored in dedicated databases related to those pipelines. As such, these additional functional annotations were retrieved from the Carbohydrate-Active enZYmes (CAZy) database (Lombard et al., 2014), the Pathosystems Resource Integration Center (PATRIC) database (Wattam et al., 2017), and the Universal Protein Resource (UniProt) database (The UniProt Consortium, 2019).

In addition, the genome annotation pipelines used by GenDB, NCBI RefSeq (NCBI prokaryotic genome annotation pipeline; Tatusova et al., 2016) and PATRIC (RASTtk; Brettin et al., 2015) represent independent methods combining gene prediction and gene annotation. Therefore, functional annotation data of these sources were combined in an in-house MySQL database specific for *A. ghanensis* LMG 23848^T and *A. senegalensis* 108B.

Comparative genomics of *Acetobacter* species based on orthogroups

From all *Acetobacter* species mentioned in the NCBI Taxonomy database (accessed May 2019), the genome sequence of 96 strains of *Acetobacter* species was available in the NCBI RefSeq database. All those genome sequences were retrieved, as well as the genome sequences of *Gluconobacter oxydans* 621H, *Komagataeibacter nataicola* RZS01, and *Escherichia coli* str. K-12 substr. MG1655 (further referred to as *E. coli*). The latter three strains were used as outgroup. Next, the *Acetobacter* genomes were ranked according to their assembly quality level, based on information in the NCBI RefSeq database. For each *Acetobacter* species, the genome with the highest assembly quality level was selected, and in the case that the genome was not from the type strain, the type strain genome was also selected. Next, OrthoFinder (Emms and Kelly, 2015) was used to predict orthogroups from the protein-encoding genes of the selected *Acetobacter* genomes and from the three outgroup

genomes. Protein identifiers from the NCBI RefSeq database were linked to gene identifiers based on the Genbank files of each genome. Subsequently, OrthoFinder was used to infer a rooted species tree based on the predicted orthogroups (Emms and Kelly, 2017, 2018).

Reconstruction of genome-scale metabolic models for *Acetobacter ghanensis* LMG 23848^T and *Acetobacter senegalensis* 108B

The relationship between genes, proteins, and reactions can be described using gene-protein-reaction (GPR) associations, linking the different entities, possibly with their stoichiometry (Thiele and Palsson, 2010). However, in practice, GPR associations are typically implemented as Boolean rules that define reaction presence based on gene presence in an annotated genome (Machado et al., 2016). Albeit potentially oversimplifying the actual GPR associations, these Boolean rules (gene-reaction rules) allow to quickly evaluate the presence of a reaction in the GEM through *in silico* gene deletions (Ebrahim et al., 2013). In the present study, this concept was exploited to predict the reaction presence based on gene presence in the annotated genomes. To convert the text Boolean expression into a symbolic rule that allows its computational assessment, the Python library SymPy was used (Meurer et al., 2017).

As a first step in the reconstruction of the GEMs for *A. ghanensis* LMG 23848^T and *A. senegalensis* 108B, the manually curated GEM of *A. pasteurianus* 386B (iAp386B454; Pelicaen et al., 2019) was used as a reference to evaluate which of the reactions of this GEM were present in the *Acetobacter* genomes considered. To minimize the number of false negative predictions of reaction presence, a separate analysis was performed, whereby only high-quality *Acetobacter* genomes with an NCBI assembly level corresponding to a complete genome were considered.

Next, the predictions obtained were used for the reconstruction of GEMs of *A. ghanensis* LMG 23848^T, further referred to as iAg23848, and of *A. senegalensis* 108B, further referred to as iAs108B. New gene-reaction rules were associated to the transferred iAp386B454 reactions. For multi-copy orthogroups, i.e., orthogroups containing multiple genes for each genome, the logic 'OR' assumption was made, expressing that these genes are co-orthologs of the *A. pasteurianus* 386B genes. Cases for which *A. pasteurianus* 386B genes occurred in the same orthogroup as the ones of *A. ghanensis* LMG 23848^T and *A. senegalensis* 108B and had a logic 'AND' relation in the iAp386B454 gene-reaction rules, were systematically checked and manually curated in the iAg23848 and iAs108B GEMs. Reactions without GPR, including spontaneous reactions as well as reactions for macromolecular biosynthesis and the iAp386B454 biomass reaction, were transferred as such to the iAg23848 and iAs108B GEMs.

Gap filling of genome-scale metabolic models and flux balance analysis

Further manual curation was performed for the iAg23848 and iAs108B GEMs in a semi-automated way. First, GEM gap filling was performed using iAp386B454 as a template. Hereto, the GEM gap filling method of CobraPy was used (Ebrahim et al., 2013), which computes the minimal amount of reactions that need to be added from the iAp386B454 template to obtain *in silico* growth. Then, gap filling results were manually curated by combining functional annotation information of *A. ghanensis* LMG 23848^T and *A. senegalensis* 108B, stored in their respective MySQL databases and in the GEMs. Only the reactions for which genome annotation evidence was found were added to the GEMs. This also included reactions necessary to reconcile *in silico* and *in vitro* growth experiments. Finally, flux balance analysis (FBA) and parsimonious FBA with biomass formation as the objective function were performed to examine the flux distributions of the newly constructed GEMs under simulated *in vitro* growth conditions. The total allowable carbon consumption flux was set to 60 c-mmol per gram of cell dry mass per h.

Presence of the glyoxylate cycle and aerobic respiratory chain reactions

To predict the presence/absence of reactions of the glyoxylate cycle and the aerobic respiratory chain, a similar analysis as described in Section 2.4 was performed but now with an *E. coli* GEM as reference. For *E. coli*, two curated reconstruction sources were leveraged, namely the EcoCyc Pathway/Genome Database embedded in Pathway Tools version 21.5, and the iJO1366 GEM of the BIGG database (Orth et al., 2011; Keseler et al., 2017).

Results

Growth experiments

Growth experiments (Table 1) under defined medium conditions, using a citrate buffer, indicated that *A. pasteurianus* 386B showed the same growth phenotype as in defined medium with a phosphate buffer. Only the addition of lactic acid as a sole carbon source could sustain the growth of *A. pasteurianus* 386B under these conditions. For *A. ghanensis* LMG 23848^T, increasing the incubation time from 48 h to 120 h allowed for growth of the bacterial population only on glucose as the sole carbon source, using a citrate buffer. In contrast, the growth phenotype of *A. senegalensis* 108B markedly differed when using a phosphate buffer or citrate buffer. Under growth conditions with a phosphate buffer, this strain only showed growth on lactic acid and citric acid as the sole carbon sources, but exchanging the phosphate buffer for a citrate buffer led to growth on all single carbon sources tested, at least after 120 h of incubation. These results indicated the

TABLE 1 Indication of bacterial population growth of strains of three different *Acetobacter* species in a modified defined medium with phosphate buffer or citrate buffer, supplemented with different carbon sources, after 48h and 48 and 120h of incubation, respectively.

Carbon source	*Acetobacter pasteurianus* 386B		*Acetobacter ghanensis* LMG 23848^T		*Acetobacter senegalensis* 108B	
	Phosphate 48 h	Citrate 48 h / 120 h	Phosphate 48 h	Citrate 48 h / 120 h	Phosphate 48 h	Citrate 48 h / 120 h
Glucose	–	– / –	–	– / +	–	+ / +
Fructose	–	– / –	–	– / –	–	+ / +
Mannitol	–	– / –	–	– / –	–	+ / +
Citric acid	–	– / –	–	– / –	+	– / +
Glycerol	–	– / –	–	– / –	–	+ / +
Lactic acid	+	+ / +	–	– / –	+	+ / +
Ethanol	–	– / –	–	– / –	–	+ / +
Acetic acid	–	– / –	–	– / –	–	+ / +

–, no growth; +, growth

influence of the medium buffer used, and the possibility of citrate co-consumption in the case that a citrate buffer was applied.

Re-annotation of the *Acetobacter ghanensis* LMG 23848^T and *Acetobacter senegalensis* 108B genomes

Functional annotation information of *A. ghanensis* LMG 23848^T and *A. senegalensis* 108B was stored in their respective MySQL databases. For *A. ghanensis* LMG 23848^T, it comprised the functional annotations of 2,698 protein-encoding genes originally annotated with GenDB, extended with 160 unique protein-encoding genes from NCBI RefSeq, and 306 unique protein-encoding genes from PATRIC. For *A. senegalensis* 108B, it comprised the functional annotations of 3,605 protein-encoding genes originally annotated with GenDB, extended with 340 unique protein-encoding genes from NCBI RefSeq, and 625 unique protein-encoding genes from PATRIC.

Comparative genomics of *Acetobacter* species based on orthogroups

The genome selection procedure resulted in 36 genomes (Table 2). Sixteen of these genomes had only a contig level quality, of which eight were type strain genomes. Based on the protein-encoding genes in these genomes, OrthoFinder predicted the presence of 6,149 orthogroups, of which 155 were orthogroups that contained at least one protein-encoding gene for each genome considered, and 98 of these orthogroups contained exactly one protein-encoding gene for each genome (so-called single-copy orthogroups).

Based on all predicted orthogroups, OrthoFinder inferred a rooted species tree (Figure 1). The outgroup genomes chosen, namely *E. coli*, *G. oxydans* 621H, and *K. nataicola* RZS01, were successfully placed outside the *Acetobacter* species subtree by OrthoFinder. Moreover, the tree locations of genomes of hereto unidentified *Acetobacter* species provided a first indication to which *Acetobacter* species they were most related to. It concerned *Acetobacter* sp. DsW_063 (isolated from a fruit fly) as *A. nitrogenifigens*, *Acetobacter* sp. DsW_54 (fruit fly) as *A. fabarum*, *Acetobacter* sp. JWB (fruit fly) as *A. pomorum*, *Acetobacter* sp. BCRC 14118 (African vinegar) as *A. ascendens* (formerly identified as *A. pasteurianus*), and *Acetobacter* sp. B6 (South Korean vinegar) as *A. pasteurianus*.

Reconstruction of genome-scale metabolic models for *Acetobacter ghanensis* LMG 23848^T and *Acetobacter senegalensis* 108B

The predicted orthogroups were used in combination with the *A. pasteurianus* iAp386B454 GEM reference to evaluate the iAp386B454 GEM reaction presence or absence in 11 high-quality *Acetobacter* genomes. The most frequent missing reactions in the central metabolism, which has been published before for *A. pasteurianus* 386B (Illeghems et al., 2013; Pelicaen et al., 2019), were the ones catalyzed by proton-translocating NAD(P)$^+$ transhydrogenase (EC 7.1.1.1; missing in *A. aceti* TMW2.1153, *A. tropicalis* BDGP1, *A. pasteurianus* Ab3, and *A. senegalensis* 108B), phosphoglucomutase (EC 5.4.2.2; missing in *A. aceti* TMW2.1153, *A. tropicalis* BDGP1, *A. pasteurianus* Ab3, and *A. senegalensis* 108B), ornithine cyclodeaminase (EC 4.3.1.12; missing in *A. persici* TMW2.1084, *A. aceti* TMW2.1153, and *A. ghanensis* LMG 23848^T), a putative periplasmic mannitol oxidation reaction (missing in *A. ascendens* LMG 1590^T, *A. aceti* TMW2.1153, and *A. pasteurianus* Ab3), ribose 5-phosphate isomerase (EC 5.3.1.6; missing in *A. persici* TMW2.1084, *A. tropicalis* BDGP1, and *A. senegalensis* 108B), and fructokinase (EC 2.7.1.4; missing in *A. ascendens* LMG 1590^T and *A. ghanensis* LMG 23848^T). Both phosphate acetyltransferase (EC 2.3.1.8) and acetate kinase (EC 2.7.2.1) were missing in *A. aceti* TMW2.1153.

Although the lactate:H$^+$ symporter was missing in *A. aceti* TMW2.1153, the genome contained genes encoding a

TABLE 2 Selection of *Acetobacter* genomes used in the OrthoFinder analysis.

Strain of *Acetobacter* species	NCBI assembly level	NCBI RefSeq identifier
Acetobacter aceti TMW2.1153	Complete genome	GCF_002005445.1_ASM200544v1
Acetobacter aceti NBRC 14818^T	Contig	GCF_004341595.1_ASM434159v1
Acetobacter ascendens LMG 1590^T	Complete genome	GCF_001766235.1_ASM176623v1
Acetobacter cerevisiae LMG 1625^T	Contig	GCF_001580535.1_ASM158053v1
Acetobacter cerevisiae LMG 1545	Contig	GCF_001581105.1_ASM158110v1
Acetobacter cibinongensis 4H-1^T	Contig	GCF_000963925.1_ASM96392v1
Acetobacter fabarum KR	Contig	GCF_002276555.1_ASM227655v1
Acetobacter ghanensis LMG 23848^T	Chromosome	GCF_001499675.1_Acetobacter_ghanensis
Acetobacter indonesiensis 5H-1^T	Scaffold	GCF_000963945.1_ASM96394v1
Acetobacter malorum CECT 7742	Scaffold	GCF_001642635.1_ASM164263v1
Acetobacter malorum LMG 1746^T	Contig	GCF_001580615.1_ASM158061v1
Acetobacter nitrogenifigens DSM 23921^T	Scaffold	GCF_000429165.1_ASM42916v1
Acetobacter okinawensis JCM 25146^T	Contig	GCF_000613865.1_ASM61386v1
Acetobacter orientalis 21F-2^T	Scaffold	GCF_000963965.1_ASM96396v1
Acetobacter orleanensis CCM 3610	Scaffold	GCF_002358055.1_ASM235805v1
Acetobacter orleanensis JCM 7639^T	Scaffold	GCF_000964205.1_ASM96420v1
Acetobacter oryzifermentans SLV-7^T	Complete genome	GCF_001628715.1_ASM162871v1
Acetobacter papayae JCM 25143^T	Contig	GCF_000613285.1_ASM61328v1
Acetobacter pasteurianus Ab3	Complete genome	GCF_001183745.1_ASM118374v1
Acetobacter pasteurianus 386B	Complete genome	GCF_000723785.2_AP1
Acetobacter pasteurianus subsp. *pasteurianus* LMG 1262^T	Scaffold	GCF_000285275.1_ASM28527v1
Acetobacter persici TMW2.1084	Complete genome	GCF_002006565.1_ASM200656v1
Acetobacter persici JCM 25330^T	Contig	GCF_000613905.1_ASM61390v1
Acetobacter pomorum BDGP5	Complete genome	GCF_002456135.1_ASM245613v1
Acetobacter senegalensis 108B	Complete genome	GCF_001499615.1_Acetobacter_senegalensis_108B
Acetobacter senegalensis LMG 23690^T	Contig	GCF_001580995.1_ASM158099v1
Acetobacter sp. B6	Contig	GCF_004014775.1_ASM401477v1
Acetobacter sp. BCRC 14118	Contig	GCF_003332175.1_ASM333217v1
Acetobacter sp. DmW_043	Contig	GCF_002153485.1_ASM215348v1
Acetobacter sp. DsW_059	Contig	GCF_002153695.1_ASM215369v1
Acetobacter sp. DsW_063	Contig	GCF_002153745.1_ASM215374v1
Acetobacter sp. DsW_54	Contig	GCF_002153575.1_ASM215357v1
Acetobacter sp. JWB	Complete genome	GCF_003323795.1_ASM332379v1
Acetobacter syzygii 9H-2^T	Scaffold	GCF_000964225.1_ASM96422v1
Acetobacter tropicalis NBRC 16470^T	Scaffold	GCF_000787635.2_ASM78763v2
Acetobacter tropicalis BDGP1	Complete genome	GCF_002549835.1_ASM254983v1

quinone-dependent (EC 1.1.5.12) and cytochrome *c*-dependent (EC 1.1.2.4) *D*-lactate dehydrogenase. This strain was originally isolated from a water kefir and other *A. aceti* strains have been typically found in an ethanol-rich habitat, examples including vinegar. The absence of the lactate:H^+ symporter in the *A. aceti* TMW2.1153 genome might indicate genome evolution toward excluding lactate as a substrate, other means of lactate transport in the cell, or, possibly, the erroneous prediction of absence of a gene encoding this function. In contrast, characteristic reactions for the *Acetobacter* genus, including the membrane-bound pyrroloquinoline quinone (PQQ)-dependent ethanol dehydrogenase (EC 1.1.5.5) and succinyl-CoA:acetate CoA-transferase (EC 2.8.3.18) were found in all high-quality *Acetobacter* genomes considered.

Combining the predicted orthogroups and the iAp386B454 GEM allowed to reconstruct GEMs for *A. ghanensis* LMG 23848^T and *A. senegalensis* 108B. GEM compositions before and after curation-based gap filling are shown in Table 3. The concomitant increase of the number of reactions and decrease of the number of dead-end metabolites indicate a successful gap filling process. A complication arose in this analysis due to the occurrence of twelve *A. pasteurianus* 386B gene identifiers in the iAp386B454 GEM, which were not present in the *A. pasteurianus* 386B NCBI RefSeq genome version used for the OrthoFinder analysis. The 10 reactions associated to these genes were computationally filtered and manually checked to see whether the presumed orthologs were present in the *A. ghanensis* LMG 23848^T and *A. senegalensis*

FIGURE 1
Rooted species tree inference by OrthoFinder. Branch lengths represent the average number of substitutions per site. Type strain genomes are indicated with an asterisk (*). For genomes for which the strain name is not indicated, the reader is referred to Table 2.

108B genomes, and if so, the reactions and associated gene-reaction rules were manually added to their respective GEMs. This was the case for D-glucose:ubiquinone oxidoreductase (EC 1.1.5.2), phosphoenolpyruvate carboxylase (EC 4.1.1.31), and 3-isopropylmalate dehydratase (EC 4.2.1.33), both for *A. ghanensis* LMG 23848^T and *A. senegalensis* 108B.

For *A. ghanensis* LMG 23848^T, a quinone-dependent *D*-lactate dehydrogenase (EC 1.1.5.12) was absent in the genome, but a cytochrome *c*-dependent enzyme (EC 1.1.2.4) was identified. No acetolactate decarboxylase (EC 4.1.1.5) was found in the *A. ghanensis* LMG 23848^T genome. Instead, a gene encoding diacetyl reductase (EC 1.1.1.303) was present. Finally, no quinone-dependent glycerol 3-phosphate dehydrogenase (EC 1.1.5.3) was found. Whereas for *A. senegalensis* 108B no proton-translocating NAD(P)$^+$ transhydrogenase (EC 7.1.1.1) was found in the genome, a soluble NAD(P)$^+$ transhydrogenase (EC 1.6.1.1) was present. Additionally, no gene could be found encoding gluconokinase (EC 2.7.1.12), possibly explaining why *A. senegalensis* 108B could not grow under defined medium conditions with glucose as the sole carbon source. The fact that citrate could sustain growth of this strain paved the way to find a genomic cause. Indeed, a putative citrate:H$^+$ symporter and a gene cluster encoding citrate lyase was found in the genome, as previously reported (Illeghems et al., 2016). The gene cluster encoding citrate lyase was also present in two *Acetobacter* species isolated from fruit or fruit-derived fermented foods, namely *A. persici* JCM 25330^T (peach fruit) and *A. malorum* CECT 7742 (strawberry vinegar). Finally, the *A. senegalensis* 108B genome encoded a phosphoenolpyruvate carboxykinase (EC 4.1.1.49), which was not found in *A. pasteurianus* 386B, thus providing another anaplerotic link between the TCA cycle and the gluconeogenesis pathway in *A. senegalensis* 108B.

Gap filling of genome-scale metabolic models and flux balance analysis

The results of the growth experiments for *A. ghanensis* LMG 23848^T and *A. senegalensis* 108B were used to fill the reaction gaps

TABLE 3 Composition of genome-scale metabolic models (GEMs) of *Acetobacter ghanensis* LMG 23848^T and *Acetobacter senegalensis* 108B after automated reconstruction and curation-based gap filling.

GEM property	*A. ghanensis* LMG 23848^T		*A. senegalensis* 108B	
	After reconstruction	After gap filling	After reconstruction	After gap filling
Compartments	2	2	2	2
Genes	306	326	339	361
Reactions	294	312	308	326
Exchange reactions	17 (6%)	17 (6%)	17 (6%)	18 (6%)
Irreversible reactions	121 (41%)	121 (41%)	132 (43%)	139 (43%)
Orphan reactions	37 (13%)	37 (13%)	37 (13%)	38 (12.0%)
Metabolites	294	297	295	298
Dead-end metabolites	26 (9%)	9 (3%)	13 (4%)	4 (1%)

in these models using the iAp386B454 GEM as a reaction repository. The FBA gap filling results indicated that 17 iAp386B454 GEM reactions were needed to obtain *in silico* growth of *A. ghanensis* LMG 23848^T with glucose as the sole carbon source. For *A. senegalensis* 108B, 10 iAp386B454 GEM reactions were necessary when growth was required with lactic acid as the sole carbon source. Manual curation allowed the addition of all but two reactions for *A. ghanensis* LMG 23848^T, for which no genomic evidence could be found. These reactions were the ones catalyzed by asparagine synthase (EC 6.3.5.4) and ornithine cyclodeaminase (EC 4.3.1.12). Both are involved in amino acid biosynthesis, the first being necessary for *L*-asparagine biosynthesis and the latter responsible for *L*-proline biosynthesis. The gene encoding the alternative *L*-proline biosynthesis enzyme NAD(P)-dependent pyrroline-5-carboxylate reductase (EC 1.5.1.2) was annotated with an internal stop codon in the NCBI RefSeq annotation. Other biosynthesis pathways for these amino acids may exist in *A. ghanensis* LMG 23848^T, since *in vitro* growth was obtained under defined medium conditions without the addition of amino acids. Conversely, for *A. senegalensis* 108B, genomic evidence was found for all gap filling results. However, this evidence had to be retrieved from genes in the NCBI RefSeq annotation, for which no amino acid sequence was available (e.g., due to a predicted frameshift) or genes only annotated in the GenDB or PATRIC genome annotation versions.

Flux balance analysis with the iAg23848 GEM on glucose as the sole carbon source did not result in growth, unless *L*-proline and *L*-asparagine were additionally available, in which case the predicted specific growth rate was 0.70 h^{-1} and the consumption of both amino acids was balanced by the protein biosynthesis reaction. The flux distribution revealed obligatory NADPH oxidation by the proton-translocating NAD(P)$^+$ transhydrogenase. However, genome annotation analysis did not support the presence of this reaction, since the *A. ghanensis* LMG 23848^T genome missed the β-subunit of this enzyme. Growth of *A. ghanensis* LMG 23848^T under defined medium conditions with glucose was only found when a citrate buffer was used. Allowing additional *in silico* consumption of citrate showed that constraining the proton-translocating NAD(P)$^+$ transhydrogenase did not prevent growth, resulting in the prediction of a specific growth rate of 0.58 h^{-1} with the glutamate synthase reaction (EC 1.4.1.13) as the largest NADPH consumer.

The iAs108B GEM was solved with FBA under two growth conditions, namely with lactic acid or with citric acid as the sole carbon sources. No additional nutrients had to be added to obtain *in silico* growth, suggesting that this model contained all reactions necessary for biomass formation. FBA with lactic acid resulted in a specific growth rate of 0.86 h^{-1}. The soluble NAD(P)$^+$ transhydrogenase produced NADPH, whereas phosphoenolpyruvate carboxykinase supplied all necessary phosphoenolpyruvate. FBA with citric acid resulted in a specific growth rate of 0.75 h^{-1}. Most of the citric acid consumed was directly used in the TCA cycle, whereas only 12% was consumed by citrate lyase. No acetate was produced by the model; all intracellular acetate produced was consumed by succinyl-CoA:acetate CoA-transferase.

Presence of the glyoxylate cycle and aerobic respiratory chain reactions

The presence of genes encoding the glyoxylate cycle enzymes was assessed in all 36 *Acetobacter* genomes examined. Presence/absence was compared to experimental data related to the growth of the strains in a defined medium containing ethanol as the sole carbon source and obtained for the type strains of a number of *Acetobacter* species (Table 4; Cleenwerck et al., 2008). For strains of eight out of 19 *Acetobacter* species that were able to grow, three species (*A. estunensis*, *A. peroxydans*, and *A. lovaniensis*) had at the time of analysis no genome sequenced, two species for which a genome sequence was available (*A. aceti* and *A. nitrogenifigens*) encoded the glyoxylate cycle, and finally, three species with a genome sequence available (*A. senegalensis*, *A. cibinongensis*, and *A. fabarum*) did not encode the glyoxylate cycle. The latter three species could thus correspond to false positive experimental results based on growth with ethanol as the sole carbon source that were obtained formerly (Table 4) and should hence be repeated, albeit that the genome sequence available for *A. fabarum* is not that from the type strain.

The enzymes involved in the aerobic respiratory chain as known for *E. coli* were present in all *Acetobacter* genomes considered, comprising NADH dehydrogenase type I (EC 7.1.1.2), NADH dehydrogenase type II (EC 1.6.5.9), cytochrome bo_3 oxidase (EC 7.1.1.3), and cytochrome *bd* oxidase (EC 7.1.1.7). Concerning NADPH metabolism, *E. coli* contains both a proton-translocating NAD(P)$^+$ transhydrogenase and a soluble NAD(P)$^+$

TABLE 4 Overview of the presence of the glyoxylate cycle enzymes in genomes of strains of *Acetobacter* species.

Acetobacter species (number of strains tested in Cleenwerck et al., 2008)	Growth on ammonium + ethanol (according to Cleenwerck et al., 2008)	Number of genomes included in the OrthoFinder analysis	Presence of a gene encoding isocitrate lyase (EC 4.1.3.1)	Presence of a gene encoding malate synthase (EC 2.3.3.9)
A. fabarum (4)	+	1	No	No
A. lovaniensis (1)	+	0	?	?
A. ghanensis (3)	–	1	No	No
A. syzygii (1)	–	0	?	?
A. pasteurianus (7)	–	3	No	No
A. pomorum (1)	–	1	No	No
A. peroxydans (2)	+	0	?	?
A. indonesiensis (2)	–	1	No	No
A. orientalis (1)	–	1	No	No
A. cibinongensis (1)	w	1	No	No
A. tropicalis (2)	–	2	No	No
A. senegalensis (3)	+	2	No	No
A. orleanensis (4)	–	2	No	No
A. malorum (1)	–	2	No	No
A. cerevisiae (4)	–	2	No	No
A. nitrogenifigens (1)	+	1	Yes	Yes
A. oeni (1)	–	0	?	?
A. aceti (4)	+	2	Yes	Yes
A. estunensis (3)	+	0	?	?

Growth, +; no growth, –; weak growth, w. If the results of only one strain are reported, this is always the type strain.
?, no genome available at the time of investigation.

transhydrogenase. From the comparative genomic analysis, it was apparent that, at least for the high-quality *Acetobacter* genomes, the presence of these enzymes was mutually exclusive. An interesting exception was *A. aceti*, for which both reactions were predicted to be present.

Discussion

The reconstruction of a GEM for *A. ghanensis* LMG 23848^T and *A. senegalensis* 108B, two candidate starter culture strains for cocoa fermentation (Illeghems et al., 2016), provided *in silico* tools to gain insights into the metabolic properties of these strains. In the current study, the GEM reconstruction process was accelerated using a semi-automated approach with experimental support. Growth experiments under defined medium conditions identified individual carbon sources that allowed the growth of *A. ghanensis* LMG 23848^T and *A. senegalensis* 108B. These growth conditions could then be used in simulations using FBA with the newly reconstructed iAg23848 and iAs108B GEMs, providing insights into the metabolic flux distributions of the models.

For *A. senegalensis* 108B, the prediction of citrate assimilation based on a previous genome analysis (Illeghems et al., 2016) was confirmed. In general, conversion of citrate present in the cocoa pulp-bean mass is ascribed to lactic acid bacteria that proliferate at the start of a cocoa fermentation process (De Vuyst and Weckx, 2016; De Vuyst and Leroy, 2020). Citrate consumption by AAB species may contribute to their survival during this more or less anaerobic stage of a cocoa fermentation process (Illeghems et al., 2016). For *A. ghanensis* LMG 23848^T, the absence of a quinone-dependent *D*-lactate dehydrogenase (EC 1.1.5.12) was probably compensated by the presence of a cytochrome *c*-dependent enzyme (EC 1.1.2.4), which probably allowed lactate consumption. However, this may be an explanation for the lower lactate consumption rate of *A. ghanensis* LMG 23848^T, compared to *A. pasteurianus* 386B, under cocoa pulp-simulating conditions (Moens et al., 2014). In general, both lactate and acetate are overoxidized during a late stage of a cocoa fermentation process (Moens et al., 2014; De Vuyst and Weckx, 2016; De Vuyst and Leroy, 2020). Additionally, no acetolactate decarboxylase (EC 4.1.1.5) was found in the *A. ghanensis* LMG 23848^T genome, although acetoin was formed (Moens et al., 2014). In *A. pasteurianus*, it has been shown that acetoin production solely depends on acetolactate decarboxylase, in contrast to the theoretically proposed acetaldehyde carboligation pathway, as found in *Saccharomyces cerevisiae* (De Ley, 1959; Gunawan et al., 2007). However, in *A. ghanensis* LMG 23848^T as well as in *A. senegalensis* 108B, yet another pathway may be responsible for acetoin formation, since in both genomes a gene encoding diacetyl reductase (EC 1.1.1.303) was present, as is the case in lactic acid bacteria (Keenan and Lindsay, 1968). Finally, no quinone-dependent glycerol 3-phosphate dehydrogenase (EC 1.1.5.3) could be found, possibly explaining why *A. ghanensis* LMG 23848^T could

not grow under defined medium conditions with glycerol as the sole carbon source.

Re-annotation of the genomes of *A. ghanensis* LMG 23848^T and *A. senegalensis* 108B proved to be critical to reconstruct their GEMs. Reaction presence predictions using the iAp386B454 GEM as a reference were successful, but led to metabolic network gaps in essential biosynthesis reactions. Without the current re-annotation effort, it would be impossible to speculate about their presence. Keeping this in mind, the mutual occurrence of genome sequence errors in query and reference genomes blurs the outcome of this functional comparative genomic analysis, since it is ultimately based on the prediction of the presence or absence of genes in the genomes considered. However, considering that genomic data are the only well-structured and publicly available data source at hand to compare the metabolic properties of *Acetobacter* species, this analysis may provide interesting insights for future research. The predicted differences in the carbon and redox metabolic potential of the *Acetobacter* species investigated revealed the possible metabolic diversity in this genus. Specifically, the presence or absence of the lactate:H^+ symporter, fructokinase, gluconokinase, ribose 5-phosphate isomerase, and citrate lyase may represent adaptations to different habitats and niches. Also, the presence or absence of a proton-translocating and soluble NAD(P)$^+$ transhydrogenase may represent an important and hitherto not sufficiently explored adaptation to the use of different carbon sources and their influence on the redox metabolism of *Acetobacter* species (Pelicaen et al., 2020). In *E. coli*, both enzymes are present, each having a specific functional role, whereby the first enzyme produces NADPH and the latter re-oxidizes excess NADPH (Sauer et al., 2004). The complete coverage of the key reactions of the aerobic respiratory chain among the *Acetobacter* genomes is a strong indication that this metabolic feature is a defining physiological factor of this genus.

The predicted presence (e.g., *A. aceti* and *A. nitrogenifigens*) or absence (e.g., *A. ghanensis*, *A. senegalensis*, and *A. pasteurianus*) of the glyoxylate cycle enzymes represented an interesting case where genomic and experimental evidence go hand in hand. Alternative pathways have been described for the assimilation of C2 compounds in microorganisms, namely the ethylmalonyl-CoA pathway and the methylaspartate cycle (Alber et al., 2006; Khomyakova et al., 2011). However, these pathways have not been found in AAB, and no genomic evidence for their presence could be found in the *Acetobacter* genomes considered. If the glyoxylate cycle is the only C2 assimilation pathway present in species of the genus *Acetobacter*, then the phenotypic test concerning the growth of an *Acetobacter* species in a medium with ethanol as the sole carbon source, commonly used to infer the taxonomy of an unknown *Acetobacter* strain, should be backed by genomic evidence. The results presented here indicate that this was indeed not the case for some *Acetobacter* species, thus questioning experimental data (Cleenwerck et al., 2008). *Acetobacter senegalensis* 108B was not able to grow under defined medium conditions with ethanol as the sole carbon source. In addition, no genomic evidence was found for the glyoxylate cycle in the re-annotated *A. senegalensis* 108B genome. The experimental results presented here are in contrast to previous results obtained for *A. senegalensis* 108B and for the type strain of *A. senegalensis* (Camu et al., 2007; Ndoye et al., 2007). Thus, this is an argument that genomic evidence should be taken into account for future species descriptions of members of the *Acetobacter* genus.

From a practical viewpoint, in fermentation processes such as vinegar production, the use of strains that can solely oxidize ethanol to acetic acid, but not assimilate it into biomass components, may be favorable (Mullins and Kappock, 2013; Sakurai et al., 2013). Similarly, for the fermentation of cocoa pulp-bean mass, the absence of the glyoxylate cycle in the genomes of *A. ghanensis* LMG 23848^T, *A. senegalensis* 108B, and *A. pasteurianus* 386B (Illeghems et al., 2013; Pelicaen et al., 2019), may represent a competitive advantage of these strains to quickly oxidize the available ethanol, produced by yeast species, to acetic acid. Genomic screening of strains may provide a more straightforward strategy to select those strains for which no evidence of the glyoxylate cycle can be found, to use them as starter cultures in such fermentation processes.

Conclusion

In the present study, the possibility of integrating two different data structures based on the same genomic data source was explored. A first data structure comprises GEMs, allowing to catalogue the entire biochemical reaction potential of a microbial strain and *in silico* metabolic flux simulations. Also, gene-reaction rules, manually curated or not, allow to explore the causal links between the genome and the reactome. A second data structure, the orthogroups, predicts the phylogenetic relatedness between protein-encoding genes from different species genomes, from which estimates of their shared function can be made. Combining the manually curated gene-reaction rules of a GEM of *A. pasteurianus* 386B and *E. coli* and a set of predicted orthogroups of a selection of *Acetobacter* genomes allowed to predict the presence of reactions that characterized the metabolism of *A. pasteurianus* 386B and *E. coli* for these *Acetobacter* species. Evaluation of biochemical reaction presence in bacterial genomes represents a new frontier in genome annotation, since this evaluation is a step closer to the actual biological functionalities that the genome encodes for. The results obtained stress the need for proper data curation and species description.

Data availability statement

The datasets presented in this study can be found in online repositories. The genome-scale metabolic models in xml format can be found at https://zenodo.org under submission number 6320681 or under DOI at https://doi.org/10.5281/zenodo.6320681.

Author contributions

RP carried out the research and drafted the manuscript. DG, SW, and LDV supervised the research and revised and edited the manuscript. All authors approved the manuscript.

Funding

The authors acknowledge financial support from the Research Council of the Vrije Universiteit Brussel (SRP7 and IOF342 projects). RP was the recipient of a PhD Fellowship strategic basic research of the Research Foundation Flanders (FWO-Vlaanderen; 1S27316N).

Conflict of interest

The authors declare that the research was conducted in the absence of any commercial or financial relationships that could be construed as a potential conflict of interest.

Publisher's note

References

Alber, B. E., Spanheimer, R., Ebenau-Jehle, C., and Fuchs, G. (2006). Study of an alternate glyoxylate cycle for acetate assimilation by Rhodobacter sphaeroides. *Mol. Microbiol.* 61, 297–309. doi: 10.1111/j.1365-2958.2006.05238.x

Arkin, A. P., Cottingham, R. W., Henry, C. S., Harris, N. L., Stevens, R. L., Maslov, S., et al. (2018). KBase: the United States Department of Energy Systems Biology Knowledgebase. *Nat. Biotechnol.* 36, 566–569. doi: 10.1038/nbt.4163

Brettin, T., Davis, J. J., Disz, T., Edwards, R. A., Gerdes, S., Olsen, G. J., et al. (2015). RASTtk: a modular and extensible implementation of the RAST algorithm for building custom annotation pipelines and annotating batches of genomes. *Sci. Rep.* 5:8365. doi: 10.1038/srep08365

Camu, N., De Winter, T., Verbrugghe, K., Cleenwerck, I., Vandamme, P., Takrama, J. S., et al. (2007). Dynamics and biodiversity of populations of lactic acid bacteria and acetic acid bacteria involved in spontaneous heap fermentation of cocoa beans in Ghana. *Appl. Environ. Microbiol.* 73, 1809–1824. doi: 10.1128/AEM.02189-06

Claudel-Renard, C., Chevalet, C., Faraut, T., and Kahn, D. (2003). Enzyme-specific profiles for genome annotation: PRIAM. *Nucleic Acids Res.* 31, 6633–6639. doi: 10.1093/nar/gkg847

Cleenwerck, I., and De Vos, P. (2008). Polyphasic taxonomy of acetic acid bacteria: an overview of the currently applied methodology. *Int. J. Food Microbiol.* 125, 2–14. doi: 10.1016/j.ijfoodmicro.2007.04.017

Cleenwerck, I., Gonzalez, A., Camu, N., Engelbeen, K., De Vos, P., and De Vuyst, L. (2008). Acetobacter fabarum sp. nov., an acetic acid bacterium from a Ghanaian cocoa bean heap fermentation. *Int. J. Syst. Evol. Microbiol.* 58, 2180–2185. doi: 10.1099/ijs.0.65778-0

Cleenwerck, I., Vandemeulebroecke, K., Janssens, D., and Swings, J. (2002). Re-examination of the genus Acetobacter, with descriptions of Acetobacter cerevisiae sp. nov. and Acetobacter malorum sp. nov. *Int. J. Syst. Evol. Microbiol.* 52, 1551–1558. doi: 10.1099/00207713-52-5-1551

Coton, M., Pawtowski, A., Taminiau, B., Burgaud, G., Deniel, F., Coulloumme-Labarthe, L., et al. (2017). Unraveling microbial ecology of industrial-scale kombucha fermentations by metabarcoding and culture-based methods. *FEMS Microbiol. Ecol.* 93:5. doi: 10.1093/femsec/fix048

De Ley, J. (1959). On the formation of acetoin by Acetobacter. *J. Gen. Microbiol.* 21, 352–365. doi: 10.1099/00221287-21-2-352

De Vuyst, L., Camu, N., De Winter, T., Vandemeulebroecke, K., Van de Perre, V., Vancanneyt, M., et al. (2008). Validation of the $(GTG)_5$-rep-PCR fingerprinting technique for rapid classification and identification of acetic acid bacteria, with a focus on isolates from Ghanaian fermented cocoa beans. *Int. J. Food Microbiol.* 125, 79–90. doi: 10.1016/j.ijfoodmicro.2007.02.030

De Vuyst, L., and Leroy, F. (2020). Functional role of yeasts, lactic acid bacteria, and acetic acid bacteria in cocoa fermentation processes. *FEMS Microbiol. Rev.* 44, 432–453. doi: 10.1093/femsre/fuaa014

De Vuyst, L., and Weckx, S. (2016). The cocoa bean fermentation process: from ecosystem analysis to starter culture development. *J. Appl. Microbiol.* 121, 5–17. doi: 10.1111/jam.13045

Díaz-Muñoz, C., Van de Voorde, D., Comasio, A., Verce, M., Hernandez, C. E., Weckx, S., et al. (2021). Curing of cocoa beans: fine-scale monitoring of the starter cultures applied and metabolomics of the fermentation and drying steps. *Front. Microbiol.* 11:616875. doi: 10.3389/fmicb.2020.616875

Ebrahim, A., Lerman, J. A., Palsson, B. Ø., and Hyduke, D. R. (2013). COBRApy: COnstraints-based reconstruction and analysis for python. *BMC Syst. Biol.* 7:74. doi: 10.1186/1752-0509-7-74

Elbourne, L. D. H., Tetu, S. G., Hassan, K. A., and Paulsen, I. T. (2017). TransportDB 2.0: a database for exploring membrane transporters in sequenced genomes from all domains of life. *Nucleic Acids Res.* 45, D320–D324. doi: 10.1093/nar/gkw1068

Emms, D. M., and Kelly, S. (2015). OrthoFinder: solving fundamental biases in whole genome comparisons dramatically improves orthogroup inference accuracy. *Genome Biol.* 16:157. doi: 10.1186/s13059-015-0721-2

Emms, D. M., and Kelly, S. (2017). STRIDE: species tree root inference from gene duplication events. *Mol. Biol. Evol.* 34, 3267–3278. doi: 10.1093/molbev/msx259

Emms, D. M., and Kelly, S. (2018). STAG: species tree inference from all genes. *bioRxiv*. doi: 10.1101/267914

Gu, C., Kim, G. B., Kim, W. J., Kim, H. U., and Lee, S. Y. (2019). Current status and applications of genome-scale metabolic models. *Genome Biol.* 20:121. doi: 10.1186/s13059-019-1730-3

Gunawan, C., Satianegara, G., Chen, A. K., Breuer, M., Hauer, B., Rogers, P. L., et al. (2007). Yeast pyruvate decarboxylases: variation in biocatalytic characteristics for (R)-phenylacetylcarbinol production. *FEMS Yeast Res.* 7, 33–39. doi: 10.1111/j.1567-1364.2006.00138.x

Huerta-Cepas, J., Forslund, K., Coelho, L. P., Szklarczyk, D., Jensen, L. J., von Mering, C., et al. (2017). Fast genome-wide functional annotation through orthology assignment by eggNOG-mapper. *Mol. Biol. Evol.* 34, 2115–2122. doi: 10.1093/molbev/msx148

Illeghems, K., De Vuyst, L., and Weckx, S. (2013). Complete genome sequence and comparative analysis of Acetobacter pasteurianus 386B, a strain well-adapted to the cocoa bean fermentation ecosystem. *BMC Genomics* 14:526. doi: 10.1186/1471-2164-14-526

Illeghems, K., Pelicaen, R., De Vuyst, L., and Weckx, S. (2016). Assessment of the contribution of cocoa-derived strains of Acetobacter ghanensis and Acetobacter senegalensis to the cocoa bean fermentation process through a genomic approach. *Food Microbiol.* 58, 68–78. doi: 10.1016/j.fm.2016.03.013

Jones, P., Binns, D., Chang, H.-Y., Fraser, M., Li, W., McAnulla, C., et al. (2014). InterProScan 5: genome-scale protein function classification. *Bioinformatics* 30, 1236–1240. doi: 10.1093/bioinformatics/btu031

Kanehisa, M., Furumichi, M., Tanabe, M., Sato, Y., and Morishima, K. (2017). KEGG: new perspectives on genomes, pathways, diseases and drugs. *Nucleic Acids Res.* 45, D353–D361. doi: 10.1093/nar/gkw1092

Kanehisa, M., Sato, Y., and Morishima, K. (2016). BlastKOALA and GhostKOALA: KEGG tools for functional characterization of genome and metagenome sequences. *J. Mol. Biol.* 428, 726–731. doi: 10.1016/j.jmb.2015.11.006

Keenan, T. W., and Lindsay, R. C. (1968). Diacetyl production and utilization by lactobacillus species. *J. Dairy Sci.* 51, 188–191. doi: 10.3168/jds.S0022-0302(68)86948-6

Keseler, I. M., Mackie, A., Santos-Zavaleta, A., Billington, R., Bonavides-Martínez, C., Caspi, R., et al. (2017). The EcoCyc database: reflecting new knowledge about Escherichia coli K-12. *Nucleic Acids Res.* 45, D543–D550. doi: 10.1093/nar/gkw1003

Khomyakova, M., Bukmez, O., Thomas, L. K., Erb, T. J., and Berg, I. A. (2011). A methylaspartate cycle in Haloarchaea. *Science* 331, 334–337. doi: 10.1126/science.1196544

Lefeber, T., Janssens, M., Camu, N., and De Vuyst, L. (2010). Kinetic analysis of strains of lactic acid bacteria and acetic acid bacteria in cocoa pulp simulation media toward development of a starter culture for cocoa bean fermentation. *Appl. Environ. Microbiol.* 76, 7708–7716. doi: 10.1128/AEM.01206-10

Lefeber, T., Janssens, M., Moens, F., Gobert, W., and De Vuyst, L. (2011). Interesting starter culture strains for controlled cocoa bean fermentation revealed by simulated cocoa pulp fermentations of cocoa-specific lactic acid bacteria. *Appl. Environ. Microbiol.* 77, 6694–6698. doi: 10.1128/AEM.00594-11

Lefeber, T., Papalexandratou, Z., Gobert, W., Camu, N., and De Vuyst, L. (2012). On-farm implementation of a starter culture for improved cocoa bean fermentation and its influence on the flavour of chocolates produced thereof. *Food Microbiol.* 30, 379–392. doi: 10.1016/j.fm.2011.12.021

Li, L., Cleenwerck, I., De Vuyst, L., and Vandamme, P. (2017). Identification of acetic acid bacteria through matrix-assisted laser desorption/ionization time-of-flight mass spectrometry and report of *Gluconobacter nephelii* Kommanee et al. 2011 and *Gluconobacter uchimurae* Tanasupawat et al. 2012 as later heterotypic synonyms of *Gluconobacter japonicus* Malimas et al. 2009 and *Gluconobacter oxydans* (Henneberg 1897) De Ley 1961 (approved lists 1980) emend. Gosselé et al. 1983, respectively. *Syst. Appl. Microbiol.* 40, 123–134. doi: 10.1016/j.syapm.2017.01.003

Lombard, V., Golaconda Ramulu, H., Drula, E., Coutinho, P. M., and Henrissat, B. (2014). The carbohydrate-active enzymes database (CAZy) in 2013. *Nucleic Acids Res.* 42, D490–D495. doi: 10.1093/nar/gkt1178

Lu, Z.-M., Wang, Z.-M., Zhang, X.-J., Mao, J., Shi, J.-S., and Xu, Z.-H. (2018). Microbial ecology of cereal vinegar fermentation: insights for driving the ecosystem function. *Curr. Opin. Biotechnol.* 49, 88–93. doi: 10.1016/j.copbio.2017.07.006

Machado, D., Herrgård, M. J., and Rocha, I. (2016). Stoichiometric representation of gene-protein-reaction associations leverages constraint-based analysis from reaction to gene-level phenotype prediction. *PLoS Comput. Biol.* 12:e1005140. doi: 10.1371/journal.pcbi.1005140

Meurer, A., Smith, C. P., Paprocki, M., Čertík, O., Kirpichev, S. B., Rocklin, M., et al. (2017). SymPy: symbolic computing in python. *Peer J. Comp. Sci.* 3:e103. doi: 10.7717/peerj-cs.103

Meyer, F. (2003). GenDB - an open source genome annotation system for prokaryote genomes. *Nucleic Acids Res.* 31, 2187–2195. doi: 10.1093/nar/gkg312

Moens, F., Lefeber, T., and De Vuyst, L. (2014). Oxidation of metabolites highlights the microbial interactions and role of Acetobacter pasteurianus during cocoa bean fermentation. *Appl. Environ. Microbiol.* 80, 1848–1857. doi: 10.1128/AEM.03344-13

Mullins, E. A., and Kappock, T. J. (2013). Functional analysis of the acetic acid resistance (aar) gene cluster in Acetobacter aceti strain 1023. *Acetic Acid Bacteria* 2:e3. doi: 10.4081/aab.2013.s1.e3

Ndoye, B., Cleenwerck, I., Engelbeen, K., Dubois-Dauphin, R., Guiro, A. T., Van Trappen, S., et al. (2007). Acetobacter senegalensis sp. nov., a thermotolerant acetic acid bacterium isolated in Senegal (sub-Saharan Africa) from mango fruit (Mangifera indica L.). *Int. J. Syst. Evol. Microbiol.* 57, 1576–1581. doi: 10.1099/ijs.0.64678-0

Orth, J. D., Conrad, T. M., Na, J., Lerman, J. A., Nam, H., Feist, A. M., et al. (2011). A comprehensive genome-scale reconstruction of Escherichia coli metabolism. *Mol. Syst. Biol.* 7:535. doi: 10.1038/msb.2011.65

Overbeek, R., Olson, R., Pusch, G. D., Olsen, G. J., Davis, J. J., Disz, T., et al. (2014). The SEED and the rapid annotation of microbial genomes using subsystems technology (RAST). *Nucleic Acids Res.* 42, D206–D214. doi: 10.1093/nar/gkt1226

Papalexandratou, Z., Cleenwerck, I., De Vos, P., and De Vuyst, L. (2009). $(GTG)_5$-PCR reference framework for acetic acid bacteria. *FEMS Microbiol. Lett.* 301, 44–49. doi: 10.1111/j.1574-6968.2009.01792.x

Papalexandratou, Z., Lefeber, T., Bahrim, B., Lee, O. S., Daniel, H.-M., and De Vuyst, L. (2013). Hanseniaspora opuntiae, Saccharomyces cerevisiae, lactobacillus fermentum, and Acetobacter pasteurianus predominate during well-performed Malaysian cocoa bean box fermentations, underlining the importance of these microbial species for a successful cocoa bean fermentation process. *Food Microbiol.* 35, 73–85. doi: 10.1016/j.fm.2013.02.015

Pelicaen, R., Gonze, D., De Vuyst, L., and Weckx, S. (2020). Genome-scale metabolic modeling of Acetobacter pasteurianus 386B reveals its metabolic adaptation to cocoa fermentation conditions. *Food Microbiol.* 92:103597. doi: 10.1016/j.fm.2020.103597

Pelicaen, R., Gonze, D., Teusink, B., De Vuyst, L., and Weckx, S. (2019). Genome-scale metabolic reconstruction of Acetobacter pasteurianus 386B, a candidate functional starter culture for cocoa bean fermentation. *Front. Microbiol.* 10:2801. doi: 10.3389/fmicb.2019.02801

Prigent, S., Nielsen, J. C., Frisvad, J. C., and Nielsen, J. (2018). Reconstruction of 24 Penicillium genome-scale metabolic models shows diversity based on their secondary metabolism. *Biotechnol. Bioeng.* 115, 2604–2612. doi: 10.1002/bit.26739

Saeki, A., Taniguchi, M., Matsushita, K., Toyama, H., Theeragool, G., Lotong, N., et al. (1997). Microbiological aspects of acetate oxidation by acetic acid bacteria, unfavorable phenomena in vinegar fermentation. *Biosci. Biotech. Bioch.* 61, 317–323. doi: 10.1271/bbb.61.317

Sakurai, K., Yamazaki, S., Ishii, M., Igarashi, Y., and Arai, H. (2013). Role of the glyoxylate pathway in acetic acid production by Acetobacter aceti. *J. Biosci. Bioeng.* 115, 32–36. doi: 10.1016/j.jbiosc.2012.07.017

Sauer, U., Canonaco, F., Heri, S., Perrenoud, A., and Fischer, E. (2004). The soluble and membrane-bound transhydrogenases UdhA and PntAB have divergent functions in NADPH metabolism of Escherichia coli. *J. Biol. Chem.* 279, 6613–6619. doi: 10.1074/jbc.M311657200

Seif, Y., Kavvas, E., Lachance, J.-C., Yurkovich, J. T., Nuccio, S.-P., Fang, X., et al. (2018). Genome-scale metabolic reconstructions of multiple salmonella strains reveal serovar-specific metabolic traits. *Nat. Commun.* 9:3771. doi: 10.1038/s41467-018-06112-5

Serres, M. H., and Riley, M. (2006). Genomic analysis of carbon source metabolism of Shewanella oneidensis MR-1: predictions versus experiments. *J. Bacteriol.* 188, 4601–4609. doi: 10.1128/JB.01787-05

Shinjoh, M., and Toyama, H. (2016). "Industrial applications of acetic acid bacteria (vitamin C and others)" in *Acetic Acid Bacteria Ecology and Physiology*. eds. K. Matsushita, H. Toyama, N. Tonouchi and A. Okamoto-Kainuma (Tokyo, Japan: Springer)

Tatusova, T., DiCuccio, M., Badretdin, A., Chetvernin, V., Nawrocki, E. P., Zaslavsky, L., et al. (2016). NCBI prokaryotic genome annotation pipeline. *Nucleic Acids Res.* 44, 6614–6624. doi: 10.1093/nar/gkw569

The UniProt Consortium (2019). UniProt: a worldwide hub of protein knowledge. *Nucleic Acids Res.* 47, D506–D515. doi: 10.1093/nar/gky1049

Thiele, I., and Palsson, B. Ø. (2010). A protocol for generating a high-quality genome-scale metabolic reconstruction. *Nat. Protoc.* 5, 93–121. doi: 10.1038/nprot.2009.203

Verduyn, C., Postma, E., Scheffers, W. A., and Van Dijken, J. P. (1992). Effect of benzoic acid on metabolic fluxes in yeasts: a continuous-culture study on the regulation of respiration and alcoholic fermentation. *Yeast* 8, 501–517. doi: 10.1002/yea.320080703

Wattam, A. R., Davis, J. J., Assaf, R., Boisvert, S., Brettin, T., Bun, C., et al. (2017). Improvements to PATRIC, the all-bacterial bioinformatics database and analysis resource center. *Nucleic Acids Res.* 45, D535–D542. doi: 10.1093/nar/gkw1017

Yamada, Y. (2016). "Systematics of acetic acid bacteria" in *Acetic Acid Bacteria Ecology and Physiology*. eds. K. Matsushita, H. Toyama, N. Tonouchi and A. Okamoto-Kainuma (Tokyo, Japan: Springer)

Yu, C.-S., Lin, C.-J., and Hwang, J.-K. (2004). Predicting subcellular localization of proteins for gram-negative bacteria by support vector machines based on n-peptide compositions. *Protein Sci.* 13, 1402–1406. doi: 10.1110/ps.03479604

frontiers | Frontiers in Microbiology

TYPE Original Research
PUBLISHED 07 December 2022
DOI 10.3389/fmicb.2022.1055010

OPEN ACCESS

EDITED BY
Viviana Corich,
University of Padua, Italy

REVIEWED BY
Salvatore La China,
University of Modena and Reggio Emilia, Italy
Severino Zara,
University of Sassari, Italy

*CORRESPONDENCE
Isidoro García-García
isidoro.garcia@uco.es

SPECIALTY SECTION
This article was submitted to Food Microbiology, a section of the journal Frontiers in Microbiology

RECEIVED 27 September 2022
ACCEPTED 21 November 2022
PUBLISHED 07 December 2022

CITATION
Román-Camacho JJ, García-García I, Santos-Dueñas IM, Ehrenreich A, Liebl W, García-Martínez T and Mauricio JC (2022) Combining omics tools for the characterization of the microbiota of diverse vinegars obtained by submerged culture: 16S rRNA amplicon sequencing and MALDI-TOF MS. *Front. Microbiol.* 13:1055010. doi: 10.3389/fmicb.2022.1055010

Combining omics tools for the characterization of the microbiota of diverse vinegars obtained by submerged culture: 16S rRNA amplicon sequencing and MALDI-TOF MS

Juan J. Román-Camacho[1], Isidoro García-García[2]*, Inés M. Santos-Dueñas[2], Armin Ehrenreich[3], Wolfgang Liebl[3], Teresa García-Martínez[1] and Juan C. Mauricio[1]

[1]Department of Agricultural Chemistry, Edaphology and Microbiology, Agrifood Campus of International Excellence ceiA3, University of Córdoba, Córdoba, Spain, [2]Department of Inorganic Chemistry and Chemical Engineering, Agrifood Campus of International Excellence ceiA3, Nano Chemistry Institute (IUNAN), University of Córdoba, Córdoba, Spain, [3]Department of Microbiology, School of Life Sciences, Technical University of Munich, Freising-Weihenstephan, Germany

Vinegars elaborated in southern Spain are highly valued all over the world because of their exceptional organoleptic properties and high quality. Among the factors which influence the characteristics of the final industrial products, the composition of the microbiota responsible for the process and the raw material used as acetification substrate have a crucial role. The current state of knowledge shows that few microbial groups are usually present throughout acetification, mainly acetic acid bacteria (AAB), although other microorganisms, present in smaller proportions, may also affect the overall activity and behavior of the microbial community. In the present work, the composition of a starter microbiota propagated on and subsequently developing three acetification profiles on different raw materials, an alcohol wine medium and two other natural substrates (a craft beer and fine wine), was characterized and compared. For this purpose, two different "omics" tools were combined for the first time to study submerged vinegar production: 16S rRNA amplicon sequencing, a culture-independent technique, and matrix-assisted laser desorption/ionization-time of flight mass spectrometry (MALDI-TOF MS), a culture-dependent method. Analysis of the metagenome revealed numerous taxa from 30 different phyla and highlighted the importance of the AAB genus *Komagataeibacter*, which was much more frequent than the other taxa, and *Acetobacter*; interestingly, also archaea from the Nitrososphaeraceae family were detected by 16S rRNA amplicon sequencing. MALDI-TOF MS confirmed the presence of *Komagataeibacter* by the identification of *K. intermedius.* These tools allowed for identifying some taxonomic groups such as the bacteria genera *Cetobacterium* and *Rhodobacter*, the bacteria species *Lysinibacillus fusiformis,* and even archaea, never to date found in this medium. Definitely, the effect of the combination of these techniques has allowed first, to confirm

the composition of the predominant microbiota obtained in our previous metaproteomics approaches; second, to identify the microbial community and discriminate specific species that can be cultivated under laboratory conditions; and third, to obtain new insights on the characterization of the acetification raw materials used. These first findings may contribute to improving the understanding of the microbial communities' role in the vinegar-making industry.

KEYWORDS

acetic acid bacteria, alcohol wine, craft beer, fine wine, metagenomics, protein fingerprinting

Introduction

The Andalusia region, located in southern Spain, has been, since immemorial times, a production area of famous and unique vinegars. Several factors influence the organoleptic properties and quality of these fermented products (Mas et al., 2014; Ho et al., 2017). First, the climate and soil factors of this Mediterranean region allow the growing of native raw materials, including grapes, cereals, and other fruits which are used for obtaining some high-quality acetification substrates such as wines (Maestre et al., 2008; Hidalgo et al., 2013; Mas et al., 2014; Román-Camacho et al., 2022). Second, the starter culture is composed of a complex community of microorganisms and does not represent an axenic culture of a single species (Li et al., 2015; Trček et al., 2016). Normally, species of the acetic acid bacteria (AAB) genera *Acetobacter* and *Komagataeibacter* (mainly relocated from *Gluconacetobacter*) predominate in the media because of their capabilities to perform, efficiently, the incomplete oxidation of the ethanol into acetic acid, as well as their tolerance to both substrate and product, and low pH (Mamlouk and Gullo, 2013; Wang et al., 2015; Qiu et al., 2021; He et al., 2022). *Acetobacter pasteurianus* is usually one of the predominant species at the beginning of the cycle, at a higher ethanol content, but *Komagataeibacter europaeus* is subsequently imposed during the rest of a submerged acetification. This results in final products with a high acetic acid content and other metabolites that influence the organoleptic properties (Andrés-Barrao et al., 2011; Zhu et al., 2018). Moreover by metagenomic and metaproteomic approaches, new non-abundant microbial groups never identified in vinegar to date, such as other typical AAB genera and lactic acid bacteria among others, have been found along with the best-adapted predominant organisms (Trček et al., 2016; Román-Camacho et al., 2020).

The development of the submerged culture systems allowed for industrializing vinegar production and enabled to efficiently control of operational variables of the system and obtaining, rapidly, higher acid final products due to the efficiency of mass transfer and continuous vigorous aeration (García-García et al., 2009, 2019; Gullo et al., 2014). Among working modes for industrial vinegar-making, the semi-continuous one is mostly imposed (De Ory et al., 2004; García-García et al., 2007, 2009; Qi et al., 2014). Here, each cycle is started by a loading phase that refills the reactor with fresh medium to the working volume without exceeding a preset ethanol concentration. Then, an exhausting stage occurs depleting the ethanol in the culture broth to a preset extent. Lastly, a part of the reactor is partially unloaded and the remaining volume is used as inoculum for the next cycle (Lee et al., 2017; Jiménez-Hornero et al., 2020). Operational variables may be controlled to maintain mean substrate (ethanol) and product (acetic acid) concentrations within appropriate ranges for AAB which, because of their high sensibility to these variations, are self-selected for the specific medium according to their growing features (García-García et al., 2009, 2019).

The microbiota participating in vinegar-making influences the features of the final products (Zhu et al., 2018; Wang et al., 2022). However, the identification of the microbial composition is often hindered by the special growing conditions and metabolic characteristics of these microorganisms, mainly AAB, which carry out their normal activity in a medium contained within industrial bioreactors (Fernández-Pérez et al., 2010; Trček and Barja, 2015; Andrés-Barrao et al., 2016; Trček et al., 2016). Because AAB not always can be isolated under laboratory conditions outside their natural environment, due to a viable but non-culturable (VBNC) state, the study of their richness and biodiversity is limited, probably ignoring key species within the microbiota (Mamlouk and Gullo, 2013; De Roos and De Vuyst, 2018). Some authors have used various "omics" approaches to facilitate these studies throughout the industrial acetification process without the necessity to isolate the microorganisms while providing massive and precise information about the microbial composition and behavior during the process (Andrés-Barrao et al., 2016; Trček et al., 2016; Wang et al., 2021). Recently, our previous work allowed us to characterize, by metaproteomics, the microbiota existing

in a submerged acetification process employing first, a synthetic alcohol wine medium as a reference raw material (Román-Camacho et al., 2020, 2021) and then, two natural substrates (Román-Camacho et al., 2022). Liquid chromatography with tandem mass spectrometry (LC-MS/MS) analyses revelated that the AAB genus *Komagataeibacter* was dominant throughout acetification, especially the species *K. europaeus* providing protein fractions above 70% of the metaproteome.

In the present work, the use of 16S rRNA amplicon sequencing, a culture-independent technique, and matrix-assisted laser desorption/ionization-time of flight mass spectrometry (MALDI-TOF MS), a culture-dependent technique, has been implemented. From these "omics" tools, the microbiota composition developing from a mixed starter culture during the course of three acetification processes, first on a synthetic alcohol wine medium and subsequently on two other natural raw materials (craft beer and fine wine), was characterized for the first time. Following this strategy, using submerged cultivation in a semi-continuous mode as a working method, the comparison of the composition of microbial profiles obtained throughout the vinegar production might both confirm our previous results based on metaproteomics as well as provide new findings in the field of vinegar industrial production.

Materials and methods

Raw materials

Three raw materials were used to perform fermentations. First, an alcoholic wine medium (AW) was prepared in the laboratory following the method of Llaguno (1991) with additional peptone (0.5 g/L) and yeast extract (0.25 g/L). Then, two natural raw materials, a high-sugar craft beer (B) (Mahou-San Miguel, Córdoba, Spain) and a dry fine wine (FW) from the Montilla-Moriles region (Bodegas Alvear S.A., Montilla, Córdoba, Spain). The fermentation media were diluted with distilled water to adjust the ethanol concentration to the working conditions [10% (v/v)]. The initial acetic acid concentration was of 0.1 ± 0.1% (w/v) for AW and 0.2 ± 0.1% (w/v) for B and FW. Additional information on the nutritional composition of natural raw materials may be found in Román-Camacho et al. (2022).

Microorganism

The first acetification (AW) was started using an inoculum consisting of a mixed culture coming from a fully active operating industrial tank (UNICO Vinagres y Salsas, S.L.L., Córdoba, Spain) making wine vinegar. A sample harvested at the final moments of the process, at the point of highest acetic acid concentration, was used as a starter culture for subsequent acetifications (B, FW). The starter culture was adapted to each raw material by a previous phase according to Román-Camacho et al. (2022).

Operating mode

Acetifications were carried out in a fully automated 8 L Frings bioreactor (Heinrich Frings GmbH & Co., KG, Bonn, Germany) at a pilot scale, operating in a semi-continuous mode which works mimicking the industrial procedures as detailed in Román-Camacho et al. (2022). In order to facilitate the understanding of the operating mode, some additional figures summarizing the process are included (**Figures 1**, **2**). A constant temperature of 31°C, a fast-loading rate of 1.3 L/h, and an air-flow rate of 7.5 L/(h L medium) were set. In the case of the beer medium, the profile was operated with a final working volume of 7 L because of excessive foaming. A detailed description of each acetification profile from a technical point of view can be found in our previous metaproteomics works (Román-Camacho et al., 2020, 2022).

Sampling

For alcohol wine acetification, sampling was carried out at three key points: at the end of fast loading (FL), at the end of discontinuous loading (DL), and just before unloading (UL). Because of a faster ethanol consumption rate in natural raw material profiles, only two points were considered; at the end of the loading stage (EL), when the final working volume is reached, and just before unloading, at the end of the ethanol exhaustion stage (UL). A total of three or four biological replicates were taken from each point in different cycles. The starting inoculum was sampled before starting the adaptation phase, after vigorous homogenization.

Metagenomics

Sample processing

Vinegar samples were harvested by directly unloading a volume of 300 mL from the acetator for each biological replicate at the sampling times aforementioned (see Section "Sampling"), dividing it into six fractions of 50 ml each, which were cooled on ice in centrifuge tubes. Cells were obtained by centrifugation and washed twice with cold sterile distilled water; the resulting cell pellets were stored at −80°C until the metagenomic procedures.

Genomic deoxyribonucleic acid extraction, purification, and quantification

Genomic DNA (gDNA) from all the samples was extracted by using a quick genomic bacterial DNA extraction kit

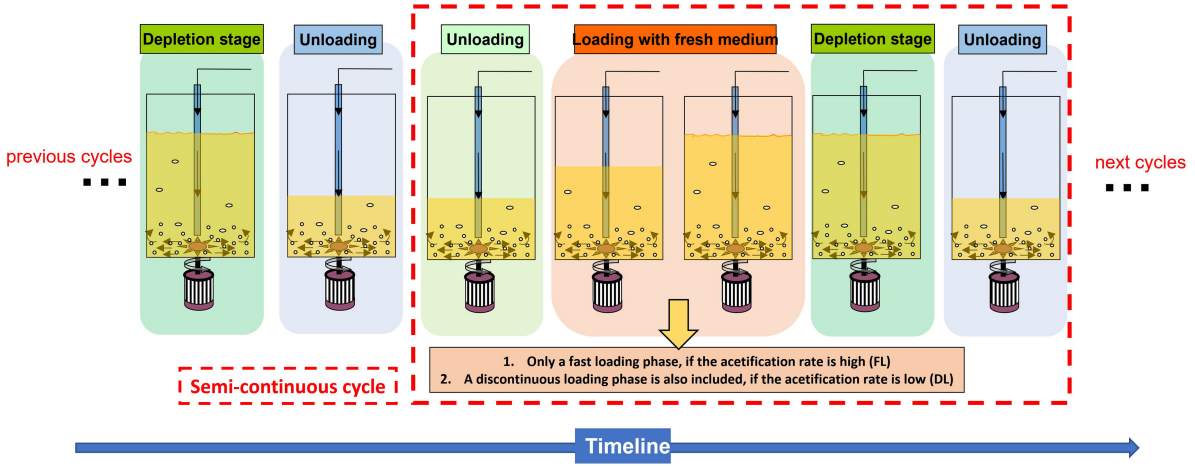

FIGURE 1
Scheme that describes the different phases that take place throughout the course of a submerged acetification process operated in a semicontinuous mode.

(Bio Knowledge Lab, S.L., Córdoba, Spain) following the instructions provided by the manufacturer. The purity and quantity of the gDNA were determined by NanoDrop ND 1000 spectrophotometer (Thermo Fisher Scientific, MA, USA).

16S rRNA sequencing

The V3-V4 region from 16S rRNA genes was amplified using the specific set of primers 341F (5′-CCTACGGGNGG CWGCAG-3′)-806R (5′-GGACTACHVGGGTWTCTAAT-3′) with barcodes (Cole et al., 2009; Caporaso et al., 2010). PCR reactions for amplicon generation were carried out with Phusion® High-Fidelity PCR Master Mix (New England Biolabs, MA, USA). PCR products were mixed with the same volume of 1 × loading buffer with SYBR green and a subsequent 2% agarose gel electrophoresis was run for the detection. Samples with a bright major band at 470 bp were selected for further experiments. PCR mixed products, obtained at equal density ratios, were purified with Qiagen Gel Extraction Kit (Qiagen, Germany). The libraries were generated with NEBNext® Ultra TM DNA Library Prep Kit for Illumina using the Illumina set of adapters F (5′-TCGTCGG CAGCGTCAGATGTGTATAAGAGACAG-3′)-R (5′-GTCTCG TGGGCTCGGAGATGTGTATAAGAGACAG-3′) and then, were quantified via Qubit and Q-PCR. The amplicon was sequenced on Illumina paired-end platform to generate 250 bp paired-end raw reads.

Raw data analysis

Raw data were firstly filtered using QIIME2 v2020.8[1] (Bolyen et al., 2019). Reads (fastq) obtained after Illumina amplicon sequencing were denoising using the DADA2 package[2] by conducting three steps: (1) trimming and truncating low-quality regions, (2) dereplicating the reads, and (3) chimera filtering (Callahan et al., 2016). After denoising, forward and reverse reads were merged into one sequence (fasta), dereplicated, and assigned to an ID, considering them as amplicon sequence variants (ASVs). The number of reads found at each filtering level is given in **Supplementary Table 1**. ASVs were grouped in operational taxonomic units (OTUs) by using the *de novo* clustering method from vsearch (Rognes et al., 2016). Clustering was carried out at 97% identity to create 97% OTUs.

The rest of the analyses were performed by using QIIME2 v2020.8. For biodiversity analysis, the core-metrics phylogenetic method, which supports computing alpha and beta diversity metrics, was used. Alpha diversity, defined as the diversity within the samples, was quantified by estimating and comparing different diversity indexes such as observed features, faith phylogenetic diversity, Shannon, and Simpson indexes. The diversity alpha rarefaction tool was applied to randomly select a different number of sequences and analyze detected OTUs at each fraction to form a rarefaction curve. Beta diversity, defined as compositional heterogeneity among samples, was represented by a Principal Coordinates Analysis (PCoA) employing the UniFrac algorithm. For taxonomic analysis, OTUs were classified by taxon using the 16S rRNA V3-V4 region SILVA database with vsearch by assigning a taxon to each OTU and generating bar plots and heatmaps with hierarchical clustering through specific QIIME2 plugins (Quast et al., 2013).

Analysis of composition microbiomes (ANCOM) was applied as a statistical tool to identify differentially abundant features across sample groups at specific taxonomic levels

1 https://qiime2.org/

2 https://github.com/benjjneb/dada2

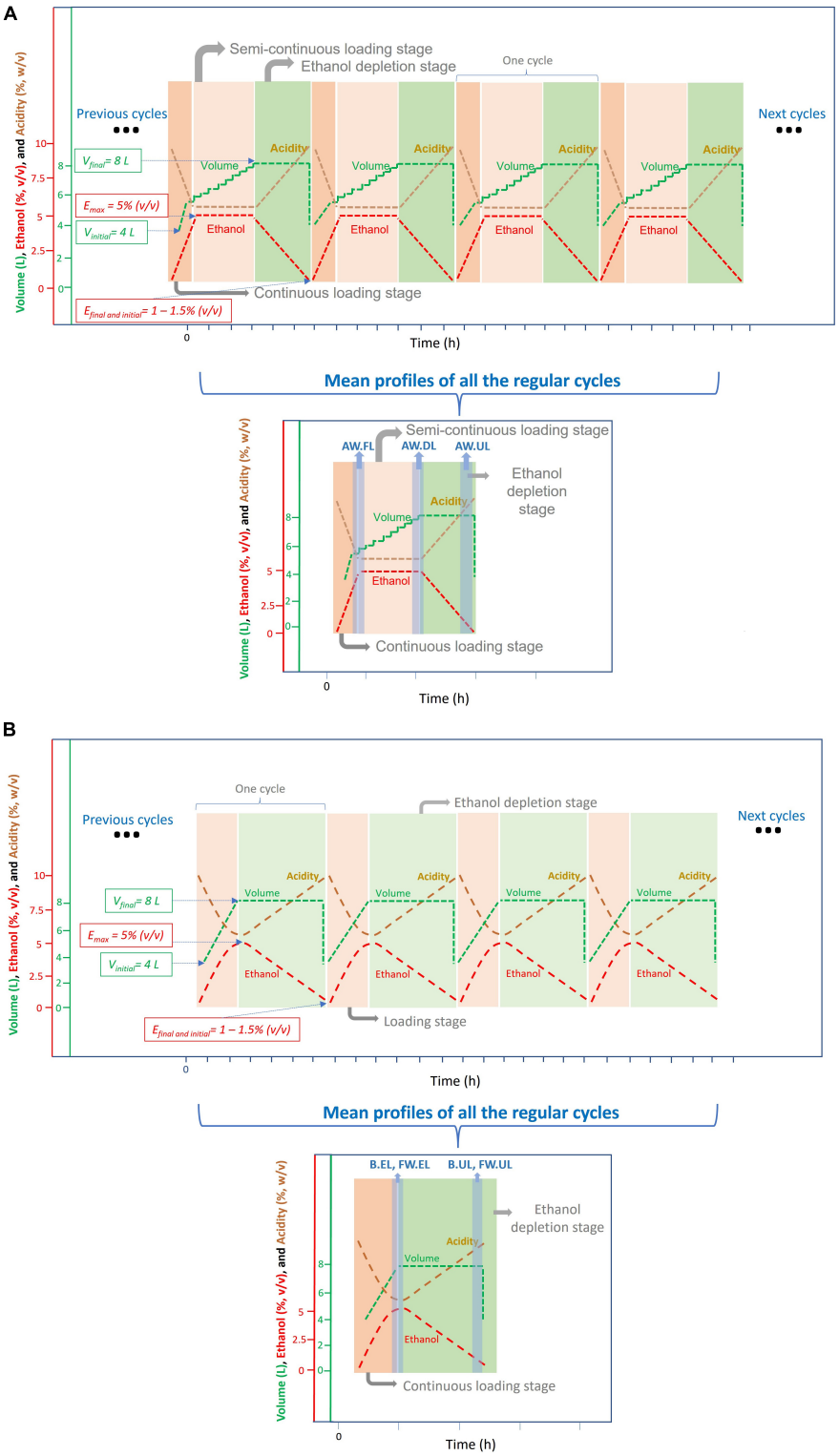

FIGURE 2
Scheme representing the operational mode used for the acetification of the different substrates; the experimental data regarding the cycle times for each acetification profile can be found in Román-Camacho et al. (2020) (for AW) and Román-Camacho et al. (2022) (for FW and B). **(A)** Submerged culture for alcohol wine vinegar (AW) production working in a semi-continuous mode. Each cycle of acetification starts by loading the tank to its working volume (8 L) without exceeding a preset ethanol concentration [5% (v/v)]. Because of a lower ethanol consumption rate in this profile, the preset ethanol concentration [5% (v/v)] is first reached (AW.FL), and therefore, an additional discontinuous loading stage (AW.DL) is necessary to reach the final working volume (8 L). When ethanol concentration is depleted to 1.0–1.5% (v/v), 50% of the
(Continued)

FIGURE 2 (Continued)
reactor content (4 L) is unloaded (AW.UL). This system is maintained for the following production cycles. **(B)** Submerged culture for the beer vinegar (B) and fine wine vinegar (FW) production working in a semi-continuous mode. Each cycle of acetification starts by loading the tank to its working volume (8 L) without exceeding a preset ethanol concentration [5% (v/v)]. Because of a higher ethanol consumption rate in these profiles, the working volume is first reached (8 L) (B.EL, FW.EL) and a discontinuous loading phase is not necessary. When ethanol concentration is depleted to 1.0–1.5% (v/v), 50% of the reactor content (4 L) is unloaded (B.UL, FW.UL). This system is maintained for the following production cycles.

(Mandal et al., 2015). The test calculates the number of ratios significantly different between ASV pairs [False Discovery Rate (FDR) with a p-value < 0.05]. The results are represented in a volcano plot, which relates the ANCOM W statistic to the center-log-ratio (CLR) for the groups, W being the number of ANCOM null hypotheses rejected for each taxon, indicating significant differences between ratios of a taxon's relative abundance to those of W for other taxa. The complete strategy for 16S rRNA amplicon sequencing is summarized in Figure 3.

Characterization of isolates by matrix-assisted laser desorption/ionization-time of flight mass spectrometry

Growing conditions

For each vinegar sample harvested from the reactor, a volume of 50 ml was centrifuged and washed as in Section "Sample processing". 1 ml of cell culture was used to perform serial dilutions in distilled sterile water and subsequently, 100 μl from each dilution were cultured in an optimized GYC medium (50 g/L glucose, 20 g/L agar, 10 g/L yeast extract, 3 g/L calcium carbonate, and 0.6% of 1:1 pure ethanol and glacial acetic acid). This medium was selected after numerous assays using different media in order to obtain a high growth efficiency (Gullo et al., 2006; De Vero and Giudici, 2013). Plates were incubated at 30 °C for 6 or 7 days. Isolates were selected attending to the phenotypical features of the grown colonies including mainly morphology, aspect, color, and size. Among three and five colonies from each phenotypic group were randomly selected to try to cover the totally different microorganisms present. Then, the isolates were both grown in a fresh tube medium and incubated again under the same conditions to obtain higher biomass before identification.

Identification of the isolates

A qualitative analysis of the isolates was performed through MALDI-TOF MS. 5–10 mg of fresh mass from each isolate were placed in 300 μl Milli-Q water and 900 μl ethanol and then vortexed until homogenization. Samples were centrifuged at 14,500 × g for 2 min, pellets were dried at room temperature (RT), and subjected to 50 μl of 70% formic acid and 50 μl of acetonitrile. After a second centrifugation, proteins were obtained in the supernatant, and 1 μl was dried in a MALDI plate subsequently coated with 1 μl of HCCA matrix (α-cyano-4-hydroxycinnamic acid) prepared in a mixture of 50% acetonitrile and 2.5% trifluoroacetic acid. Samples were again dried at RT.

Dried samples were analyzed with MALDI-TOF/TOF "ULTRAFLEXTREME" (Bruker Daltonics, Bremen, Germany) equipment. Obtained spectra were treated with MALDI Biotyper Compass (MBT Compass; Bruker, MA, United States) software, calibrating the spectra before searching and matching, automatizing the measures and obtaining the identifications. Spectra were compared with reference profiles from the MBT Compass Library (Bruker) and finally, score values ≥ 1.70 were considered.

Results

Qualitative analysis

A total of 12,443 unique ASVs were detected after performing strict quality control. After clustering and chimera filtering, a total of 6,187 unique OTUs were found at 97% identity in, at least, one out of a total of 26 samples. The distribution of the unique OTUs within samples was analyzed through Venn diagrams to obtain an overview of the qualitative metagenome for each acetification profile, see Figure 4.

For alcohol wine vinegar (AW, Figure 4A), a total of 561 OTUs were found throughout the acetification. Of them, 132 (23.5%), 61 (10.9%), and 79 (14.1%) were specific to AW.FL, AW.DL, and AW.UL phases, respectively. The highest amount of OTUs was located in the central common area for the three time points of sampling (148, 26.4%). For beer vinegar (B, Figure 4B), a total of 656 OTUs were found containing 256 (39.0%) common ones at the end of loading as well as just before unloading. In this case, the highest fraction of sampling point specific OTUs corresponded to B.EL with 325 (49.6%) contrasting with a much lower number for B.UL with only 75 (11.4%). For fine wine vinegar (FW, Figure 4C), 638 OTUs were detected in total, with 256 (40.1%) OTUs at both sampling time points, while 223 (35.0%) and 159 (24.9%) were specific

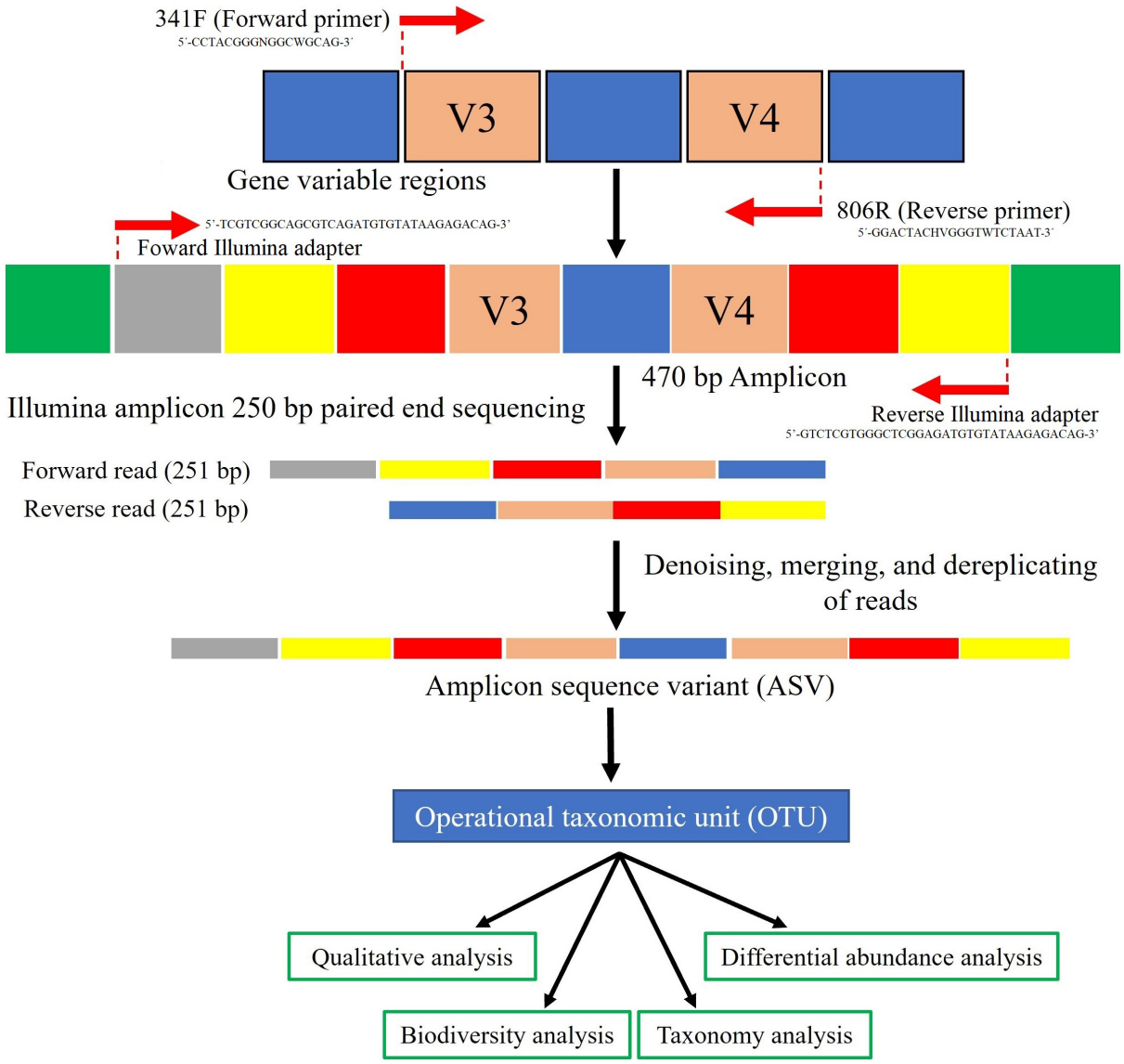

FIGURE 3
Flow diagram representing the strategy employed for 16S rRNA amplicon sequencing and raw data processing. Reads were denoising by the DADA2 package (https://github.com/benjjneb/dada2) and the rest of the procedures using QIIME2 v2020.8 (https://qiime2.org/).

to FW.EL and FW.UL, respectively, in this matrix. In general, an important fraction of OTUs was common throughout each acetification although, regarding sampling times, OTUs were more abundant at the end of loading periods (EL), especially in beer vinegar. Fine wine vinegar exhibited a higher proportion of OTUs at the final moments of the acetification (UL), amounting to around 25%, while the other profiles were characterized by a lower OTU diversity at this time point, between 10 and 15%, see **Figure 4**. It is also worth noting that analysis of the inoculum samples revealed a total of 919 unique OTUs, a higher number than in any sample throughout the acetification processes.

Biodiversity analysis

The study of the biodiversity degree, provided by the amount of detected OTUs and how they are distributed both within samples and between them, is described in the following. Alpha diversity within the samples was determined through quantification by different diversity indexes including observed features, Faith phylogenetic diversity, Shannon, and Simpson indexes, see **Table 1**. Inoculum samples provided the highest biodiversity values in all indexes, far above acetification matrices. For alcohol vinegar (AW), the diversity pattern was similar to that shown for the OTU distribution (see

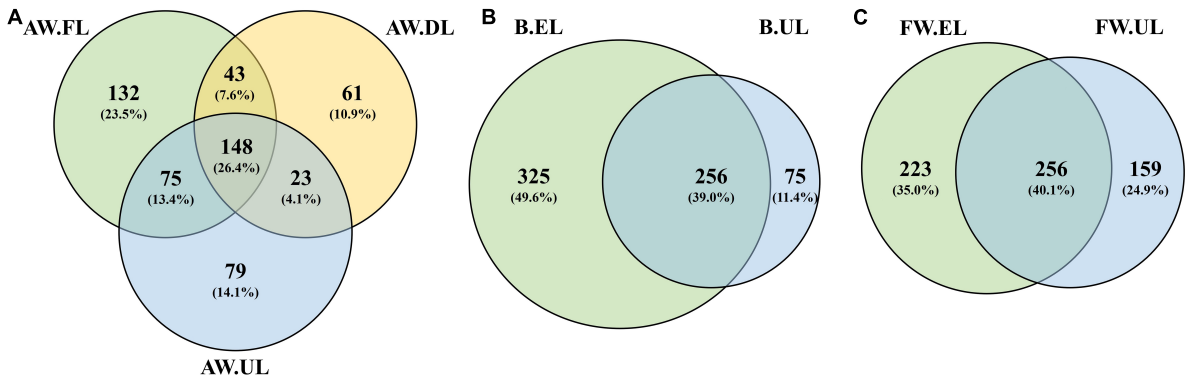

FIGURE 4
Venn diagrams representing the number of valid unique OTUs present within samples for each acetification profile. **(A)** Alcohol wine vinegar; **(B)** beer vinegar; **(C)** fine wine vinegar. AW, alcohol wine; B, beer; FW, fine wine; EL, end of loading phase (FL, fast loading; DL, discontinuous loading); UL, just before unloading.

Figure 4), higher at the beginning of the process (AW.FL) with a subsequent strong decrease (AW.DL) before finally increasing again but without reaching initial levels (AW.UL). For fine wine vinegar (FW), diversity was slightly higher at the end of loading period (FW.EL) compared to the sampling point just before unloading (FW.UL) while for beer vinegar (B), diversity was much higher at the final moments of the process (B.UL). These results are represented in an alpha rarefaction plot generated by randomly selecting a different number of sequences and analyzing detected OTUs at each fraction to form a rarefaction curve. The Shannon index was selected as the quantitative measure to represent the biodiversity of each sample, individually, thus connecting the median values of the metric distribution across the sampling depths, see Figure 5A.

Beta diversity analyses were carried out by selecting the UniFrac algorithm both at a qualitative (unweighted) and quantitative (weighted) level and represented by a Principal Coordinates Analysis (PCoA), see Figures 5B,C. These results show a bi-dimensional matrix in which each sample is a point and the distance between them indicates the similarity between samples (closer together more similarity). The size of the points represents the diversity of Shannon ranging from level 1 to 4. The unweighted matrix (Figure 5B) showed no aggrupation of the samples which were widely distributed throughout the plot while the weighted matrix (Figure 5C) showed a very close aggrupation of most samples from each acetification profile at the bottom left although samples from the starting inoculum were particularly diverse and separated from the rest of the samples. These results might indicate that the OTUs' frequency plays a bigger role in the samples than the OTUs' presence/absence. From a quantitative point of view, the raw material used for making vinegar did not cause significant variations in the diversity of samples from the three acetification processes, as can be observed in their closed aggrupation.

TABLE 1 Alpha diversity indexes for quantification of the biodiversity degree within the vinegar samples.

Sample	Observed feat.	Faith ph.	Shannon	Simpson
Inoculum	2417 ± 784	159.3 ± 8.0	3.40 ± 1.30	0.434 ± 0.154
AW.FL	332 ± 94	49.8 ± 14.5	0.43 ± 0.16	0.067 ± 0.026
AW.DL	198 ± 56	33.6 ± 3.3	0.27 ± 0.10	0.042 ± 0.016
AW.UL	294 ± 52	42.5 ± 7.7	0.36 ± 0.04	0.054 ± 0.006
B.EL	258 ± 30	41.6 ± 4.2	0.34 ± 0.06	0.052 ± 0.009
B.UL	720 ± 197	72.9 ± 15.6	0.73 ± 0.20	0.105 ± 0.029
FW.EL	450 ± 138	52.6 ± 9.0	0.61 ± 0.19	0.104 ± 0.025
FW.UL	359 ± 158	51.9 ± 7.7	0.50 ± 0.21	0.079 ± 0.029

AW, alcohol wine; B, beer; FW, fine wine; EL, end of loading phase (FL, fast loading; DL, discontinuous loading); UL, just before unloading.

Taxonomy analysis

The assignment of a taxon to each OTU found in the vinegar samples enabled the identification of the taxon composition within the metagenome. The total OTUs were first clustered in a heatmap obtained through the QIIME2 heatmap plugin and then also depicted in a bar plot obtained through the QIIME2 taxa bar plot plugin. In the heatmap, the taxa were grouped by hierarchical clustering and represented at the phylum level for each sample including their frequency (log10), see Figure 6. The results indicated that Proteobacteria (96.41%) was the most frequent phylum throughout the three acetification profiles (AW, B, FW), far above the rest of the phyla and being less abundant in the inoculum samples. For this reason, this group built a separate cluster from the rest of the taxonomic groups. None of the remaining phyla contributed a mean frequency ≥ 1%. Interestingly, the second most frequent phylum was Thaumarchaeota (0.69%) belonging to the archaea; with less mean frequency, another two archaeal phyla were found in this

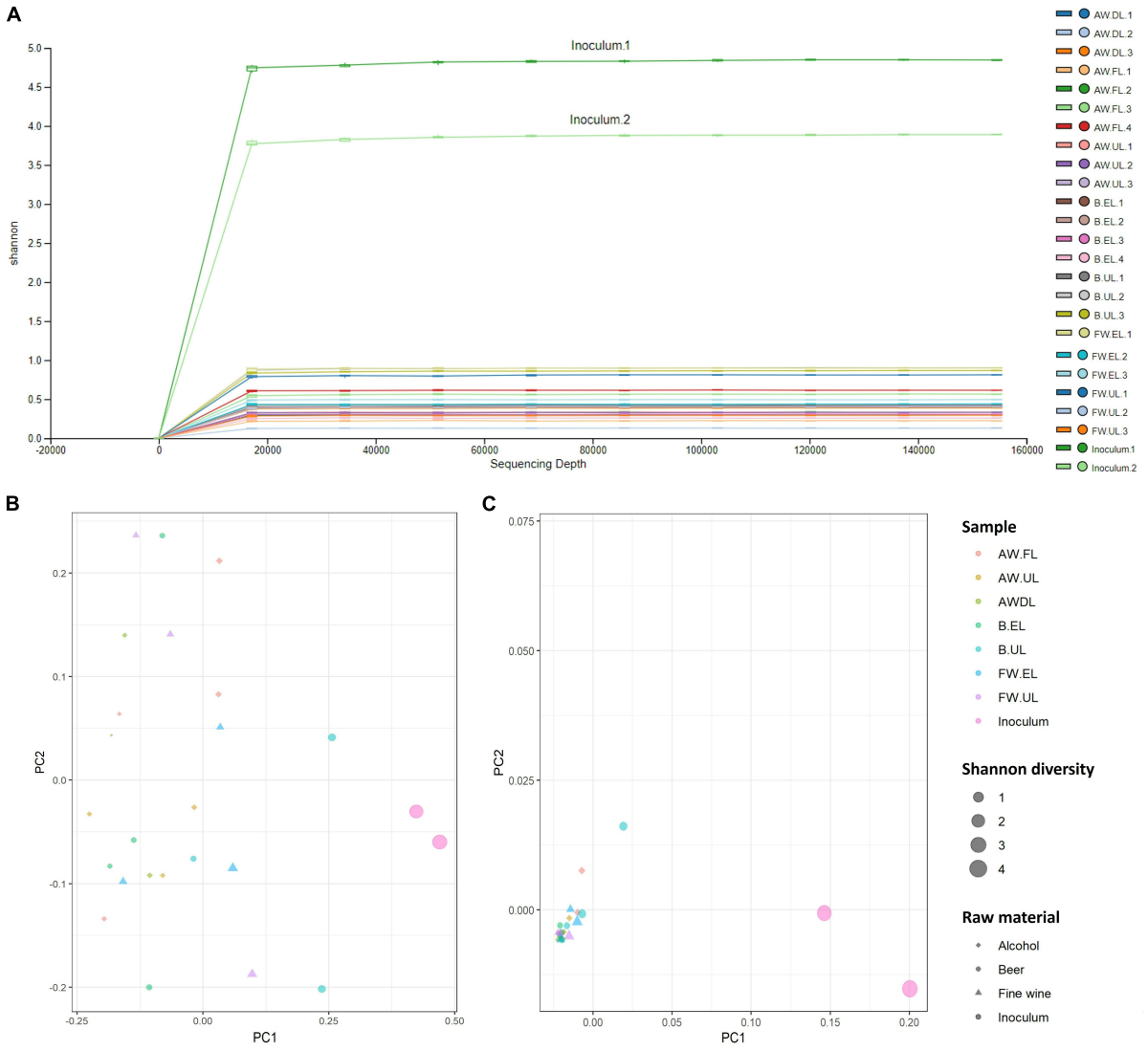

FIGURE 5
(A) Alpha rarefaction plot that shows the Shannon rarefaction curve as a biodiversity quantitative index. The box plots represent the distribution of the Shannon metric for each group of samples at each even sampling depth. The lower and upper whiskers of the box are the 9th and 91st percentiles, respectively, while lower and upper extents are the 25th and 75th percentiles; the horizontal bar through the middle is the median value. The line chart connects the medians of the metric distribution across sampling depths. **(B,C)** Principal Coordinates Analysis (PCoA) by using the unweighted **(B)** and weighted **(C)** UniFrac algorithm. Each sample is represented as a dot in a bi-dimensional matrix and the distance between dots indicates the similarity between samples (closer together more similarity). The color, size, and shape of dots represent sampling time, Shannon diversity, and raw material, respectively. AW, alcohol wine; B, beer; FW, fine wine; EL, end of loading phase (FL, fast loading; DL, discontinuous loading); UL, just before unloading.

study, Euryarchaeota (0.04%) and Nanoarchaeaeota (0.01%). Some of the following most frequent taxa which conformed to a closer cluster were the bacterial phyla Bacteroidetes (0.54%), Firmicutes (syn. Bacillota) (0.51%), Actinobacteria (0.42%), Verrucomicrobia (0.27%), Acidobacteria (0.24%), Chloroflexi (0.24%) and Fusobacteria (0.22%). In general lines for these taxonomic groups, inoculum samples showed higher frequencies than any of the acetification process samples, following the results obtained in the biodiversity analysis. It is also worth mentioning that around 30 different phyla were identified by 16S rRNA gene amplicon sequencing, see Figure 6.

The bar plot shows the relative frequency (%) that the main taxonomic groups contribute to each sample, see Figure 7. To complement the results of the heatmap and hierarchical clustering analysis, the taxa were also identified at the genus level. The acetic acid bacteria genera *Acetobacter* and *Komagataeibacter* were the main representatives of Proteobacteria. In general, *Komagataeibacter* was the most frequent taxon of the vinegar metagenomes, amounting

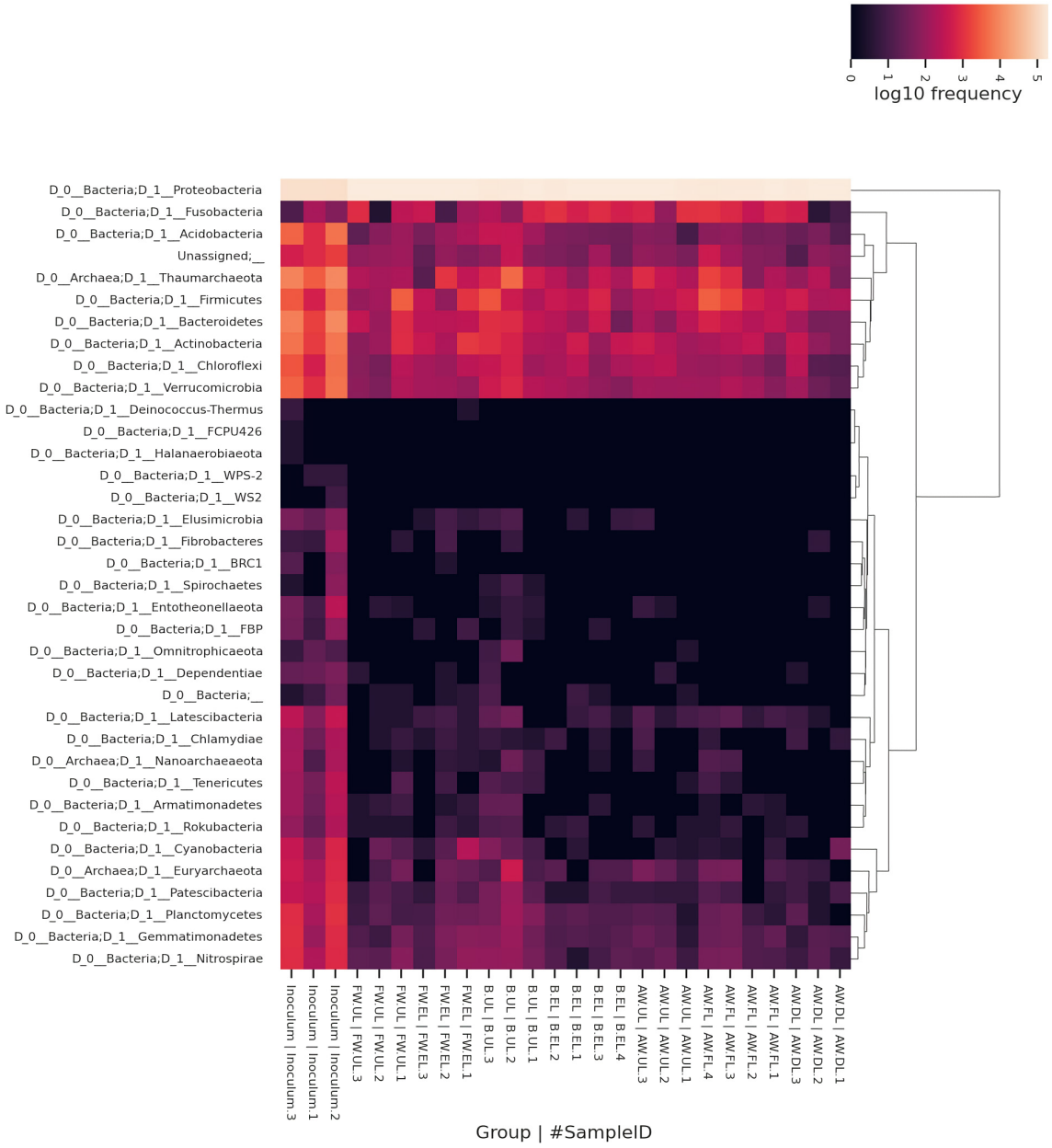

FIGURE 6
Heatmap clustering the metagenome taxonomy based on OTUs that comprise each taxon represented up to the phylum level as a maximum specificity. Taxa were grouped by hierarchical clustering for all samples according to their frequency (log10). AW, alcohol wine; B, beer; FW, fine wine; EL, end of loading phase (FL, fast loading; DL, discontinuous loading); UL, just before unloading.

to around 90% of the total OTUs. In the samples of the starter inoculum, the biodiversity was higher, but still *Komagataeibacter* contributed around 60–90% of the OTUs, while in the acetification samples (AW, B, FW) the predominance of the genus increased, irrespective of the raw material and the sampling time, to about 90–95%. *Acetobacter* was one of the most frequent taxa of the less abundant microbiota, especially in FW vinegar, accounting for up to 2% of the total OTUs in the FW.EL samples as well as being present in the rest of the samples. Moreover, a high difference in the number of total OTUs assigned to *Komagataeibacter* (431) and *Acetobacter* (3) might result in a significant difference in the diversity of species within the two AAB genera. Apart from these two genera, no other taxa from the acetic acid bacteria group were found among the main ones although a few other Acetobacteraceae members (e.g., *Acidiphilium*, *Craurococcus*, *Gluconacetobacter*, *Gluconobacter*, *Roseomonas*) were identified at very low frequency among the sequence

reads (see **Supplementary Table 2**). The archaeal group Thaumarchaeota was found to occur as unique OTUs mainly assigned to the Nitrososphaeraceae family accounting for about 2–5% of the total metagenome in inoculum samples but were also widely found in the acetification samples. The presence of archaea in vinegar is little known and their role in the microbial community may be an object of future study. Regarding the rest of the bacterial groups of the non-abundant metagenome, the OTUs were mainly assigned to *Cetobacterium* and *Rhodobacter*, present in most of the vinegar samples, as well as *Bacillus* and *Sphingomonas*, mostly contained in specific samples of inoculum, AW, and FW. Of the microbial phyla, Proteobacteria (including the genera *Komagataeibacter, Acetobacter, Rhodobacter, Sphingomonas*) and Fusobacteria (*Cetobacterium*) provided the most frequent genera, although many other microbial groups were identified as contributing but with merely very low fractions of the total OTUs. The list of the total OTUs with the taxon assigned to each of them, including those conforming to a minor fraction of taxa (see gray color in **Figure 7**) is available in **Supplementary Table 2**.

Differential abundance analysis

The abundance differences between the three acetification profiles and sampling times within each one of them were studied through ANCOM statistics. **Figure 8** represents volcano plots with a total of six matrices (A-F) showing these differences according to the distribution of the taxa (displayed as dots) throughout each matrix. The abundance of the taxa is measured through the relationship between the ANCOM *W* statistic to the center-log-ratio (CLR). **Figures 8A–C** shows the alcohol wine (AW), beer (B), and fine wine (FW) acetification profiles, respectively. The AW profile (**Figure 8A**) and FW profile (**Figure 8C**) barely revealed abundance differences, although both showed a couple of taxa with slightly higher *W* values than the rest [AW: *Conexibacter* ($W = 4$), Anaerolineaceae ($W = 3$); FW: *Microvirga* ($W = 18$), Betaproteobacteriales ($W = 9$)]. The B profile (**Figure 8B**) exhibited more abundance differences, as reflected in a more pronounced distribution of taxa in the matrix, highlighting some taxa such as the phylum Acidobacteria ($W = 39$) and the family Anaerolineaceae ($W = 25$) among others. The end of loading (**Figure 8D**) and just prior to unloading (**Figure 8E**) samples showed low relative abundance differences among the taxa, however, the genus *Acetobacter* stood out (located at the top right of both matrices) with much higher *W* values than the rest of the taxa in its matrix, particularly among the end of the loading samples (EL), reaching a statistically significant level ($W = 230$). Analysis of the relationship between the highly different samples from starter culture and final products revealed numerous taxa with significant abundance differences highlighting the genus *Aeromonas* ($W = 166$) and the family Pedosphaeraceae ($W = 140$) among others (**Figure 8F**).

Identification of isolates by protein fingerprinting using matrix-assisted laser desorption/ionization time of flight mass spectrometry

A total of 31 isolates were selected for identification after a morphological study of their colonies. Of them, 21 isolates were identified with high (2.00–3.00) or medium (1.99–1.70) confidence; 12 were from alcohol wine vinegar, 6 from beer vinegar, and 3 from fine wine vinegar. No acetic acid bacteria could be isolated on the solid medium from AW vinegar and the 12 isolates belonged to the gram-positive bacteria, *Lysinibacillus fusiformis*. A total of 7 isolates of acetic acid bacteria were obtained from samples at different phases from the acetification of natural media (B, FW), all of them belonging to the species *Komagataeibacter intermedius*. Another two strains of the bacteria species *L. fusiformis* were isolated from the FW vinegar samples. The complete list of species identified among the 31 isolates can be found in **Table 2**.

Discussion

The well-known 16S rRNA amplicon sequencing and MALDI-TOF MS techniques have allowed for comparing the microbial composition of three acetification profiles avoiding the risk of ignoring some unculturable or hardly culturable microorganisms under controlled laboratory conditions, as other author have previously reported in vinegar making (Fernández-Pérez et al., 2010; Vegas et al., 2010; Kim et al., 2013; Trček et al., 2016; Peters et al., 2017; Imchen et al., 2019; Rizo et al., 2020). In this work, these aspects are mainly based on the use of three raw materials as acetification substrates with different nutritional features which may influence the microbiota composition and diversity.

The qualitative and biodiversity analyses yielded some evidence based on the number and distribution of OTUs which might clarify fundamental aspects of the characterization of these raw materials and operating conditions (**Figures 4**, **5**). Although significant numbers of OTUs common to all samples of each acetification process were shown, also high numbers of specific OTUs were found at the end of the loading, especially in beer vinegar. Under our working conditions in which a semi-continuous submerged fermentation is performed, the loading phase refills the tank with fresh medium coming from each raw material. At the end of this phase, the moment of highest ethanol concentration and lowest acidity level of the cycle is reached (García-García et al., 2019; Jiménez-Hornero et al., 2020; Román-Camacho et al., 2022). In this

10.3389/fmicb.2022.1055010

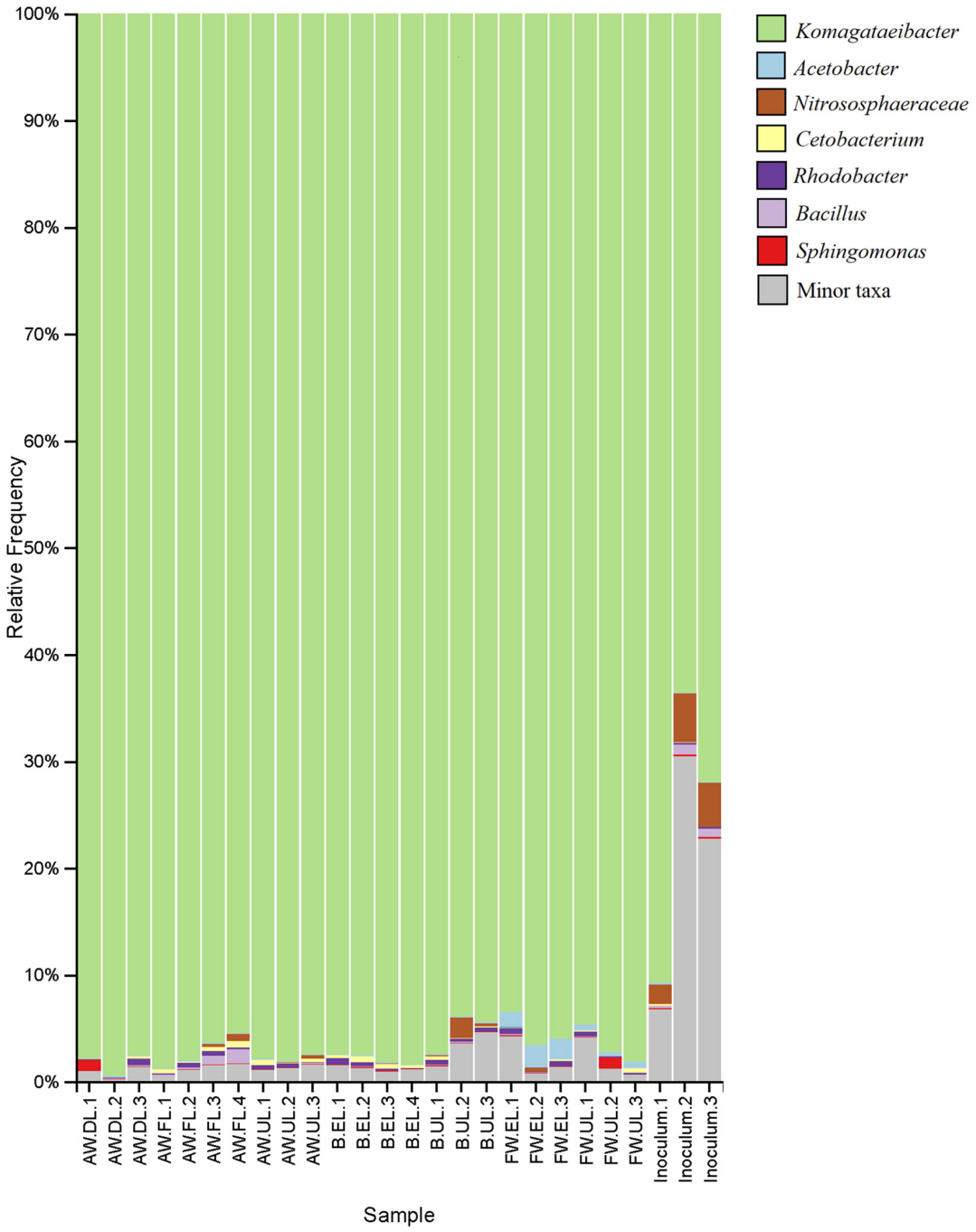

FIGURE 7
Taxonomy bar plot showing the assignment of the total OTUs to the main taxa of the vinegar metagenome. The relative frequency (%) of OTUs provided by the taxa to each sample is represented up to the genus level as a maximum specificity. The list of taxa assigned to each one of the total OTUs, including the main taxa and those conforming to a minor fraction (see gray color) can be found in **Supplementary Table 2**. AW, alcohol wine; B, beer; FW, fine wine; EL, end of loading phase (FL, fast loading; DL, discontinuous loading); UL, just before unloading.

milder environment, this point may be characterized by a higher diversity of microorganisms and, consequently, unique OTUs. Conversely, at the final period of the acetification, both the highest acetification rates and final acidity levels are achieved thus favoring the growth of, exclusively, the best-adapted microbiota (Wang et al., 2015; Andrés-Barrao et al., 2016; Zhu et al., 2018). This event might explain the considerable number of OTUs at the final stage of the process for FW vinegar, a highly efficient acetification substrate (Román-Camacho et al., 2022). The higher number of OTUs could

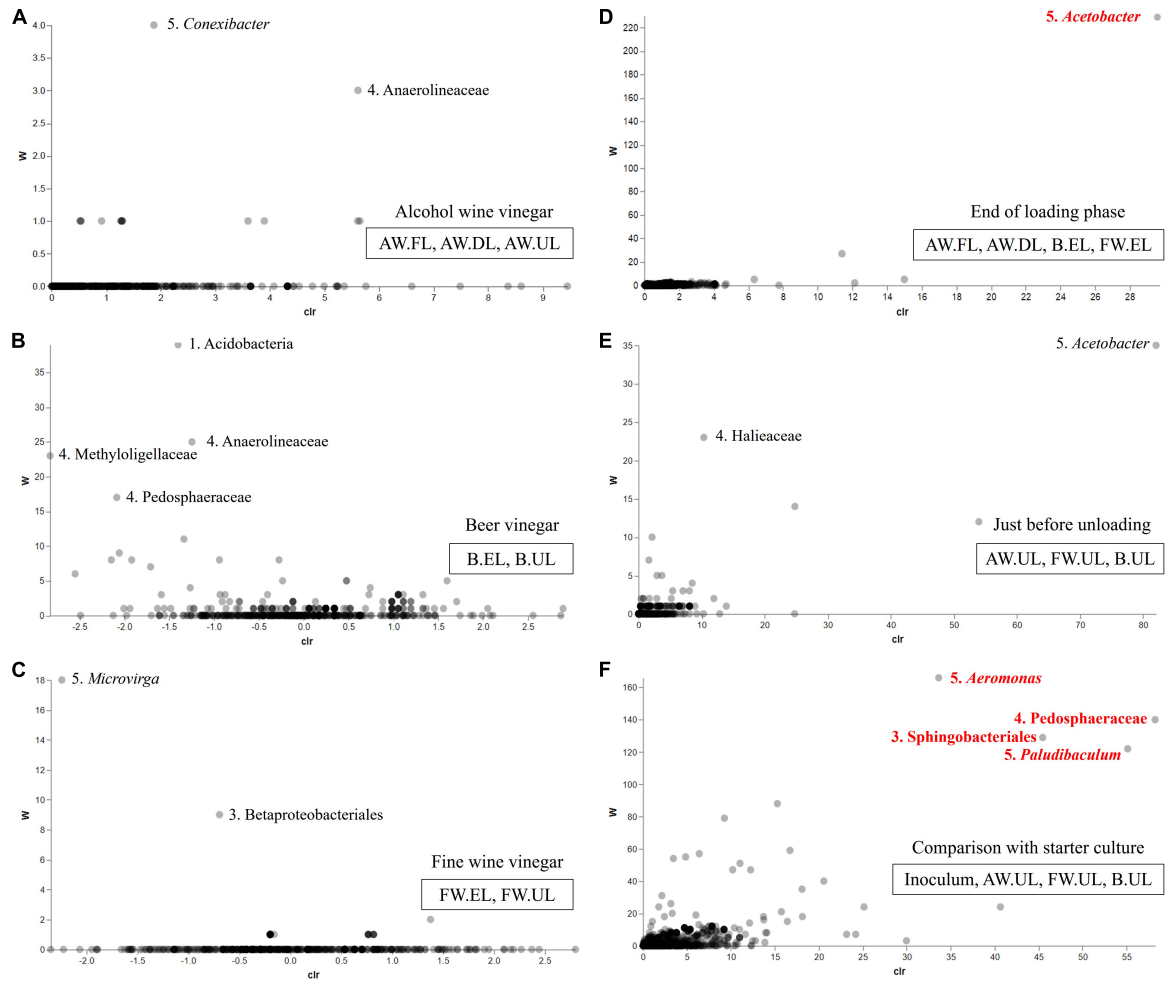

FIGURE 8
Volcano plot which represents abundance differences of vinegar metagenome through the relationship of the ANCOM *W* statistic to the center-log-ratio (CLR) for the sample groups: **(A)** alcohol wine vinegar (AW.FL, AW.DL, AW.UL); **(B)** beer vinegar (B.EL, B.UL); **(C)** fine wine vinegar (FW.EL, FW.UL); **(D)** end of the loading phase (AW.FL, AW.DL, B.EL, FW.EL); **(E)** just before unloading (AW.UL, B.UL, FW.UL); **(F)** comparison with the starter culture (inoculum, AW.UL, B.UL, FW.UL). *W* statistic is the number of ANCOM null hypotheses rejected for each taxon, indicating significant differences between ratios of a taxon's relative abundance to those of *W* for other taxa (FDR with a p-value < 0.05). Taxa are displayed as dots distributed along the matrix and numbers next to highlighted taxa indicate the taxonomical category (1. Phylum, 2. Class, 3. Orden, 4. Family, 5. Genus). Those taxa with significant abundance differences are displayed in red color.

be associated with higher diversity levels in the case of AW and FW vinegar, whereas the opposite occurred for B vinegar: the biodiversity study revealed a lower diversity level at B.EL and an increase at B.UL. Sudden changes caused by the addition of fresh medium might establish a specific dominant microbiota that exploit the nutrients provided particularly by the beer medium, such as fermentable sugars and amino acids (Román-Camacho et al., 2022). Other components such as those containing hops have demonstrated a high antimicrobial ability against the growth of several bacteria and molds, which might promote lower diversity when the beer medium is added (Rodhouse and Carbonero, 2019; Tronina et al., 2020). So, the particular features associated with each raw material apparently influence the number and distribution of OTUs in the vinegar metagenome.

On the other hand, the inoculum exhibited the highest number and biodiversity of OTUs according to the alpha and beta diversity analyses performed, far above the vinegar-making samples (**Table 1** and **Figure 5**). It is worth noting that the original starter culture came from a previous acetification process for making wine vinegar which was first used for starting the alcohol wine acetification, which subsequently served as a starter for the acetification of natural raw materials (Román-Camacho et al., 2020, 2022). Under this working system, the microbiota comprising the starter culture are subjected to diverse environmental changes due to the switching to different media. This situation might explain the high biodiversity in

TABLE 2 List of selected vinegar isolates for identification by MALDI-TOF MS analysis.

Isolated	Species	Appearance	Sampling time	Medium	Score
1	*L. fusiformis*	Other bacteria	AW.FL	GYC	2.11
2	*L. fusiformis*	Other bacteria	AW.FL	GYC	1.79
3	*L. fusiformis*	Other bacteria	AW.FL	GYC	2.13
4	*L. fusiformis*	Other bacteria	AW.FL	GYC	1.78
5	*L. fusiformis*	Other bacteria	AW.FL	GYC	2.08
6	*L. fusiformis*	Other bacteria	AW.DL	GYC	2.19
7	*L. fusiformis*	Other bacteria	AW.DL	GYC	2.15
8	*L. fusiformis*	Other bacteria	AW.DL	GYC	2.11
9	No identified	Other bacteria	AW.DL	GYC	1.59
10	*L. fusiformis*	Other bacteria	AW.UL	GYC	2.14
11	*L. fusiformis*	Other bacteria	AW.UL	YPD	2.28
12	*L. fusiformis*	Other bacteria	AW.UL	YPD	2.29
13	*L. fusiformis*	Other bacteria	AW.UL	GYC	2.23
14	No identified	Other bacteria	AW.UL	GYC	1.62
15	No identified	Other bacteria	AW.UL	GYC	1.43
16	*K. intermedius*	AAB	B.EL	GYC	1.80
17	*K. intermedius*	AAB	B.EL	GYC	1.70
18	No identified	AAB	B.EL	GYC	1.34
19	No identified	AAB	B.EL	GYC	1.54
20	No identified	AAB	B.EL	GYC	1.54
21	*K. intermedius*	AAB	B.EL	GYC	1.71
22	*K. intermedius*	AAB	B.EL	GYC	1.81
23	No identified	AAB	B.UL	GYC	1.51
24	*K. intermedius*	AAB	B.UL	GYC	1.86
25	No identified	AAB	B.UL	GYC	1.58
26	*K. intermedius*	AAB	B.UL	GYC	1.87
27	*L. fusiformis*	Other bacteria	FW.EL	GYC	2.25
28	No identified	AAB	FW.UL	GYC	1.62
29	No identified	AAB	FW.UL	GYC	1.54
30	*K. intermedius*	AAB	FW.UL	GYC	1.72
31	*L. fusiformis*	Other bacteria	FW.UL	GYC	2.22

AW, alcohol wine; B, beer; FW, fine wine; EL, end of loading phase (FL, fast loading; DL, discontinuous loading); UL, just before unloading. AAB, acetic acid bacteria.
Score values represent the confidence degree for the identification of each isolate. High-confidence (2.00–3.00, green color); medium-confidence (1.99–1.70, yellow color); low-confidence or no organism identification possible (0.00–1.69, red color).

the starting inoculum and its progressive loss in vinegar-making samples which would vary depending on the raw material. Peng et al. (2015) determined a decrease in the alpha diversity throughout acetic acid fermentation of Chinese vinegar produced by solid-state fermentation and using 454 pyrosequencing.

In order to carry out a more complete taxonomic study that will facilitate a more accurate identification of the vinegar microbiota, 16S rRNA amplicon sequencing and MALDI-TOF MS were applied. The analysis revealed that Proteobacteria was the most frequent taxon including the acetic acid bacteria (AAB) genera *Acetobacter* and *Komagataeibacter* (**Figures 6**, **7**). The latter was the most predominant genus of the metagenome, far above all other taxa in- or outside of the Proteobacteria. Indeed, the high number of *Komagataeibacter* OTUs (431) found among the sequence reads could lead to a higher diversity of the present species within the genus (**Supplementary Table 2**). Several studies have demonstrated the suitability of some *Komagataeibacter* species for adaptation and survival throughout industrial acetification due to their physiological and growth characteristics, including high ethanol preference, high acetic acid-producing capability, withstanding both low [7–9% (w/v)] and high [10–20% (w/v)] acidity levels, and a constant oxygen requirement (Yamada et al., 2012; Gullo et al., 2014; Qiu et al., 2021; He et al., 2022). Metagenomics studies applied to the elaboration of vinegar by traditional surface culture (Valera et al., 2015; Peters et al., 2017; Milanović et al., 2018) and industrial submerged culture (Trček et al., 2016) have highlighted the presence and function of *Komagataeibacter*, particularly species such as *K. europaeus*,

K. intermedius, *K. hansenii*, *K. nataicola*, *K. rhaeticus*, and *K. xylinus*. Furthermore, *Komagataeibacter* has been reported in other omics approaches such as transcriptomics (Wang et al., 2021) and metaproteomics (Andrés-Barrao et al., 2016), including our previous works in which the genus accounted for around 90% of total proteins allowing to confirm these results (Román-Camacho et al., 2020, 2021, 2022). Despite the well-known difficulty to recover AAB on solid culture media from industrial bioreactors (Mamlouk and Gullo, 2013; Vegas et al., 2013), MALDI-TOF MS protein fingerprinting succeeded in identifying 7 isolates as the AAB species *K. intermedius*, from FW and B vinegars. This milestone was also achieved by Andrés-Barrao et al. (2013) in industrial vinegar production.

Acetobacter was the other AAB genus identified by amplicon sequencing, one of the most prominent taxa of the non-abundant microbiota, mainly in FW vinegar (**Figure 7**). In contrast to *Komagataeibacter*, *Acetobacter* may lack either the molecular mechanisms of adaptation to a nutritionally poor medium such as AW or the capability to assimilate the excess sugars from the B medium (Román-Camacho et al., 2022). Despite this, the results of differential abundance analysis suggested that *Acetobacter* exhibited a strong ability to survive throughout the process (**Figure 8**). Most molecular studies have demonstrated that *Acetobacter* species are normally damaged at acidity levels higher than 8–10% (w/v), so they are usually found in wine, cereal, and balsamic traditional vinegars and early stages of those produced by submerged culture, with *A. pasteurianus* being the most reported one due to its notable production of and high resistance to acetic acid (Gullo and Giudici, 2008; Andrés-Barrao et al., 2011, 2013; Gullo et al., 2014; Zhang et al., 2015; Wu et al., 2017). It is worth noting that similar frequencies for *Acetobacter* to those obtained in this analysis (around 2–3%) were showed in our metaproteomic approaches for the same media (Román-Camacho et al., 2020, 2021, 2022). Despite the use of an optimized medium for AAB, none of the isolates were identified as *Acetobacter* by MALDI-TOF MS, which would indicate that these bacteria may be present in a "viable but non-culturable" (VBNC) state in competition with other microbial groups (De Roos and De Vuyst, 2018; Milanović et al., 2018).

On the other hand, 16S rRNA amplicon sequencing revealed the presence of archaea from the phylum Thaumarchaeota with, more specifically, members of the Nitrososphaeraceae family as the main representatives (**Figures 5**, **7**). To our knowledge, no studies have reported the presence of archaea in industrially produced vinegar, and only Wu et al. (2017) reported by metagenomics "shotgun" sequencing that around 8% of a traditional cereal vinegar microbiota were identified as archaea. Nitrososphaeraceae has been recently found as a part of microbial communities of marine water surfaces and soils by metagenomics and metatranscriptomics (Clark et al., 2021; Jain and Krishnan, 2021). These microorganisms obtain energy by oxidizing ammonia to nitrite aerobically, thereby fixing CO_2, but growth depends on the addition of small amounts of organic acids (Stieglmeier et al., 2014). Future studies based on functional analyses will be necessary to clarify the physiology and role of these archaea in a medium such as vinegar, both in the raw material and throughout the acetification process.

Many other groups of bacteria, different from AAB, were also identified by 16S rRNA amplicon sequencing. Regarding *Cetobacterium* and *Rhodobacter*, no reports in vinegar have been found for these microorganisms, but because they were present in most of the samples, mainly in those taken along the acetification process, they might play a prominent role in the microbial community. These genera have been associated with the use of diverse strategies for the production and assimilation of acetate, respectively (Erkal et al., 2019; Bhute et al., 2020; Xie et al., 2022). Conversely, the presence of *Bacillus* (e.g., *Bacillus amyloliquefaciens*) has been previously reported in vinegar, concretely, Zhang et al. (2017) showed that they may contribute to the production of acetoin and tetramethylpyrazine, thus enhancing the organoleptic properties, mainly the flavor, of final Chinese vinegars. Moreover, a high concurrence of *Bacillus* was found in biofilms of strawberry vinegar (Valera et al., 2015) and seed vinegar (Milanović et al., 2018). *Sphingomonas* were reported in vinegar for the first time in surface vinegar and, due to the ability of some species to produce extracellular polysaccharides, its presence was attributed to the contribution to the vinegar biofilm formation (Huang et al., 2016; Milanović et al., 2018). To our knowledge, this is the first time that these bacterial genera are identified in submerged culture vinegar, however, further assays could facilitate a better understanding of the strategies used for minor fractions of these microorganisms to survive throughout acetification.

In addition to AAB, other microorganisms were identified both by 16S rRNA amplicon sequencing and MALDI-TOF MS and, particularly, by the latter method (**Table 2**). These isolates belonged mainly to an endophyte bacteria named *L. fusiformis*, which was widely reported in AW vinegar and some samples of FW vinegar. Although this microorganism has not been well-studied, some works have detailed its role in the production of acetic acid for enhancing signaling pathways to respond to different stressors in plants (Goud et al., 2014; Zhu et al., 2021). Furthermore, one single OTU has been associated with the *Lysinibacillus* genus through 16S rRNA amplicon sequencing (**Supplementary Table 2**). Despite the low frequency displayed in metagenomics, this microorganism may present appropriate growing conditions for the development in solid media, although its role in the submerged vinegar production requires further studies.

Conclusion

A strategy applying two different "omics" tools has been carried out to identify the present microbiota during the

submerged acetification process of three different raw materials, a synthetic medium and two natural substrates. Metagenomics by 16S rRNA amplicon sequencing and protein fingerprinting by MALDI-TOF MS were implemented, leading to novel results about the microbial composition of vinegar. Metagenomics revealed that along the time courses of the three acetification processes studied, the vinegar microbiota was mainly composed of the AAB genus *Komagataeibacter*, which dramatically outnumbered the rest of the taxa, and a minor fraction of microorganisms including the AAB genus *Acetobacter*, many other groups of bacteria, and even microorganisms belonging to the archaea, mainly Nitrososphaeraceae. Regarding AAB groups, these results allowed us to confirm the composition of the predominant microbiota obtained in our previous metaproteomics approaches. MALDI-TOF MS also confirmed the dominance of *Komagataeibacter* allowing the identification of a specific species, *K. intermedius*. 16S rRNA amplicon sequencing has allowed the detection of a larger number of taxonomic groups, up to genus level, than most DNA-based methods used during the production of vinegar. MALDI-TOF MS may be an easy, cheap, and quick method to complement the identification analysis, allowing to reach the species or strain level. However, the cultivability of the microorganisms in solid media as well as comprehensive databases to compare the peptide mass fingerprints are necessary. The combination of a culture-independent technique and a culture-dependent method, as done in the present work, allows the generation of a broader picture of the industrial production of vinegar. The finding of, not only the main AAB group responsible for the acetification but also of new microbial groups, such as other bacteria and archaea, which were not reported to date in industrial vinegar produced by submerged culture, encourages to perform further studies to understand their role in the microbial community. In addition, new insights on the characterization of the raw materials used have been obtained. This combined "omics" approach may have a biotechnological potential for the vinegar-making industry and even in other related food microbiology fields.

Data availability statement

The data presented in this study are deposited in the Sequence Read Archive (SRA) repository (NCBI), accession number: PRJNA891065 (https://www.ncbi.nlm.nih.gov/sra/).

Author contributions

JR-C: methodology, validation, formal analysis, data curation, writing—original draft preparation, and visualization. IG-G and JM: conceptualization, investigation, resources, writing—review and editing, supervision, project administration, and funding acquisition. IS-D: methodology, validation, formal analysis, conceptualization, and visualization. AE and WL: validation and supervision. TG-M: conceptualization, data curation, validation, and supervision. All authors contributed to the article and approved the submitted version.

Funding

This study was co-financed by the "Junta de Andalucía" and the European Regional Development Fund, ERDF (FEDER), Ref. PY20_00590 and PID2021-127766OB-I00 from Spanish Ministry of Science and Innovation (MICINN/European Union FEDER).

Acknowledgments

Kind help of the staff of Bio Knowledge Lab, S.L. for providing the gDNA extraction kit and performing the 16S rRNA amplicon sequencing as well as the staff of the Proteomics Unit at the Central Research Support Service (SCAI) of the University of Córdoba for performing the identification of isolates by MALDI-TOF MS is gratefully acknowledged. Also, a special mention to Irene Sánchez-León for her kind collaboration in quantifying the gDNA. Finally, we would like to express our gratitude to Alvear winery and Mahou San Miguel Group, production Center of Córdoba, for supplying us the fine wine and craft beer, respectively.

Conflict of interest

The authors declare that the research was conducted in the absence of any commercial or financial relationships that could be construed as a potential conflict of interest.

Publisher's note

Supplementary material

The Supplementary Material for this article can be found online at: https://www.frontiersin.org/articles/10.3389/fmicb.2022.1055010/full#supplementary-material

References

Andrés-Barrao, C., Benagli, C., Chappuis, M., Ortega-Pérez, R., Tonolla, M., and Barja, F. (2013). Rapid identification of acetic acid bacteria using MALDI-TOF mass spectrometry fingerprinting. *Syst. Appl. Microbiol.* 36, 75–81. doi: 10.1016/j.syapm.2012.09.002

Andrés-Barrao, C., Saad, M. M., Cabello-Ferrete, E., Bravo, D., Chappuis, M. L., Ortega-Pérez, R., et al. (2016). Metaproteomics and ultrastructure characterization of *Komagataeibacter* spp. involved in high-acid spirit vinegar production. *Food Microbiol.* 55, 112–122. doi: 10.1016/j.fm.2015.10.012

Andrés-Barrao, C., Weber, A., Chappuis, M. L., Theiler, G., and Barja, F. (2011). Acetic acid bacteria population dynamics and natural imposition of *Gluconacetobacter europaeus* during submerged vinegar production. *Arch. Sci.* 64, 99–114.

Bhute, S. S., Escobedo, B., Haider, M., Mekonen, Y., Ferrer, D., Hillyard, S. D., et al. (2020). The gut microbiome and its potential role in paradoxical anaerobism in pupfishes of the Mojave Desert. *Anim. Microbiome* 2:20. doi: 10.1186/s42523-020-00037-5

Bolyen, E., Rideout, J. R., Dillon, M. R., Bokulich, N. A., Abnet, C. C., Al-Ghalith, G. A., et al. (2019). Reproducible, interactive, scalable and extensible microbiome data science using QIIME 2. *Nat. Biotechnol.* 37, 852–857. doi: 10.1038/s41587-019-0209-9

Callahan, B. J., McMurdie, P. J., Rosen, M. J., Han, A. W., Johnson, A. J. A., and Holmes, S. P. (2016). DADA2: High-resolution sample inference from Illumina amplicon data. *Nat. Methods* 13, 581–583. doi: 10.1038/nmeth.3869

Caporaso, J. G., Lauber, C. L., Walters, W. A., Berg-Lyons, D., Lozupone, C. A., Turnbaugh, P. J., et al. (2010). Global patterns of 16S rRNA diversity at a depth of millions of sequences per sample. *PNAS* 108, 4516–4522. doi: 10.1073/pnas.1000080107

Clark, I. M., Hughes, D. J., Fu, Q., Abadie, M., and Hirsch, P. R. (2021). Metagenomic approaches reveal differences in genetic diversity and relative abundance of nitrifying bacteria and archaea in contrasting soils. *Sci. Rep.* 11:15905. doi: 10.1038/s41598-021-95100-9

Cole, J. R., Wang, Q., Cardenas, E., Fish, J., Chai, B., Farris, R. J., et al. (2009). The Ribosomal Database Project: Improved alignments and new tools for rRNA analysis. *Nucleic Acids Res.* 37, 141–145. doi: 10.1093/nar/gkn879

De Ory, I., Romero, L. E., and Cantero, D. (2004). Operation in semi-continuous with a closed pilot plant scale acetifier for vinegar production. *J. Food Eng.* 63, 39–45. doi: 10.1016/S0260-8774(03)00280-2

De Roos, J., and De Vuyst, L. (2018). Acetic acid bacteria in fermented foods and beverages. *Curr. Opin. Biotechnol.* 49, 115–119. doi: 10.1016/j.copbio.2017.08.007

De Vero, L., and Giudici, P. (2013). Significance and management of acetic acid bacteria culture collections. *Acetic Acid Bact.* 2:e9. doi: 10.4081/aab.2013.s1.e9

Erkal, N. A., Eser, M. G., Özgür, E., Gündüz, U., Eroglu, I., and Yücel, M. (2019). Transcriptome analysis of *Rhodobacter capsulatus* grown on different nitrogen sources. *Arch. Microbiol.* 201, 661–671. doi: 10.1007/s00203-019-01635-x

Fernández-Pérez, R., Torres, C., Sanz, S., and Ruiz-Larrea, F. (2010). Strain typing of acetic acid bacteria responsible for vinegar production by the submerged elaboration method. *Food Microbiol.* 27, 973–978. doi: 10.1016/j.fm.2010.05.020

García-García, I., Cantero-Moreno, D., Jiménez-Ot, C., Baena-Ruano, S., Jiménez-Hornero, J., Santos-Dueñas, I., et al. (2007). Estimating the mean acetification rate via on-line monitored changes in ethanol during a semi-continuous vinegar production cycle. *J. Food Eng.* 80, 460–464. doi: 10.1016/j.jfoodeng.2006.05.028

García-García, I., Jiménez-Hornero, J. E., Santos-Dueñas, I. M., González-Granados, Z., and Cañete-Rodríguez, A. M. (2019). "Modeling and optimization of acetic acid fermentation," in *Advances in Vinegar Production*, ed. A. Bekatorou (Madrid: Taylor & Francis Group), doi: 10.1201/9781351208475

García-García, I., Santos-Dueñas, I. M., Jiménez-Ot, C., Jiménez-Hornero, J. E., and Bonilla-Venceslada, J. L. (2009). "Vinegar Engineering," in *Vinegars of the World*, eds L. Solieri and P. Giudici (Milano: Springer), doi: 10.1007/978-88-470-0866-3_6

Goud, R. K., Sarkar, O., Chiranjeevi, P., and Venkata-Mohan, S. (2014). Bioaugmentation of potent acidogenic isolates: A strategy for enhancing biohydrogen production at elevated organic load. *Bioresour. Technol.* 165, 223–232. doi: 10.1016/j.biortech.2014.03.049

Gullo, M., Caggia, C., De Vero, L., and Giudici, P. (2006). Characterization of acetic acid bacteria in "traditional balsamic vinegar". *Int. J. Food Microbiol.* 106, 209–212. doi: 10.1016/j.ijfoodmicro.2005.06.024

Gullo, M., and Giudici, P. (2008). Acetic acid bacteria in traditional balsamic vinegar: Phenotypic traits relevant of starter cultures selection. *Int. J. Food Microbiol.* 125, 46–53. doi: 10.1016/j.ijfoodmicro.2007.11.076

Gullo, M., Verzelloni, E., and Canonico, M. (2014). Aerobic submerged fermentation by acetic acid bacteria for vinegar production: Process and biotechnological aspects. *Process Biochem.* 49, 1571–1579. doi: 10.1016/j.procbio.2014.07.003

He, Y., Xie, Z., Zhang, H., Liebl, W., Toyama, H., and Chen, F. (2022). Oxidative fermentation of acetic acid bacteria and its products. *Front. Microbiol.* 13:879246. doi: 10.3389/fmicb.2022.879246

Hidalgo, C., Torija, M. J., Mas, A., and Mateo, E. (2013). Effect of inoculation on strawberry fermentation and acetification processes using native strains of yeast and acetic acid bacteria. *Food Microbiol.* 34, 88–94. doi: 10.1016/j.fm.2012.11.019

Ho, C. W., Lazim, A. M., Fazry, S., Zaki, U. K. H. H., and Lim, S. J. (2017). Varieties, production, composition and health benefits of vinegars: A review. *Food Chem.* 221, 1621–1630. doi: 10.1016/j.foodchem.2016.10.128

Huang, H., Wu, M., Yang, H., Li, X., Ren, M., Li, G., et al. (2016). Structural and physical properties of sanxan polysaccharide from *Sphingomonas sanxanigenens*. *Carbohydr. Polym.* 144, 410–418. doi: 10.1016/j.carbpol.2016.02.079

Imchen, M., Kumavath, R., Vaz, A. B. M., Góes-Neto, A., Barh, D., Ghosh, P., et al. (2019). 16S rRNA gene amplicon based metagenomic signatures of rhizobiome community in rice field during various growth stages. *Front. Microbiol.* 10:2103. doi: 10.3389/fmicb.2019.02103

Jain, A., and Krishnan, K. P. (2021). Marine Group-II archaea dominate particle-attached as well as free-living archaeal assemblages in the surface waters of Kongsfjorden, Svalbard, Arctic Ocean. *Antonie Van Leeuwenhoek* 114, 633–647. doi: 10.1007/s10482-021-01547-1

Jiménez-Hornero, J. E., Santos-Dueñas, I. M., and García-García, I. (2020). Modelling acetification with Artificial Neural Networks and comparison with alternative procedures. *Processes* 8:749. doi: 10.3390/pr8070749

Kim, M., Lee, K. H., Yoon, S. W., Kim, B. S., Chun, J., and Yi, H. (2013). Analytical tools and databases for metagenomics in the next-generation sequencing era. *Genom. Inform.* 11, 102–113. doi: 10.5808/GI.2013.11.3.102

Lee, S., Lee, J. A., Park, G. G., Jang, J. K., and Park, Y. S. (2017). Semi-continuous fermentation of onion vinegar and its functional properties. *Molecules* 22:1313. doi: 10.3390/molecules22081313

Li, S., Li, P., Feng, F., and Luo, L. X. (2015). Microbial diversity and their roles in the vinegar fermentation process. *Appl. Microbiol. Biotechnol.* 99, 4997–5024. doi: 10.1007/s00253-015-6659-1

Llaguno, C. (1991). "Definición y tipos de vinagre," in *El Vinagre De Vino*, eds C. Llaguno and M. C. Polo (Madrid: Consejo Superior de Investigaciones Científicas (CSIC)), 133–145.

Maestre, O., Santos-Dueñas, I. M., Peinado, R., Jiménez-Ot, C., García-García, I., and Mauricio, J. C. (2008). Changes in amino acid composition during wine vinegar production in a fully automatic pilot acetator. *Process Biochem.* 43, 803–807. doi: 10.1016/j.procbio.2008.03.007

Mamlouk, D., and Gullo, M. (2013). Acetic acid bacteria: Physiology and carbon sources oxidation. *Indian J. Microbiol.* 53, 377–384. doi: 10.1007/s12088-013-0414-z

Mandal, S., Van Treuren, W., White, R. A., Eggesbø, M., Knight, R., and Peddada, S. D. (2015). Analysis of composition of microbiomes: A novel method for studying microbial composition. *Microb. Ecol. Health Dis.* 26:27663. doi: 10.3402/mehd.v26.27663

Mas, A., Torija, M. J., García-Parrilla, M. C., and Troncoso, A. M. (2014). Acetic acid bacteria and the production and quality of wine vinegar. *Sci. World J.* 2014:394671. doi: 10.1155/2014/394671

Milanović, V., Osimani, A., Garofalo, C., De Filippis, F., Ercolini, D., Cardinali, F., et al. (2018). Profiling white wine seed vinegar bacterial diversity through viable counting, metagenomic sequencing and PCR-DGGE. *Int. J. Food Microbiol.* 286, 66–74. doi: 10.1016/j.ijfoodmicro.2018.07.022

Peng, Q., Yang, Y., Guo, Y., and Han, Y. (2015). Analysis of bacterial diversity during acetic acid fermentation of tianjin duliu aged vinegar by 454 pyrosequencing. *Curr. Microbiol.* 71, 195–203. doi: 10.1007/s00284-015-0823-9

Peters, B., Mientus, M., Kostner, D., Daniel, R., Liebl, W., and Ehrenreich, A. (2017). Expression of membrane-bound dehydrogenases from a mother of vinegar metagenome in *Gluconobacter oxydans*. *Appl. Microbiol. Biotechnol.* 101, 7901–7912. doi: 10.1007/s00253-017-8479-y

Qi, Z., Yang, H., Xia, X., Quan, W., Wang, W., and Yu, X. (2014). Achieving high strength vinegar fermentation via regulating cellular growth status and aeration strategy. *Process Biochem*. 49, 1063–1070. doi: 10.1016/j.procbio.2014.03.018

Qiu, X., Zhang, Y., and Hong, H. (2021). Classification of acetic acid bacteria and their acid resistant mechanism. *AMB Express* 11:29. doi: 10.1186/s13568-021-01189-6

Quast, C., Pruesse, E., Yilmaz, P., Gerken, J., Schweer, T., Yarza, P., et al. (2013). The SILVA ribosomal RNA gene database project: Improved data processing and web-based tools. *Nucleic Acids Res*. 41, 590–596. doi: 10.1093/nar/gks1219

Rizo, J., Guillén, D., Farrés, A., Díaz-Ruiz, G., Sánchez, S., Wacher, C., et al. (2020). Omics in traditional vegetable fermented foods and beverages. *Crit. Rev. Food Sci. Nutr*. 60, 791–809. doi: 10.1080/10408398.2018.1551189

Rodhouse, L., and Carbonero, F. (2019). Overview of craft brewing specificities and potentially associated microbiota. *Crit. Rev. Food Sci. Nutr*. 59, 462–473. doi: 10.1080/10408398.2017.1378616

Rognes, T., Flouri, T., Nichols, B., Quince, C., and Mahé, F. (2016). VSEARCH: A versatile open source tool for metagenomics. *Peerj* 4:e2584. doi: 10.7717/peerj.2584

Román-Camacho, J. J., Mauricio, J. C., Santos-Dueñas, I. M., García-Martínez, T., and García-García, I. (2021). Functional metaproteomic analysis of alcohol vinegar microbiota during an acetification process: A quantitative proteomic approach. *Food Microbiol*. 98:103799. doi: 10.1016/j.fm.2021.103799

Román-Camacho, J. J., Mauricio, J. C., Santos-Dueñas, I. M., García-Martínez, T., and García-García, I. (2022). Unraveling the role of acetic acid bacteria comparing two acetification profiles from natural raw materials: A quantitative approach in *Komagataeibacter europaeus*. *Front. Microbiol*. 13:840119. doi: 10.3389/fmicb.2022.840119

Román-Camacho, J. J., Santos-Dueñas, I. M., García-García, I., Moreno-García, J., García-Martínez, T., and Mauricio, J. C. (2020). Metaproteomics of microbiota involved in submerged culture production of alcohol wine vinegar: A first approach. *Int. J. Food Microbiol*. 333:108797. doi: 10.1016/j.ijfoodmicro.2020.108797

Stieglmeier, M., Klingl, A., Alves, R. J. E., Rittmann, S. K. M. R., Melcher, M., Leisch, N., et al. (2014). Nitrososphaera viennensis gen. nov., sp. nov., an aerobic and mesophilic, ammonia-oxidizing archaeon from soil and a member of the archaeal phylum *Thaumarchaeota*. *Int. J. Syst. Evol. Microbiol*. 64, 2738–2752. doi: 10.1099/ijs.0.063172-0

Trček, J., and Barja, F. (2015). Updates on quick identification of acetic acid bacteria with a focus on the 16S–23S rRNA gene internal transcribed spacer and the analysis of cell proteins by MALDI-TOF mass spectrometry. *Int. J. Food Microbiol*. 196, 137–144. doi: 10.1016/j.ijfoodmicro.2014.12.003

Trček, J., Mahnič, A., and Rupnik, M. (2016). Diversity of the microbiota involved in wine and organic apple cider submerged vinegar production as revealed by DHPLC analysis and next-generation sequencing. *Int. J. Food Microbiol*. 223, 57–62. doi: 10.1016/j.ijfoodmicro.2016.02.007

Tronina, T., Popłoński, J., and Bartmańska, A. (2020). Flavonoids as phytoestrogenic components of hops and beer. *Molecules* 25:4201. doi: 10.3390/molecules25184201

Valera, M. J., Torija, M. J., Mas, A., and Mateo, E. (2015). Acetic acid bacteria from biofilm of strawberry vinegar visualized by microscopy and detected by complementing culture-dependent and culture-independent techniques. *Food Microbiol*. 46, 452–462. doi: 10.1016/j.fm.2014.09.006

Vegas, C., González, A., Mateo, E., Mas, A., Poblet, M., and Torija, M. J. (2013). Evaluation of representativity of the acetic acid bacteria species identified by culture-dependent method during a traditional wine vinegar production. *Food Res. Int*. 51, 404–411. doi: 10.1016/j.foodres.2012.12.055

Vegas, C., Mateo, E., González, A., Jara, C., Guillamón, J. M., Poblet, M., et al. (2010). Population dynamics of acetic acid bacteria during traditional wine vinegar production. *Int. J. Food Microbiol*. 138, 130–136. doi: 10.1016/j.ijfoodmicro.2010.01.006

Wang, B., Shao, Y., and Chen, F. (2015). Overview on mechanisms of acetic acid resistance in acetic acid bacteria. *World J. Microbiol. Biotechnol*. 31, 255–263. doi: 10.1007/s11274-015-1799-0

Wang, D., Wang, M., Cao, L., Wang, X., Sun, J., Yuan, J., et al. (2022). Changes and correlation of microorganism and flavor substances during persimmon vinegar fermentation. *Food Biosci*. 46:101565. doi: 10.1016/j.fbio.2022.101565

Wang, L., Hong, H., Zhang, C., Huang, Z., and Guo, H. (2021). Transcriptome analysis of *Komagataeibacter europaeus* CGMCC 20445 responses to different acidity levels during acetic acid fermentation. *Pol. J. Microbiol*. 70, 305–313. doi: 10.33073/pjm-2021-027

Wu, L. H., Lu, Z. M., Zhang, X. J., Wang, Z. M., Yu, Y. J., Shi, J. S., et al. (2017). Metagenomics reveals flavour metabolic network of cereal vinegar microbiota. *Food Microbiol*. 62, 23–31. doi: 10.1016/j.fm.2016.09.010

Xie, M., Xie, Y., Li, Y., Zhou, W., Zhang, Z., Yang, Y., et al. (2022). Stabilized fermentation product of *Cetobacterium somerae* improves gut and liver health and antiviral immunity of zebrafish. *Fish Shellfish Immunol*. 120, 56–66. doi: 10.1016/j.fsi.2021.11.017

Yamada, Y., Yukphan, P., Lan-Vu, H. T., Muramatsu, Y., Ochaikul, D., Tanasupawat, S., et al. (2012). Description of *Komagataeibacter* gen. nov., with proposals of new combinations (*Acetobacteraceae*). *J. Gen. Appl. Microbiol*. 58, 397–404. doi: 10.2323/jgam.58.397

Zhang, L., Huang, J., Zhou, R., and Wu, C. (2017). Evaluating the feasibility of fermentation starter inoculated with *Bacillus amyloliquefaciens* for improving acetoin and tetramethylpyrazine in Baoning bran vinegar. *Int. J. Food Microbiol*. 255, 42–50. doi: 10.1016/j.ijfoodmicro.2017.05.021

Zhang, Z., Ma, H., Yang, Y., Dai, L., and Chen, K. (2015). Protein profile of *Acetobacter pasteurianus* HZ3-21. *Curr. Microbiol*. 70, 724–729. doi: 10.1007/s00284-015-0777-y

Zhu, L., Guo, J., Sun, Y., Wang, S., and Zhou, C. (2021). Acetic acid-producing endophyte *Lysinibacillus fusiformis* orchestrates jasmonic acid signaling and contributes to repression of cadmium uptake in tomato plants. *Front. Plant Sci*. 12:670216. doi: 10.3389/fpls.2021.670216

Zhu, Y., Zhang, F., Zhang, C., Yang, L., Fan, G., Xu, Y., et al. (2018). Dynamic microbial succession of Shanxi aged vinegar and its correlation with flavor metabolites during different stages of acetic acid fermentation. *Sci. Rep*. 8:8612. doi: 10.1038/s41598-018-26787-6

Frontiers in Microbiology

Explores the habitable world and the potential of microbial life

The largest and most cited microbiology journal which advances our understanding of the role microbes play in addressing global challenges such as healthcare, food security, and climate change.

Discover the latest Research Topics

See more →

Frontiers

Avenue du Tribunal-Fédéral 34
1005 Lausanne, Switzerland
frontiersin.org

Contact us

+41 (0)21 510 17 00
frontiersin.org/about/contact